

UNCLASSIFIED

AD NUMBER
AD390359
CLASSIFICATION CHANGES
TO: unclassified
FROM: confidential
LIMITATION CHANGES
TO: Approved for public release, distribution unlimited
FROM: Distribution authorized to U.S. Gov't. agencies and their contractors; Critical Technology; MAY 1968. Other requests shall be referred to Air Force Rocket Propulsion Lab., Edwards AFB, CA.
AUTHORITY
31 May 1980, DoDD 5200.10; AFPRL ltr, 5 Feb 1986

THIS PAGE IS UNCLASSIFIED

AD 390 359

AUTHORITY:

AFRPL

14 Feb 86



THIS REPORT HAS BEEN DELIMITED
AND CLEARED FOR PUBLIC RELEASE
UNDER DOD DIRECTIVE 5200.20 AND
NO RESTRICTIONS ARE IMPOSED UPON
ITS USE AND DISCLOSURE.

DISTRIBUTION STATEMENT A

APPROVED FOR PUBLIC RELEASE;
DISTRIBUTION UNLIMITED.

SECURITY

MARKING

The classified or limited status of this report applies to each page, unless otherwise marked.

Separate page printouts MUST be marked accordingly.

THIS DOCUMENT CONTAINS INFORMATION AFFECTING THE NATIONAL DEFENSE OF THE UNITED STATES WITHIN THE MEANING OF THE ESPIONAGE LAWS, TITLE 18, U.S.C., SECTIONS 793 AND 794. THE TRANSMISSION OR THE REVELATION OF ITS CONTENTS IN ANY MANNER TO AN UNAUTHORIZED PERSON IS PROHIBITED BY LAW.

NOTICE: When government or other drawings, specifications or other data are used for any purpose other than in connection with a definitely related government procurement operation, the U.S. Government thereby incurs no responsibility, nor any obligation whatsoever; and the fact that the Government may have formulated, furnished, or in any way supplied the said drawings, specifications, or other data is not to be regarded by implication or otherwise as in any manner licensing the holder or any other person or corporation, or conveying any rights or permission to manufacture, use or sell any patented invention that may in any way be related thereto.

CONFIDENTIAL

AFRPL-TR-68-20

ADVANCED MANEUVERING PROPULSION
TECHNOLOGY PROGRAM
(SECOND QUARTERLY PROGRESS REPORT)

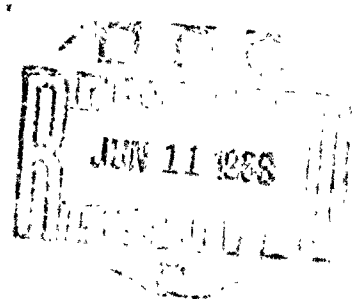
Rocketdyne
A Division of North American Rockwell Corporation
6633 Canoga Ave.
Canoga Park, California

Technical Report AFRPL-TR-68-20

May 1968

Group 4
Downgraded at 3-Year Intervals
Declassified After 12 Years

THIS MATERIAL CONTAINS INFORMATION AFFECTING THE NATIONAL
DEFENSE OF THE UNITED STATES WITHIN THE MEANING OF THE
ESPIONAGE LAWS, TITLE 18 U.S.C., SECTIONS 793 AND 794, THE
TRANSMISSION OR REVELATION OF WHICH IN ANY MANNER TO AN
UNAUTHORIZED PERSON IS PROHIBITED BY LAW.



In addition to security requirements which must be met, this document is subject to special export controls and each transmittal to foreign governments or foreign nationals may be made only with prior approval of AFRPL (RPPR/STINFO), Edwards, California, 93523.

Air Force Rocket Propulsion Laboratory
Air Force Systems Command
United States Air Force
Edwards Air Force Base, California

CONFIDENTIAL

390359

AD390359

Qualified users may obtain copies of this report from the Defense Documentation Center.

Reproduction Notice. This report may be reproduced to satisfy needs of U.S. Government agencies. No other reproduction is authorized except with permission of AFRPL.

When U.S. Government drawings, specifications, or other data are used for any purpose other than a definitely related Government procurement operation, the Government thereby incurs no responsibility nor any obligation whatsoever, and the fact that the Government may have formulated, furnished, or in any way supplied the said drawings, specifications, or other data is not to be regarded by implication or otherwise, as in any manner licensing the holder or any other person or corporation, or conveying any rights or permission to manufacture, use, or sell any patented invention that may in any way be related thereto.

ERRATA SHEET FOR
ADVANCED MANEUVERING PROPULSION TECHNOLOGY PROGRAM
(SECOND QUARTERLY PROGRESS REPORT)

Rocketdyne No. R-7380-2
ATRPL TR-68-20

NOTE TO RECIPIENTS OF THE ABOVE REPORT:

Delete Figures 46 and 47 from Appendix II. These figures appear on pages 104 and 106 of Appendix II.

CONFIDENTIAL

AFRPL-TR-68-20

25

ADVANCED MANEUVERING PROPULSION
TECHNOLOGY PROGRAM
(SECOND QUARTERLY PROGRESS REPORT)

ROCKETDYNE
A Division of North American Rockwell Corporation
6633 Canoga Ave.
Canoga Park, California

Technical Report AFRPL-TR-68-20

May 1968

Group 4
Downgraded at 3-Year Intervals
Declassified After 12 Years

THIS MATERIAL CONTAINS INFORMATION AFFECTING THE NATIONAL
DEFENSE OF THE UNITED STATES WITHIN THE MEANING OF THE
ESPIONAGE LAWS, TITLE 18 U.S.C., SECTIONS 793 AND 794, THE
TRANSMISSION OR REVELATION OF WHICH IN ANY MANNER TO AN
UNAUTHORIZED PERSON IS PROHIBITED BY LAW.

In addition to security requirements which must be met, this document is subject to special export controls and each transmittal to foreign governments or foreign nationals may be made only with prior approval of AFRPL (RPPR/STINFO), Edwards, California, 93523.

Air Force Rocket Propulsion Laboratory
Air Force Systems Command
United States Air Force
Edwards Air Force Base, California

CONFIDENTIAL

CONFIDENTIAL

ABSTRACT

- (C) Analysis and design effort on the Advanced Maneuvering Propulsion System (AMPS) progressed satisfactorily during the second quarterly period. Engine system analyses of start and cutoff sequencing, thrust vs mixture ratio operating range, and operational requirements were conducted. Thrust chamber, turbopump, and control subsystem design analysis were performed. Propellant feed system analysis and design effort was accomplished on the propellant tanks, outer shroud and tank supports, insulation, and pressurization subsystems.
- (C) Engine critical component demonstration testing was accomplished on the main engine thrust chamber segment hardware. Forty firing tests were accomplished with the 5-inch solid-wall segment configuration over a chamber pressure range of 650 psia to 72 psia, which meets the design requirement.

CONTENTS

Foreword	ii
Abstract	iii
Introduction	1
Summary	
<u>Task I - Engine System Analysis and Design</u>	13
1. Engine System	13
a. Engine Sequencing Analysis	14
b. Thrust and Mixture Ratio Envelope	25
c. Engine Influence Coefficients	36
d. Purge Requirements for the AMPS Engine	41
e. Instrumentation	54
f. AMPS Engine Base Flow Analysis	55
g. Accessory Provisions	63
h. Manned Mission	63
i. Design	65
2. Thrust Chamber Analysis and Design	73
a. Segment Thrust Chamber Assembly	73
b. Thrust Chamber Cooling	76
3. Turbopump Analysis and Design	93
a. Design Analysis	93
b. Critical Speed Analysis	99
c. Operating Limits	109
4. Control Analysis and Design	109
a. Valve Actuation	110
b. Control System Computer Model	113
5. Technology Assessment	123
<u>Task II - Critical Engine Component Demonstration Testing</u>	127
1. Segment Thrust Chamber Design and Fabrication	127
a. 5-Inch Solid-Wall Thrust Chamber Segment	127
b. 5-Inch Tubular-Wall Thrust Chamber Segment	127
c. 30-Degree Solid-Wall Thrust Chamber Segment	131
d. 30-Degree Tubular-Wall Thrust Chamber Segment	131

2. Injector Design and Fabrication	131
a. 5-Inch Segment Injectors	135
b. 30-Degree Injectors	140
3. Segment Thrust Chamber Testing	140
a. 5-Inch Solid-Wall Thrust Chamber Segment Testing	140
b. 5-Inch Tubular-Wall Thrust Chamber Segment Test	153
c. Thrust Chamber Segment Test Summary	155
d. Injector Face Heat Flux Data Analysis	157
e. Injector Performance	159
f. Chamber Wall Heat Transfer	164
4. Turbopump Bearing and Seal Program	164
5. Facility Operation and Preparation	170
a. Victor Test Stand	170
b. Nevada Field Laboratory Test Facility Design Modification	175
<u>Task III - Propellant Feed System Analysis and Design</u>	179
<u>References</u>	183
<u>Appendix I, Convair Task III Results for</u> <u>Second Quarterly Period</u>	
<u>Appendix II, Lockheed Task III Results for</u> <u>Second Quarterly Period</u>	

ILLUSTRATIONS

1. System Characteristics	3
2. Engine System for Advanced Maneuvering Propulsion System . .	4
3. AMPT Program Milestones	6
4. AMPT Phase 1 Program	7
5. Main Thrust Chamber Segment Approach	10
6. Predicted Thrust During Transition from Main to Secondary Engines	17
7. Fuel Temperature and Density at Pump Discharge During Main Engine Start	20
8. Main Engine Chamber Pressure and Pump Flowrates During Start	24
9. Flow Chart for Thrust and Mixture Ratio Envelope Evaluation .	27
10. Operating Requirements for Main Engine Pumps	29
11. Flowrate Requirements for Main Engine Propellants	30
12. Inlet Conditions for Main Engine Hot-Gas Valve	31
13. Differential Pressure Requirements for Main Engine Oxidizer Turbine Hot-Gas Valve	32
14. Differential Pressure Requirements for Main Engine Fuel Turbine Hot-Gas Valve	33
15. Main Engine Performance	34
16. Operating Envelopes for Main Engine Propellant Pumps . . .	35
17. AMPS Engine Start and Cutoff Control Logic With One Turbine Valve	47
18. AMPS Engine Start and Cutoff Control Logic With Two Turbine Hot-Gas Valves	49
19. Flow Field of Typical Aerospike Nozzle	56
20. Water Table	58
21. AMPS Model Installed in Water Table With Sluice-Generated Primary Flow	59
22. Primary Flowpath for AMPS Engine Base Region	60

CONFIDENTIAL

23. Secondary Flow Paths for AMPS Engine Base Region	61
24. Turbine Exhaust Base Injection Technique to Restrict Base Flow Recirculation Into the Bell Chamber	64
25. AMPS Main Engine Turbine Exhaust Distribution Manifold	67
26. AMPS Main Engine Turbine Exhaust Duct	68
27. Secondary Engine Thrust Chamber Simulator	69
28. Main Fuel Distribution Manifold	70
29. Interim Thrust Mount and Oxidizer Distribution Manifold	71
30. AMPS Main Engine Oxidizer Duct and Manifold	72
31. Candidate Cooling Paths for Main Engine Thrust Chamber	78
32. Main Thrust Chamber Coolant Flowrate vs Chamber Pressure	79
33. Relationship of Wall Position to Stanton and Prandtl Numbers	82
34. Heat Transfer Coefficient Profile at 370- and 650-psia Chamber Pressure	83
35. Temperature Profile for Tube Outer Body at 650-psia Chamber Pressure	85
36. Temperature Profile for Tube Inner Body at 650-psia Chamber Pressure	86
37. Temperature Profile for Tube Inner Body at 370-psia Chamber Pressure	87
38. Heat Flux Profile for Tubes at 650-psia Chamber Pressure	89
39. Heat Flux Profile for Tubes at 370-psia Chamber Pressure	90
40. Available Injector Pressure Drop vs Thrust Chamber Inlet Pressure	91
41. Total Coolant Heat Load vs Chamber Pressure	92
42. Main Engine Oxidizer Turbopump	94
43. Main Engine Fuel Turbopump	95
44. Main Engine Turbopump Critical Speed vs Bearing Spring Rate	102
45. Rotation Path for Pump Shaft	103
46. Main Engine Oxidizer Turbopump Shaft Shape for "Free-Free" Mode	104

CONFIDENTIAL

47. Main Engine Oxidizer Turbopump Shaft Shape for Turbine-End Bearing "Stick" Mode (100,000 lb/in. spring rate)	106
48. Main Engine Oxidizer Turbopump Shaft Shape for Inducer-End Bearing "Stick" Mode	107
49. Main Engine Oxidizer Turbopump Shaft Shape for Turbine-End Bearing "Stick" Mode (1,000,000 lb/in. spring rate)	108
50. Comparison of Valve Actuation Weights	112
51. Engine Mixture Ratio and Chamber Pressure Control Schemes for Hydrogen Bleed Engine Cycle	114
52. Main Engine Control by One Hot-Gas Valve and Two Cavitating Venturi Valves	115
53. Main Engine Control Response With One Hot-Gas Valve and Two Cavitating Venturi Valves	117
54. Main Engine Control With One Hot-Gas Valve and Two Butterfly Propellant Valves	119
55. Main Engine Control With Two Turbine Hot-Gas Valves Only	120
56. Positive Mixture Ratio Error vs Chamber Pressure Ramp Rate	122
57. 5-Inch Solid Wall Segment for G_c Combustion Chamber Contour	129
58. 5-Inch Tubular-Wall Segment Assembly Without Injector	130
59. 30-Degree Solid-Wall Thrust Chamber Segment	132
60. Main Engine Thrust Chamber Tubular-Wall Segments	133
61. Modified 5-Inch Triplet Injector Segment	136
62. 5-Inch Fan Injector Segment	137
63. 5-Inch Concentric Orifice Injector	138
64. Modified 5-Inch Fan Injector	139
65. 30-Degree Fan Injector Segment	141
66. Fan Injector With Radial Drilled Propellant Feed Passages	142
67. Critical Component Demonstration Test Schedule	143
68. 5-Inch Solid-Wall Thrust Chamber Segment at Victor Test Stand	147
69. 5-Inch Triplet Injector U/N 3 With Repair	152
70. 5-Inch Tubular-Wall Thrust Chamber Segment	154
71. Heat Flux Distribution Measured in Contour K and G_c Contour Solid-Wall Thrust Chambers	156

CONFIDENTIAL

72.	Fan Injector U/N 2 After Test 50	158
73.	Heat Flux vs Chamber Pressure Showing Quality of Fluorine Injected on a Bulk Basis	160
74.	5-Inch Fan Injector Orifice Pressure Drop vs Flowrate	161
75.	Performance During Solid-Wall Segment Tests 38 Through 46	164
76.	Characteristic Velocity Efficiency vs Oxidizer Flowrate Divided by Fuel Momentum Flux	165
77.	Oxidizer Bearing and Seal Tester Design	166
78.	Oxidizer Turbopump Seal Designs	168
79.	Main Engine Oxidizer Pump Turbine Seal Design	169
80.	Oxidizer Injection Pressure During Start of Test 36	172
81.	Schematic of Gaseous Fluorine Storage Facility	176
82.	Task III Schedule	181

x

CONFIDENTIAL

CONFIDENTIAL

TABLES

1. Effect of Fuel System Thermal Variations on Engine Start Time	22
2. Main Engine Influence Coefficients for Full Thrust Operation	37
3. Main Engine Influence Coefficients for 9:1 Throttled Operation	38
4. Secondary Engine Influence Coefficients for Full Thrust Operation	39
5. Secondary Engine Influence Coefficients for 9:1 Throttled Operation	40
6. Engine System Purge Requirements	42
7. Total Engine System Operational Purge Fluid Requirements for Extreme Duty Cycles	50
8. Coolant Flowrates for Candidate Main Thrust Chamber Coolant Circuits	80
9. Calculated Values for Main Engine LH ₂ Inducer and Impeller	98
10. Main Engine Oxidizer Pump Bearing Specification	100
11. Additions to Table 18 of First Quarterly Report (R-7380-2)	124
12. Status of Task II Thrust Chamber Design, Fabrication, and Test	128
13. 5-Inch Segment Injector Design Characteristics	134
14. 5-Inch Injector and Solid-Wall Segment Thrust Chamber Test Summary	144
15. Chemical Analysis of Fluorine and Hydrogen at Victor Test Stand	174

CONFIDENTIAL

INTRODUCTION

- (C) The Advanced Maneuvering Propulsion System (AMPS) is a high-energy system utilizing LF_2/LH_2 propellants. The system concept is illustrated in Fig. 1 with some of the basic design parameters for the Advanced Development Program (ADP) together with some of the design variations being considered separately.
- (C) The engine configuration (Fig. 2) utilizes concentric thrust chambers. The outer main thrust chamber (30,000 pounds of thrust) incorporates the toroidal-aerodynamic spike design concept. The inner secondary thrust chamber (3300 pounds of thrust) is a bell-type design. The thrust chambers are fed from independent turbopumps which are driven by hot gases from each thrust chamber. Each thrust chamber can be throttled over a 9:1 thrust range, which gives the engine system an overall throttle ratio of 81:1. The normal mode of operation is for the thrust chambers to fire one at a time, although both chambers can fire simultaneously if desired.
- (C) The propellant feed system consists of the main propellant tankage; thermal conditioning and support structures; zero gravity expulsion system, fill, vent, feed, and drain lines; propellant management system; and a pressurization system. The 18,000-pound payload (20,000 pounds total) is compatible with the present Titan IIID launch vehicle for polar orbit launches from the Western Test Range. A gimbal angle of ± 10 degrees was selected to provide the capability for rapid turning maneuvers. System thermal design provides the capability of at least 14 days in orbit with no fluorine loss and with very little or no hydrogen loss, depending on the mission duty cycle.
- (C) The Advanced Maneuvering Propulsion Technology (AMPT) Advanced Development Program consists of two phases. Phase I, the current program effort for a 24-month period, includes the following three tasks.

Task I, Engine Analysis and Design
Task II, Engine Critical Component Demonstration Testing
Task III, Propellant Feed System Analysis and Design

(U) Effort on Tasks I and II was initiated 1 November 1967. Task III, being performed by two vehicle company subcontractors (General Dynamics/Convair and Lockheed Missiles and Space Company), was initiated 1 December 1967.

CONFIDENTIAL

DESIGN POINT FOR ADP	DESIGN VARIATIONS BEING CONSIDERED
18,000	10,000 TO 75,000
2,000	1,000 TO 25,000
30,000	VARIATIONS WITH STAGE SIZE & APPLICATION
TITAN III C WITHOUT TRANSTAGE	FAMILY OF LAUNCH VEHICLES
14 DAYS (NO F ₂ VENTING)	UP TO 180 DAYS
30 MINIMUM	VARIATIONS WITH MISSION REQUIREMENTS
• NO F ₂ VENTING • H ₂ VENTING & TOPPING	NEAR INSTANT LAUNCH READINESS
• NO SUBORBITAL BURN • 100 NM, CIRCULAR POLAR ORBIT	DEPENDENT ON APPLICATION

PROPULSION SYSTEM WEIGHT, LB

PAYLOAD WEIGHT, LB

THRUST (MAXIMUM), LB

LAUNCH VEHICLE

SPACE RESIDENCE TIME

RESTARTS

PAD HOLD CAPABILITY

FLIGHT PLAN

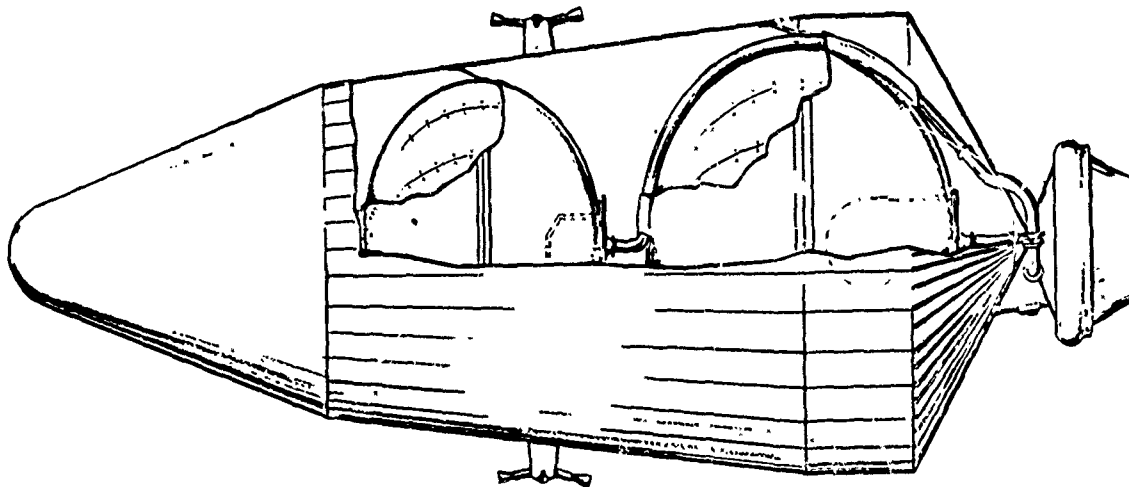
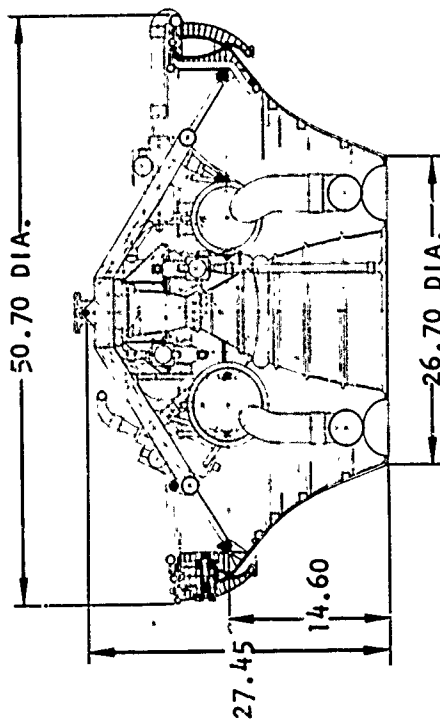
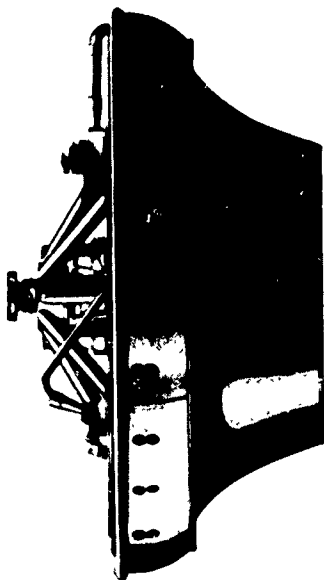


Figure 1. System Characteristics

CONFIDENTIAL

CONFIDENTIAL



PARAMETER	MAIN ENGINE	SECONDARY ENGINE
THRUST, POUNDS	30,000	3,300
CHAMBER PRESSURE, PSIA	650	750
VACUUM SPECIFIC IMPULSE, SECONDS	460	457.5
MIXTURE RATIO, O/F	12:1	12:1
THROTTLE RATIO	9:1	9:1
AREA RATIO	60:1	60:1

Figure 2. Engine System for Advanced Maneuvering Propulsion System

4
CONFIDENTIAL

CONFIDENTIAL

SUMMARY

(U) This report presents the work accomplished and the technical results obtained during the second quarterly period of 1 February 1968 to 30 April 1968. The major milestones of the program are shown in Fig. 3, and the basic program schedule is shown in Fig. 4. The hardware items indicated in Fig. 4 are described in the discussion of the Task II effort.

(U) The program is progressing satisfactorily with significant accomplishments being made in each of the three major tasks. The tasks are summarized below.

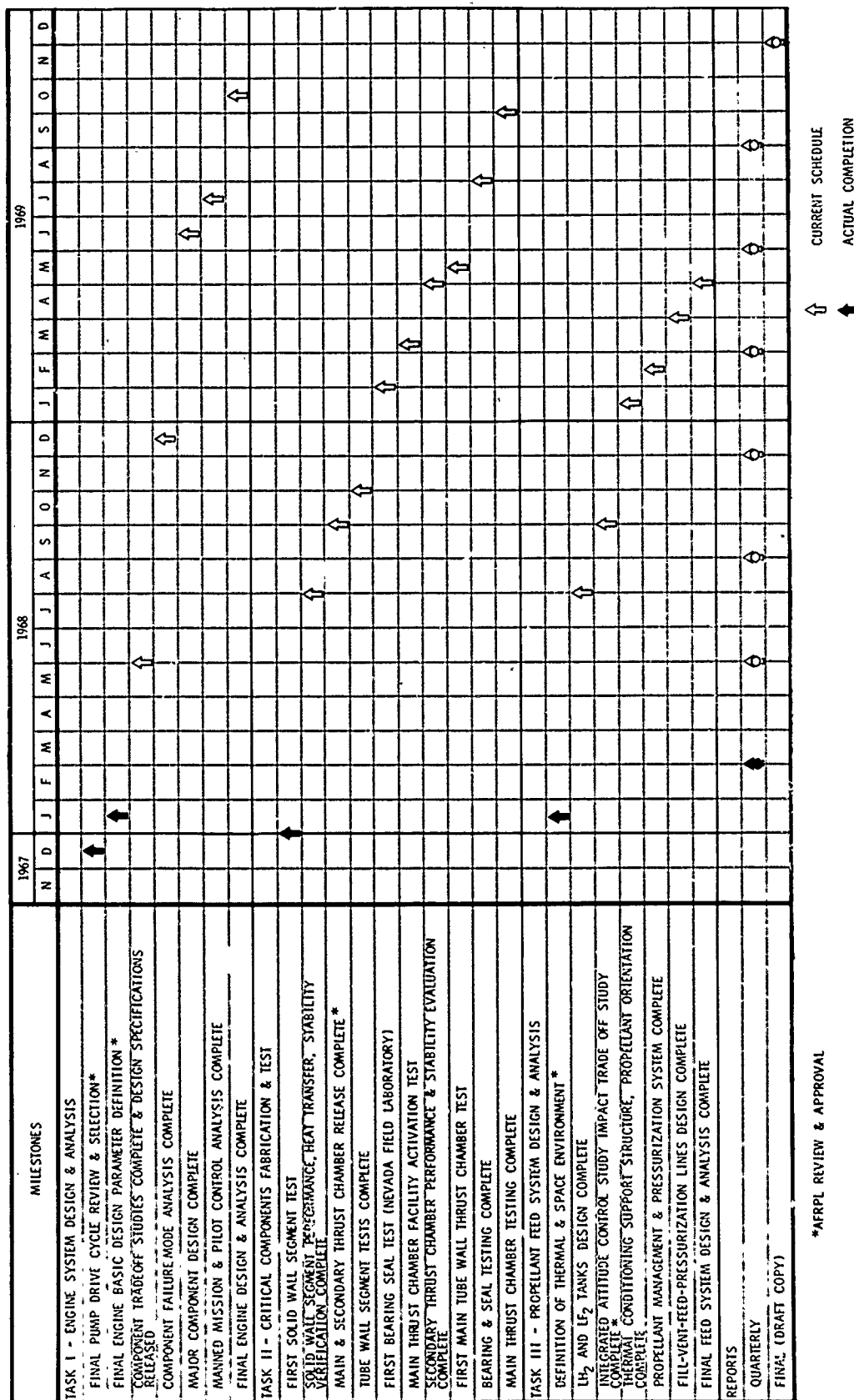
1. TASK I - ENGINE ANALYSIS AND DESIGN

(U) Work accomplished in Task I includes analysis and design effort for the engine system, thrust chambers, turbopumps, and engine controls.

(C) Engine system start and cutoff sequencing analysis continued and included considerations of the transition from main to secondary engine operation, and requirements for thermal conditioning of the main engine to achieve a rapid start under all possible operating conditions. Thermal conditioning methods investigated to reduce the effect of a relatively "warm" fuel pump (after an extended coast period) included use of an internal Kel-F coating in the fuel pump and the use of a larger-flow-area fuel control valve, located downstream of the pump.

(C) Analysis was conducted on the main engine to define the thrust vs mixture ratio envelope within which the engine is capable of operating. The present goal for mixture ratio limits is from 9:1 to 13:1, which is anticipated to be adequate for system propellant utilization requirements. The analyses to date indicate that the oxidizer and fuel turbopumps impose no restrictions on engine operation over the desired range.

CONFIDENTIAL

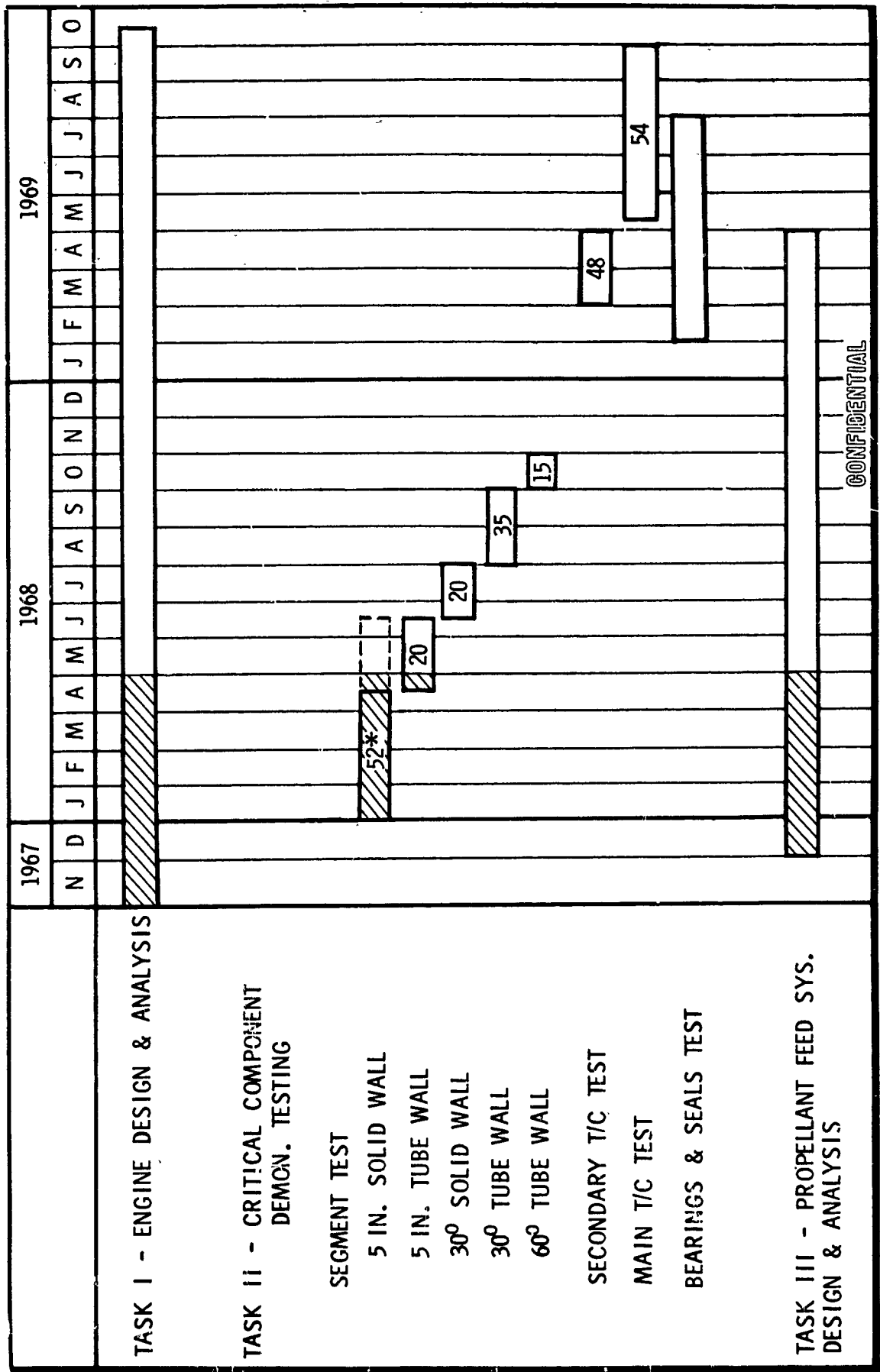


*AFRPL REVIEW & APPROVAL

Figure 3. AMPT Program Milestones

6
CONFIDENTIAL

CONFIDENTIAL



*NO. OF FIRING TESTS

Figure 4. AMPT Phase 1 Program

7
CONFIDENTIAL

CONFIDENTIAL

- (C) Engine operational analyses continued and included establishing tables of preliminary influence coefficients and definition of purge gas and instrumentation requirements. Investigation of base heating effects from recirculation of main engine primary flow gases into the thrust chamber cavity of the secondary engine was accomplished. By proper orientation of the injected turbine exhaust gases from the main engine, it was determined that the base area temperatures can be maintained at approximately the temperature of the turbine exhaust gas (640 F).
- (U) Engine design activity continued and included preparation of engine interconnect layout drawings and design specifications for engine components.
- (U) Main thrust chamber heat transfer analysis continued utilizing the test results from the Task II, 5-inch segment firings. Several different cooling circuits were analyzed for the inner body, outer body, and baffles.
- (C) Refinements to the main engine turbopump designs were established. A common turbine configuration has been selected for the oxidizer and fuel pumps with corresponding pressure ratios of 7.6:1 and 10:1. Pump shaft critical speed analyses were conducted for the present configurations, and the shaft normalized mode shapes were defined. Bearing specifications were prepared from these analyses.
- (U) Control system analysis continued using the mathematical analog computer model. Several control systems considered were: (1) one turbine hot-gas valve and two variable-area cavitating-venturi liquid control valves, (2) one turbine hot-gas valve and two square law liquid control valves, and (3) two turbine hot-gas valves and no liquid control valves. It was concluded that any one of these systems can provide adequate control of the engines, and the final selection would primarily depend on other factors.

2. TASK II - CRITICAL ENGINE COMPONENT DEMONSTRATION TESTING

- (C) This task is to provide for design, fabrication, and test of critical engine component hardware to demonstrate performance and determine solutions

CONFIDENTIAL

to potential design and fabrication problems. The critical components include segments of the main engine thrust chamber, complete main thrust chamber, solid-wall secondary thrust chamber, and main and secondary LF_2 pump bearings and seals. The main chamber segment approach is illustrated in Fig. 5, and was discussed in the First Quarterly Report (AFBPL-TR-68-17).

a. SEGMENT EVALUATION

- (C) Forty hot-firing tests were accomplished with the 5-inch solid-wall segment hardware during this report period, bringing the total number of tests to 50. Chambers with the G_c and the K wall contours were tested with both the triplet and fan injector designs. These tests covered the complete chamber pressure design range of 650 psia to 72 psia. Test durations up to 20 seconds were demonstrated with an accumulated duration of 104 seconds. Combustion was stable during all tests.
- (C) Data from these tests defined the heat transfer and performance characteristics of each of the configurations and resulted in the selection of the G_c chamber contour and the fan injector for the subsequent 30-degree segment and complete main chamber designs.
- (C) One test was accomplished with the 5-inch tubular wall chamber segment. The chamber and injector were damaged as a result of a facility malfunction.
- (U) Design refinements for fabrication simplification and improved operating characteristics have been incorporated into the basic 5-inch fan injector configuration. Two additional injectors incorporating these improvements are being fabricated and will be tested early in the next report period.
- (U) Design of the 30-degree solid-wall and tubular-wall segment chambers was completed, and fabrication is in progress. Design of the first 30-degree segment injector was completed, and fabrication of this unit was started. Design of the second unit is approximately 80-percent complete. Testing of the 30-degree solid-wall segment is scheduled to start during the next report period.

CONFIDENTIAL

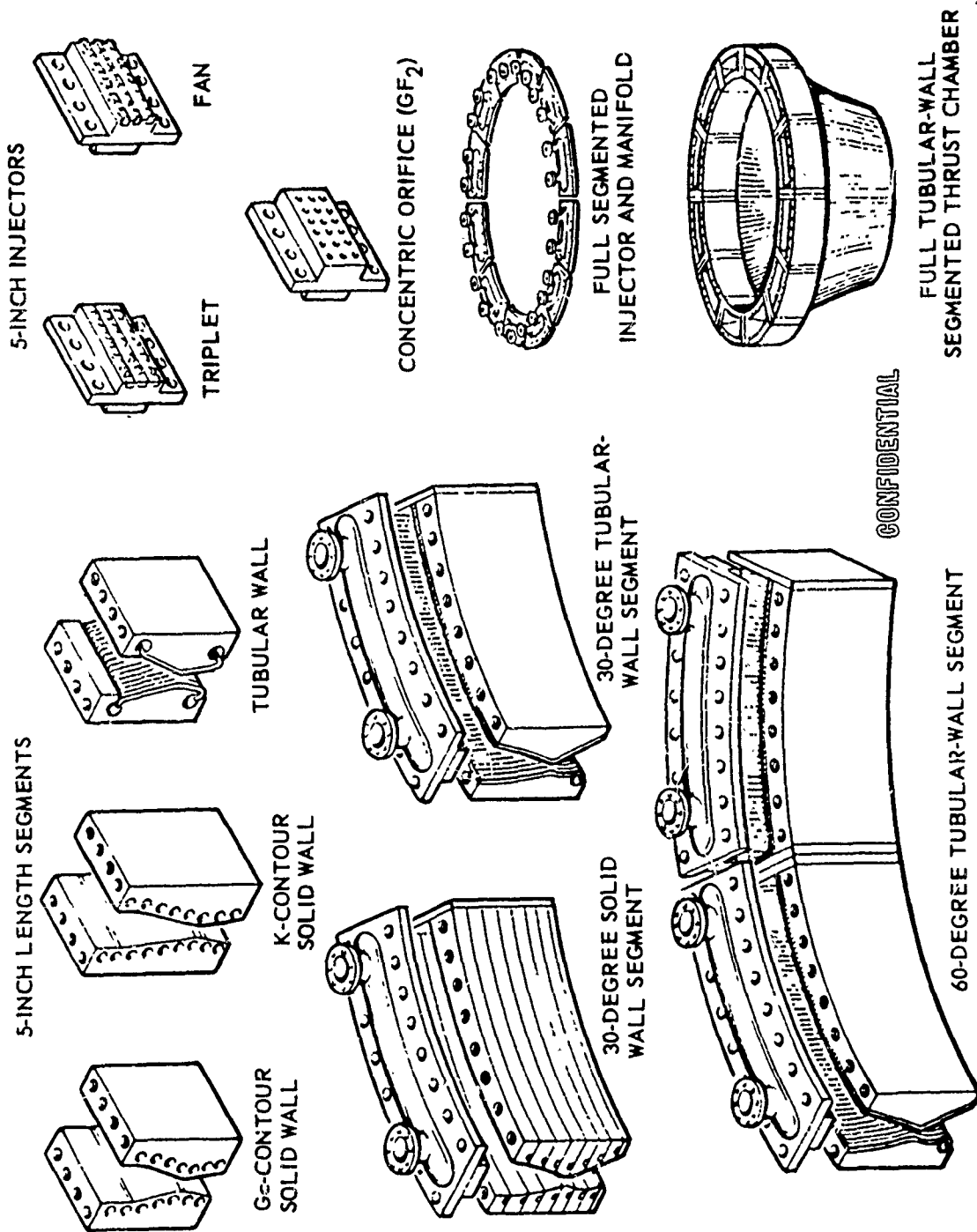


Figure 5. Main Thrust Chamber Segment Approach

CONFIDENTIAL

b. OXIDIZER PUMP BEARINGS AND SEALS EVALUATION

- (U) The design layout for the oxidizer pump bearing and seal tester was completed, and detail design was initiated. The tester design has the provisions for testing the bearing and seal sizes of both the main engine and secondary engine oxidizer pumps. The main engine seal package consisting of face-riding primary oxidizer and turbine gas seals and a shaft-riding intermediate seal was selected as the primary configuration. Alternate designs are also planned for test evaluation.

3. TASK III - PROPELLANT FEED SYSTEM ANALYSIS AND DESIGN

- (U) This task provides for analysis and design of an advanced propellant feed system to be integrated with the advanced engine design resulting from Tasks I and II. The task is being conducted by two selected subcontractors: General Dynamics/Convair and Lockheed Missiles and Space Company.
- (U) Major emphasis by both subcontractors during this second report period was on the propellant tank, thermal conditioning, and support structure subsystems. Propellant tank shape optimizations, material selections and fabrication method evaluations were conducted. Outer structural shroud configurations were defined and candidate materials and type of construction were evaluated. Design of the propellant tanks, support structure, and outer shroud is to be completed during the next quarterly period.
- (U) Insulation optimization analysis continued with candidate insulation types, location, number of layers, etc. being analyzed. The location of the insulation on the propellant tanks was shown to be superior to location on the outer shroud.
- (U) Work also progressed on the pressurization subsystem optimization and configuration definition. Work was started on the propellant orientation and integrated attitude control subsystems and the fill, vent, feed, and pressurization lines.

CONFIDENTIAL

TASK I - ENGINE SYSTEM ANALYSIS AND DESIGN

(U) This task provides for analysis and design of the complete engine system. Test results obtained during the critical component testing (Task II) are used in applicable areas for the final engine system design.

(U) The subtasks in Task I include analysis and design efforts for the engine system, thrust chambers, turbopumps, and controls. The progress accomplished in each of these areas during the second quarterly period is discussed in the following sections.

1. ENGINE SYSTEM

(U) Engine system analyses in the second quarterly report period included the following effort:

1. Additional effort in start sequence and transient operation of the main engine
2. Initiation of effort to define the main engine thrust vs mixture ratio operating envelope
3. Definition of the engine system purge requirements
4. Identification of instrumentation requirements for the main engine
5. Establishment of the initial set of influence coefficients for the engine system
6. Evaluation of the base recirculation flow of the main engine thrust chamber in the base region and in the nonoperating secondary engine thrust chamber cavity
7. Continuation of design effort to define the engine system configuration
8. Initiation of effort to evaluate the man-in-the-loop aspects of the engine system control
9. Initiation of effort to define engine accessory requirements

CONFIDENTIAL

a. ENGINE SEQUENCING ANALYSIS

(U) Analysis of the engine start and cutoff sequencing procedures was conducted to evaluate the previously established control logic and to optimize the timing of the individual control functions. The start sequencing studies include analytical evaluations of engine system thermal conditioning requirements, purge system effects, and variations on the basic control system configuration. Initial studies have concentrated on the main engine start characteristics. Main engine cutoff control system requirements will be investigated upon completion of the start analysis. Secondary engine start and cutoff control system requirements will be analyzed subsequently.

(U) Effort during this report period was directed toward revisions of the basic engine dynamics computer model to include a more detailed description of the engine system and to include feed system priming and thermal conditioning effects. Main engine thermal conditioning studies have been completed, and optimization of the start sequencing procedure was completed for the basic control system configuration. Preliminary studies have been made of the operational aspects of the transition between the main and secondary engine to determine what requirements this may impose on the start and cutoff sequencing control system.

(1) Computer Program Revisions

(U) The basic digital computer program which is used in analyzing the engine start dynamics was established in the first report period. However, various modifications were required to provide a more exact description of the engine system configuration and operating characteristics. The following outline provides a brief description of the major modifications that have been incorporated in the computer program. Other modifications of a lesser nature are periodically being made to investigate various control system perturbations and system effects that are of interest.

CONFIDENTIAL

1. Improved description of the fuel pump and high-pressure ducting, including the addition of heat transfer between the pump and fluid
2. Addition of two-dimensional heat transfer within the pump to include the effects of thermal conductivity of the pump metal upon the heat transfer to the fluid
3. Improved description of the two-stage fuel pump, where each stage is treated separately
4. Capability of thermally isolating the pump components and/or high-pressure ducting from the fluid by use of a low-conductivity coating
5. Addition of variable area cavitating venturies in the fuel and oxidizer feed lines
6. Addition of closed-loop mainstage controls which govern the positions of the fuel and oxidizer cavitating venturi valves and the hot-gas valve during start and mainstage

(2) Transition Between Main and Secondary Engine

(U) In certain mission applications there is a requirement for continuous engine throttling in thrust regions where it is necessary to switch from the main engine to the secondary engine. A brief evaluation of the impact of this consideration on the control system start and cutoff logic and sequencing was conducted.

(U) Under the most severe of engine operating conditions, there could be a significant time lag between the time when the main engine is shut down and the secondary engine is brought up to full thrust unless special provisions are made. This time lag is due to the possible requirement for engine chilldown, a helium purge of the secondary engine feed system before startup, and the nominal start transient time.

CONFIDENTIAL

(C) An estimate was made of the AMPS engine switching time lag for a rendezvous mission application based on the preliminary engine start and cutoff transients presented in the previous quarterly report. This estimate assumed that the secondary engine start signal would occur simultaneously with the main engine cutoff signal. An estimate of the delivered engine thrust vs time is shown in Fig. 6 for the main and secondary engines. The dotted line indicates the total thrust produced during the overlap period when both engines are producing thrust. The total time lag between cutoff and the re-establishment of thrust is seen to be approximately 2 seconds. This time lag is satisfactory for a near-optimum rendezvous approach trajectory based on the studies of Ref. 3 and 4. The results of this study for these type missions indicate that special control system provisions are unnecessary for the main/secondary engine throttling transition; however, they would be provided if other type missions dictate the need.

(U) Upon completion of the current engine start and cutoff sequencing studies, a more exact description of the engine system operating characteristics during this transition will be defined and will include the effects of system priming, thermal conditioning, purge requirements, and the selected control system configuration.

(3) Main Engine Thermal Conditioning Requirements

(U) A study has been completed to determine the effects of fuel feed system thermal conditioning upon the main engine's start transient.

(C) The analysis was conducted with the use of the digital computer model of the engine start dynamics. Simulated tank-head engine starts were made with fuel and oxidizer tank pressures of 70 psia and 65 psia, respectively. The lower oxidizer tank pressure was used to prevent high mixture ratio excursions during priming of the oxidizer feed system. The main stage tank pressures were assumed to be 70 psia in both tanks.

CONFIDENTIAL

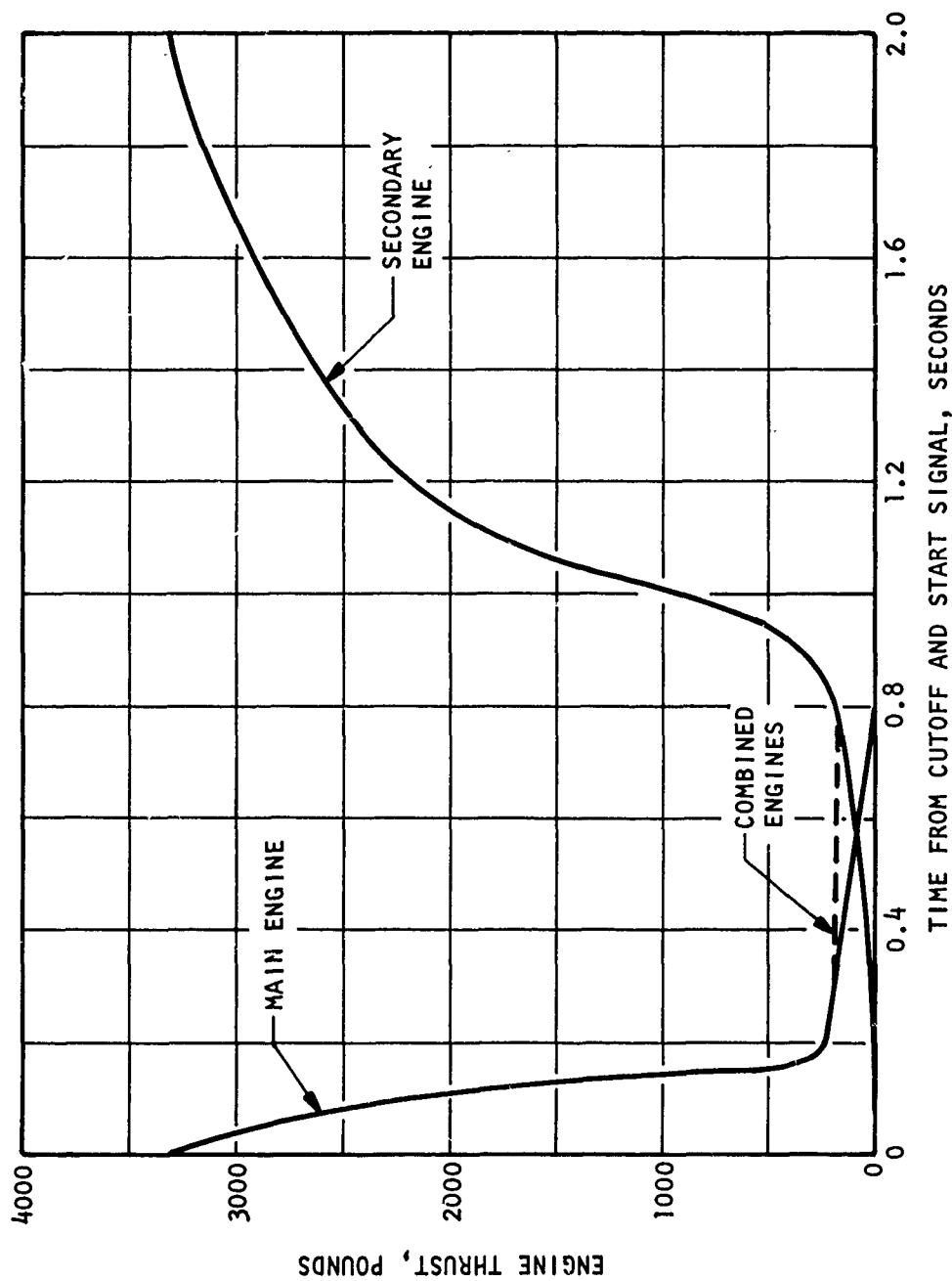


Figure 6. Predicted Thrust During Transition from Main to Secondary Engines

CONFIDENTIAL

CONFIDENTIAL

(C) Future start model analysis will investigate the tank-head start with equal tank pressures and with the oxidizer side throttled to achieve the same effect as the reduced oxidizer tank pressure. The thermal conditioning start analysis was conducted for starts to full thrust at an engine mixture ratio of 12:1.

(C) Engine thermal conditioning requirements were investigated for two extremes of initial feed system thermal conditions. The first case simulated an immediate restart; the pumps would be at the propellant liquid temperatures and the thrust chamber would be at an average bulk temperature of approximately 1000 F. The second case simulated the engine thermal conditions after attaining equilibrium during an orbital coast period. This latter case represents the most stringent thermal conditioning requirements, because the pumps and thrust chamber temperature would be approximately 60 F. It has been determined that the initial pump temperatures will always be within these approximate extremes. The analytical model used in establishing the pump thermal conditions was verified by comparison with analytical predictions and actual engine firings studied under contract NAS 8-20324, "Thermodynamic Improvements in Liquid Hydrogen Turbopumps." The results of the current AMPS analysis were found to correlate closely with the results of the previous studies.

(C) With the fuel pump and ducting at liquid hydrogen temperatures, the engine will reach full mainstage in approximately 2.0 seconds. However, with the warm pump and ducting, the engine will require approximately 4.3 seconds to reach mainstage. The warmer pump and ducting increases the engine start time by lengthening the time before the pump begins to generate positive head and by reducing the fuel flowrate through the system.

(U) The vaporization of the hydrogen entering the "warm" pump results in increased resistance to liquid flow by the downstream feed system components such as the hydrogen control valves and cooling jacket tube bundle. Thermal conditioning requirements of the oxidizer feed system were found to be nonrestrictive relative to the fuel feed system.

CONFIDENTIAL

(U) Several methods were considered to reduce the magnitude of the heat flux transferred to the fuel and/or reduce the effect of the hardware temperature upon the start time. Methods of reducing the downstream resistance to flow were also investigated. The following system variations were considered:

1. A 0.002-inch Kel-F coating on the rotating parts of the fuel pump
2. A 0.010-inch Kel-F coating on the high-pressure ducting and non-rotating parts of the fuel pump
3. A 0.002-inch Kel-F coating on the rotating parts of the fuel pump plus a 0.010-inch Kel-F coating on the ducting and non-rotating parts of the fuel pump
4. Replacement of the fuel cavitating venturi with a large flow area valve

(U) It can be seen in Fig. 7 that the amount and location of the Kel-F coating, or any other low conductivity coating, determines how effectively the fuel is thermally isolated from the metal and how quickly the fuel reaches liquid temperatures. Once the fuel has reached liquid temperatures, the fuel density in the feed system is dependent upon the pressure generated by the pump. Thus, pump speed buildup will influence how quickly liquid densities are attained. Figure 7 also shows fuel density at the pump discharge for each of the system alterations considered.

(U) Chillover and priming of the fuel system is hampered by choking of the cavitating venturi with gaseous and two-phase flow. Thus, a chillover was made with the cavitating venturi replaced by a low-resistance butterfly valve. The results of this change are included in Fig. 7. Use of the butterfly valve instead of the cavitating venturi reduced chillover and fuel pump prime by approximately 1.0 second. The 1.0-second gain in start time was achieved by increasing the amount of fuel flow through the system in the early phase of engine start.

CONFIDENTIAL

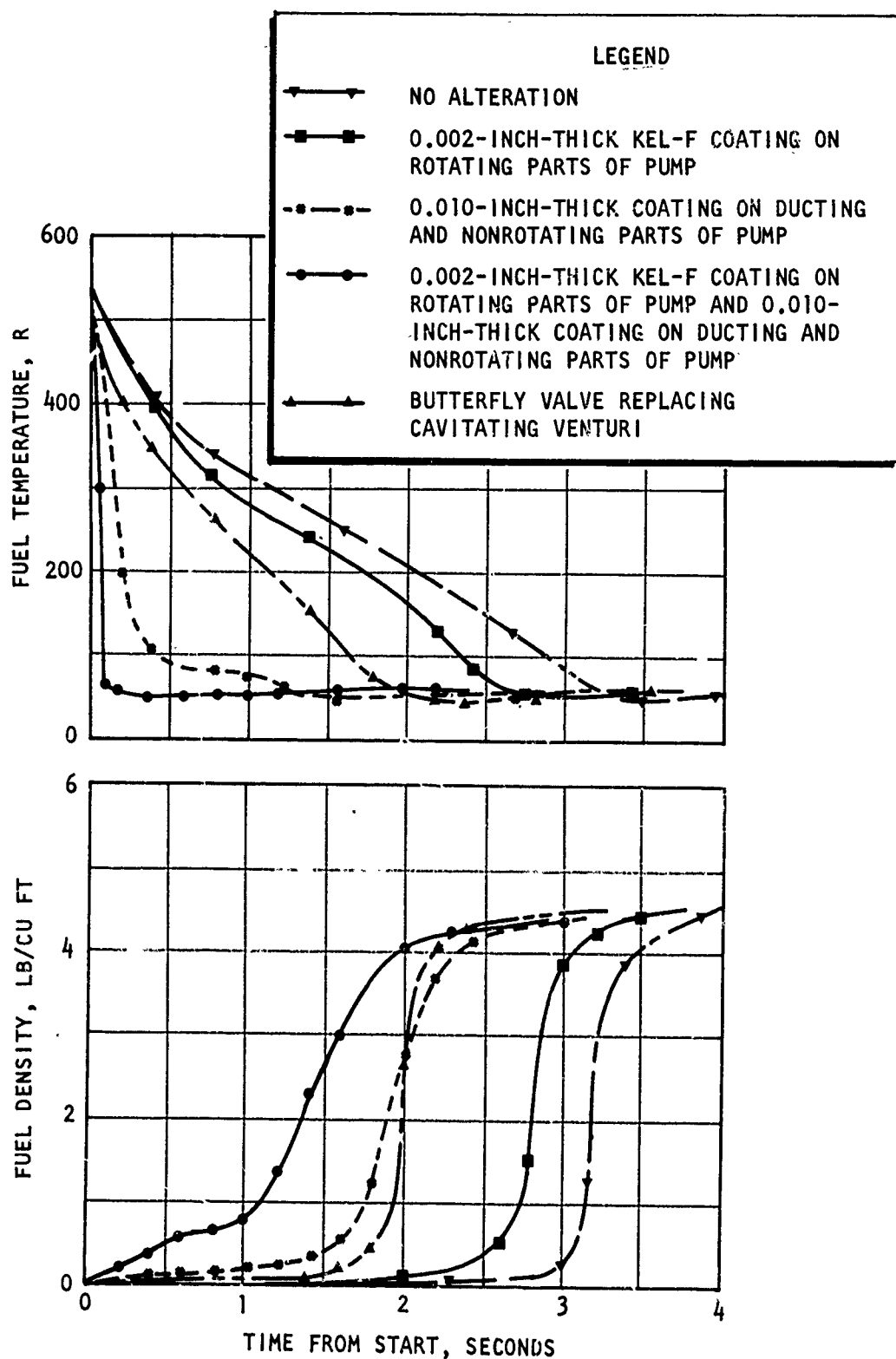


Figure 7. Fuel Temperature and Density at Pump Discharge During Main Engine Start

CONFIDENTIAL

CONFIDENTIAL

(U) Using the same engine sequence for each of the above system variations, the total elapsed time from start to mainstage is given in Table 1.

(U) Other fuel feed system variations will be investigated for possible methods of reducing the difference in start time for the two extremes in feed system thermal condition. The advantages of incorporating a bypass of the thrust chamber coolant lines during the hydrogen lead are being evaluated in current studies. This bypass would greatly reduce the resistance to flow by transferring the initially vaporized hydrogen directly to the injector manifold. Estimates indicate that the "warm" start can be accomplished in approximately 2.2 seconds with the low ΔP fuel valve and a bypass around the cooling jacket.

(U) An alternate control system configuration, using two hot-gas turbine control valves, may also provide a benefit for the "warm" start condition through greater sequencing flexibility during the start transient. This is also currently being investigated.

(4) Start Sequencing Optimization

(U) A start sequencing control system optimization has been completed for the main engine using a single hot-gas turbine control valve. The optimization analysis had the primary objectives of providing a rapid start with little or no overshoot of pump speed or chamber pressure, maintaining engine mixture ratio within a tolerable range for thrust chamber cooling considerations, and providing control function signals that are independent of initial engine thermal conditions. That is, the control system will automatically compensate for variations in initial thermal conditions by taking the sequencing function signals from selected engine system operating parameters. A further requirement is that the above engine starting features be achieved at starts to any thrust level within the throttling range.

CONFIDENTIAL

TABLE 1

EFFECT OF FUEL SYSTEM THERMAL VARIATIONS ON ENGINE START TIME

Fuel System Variation	Engine Start Time, seconds	
	Instant Restart	Start After Long Coast Period
No Alteration	2.0	4.3
0.002-Inch-Thick Kel-F Coating on Rotating Parts of Pump	2.0	3.9
0.010-Inch-Thick Kel-F Coating on Ducting and Nonrotating Parts of Pump	2.0	3.0
0.002-Inch-Thick Kel-F Coating on Rotating Parts of Pump, and 0.010-Inch-Thick Kel-F Coating on Ducting and Nonrotating Parts of Pump	2.0	2.49
Butterfly Valve		2.81

CONFIDENTIAL

(C) The analysis was started by assuming the basic start sequencing control logic that was presented in the previous quarterly report. Tank-head starts were simulated with the aid of the computerized engine dynamic start model. Start characteristics were evaluated with both cold and warm initial conditions. Full thrust chamber pressure was 650 psia with a mixture ratio of 12:1. A cavitating venturi was used for the oxidizer flow-control valve and a large flow area valve was used for the fuel flow valve. Both oxidizer and fuel turbine flow was controlled by a single hot-gas valve.

(C) The main chamber pressure and pump flowrates as a function of time during the start transient are shown in Fig. 8. The results shown in Fig. 8 are representative of the optimized start sequence for the single hot-gas valve system. The following sequence was established for the illustrated starts.

1. Main fuel and oxidizer valves opened at engine start
2. Fuel-control valve opened to mainstage position at engine start
3. Hot-gas valve opened to +200 percent of mainstage at engine start
4. Oxidizer control valve opened to 35 percent of mainstage when fuel injection pressure reaches 50 psia (liquid is in pump)
5. Fuel control valve, oxidizer control valve, and hot-gas valve turned over to mainstage controls when oxidizer injection pressure reaches 200 psia (oxidizer ducting primed)

(U) The results shown in Fig. 8 indicate that the following basic engine start objectives can be achieved with this sequence.

1. Rapid starts can be achieved.
2. Warm pump starts can be achieved, which are faster than shown, by utilizing the previously discussed feed system variations to improve thermal conditioning effects.

CONFIDENTIAL

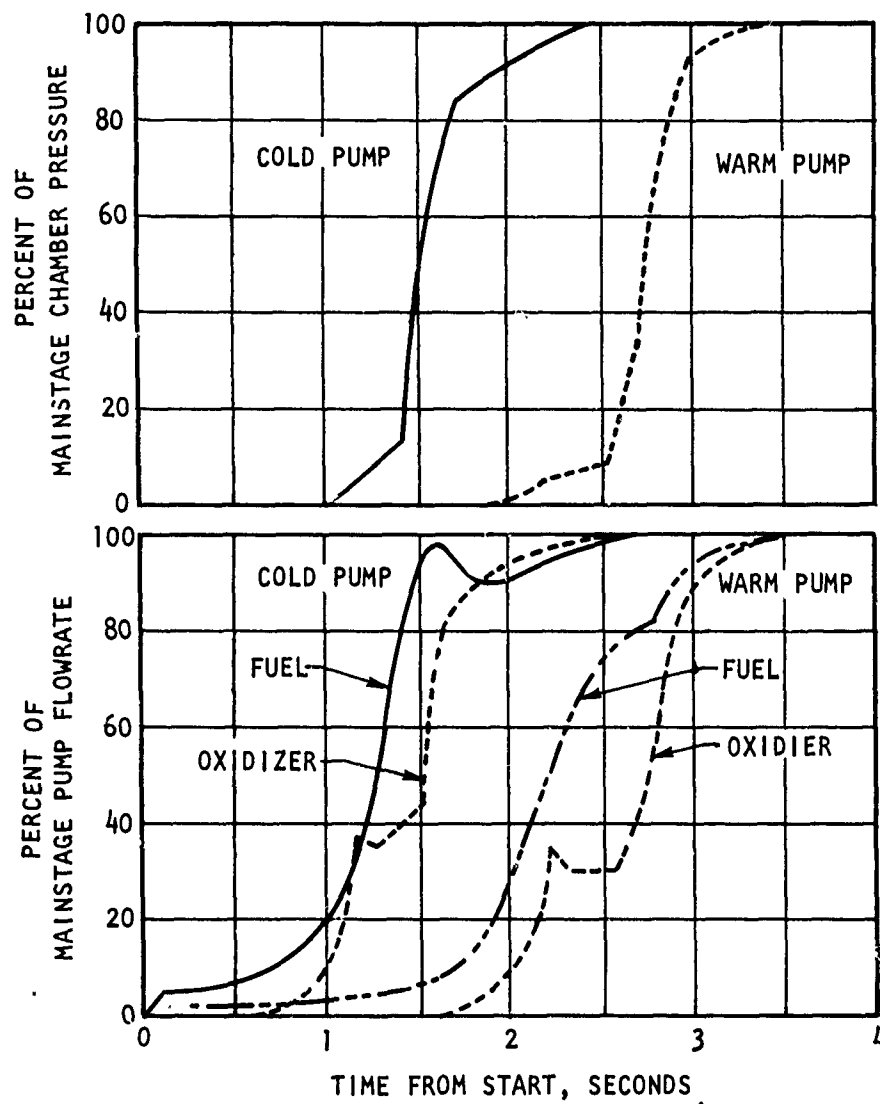


Figure 8. Main Engine Chamber Pressure and Pump Flowrates During Start

CONFIDENTIAL

CONFIDENTIAL

3. Good thrust control is obtained.
4. No overshoot occurs.
5. Engine mixture ratio is maintained at or below the mainstage command valve through the start transient.

b. THRUST AND MIXTURE RATIO ENVELOPE

(C) An engine system study is currently in progress to define the range of thrust and mixture ratios within which the engine is capable of operation. Previous component and engine system design and operational studies have been conducted at the nominal engine mixture ratio of 12:1 and over the required throttling thrust range. However, recent mixture ratio selection and propellant storage studies have indicated that off-design mixture ratio operation will be required to accomplish the range of possible mission applications with a maximum performance capability. This requires that the engine system be capable of operation over a range of mixture ratios at any thrust level within the required throttling range. The exact limits of the required mixture ratio excursions are not known at present as the propellant management subsystem studies have not been completed (Task III). However, previous studies concerned with AMPS mixture ratio selection, propellant storage capability, and propellant utilization requirements, have indicated that for efficient propellant utilization, the engine must be capable of operating three mixture ratio units below the nominal design. It was also determined that the capability of operating slightly above nominal mixture ratio is also required to ensure complete propellant depletion.

(C) Based on these earlier findings, engine and component thrust and mixture ratio envelope studies are being conducted over a mixture ratio range of from 9:1 to 13:1 and over the required thrust range for both the main and secondary engine. It is anticipated that this mixture ratio range will be adequate for the propellant utilization requirements.

CONFIDENTIAL

(1) Method of Analysis

(U) A flow chart describing the various steps involved in this study is shown in Fig. 9. The analysis was begun by conducting an engine system power balance and performance analysis for a range of engine thrust levels and mixture ratios. The current engine and component design and operating parameters were input to this analysis along with the current pump and turbine operating maps, predicted thrust chamber efficiencies, and regenerative cooling heat transfer values.

(U) The results of this analysis provide detailed information pertaining to the engine system and component operating range, such as, propellant flowrates, turbine flowrates, valve pressure drop requirements, and turbine speeds vs thrust and mixture ratio. This information then establishes the ideal or desired range of operating conditions for each of the engine system components over the range of thrust and mixture ratio considered. This information is then fed into the individual component design and analysis studies to indicate the desired operating range in speed, pressure drop, flowrate, and pump head rise. Where this operating range cannot be satisfied without seriously compromising the design, the restrictions imposed by that specific component are imposed on the engine system operating range. The net result will be to define the thrust vs mixture ratio envelope within which the overall engine system is capable of operation.

(2) Results

(U) This study is currently in progress, and is scheduled for completion in the next reporting period. The engine power balance and performance analysis has been completed for the main and secondary engines over their respective thrust and mixture ratio ranges. The results of this analysis have been evaluated to determine the desired range of operating conditions and design requirements for each of the system components. An example of

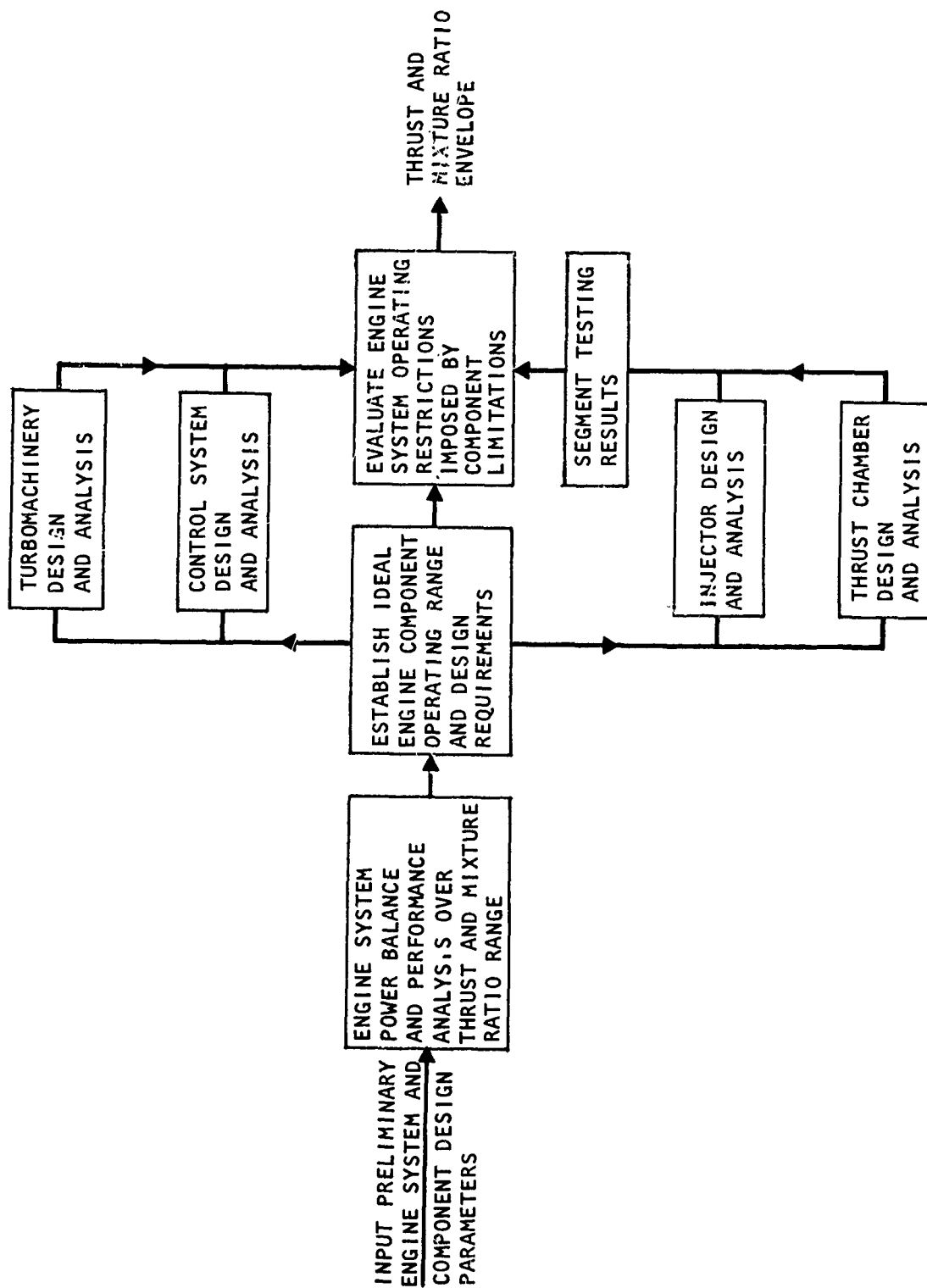


Figure 9. Flow Chart for Thrust and Mixture Ratio Envelope Evaluation

CONFIDENTIAL

the type of information that is obtained from this analysis is presented in Fig. 10 through 15, which show the operating ranges of the main engine fuel and oxidizer pumps and the turbine hot-gas valve to satisfy the required range of thrust and mixture ratio.

(U) This information has been generated for two variations of the turbine gas drive system; that of a single hot-gas valve controlling the hot-gas flow to both turbines, or a separate valve for each turbine. This option results in differences in the oxidizer turbine flowrates and pump discharge pressure for off-design mixture ratio operation. These two alternatives are currently being studied to determine their impact on the overall engine system and control system requirements.

(U) Other component design and analysis studies currently in progress will indicate any limitations on the desired engine operational range.

(C) The main engine pump design studies have furnished pump maps (head vs flow curves) indicating permissible regions of operation. The required operating regions from the engine power balance analysis were then superimposed on these maps. The results are shown in Fig. 16 for the main engine oxidizer and fuel pumps. The required operating regions are shown for the oxidizer pump with either single or dual turbine hot-gas control valves. The fuel pump is unaffected by this option. The results shown in Fig. 16 indicate that the oxidizer and fuel pumps will not impose any restrictions on engine operation between thrust levels of 30,000 and 3330 pounds and mixture ratios of 9:1 to 13:1.

(U) Thrust chamber cooling studies are currently being conducted based on the results of the solid-wall segment testing of Task II. The results of this analysis will also be evaluated to determine any restrictions on the permissible range of engine operation due to regenerative cooling limitations. Items of interest will be: cooling jacket ΔP , coolant bulk temperature rise, and gas-side tube wall temperatures vs thrust and mixture ratio.

CONFIDENTIAL

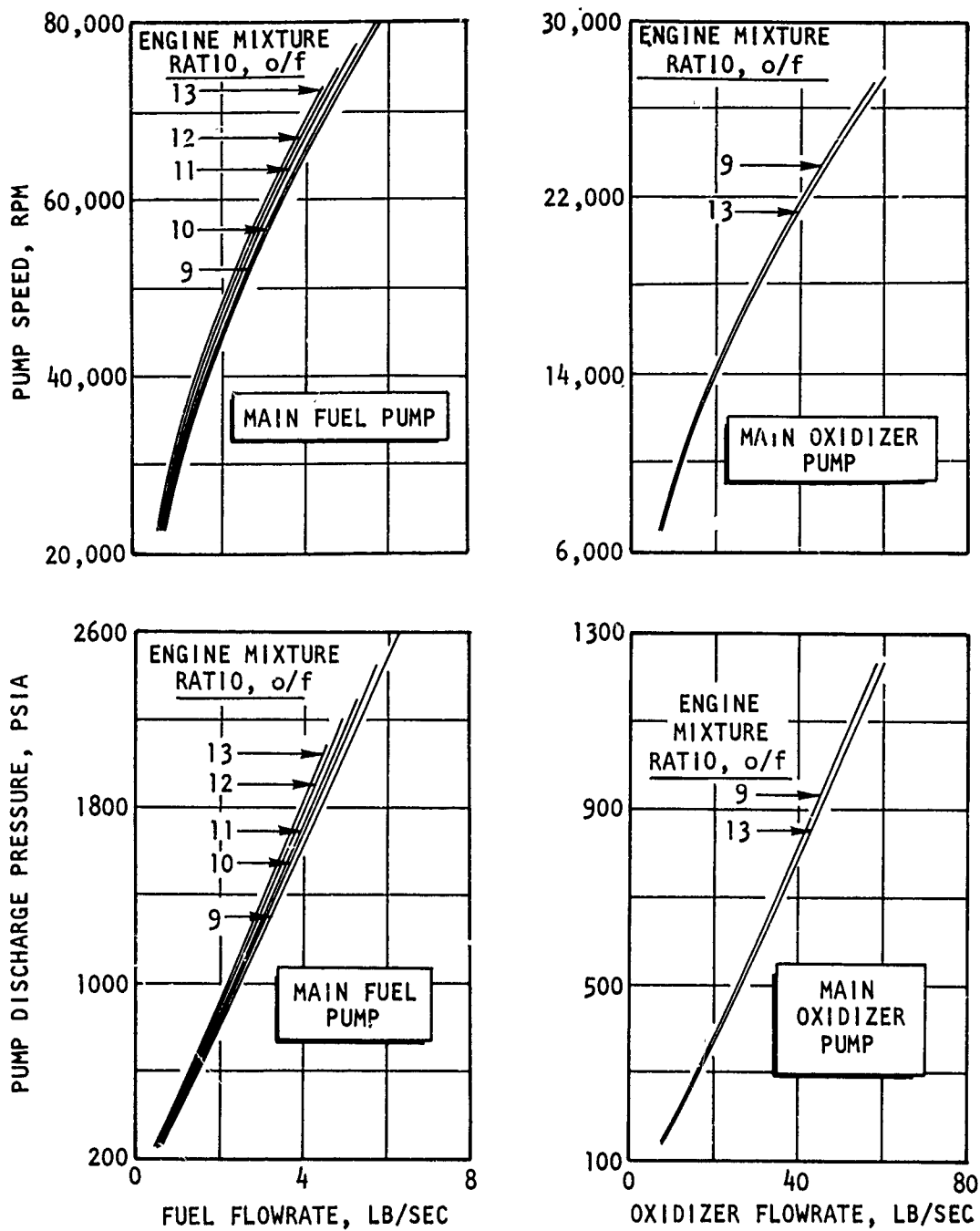


Figure 10. Operating Requirements for Main Engine Pumps

CONFIDENTIAL

CONFIDENTIAL

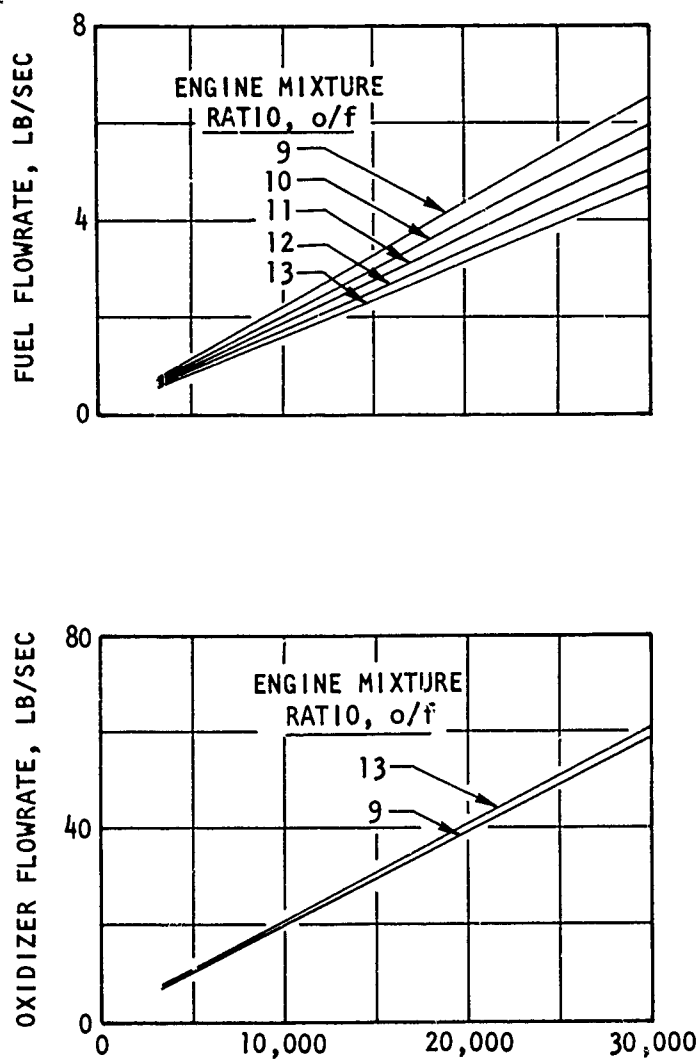


Figure 11. Flowrate Requirements for Main Engine Propellants

CONFIDENTIAL

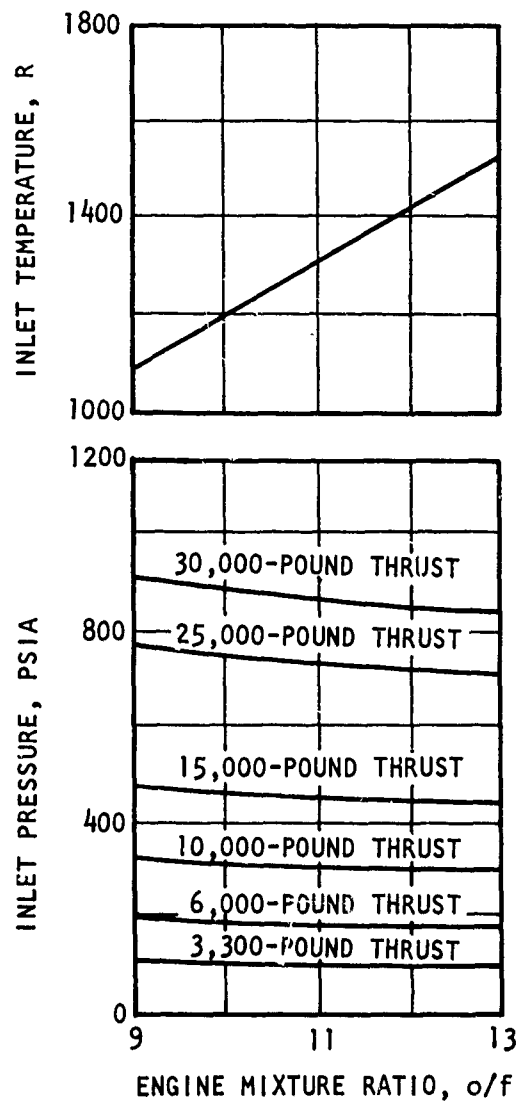


Figure 12. Inlet Conditions for Main Engine Hot-Gas Valve

CONFIDENTIAL

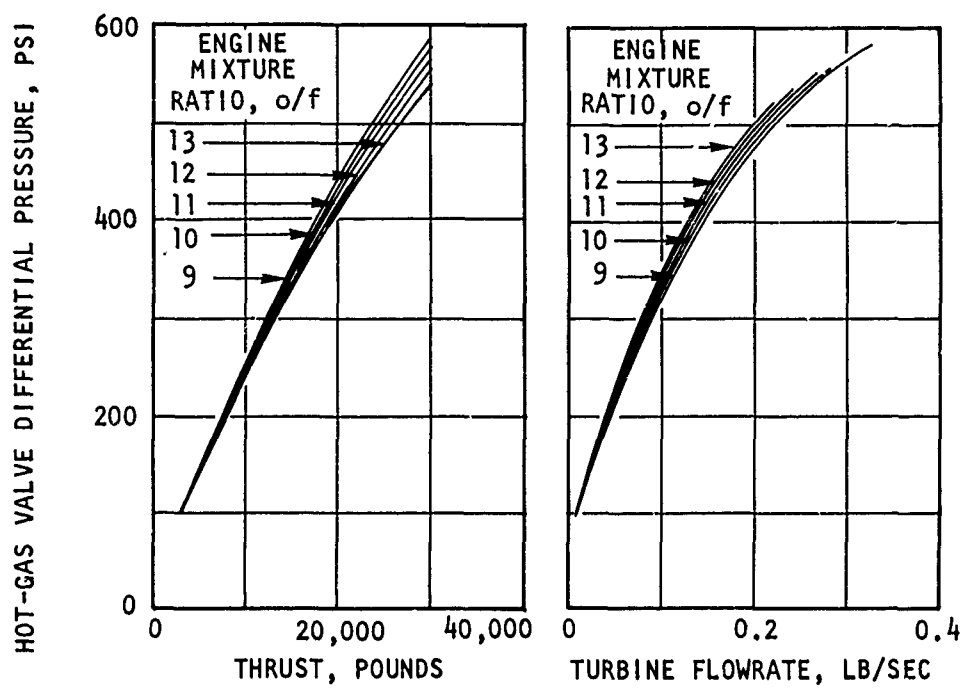


Figure 13. Differential Pressure Requirements for Main Engine Oxidizer Turbine Hot-Gas Valve

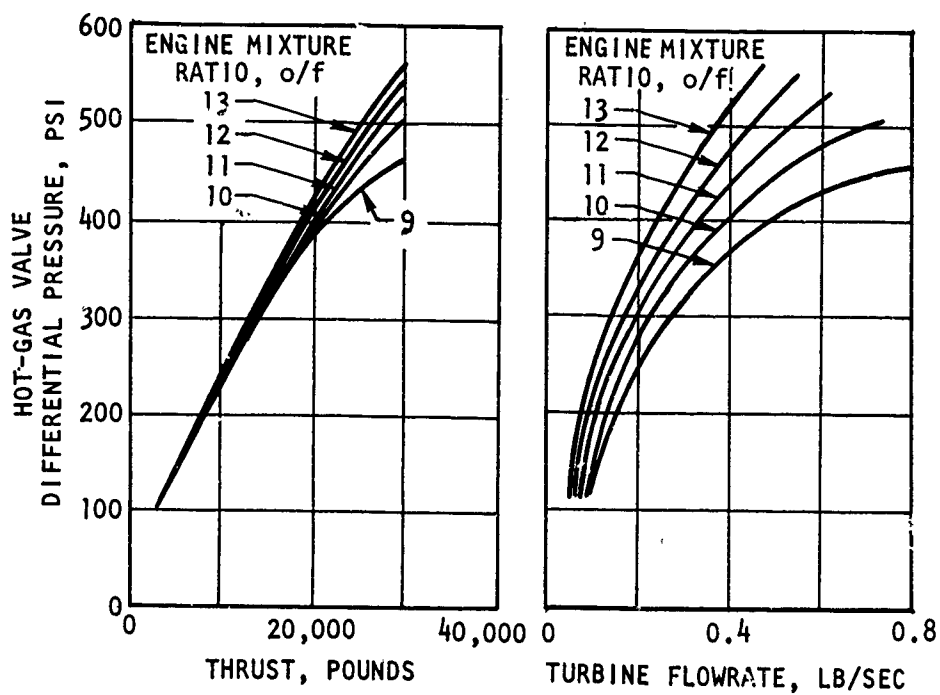


Figure 14. Differential Pressure Requirements for Main Engine Fuel Turbine Hot-Gas Valve

CONFIDENTIAL

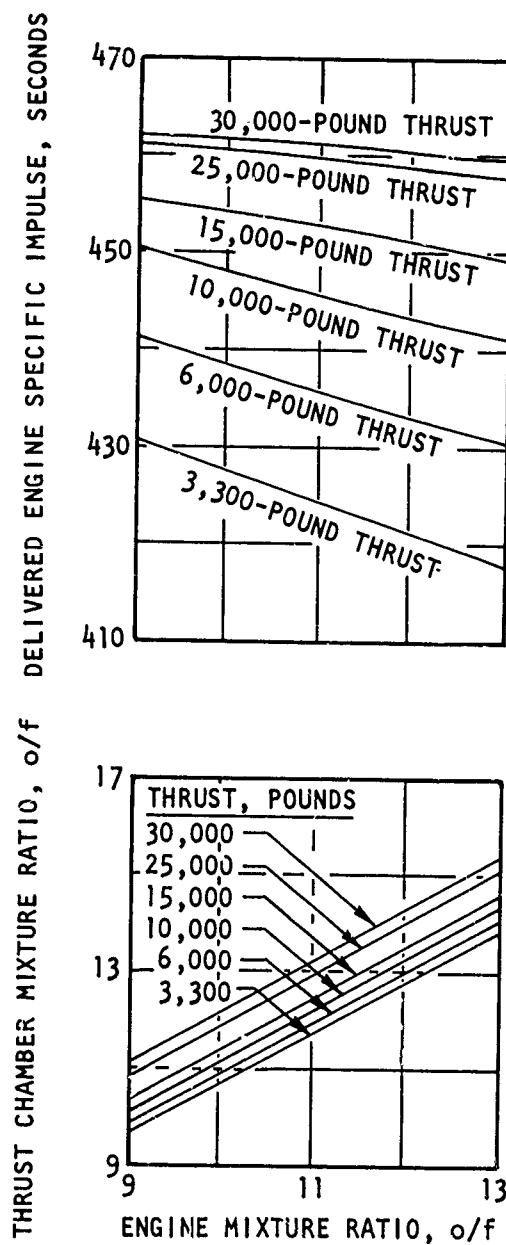


Figure 15. Main Engine Performance

CONFIDENTIAL

CONFIDENTIAL

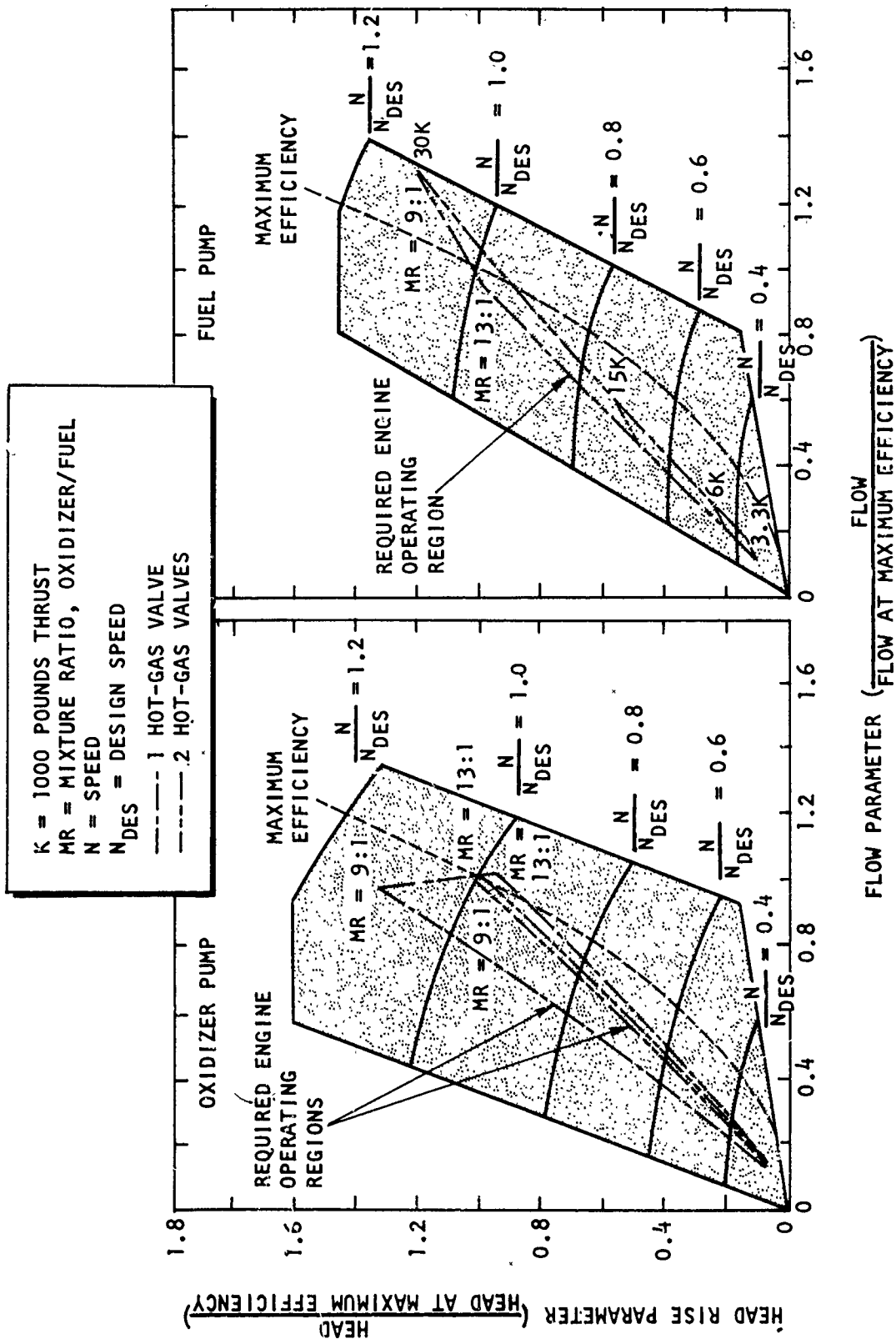


Figure 16. Operating Envelopes for Main Engine Propellant Pumps

CONFIDENTIAL

CONFIDENTIAL

(U) Injector design and analysis studies in conjunction with the segment testing results may also indicate other operational restrictions on the engine system. Current investigations are concerned with injector ΔP , injection velocity, and injector face heat flux vs thrust and mixture ratio.

(U) Control system studies are being conducted to investigate single vs dual hot-gas valve advantages as well as other control system operating capabilities over the thrust and mixture ratio range.

(U) At the conclusion of these component studies, the results will be combined to define the permissible range of thrust and mixture ratio operation for the overall engine system.

c. ENGINE INFLUENCE COEFFICIENTS

(C) A set of preliminary engine influence coefficients (Tables 2 through 5) were prepared for the main and secondary engine at their respective full and 9:1 throttled thrust operating levels and, in both cases, at the nominal design mixture ratio of 12:1. The selected independent variables include external engine effects such as propellant inlet pressure and temperature conditions, and internal engine design or operating conditions such as system pressure drop and coolant bulk temperature rise. The system pressure drop effect is characterized by the oxidizer or fuel injector ΔP , and may be interpreted to have the same percentage effect. The analysis was conducted based on the assumption that the control system would always maintain the command thrust and mixture ratio value with any system perturbation. Based on this assumption, engine thrust and mixture ratio remain constant, and the delivered engine specific impulse becomes the primary dependent variable. Other dependent variables are presented to indicate the effect of the independent variables on engine system component operating characteristics such as pump and turbine speeds, flow-rates, and horsepower requirements. The data in Tables 2 through 5 show that there is minimal effect realized by varying any one independent

CONFIDENTIAL

TABLE 2
MAIN ENGINE INFLUENCE COEFFICIENTS FOR FULL THRUST OPERATION

<u>Independent Variable</u>	<u>Nominal Value</u>	<u>Remarks</u>
Fuel Pump Inlet Pressure, psia	60	A 1-percent increase in any independent variable causes a percentage change in each dependent variable. The magnitude of change in dependent variables is listed below.
Oxidizer Pump Inlet Pressure, psia	45	
Fuel Pump Inlet Temperature, R	40	
Oxidizer Pump Inlet Temperature, R	153	
Fuel Injector Pressure Drop, psi	201.3	
Oxidizer Injector Pressure Drop, psi	325.7	
Coolant Bulk Temperature Rise, R	1432	

Dependent Variable	Percent Change Caused by 1-Percent Increase In:						
	Fuel Pump Inlet Pressure	Oxidizer Pump Inlet Pressure	Fuel Pump Inlet Temperature	Oxidizer Pump Inlet Temperature	Fuel Injector Pressure Drop	Oxidizer Injector Pressure Drop	Coolant Bulk Temperature Rise
Engine Specific Impulse	0.000	0.000	-0.002	-0.001	-0.001	-0.001	0.014
Thrust Chamber Mixture Ratio	-0.003	-0.001	0.022	0.017	0.009	0.014	-0.119
Oxidizer Pump Speed	-0.003	-0.015	0.000	0.262	0.000	0.126	-0.004
Fuel Pump Speed	-0.016	0.000	0.214	0.000	0.045	0.000	0.000
Oxidizer Pump Horsepower	0.000	-0.038	0.001	0.452	0.000	0.317	-0.017
Fuel Pump Horsepower	-0.034	0.000	0.361	0.000	0.104	0.000	-0.009
Oxidizer Pump Discharge Pressure	0.000	0.000	0.000	0.029	0.000	0.309	-0.003
Fuel Pump Discharge Pressure	0.000	0.000	0.021	-0.001	0.107	-0.001	0.005
Oxidizer Turbine Flowrate	-0.004	-0.022	0.000	0.216	0.017	0.181	-0.638
Fuel Turbine Flowrate	-0.019	-0.003	0.164	0.031	0.065	0.025	-0.641

CONFIDENTIAL

CONFIDENTIAL

TABLE 3

MAIN ENGINE INFLUENCE COEFFICIENTS FOR 9:1 THROTTLED OPERATION

<u>Independent Variable</u>	<u>Nominal Value</u>	<u>Remarks</u>
Fuel Pump Inlet Pressure, psia	60	A 1-percent increase in any independent variable causes a percentage change in each dependent variable. The magnitude of change in dependent variables is listed below.
Oxidizer Pump Inlet Pressure, psia	45	
Fuel Pump Inlet Temperature, R	40	
Oxidizer Pump Inlet Temperature, R	153	
Fuel Injector Pressure Drop, psi	27.3	
Oxidizer Injector Pressure Drop, psi	39.5	
Coolant Bulk Temperature Rise, R	1407	

Dependent Variable	Percent Change Caused by 1-Percent Increase In:						
	Fuel Pump Inlet Pressure	Oxidizer Pump Inlet Pressure	Fuel Pump Inlet Temperature	Oxidizer Pump Inlet Temperature	Fuel Injector Pressure Drop	Oxidizer Injector Pressure Drop	Coolant Bulk Temperature Rise
Engine Specific Impulse	0.001	0.001	0.000	0.000	0.000	-0.001	0.006
Thrust Chamber Mixture Ratio	-0.011	-0.009	0.003	0.002	0.006	0.009	-0.034
Oxidizer Pump Speed	0.000	-0.227	0.000	0.219	0.000	0.234	-0.002
Fuel Pump Speed	-0.157	0.001	0.202	0.000	0.082	-0.001	0.000
Oxidizer Pump Horsepower	0.000	-0.631	0.000	0.285	0.000	0.653	-0.008
Fuel Pump Horsepower	-0.394	0.001	0.273	0.000	0.210	-0.001	-0.003
Oxidizer Pump Discharge Pressure	0.000	0.000	0.000	0.004	0.000	0.333	-0.075
Fuel Pump Discharge Pressure	0.001	0.001	0.002	0.000	0.123	-0.001	0.000
Oxidizer Turbine Flowrate	-0.046	-0.346	-0.004	0.063	0.020	0.352	-0.542
Fuel Turbine Flowrate	-0.225	-0.036	0.065	0.010	0.124	0.042	-0.540

CONFIDENTIAL

CONFIDENTIAL

TABLE 4

SECONDARY ENGINE INFLUENCE COEFFICIENTS FOR FULL THRUST OPERATION

<u>Independent Variable</u>	<u>Nominal Value</u>	<u>Remarks</u>
Fuel Pump Inlet Pressure, psia	60	A 1-percent increase in any independent variable causes a percentage change in each dependent variable. The magnitude of change in dependent variables is listed below.
Oxidizer Pump Inlet Pressure, psia	45	
Fuel Pump Inlet Temperature, R	40	
Oxidizer Pump Inlet Temperature, R	153	
Fuel Injector Pressure Drop, psi	243.8	
Oxidizer Injector Pressure Drop, psi	374.7	
Coolant Bulk Temperature Rise, R	576	

Dependent Variable	Percent Change Caused by 1-Percent Increase In:						
	Fuel Pump Inlet Pressure	Oxidizer Pump Inlet Pressure	Fuel Pump Inlet Temperature	Oxidizer Pump Inlet Temperature	Fuel Injector Pressure Drop	Oxidizer Injector Pressure Drop	Coolant Bulk Temperature Rise
Engine Specific Impulse	0.000	0.000	0.001	0.000	0.000	0.000	0.002
Thrust Chamber Mixture Ratio	-0.002	-0.001	0.028	0.012	0.008	0.010	0.017
Oxidizer Pump Speed	0.000	-0.013	0.000	0.264	0.000	0.120	-0.002
Fuel Pump Speed	-0.019	0.000	0.268	0.000	0.063	0.000	-0.001
Oxidizer Pump Horsepower	0.002	-0.032	0.001	0.456	0.000	0.299	-0.003
Fuel Pump Horsepower	-0.028	0.012	0.525	0.012	0.147	0.012	0.008
Oxidizer Pump Discharge Pressure	0.000	0.000	-0.002	0.024	-0.001	0.303	-0.001
Fuel Pump Discharge Pressure	-0.001	0.000	0.041	0.041	0.178	0.000	-0.001
Oxidizer Turbine Flowrate	-0.002	0.014	0.014	0.209	0.006	0.180	-0.117
Fuel Turbine Flowrate	-0.024	-0.001	0.282	0.282	0.082	0.010	-0.126

CONFIDENTIAL

CONFIDENTIAL

TABLE 5

SECONDARY ENGINE INFLUENCE COEFFICIENTS FOR 9:1 THROTTLED OPERATION

<u>Independent Variable</u>	<u>Nominal Value</u>	<u>Remarks</u>
Fuel Pump Inlet Pressure, psia	60	A 1-percent increase in any independent variable causes a percentage change in each dependent variable. The magnitude of change in dependent variables is listed below.
Oxidizer Pump Inlet Pressure, psia	45	
Fuel Pump Inlet Temperature, R	40	
Oxidizer Pump Inlet Temperature, R	153	
Fuel Injector Pressure Drop, psi	28.9	
Oxidizer Injector Pressure Drop, psi	44.4	
Coolant Bulk Temperature Rise, R	890	

Dependent Variable	Percent Change Caused by 1-Percent Increase In:						
	Fuel Pump Inlet Pressure	Oxidizer Pump Inlet Pressure	Fuel Pump Inlet Temperature	Oxidizer Pump Inlet Temperature	Fuel Injector Pressure Drop	Oxidizer Injector Pressure Drop	Coolant Bulk Temperature Rise
Engine Specific Impulse	0.030	0.000	0.000	0.000	0.000	0.000	0.001
Thrust Chamber Mixture Ratio	-0.011	-0.008	0.004	0.002	-0.006	0.009	0.014
Oxidizer Pump Speed	0.000	-0.192	0.000	0.208	-0.001	0.222	-0.001
Fuel Pump Speed	0.267	0.000	0.217	0.000	0.147	-0.001	-0.001
Oxidizer Pump Horsepower	0.001	-0.518	0.000	0.274	-0.001	0.601	-0.002
Fuel Pump Horsepower	-0.648	0.001	0.339	0.000	0.362	-0.001	-0.001
Oxidizer Pump Discharge Pressure	0.001	0.030	-0.001	0.003	0.000	0.677	-0.001
Fuel Pump Discharge Pressure	0.000	0.900	0.005	0.000	0.197	-0.001	-0.001
Oxidizer Turbine Flowrate	-0.022	-0.310	0.005	0.067	0.014	0.359	-0.160
Fuel Turbine Flowrate	-0.371	-0.020	0.118	-0.004	0.207	0.023	-0.162

40
CONFIDENTIAL

CONFIDENTIAL

variable. This should be expected with an engine utilizing both thrust and mixture ratio control. The influence coefficients were generated based on the engine basic design parameters and the pump and turbine maps which were presented in the first quarterly report (AFRPL-TR-68-17). A refined evaluation of the important engine influence coefficients will be conducted when the engine system design has been more nearly finalized. At that time, a double precision computerized analysis will be used to provide a greater degree of accuracy.

d. PURGE REQUIREMENTS FOR THE AMP'S ENGINE

(U) To define the inert fluid requirements for the engine system, a purge requirements analysis of the engine system was conducted. This analysis necessitated consideration of the properties of the propellants used, engine operational requirements, serviceability, engine and component configurations, orientation of hardware, and residual propellant expulsion rates.

(U) From the analysis, the total purge fluid requirements were estimated. These are summarized in Table 6. The following discussion presents the analysis conducted in arriving at these estimates.

(U) The approach taken in the analysis was to define the hardware decontamination necessary strictly on the basis of hardware storage, then to define the requirements necessary to restart the engine, and, finally, to evaluate various methods to minimize the impact of these requirements on the restart capability of the engine.

(1) Decontamination for Storage

(U) As the fuel and oxidizer are cryogenic, no major problem is expected with regard to decontamination for purposes of hardware storage. However,

CONFIDENTIAL

TABLE 6

ENGINE SYSTEM PURGE REQUIREMENTS

Item	Purge Medium	Regulated Purge Pressure, psia	Purge Flowrate, scfm	Purge Temperature, R
<u>Main Engine Operation</u>				
Oxidizer System	Helium	750	75	>180
Fuel System	Helium	750	100	
Oxidizer Pump Seal	Helium	750	4.4	>180
<u>Secondary Engine Operation</u>				
Oxidizer System	Helium	750	Not defined	>180
Fuel System	Helium	750	Not defined	
Oxidizer Pump Seal	Helium	750	1.0	>180
<u>Main and Secondary Engine Ground Test</u>				
Fuel System Standby	Gaseous Nitrogen	750	~1	Ambient
Oxidizer System Standby	Gaseous Nitrogen	750	~1	Ambient

CONFIDENTIAL

the propellants exhausting into the thrust chamber would result in finite thrust until all propellants were dissipated. Given sufficient time, both propellants in the propellant feed system would dissipate to the atmosphere through the thrust chamber and leave no residual which would require special treatment (i.e., draining, flushing, etc.) to expel. Also, there are sufficient sources in all situations of operation to provide the necessary heat to vaporize the residual. The ground operation presents the greatest problem in this regard because of the gravitational conditions which tend to "puddle" the fluids at low points. As the result of "puddling" evaporation of residuals would be retarded because of the increased amount of heat transfer required at the low points. In a zero gravity environment, the evaporation would be uniform throughout uniform volumes. A hypothetical case was assumed where all of the residual oxidizer for the main engine (0.116 cu ft) was contained in 1-inch x 0.085-inch stainless steel tubes with a zero gravity field. It was found that under the probable environment imposed following engine shutdown it would require in excess of 100 seconds for the oxidizer to evaporate. Less time would be required for evaporating the fuel because the majority of the residual fuel would be in the vapor state at engine shutdown, and the heat input required to vaporize the remainder would be much less than that required to vaporize the oxidizer.

(2) Engine Restart Conditions

(U) From the standpoint of the start sequences contemplated for the AMPS engines, where a significant fuel lead is to be used, it becomes apparent that the oxidizer system could become primed with fuel before the oxidizer valve opened. The result would be that combustion would occur upstream of the oxidizer injector. This could be avoided if a gas purge was introduced into the oxidizer system during the period of fuel lead. The magnitude or location of entry for this purge is not critical as its purpose is to merely provide a positive pressure at the oxidizer injector; however, both magnitude and location become important if one engine has been operating

CONFIDENTIAL

and the other engine is started. Because the turbine gas is to be expelled into the base region, it is expected that the atmosphere in the nonoperating engine fuel and oxidizer systems could be fuel rich. Consequently, it is important that the entire oxidizer system is purged free of fuel prior to opening the main oxidizer valve (MOV). In the case of restarting the engine immediately after shutdown, it is assumed that virtually no propellant evaporation would occur, and the engine propellant system would be fully primed at the time engine start would be required. To avert preignition with the residual propellants, procedures are required which would produce an inert chamber atmosphere during fuel system prime.

(3) Minimization of Effect of System Purges

(U) Analyses were made to evaluate and reduce the impact of the required purges on the restart capability. An initial analysis was made to determine the rate at which oxidizer expulsion could occur. For this analysis a 100-scfm helium purge, with an entry point immediately downstream of the main oxidizer shutoff valve, was assumed. In this configuration, the entire engine oxidizer system (≈ 0.116 cu ft) would be purged free of oxidizer. For the calculation it was assumed that the properties of the oxidizer would be the same as mainstage until the expulsion was complete, and there would be virtually no mixing of the oxidizer and purge gas. In a zero gravity field, this would probably be a good assumption. With the influence of gravity (or axial thrust) it is expected that the purge would not be as effective. A calculation was made to estimate the effect of heat transfer on the effectiveness of the purge. It was assumed that the purge gas was supplied at a temperature of 400 F and a pressure of 750 psia and dropped to 150 R and 25 psia upon entering the engine. The change in enthalpy between the two conditions is 400 Btu/lb. On the basis of the 100-scfm (0.0174 lb/sec) purge flowrate, the heat available for heating the oxidizer is 7 Btu/sec. Since the heat of vaporization for the oxidizer is approximately 80 Btu/lb, it becomes apparent that the heat input from the purge gas is relatively insignificant.

CONFIDENTIAL

(C) A potential problem recognized in the purge procedure is that to expel all the oxidizer with a zero chamber pressure, it is necessary to have no fuel flow. Consequently, it is required that the mixture ratio increase through stoichiometric and, thereby, expose the chamber to a short period of high combustor chamber temperature. To assess the magnitude of this problem, a heat balance was made using the data (film coefficient, heat flux, etc.) derived from the 5-inch (G_c contour) segment testing. The data used was that produced during 70-psia chamber pressure operation. The tube wall temperatures (gas and coolant) and coolant wall film coefficients were computed on the basis of combustion temperature, coolant temperature, and heat flux at the nominal mixture ratio. It was assumed that the coolant temperature and gas and coolant film coefficients would remain the same, and the heat balance was computed for stoichiometric mixture ratio. The gas-side tube wall temperature increase as a result of the mixture ratio increase was computed to be 20 R (1680 R to 1700 R). It is probably optimistic to assume constant wall film coefficients; however, this may be approached if the main fuel valve is left open until the oxidizer purge is completed.

(C) Because of the uncertainty associated with the oxidizer-rich purge, an analysis was made to define a purge which would avoid the high mixture ratio condition. A fuel flowrate is required during the oxidizer expulsion which will maintain the thrust chamber mixture ratio at or below the nominal operating mixture ratio. The maximum fuel weight contained in the fuel system volume (0.26 cu ft) is approximately 0.6 pound and could be as little as 0.5 pound. It is observed that the residual propellant mixture ratio would be in the range of approximately 17:1 to 20:1. It became evident that to maintain the mixture ratio during purging at or below the nominal operating mixture ratio, the fuel shutoff valve cannot be closed simultaneously with the oxidizer shutoff valve. Two basic approaches to the problem were made. The first approach considered a single hot-gas valve to control fuel and oxidizer turbine flow. This valve would be closed at the cutoff signal. The main oxidizer valve would also be closed but the main fuel valve would remain open until the oxidizer was purged from the

CONFIDENTIAL

system. Assuming a fuel pump discharge pressure of 50 psia (tank pressure of 70 psia), chamber pressure of 20 psia, and the fuel density temperature profile remaining unchanged from engine operation to purge operation, it was found that fuel weight flowrate would be 0.245 lb/sec. Assuming a 10:1 mixture ratio, it would require 4.4 seconds to expel the oxidizer from the 0.116 cu ft system volume. The helium purge required to provide this expulsion rate was computed to be 5.3 scfm.

(U) Restart of the engine could be accomplished at any time during the sequence since the fuel system would be primed and in the same condition required for signalling the hot-gas valve and oxidizer valve to open during a "normal" start sequence. The start and cutoff control logic for this configuration is shown in Fig. 17. This control logic is basically the same logic that was presented in the first quarterly progress report (Ref. 1); however, some modifications were required as the result of the purge analysis.

(C) The major disadvantage of this cutoff purge configuration appears to be that the propellant flowrates for the period of the oxidizer purge (4.4 seconds) are small and result in an extremely low injection velocity. Analyses have indicated that excessively low injector flowrates may cause injector overheating. Consequently, a purge of this magnitude could only be used if subsequent testing reveals that these flowrates cause no injector heating problem.

(C) The second approach considered for providing adequate fuel flow during the purge involves two turbine hot-gas valves. Since allowable expulsion flowrate of the residual oxidizer following cutoff is a function of the fuel flowrate (lower than nominal mixture ratio), it was rationalized that the fuel flowrate could be maintained at the full throttled thrust level during the period of oxidizer expulsion if the hot-gas valve controlling the fuel turbine flowrate was left open until the oxidizer was expelled. With this fuel flowrate, the oxidizer flowrate could also be maintained at a compatible flowrate during residual expulsion. Computations revealed that under these conditions the oxidizer expulsion time

CONFIDENTIAL

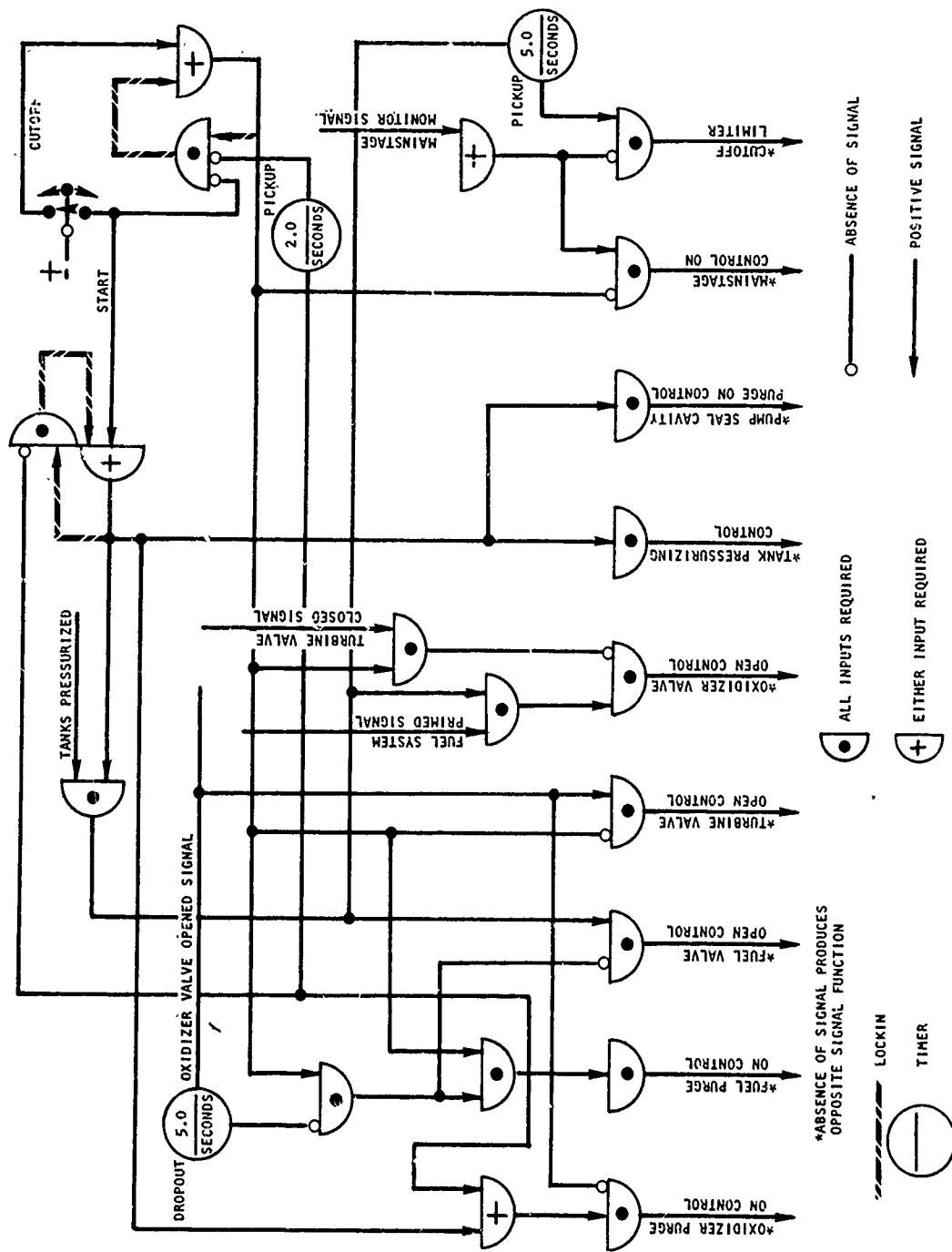


Figure 17. AMPS Engine Start and Cutoff Control Logic With One Turbine Valve

CONFIDENTIAL

CONFIDENTIAL

would be less than 2.0 seconds. During the purge, the injection velocities of the propellants would be comparable to the velocities achieved during full throttled operation. Therefore, injector face heating would be no problem with this purge configuration. As in the case of the first approach, there would be no restraint on restarting the engine as the result of the purge. The main difference in this sequence when compared to a normal start is that the atmosphere in the thrust chamber could be abnormally fuel rich (e.g., in the case of total oxidizer expulsion at the time of restart signal), and the power available to the oxidizer turbine would possibly be greater than usual. It is anticipated that the restart would be faster than normal; however, no problems are anticipated as a result of the condition. The control logic for this start and cutoff purge sequence, including the two hot-gas valves, is shown in Fig. 18.

(U) After weighing the alternatives, it was concluded that the two hot-gas valve configuration permitted definition of the best purge configuration for the AMPS engine. The system provides a method for unlimited restart capability and, at the same time, avoids the question of the effect of low injection velocities on injector heating.

(U) Total fluid requirements for the oxidizer system purge were computed as a function of the maximum number of starts and restarts required of the main engine using the two hot-gas valve configurations. With this criteria, it is estimated that approximately 250 scf of helium is required (Table 7). The thermal conditioning of the purge is to be such that the oxidizer does not freeze (≈ 82 R) when helium gas is introduced into the oxidizer system. The calculations were made with an assumed temperature of 200 R. The purge is to be supplied to the engine from a regulated pressure source combined with proper orificing to meet the flow requirements.

(U) Because secondary engine volumes have not been defined, it was not possible to make similar analysis with respect to the oxidizer system purge requirements. However, in the interest of determining preliminary

CONFIDENTIAL

CONFIDENTIAL

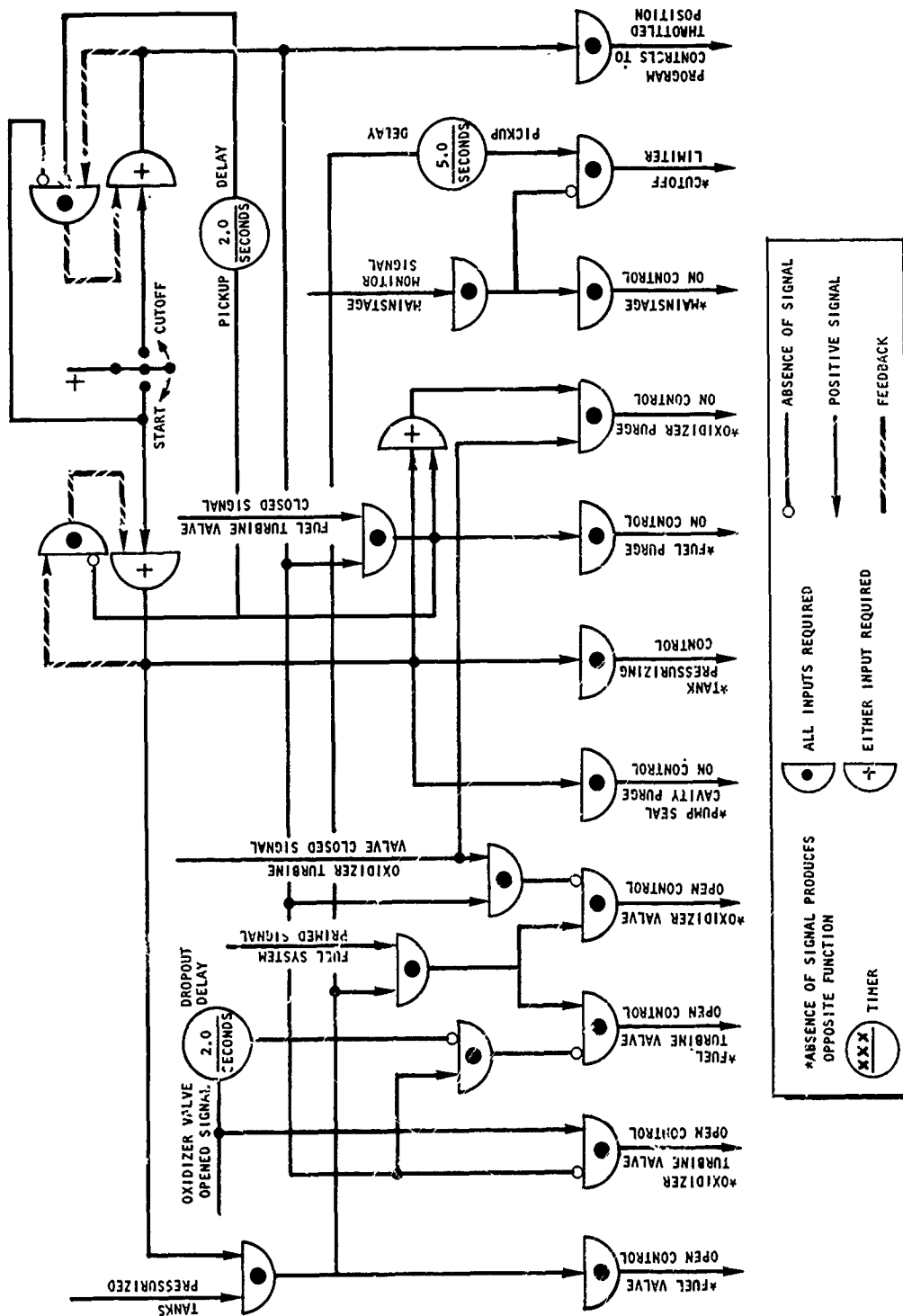


Figure 18. AMPS Engine Start and Cutoff Control Logic With Two Turbine Hot-Gas Valves

CONFIDENTIAL

CONFIDENTIAL

TABLE 7

TOTAL ENGINE SYSTEM OPERATIONAL PURGE FLUID REQUIREMENTS FOR EXTREME DUTY CYCLES

<u>Main Engine (31 Starts; Maximum Duration)</u>	<u>Helium Purge Volume, scf</u>
Oxidizer System	250
Fuel System	100
Pump Seal Purge	<u>150</u>
Total	500
<u>Secondary Engine (31 Starts; Maximum Duration)</u>	
Oxidizer System	125
Fuel System	50
Pump Seal Purge	<u>300</u>
Total	475
<u>Total AMPS Engine (29 Short Main Engine Burns With 1 Long Secondary Engine Burn)</u>	~650

CONFIDENTIAL

requirements, a volume of 100 cu in. was estimated. By scaling the purge requirement from the main engine as a linear function of volume, the total purge fluid requirements for the secondary engine were estimated to be 125 scf.

(U) Although the pressure value of the regulated source is not particularly critical, it is important to maintain the number of accessory requirements at a minimum. Consequently, a regulated pressure source of 750 psia was identified as the purge source because the pneumatic pressure planned for engine valve actuators is 750 psia. It is possible that the same regulator could be used for both purposes.

(3) Fuel System Purge Requirements

(U) Although there is no requirement for purging the fuel system from the standpoint of hardware storage, the use of a purge after shutdown is advantageous to minimize the time interval in which the residual fuel expels from the thrust chamber. If the propellant is permitted to boil off, a finite residual thrust will be present until the boiloff is completed. Using the same approach that was used for the oxidizer system, it is estimated that the time required for the residual fuel (225 cu in. at 3.9 lb/cu ft) to evaporate would be in excess of 90 seconds. By supplying a 100 scfm helium purge, it is estimated that expulsion of residual fuel can be accomplished in slightly more than 1.0 second.

(U) Inclusion of the fuel system purge in the cutoff sequence puts no restraint on the restart capability, and the purge can be overridden by an engine start signal. This control is included in the logic presented in Fig. 17 and 18.

(C) The fluid requirements of the purge were computed based on the maximum number of starts required (31 starts) and for a 2-second purge following each engine shutdown sequence (Table 7). The total volume requirement was 100 scf for the main engine.

(U) Estimating the fuel system volume for the secondary engine to be half that of the main engine results in a 50 scf fluid requirement for the secondary engine fuel purge.

(U) There is no temperature requirement for the purge (50 R was used for the calculations). The purge is to be supplied from a regulated source pressure and combined with proper orificing to meet the flow requirements. The entry point of the purge to the engine is to be immediately downstream of the fuel shutoff valve.

(4) Turbopump Seal Cavity Purge

(U) Purge requirements for scavenging and pressurizing the cavity between the main engine oxidizer pump seal and turbine seal have been specified to be 7500 scim helium during operation and 1500 scim helium during static conditions with propellants in the pump. The resulting seal cavity pressure for these flowrates was computed to be approximately 50 psia. Analyzing these requirements with respect to the anticipated start and cutoff sequences of the main engine it is concluded that a dual requirement for operation of the engine is not warranted. This conclusion is based on the fact that under present operating concepts, fuel and oxidizer will be present in the seal area only while the pumps are turning, except for brief periods during start and cutoff. However, it appears that it would be impractical to attempt to program a static purge of different magnitude than the operating purge for these brief periods (in the order of 1.0 second). Consequently, a 7500 scim helium purge was identified for the main engine oxidizer pump seal cavity. To program the purge on and off so that it is consistent with the engine sequencing, the purge is to be sequenced on with the signal to pressurize the propellant tanks, and off with termination of the oxidizer system purge following engine cutoff. This would provide the control logic presently shown for the main tank pressurizing control (Fig. 17 and 18). The logic would provide 750 scim helium flow at any time that oxidizer was in the pump. The purge described is to be used for the Phase II engine configuration.

(U) The secondary engine oxidizer pump seal purge logic would be the same, but the magnitude would be 1500 scim.

(U) Maximum fluid requirements for providing the purge are based on the possibility of only secondary engine starts combined with maximum duration (minimum thrust) of operation. With these conditions, approximately 300 scf helium would be required for operation (Table 7). In event the main engine operated for a maximum duration (minimum thrust), 150 scf would be required. The conditioning requirements for the purge prior to entry into the seal cavity are that the supply pressure is a regulated pressure and, to avoid formation of fluid in the cavity, the gas temperature of the purge must be above the saturation temperature of the oxidizer. In the case of a 50 psia cavity pressure, the temperature would be above 180 R (200 R was assumed for the calculations).

(5) Ground Requirements

(U) Because the immediate task is directed toward ground testing of the AMPS engine during the Phase II effort, it is necessary to define those procedures which are unique to the ground operation. The altitude environment (100,000 feet) of the engine is to be simulated during the actual test firing. It is assumed that the environment will be maintained sufficiently long before and after engine start to permit effecting the operational purges defined previously. Since ground testing of the AMPS engine is to be accomplished in confinement of an environment chamber, it is imperative that the atmosphere inside the chamber be maintained at a neutral atmosphere as nearly as possible to reduce the possibility of damage to the facility. To accomplish this, both oxidizer and fuel systems of the engine are to be purged free of propellants prior to shutdown of the altitude environment. The purges defined for the fuel and oxidizer systems in previous paragraphs will satisfy this requirement.

(U) Since both systems will be cold following engine tests, and the environment exposure of the systems will eventually be that of the test

site environment, it will be necessary to provide continuous purges in both fuel and oxidizer systems during all periods of nonfiring conditions to maintain moisture control. Moisture in either system could result in severe damage either as a result of ice formation in the fuel system and ice formation or combustion in the oxidizer system.

(U) Following periods of engine maintenance during which the purges are required to be shut off, it will be necessary to take other contamination prevention measures (e.g., purge and passivation). The magnitude of the standby purges is not critical since their only purpose is to prevent moisture or other contaminants from entering the propellant systems. These purges appear to be the only operational requirement unique to ground testing the AMPS engine.

e. INSTRUMENTATION

(U) An evaluation was made of the AMPS main engine to generally define instrumentation requirements for the Phase II engine. This effort was made so that the instrumentation ports, position indicators, switches, etc., could be included in the initial component and engine design. In the evaluation, consideration was given to minimize the number of potential leakage points and at the same time provide the capability of performing detailed performance and diagnostic analyses. Consideration was also given to the establishment of basic instrumentation which would be used during all levels of operation (component, subengine, etc.) and used for direct comparison analyses at the various levels.

(U) From the standpoint of instrumentation, the segmentation approach of the main engine thrust chamber creates a configuration which is made up of 12 compartments. Consequently, it was concluded that the initial approach would be to provide the capability to record propellant pressure and temperatures in each of the 12 segments.

(U) There is a need for determining the heating conditions of the base region (and secondary engine thrust chamber) during operation of the main engine. To evaluate these conditions, instrumentation has been qualitatively defined for determining temperatures and the heat flux exposure of this region during the Phase I thrust chamber test program.

f. AMPS ENGINE BASE FLOW ANALYSIS

(U) An investigation was conducted to evaluate the effect of recirculation of the main engine thrust chamber primary combustion gas into the bell thrust chamber when the main thrust chamber is firing.

(U) The flow field of a typical aerospike engine firing at high altitude is illustrated in Fig. 19. Low-velocity gases in the nozzle base region cannot negotiate the pressure rise at the recompression shock and, as a result, these gases are turned back toward the base. The gas in the base region forms a natural recirculation pattern, with the central core of the flow moving toward and stagnating at the center of the base. Cold-flow model tests investigating base recirculation have been performed on a number of aerospike configurations. Also, an extensive water table study investigating base recirculation phenomena has been performed.

(U) From these studies, it has been concluded that if no low-temperature secondary bleed gas is exhausted into the aerospike base, the temperature of the recirculating gas is near the primary combustion temperature. Introduction of low-temperature secondary gas into the base strongly affects the base recirculation pattern and influences the temperature of the gas in the base cavity. With the proper secondary flow and orientation of injection for a particular base configuration, the base temperature can be maintained near the temperature of the secondary flow.

(U) To evaluate the effect of the secondary flow (1 percent of primary) on the recirculation pattern of the main engine thrust chamber, Rocketdyne's

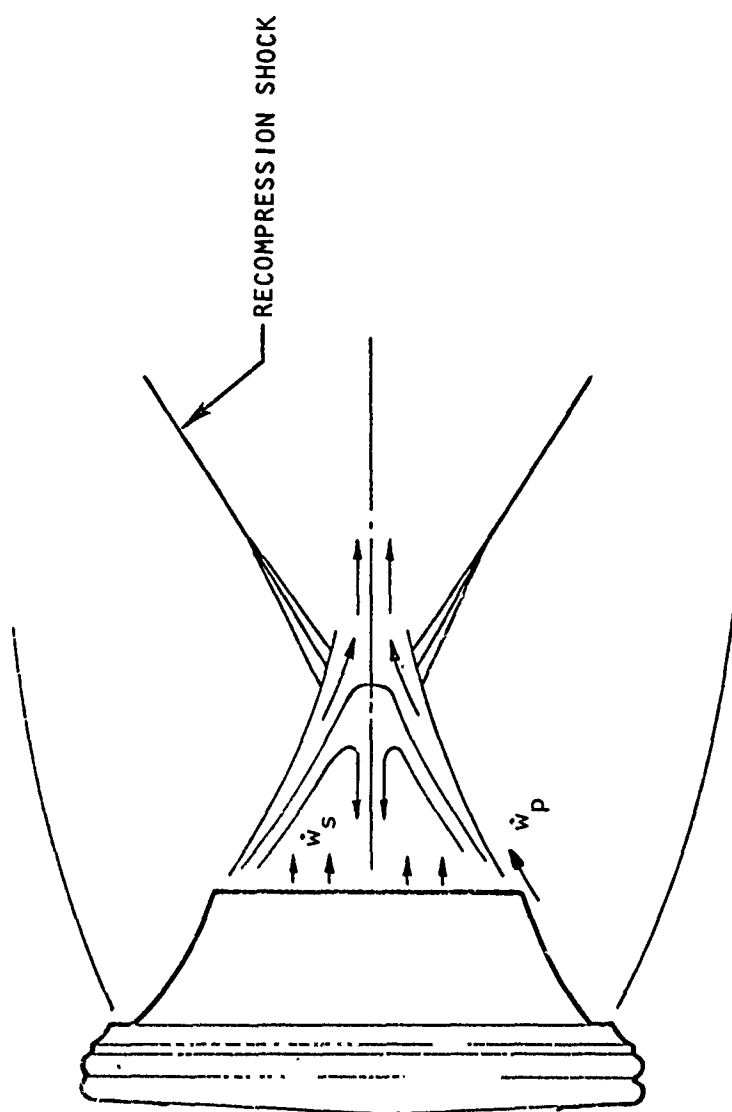


Figure 19. Flow Field of Typical Aerospike Nozzle

water table facility (located at the Rocket Nozzle Test Facility at Los Angeles Division of North American Rockwell Corporation) was used. In previous water table tests, it was indicated that directing the secondary flow to oppose the natural recirculation of the fluid in the base region tended to retard entry into the base cavity of the mixture of primary and secondary fluids circulating from the base jet boundary shear layer. The success of this test method to qualitatively reproduce trends observed with cold-flow air testing suggested that the water table could be used quickly and successfully to simulate the circulation of gases in the secondary engine bell chamber and base region.

(U) The water table (Fig. 20) can be used to simulate two-dimensional supersonic flow of a gas, because of the properties of surface waves on a sheet of shallow water. The hydraulic analogy to compressible gas flow rests on a similarity of equations of a constant-density inviscid liquid flowing in a shallow, horizontal, open channel of rectangular cross section, where the free surface curvature is small compared with the depth; and the isentropic flow of a perfect gas with specific heat ratio $\gamma = 2$, in a two-dimensional channel of rectangular cross section with no discontinuities in the flow.

(U) To simulate gas recirculation in the main engine base region, an AMPS model (Fig. 21) was installed on the water table. The model was placed on the glass floor plate as shown in Fig. 22 and 23. Two strips of formed aluminum were inserted into the base cavity; the inner strip to simulate the secondary engine bell chamber and the outer strip to form a channel which would permit injection of secondary flow. Weights were placed on the aluminum strips to prevent movement during water flow conditions. During flow conditions, white foam particles were scattered over the water surface, and still photographs were taken from which flow paths could be identified. A 2.5-inch head of water was established upstream of the model. This head simulates the primary stagnation pressure associated with the combustion chamber of a real engine. A variable-height sluice gate permitted the establishment of the model primary flow field with proper Mach number simulation. The primary flow path can be observed in Fig. 22.

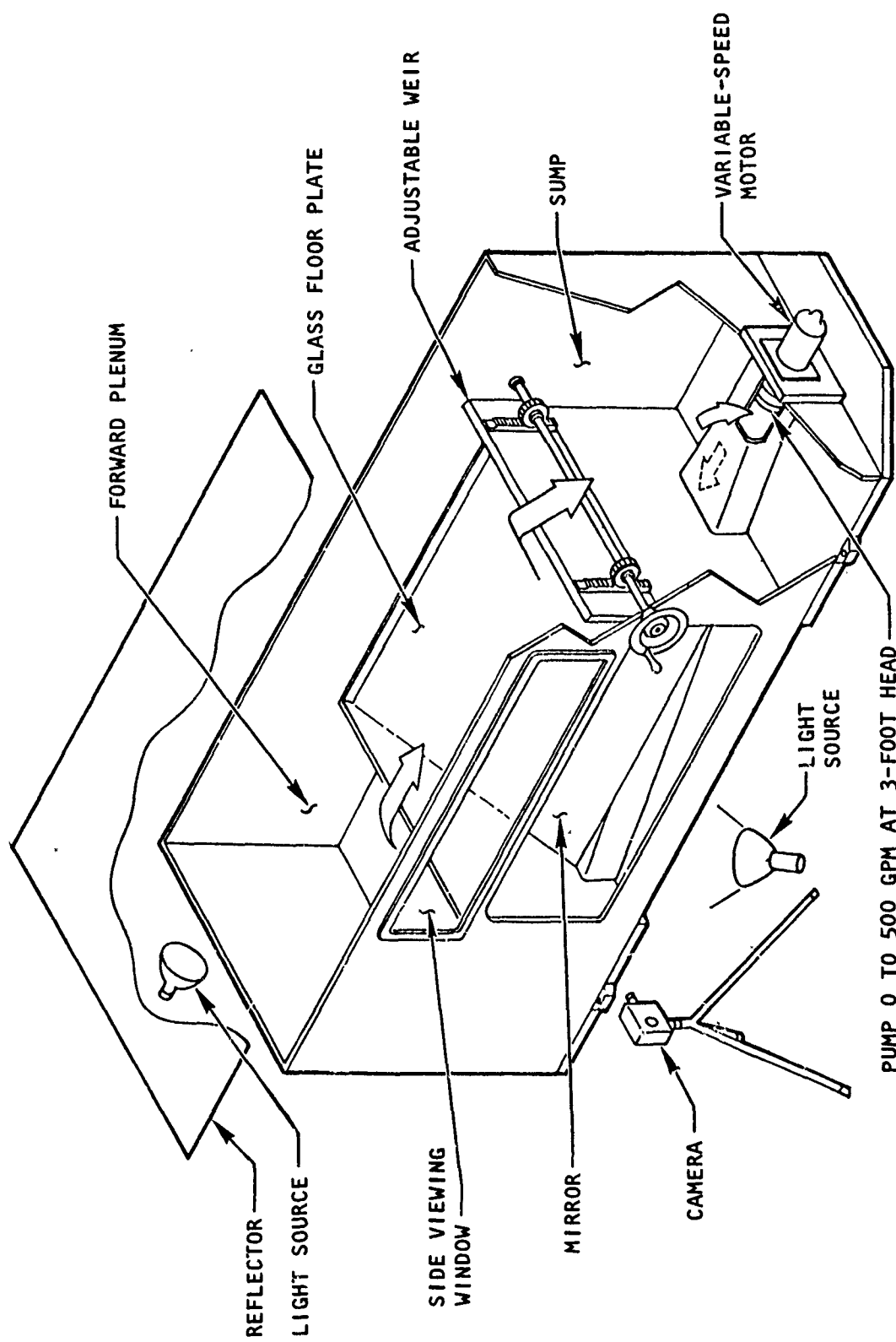


Figure 20. Water Table

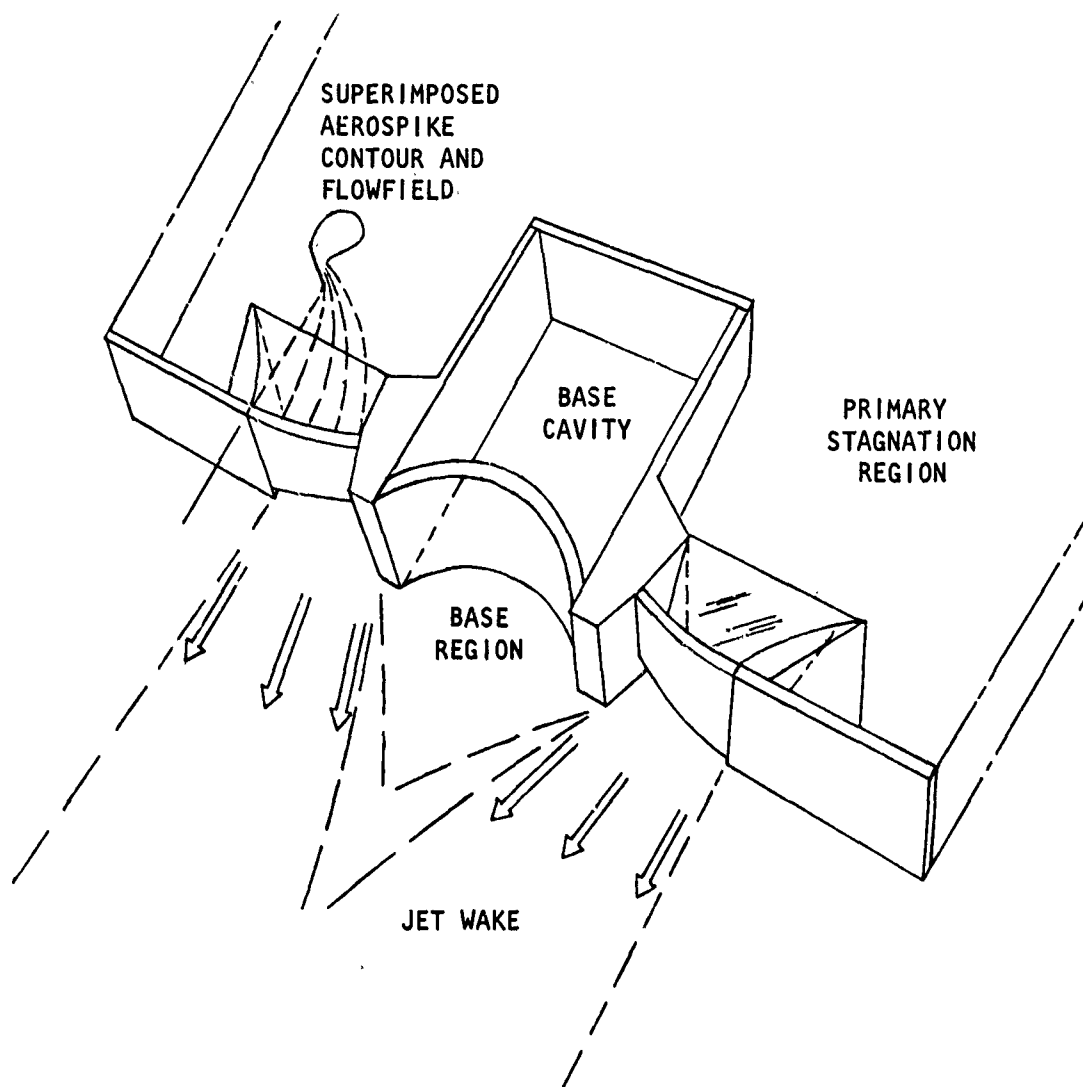
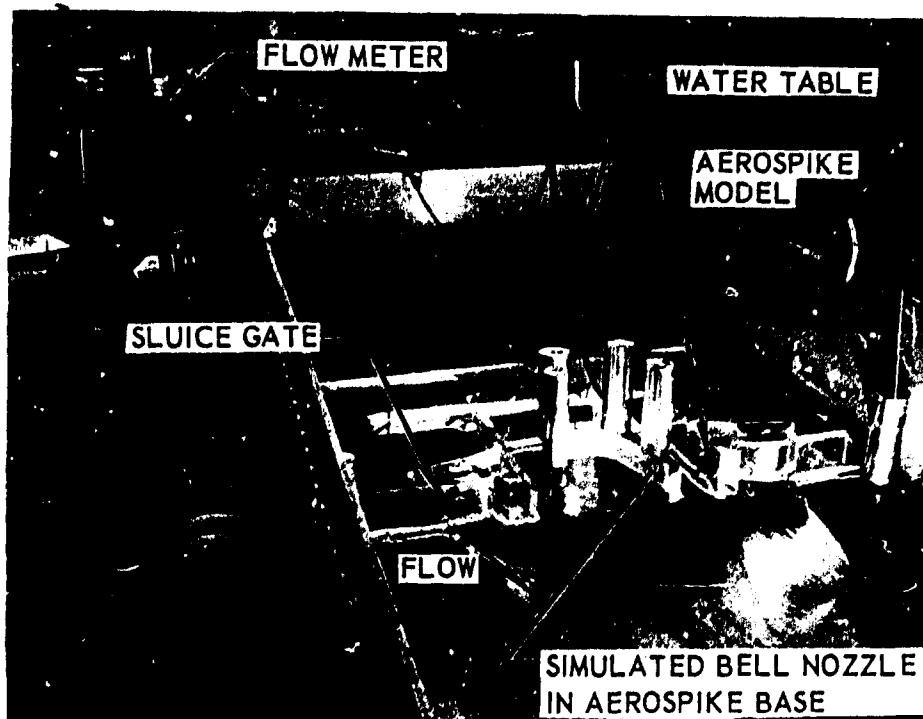
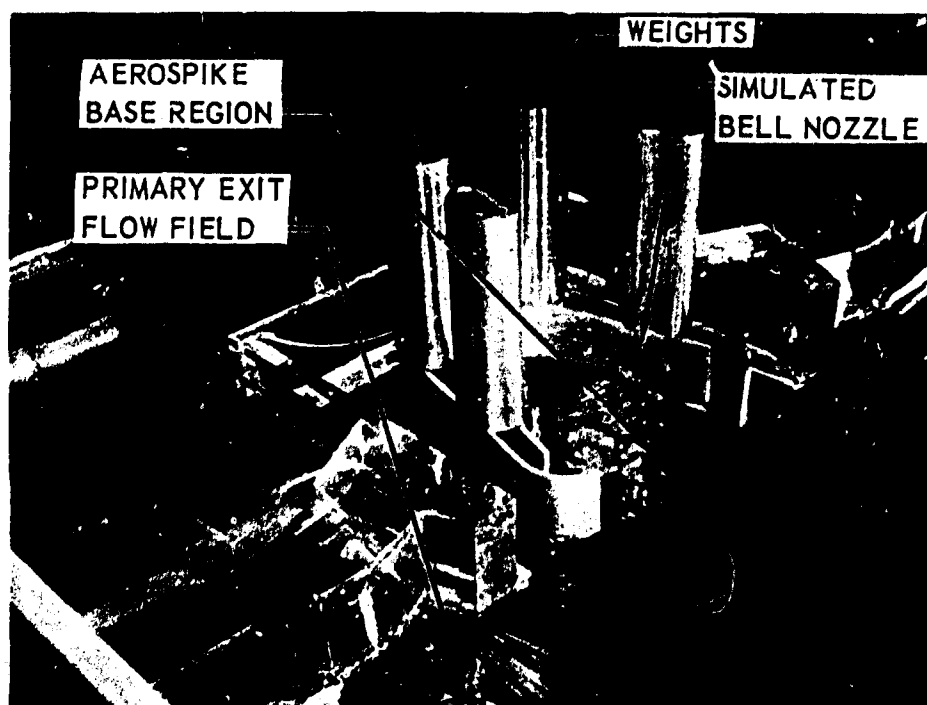


Figure 21. AMPS Model Installed in Water Table With Sluice-Generated Primary Flow



Water Table With
Simulated AMPS
Engine Base
Region



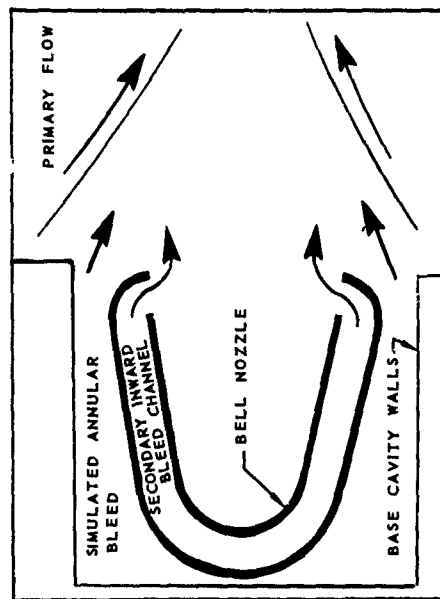
AMPS Engine
Base Region

Figure 22. Primary Flowpath for AMPS Engine Base Region

CONFIDENTIAL

AMPS BASE RECIRCULATION
WATER TABLE SIMULATION

333-247
5-68



FLOW SKETCH



ZERO SECONDARY FLOW



1-PERCENT ANNULAR SECONDARY FLOW



1-PERCENT RADIAL SECONDARY FLOW

Figure 23. Secondary Flow Paths for AMPS
Engine Base Region

CONFIDENTIAL

CONFIDENTIAL

(U) Four secondary flow combinations were used: (1) zero secondary flow, (2) annular (or axial) bleed, (3) inward (radial) bleed, and (4) a combination of the two bleed flows. Figure 23 shows a sketch of the flow paths associated with these combinations.

(U) In the case of no secondary flow, although a strong natural recirculation pattern was established, very little motion occurred within the bell. In the case of pure axial secondary flow (1 percent of primary flow), it is observed that the primary gas circulates into the region that simulates the secondary thrust chamber cavity. Upon comparing the results of axial secondary flow with no secondary flow, it appears that the presence of pure axial flow may actually promote penetration of the recirculation gases into the bell chamber region. The actual gases in the recirculation flow would be a mixture of secondary gases and primary gases. The temperature of these gases is not known since there is no data to identify the amount of mixing. However, it is probable that the temperature would be excessive.

(C) Figure 23 shows a simulation of 1-percent secondary flow directed radially toward the thrust chamber centerlines. The natural recirculation, still a mixture of primary and secondary fluids, has been forced away from the bell cavity. As shown in Fig. 23, the particles are nearly motionless in the bell and in the region immediately aft the bell. The pattern suggests that the temperature of the gases in the bell chamber cavity would be approximately equal to the stagnation temperature of the secondary gas (≈ 640 F).

(U) On other aerospike thrust chamber test programs, the base region has been successfully protected with the use of secondary flow; however, there have been no gas temperature data obtained to define the environment. It has been generally assumed from the test results that where secondary flow has provided a buffer zone, the gas temperature at the base plate has been near the secondary gas temperature.

CONFIDENTIAL

(C) From this study, it was concluded that to maintain the gas temperature at the base of the AMPS engine at a relatively low temperature (≈ 640 F) during firing of the main engine, it will be necessary to provide a secondary flow which has a radial injection component (Fig. 24).

(U) The results of this study are to be confirmed during the main thrust chamber test series of the Task II effort. A bell chamber simulation has been designed (Engine Design section) to house the instrumentation required to determine the environment of the base region.

g. ACCESSORY PROVISIONS

(U) Investigation of the engine accessory requirements was started. The study will consist of the evaluation of system requirements for auxiliary power and the description of engine mounted accessory components. Typical components could be accumulators, regulators, hydraulic pumps, electric motors, heat exchangers, etc. Initial effort will be directed toward definition of preliminary engine fluid requirements and methods to supply the required pressure and flow and to define preliminary engine gimbal system requirements. This effort will be coordinated with each of the Task III propellant feed system subcontractors.

h. MANNED MISSION

(U) Effort was initiated to evaluate the relationship of man and the AMPS engine system in a manned mission application. The present effort is primarily concerned with the influence of man-in-the-loop control system. Initial effort is concentrated on evaluation of the results of the X-15 program and its application to the AMPS program. Additional effort will include review and evaluation of other manned space programs (i.e., Apollo).

CONFIDENTIAL

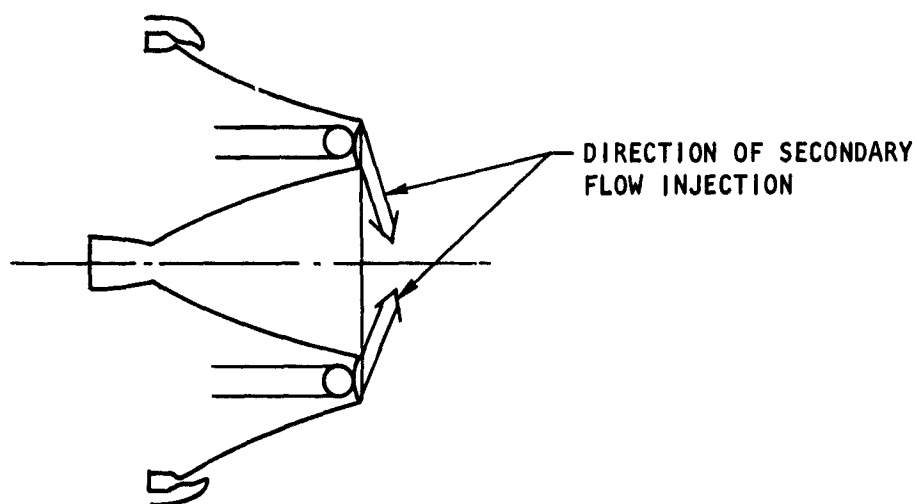


Figure 24. Turbine Exhaust Base Injection Technique to Restrict Base Flow Recirculation Into the Bell Chamber

64
CONFIDENTIAL

i. DESIGN

(U) Engine design effort in the second quarter consisted of preparing design specifications for engine components and preparing layouts of engine interconnects. The design specifications for the engine system components were completed to the extent of defining loads and functions. The specifications which were prepared are as follows:

1. Engine Thrust Mount Assembly
2. Base Closure
3. Main Engine Fuel Turbine Exhaust Duct
4. Main Engine Oxidizer Turbine Exhaust Duct
5. Main Oxidizer Turbopump Mount
6. Main Fuel Turbopump Mount
7. Secondary Engine High-Pressure Oxidizer Line
8. Secondary Engine Oxidizer Inlet Line
9. Gimbal Bearing Simulator
10. Secondary Engine Tapoff Y-Duct
11. Secondary Engine Tapoff Duct
12. Secondary Engine Oxidizer Turbopump Mount
13. Secondary Engine Oxidizer Turbine Exhaust Duct
14. Secondary Engine High-Pressure Fuel Duct
15. Secondary Engine Fuel Turbopump Mount
16. Secondary Engine Fuel Turbine Exhaust Duct
17. Secondary Engine Fuel Inlet Line
18. Main Engine Turbine Gas Bleed Y-Duct
19. Main Engine Turbine Gas Bleed Duct
20. Main Engine Fuel Transfer Lines
21. Main Engine Coolant Transfer Lines

CONFIDENTIAL

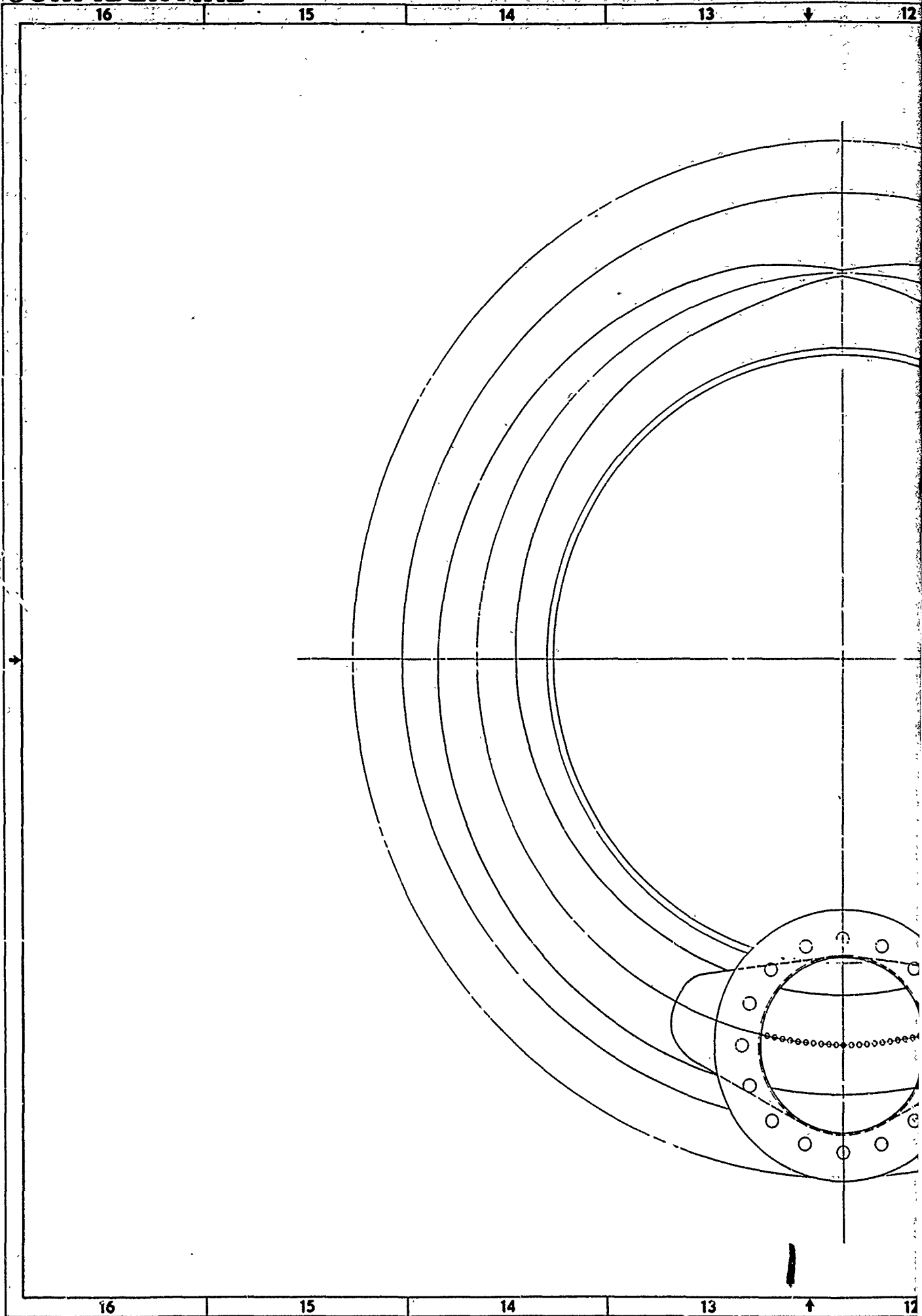
(C) Design analyses and layouts were completed for the main engine turbine exhaust manifold. The design (Fig. 25) utilizes a continuous taper manifold with 285 holes 0.125 inch diameter, to provide a uniform pressure distribution around the full circumference of the base region. Attachment details of the manifold to the base plate have not been defined pending a more detailed design definition of the main engine thrust chamber backup structure.

(U) In the layout shown in Fig. 25, the exhaust duct is shown to provide a radial velocity component to the secondary gases. The duct configuration and gas injection direction will be evaluated during the testing in Phase I. Figure 26 is a layout of the turbine exhaust duct which transports the secondary gases from the turbines to the exhaust manifold.

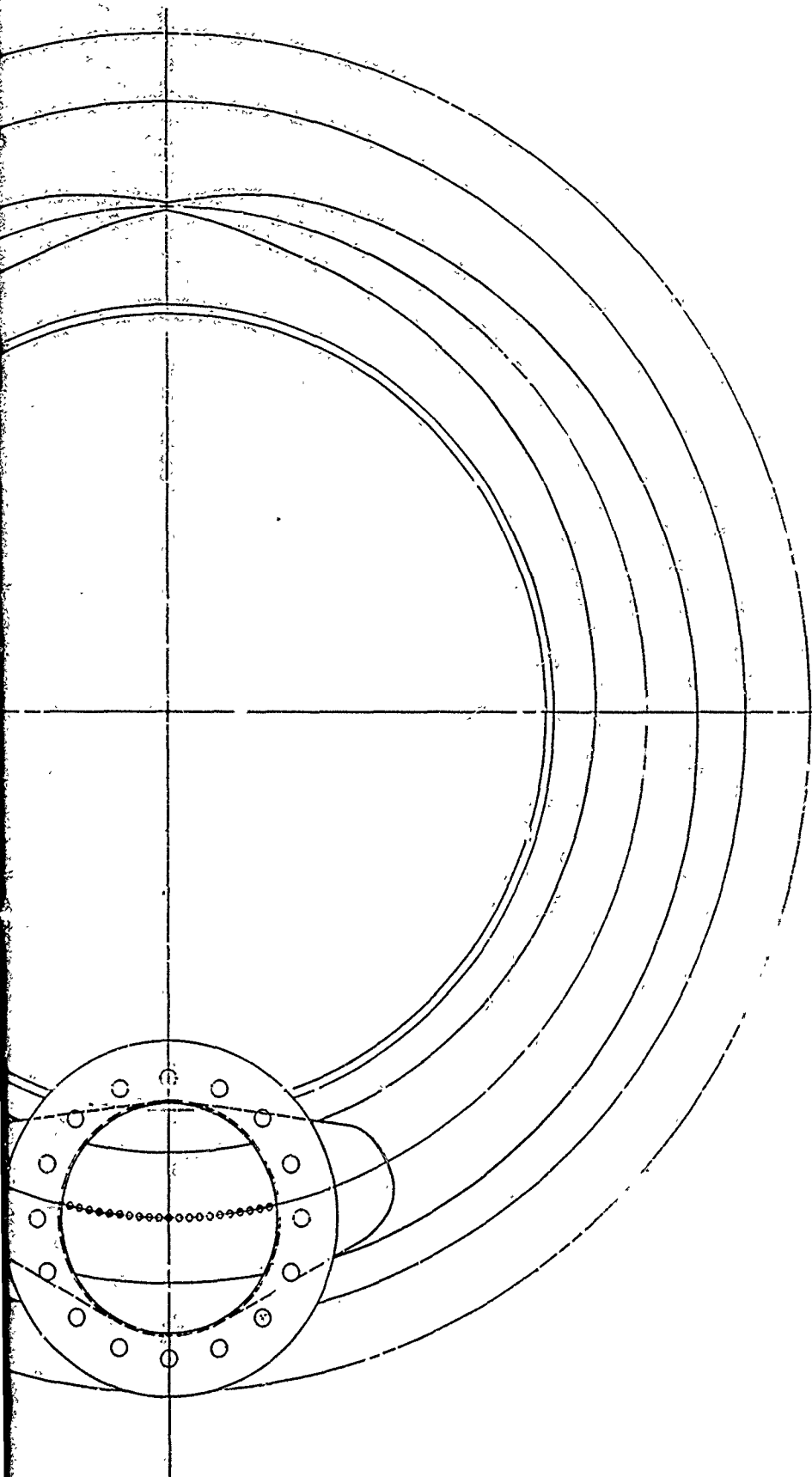
(U) A design layout of a secondary engine thrust chamber simulator was completed (Fig. 27). This simulator is intended for use in Phase I main thrust chamber testing as well as Phase II main engine testing. It is planned to utilize temperature and pressure measuring devices from which the heat load to the secondary engine thrust chamber can be determined.

(U) Additional analyses of the main engine thrust mount and propellant manifolding resulted in a more detailed description and some changes to the configurations which were presented in the first quarterly report. A tradeoff was made for the oxidizer and fuel distribution manifold profiles for tapered, stepped, and constant area configurations. It was concluded that stepped manifolds in both cases (Fig. 28 and 29) would produce the flow distribution to provide even priming and pressure profiles for satisfactory engine operation. The stepped configuration proved to be best suited since it would produce the same effect as the tapered configuration in this particular application and can be manufactured at considerably less cost than the tapered manifold. The orificed configuration was ruled out because of the uneven pressure profile inherent in the design.

CONFIDENTIAL



12 11 10 9 8



ROCKWELL
A DIVISION OF NORTH AMERICAN ROCKWELL CORPORATION
GARDEN CITY, CALIFORNIA • GARDEN CITY, NEW YORK
CODE IDENT 82453 FRAME 1

2

12 11 10 9 8

8

7

6

5

4

3

SECONDARY THRUST CHAMBER

AFT

EXHAUST INLET

EXHAUST DUCT

DISTRIBUTION MANFOLD

PRIMARY THRUST CHAMBER

NOTE: UNLESS OTHERWISE SPECIFIED

2

3

8

7

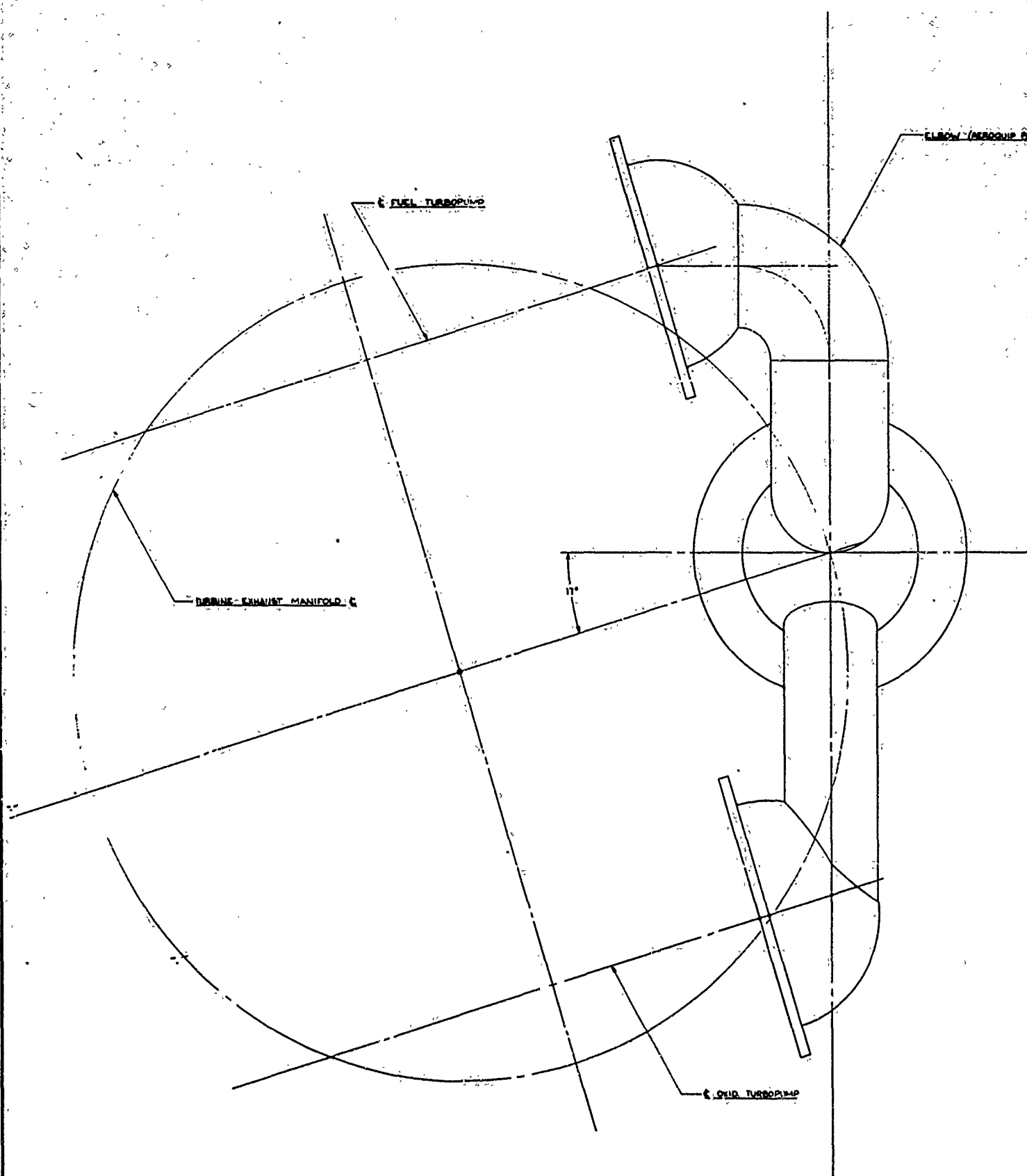
6

5

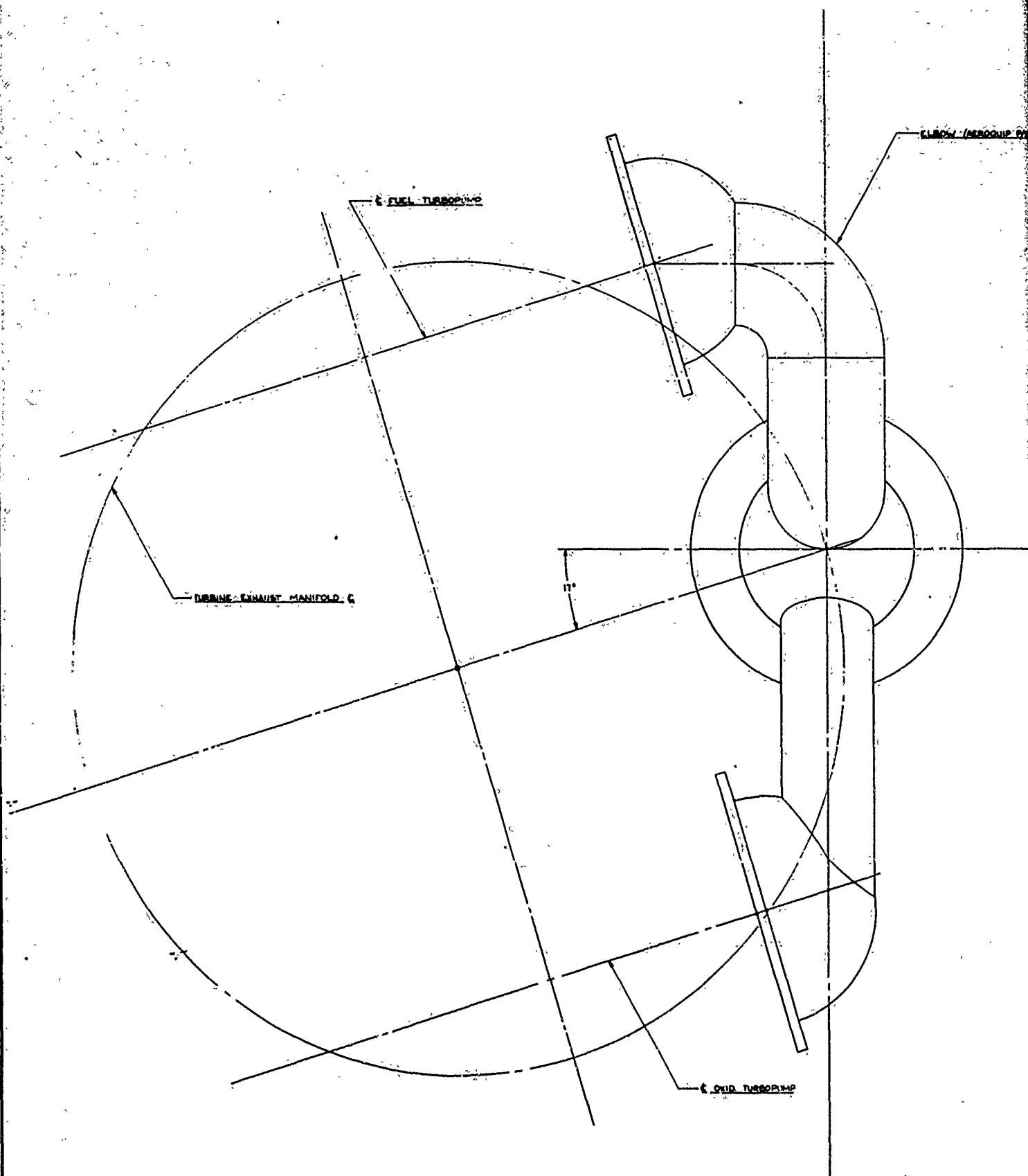
4

3

CONFIDENTIAL



CONFIDENTIAL



18

17

16

15

41

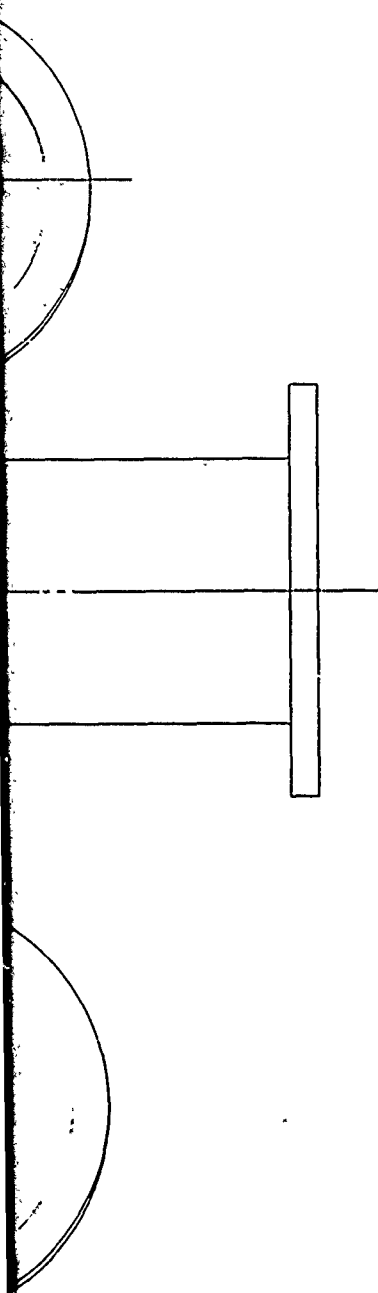


Figure 26. AMPS Main Engine Turbine Exhaust Duct

68

BROOKLYN
A DIVISION OF NORTH AMERICAN AVIATION, INC.
BOSTON, MASS. 02108 • BOSTON, MASS. 02108
CODE 1001 01607 NAME ONE SHEET

CONFIDENTIAL

2

18

17

16

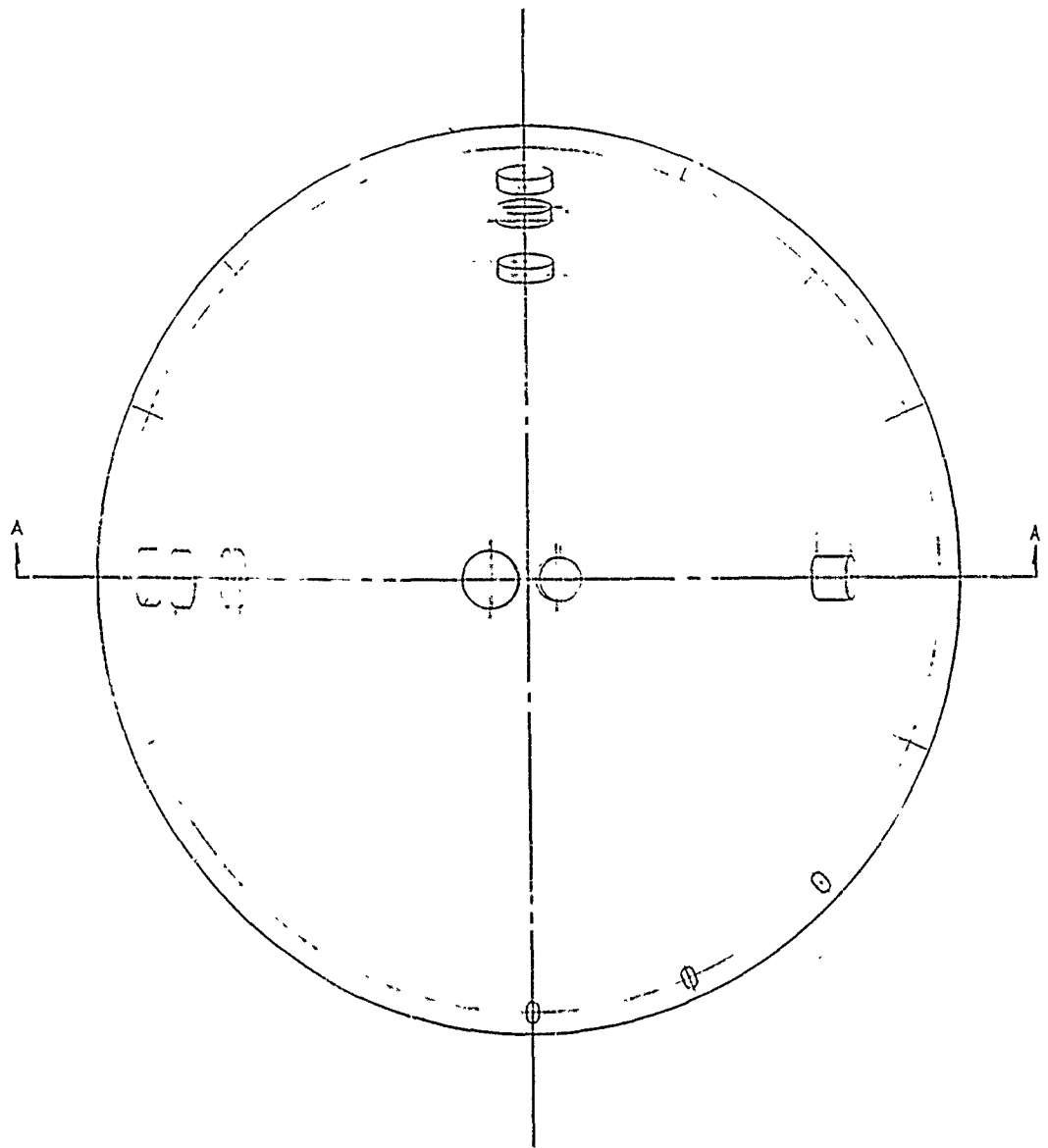
15

b

3

8 7 ↓

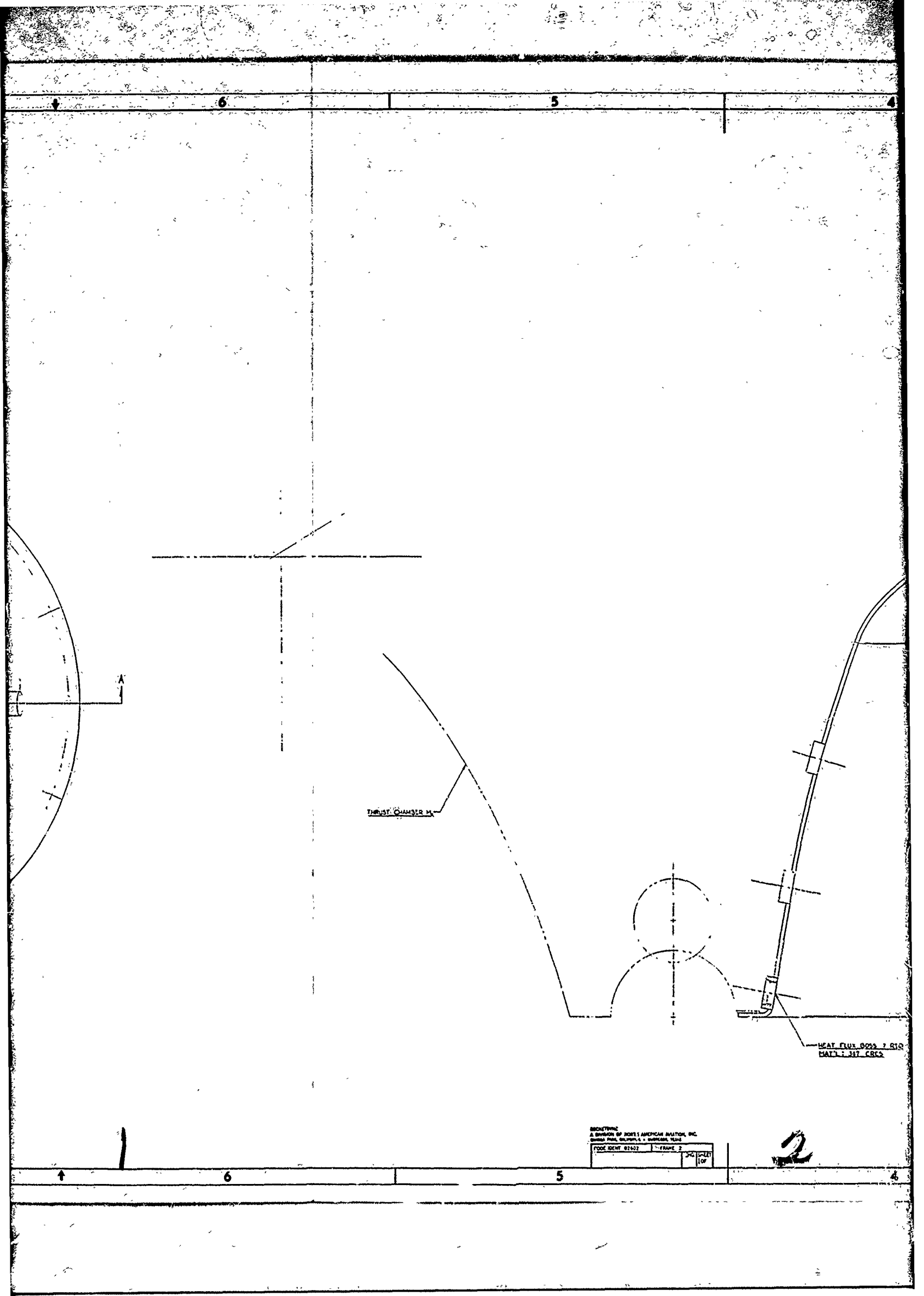
CONFIDENTIAL

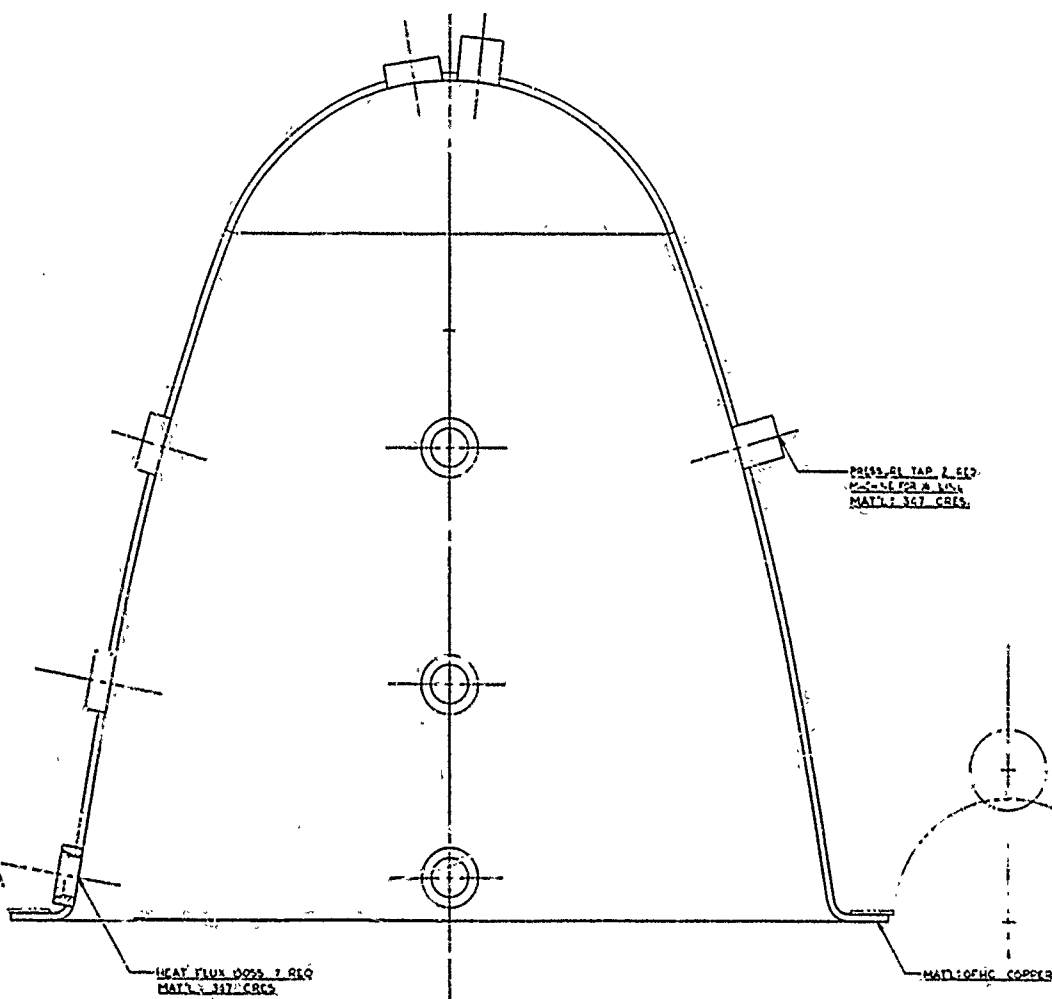


8

7

↑





SECTION A-A

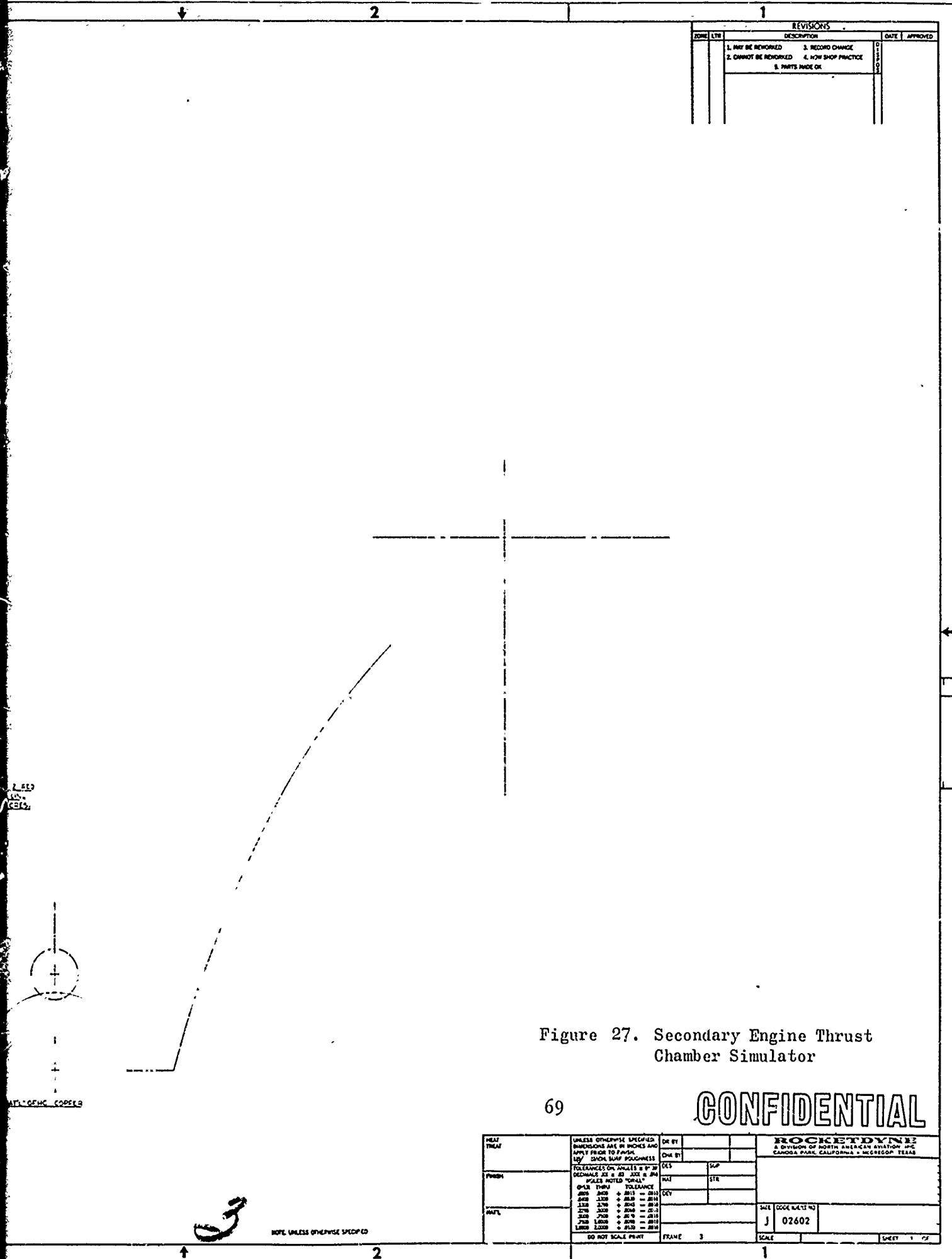


Figure 27. Secondary Engine Thrust Chamber Simulator

69

CONFIDENTIAL

HEAT TREAT	UNLESS OTHERWISE SPECIFIED, DIMENSIONS ARE IN INCHES AND APPLY PRIOR TO FINISH. SURF. FINISH: 32 RMS. SURF. TOUGHNESS: 100. FINISH: 32 RMS. SURF. TOUGHNESS: 100. FINISH: 32 RMS. SURF. TOUGHNESS: 100.	DR BY	CHK BY	DATE	APPROVED
FINISH	UNLESS OTHERWISE SPECIFIED, DIMENSIONS ARE IN INCHES AND APPLY PRIOR TO FINISH. SURF. FINISH: 32 RMS. SURF. TOUGHNESS: 100. FINISH: 32 RMS. SURF. TOUGHNESS: 100. FINISH: 32 RMS. SURF. TOUGHNESS: 100.	DR BY	CHK BY	DATE	APPROVED
DATE	UNLESS OTHERWISE SPECIFIED, DIMENSIONS ARE IN INCHES AND APPLY PRIOR TO FINISH. SURF. FINISH: 32 RMS. SURF. TOUGHNESS: 100. FINISH: 32 RMS. SURF. TOUGHNESS: 100. FINISH: 32 RMS. SURF. TOUGHNESS: 100.	DR BY	CHK BY	DATE	APPROVED
SCALE	UNLESS OTHERWISE SPECIFIED, DIMENSIONS ARE IN INCHES AND APPLY PRIOR TO FINISH. SURF. FINISH: 32 RMS. SURF. TOUGHNESS: 100. FINISH: 32 RMS. SURF. TOUGHNESS: 100. FINISH: 32 RMS. SURF. TOUGHNESS: 100.	DR BY	CHK BY	DATE	APPROVED
FRAME	UNLESS OTHERWISE SPECIFIED, DIMENSIONS ARE IN INCHES AND APPLY PRIOR TO FINISH. SURF. FINISH: 32 RMS. SURF. TOUGHNESS: 100. FINISH: 32 RMS. SURF. TOUGHNESS: 100. FINISH: 32 RMS. SURF. TOUGHNESS: 100.	DR BY	CHK BY	DATE	APPROVED

ROCKETDYNE
A DIVISION OF NORTH AMERICAN AVIATION, INC.
CANOGA PARK, CALIFORNIA 91309

DATE CODE DATE NO

J 02602

SCALE

1

SHEET 1 OF 2

CONFIDENTIAL

12

11

10

MANIFOLD MAX. DIA.

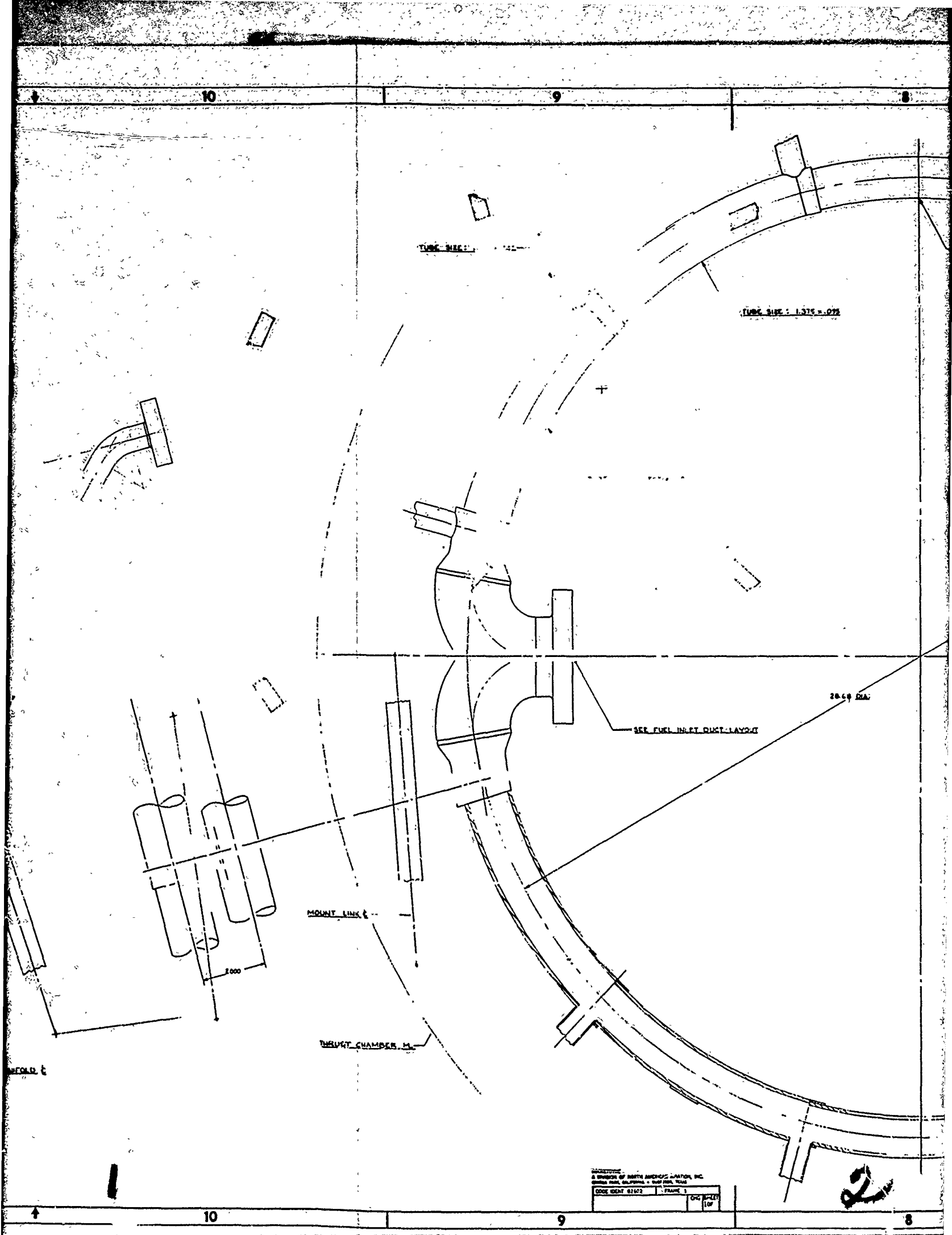
BOUNT LINK

MANIFOLD E

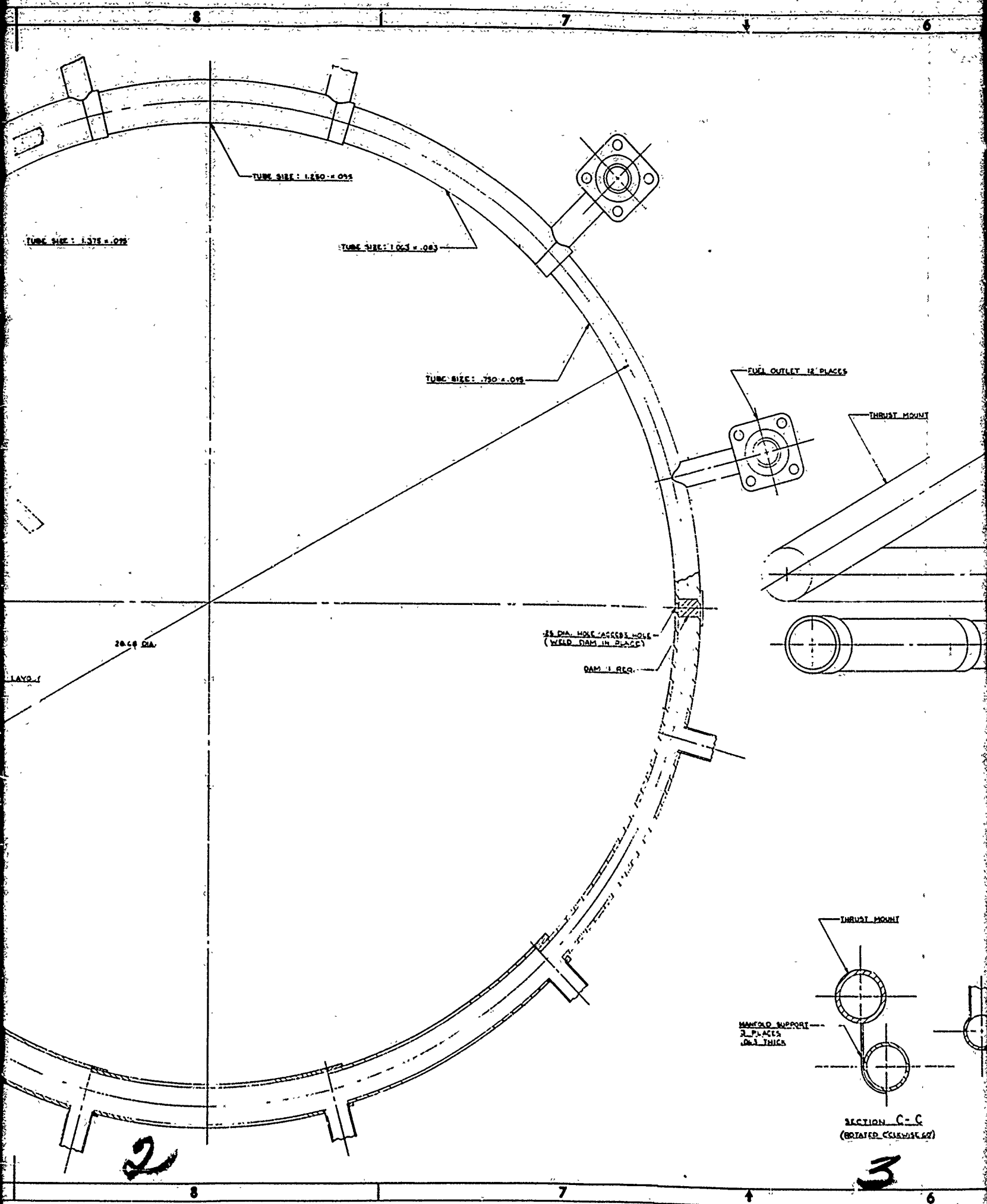
12

11

10



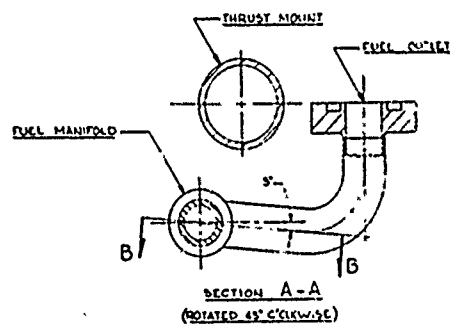
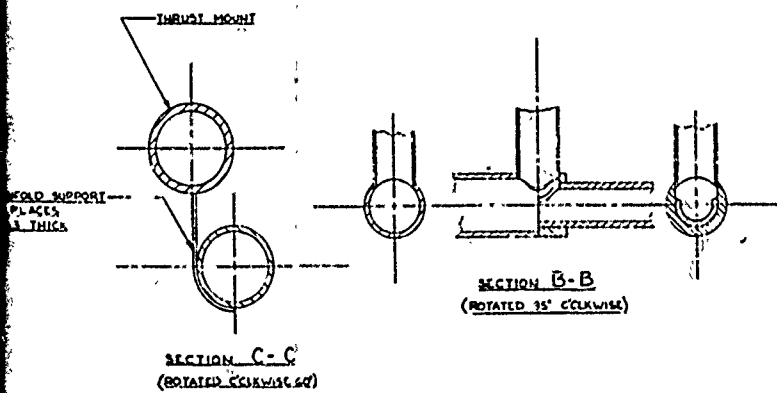
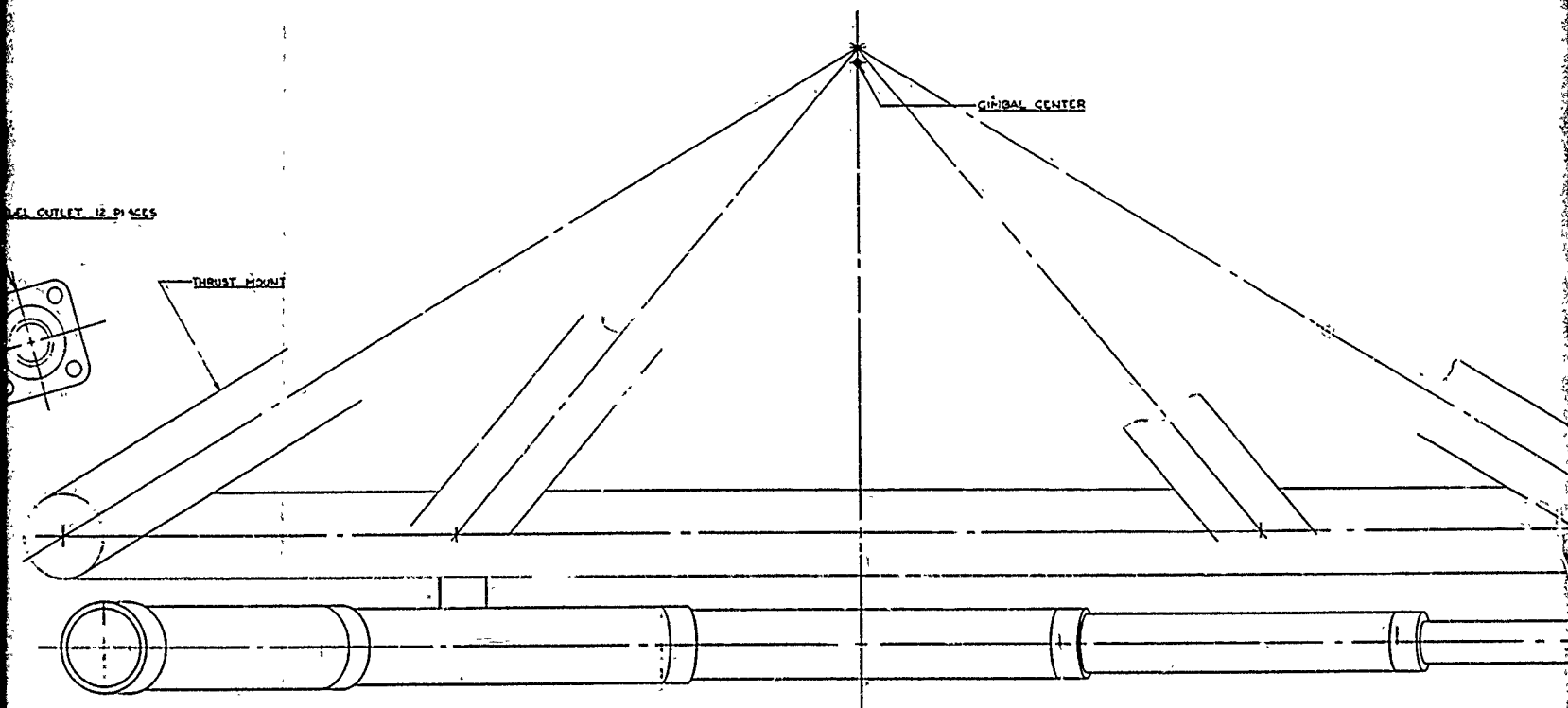
PROTOTYPE
A DIVISION OF NORTH AMERICAN LAMSON, INC.
3000 ROAD, CALIFORNIA - BURBANK, TEXAS
CODE IDENT 01602 - FRAME 1
ONE SHEET
OF



6

5

4



REDUCTION
A DIVISION OF NORTH AMERICAN AVIATION, INC.
CHULA VISTA, CALIFORNIA 92011

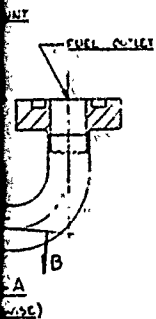
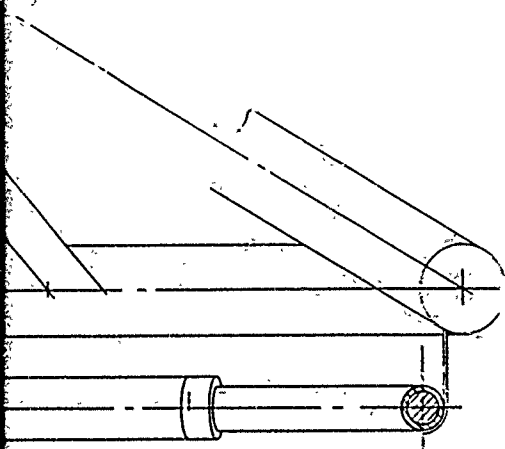
CODE IDENT 02602 FRAME 2

ONE SHEET
10"

6

5

4



4

5

NOTE: UNLESS OTHERWISE SPECIFIED

CONFIDENTIAL

12

11

↓

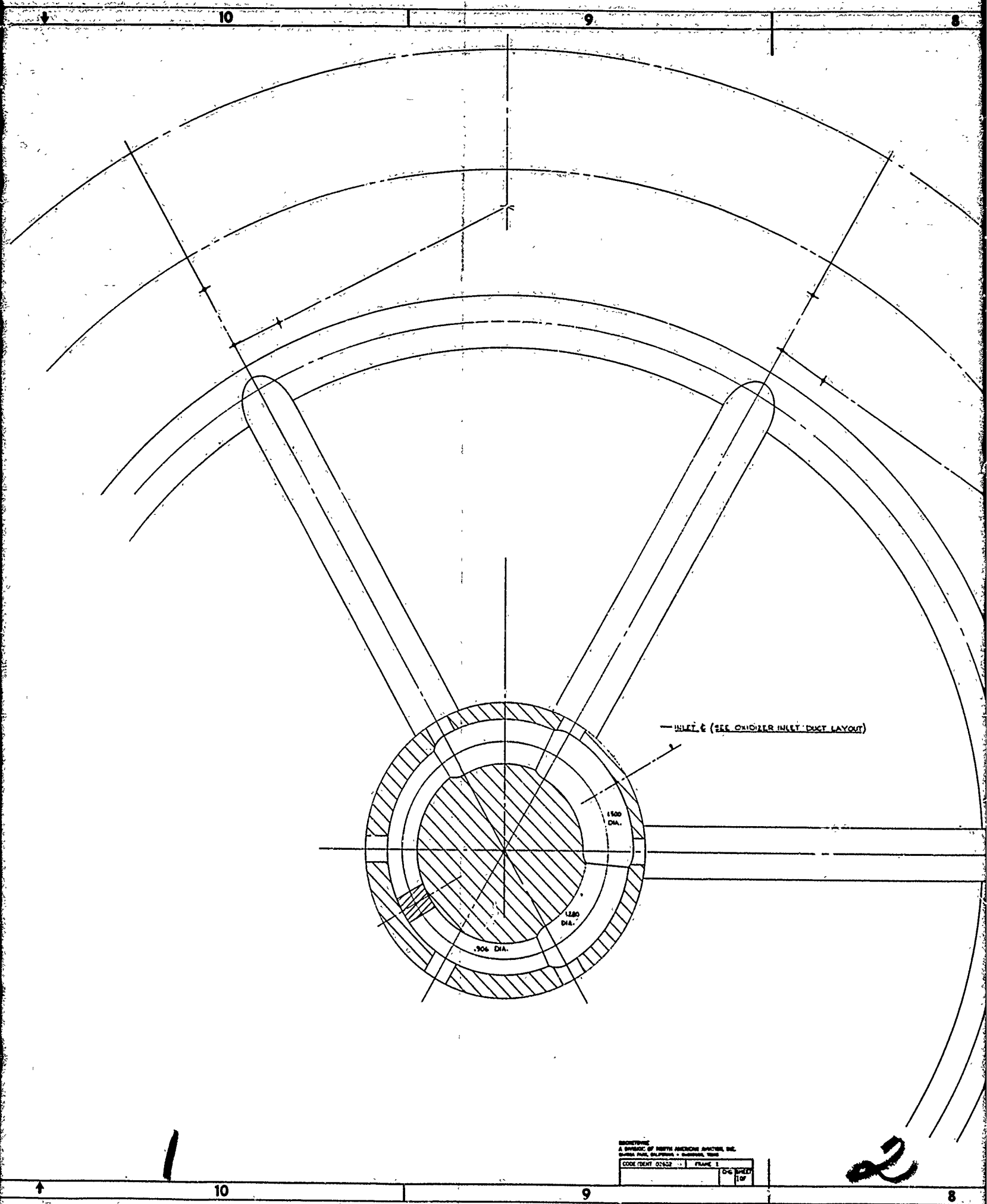
→

12

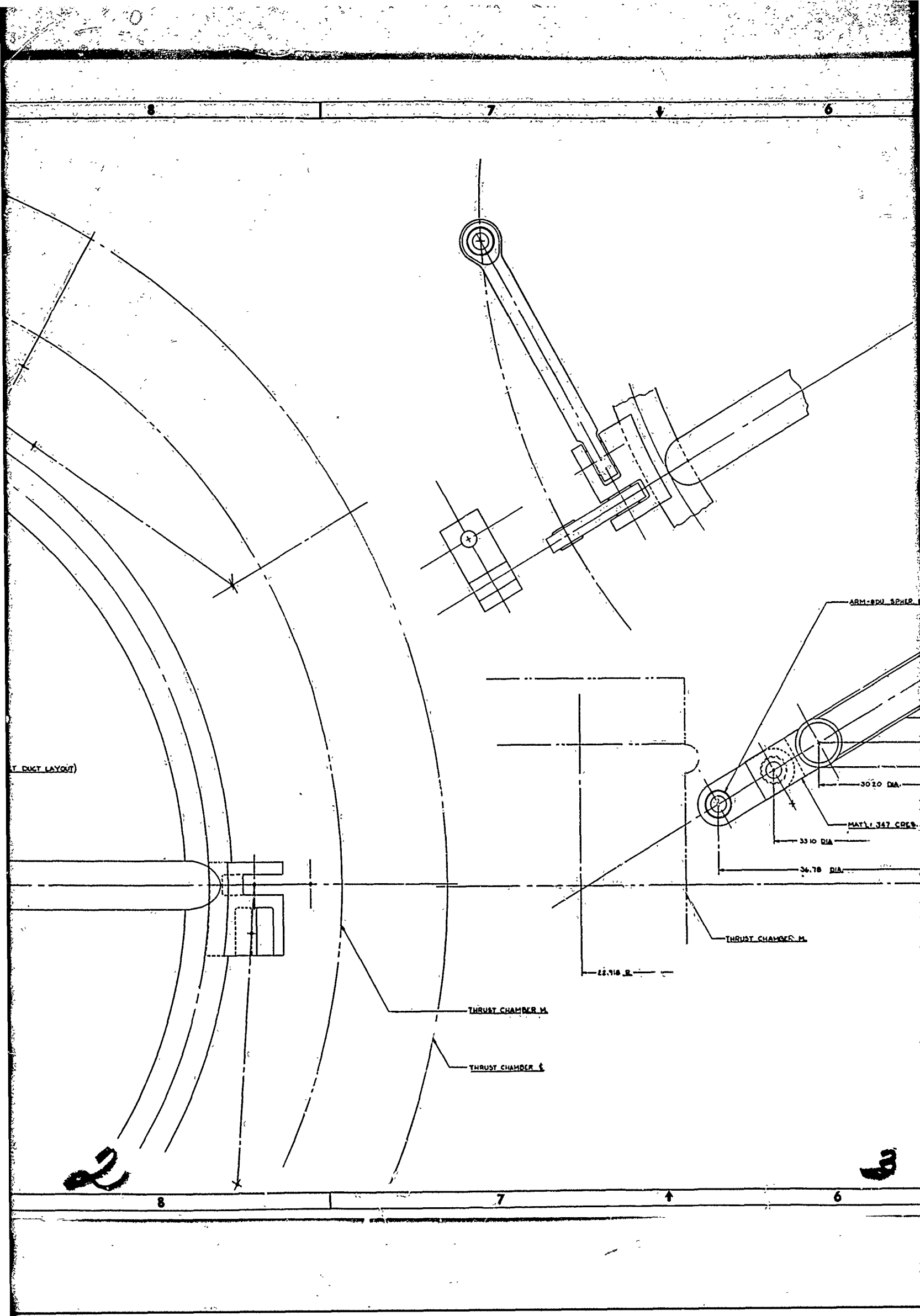
11

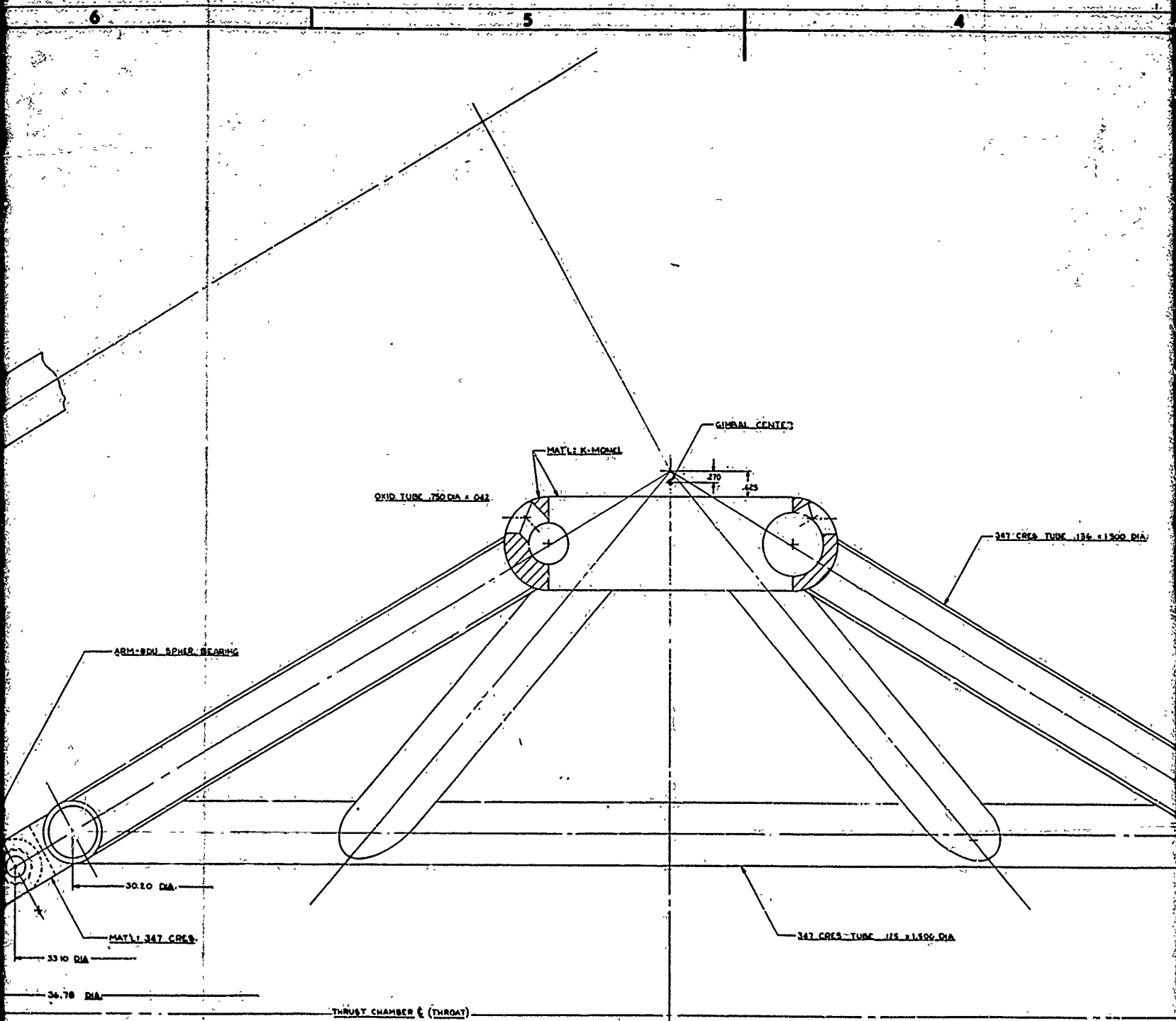
↑

1



ENGINEERING
A DIVISION OF NORTH AMERICAN AVIATION, INC.
DALLAS, TEXAS
CODE 02452 PLANE 1
D-6 SPEED
110





WAGNER H.

ROCKETDOME
A DIVISION OF NORTH AMERICAN AVIATION, INC.
GARDEN CITY, CALIFORNIA - 91506, U.S.A.
CODE IDENT 02602 FRAME 3

ONE SHEET
OF

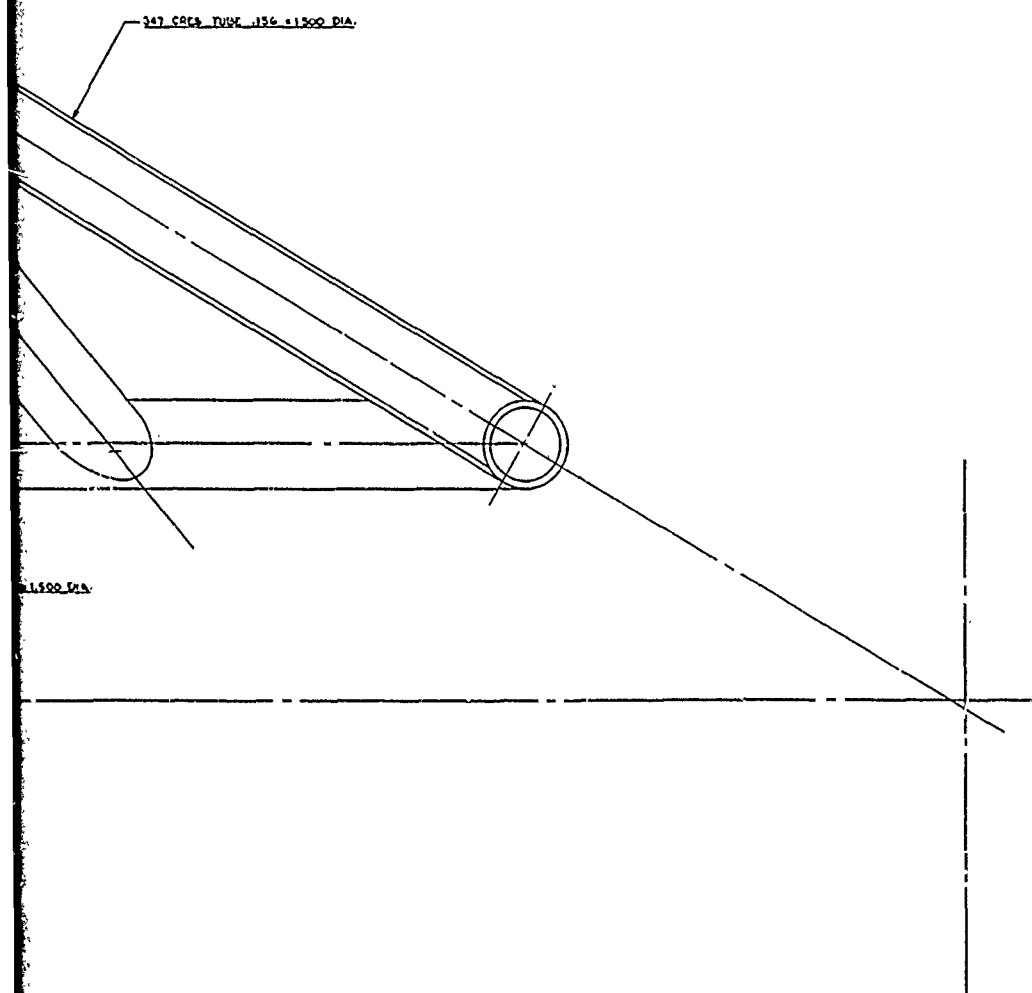


Figure 29.

71

HEAT TREAT	UNLESS OTHERWISE SPECIFIED, ALL DIMENSIONS ARE TO BE HAD TO THE TOLERANCES SHOWN.
FINISH	OVER THE ENTIRE SURFACE UNLESS OTHERWISE SPECIFIED.
NOTE	1. ALL DIMENSIONS ARE TO BE HAD TO THE TOLERANCES SHOWN.

NOTE: UNLESS OTHERWISE SPECIFIED

1		REVISIONS		DATE		APPROVED	
DATE	BY	DESCRIPTION	DATE	BY	DATE	BY	DATE
		1. MAY BE REWORKED					
		2. CANNOT BE REWORKED					
		3. RECORD CHANGE					
		4. NOW SHOP PRACTICE					
		5. PARTS MADE OK					

Figure 29. Interim Thrust Mount and Oxidizer Distribution Manifold

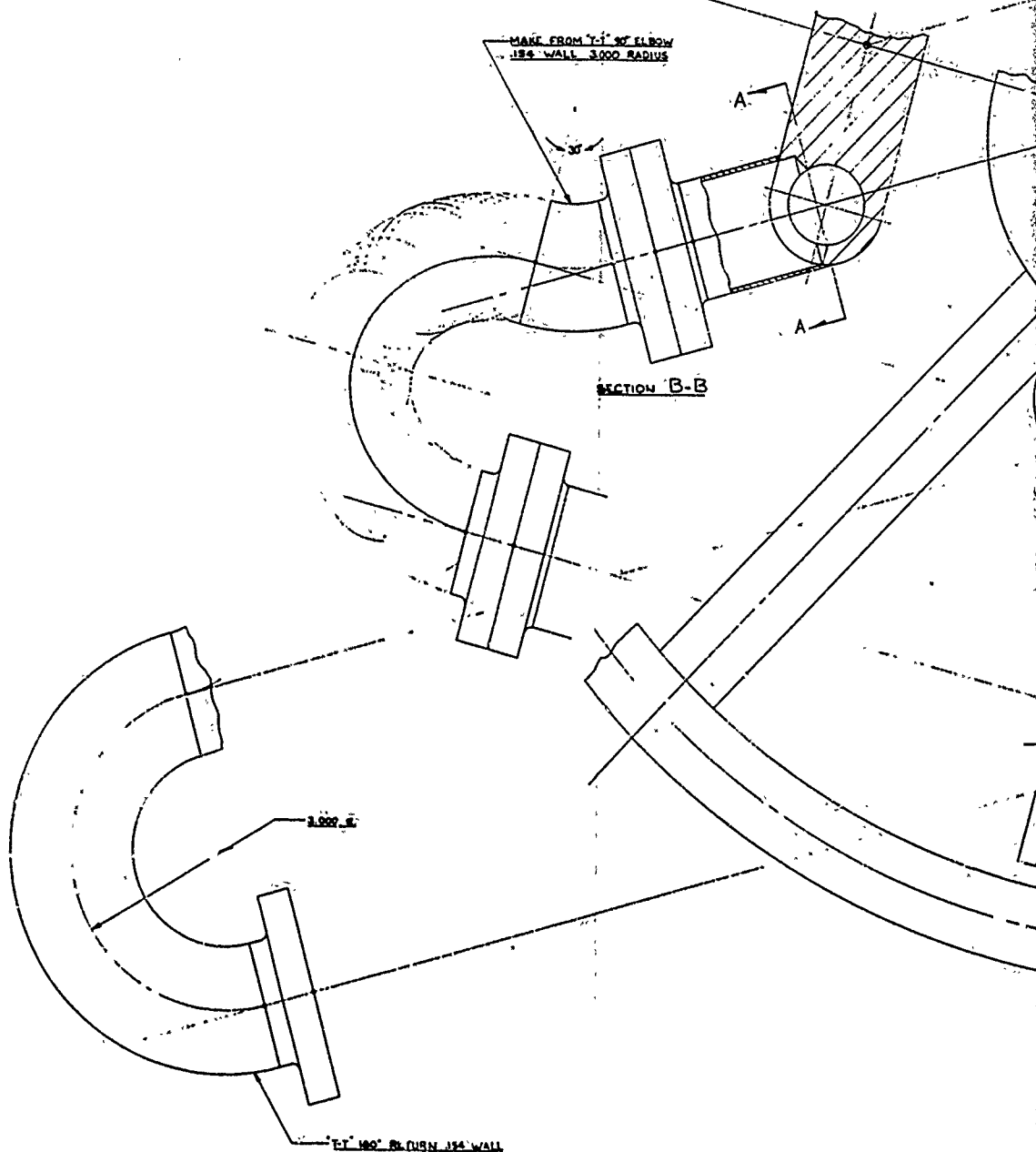
71

CONFIDENTIAL

HEAD TREAT	UNLESS OTHERWISE SPECIFIED: DIMENSIONS ARE IN INCHES AND APPLY PEG TO FINISH BY BACK SURF. ROUGHNESS	DR BY	11	DEL	11	ROCKETDYNE A DIVISION OF NORTH AMERICAN AVIATION, INC. CANOGA PARK, CALIFORNIA • WHEATSGO, TEXAS
FINISH	TOLERANCES ON ANGLES & 9" R DIMENSIONS 2X & 20" 20X & 20" HOLD NOTED "DEAL"	CHK BY		DEL	11	THRUST MOUNT & OXIDIZER DISTRIBUTION MANIFOLD, INTERIM
MAT'L	OVER THRU TOLERANCE .005 .005 + .005 - .005 .010 .010 + .010 - .010 .020 .020 + .020 - .020 .030 .030 + .030 - .030 .040 .040 + .040 - .040 .050 .050 + .050 - .050 .060 .060 + .060 - .060 .070 .070 + .070 - .070 .080 .080 + .080 - .080 .090 .090 + .090 - .090 .100 .100 + .100 - .100 .120 .120 + .120 - .120 .150 .150 + .150 - .150 .200 .200 + .200 - .200 .250 .250 + .250 - .250 .300 .300 + .300 - .300 .350 .350 + .350 - .350 .400 .400 + .400 - .400 .450 .450 + .450 - .450 .500 .500 + .500 - .500 .550 .550 + .550 - .550 .600 .600 + .600 - .600 .650 .650 + .650 - .650 .700 .700 + .700 - .700 .750 .750 + .750 - .750 .800 .800 + .800 - .800 .850 .850 + .850 - .850 .900 .900 + .900 - .900 .950 .950 + .950 - .950 1.000 1.000 + 1.000 - 1.000 1.200 1.200 + 1.200 - 1.200 1.500 1.500 + 1.500 - 1.500 2.000 2.000 + 2.000 - 2.000 2.500 2.500 + 2.500 - 2.500 3.000 3.000 + 3.000 - 3.000 3.500 3.500 + 3.500 - 3.500 4.000 4.000 + 4.000 - 4.000 4.500 4.500 + 4.500 - 4.500 5.000 5.000 + 5.000 - 5.000 5.500 5.500 + 5.500 - 5.500 6.000 6.000 + 6.000 - 6.000 6.500 6.500 + 6.500 - 6.500 7.000 7.000 + 7.000 - 7.000 7.500 7.500 + 7.500 - 7.500 8.000 8.000 + 8.000 - 8.000 8.500 8.500 + 8.500 - 8.500 9.000 9.000 + 9.000 - 9.000 9.500 9.500 + 9.500 - 9.500 10.000 10.000 + 10.000 - 10.000 12.000 12.000 + 12.000 - 12.000 15.000 15.000 + 15.000 - 15.000 20.000 20.000 + 20.000 - 20.000 25.000 25.000 + 25.000 - 25.000 30.000 30.000 + 30.000 - 30.000 35.000 35.000 + 35.000 - 35.000 40.000 40.000 + 40.000 - 40.000 45.000 45.000 + 45.000 - 45.000 50.000 50.000 + 50.000 - 50.000 55.000 55.000 + 55.000 - 55.000 60.000 60.000 + 60.000 - 60.000 65.000 65.000 + 65.000 - 65.000 70.000 70.000 + 70.000 - 70.000 75.000 75.000 + 75.000 - 75.000 80.000 80.000 + 80.000 - 80.000 85.000 85.000 + 85.000 - 85.000 90.000 90.000 + 90.000 - 90.000 95.000 95.000 + 95.000 - 95.000 100.000 100.000 + 100.000 - 100.000 120.000 120.000 + 120.000 - 120.000 150.000 150.000 + 150.000 - 150.000 200.000 200.000 + 200.000 - 200.000 250.000 250.000 + 250.000 - 250.000 300.000 300.000 + 300.000 - 300.000 350.000 350.000 + 350.000 - 350.000 400.000 400.000 + 400.000 - 400.000 450.000 450.000 + 450.000 - 450.000 500.000 500.000 + 500.000 - 500.000 550.000 550.000 + 550.000 - 550.000 600.000 600.000 + 600.000 - 600.000 650.000 650.000 + 650.000 - 650.000 700.000 700.000 + 700.000 - 700.000 750.000 750.000 + 750.000 - 750.000 800.000 800.000 + 800.000 - 800.000 850.000 850.000 + 850.000 - 850.000 900.000 900.000 + 900.000 - 900.000 950.000 950.000 + 950.000 - 950.000 1000.000 1000.000 + 1000.000 - 1000.000 1200.000 1200.000 + 1200.000 - 1200.000 1500.000 1500.000 + 1500.000 - 1500.000 2000.000 2000.000 + 2000.000 - 2000.000 2500.000 2500.000 + 2500.000 - 2500.000 3000.000 3000.000 + 3000.000 - 3000.000 3500.000 3500.000 + 3500.000 - 3500.000 4000.000 4000.000 + 4000.000 - 4000.000 4500.000 4500.000 + 4500.000 - 4500.000 5000.000 5000.000 + 5000.000 - 5000.000 5500.000 5500.000 + 5500.000 - 5500.000 6000.000 6000.000 + 6000.000 - 6000.000 6500.000 6500.000 + 6500.000 - 6500.000 7000.000 7000.000 + 7000.000 - 7000.000 7500.000 7500.000 + 7500.000 - 7500.000 8000.000 8000.000 + 8000.000 - 8000.000 8500.000 8500.000 + 8500.000 - 8500.000 9000.000 9000.000 + 9000.000 - 9000.000 9500.000 9500.000 + 9500.000 - 9500.000 10000.000 10000.000 + 10000.000 - 10000.000 12000.000 12000.000 + 12000.000 - 12000.000 15000.000 15000.000 + 15000.000 - 15000.000 20000.000 20000.000 + 20000.000 - 20000.000 25000.000 25000.000 + 25000.000 - 25000.000 30000.000 30000.000 + 30000.000 - 30000.000 35000.000 35000.000 + 35000.000 - 35000.000 40000.000 40000.000 + 40000.000 - 40000.000 45000.000 45000.000 + 45000.000 - 45000.000 50000.000 50000.000 + 50000.000 - 50000.000 55000.000 55000.000 + 55000.000 - 55000.000 60000.000 60000.000 + 60000.000 - 60000.000 65000.000 65000.000 + 65000.000 - 65000.000 70000.000 70000.000 + 70000.000 - 70000.000 75000.000 75000.000 + 75000.000 - 75000.000 80000.000 80000.000 + 80000.000 - 80000.000 85000.000 85000.000 + 85000.000 - 85000.000 90000.000 90000.000 + 90000.000 - 90000.000 95000.000 95000.000 + 95000.000 - 95000.000 100000.000 100000.000 + 100000.000 - 100000.000 120000.000 120000.000 + 120000.000 - 120000.000 150000.000 150000.000 + 150000.000 - 150000.000 200000.000 200000.000 + 200000.000 - 200000.000 250000.000 250000.000 + 250000.000 - 250000.000 300000.000 300000.000 + 300000.000 - 300000.000 350000.000 350000.000 + 350000.000 - 350000.000 400000.000 400000.000 + 400000.000 - 400000.000 450000.000 450000.000 + 450000.000 - 450000.000 500000.000 500000.000 + 500000.000 - 500000.000 550000.000 550000.000 + 550000.000 - 550000.000 600000.000 600000.000 + 600000.000 - 600000.000 650000.000 650000.000 + 650000.000 - 650000.000 700000.000 700000.000 + 700000.000 - 700000.000 750000.000 750000.000 + 750000.000 - 750000.000 800000.000 800000.000 + 800000.000 - 800000.000 850000.000 850000.000 + 850000.000 - 850000.000 900000.000 900000.000 + 900000.000 - 900000.000 950000.000 950000.000 + 950000.000 - 950000.000 1000000.000 1000000.000 + 1000000.000 - 1000000.000 1200000.000 1200000.000 + 1200000.000 - 1200000.000 1500000.000 1500000.000 + 1500000.000 - 1500000.000 2000000.000 2000000.000 + 2000000.000 - 2000000.000 2500000.000 2500000.000 + 2500000.000 - 2500000.000 3000000.000 3000000.000 + 3000000.000 - 3000000.000 3500000.000 3500000.000 + 3500000.000 - 3500000.000 4000000.000 4000000.000 + 4000000.000 - 4000000.000 4500000.000 4500000.000 + 4500000.000 - 4500000.000 5000000.000 5000000.000 + 5000000.000 - 5000000.000 5500000.000 5500000.000 + 5500000.000 - 5500000.000 6000000.000 6000000.000 + 6000000.000 - 6000000.000 6500000.000 6500000.000 + 6500000.000 - 6500000.000 7000000.000 7000000.000 + 7000000.000 - 7000000.000 7500000.000 7500000.000 + 7500000.000 - 7500000.000 8000000.000 8000000.000 + 8000000.000 - 8000000.000 8500000.000 8500000.000 + 8500000.000 - 8500000.000 9000000.000 9000000.000 + 9000000.000 - 9000000.000 9500000.000 9500000.000 + 9500000.000 - 9500000.000 10000000.000 10000000.000 + 10000000.000 - 10000000.000 12000000.000 12000000.000 + 12000000.000 - 12000000.000 15000000.000 15000000.000 + 15000000.000 - 15000000.000 20000000.000 20000000.000 + 20000000.000 - 20000000.000 25000000.000 25000000.000 + 25000000.000 - 25000000.000 30000000.000 30000000.000 + 30000000.000 - 30000000.000 35000000.000 35000000.000 + 35000000.000 - 35000000.000 40000000.000 40000000.000 + 40000000.000 - 40000000.000 45000000.000 45000000.000 + 45000000.000 - 45000000.000 50000000.000 50000000.000 + 50000000.000 - 50000000.000 55000000.000 55000000.000 + 55000000.000 - 55000000.000 60000000.000 60000000.000 + 60000000.000 - 60000000.000 65000000.000 65000000.000 + 65000000.000 - 65000000.000 70000000.000 70000000.000 + 70000000.000 - 70000000.000 75000000.000 75000000.000 + 75000000.000 - 75000000.000 80000000.000 80000000.000 + 80000000.000 - 80000000.000 85000000.000 85000000.000 + 85000000.000 - 85000000.000 90000000.000 90000000.000 + 90000000.000 - 90000000.000 95000000.000 95000000.000 + 95000000.000 - 95000000.000 100000000.000 100000000.000 + 100000000.000 - 100000000.000 120000000.000 120000000.000 + 120000000.000 - 120000000.000 150000000.000 150000000.000 + 150000000.000 - 150000000.000 200000000.000 200000000.000 + 200000000.000 - 200000000.000 250000000.000 250000000.000 + 250000000.000 - 250000000.000 300000000.000 300000000.000 + 300000000.000 - 300000000.000 350000000.000 350000000.000 + 350000000.000 - 350000000.000 400000000.000 400000000.000 + 400000000.000 - 400000000.000 450000000.000 450000000.000 + 450000000.000 - 450000000.000 500000000.000 500000000.000 + 500000000.000 - 500000000.000 550000000.000 550000000.000 + 550000000.000 - 550000000.000 600000000.000 600000000.000 + 600000000.000 - 600000000.000 650000000.000 650000000.000 + 650000000.000 - 650000000.000 700000000.000 700000000.000 + 700000000.000 - 700000000.000 750000000.000 750000000.000 + 750000000.000 - 750000000.000 800000000.000 800000000.000 + 800000000.000 - 800000000.000 850000000.000 850000000.000 + 850000000.000 - 850000000.000 900000000.000 900000000.000 + 900000000.000 - 900000000.000 950000000.000 950000000.000 + 950000000.000 - 950000000.000 1000000000.000 1000000000.000 + 1000000000.000 - 1000000000.000 1200000000.000 1200000000.000 + 1200000000.000 - 1200000000.000 1500000000.000 1500000000.000 + 1500000000.000 - 1500000000.000 2000000000.000 2000000000.000 + 2000000000.000 - 2000000000.000 2500000000.000 2500000000.000 + 2500000000.000 - 2500000000.000 3000000000.000 3000000000.000 + 3000000000.000 - 3000000000.000 3500000000.000 3500000000.000 + 3500000000.000 - 3500000000.000 4000000000.000 4000000000.000 + 4000000000.000 - 4000000000.000 4500000000.000 4500000000.000 + 4500000000.000 - 4500000000.000 5000000000.000 5000000000.000 + 5000000000.000 - 5000000000.000 5500000000.000 5500000000.000 + 5500000000.000 - 5500000000.000 6000000000.000 6000000000.000 + 6000000000.000 - 6000000000.000 6500000000.000 6500000000.000 + 6500000000.000 - 6500000000.000 7000000000.000 7000000000.000 + 7000000000.000 - 7000000000.000 7500000000.000 7500000000.000 + 7500000000.000 - 7500000000.000 8000000000.000 8000000000.000 + 8000000000.000 - 8000000000.000 8500000000.000 8500000000.000 + 8500000000.000 - 8500000000.000 9000000000.000 9000000000.000 + 9000000000.000 - 9000000000.000 9500000000.000 9500000000.000 + 9500000000.000 - 9500000000.000 10000000000.000 10000000000.000 + 10000000000.000 - 10000000000.000 12000000000.000 12000000000.000 + 12000000000.000 - 12000000000.000 15000000000.000 15000000000.000 + 15000000000.000 - 15000000000.000 20000000000.000 20000000000.000 + 20000000000.000 - 20000000000.000 25000000000.000 25000000000.000 + 25000000000.000 - 25000000000.000 30000000000.000 30000000000.000 + 30000000000.000 - 30000000000.000 35000000000.000 35000000000.000 + 35000000000.000 - 35000000000.000 40000000000.000 40000000000.000 + 40000000000.000 - 40000000000.000 45000000000.000 45000000000.000 + 45000000000.000 - 45000000000.000 50000000000.000 50000000000.000 + 50000000000.000 - 50000000000.000 55000000000.000 55000000000.000 + 55000000000.000 - 55000000000.000 60000000000.000 60000000000.000 + 60000000000.000 - 60000000000.000 65000000000.000 65000000000.000 + 65000000000.000 - 65000000000.000 70000000000.000 70000000000.000 + 70000000000.000 - 70000000000.000 75000000000.000 75000000000.000 + 75000000000.000 - 75000000000.000 80000000000.000 80000000000.000 + 80000000000.000 - 80000000000.000 85000000000.000 85000000000.000 + 85000000000.000 - 85000000000.000 90000000000.000 90000000000.000 + 90000000000.000 - 90000000000.000 95000000000.000 95000000000.000 + 95000000000.000 - 95000000000.000 100000000000.000 100000000000.000 + 100000000000.000 - 100000000000.000 120000000000.000 120000000000.000 + 120000000000.000 - 120000000000.000 150000000000.000 150000000000.000 + 150000000000.000 - 150000000000.000 200000000000.000 200000000000.000 + 200000000000.000 - 200000000000.000 250000000000.000 250000000000.000 + 250000000000.000 - 250000000000.000 300000000000.000 300000000000					

14 13 12 11 10

CONFIDENTIAL



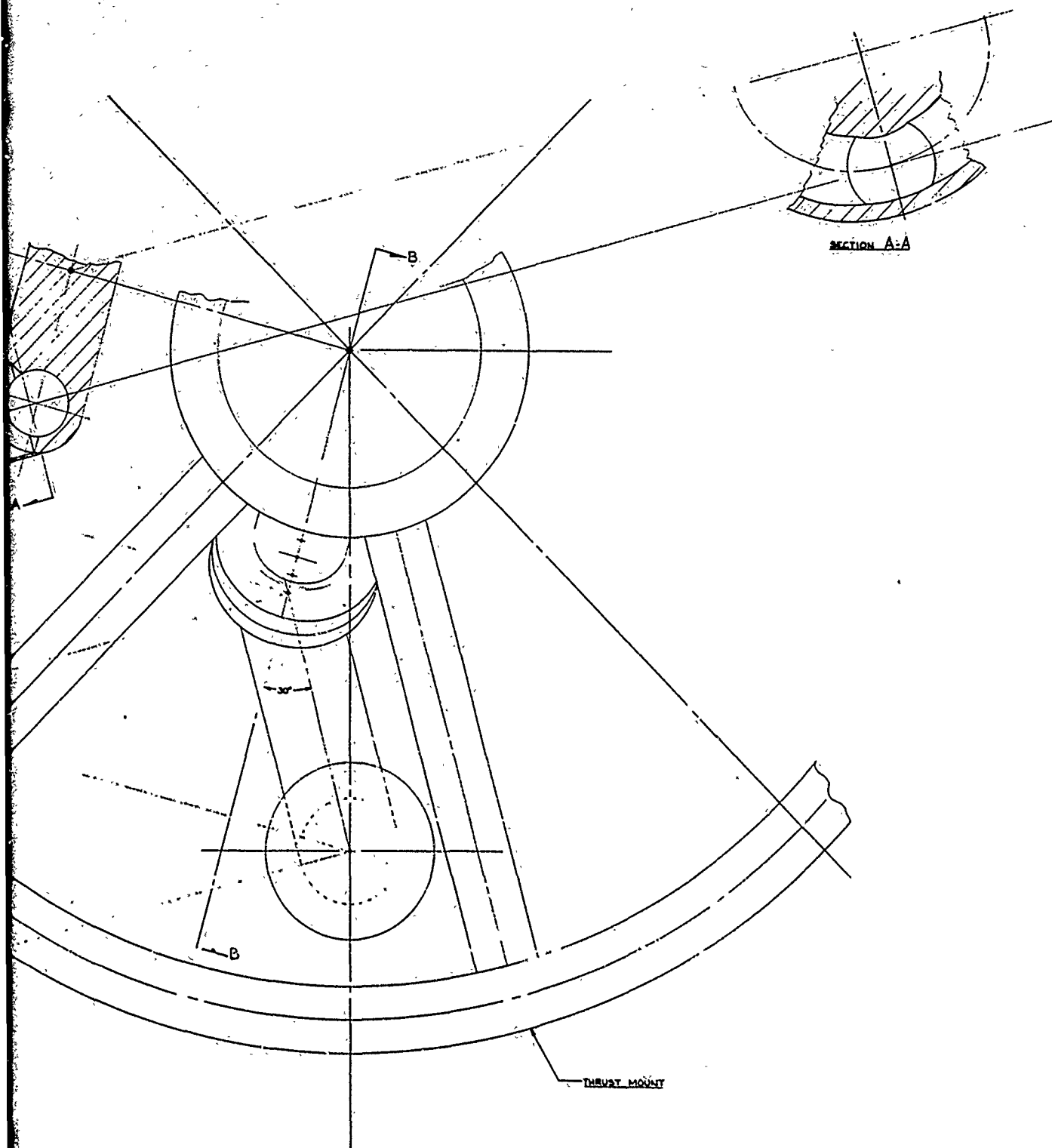
14

13

12

11

10



1

ENGINEERING
A DIVISION OF NORTH AMERICAN AVIATION, INC.
CHICAGO, ILL. 60646 • 1960 FEB. 10

DRWG NO. 62403	FRAME 2
CHG. (MKT)	

2

6	5	4	3	2
---	---	---	---	---

1. INC. 10
2. 10.000

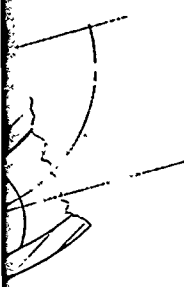


Figure 30. AMPS Main Eng
Duct and Mani

72

GO

NEAT TOLER	UNLESS OTHERWISE SPECIFIED DIMENSIONS ARE IN INCHES AND APPLY PRIOR TO FINISH 100' BACK SAMP. ROUGHNESS	DR BY	
FINISH	TOLERANCES ON ANGLES 90° ± 30° HOLDING POWER "HOLD"	CHK BY	
INT'L	OVER TOLU 2.000 ± .010 1.500 ± .008 1.000 ± .006 0.500 ± .004 0.250 ± .002 0.125 ± .001 0.062 ± .0005 0.031 ± .0002 0.015 ± .0001 0.007 ± .00005 0.003 ± .00002 0.001 ± .00001	DATE	REV
	DO NOT SCALE PRINT	FRAME	3

NOTE: UNLESS OTHERWISE SPECIFIED

6	5	4	3	2
---	---	---	---	---

CONFIDENTIAL

(U) Stress analysis of the main engine thrust structure resulted in separating the oxidizer feeder lines and the fuel distribution manifold from the engine thrust structure. Since the unitized configuration of the thrust structure housing and propellant manifolds (first quarterly report) is attractive from packaging aspects, it will be re-evaluated after engine vibratory loads are defined.

(U) Figure 30 shows the attachment of the oxidizer duct to the distribution manifold. Effort in the next report period will include initiation of engine packaging methods and additional interconnect definition.

2. THRUST CHAMBER ANALYSIS AND DESIGN

(U) In the previous report period, the geometric configuration of the main thrust chamber was defined, and a preliminary analysis was made to define the expected heat transfer and fluid dynamics. In this report period, analyses were conducted on this configuration utilizing the data that were generated during the 5-inch thrust chamber segment testing of Task II. Additionally, effort was initiated to evaluate candidate backup structures for the main engine thrust chamber.

(U) The secondary thrust chamber analysis and design effort will be started during the next quarterly report period.

a. SEGMENT THRUST CHAMBER ASSEMBLY

(U) A segmented, supersonic-baffle, main thrust chamber concept was adopted during the first quarter after a re-evaluation of the major development tasks, hardware utilization, and combustion stability characteristics.

(C) The segmented approach will permit the early evaluation of the basic building blocks of the full thrust chamber assembly which will

⁷³
CONFIDENTIAL

CONFIDENTIAL

be assembled from 12 30-degree segments and a nonsegmented detachable aerospike nozzle. Each segment will have an individual, manifolded propellant supply and independent support structure that is fastened at the flanged interface of the supersonic baffles. A segment is removable by removing the propellant lines, the bolts at the structural tie between segments, and the bolts from that portion of the aerospike nozzle in line with the segment.

(1) Structural Design Considerations

(C) The basic design considerations for the structural support of these segments are to restrain the throat deflection within acceptable limits, to effectively use materials to minimize the weight, and to use known manufacturing techniques to facilitate their fabrication. A stress analysis tradeoff study was made which considered weight, number of segments, and throat deflection. The results indicated that a 12-segment design was optimum and the throat deflection for this design would be less than 2.0 percent of the throat gap. Various designs for aerospike thrust chamber support structures, such as "C" clamp, hoop tension, subsonic baffles, and supersonic baffles have previously been investigated. Studies of the backup structure for the aerospike thrust chamber under contract AF04(611)-11617 indicated that a either rib- or honeycomb-type structure would provide adequate rigidity to the assembly to control throat gap. Also, it was indicated that fabrication and weight of the two assembly types were comparable. However, analysis indicated that loads predicted for the backup structure are greater than those in which honeycomb designs are generally used.

(C) The use of supersonic baffles as structural ties between the inner-to-outer body can effectively control throat area changes. The supersonic baffle design basically consists of an inner and outer ring joined together with equally spaced radial ties. The combustion chamber pressure acts between the two rings, applying radial outward loading on the outer

CONFIDENTIAL

ring, and radial inward loading on the inner ring. The pressure loads between the supersonic radial baffle ties are restrained by the ring segments acting as fixed-end beams. The loads transfer through the ring and react as a tension load across the baffle ties. The use of 12 such baffles results in a good basic structural ring design. In addition to controlling throat deflection, the design is lightweight, and is conducive to several conventional manufacturing techniques.

(U) Several types of beam structures are being considered for use with the supersonic baffle design such as I-beams, open face "egg crate," and box beams. The optimum choice will be determined by a detailed consideration of manufacturing methods, cost, and weight.

(2) Thrust Chamber Configuration Tradeoff Analysis

(U) The following items are being evaluated as concepts to be utilized within the overall thrust chamber assembly design.

1. An injector assembly that is an integral component, and contains only a minimum of braze or weld joints; in particular, no braze or weld joints between adjacent dissimilar propellant passages. Additional considerations being evaluated for the injector include use of hydrogen regenerative coolant that is transferred from the outer body to the inner body through the injector. This fuel can be used as supplementary coolant for the injector in addition to the injector propellant coolant. It performs two basic functions; (1) cooling the injector face, and (2) removing heat that would be transferred in the oxidizer. Also under consideration is an injector face which would be made flat to reduce manufacturing costs and obtain minimum face heat transfer areas.

The above considerations would only be included if a need became apparent and they are proved successful in the 5-inch segment testing in Task II.

CONFIDENTIAL

2. A nozzle-to-thrust chamber joint and seal design that would incorporate an integral feed system across the joint and, (1) regeneratively cool the seal region, (2) provide a smooth contour on the hot-gas surface to prevent recirculation and stagnation heat transfer, and (3) be adaptable to easy segment refurbishment or replacement
3. A regeneratively cooled baffle design with cooling passages formed by electrical discharge machining and an electroformed face sheet: the feed manifolds would be integral, provide ease of sealing, versatility of feed circuits, and optimum use of baffle coolant.

b. THRUST CHAMBER COOLING

(U) A heat transfer analysis was conducted for the main engine thrust chamber using empirical data obtained from the solid-wall thrust chamber segment test of Task II.

(U) Factors that influence these data have led to the conclusion that the results of this initial heat transfer analysis are conservative. The data were obtained from tests in which the U/N 1 fan injector was used. Subsequent developments have led to increasing the propellant injection velocities and thereby reducing the total integrated heat load to the thrust chamber coolant. Also, upon comparison of the water-cooled, solid-wall segment tests of the previous contract (AF04(611)-11617) to the subsequent tube-wall tests of that same contract, it was found that the integrated heat load at the low chamber pressures in the tube-wall configuration were lower than predicted from the solid-wall segment tests. A direct comparison with the AMPS and the previous contract data in this regard is not possible because unheated hydrogen had been used on the previous program for the solid-wall segment tests.

CONFIDENTIAL

(C) The results presented in following discussions relate to thrust chamber pressures from 650 to 370 psia. The analysis for pressures down to 70 psia chamber pressure is not presented since the analysis was not completed. This analysis and additional analyses with the current injector designs are to continue in the next report period.

(1) Configuration

(C) The analysis was conducted on the G_c chamber contour with the inner and outer body each constructed of 927 nickel tubes of 0.016-inch wall thickness and having a minimum unformed tube outside diameter of 0.072 inch. Three flow configurations were considered (Fig. 31), all of which use 15 percent of the total engine fuel flow to pass through the baffles. In the parallel-series (P-S) and series-parallel (S-P) configurations, 85 percent of the flow has a parallel pass through the outer tube body (P-S) and inner tube body (S-P), respectively. The combined flow (100 percent) passes through all of the remaining tube circuits. In the all-parallel (ALL-P) configuration, 85 percent of the total fuel flow passes through both outer and inner bodies before recombining with the 15-percent baffle flow.

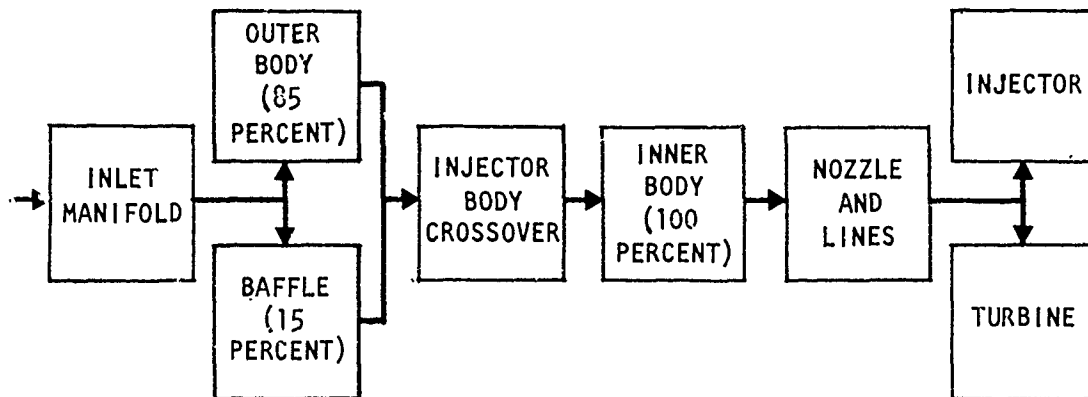
(U) The effect of contouring the back side of the tubes where maximum tube-wall temperatures occurred was also investigated. The length of the contoured portions of the tubes was 0.6 inch or less. The objective in contouring the tube was to reduce the tube inside cross-sectional area and improve cooling by increasing the coolant mass velocity.

(2) Heat Transfer Data

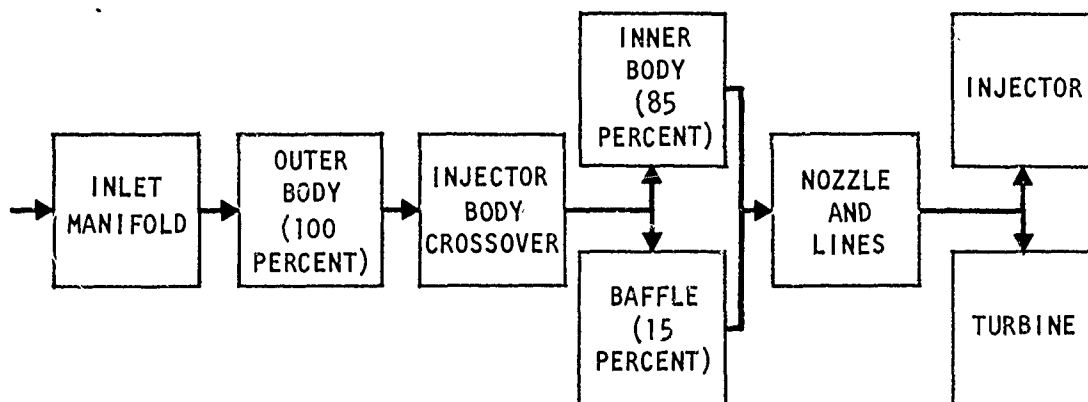
(C) The numerical values used for coolant flowrate in the analysis are presented in Fig. 32 as a linear function of chamber pressure. The specific values for 370 psia and 650 psia chamber pressure are shown in Table 8. These values represent either 100 percent of the flow or 85 percent of the flow corresponding to the particular flow path being considered.

CONFIDENTIAL

1. PARALLEL - SERIES CIRCUIT (P-S)



2. SERIES - PARALLEL CIRCUIT (S-P)



3. ALL - PARALLEL CIRCUIT (ALL P)

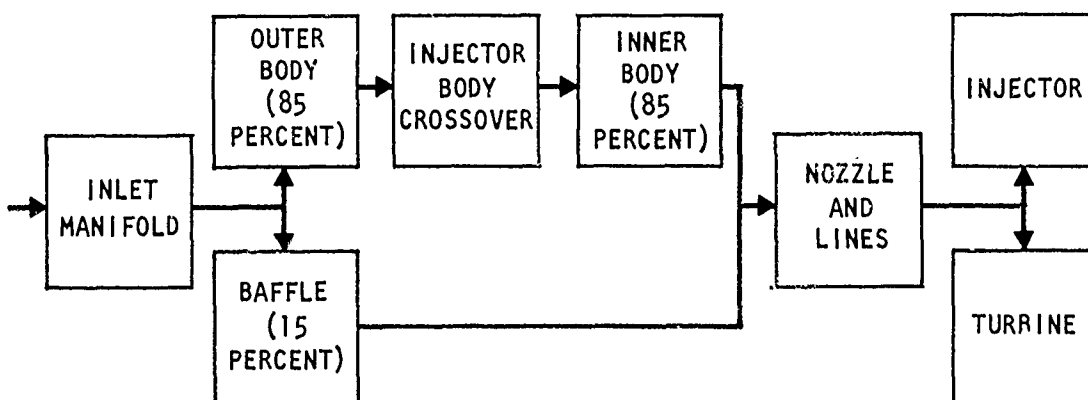


Figure 31. Candidate Cooling Paths for Main Engine Thrust Chamber

CONFIDENTIAL

CONFIDENTIAL

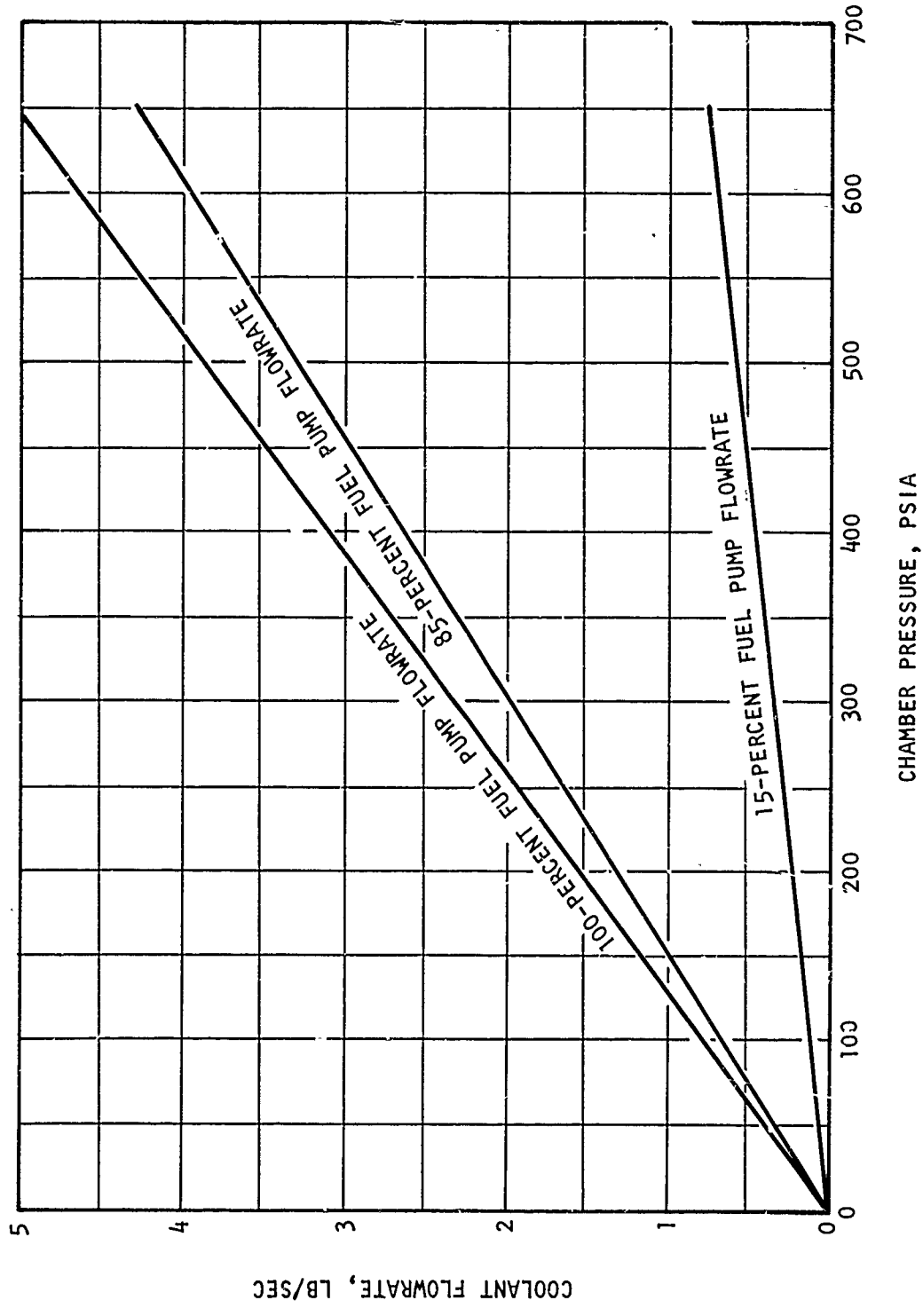


Figure 32. Main Thrust Chamber Coolant Flowrate vs Chamber Pressure

CONFIDENTIAL

CONFIDENTIAL

TABLE 8
COOLANT FLOW-RATES FOR CANDIDATE
MAIN THRUST CHAMBER COOLANT CIRCUITS

Chamber Pressure, psia	Configuration	Outer-Body Flowrate		Inner-Body Flowrate		Baffle Flowrate	
		lb/sec	Percent of Engine Flowrate	lb/sec	Percent of Engine Flowrate	lb/sec	Percent of Engine Flowrate
650	Parallel-Series	5.10	100	4.335	85	0.765	15
	Series-Parallel	4.335	85	5.10	100	0.765	15
	All-Parallel	4.335	85	4.335	85	0.765	15
370	Parallel-Series	2.903	100	2.467	85	0.436	15
	Series-Parallel	2.467	85	2.903	100	0.436	15
	All-Parallel	2.467	85	2.467	85	0.436	15

CONFIDENTIAL

(C) The surface heat transfer coefficient on the combustion side of the tubes was obtained by analyses of the data from the water-cooled, solid-wall, G_c contour chamber segment test firings. The tests evaluated to date were conducted at chamber pressures of 644 psia and 374 psia. The observed heat fluxes and gas-side conditions were reduced to curves relating axial distance from the throat to Stanton Number (St) and Prandtl Number (Pr). These are shown in Fig. 33. The product, $St \times Pr^{2/3}$, is relatively constant with changing chamber gas-side conditions because it reduces in most cases to $St \times Pr^{2/3} = \frac{f}{2}$ where f = friction factor.

(U) The curve of $St \times Pr^{2/3}$ vs axial position was used in the analysis to estimate surface heat transfer coefficients (h_g) on the combustion gas side of the inner and outer tube bodies using the relation $h_g \propto (St \times Pr^{2/3})$.

where:

$$St = \frac{h_g}{\rho V C_p}$$

$$Pr = \frac{C_p \mu}{k}$$

k = thermal conductivity

C_p = specific heat

ρ = density

V = velocity

μ = viscosity

(U) The gas-side film coefficients (h_g) used in the analysis are shown in Fig. 34. Interpolation between the test data points was accomplished to complete the curves. The tests were conducted at chamber pressures of 644 psia and 374 psia; however, the data were analyzed at pressures of 650 psia and 370 psia, respectively.

CONFIDENTIAL

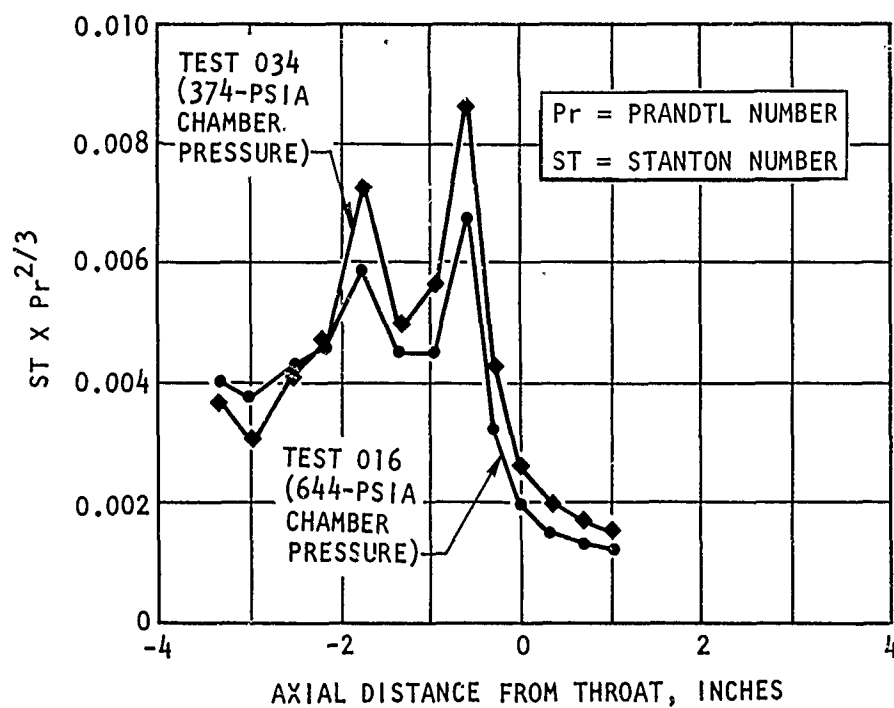


Figure 33. Relationship of Wall Position to Stanton and Prandtl Numbers

CONFIDENTIAL

CONFIDENTIAL

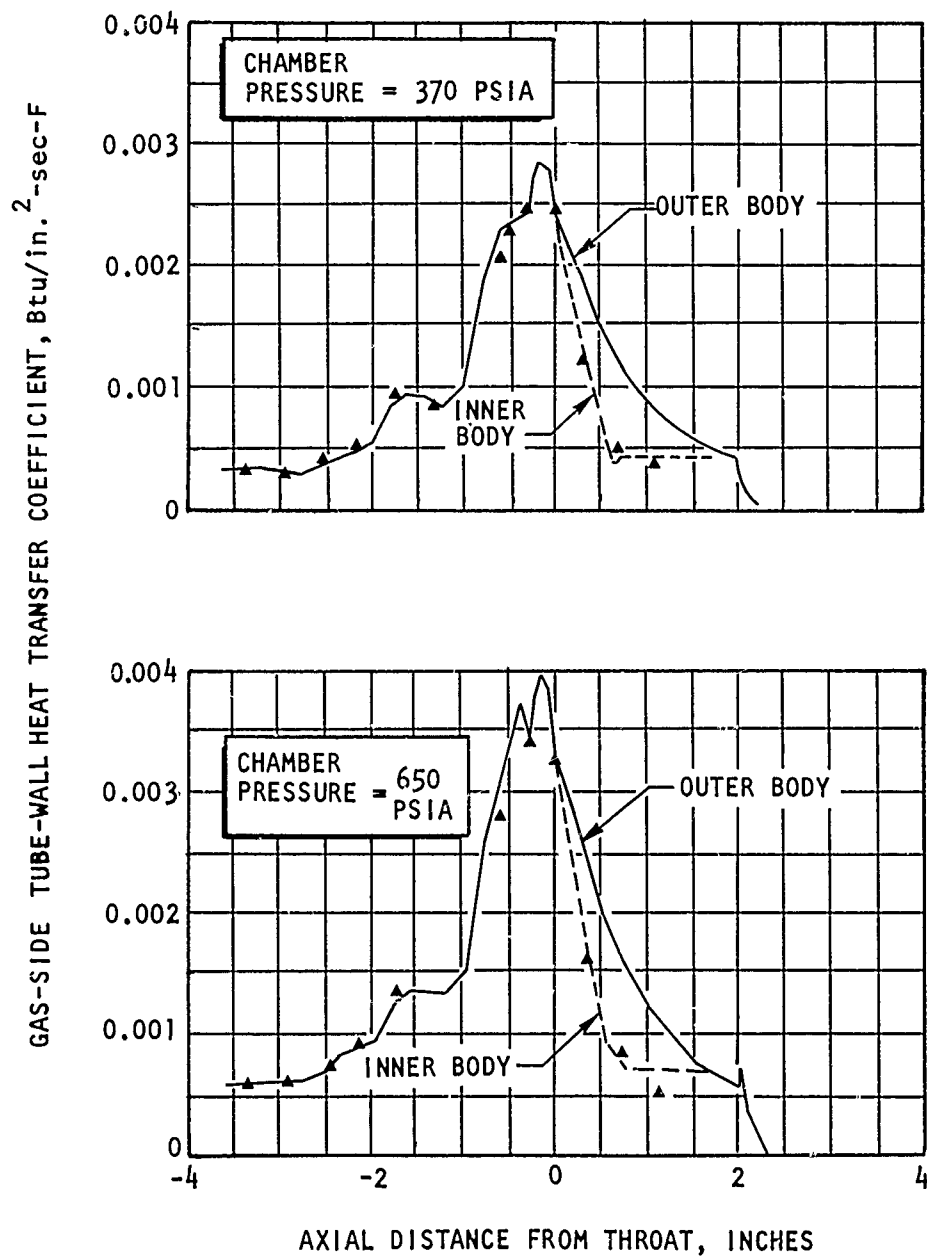


Figure 34. Heat Transfer Coefficient Profile at 370- and 650-psia Chamber Pressure

CONFIDENTIAL

CONFIDENTIAL

(3) Results of Analysis

(C) The tube gas-side wall temperature profiles of the outer and inner tube bodies for 650 psia chamber pressure are shown in Fig. 35 and 36 for the flowrates of the three candidate configurations (Table 8). Figure 35 presents the predicted up-pass and down-pass gas-side tube wall temperature profile for the outer body at 650 psia chamber pressure. The 5.10 lb/sec flow is for the series-parallel flow configuration and the 4.335 lb/sec flow is for the parallel-series and all-parallel flow configurations (Fig. 31).

(C) Figure 36 presents the tube wall temperature profiles for the inner body at 650 psia chamber pressure. The 5.10 lb/sec flow corresponds to the series-parallel configuration and the 4.335 lb/sec flowrate corresponds to the parallel-series and all-parallel configurations. The effect of contouring the tubes, as previously discussed, is shown in Fig. 36. Typical results of the 370 psia chamber pressure analyses are presented in Fig. 37 for the inner body.

(U) There are several characteristics common to all the profiles: (1) A peaking just prior to the throat that is a result of the input combustion side surface heat transfer coefficients peaking at that point, and (2) the improvement in coolant-side surface heat transfer coefficient due to curvature causing the large dip in the profiles for the first 0.35-inch downstream of the throat on the down-passes and the similar effect for 0.35-inch upstream of the throat on the up-passes. A third common characteristic of all the tube-wall temperature profiles are the steep gradients and sharp peaks near the throat. These are the result of a heat flux condition where heat flow is neglected in the axial direction of the tubes, and rapid changes are occurring axially in combustion gas and coolant properties. In the actual case, there is some axial heat transfer and would result in reducing the computed throat heat flux.

CONFIDENTIAL

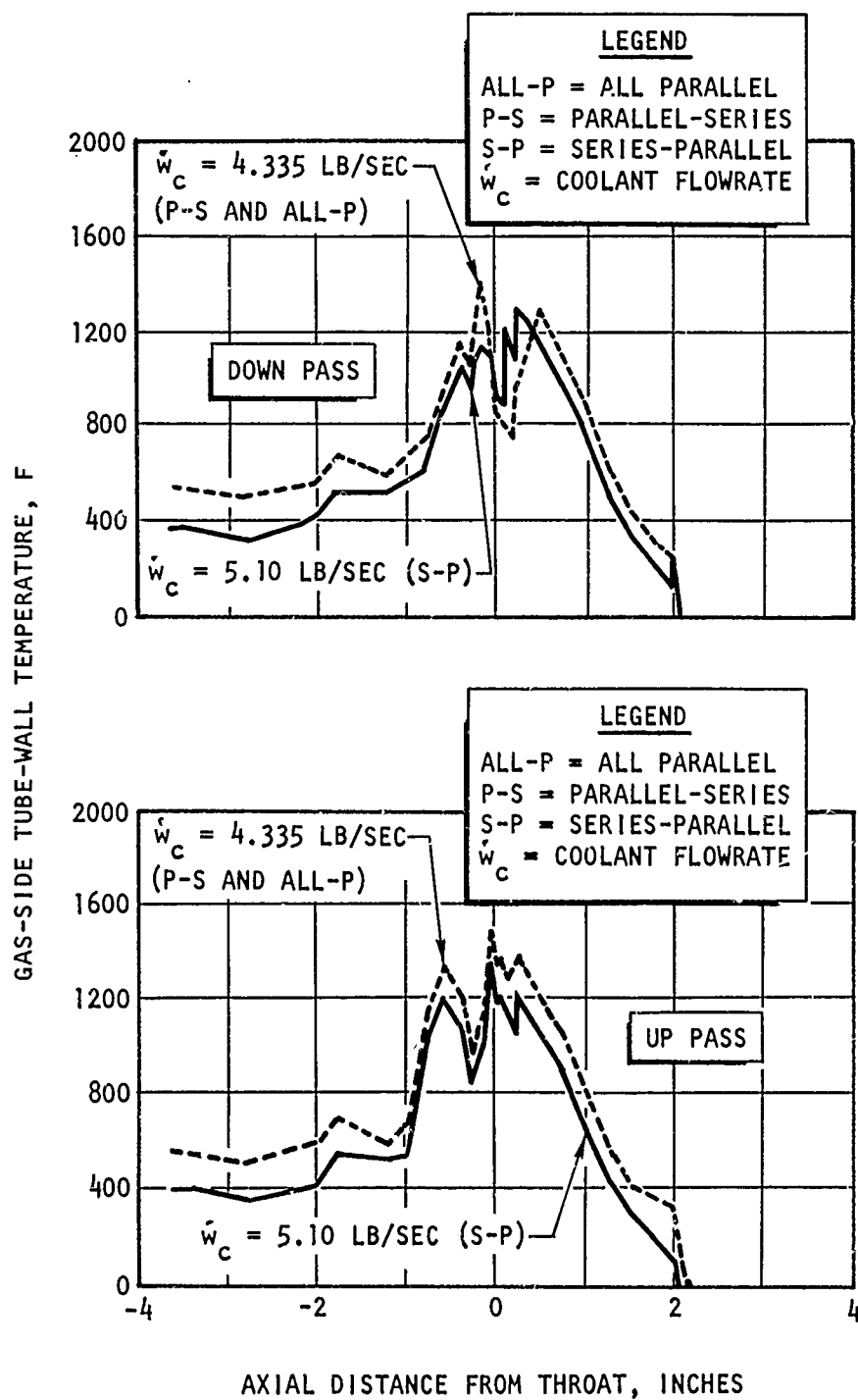


Figure 35. Temperature Profile for Tube Outer Body at 650-psia Chamber Pressure

CONFIDENTIAL

CONFIDENTIAL

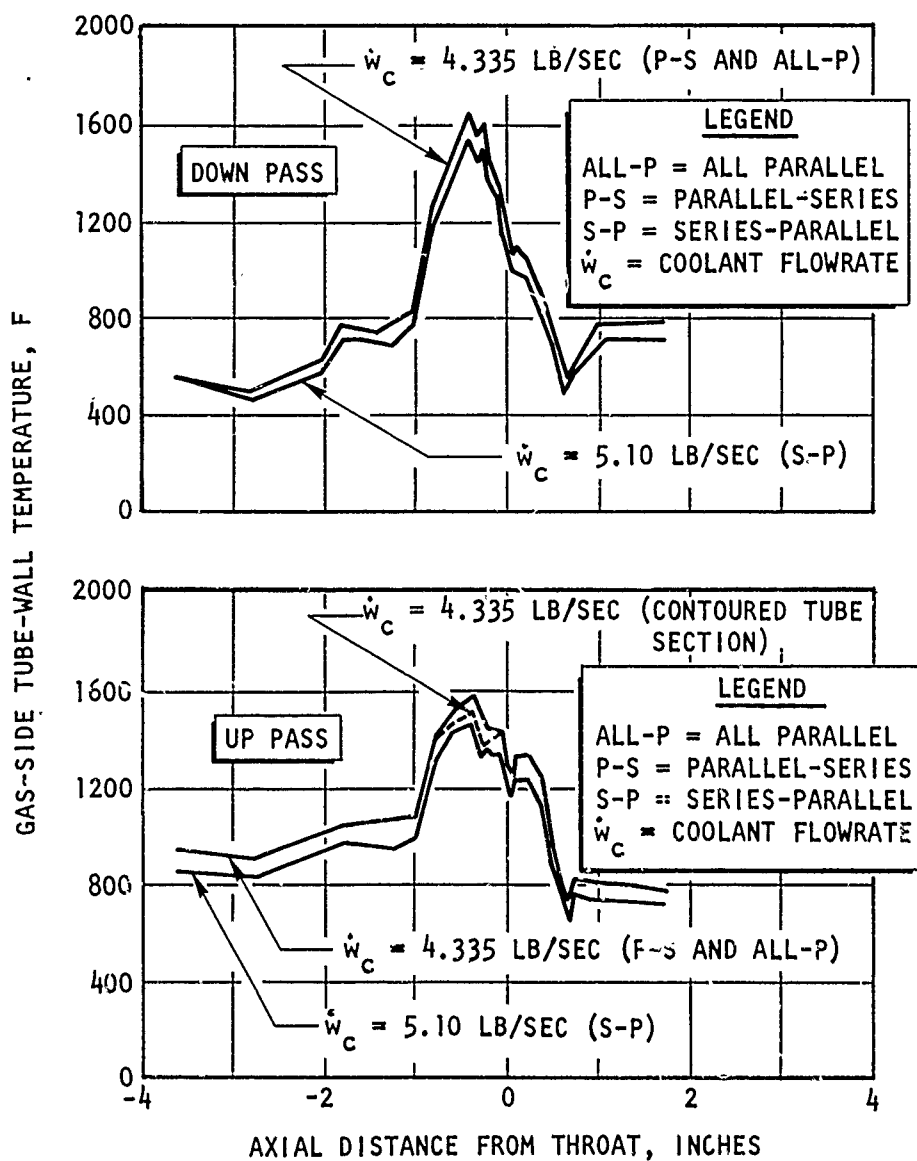


Figure 36. Temperature Profile for Tube Inner Body at 650-psia Chamber Pressure

CONFIDENTIAL

CONFIDENTIAL

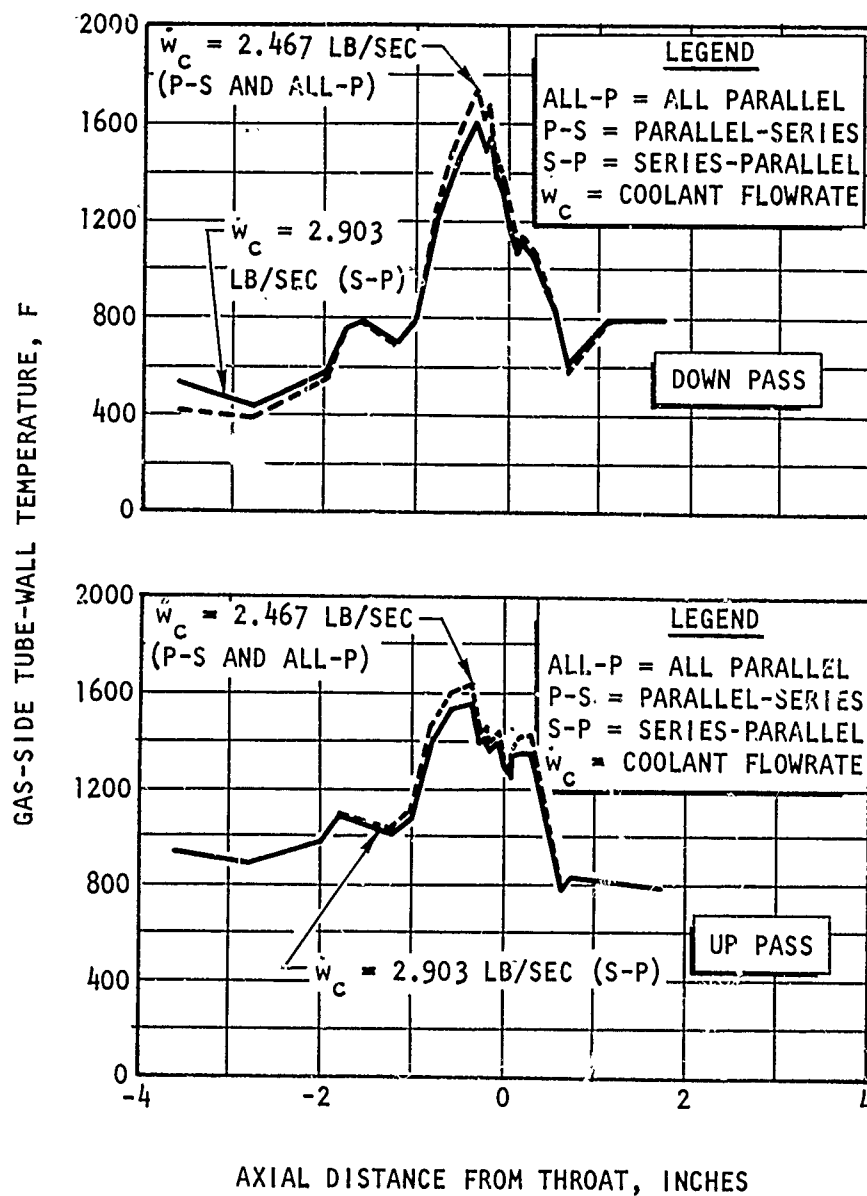


Figure 37. Temperature Profile for Tube Inner Body at 370-psia Chamber Pressure

CONFIDENTIAL

CONFIDENTIAL

(U) The rise to a new peak downstream of the throat in the outer body downpass profiles (Fig. 35) is a result of the coolant-side heat transfer coefficient being sensitive to the rapid increase in tube diameter (decreasing velocity) of this pass.

(C) The gas-side tube wall heat flux profiles for 650 psia and 370 psia chamber pressures (Fig. 38 and 39) are essentially of the same shape as the combustion-side surface heat transfer coefficient profiles shown in Fig. 34. This is because 90 percent of the total heat flow resistance is contained in this coefficient. The effect of the coolant-side heat transfer coefficient is evidenced in the small difference, for a given tube body, between the profiles of a down-pass and an up-pass. Coolant flowrate (over the range of from 85 to 100 percent of engine flowrate) has negligible effect on the heat flux profiles for a given chamber pressure.

(U) For these analyses it was found that there are several possible cooling circuits that result in suitable wall temperatures, heat loads, and pressure profiles. The series-parallel circuit, however, gives generally lower gas-side wall temperatures over the wall profile than the other cooling circuits do. The circuit for the main engine thrust chamber will be selected upon completion of the analysis involving the full range of operation for the engine, and will include data obtained from tests on the tube-wall thrust chamber segments.

(C) The pressure drop available to the injector is shown in Fig. 40 as a function of thrust chamber inlet pressure for the three cooling circuits at chamber pressures of 650 psia and 370 psia.

(U) In the heat transfer analysis, based on the solid-wall segment tests, it was found that the coolant heat load does not vary linearly with chamber pressure (Fig. 41). This was also found to be the case in the previous contract (AF04(611)-11617) in tests on water-cooled, solid-wall thrust chamber segments. However, the relationship was found to be linear when

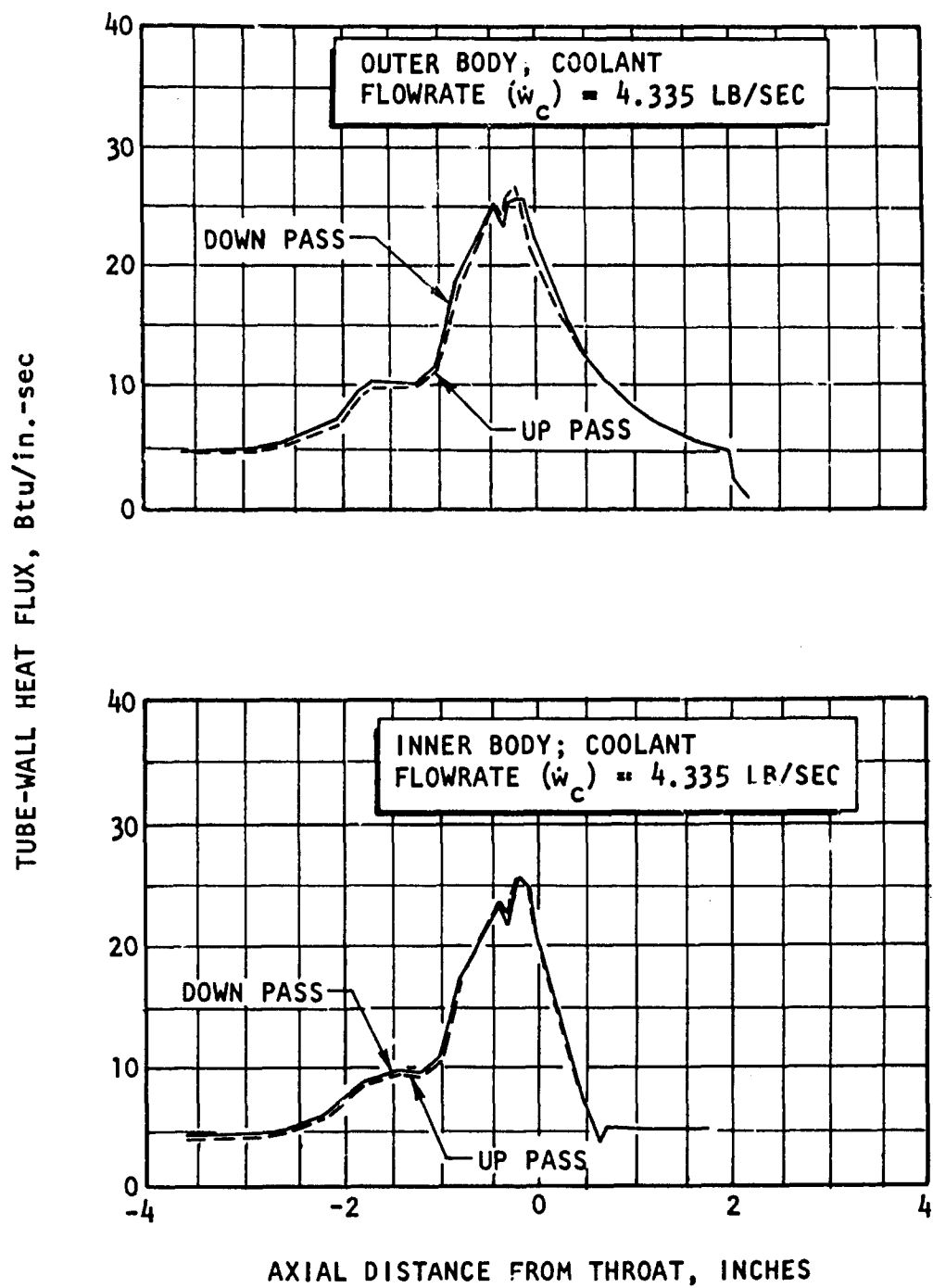


Figure 38. Heat Flux Profile for Tubes at 650-psia Chamber Pressure

CONFIDENTIAL

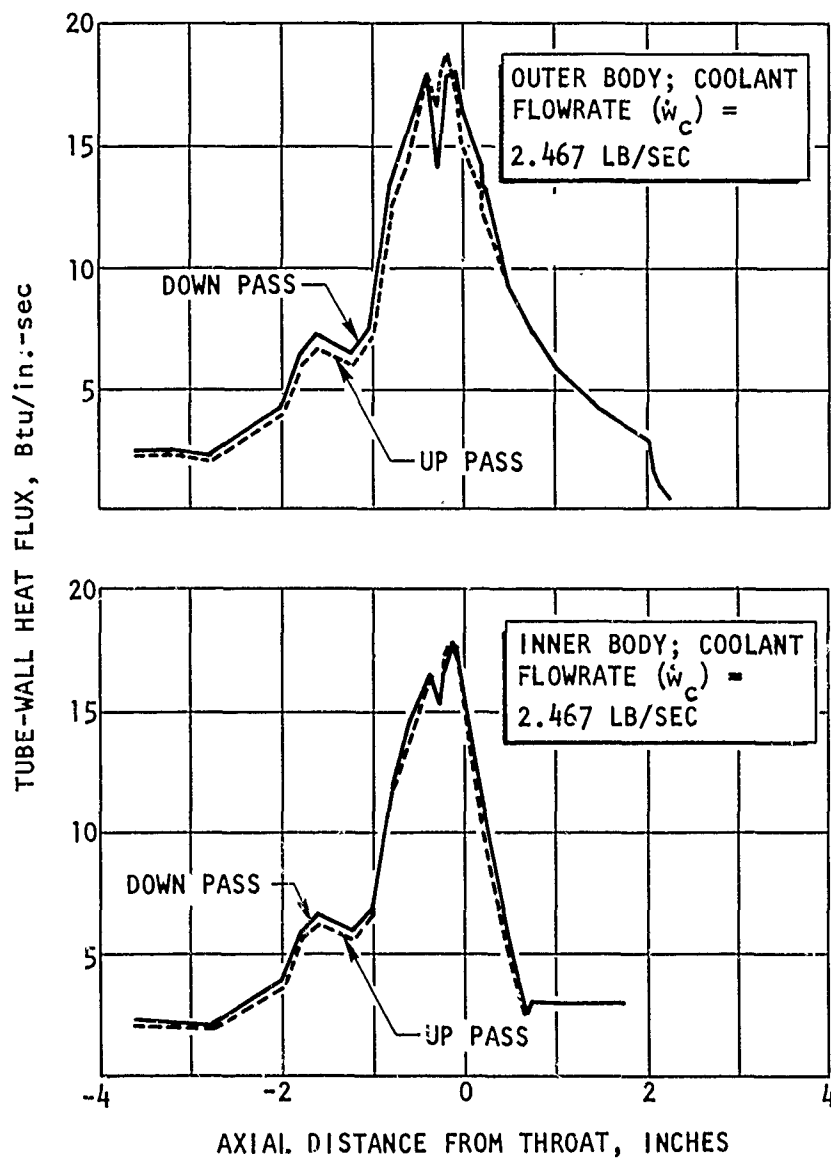


Figure 39. Heat Flux Profile for Tubes at 370-psia Chamber Pressure

CONFIDENTIAL

CONFIDENTIAL

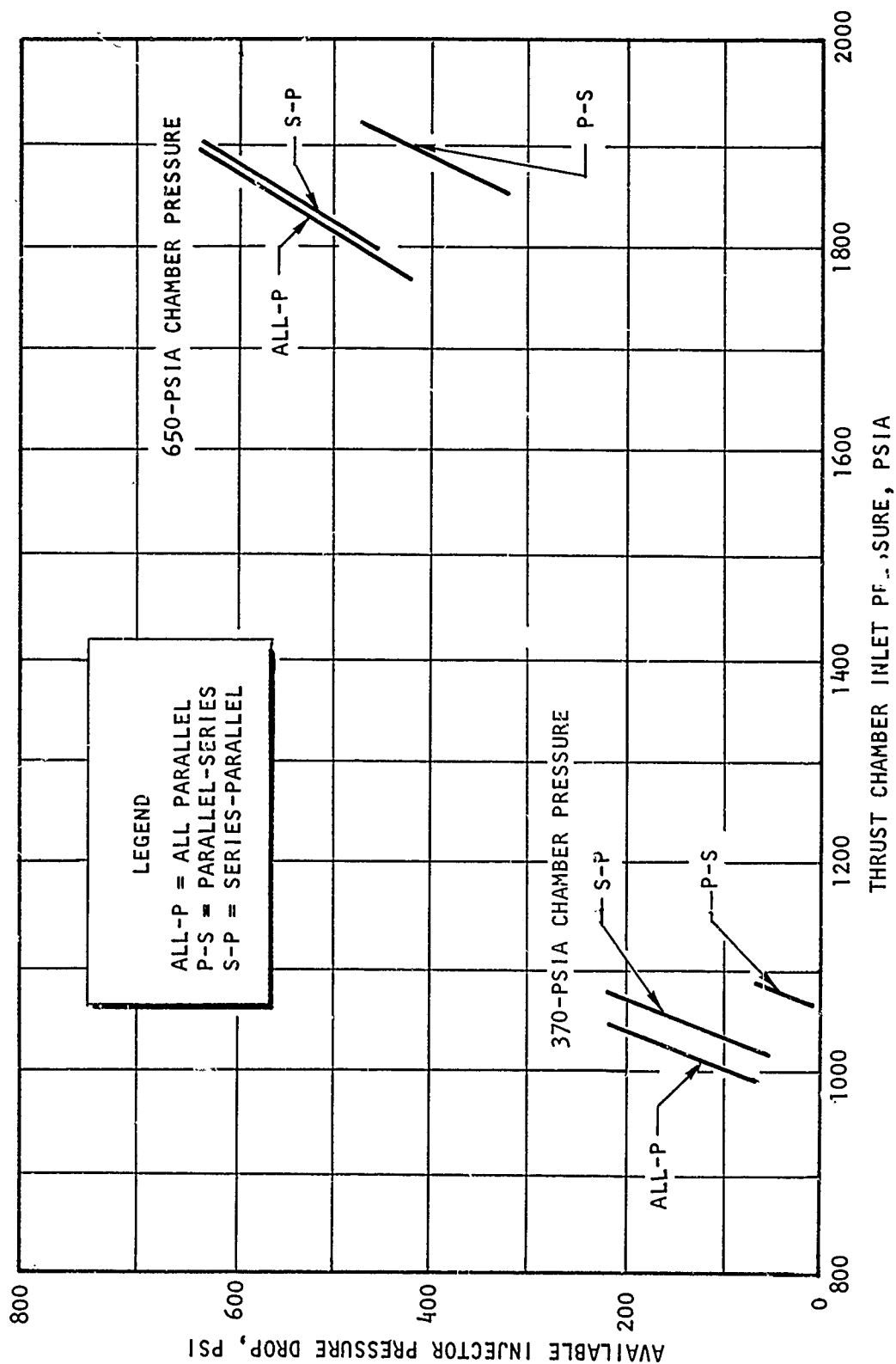


Figure 40. Available Injector Pressure Drop vs Thrust Chamber Inlet Pressure
(All Cooling Circuits)

CONFIDENTIAL

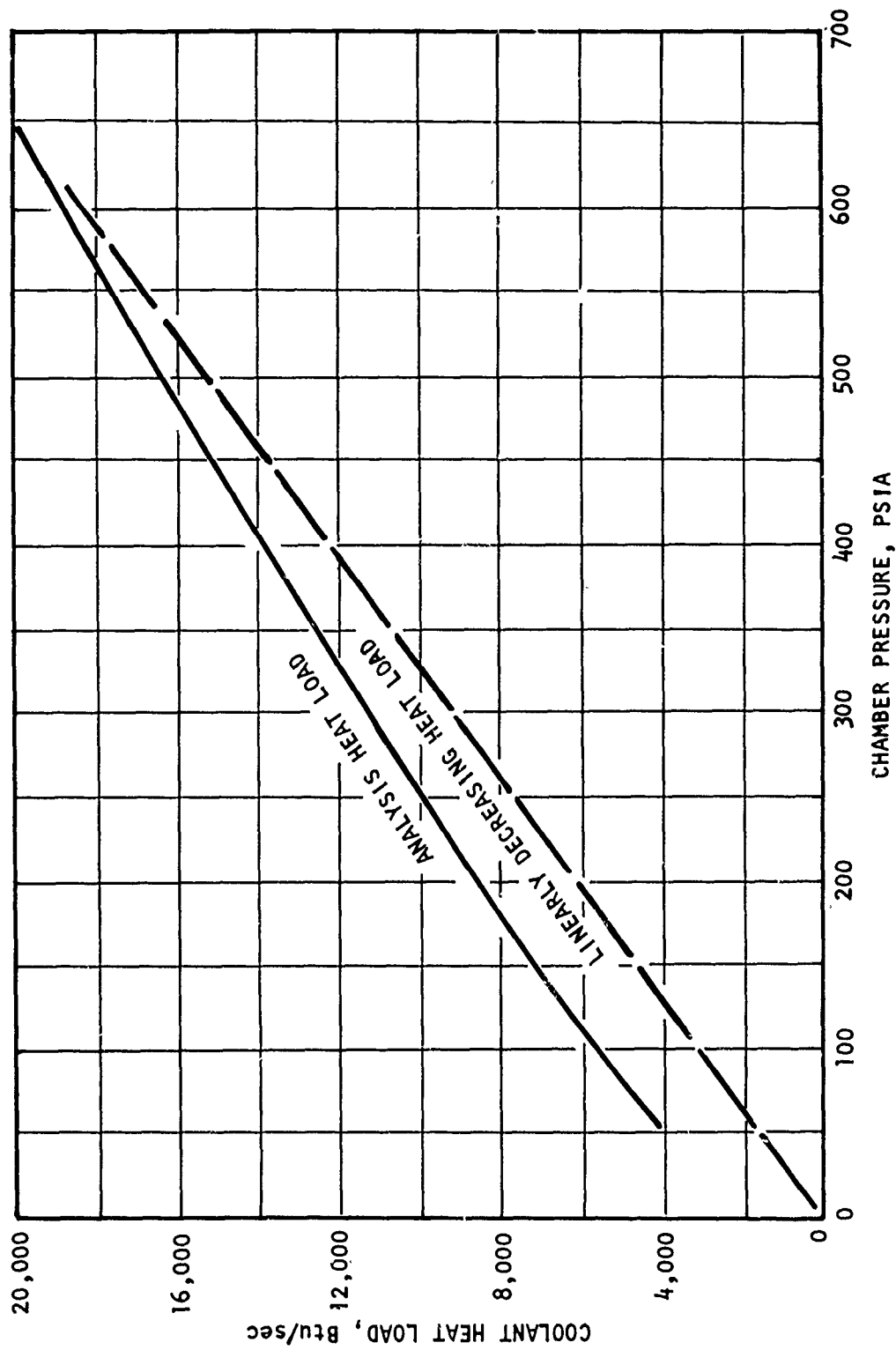


Figure 41. Total Coolant Heat Load vs Chamber Pressure (All-Parallel Cooling Circuit)

CONFIDENTIAL

CONFIDENTIAL

the analysis was accomplished using tube-wall segment test data. A linear relationship is required to obtain constant fuel injection temperatures as the propellant flow has a near-linear relationship with chamber pressure. The variation in injection temperature is to be evaluated in detail as further segment test data become available.

3. TURBOPUMP ANALYSIS AND DESIGN

(U) The main engine turbopump analysis and design effort during this report period included preliminary structural analysis, with resulting design refinements, pump component sizing, and additional critical speed analysis.

(U) The secondary engine turbopump analysis and design effort will be started during the next quarterly report period.

a. DESIGN ANALYSIS

(C) Design layout work continued on both main engine turbopumps. The configuration of the assemblies at the close of the report period is shown in Fig. 42 and 43. Notable changes from the configurations which were presented in the first quarterly progress report (AFRPL-TR-68-17) are the turbine wheels designs. Originally, it has been planned to mount the two-stage turbine on a common hub with the two stages joining in a "Y." Stress analyses of the fuel turbine indicated that the loads in the Y were excessive. Consequently, the design was modified to the dual hub configuration shown in Fig. 42. Although the oxidizer turbine stress loads were acceptable, it was decided that in the interest of maintaining common similarity in the design of the two turbines that the oxidizer turbine design would also be changed (Fig. 43). The resulting pressure ratio of the oxidizer turbine is 7.6:1.

CONFIDENTIAL

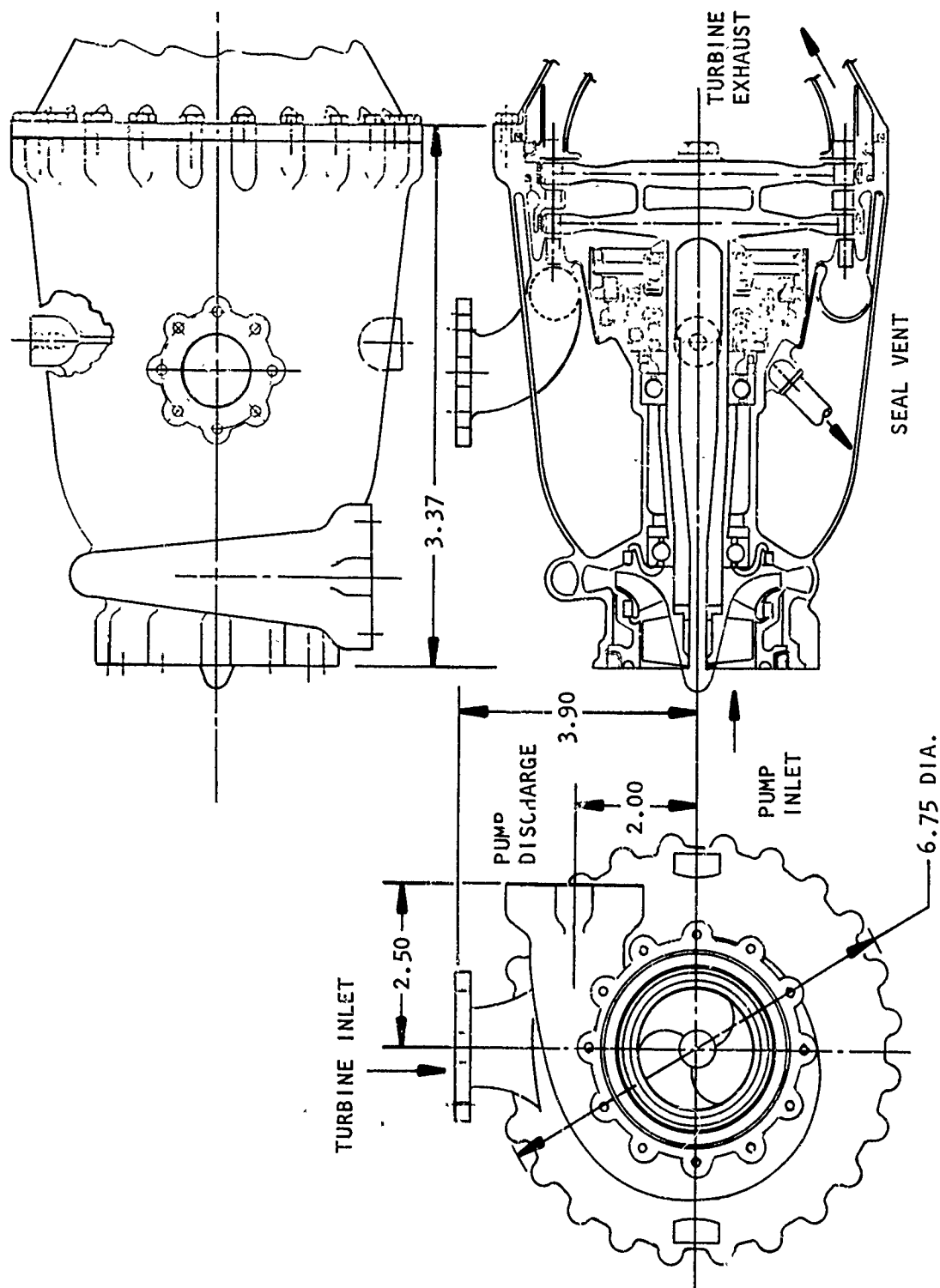


Figure 42. Main Engine Oxidizer Turbopump

CONFIDENTIAL

CONFIDENTIAL

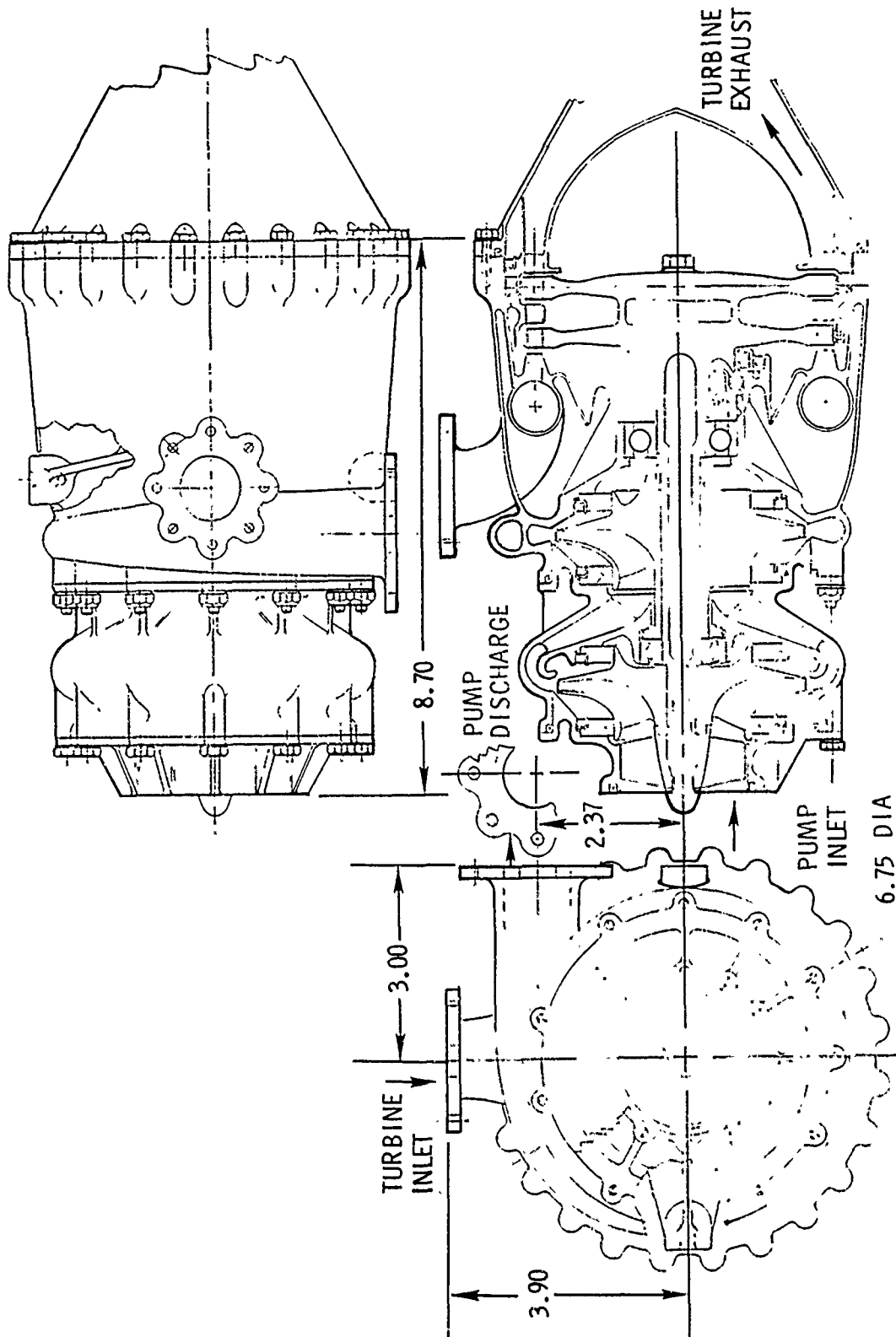


Figure 43. Main Engine Fuel Turbopump

CONFIDENTIAL

CONFIDENTIAL

(C) In making the decisions for identical fuel and oxidizer pump turbines, a tradeoff was made considering two alternatives. The first alternative was to use two turbines of similar design both with a 10:1 pressure ratio. The turbine flowrates required for operating the oxidizer and fuel pumps at the full thrust level for this configuration were 0.35 lb/sec and 0.42 lb/sec, respectively.

(C) The flowrates required for the 10:1 fuel turbine and 7.6:1 oxidizer turbine were determined to be 0.42 lb/sec and 0.33 lb/sec, respectively. Since there is virtually no difference in the required flowrate for the two configurations, it was concluded that identical turbines could be used for both pumps.

(U) Preliminary sizing calculations have been made for the main engine liquid hydrogen pump to indicate the magnitude of the major parameters required to define the pump components. The results of these calculations indicated those areas which appeared to be more critical from the standpoint of being able to meet the required hydrodynamic performance. Design studies were initiated to investigate these more critical areas and, eventually, to establish an acceptable design. Further design studies were initiated to indicate an optimum hydrodynamic design. The areas studied and some of the preliminary calculations are given below.

(C) The first-stage liquid hydrogen pump consists of an inducer, an impeller, and an appropriate first-stage diffusion system with a first-stage to second-stage crossover passage. The inducer is a low-head inducer with cylindrical tip and contoured hub. The impeller design tradeoff included flowrate, pump speed, impeller diameter, impeller tip width, and impeller back-discharge angle. The flowrate is relatively low and results a low impeller flow coefficient. Head requirement (ΔH), flow coefficient (ψ) and impeller tip speed (U_t) have the following relationship:

$$\Delta H \sim \psi U_t^2$$

CONFIDENTIAL

(C) From this relationship, it is evident that for a given head requirement a high impeller blade tip speed is required if the flow coefficient is low. This can be accomplished by either a larger diameter impeller or by increasing the pump speed. Fabrication can become a problem if the impeller tip width to impeller diameter becomes too small. In the tradeoff, a ratio of 0.03 was selected together with a pump speed of 75,000 rpm at the full-thrust operating level. The impeller blade discharge angle was selected to be 40 degrees (measured from the tangential direction). The selection was made to provide a reasonable negative H-Q curve slope for the pump and still maintain fabrication capability. A steep slope (produced by a smaller angle) is desirable from the standpoint of engine control since it produces a relatively high gain. On the other hand, fabrication of the impeller becomes a problem if the angle is small enough to make the blade width to effective impeller diameter too small. Decreasing the angle (increasing spiral length) has the same effect as increasing the impeller diameter. The results of the preliminary calculations for the inducer and impeller are given in Table 9.

(U) As the flow leaves the impeller, it has a high velocity and a low angle (measured from the tangential). This velocity must be diffused to a value acceptable as an inlet velocity in the second-stage impeller. It would be desirable from the standpoint of design simplicity to design the second-stage impeller identical to the first-stage impeller. Consequently, the inlet velocity of the second-stage impeller should match that of the first-stage impeller. This includes some prewhirl developed by the first-stage inducer. With these considerations, the requirements of the diffusion system and crossover ducts are defined. The efficiency of the turbopump will depend to a large degree on the performance of this diffusion system. As a result, several diffusion systems are being studied and will be compared to arrive at the best design. The diffusion systems being investigated for the first stage are:

1. The flow passes radially outward through a vaned diffuser, making a 180-degree turn through an internal axisymmetric bend, and

CONFIDENTIAL

TABLE 9

CALCULATED VALUES FOR MAIN ENGINE LH₂ INDUCER AND IMPELLER

Parameter	Inducer	Impeller
Inlet Tip Diameter, inches	2.1	2.1
Inlet Hub Diameter, inches	0.63	1.5
Inlet Tip Blade Angle, degrees	7.0	11.1
Discharge Tip Diameter, inches	2.1	4.1
Discharge Hub Diameter, inches	1.5	4.1
Discharge Blade Angle, degrees	12.0	40
Number of Blades	3	20
Head Coefficient	0.10	0.609
Flow Coefficient	0.0704 (inlet)	0.098 (discharge)
Discharge Tip Blade Velocity, ft/sec	687	1342
Discharge Tip Fluid Whirl Velocity, ft/sec	114	1018
Discharge Tip Fluid Axial Velocity, ft/sec	112.3	131.4
Euler Head, feet	2440	40,000

passing radially inward through a two-stage stator row in an internal axisymmetric return channel.

2. Same as (1), except that a single stator is used in the return channel.
3. Same as (1), except the flow passes radially outward through a vaneless space rather than through a vaned diffuser.
4. The flow passes radially outward through a vaned diffuser and enters a twin volute which feeds conical diffusers and external crossover passages to the second stage.
5. The flow passes directly from the impeller to a twin volute which feeds conical diffusers and external crossover passages.

Systems (4) and (5) permit the two stages of the impeller to be back-to-back.

(U) Two variations have been considered for the diffusion system of the second stage of the pump.

1. Vaned diffuser with a double-tongue volute
2. Vaneless diffuser with a double-tongue volute

(U) There are advantages and disadvantages to each of the variations of these two diffusion systems. The investigation of these is continuing, and primary emphasis during the next report period will be centered on calculating the losses and efficiency of these various diffusion systems.

(U) Sizing of the main engine oxidizer pump bearings was completed. The design specification is presented in Table 10. Additional sizing of the oxidizer pump is to be completed in the next report period.

b. CRITICAL SPEED ANALYSIS

(U) In the first quarterly progress report, the critical speed characteristics were presented for the main engine oxidizer pump. With the change

CONFIDENTIAL

TABLE 10

MAIN ENGINE OXIDIZER PUMP BEARING SPECIFICATION

Item	Position	
	Turbine	Pump
Type	Angular Contact Ball Bearing	Angular Contact Ball Bearing
Basic Size		
Bor , millimeters	25	20
OD, millimeters	47	42
Width, millimeters	12	12
Class*	5	5
Ball Complement		
Number of Balls	13	11
Ball Diameter, inches	1/4	1/4
Pitch Diameter, inches	1.42	
Initial Contact Angle, degrees	25	25
Race Curvature, percent of ball radius		
Inner	52	52
Outer	53	53
Cage		
OD	0.015	0.013
Pocket	0.020	0.020
Materials (Tentative)		
Balls	440-C	440-C
Races	440-C	440-C
Cage	K-Monel	K-Monel
DN at 28,000 rpm	700,000	560,000

*Annular Bearing Engineering Committee

CONFIDENTIAL

CONFIDENTIAL

in turbine wheel design as discussed in the previous pages, the critical speed characteristics also changed. Critical speed characteristics were defined during the subject report period for the present fuel and oxidizer pump designs. These are presented in Fig. 44.

(U) The item having a large effect on sizing the bearing and seals is the critical speed of the rotating parts. In addition to those shaft speeds which are generally identified with shaft bending, "dump speeds" are identifiable to a phenomenon identified as "whirl." Generally, whirl is ignored in design of a pump since there is no accompanying shaft bending. Although no problems are anticipated with whirl on the AMPS engines, they have been identified to assist in selection of bearing sizes and bearing spring rates.

(U) When whirl exists, the rotating assembly orbits about the bearing geometric centerline. Each point on the rotating assembly (rotor) centerline describes a circular path about the bearing geometric centerline, as indicated in Fig. 45. However, whirl does not always occur at a particular speed for two reasons: (1) bearing clearances tend to prevent simple spring-mass resonance, and (2) the fluid pumped provides damping which can limit the rotor motion amplitudes to acceptable values.

(C) For the main engine primary fuel and oxidizer turbopumps there are two speed areas which were investigated. The first area is the "free-free" mode critical speed in which the bearings are not loaded and the shaft rotates in its bent shape about the bearing geometric centerline. The free-free mode is a function of shaft stiffness and weight only. The free-free critical speed is maintained above maximum operating speed by securing maximum shaft stiffness and minimum weight. The free-free critical speeds are estimated to be 318,000 rpm for the oxidizer turbopump and 157,000 rpm for the fuel turbopump. Both free-free critical speeds are sufficiently high to prevent any critical speed problems. Figure 46 presents the free-free shaft mode shape for the oxidizer pump rotating at its critical speed.

CONFIDENTIAL

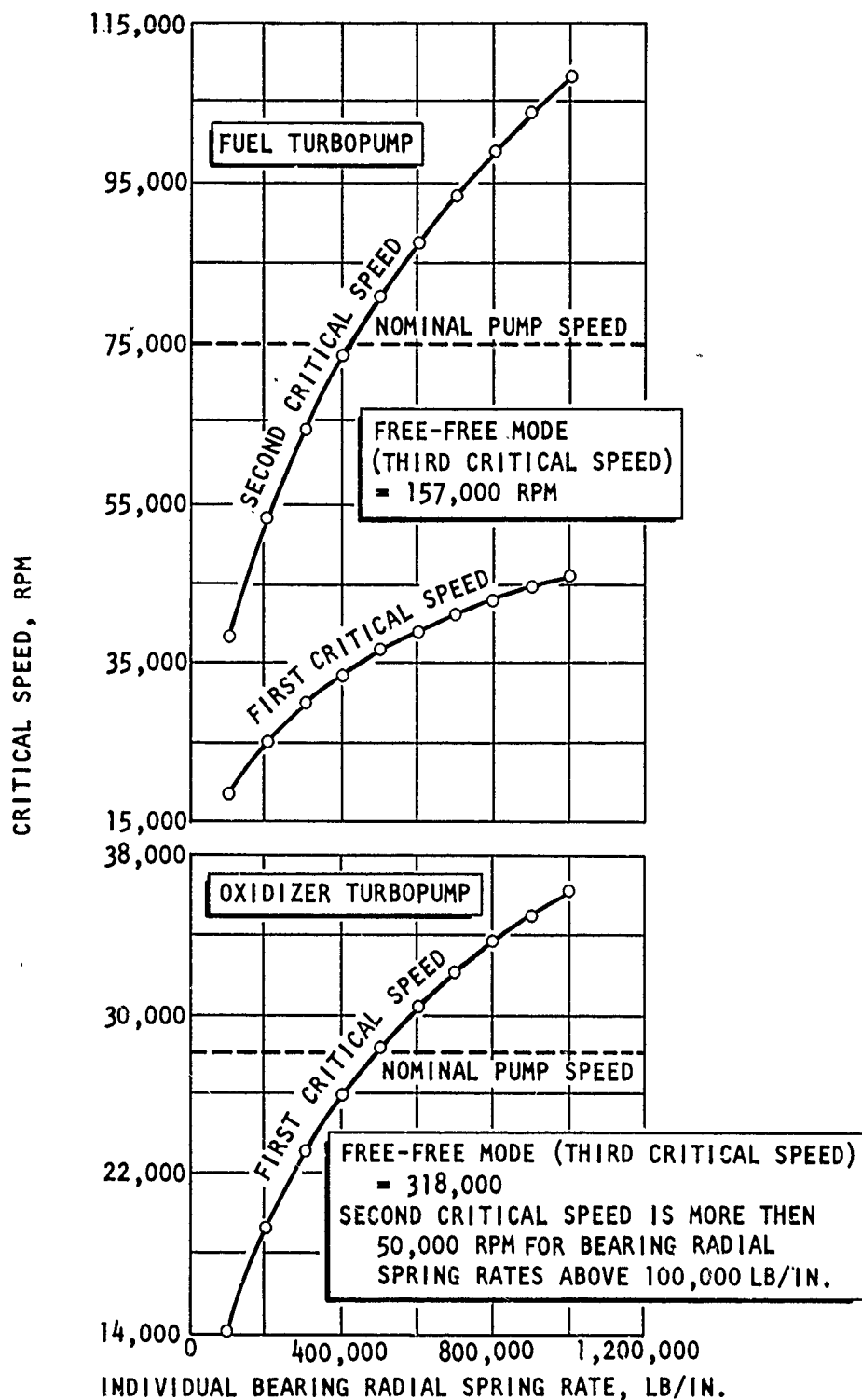


Figure 44. Main Engine Turbopump Critical Speed vs Bearing Spring Rate

CONFIDENTIAL

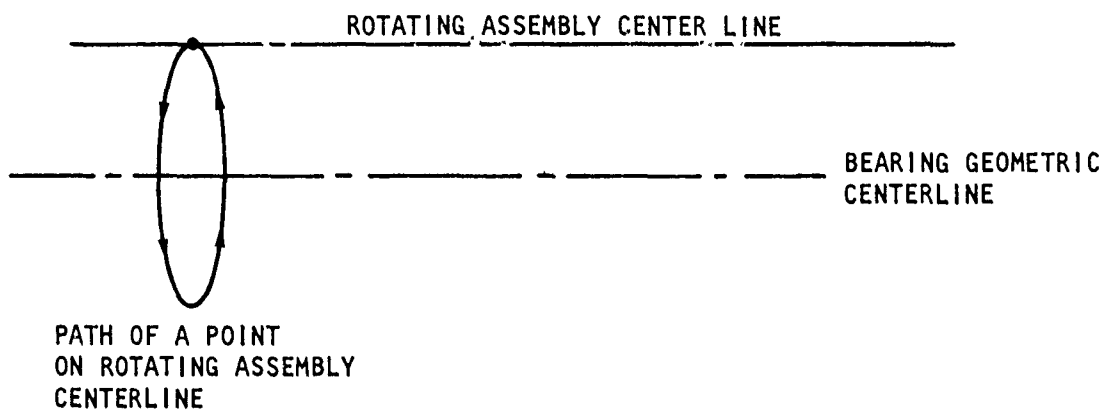


Figure 45. Rotation Path for Pump Shaft

CONFIDENTIAL

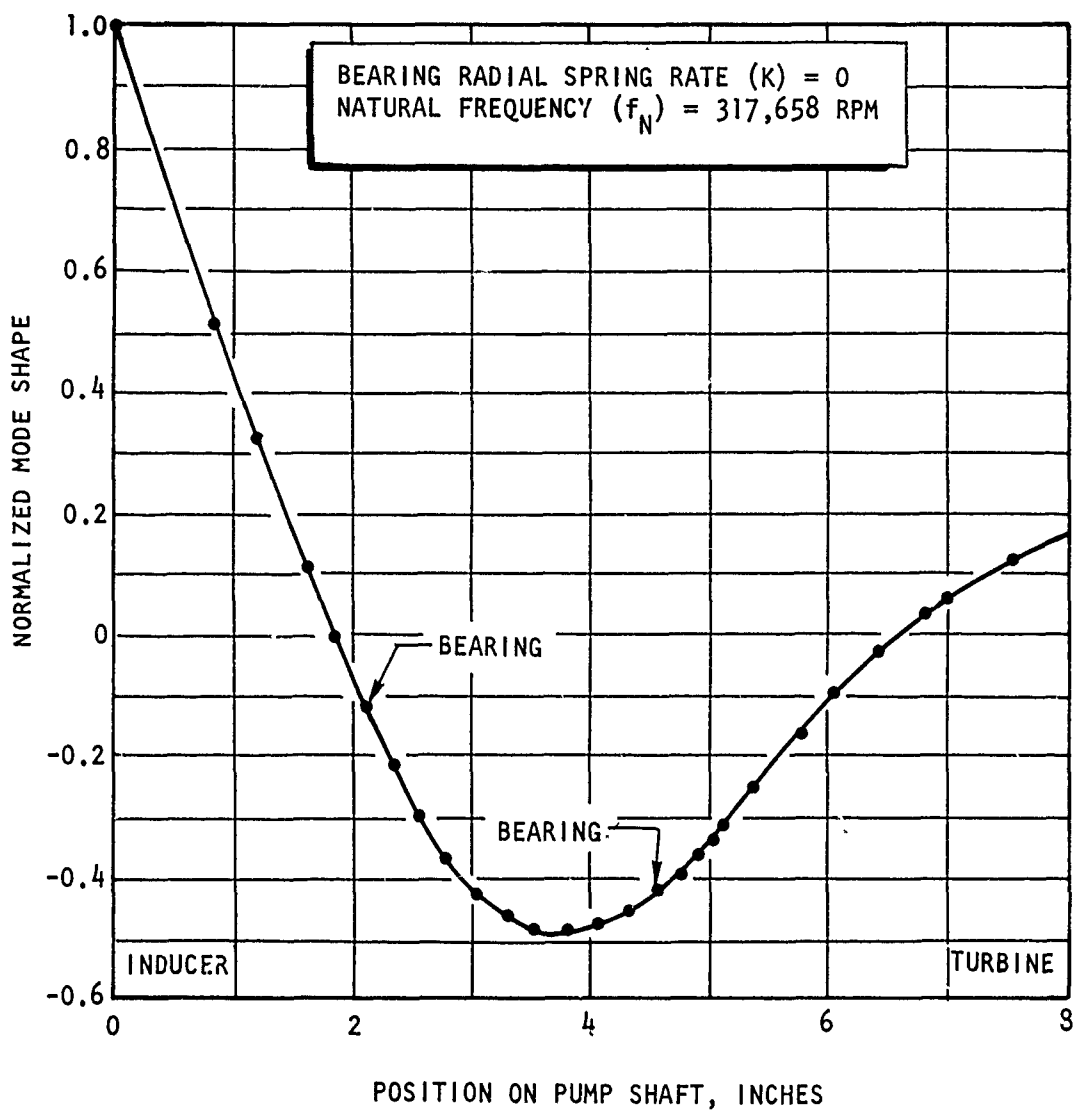


Figure 46. Main Engine Oxidizer Turbopump Shaft Shape for "Free-Free" Mode

CONFIDENTIAL

CONFIDENTIAL

(U) The second area is those speeds associated with whirl and called the "stick" modes in which the rotor remains unbent and whirls about the bearing centerline. In this condition, the bearing radial spring rate becomes a key parameter since the transfer of load from the bearing cage to the balls could be significantly changed if the bearing spring rate was not great enough.

(C) There are two stick mode speeds, both well below the free-free critical speed. One is identified by holding the shaft rigid at one bearing and permitting the other end to whirl. The second is identified by holding the shaft rigid at the opposite bearing and permitting the first end to whirl. The main oxidizer turbopump shaft mode shapes for these conditions are shown in Fig. 47 and 48 for bearing spring rates of 100,000 lb/in. Figure 49 shows the first stick mode for a bearing spring rate of 1,000,000 lb/in. The primary oxidizer pump can have its first stick mode below, at, or above the engine full-thrust operating speed of 28,000 rpm, depending upon bearing radial spring rate. The first stick mode speed increases with increasing spring rate. The spring rate is a complicated function of many parameters, and is currently being evaluated. It is desired to provide sufficiently high spring rate so as to place the first stick mode well above 28,000 rpm.

(C) The primary fuel turbopump will have both its stick modes below the nominal speed of 75,000 rpm, for any reasonable value of spring rate. The bearings will be designed with sufficient flexibility to keep both stick modes well below 75,000 rpm, but rigid enough to prevent excessive adverse bearing load. Additional analysis will be performed after the bearing designs are determined. In particular, the spring rate will be mapped vs all necessary variables to ensure proper speed characteristics. The bearing clearances will be optimized and balancing requirements will be established.

CONFIDENTIAL

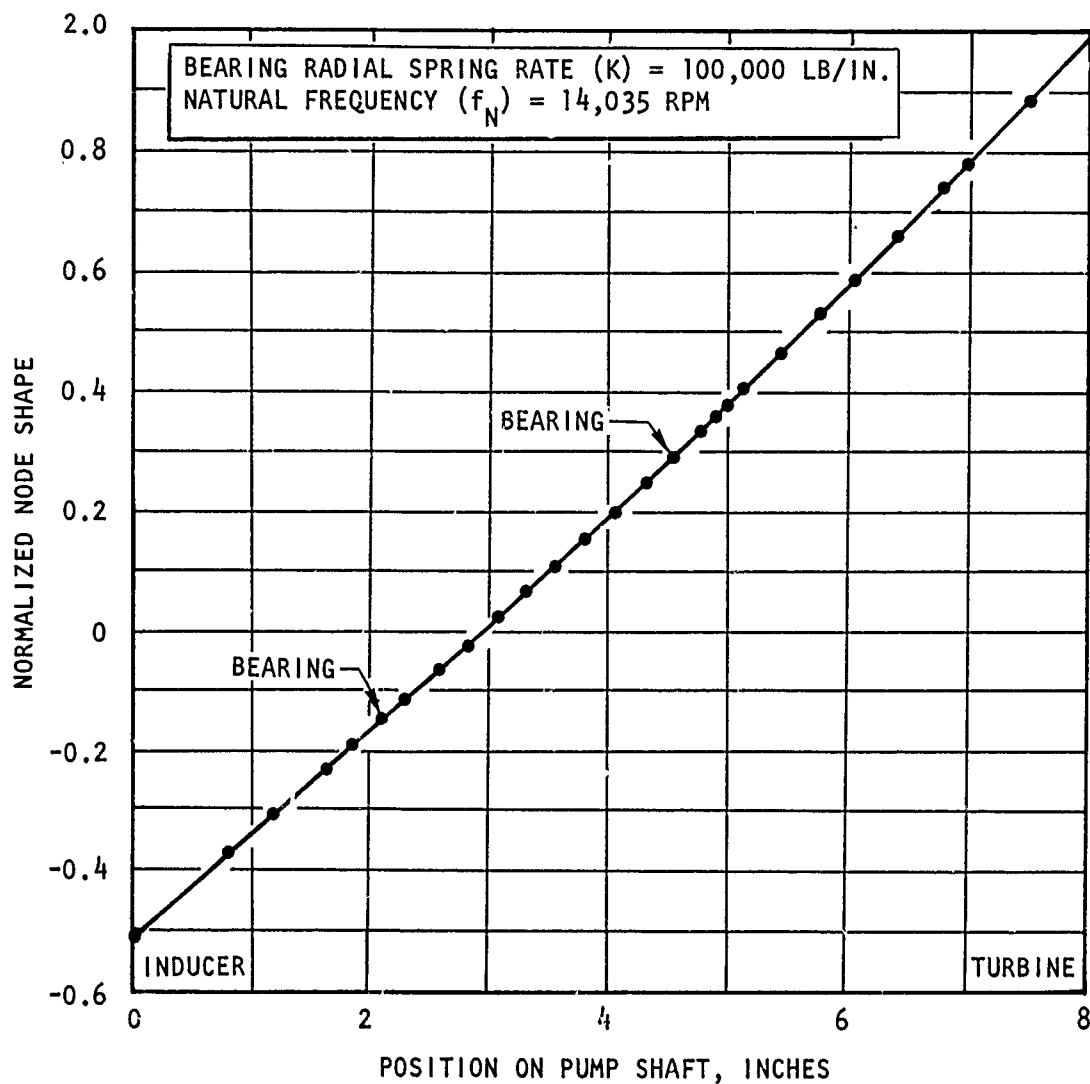


Figure 47. Main Engine Oxidizer Turbopump Shaft Shape for Turbine-End Bearing "Stick" Mode (100,000 lb/in. spring rate)

CONFIDENTIAL

CONFIDENTIAL

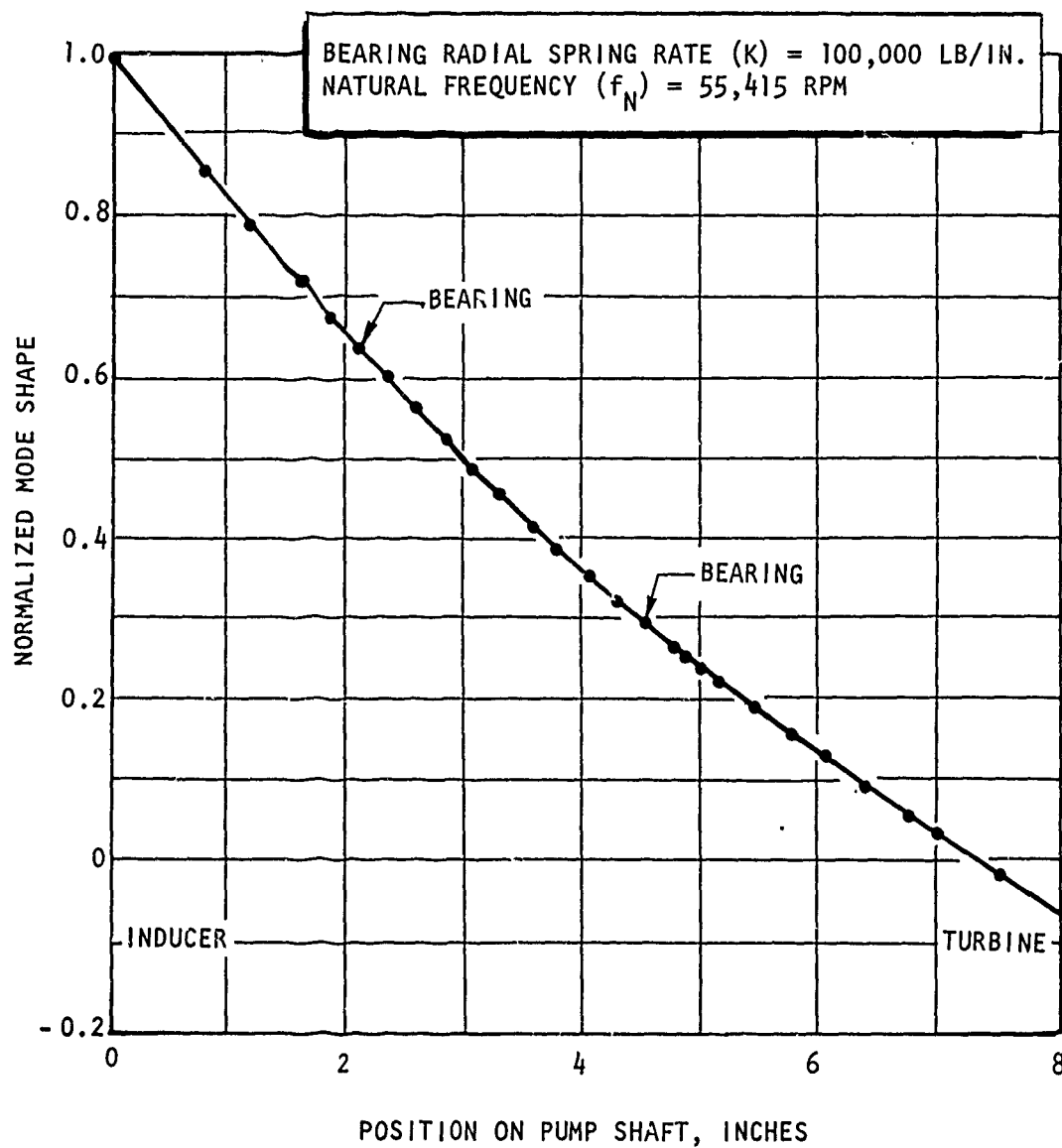


Figure 48. Main Engine Oxidizer Turbopump Shaft Shape for Inducer-End Bearing "Stick" Mode

CONFIDENTIAL

CONFIDENTIAL

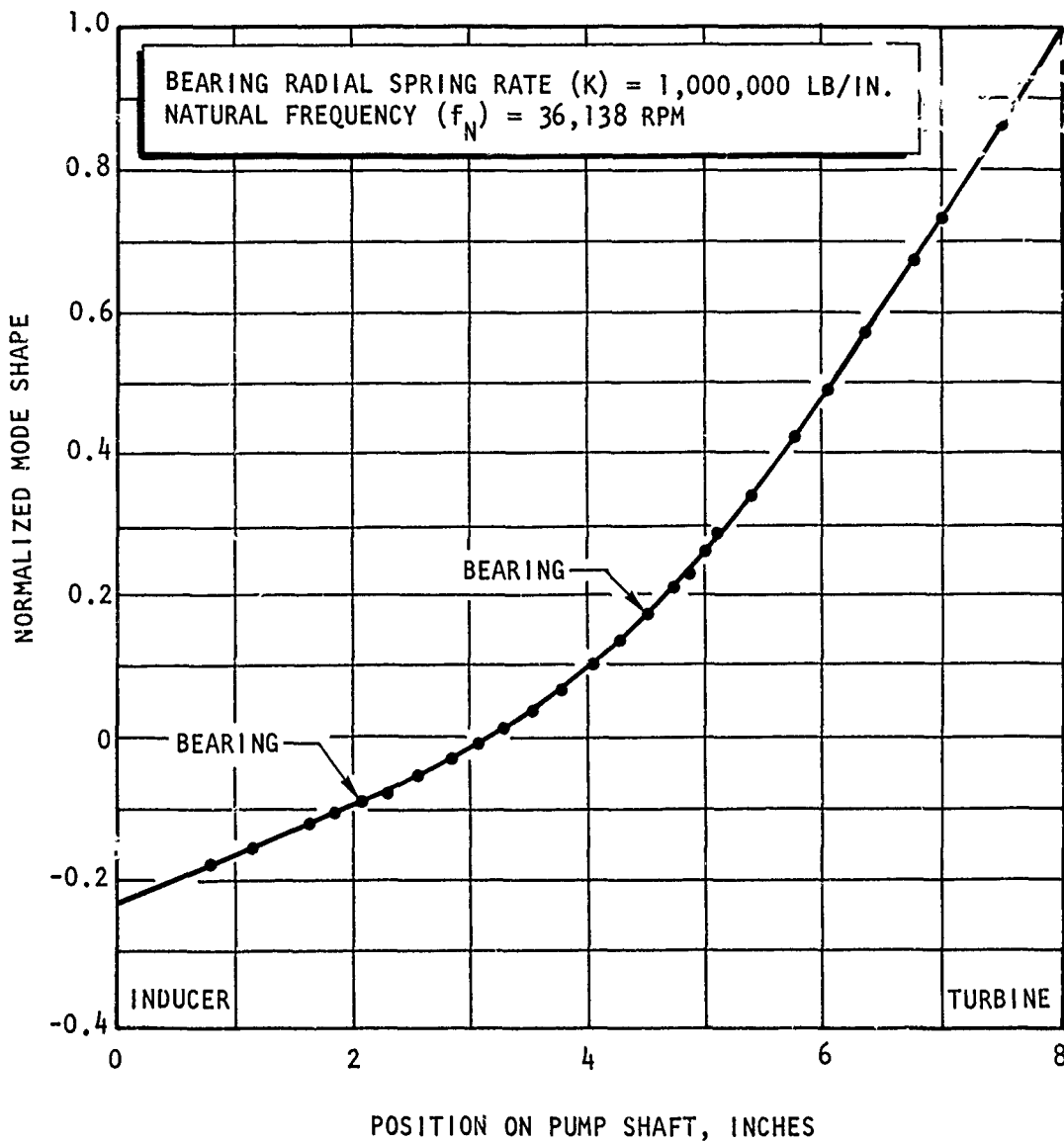


Figure 49. Main Engine Oxidizer Turbopump Shaft Shape for Turbine-End Bearing "Stick" Mode (1,000,000 lb/in. spring rate)

CONFIDENTIAL

c. OPERATING LIMITS

(U) To define the operating limits of the main engine fuel and oxidizer pumps, hydrodynamic features and stress limits are considered. The operating envelopes presented in the Engine Analysis section of this report were determined by the following criteria:

1. The maximum head rise of the pump is dictated by stress limitations in the volute structure.
2. The maximum speed in rpm is also set by stress limitations due to centrifugal forces in the pump and turbine.
3. The maximum flow of the pump is set hydrodynamically in regard to cavitation.
4. The minimum flow of the pump is also set hydrodynamically in regard to surging.

4. CONTROL ANALYSIS AND DESIGN

(U) During the first quarterly report period, preliminary design specifications were established for the main engine control valves, and a weight tradeoff was made of flow area vs valve weight for the four engine liquid line valves. Also, a tradeoff was made in which it was concluded that pneumatic actuation of the main propellant shutoff valves was preferable to electrical actuation. Using these data, the design specifications for the main shutoff valves of the main engine were prepared during this report period. Also, a similar weight vs actuation method was conducted for the liquid control valves. Additionally, effort was directed toward evaluation of the engine control system with use of the mathematical analog model. The basic model was constructed for an analog computer during the first quarterly report period.

(U) The secondary engine control system analysis and design effort will be started during the next quarterly report period.

CONFIDENTIAL

a. VALVE ACTUATION

(1) Control Valves

(U) As previously shown in the AMPS first quarterly progress report, analysis of the relative weight of the power supplies for pneumatic and electrical valve power actuation systems indicates a significant weight advantage for electrical power over pneumatic power for missions requiring relatively long and numerous valve operational times.

(C) The total energy requirement for valve power actuation is dependent on actual mission definition. Weight estimates were made using the present control valve configuration (i.e., two liquid control valves and one hot-gas valve) and assuming:

1. 6 nonevasive rendezvous
2. 12 main engine starts and 393 seconds operation
3. 18 small engine starts and 2766 seconds operation
4. 10-percent standby power (for electrical and pneumatic)
5. 30 watt-hours per pound battery weight efficiency
6. 3.2 watt-hours per pound for helium stored at a pressure of 3000 psi and a temperature of 40 R and used at a pressure of 750 psi and a temperature of 500 R
7. 2 pounds/horsepower was used for electric motors operated intermittently (rated 6 pounds/horsepower for continuous duty)

(C) The resulting power supply weight estimates for the two candidate systems were:

Electrical	39.3 pounds
Pneumatic	104 pounds

CONFIDENTIAL

(C) Weight vs mission time (3159 seconds total) is plotted in Fig. 50. The curves were obtained by applying ratios to the above basic figures. However, since electrical actuators for the power range required (25 watts) weigh slightly more than equivalent pneumatic actuators, the net weight advantage will be slightly smaller than indicated by the power source tradeoff.

(U) It was concluded from the study that for some mission descriptions (total engine operating time ≈ 1400 seconds) electrical actuation of the engine control valves provided a system weight advantage over a pneumatic actuating system. Further analysis is required to define all contributing factors for selection of the control system.

(2) Main Propellant Valve Actuation

(U) From Fig. 50 it is indicated that a pneumatic system would be superior from a weight standpoint for mission times somewhere below 1000 to 1400 seconds, while the electrical system would be best for mission times above that. Based on these results and previous study (first quarterly report), pneumatic actuation was selected for the main propellant valves for the following reasons:

1. Fast response: opening and closing times of the order of 150 milliseconds or less are easily obtainable with no weight penalty.
2. Actuation control by solenoid valves is a highly developed technique.
3. Low standby power is needed, which results in a small increment of pneumatic supply weight and utilizes the weight advantage of the pneumatic actuator over the electrical actuator.

CONFIDENTIAL

CONFIDENTIAL

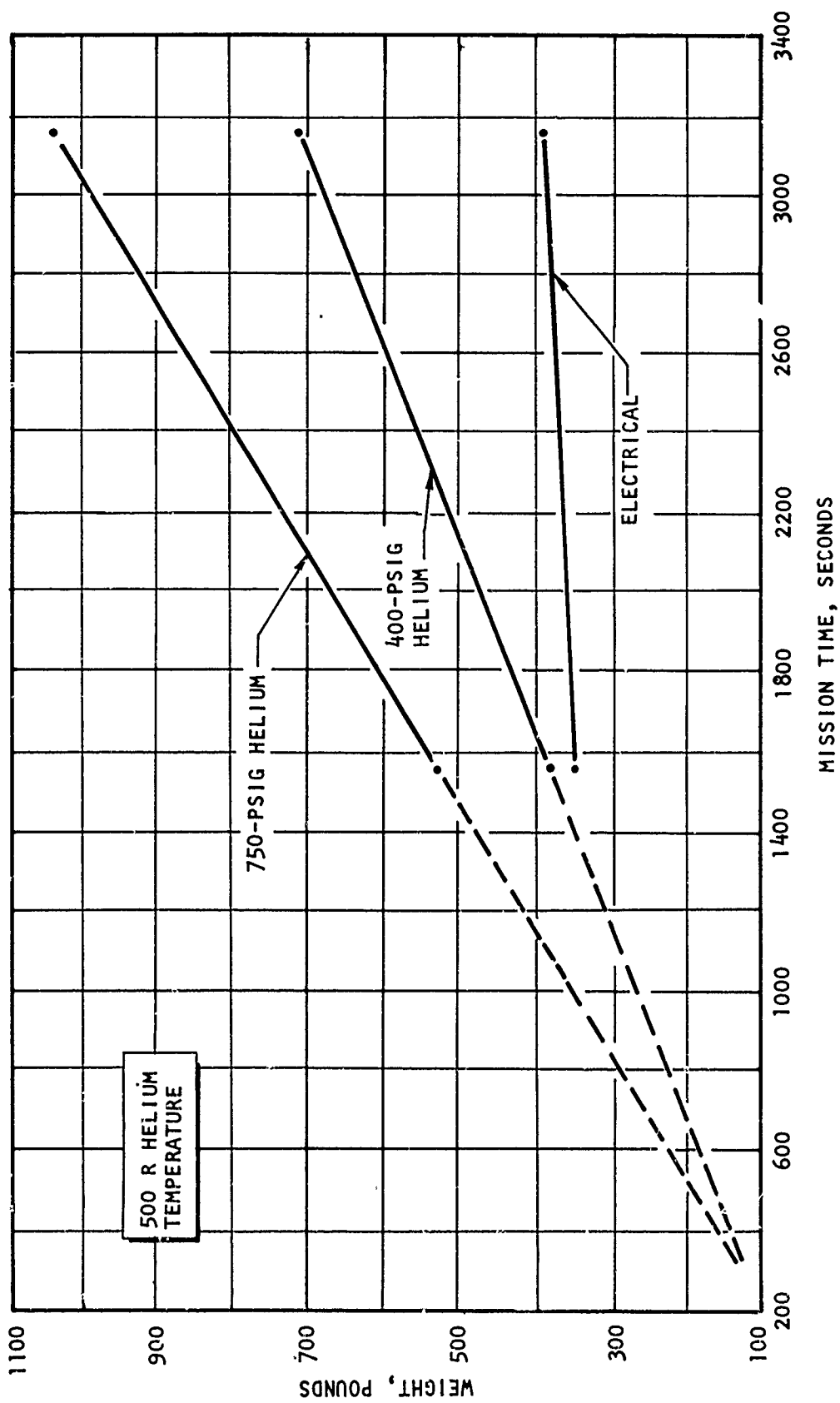


Figure 50. Comparison of Valve Actuation Weights (Liquid Control Valves)

CONFIDENTIAL

CONFIDENTIAL

b. CONTROL SYSTEM COMPUTER MODEL

(U) The analog computer model is a simulation of the main engine with chamber pressure (P_c) and engine mixture ratio (MR_e) controls. Low-frequency (order of <10 cps) engine and control component dynamics equations are mechanized for the model. The model has been updated as more accurate information has become available or design changes have been made. At present, two linked analog computers are being utilized.

(U) The hydrogen bleed (hydrogen tapoff) engine cycle was used as the basic engine cycle for the control studies. Three configurations of hot-gas valves and liquid-propellant control valves (Fig. 51) were simulated for control of chamber pressure and mixture ratio.

1. One hot-gas valve for turbine speed control and two variable-area cavitating venturis to control liquid propellant flow
2. One hot-gas valve and two butterfly valves
3. Two hot-gas valves only (one for each turbine)

(U) For each case, basic engine response, stability, and ability to control over the entire chamber pressure and mixture ratio envelope were explored. Preliminary selection of control gains and compensation were made, but were not idealized. Control optimization will be accomplished only for the configuration finally selected because this is a very time-consuming process. The intent of the current effort was to identify the controls systems which could be used to provide adequate control for the main engine. Predicted engine system response to chamber pressure command ramps and steps, mixture ratio command steps, and chamber pressure perturbation at various chamber pressures and mixture ratio levels were recorded for each system.

(C) Figure 52 shows step responses around chamber pressure levels of 60 percent and 20 percent for the one hot-gas valve and two cavitating venturi control valve simulation. The initial error observed in Fig. 52

CONFIDENTIAL

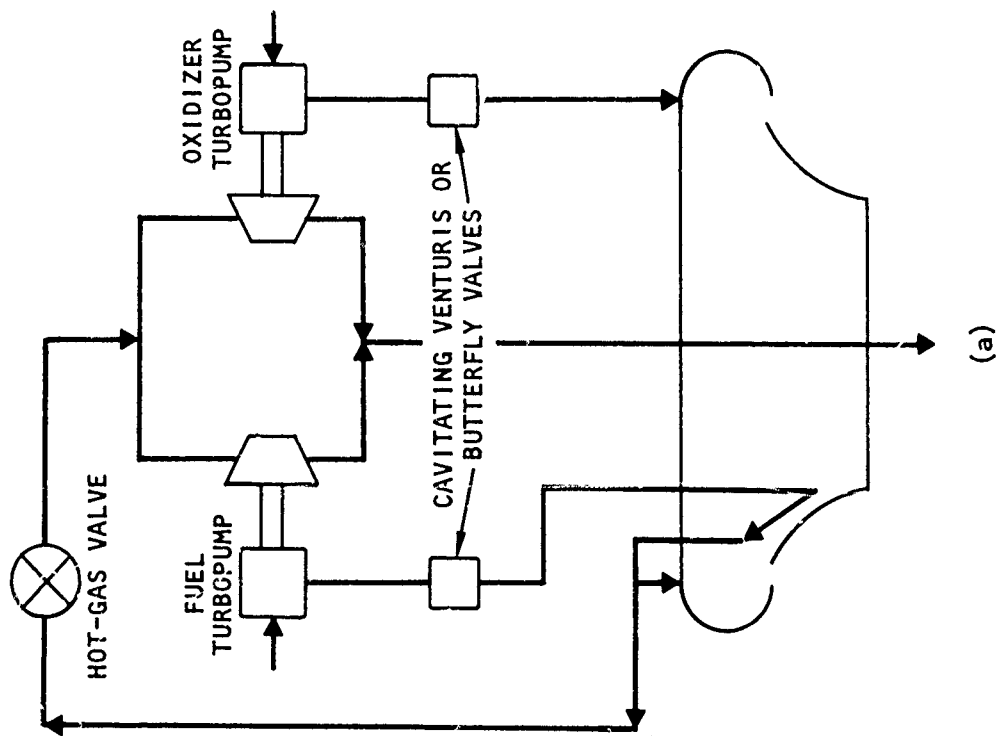
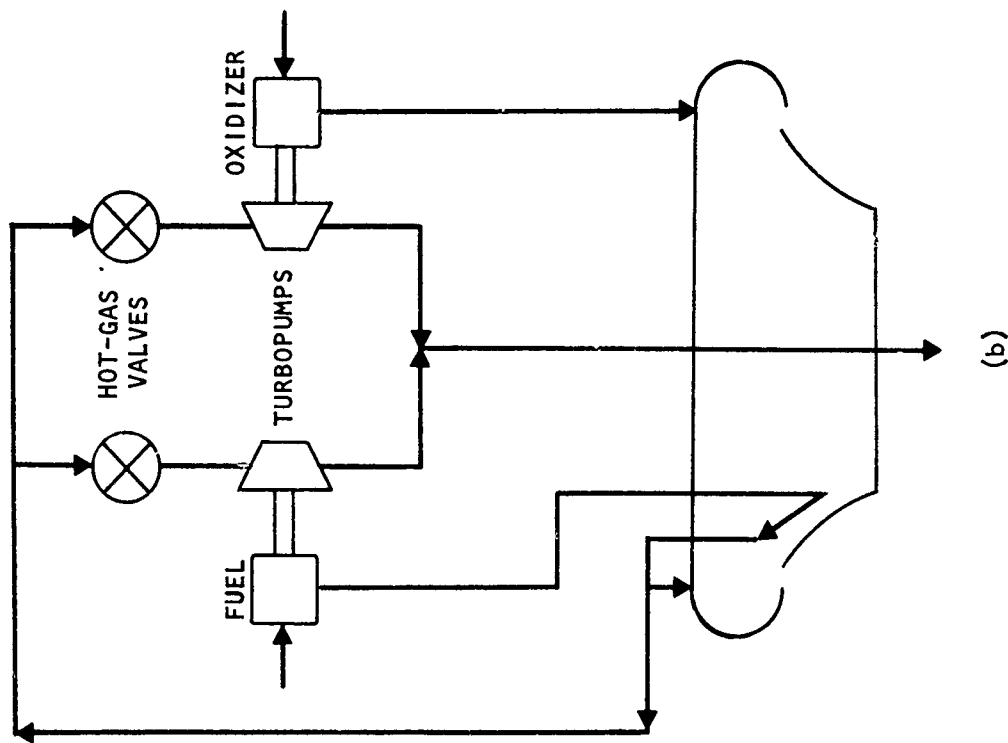


Figure 51. Engine Mixture Ratio and Chamber Pressure Control Schemes for Hydrogen Bleed Engine Cycle

CONFIDENTIAL

CONFIDENTIAL

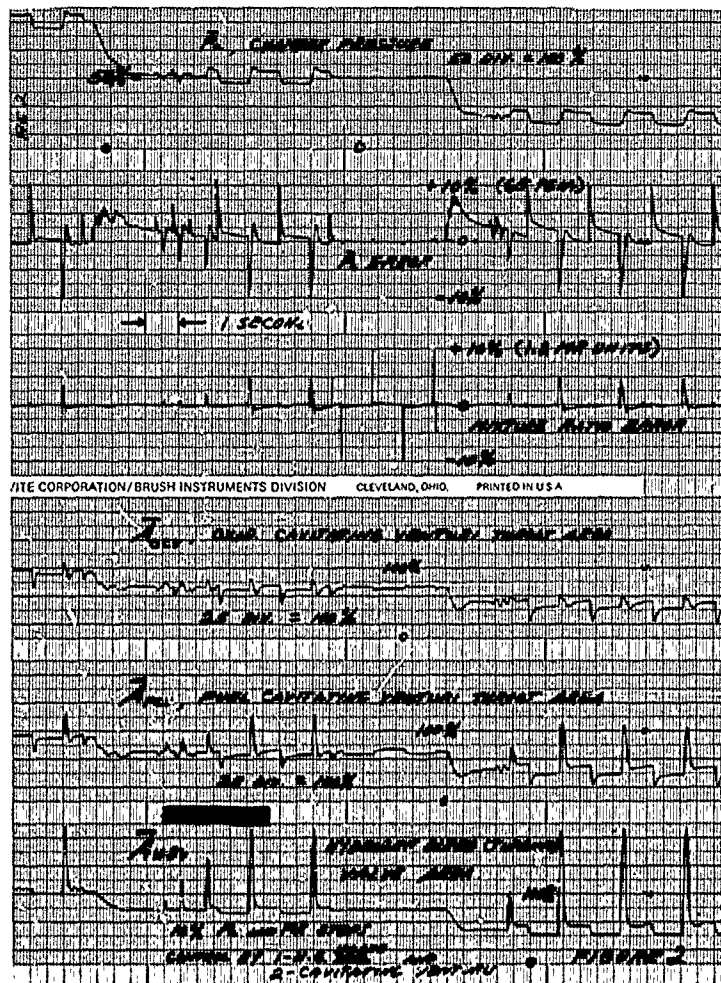


Figure 52. Main Engine Control by One Hot-Gas Valve and Two Cavitating Venturi Valves

CONFIDENTIAL

CONFIDENTIAL

for a step command is, of course, the full value of the step. The command to each cavitating venturi was the sum of the commands from the mixture ratio and chamber pressure controls. The hot-gas valve area was also scheduled as a function of both chamber pressure and mixture ratio so that the turbine input power would be at the proper steady-state level. In addition, for dynamic compensation, the hot-gas valve was opened an additional amount by the chamber pressure error signal whenever chamber pressure was less than the command. This was necessary to accelerate the turbopump speed buildup and flowrate. The variables presented, commensurate with the desired ramp rates, are normalized about their nominal value at full thrust (30K) and an engine mixture ratio of 12:1. The hot-gas valve area was limited to twice the nominal area, or 200 percent. Note in Fig. 52 that 200 percent was almost attained during the chamber pressure command step tests.

(U) Note, also, that there is some interaction between the two controls. This is always the case when each control component affects each controlled variable. One purpose of control optimization is to reduce such interaction to a reasonable minimum. In this particular case, mixture ratio command steps here have little effect on chamber pressure error, but chamber pressure steps do temporarily perturb mixture ratio.

(C) Figure 53 shows the response of the main engine to various chamber pressure command rates between chamber pressure levels of 10 and 100 percent. Valve area limits for these tests were set at 110 percent for the oxidizer cavitating venturi, 130 percent for the fuel cavitating venturi, and 200 percent for the hot-gas valve. Note that the fuel venturi came out of cavitation (i.e., throat pressure exceeded vapor pressure) for about 0.5 second during each ramp even though the turbine hot-gas valve was wide open at double nominal area. As the fuel turbopump speed increased so that enough output pressure was developed, the fuel venturi went back to cavitating flow. Aside from this factor, the control system consisting of a single hot-gas valve and cavitating venturi liquid control valves appears to provide adequate engine control.

CONFIDENTIAL

CONFIDENTIAL

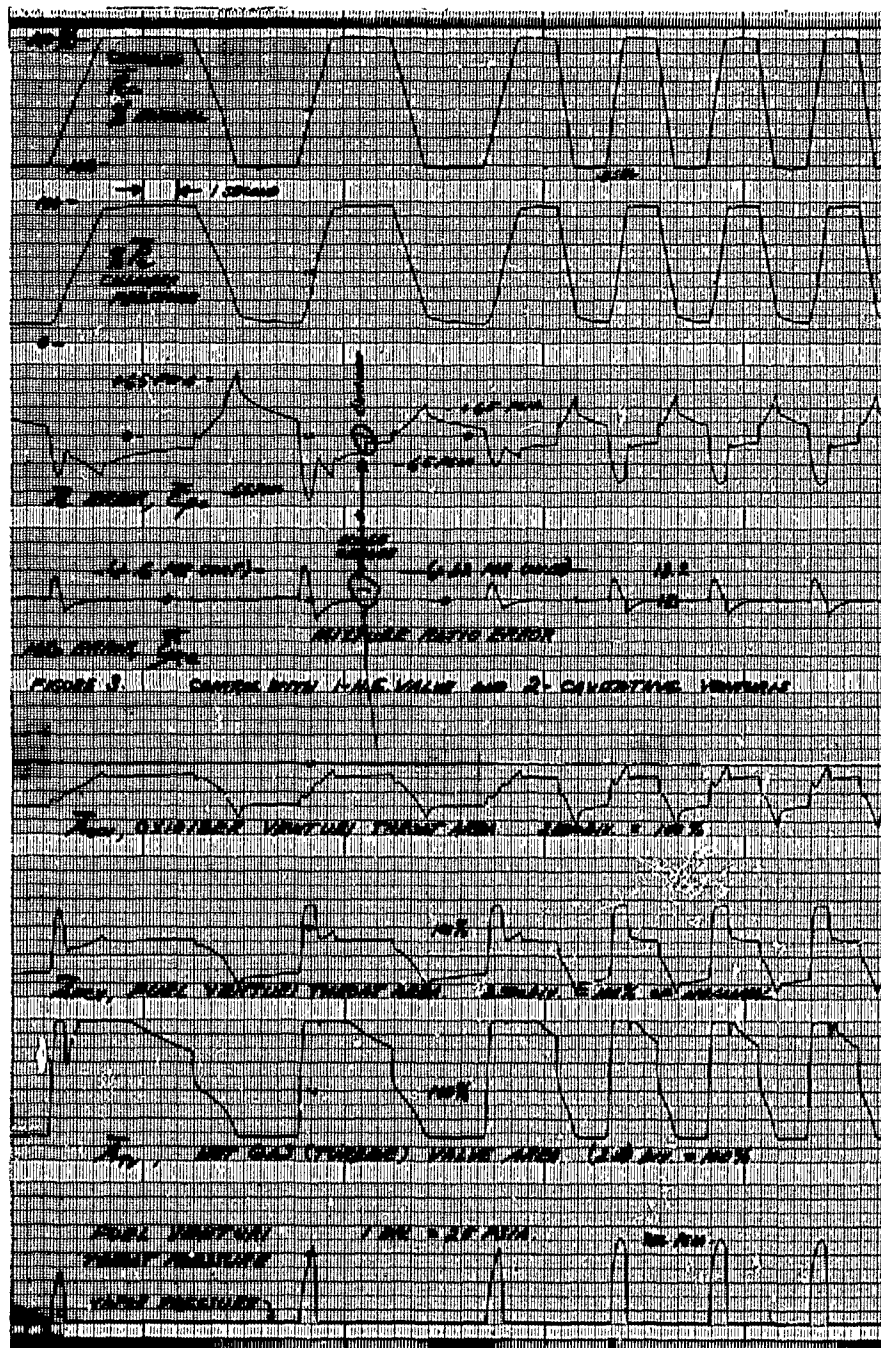


Figure 53. Main Engine Control Response With One Hot-Gas Valve and Two Cavitating Venturi Valves

CONFIDENTIAL

(U) Next, two butterfly propellant valves were simulated in place of the two variable-area cavitating venturis. Figure 54 shows chamber pressure and chamber pressure and mixture ratio errors in response to various chamber pressure command ramp rates. The errors in chamber pressure and mixture ratio are greater than those produced during the cavitating venturi simulation, but could be substantially reduced by various methods of control compensation. It was concluded that an adequate control system could be developed using control valves that obey the $\Delta P \sim \dot{W}^2$ relationship.

(U) Figure 55 shows ramp response for mixture ratio and chamber pressure control by two turbine-control valves only (no liquid-propellant control valves). To reduce the maximum (high) transient mixture ratio error for this configuration required that the chamber pressure error signal be utilized to increase the valve area command to the fuel turbine hot-gas valve. The results of these runs indicated that a control system consisting of only turbine control could be developed to provide adequate control for the main engine.

(U) Some general comparisons between the three control concepts can be made. Detailed comparisons are not valid, however, because none of the controls were optimized and neither were they in the same state of development or improvement. In general, the hot-gas valves only system does not appear to have the maximum response capability of either system with liquid propellant valves. There may also be a little less gain and phase margin at minimum thrust. The computer study indicates that each of the three methods are suitable for chamber pressure and mixture ratio control. The two hot-gas valves only approach offers a simpler control system than either approach using liquid control valves since there are less components to control. The final decision, however, must be based upon additional factors.

(U) Figure 56 shows the maximum increase in mixture ratio as a function of ramp rates for the first and third concepts discussed. The second concept was not included because particular attention was not given to

CONFIDENTIAL

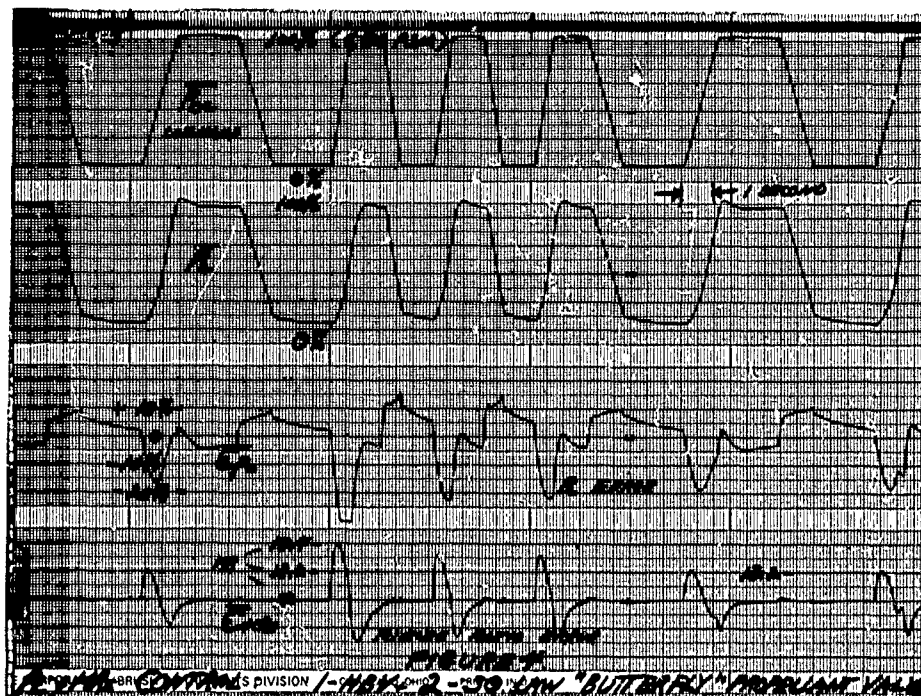


Figure 54. Main Engine Control With One Hot-Gas Valve and Two Butterfly Propellant Valves

CONFIDENTIAL

○



}

CONFIDENTIAL

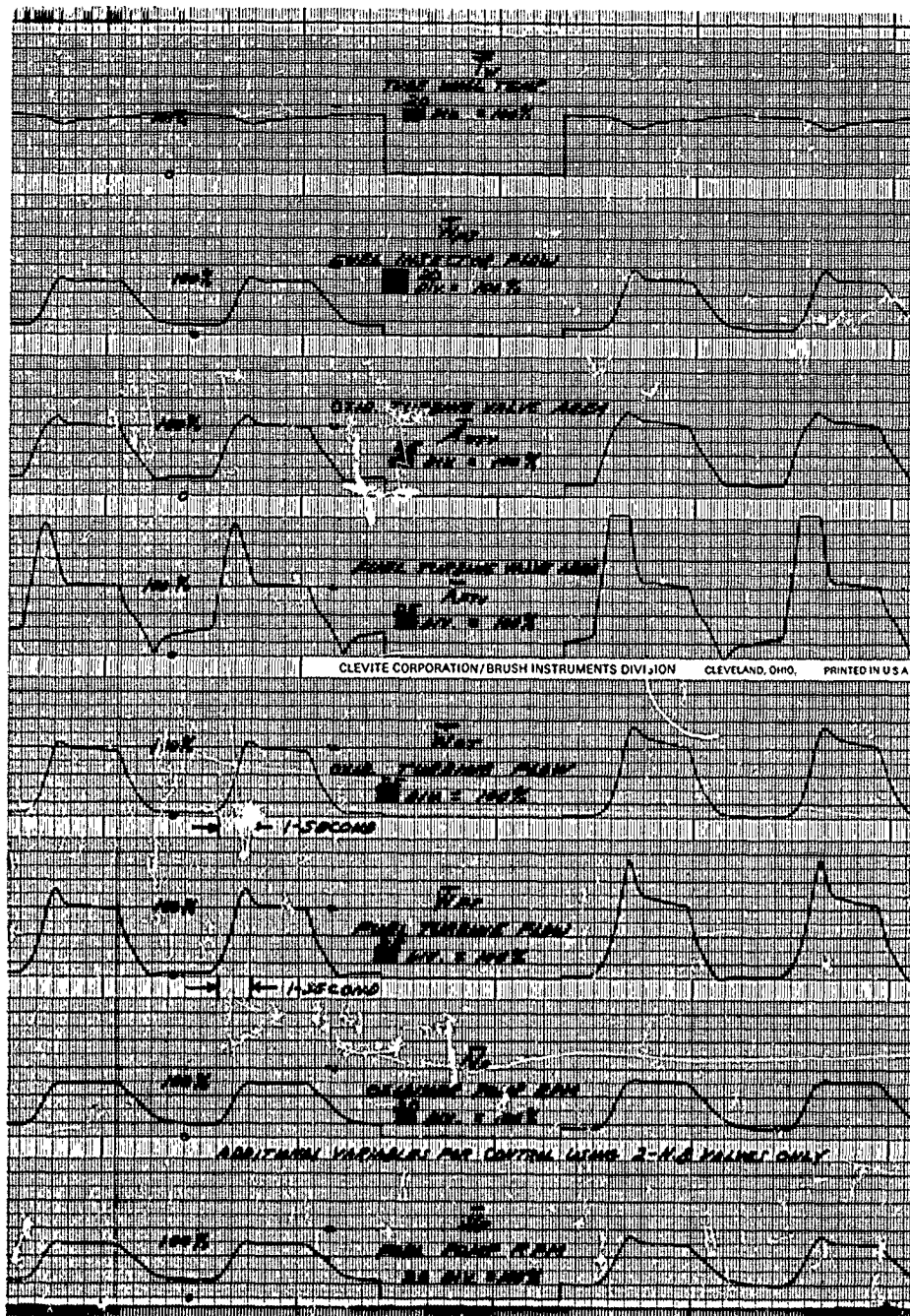


Figure 55. (Concluded)

CONFIDENTIAL

CONFIDENTIAL

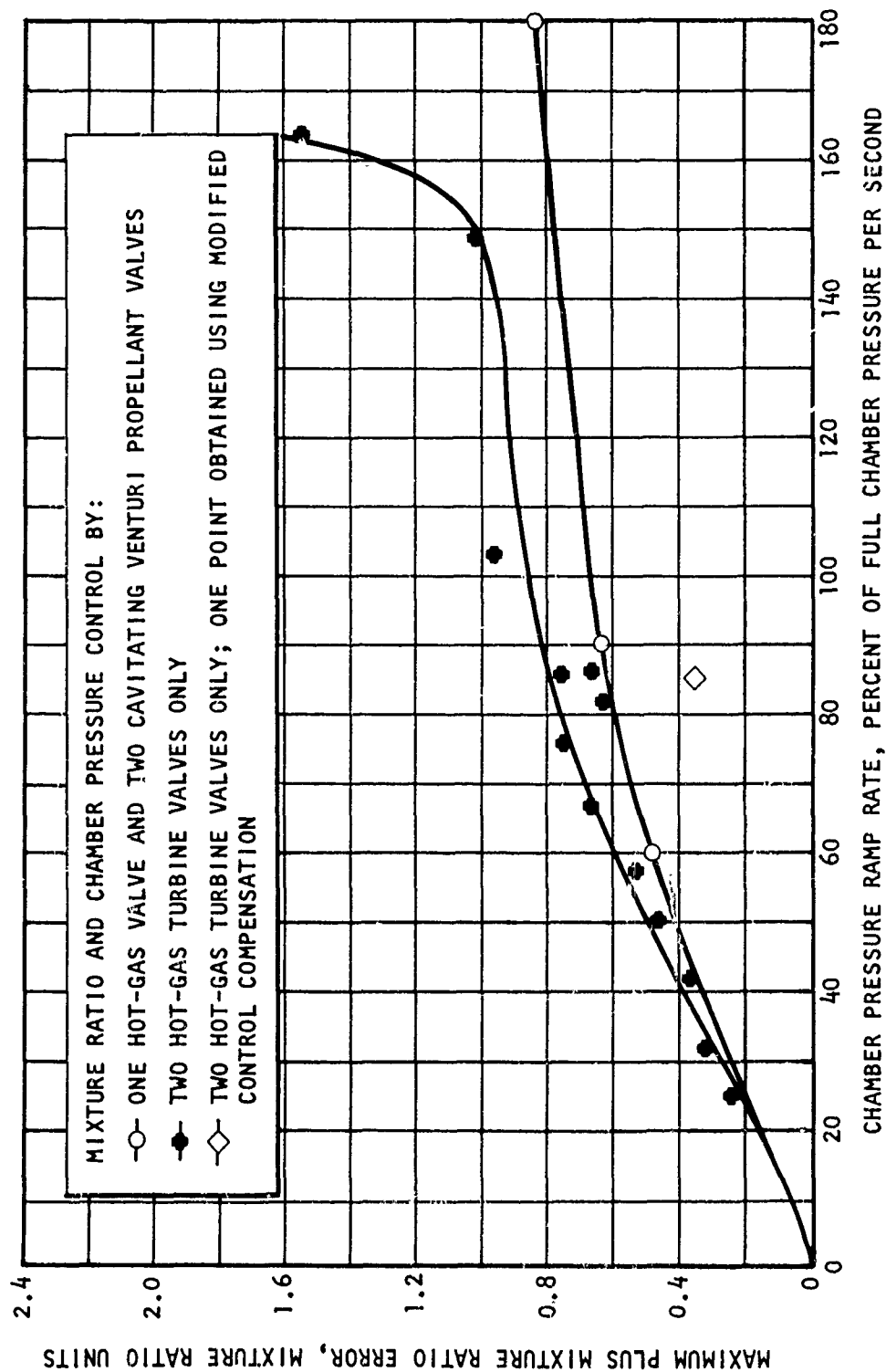


Figure 56. Positive Mixture Ratio Error vs Chamber Pressure Ramp Rate

CONFIDENTIAL

CONFIDENTIAL

mixture ratio during this series of tests. This relationship is of interest because the thrust chamber tube-wall temperatures are increased at high engine mixture ratios. The curves are comparable, but both can probably be lowered (less mixture ratio error) through control optimization. This was accomplished for one test point using the two hot-gas valves only configuration. This method and others will be investigated further in the next quarterly period.

5. TECHNOLOGY ASSESSMENT

(U) Evaluation of related program results achieved both at Rocketdyne and other agencies was continued. The documents listed in the first quarterly progress report are used as reference material and are continually analyzed as they apply to particular aspects of the current effort. Additionally, evaluations were made of program reports involving thermal conditioning of hydrogen pumps and component and engine test programs in which fluorine was used as the oxidizer. The reports listed in Table 11 present the current list of reference material being utilized.

(U) A review of the work accomplished on contract NAS8-20324, "Thermodynamic Improvements in Liquid Hydrogen Turbopumps," was conducted to provide comparative results and information for the AMPS engine start analysis and thermal conditioning studies. The Rocketdyne report of this work (R-7138) provides both experimental and analytical results pertaining to the thermal conditioning requirements and design recommendations for liquid hydrogen pumps. Detailed information is presented describing pump thermal design and analysis techniques, two-phase flow analysis, material characteristics, precondition and thermal protection techniques, and a review of the thermal conditioning characteristics of existing liquid hydrogen pumps.

CONFIDENTIAL

CONFIDENTIAL

TABLE 11

ADDITIONS TO TABLE 18 OF FIRST QUARTERLY REPORT (R-7380-2)

Area of Interest	Document Number	Document Title
Engine Systems and Turbomachinery	R-7138 July 1967	Thermodynamic Improvements in Liquid Hydrogen Turbopumps
Injectors	AFRPL-TR-66-43 7 March 1966	Final Report of High Energy Advanced Throttling Concept Study
Engine Systems, Turbomachinery, and Valves	CR 72074 21 October 1966	Research on a Hydrogen-Fluorine Propulsion System
Turbomachinery	R-5889 9 January 1964	Atlas Mark 4 Turbopump Seal FLOX Test Program
Valves	AFRPL-TR-68-03	Liquid Fluorine Shutoff Valve Development
Turbomachinery	NASA TND 2453	Friction Wear and Dynamic Seal Studies in LF_2 and LO_2

CONFIDENTIAL

(U) Effort conducted under NASA and AFRL contracts (NAS-754, NASA 3-3239, and AF04(611)-9965), and NASA effort reported in NASA TND 2543, were reviewed to further assess the approach taken in the current AMPS engine and component design with those which proved to be successful or were recommended on these earlier programs.

(C) An evaluation is presently being made of the test results of the 2-inch liquid fluorine shutoff valve of contract AF04(611)-10925.

CONFIDENTIAL

TASK II - CRITICAL ENGINE COMPONENT DEMONSTRATION TESTING

(U) This task provides for design, fabrication, and test of critical engine component hardware to determine performance and demonstrate solutions to potential design and fabrication problems. The critical components include segments of the main thrust chamber, complete main thrust chambers, solid-wall secondary thrust chambers, and oxidizer pump bearings and seals.

1. SEGMENT THRUST CHAMBER DESIGN AND FABRICATION

(U) Evaluation of injector patterns and combustion chamber geometry variations are being accomplished in 5-inch length segment hardware. These tests provide data necessary to define the contour and injector configuration for the subsequent 30-degree segments and full main thrust chamber designs. A summary of the hardware design, fabrication, and test status is presented in Table 12.

a. 5-INCH SOLID-WALL THRUST CHAMBER SEGMENT

(U) Fabrication of the second G_c contour, solid-wall thrust chamber segment was completed. The first G_c contour chamber and a K-contour thrust chamber segment were completed in the previous report period. The G_c contour chamber shown in Fig. 57 illustrates the geometry and cooling passage arrangement.

b. 5-INCH TUBULAR-WALL THRUST CHAMBER SEGMENT

(C) Fabrication of the 5-inch tubular wall thrust chamber segment was completed during this report period. The completed assembly is shown in Fig. 58.

CONFIDENTIAL

TABLE 12
STATUS OF TASK II THRUST CHAMBER DESIGN, FABRICATION, AND TEST

Hardware	Design Status	Fabrication Status	Test Status
5-Inch Solid-Wall Chamber Segment (G), U/N 1	Complete	Complete	32 Tests, Throat Area Deterioration
5-Inch Solid-Wall Chamber Segment (G), U/N 2	Complete	Complete	7 Tests, Throat Melted (Because of Insufficient Coolant Water)
5-Inch Solid-Wall Chamber Segment (K), U/N 1	Complete	Complete	8 Tests, No Damage
5-Inch Triplet Injector Segment, U/N 1	Complete	Complete	3 Tests, Face Overheated
5-Inch Triplet Injector Segment, U/N 2	Complete	Complete	4 Tests, Face Overheated
5-Inch Triplet Injector Segment, U/N 3	Complete	Complete	10 Tests, Structural Failure of Injector
5-Inch Fan Injector Segment, U/N 1	Complete	Complete	18 Tests, Face Overheated
5-Inch Fan Injector Segment, U/N 2	Complete	Complete	14 Tests, Damaged During Test 051
5-Inch GF ₂ Injector Segment, U/N 1	Complete	Complete	No Tests to Date
5-Inch Fan Injector Segment, U/N 3	Complete	90-Percent Complete	No Tests to Date
5-Inch Tubular-Wall Chamber Segment	Complete	Complete	Damaged During Test 051
30-Degree Solid-Wall Chamber Segment	Complete	75-Percent Complete	No Tests to Date
30-Degree Tubular-Wall Chamber Segment	Complete	50-Percent Complete	No Tests to Date
30-Degree Injector Segment, U/N 1	Complete	15-Percent Complete	No Tests to Date
30-Degree Injector Segment, U/N 2	80-Percent Complete	Material on Hand	No Tests to Date
Main Tubular-Wall Thrust Chamber Assembly	20-Percent Complete	In Planning, Material Ordered	No Tests to Date
Secondary Solid-Wall Thrust Chamber	Preliminary Design	In Planning	No Tests to Date
Secondary Injector	Preliminary Design	In Planning	No Tests to Date

CONFIDENTIAL

CONFIDENTIAL

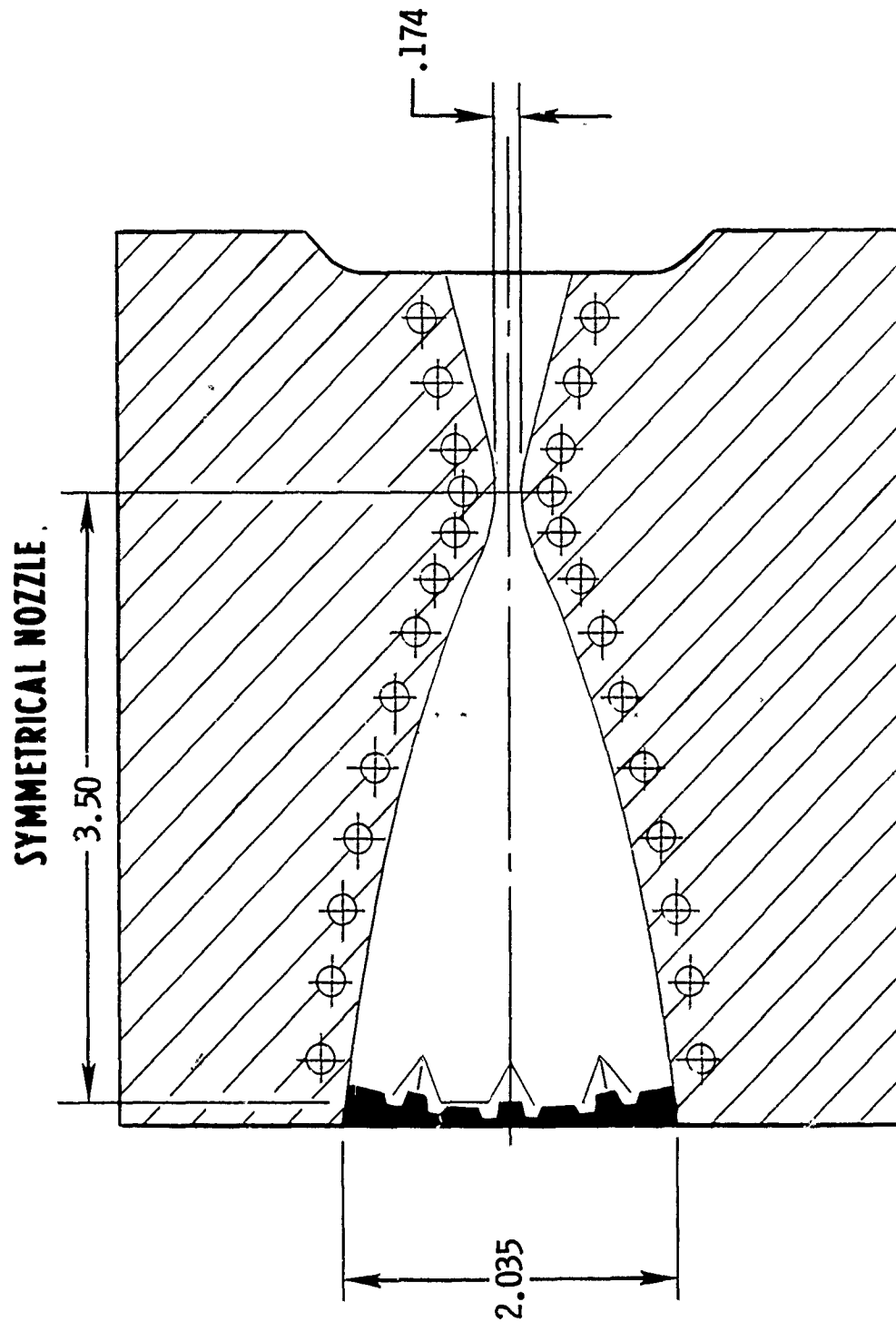
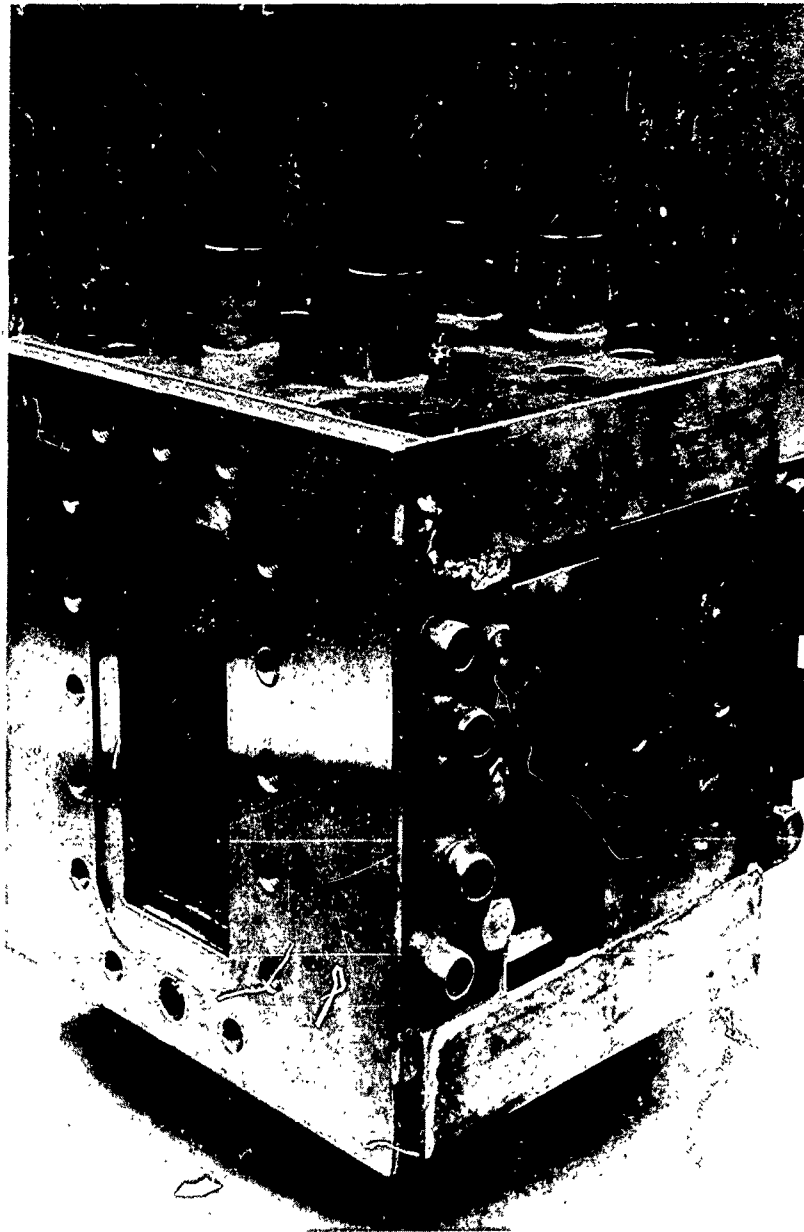


Figure 57. 5-Inch Solid-Wall Segment for G_c Combustion Chamber Contour

CONFIDENTIAL

CONFIDENTIAL



1EH32-4/23/68-C1F

Figure 58. 5-Inch Tubular-Wall Segment Assembly
Without Injector

CONFIDENTIAL

CONFIDENTIAL

The tubes for the 5-inch segment and main chamber are fabricated of Nickel 200. The thrust chamber is a furnace-brazed assembly that consists of water-cooled copper side plates and two identical tubular wall halves. The tubular wall halves are independent, and can be cooled separately (parallel) or in series. The tubular walls are tube panels that consist of tapered and formed tubes electron-beam welded together in a flat condition and then contour formed and brazed to a backup structure.

c. 30-DEGREE SOLID-WALL THRUST CHAMBER SEGMENT

(U) Design of the 30-degree, solid-wall segment is complete (Fig. 59), and fabrication is in progress. The segment is curved with the internal combustion chamber geometry duplicating that of 30-degree tubular wall segment. The combustion chamber walls and end plates are both water cooled.

d. 30-DEGREE TUBULAR-WALL THRUST CHAMBER SEGMENT

(U) Design of the 30-degree tubular wall thrust chamber (Fig. 60) was completed and fabrication was started. The outer segment body machining is completed and it is ready for tube stacking. Tube tapering and forming was completed.

2. INJECTOR DESIGN AND FABRICATION

(U) Six 5-inch injectors have been fabricated; five of these have been tested. Comparison of the basic injector types, triplet and fan, resulted in the fan pattern being selected as the basic design for the 30-degree injector. A comparison of the design details for all the injectors fabricated or in the process of being fabricated is presented in Table 13.

CONFIDENTIAL

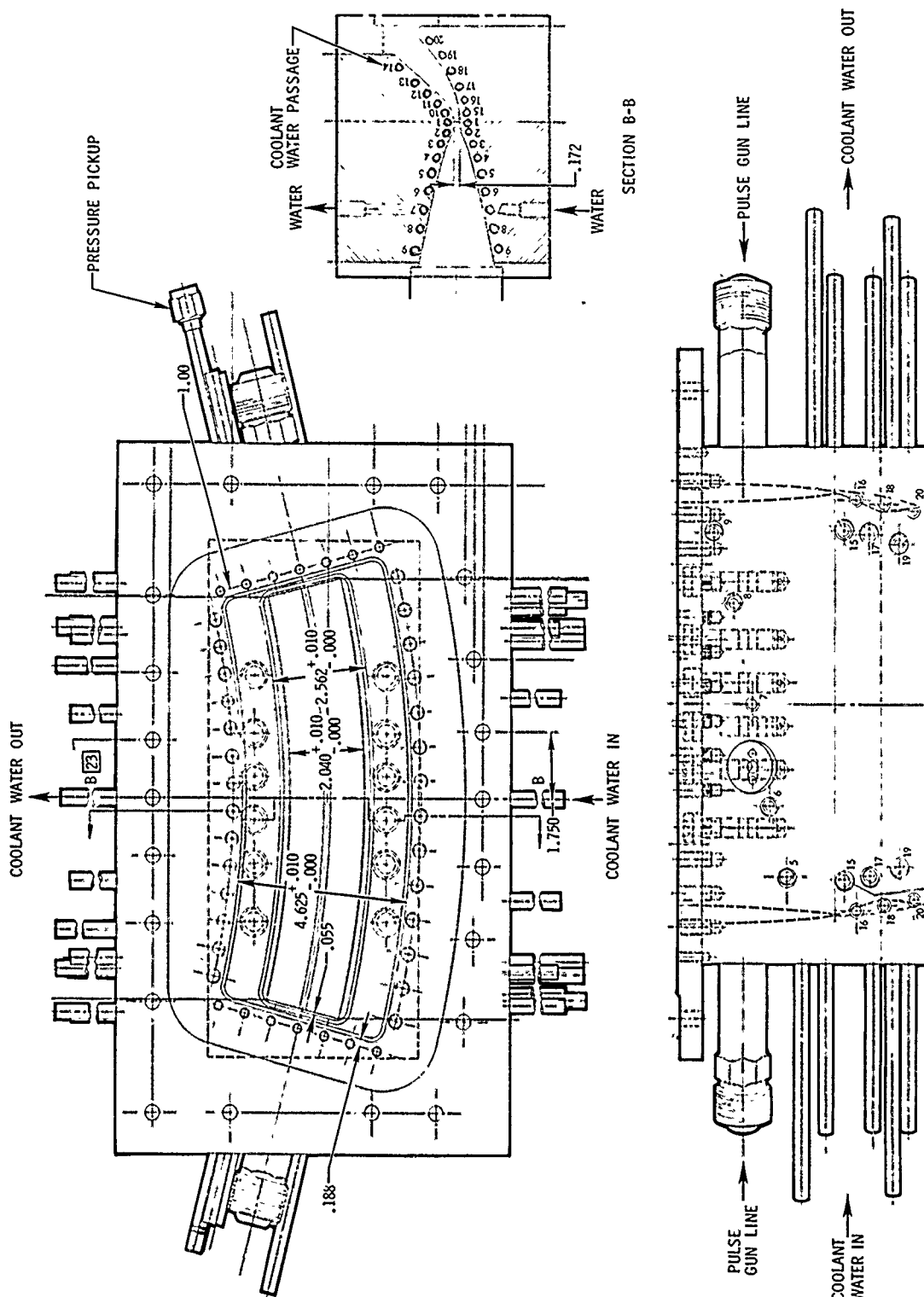


Figure 59. 30-Degree Solid-Wall Thrust Chamber Segment

CONFIDENTIAL

CONFIDENTIAL

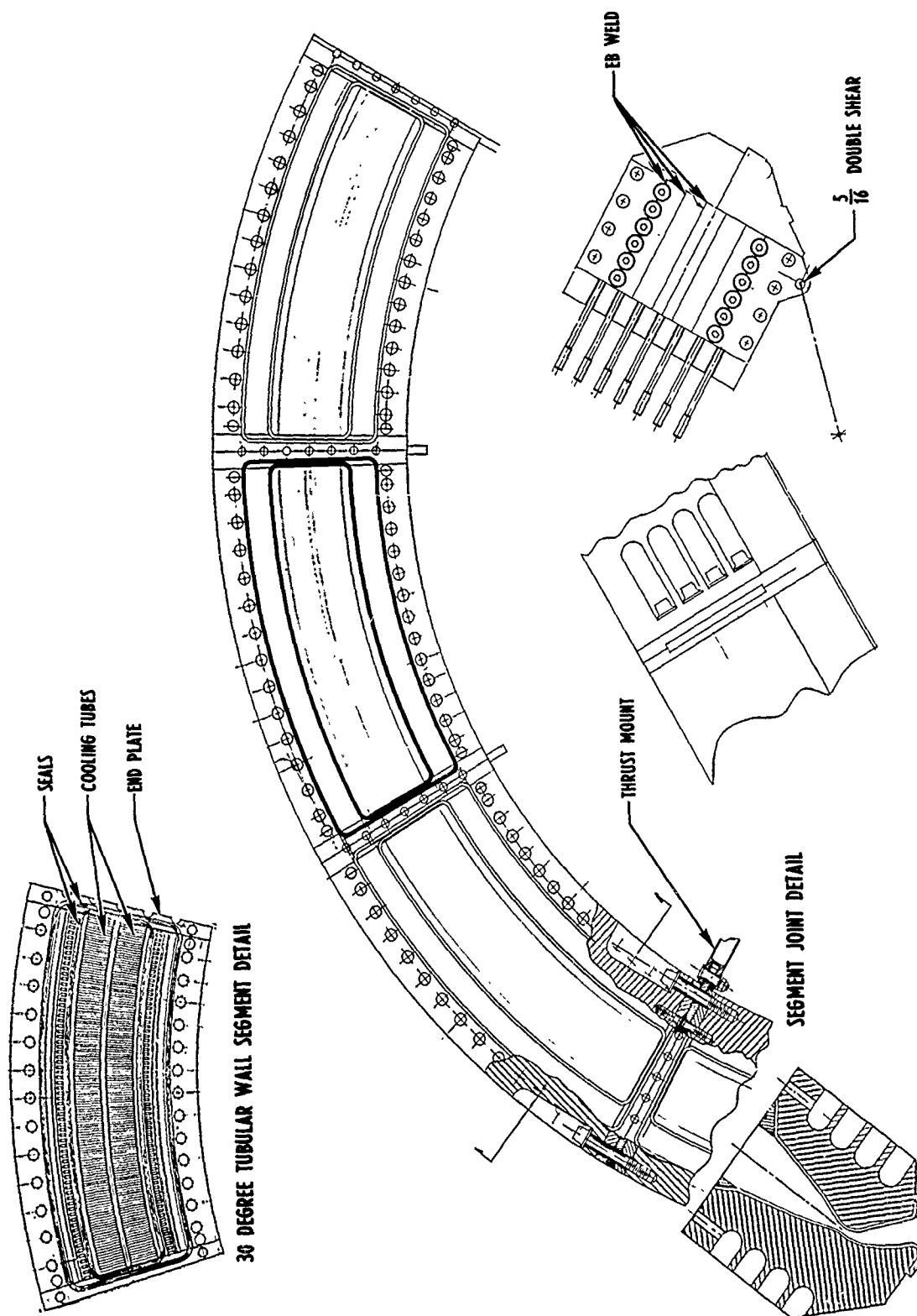


Figure 60. Main Engine Thrust Chamber Tubular-Wall Segments

CONFIDENTIAL

CONFIDENTIAL

TABLE 13
5-INCH SEGMENT INJECTOR DESIGN CHARACTERISTICS

Item	Triplet U/N 1	Triplet U/N 2	Triplet U/N 3	Fan U/N 1	Fan U/N 2	Fan U/N 3	Concentric Orifice U/N 1
Orifice Diameter Size, inches							
Fuel	0.0483	0.0483	0.035	0.026 & 0.037	0.018 & 0.028	0.018 & 0.028	0.008 Annulus
Oxidizer	0.020	0.020	0.018	0.016	0.016	0.015	0.033
Number of Orifices							
Fuel	39	39	48	117	117	117	33
Oxidizer	78	82	96	156	156	156	33
Total Orifice Area, sq in.							
Fuel	0.07133	0.07133	0.04618	0.0833	0.04386	0.04386	0.09265
Oxidizer	0.0245	0.02576	0.02443	0.0314	0.03140	0.02757	0.02822
Impingement Length-to-Diameter Ratio							
Fuel	2.98	2.98	5.20	5.9 & 8.4	7.8 & 12.2	7.8 & 12.2	--
Oxidizer	13.6	13.6	16.81	3.9 & 23.4	3.9 & 23.4	2.5 & 20.4	--
Included Impingement Angle (Oxidizer), degrees							
Preimpingement, Oxidizer	--	--	--	55	55	55	--
Final Impingement With Fuel Showerhead	68	68	60	65	65	65	--
Impingement Distance (Fuel Orifice Face to Impingement Point), inches							
	0.144	0.144	0.182	0.219	0.219	0.219	--
Number of Strips	3	3	3	3	3	3	3 (rows)
Number of Elements	39	39	48	39	39	39	33
Injector Face Size, inches	2 x 5	2 x 5	2 x 5	2 x 5	2 x 5	2 x 5	2 x 5
Curcuated Pressure Drop at 650-psia Chamber Pressure, psid							
Fuel	216	216	350	202	350	350	100
Oxidizer	316	316	316	272	272	350	306
Injection Density (elements/sq in.)	3.9	3.9	4.8	3.9	3.9	3.9	3.3
Element-to-Wall Cant Angle, degrees	30	30	30	30	30	30	--

CONFIDENTIAL

CONFIDENTIAL

Fabrication of triplet injectors U/N 1 and U/N 2 and fan injector U/N 1 was completed in the previous report period.

a. 5-INCH SEGMENT INJECTORS

(U) The third triplet injector design, U/N 3, was modified from the first and second triplet injectors. The fuel orifices were drilled to smaller diameter, feed control webs were added to increase the oxidizer feed velocity, and turbulence inducers were installed in the oxidizer strip to produce uniform temperature across the feed passage. The injector is shown in Fig. 61.

(U) The second fan injector was modified similarly to the third triplet injector and is shown in Fig. 62.

(U) Fabrication of the concentric orifice injector segment was completed and the injector is shown in Fig. 63.

(U) Design details of these injectors were discussed in the first quarterly report.

(C) Design of the third fan injector was completed and fabrication is 90-percent complete. The design (Fig. 64) has been modified from the first two fan injectors in that the oxidizer orifices have been drilled to a smaller diameter, and the oxidizer protrusions have been removed from the injector face. These changes were made to improve cooling.

(U) Flow tests were completed on the third triplet injector, the second and third fan injector, and the concentric orifice injector. All injectors were flow calibrated and cleaned prior to hot firing, as described in the previous quarterly report.

CONFIDENTIAL

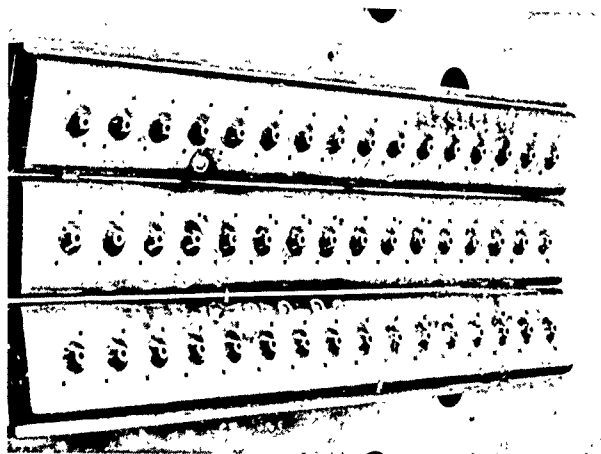
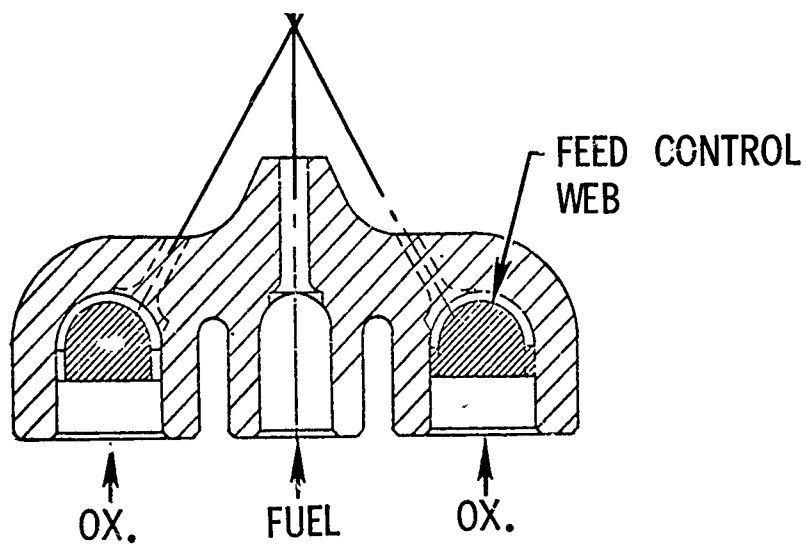


Figure 61. Modified 5-Inch Triplet Injector Segment (U/N 3)

CONFIDENTIAL

CONFIDENTIAL

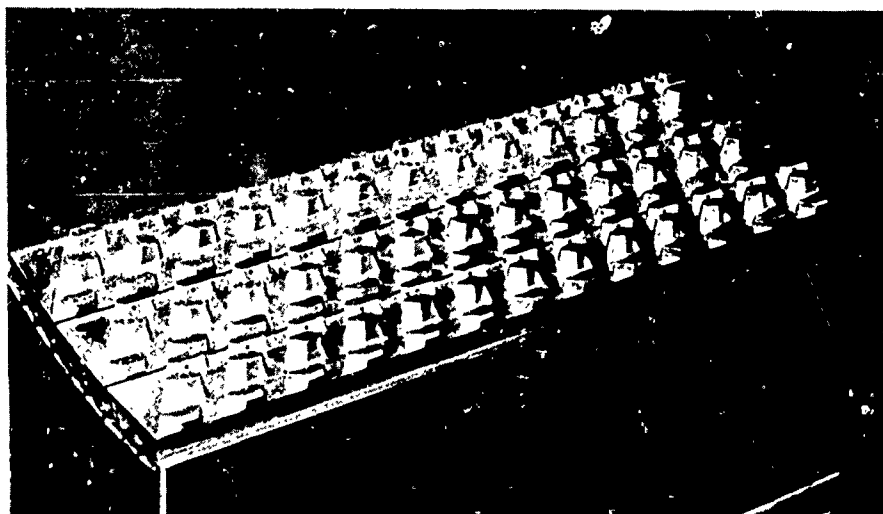
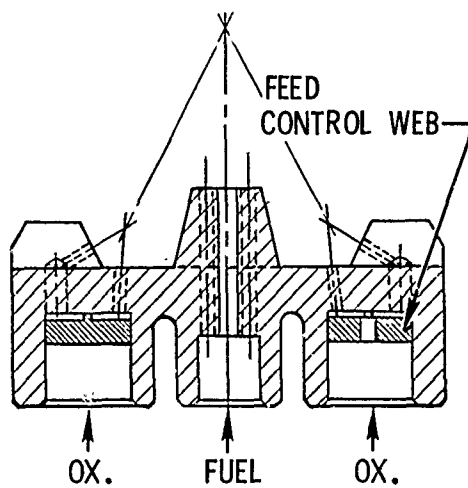


Figure 62. 5-Inch Fan Injector Segment (U/N 2)

CONFIDENTIAL

CONFIDENTIAL

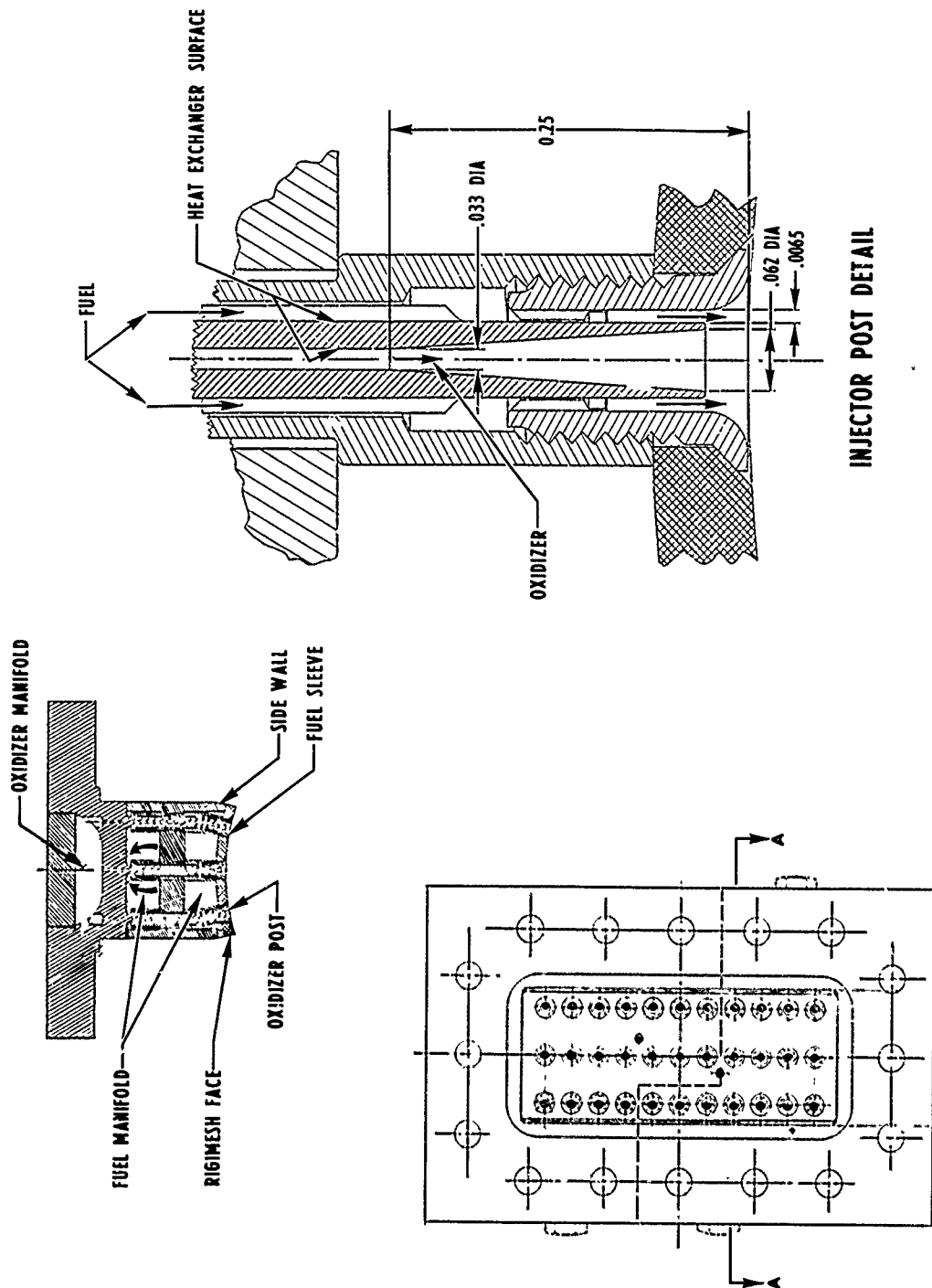


Figure 63. 5-Inch Concentric Orifice Injector

CONFIDENTIAL

CONFIDENTIAL

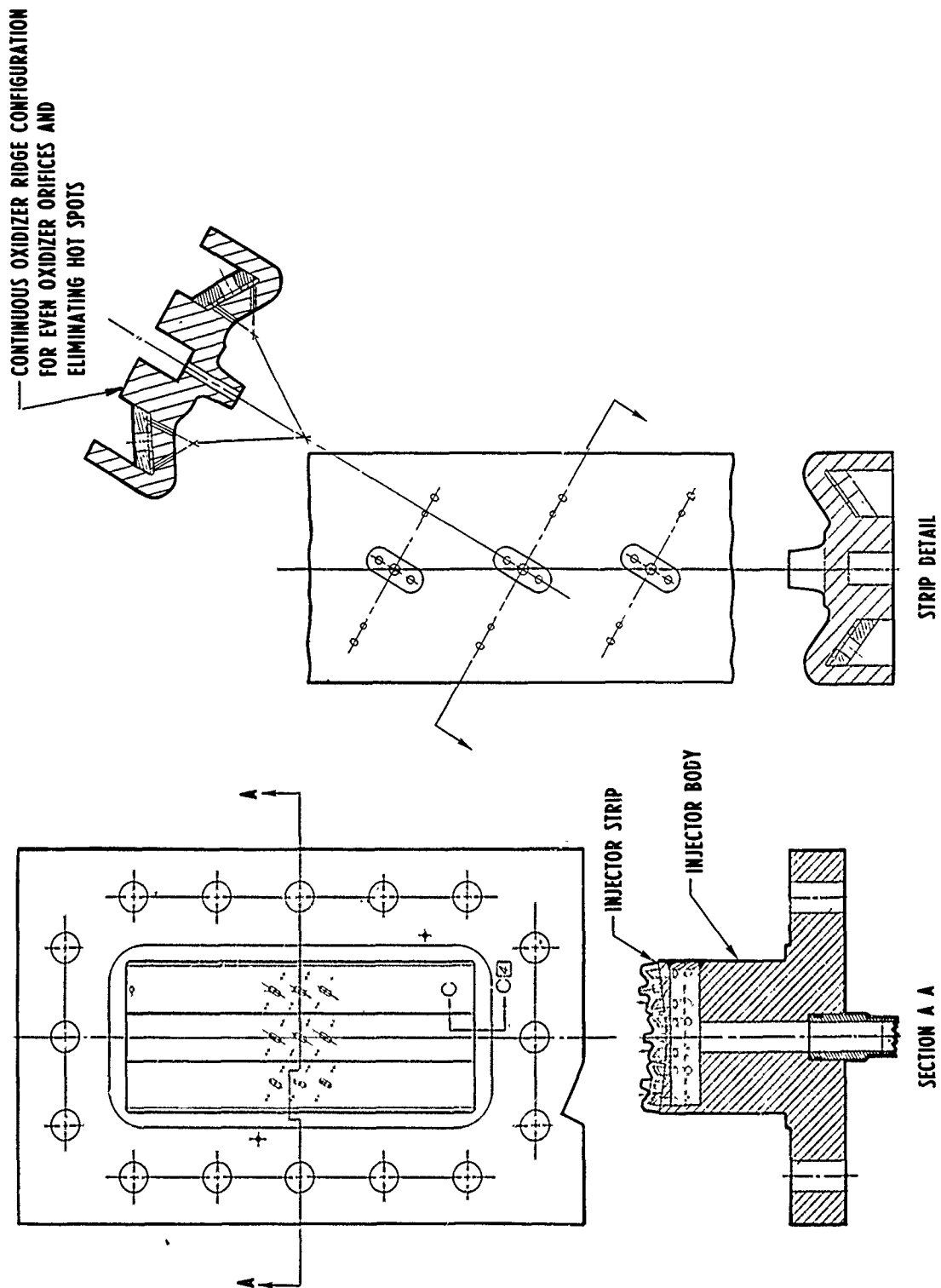


Figure 64. Modified 5-Inch Fan Injector (U/N 3)

CONFIDENTIAL

CONFIDENTIAL

b. 30-DEGREE INJECTORS

(U) Design of the first 30-degree segment injector (U/N 1) was completed and fabrication was initiated. This design, shown in Fig. 65, is basically the same configuration as the second 5-inch fan injector (U/N 2).

(U) A modified design approach is being considered for the second unit, which permits fabrication of the injector without furnace brazing or extensive welding. The design (Fig. 66) utilizes radially drilled feed passages for both propellants. Fabrication of an injector of this configuration will depend on the satisfactory results of a 5-inch segment prototype which is planned for evaluation.

3. SEGMENT THRUST CHAMBER TESTING

(U) A building block segment approach has been established to develop the main thrust chamber assembly. Tests are to be accomplished in sequence; first with 5-inch segments, then, with 30-degree and 60-degree segments before the complete thrust chamber is tested. The planned test schedule is shown in Fig. 67.

a. 5-INCH SOLID-WALL THRUST CHAMBER SEGMENT TESTING

(U) A total of 40 5-inch solid-wall segment tests were accomplished during this report period. The test data is presented in Table 14 and discussed in the following paragraphs. The initial 10 tests were reported in the first quarterly progress report. A test stand installation and firing is shown in Fig. 68.

(1) Tests 011 through 017

(C) The test hardware assembly consisted of the fan injector (U/N 1) and the G_c contour, solid-wall thrust chamber (U/N 1). The test objectives were:

1. Evaluation of injector face heat transfer and cooling capability

CONFIDENTIAL

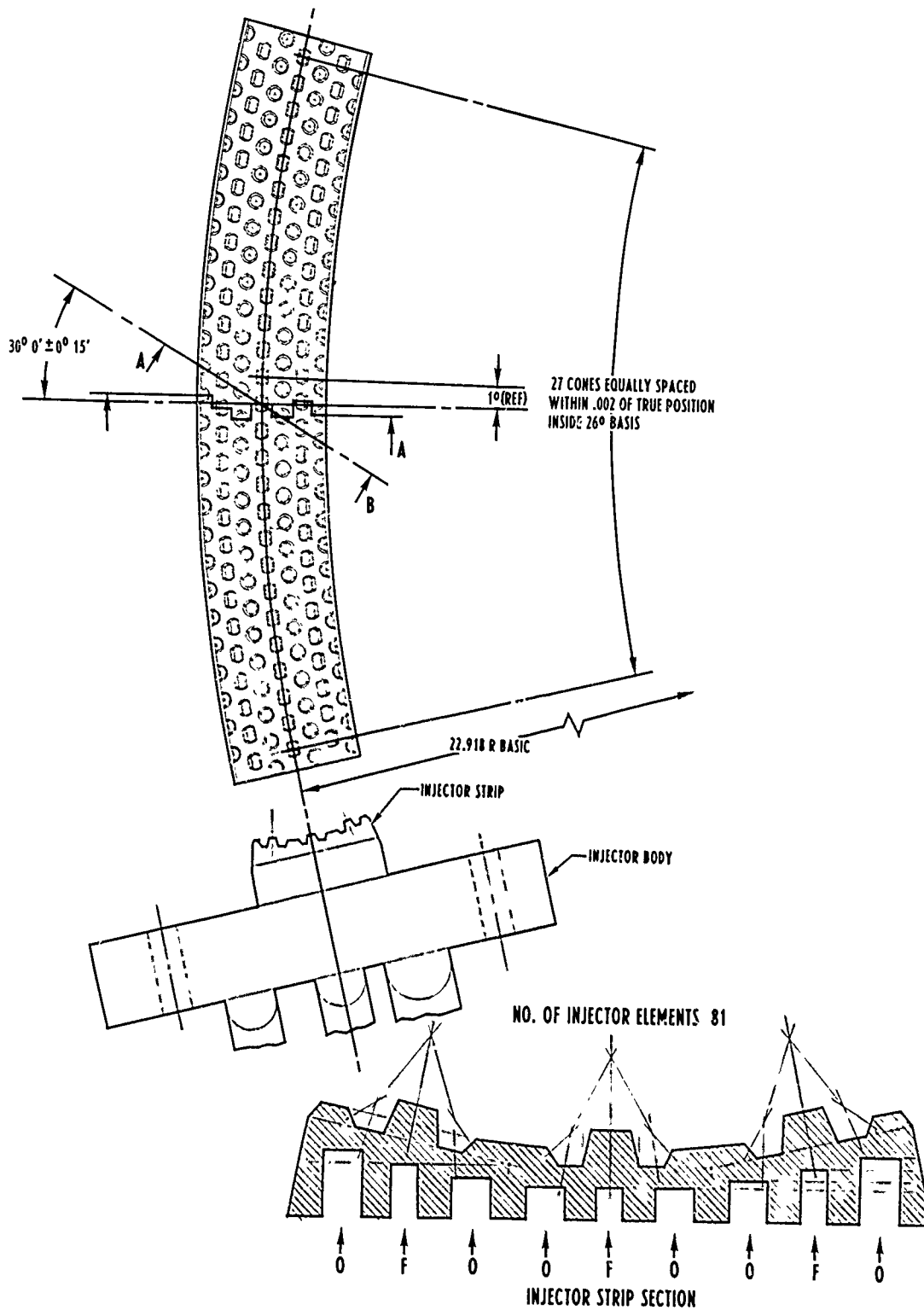


Figure 65. 30-Degree Fan Injector Segment (U/N 1)

CONFIDENTIAL

CONFIDENTIAL

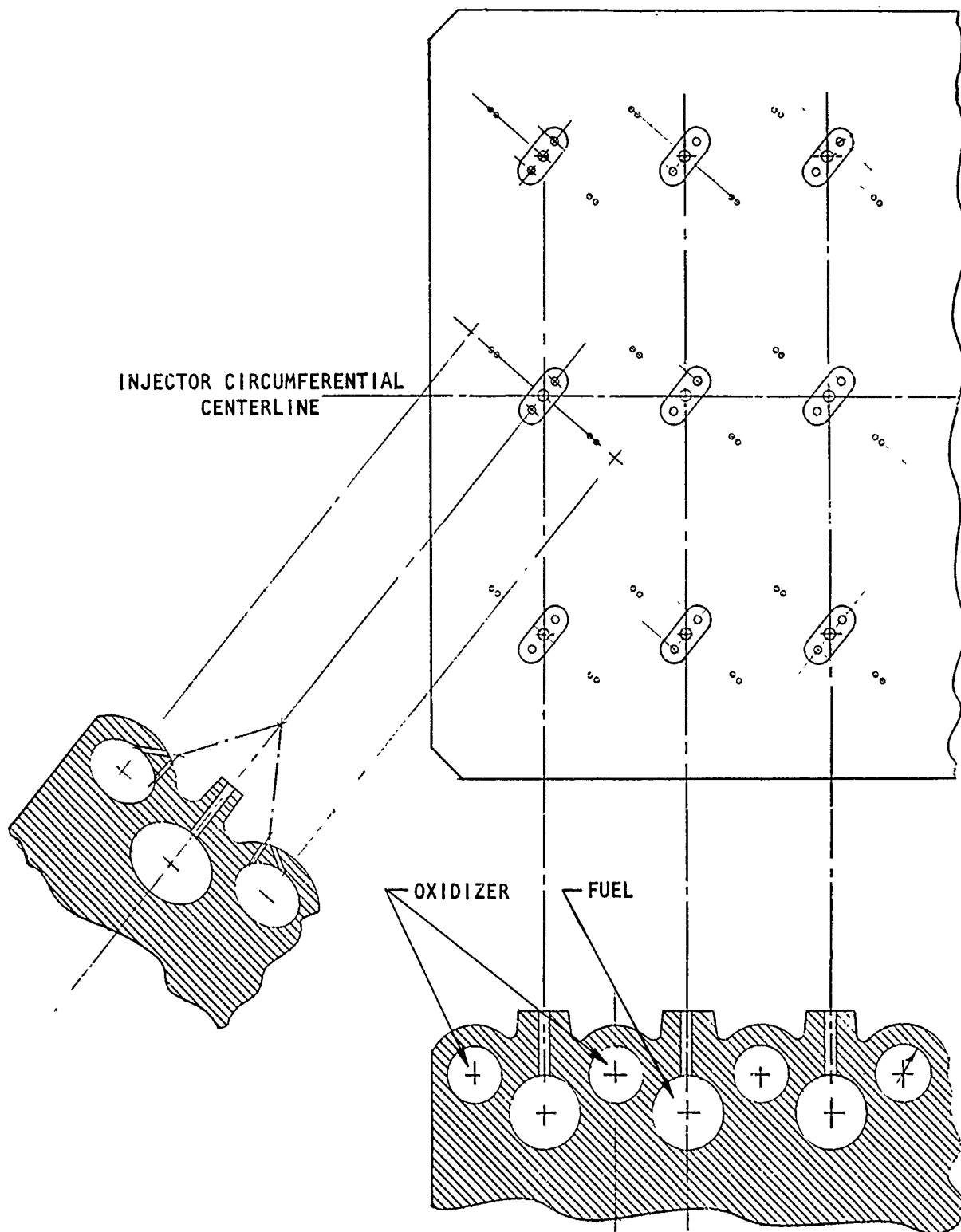
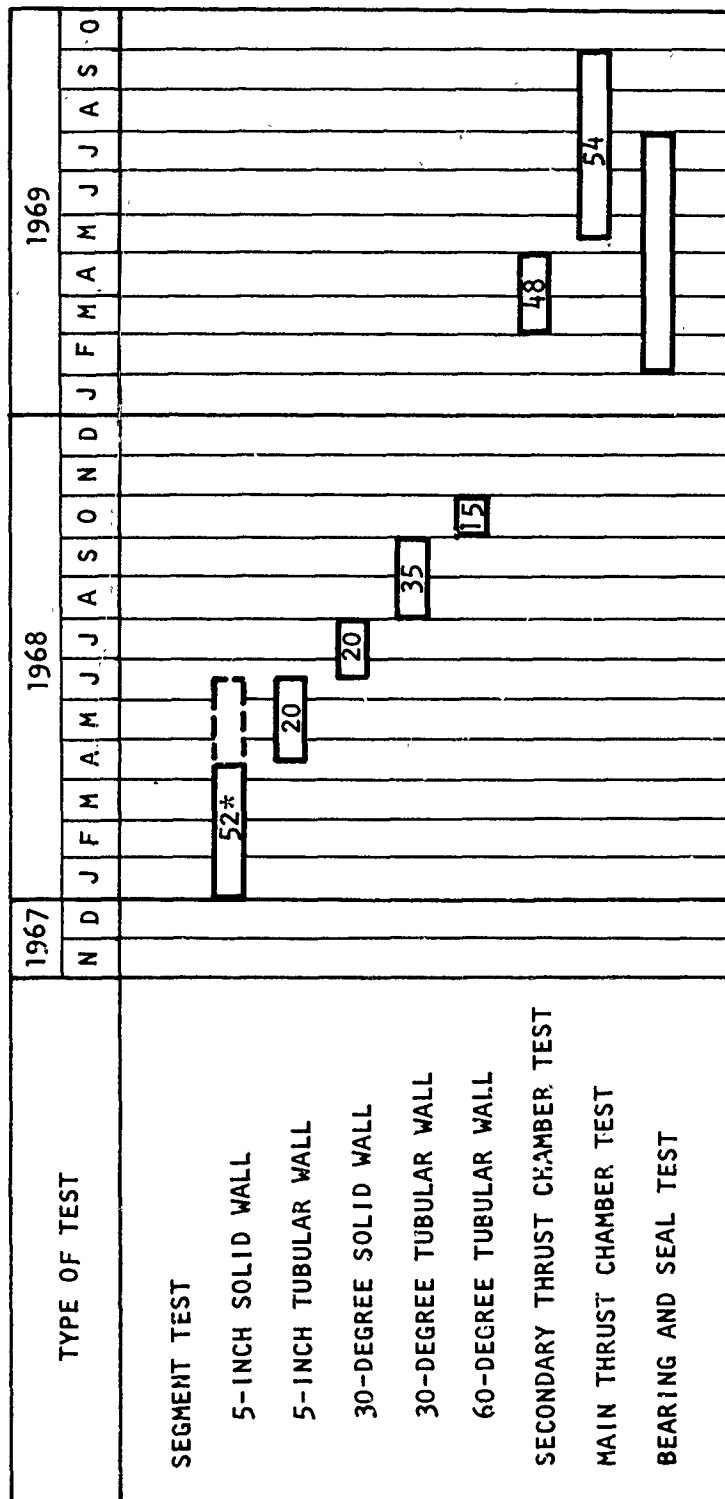


Figure 66. Fan Injector With Radial Drilled Propellant Feed Passages

CONFIDENTIAL

CONFIDENTIAL



* NUMBER OF FIRING TESTS PLANNED

Figure 67. Critical Component Demonstration Test Schedule

CONFIDENTIAL

CONFIDENTIAL

TABLE 14
5-INCH INJECTOR AND SOLID-WALL SEGMENT THRUST CHAMBER TEST SUMMARY

Test Date, No. 1968	Chamber Segment	Injector	Test Duration, seconds	Chamber Pressure, psia	Injector Flow, lb/sec	Mixture Ratio, o/f	Fuel Injection Temperature, °R	Throat Heat Flux Btu/sq in.-sec	Injector-End Heat Flux Btu/sq in.-sec	Characteristic Velocity (From Chamber Pressure), ft/sec	Corrected Characteristic Velocity Efficiency, Percent		Momentum Ratio $\frac{V_o}{V_{eff}} \times 10^3$	Remarks
											From Chamber Pressure	From Thrust		
1 1-5	C #1	Triplet U/S 1	0.6	350	0.91	8.1	Instrument Malfunction	11.7	2.97	—	—	—	—	No Hardware Damage
2 1-5	C #1	Triplet U/S 1	1.6	355	0.94	8.4	Instrument Malfunction	13.4	3.65	*	*	*	*	Slight Injector Face Overheating
3 1-9	C #1	Triplet U/S 1	2.2	345	0.91	9.1	1083	14.05	10.1	*	*	*	*	Injector Face Overheated
4														
5														
6														
Facility Checkout tests With Stand Activation Hardware														
7 1-19	C #1	Triplet U/S 2	1.0	337	1.11	12.7	798	12.1	3.9	*	*	*	*	Slight Injector Face Overheating
8 1-23	C #1	Triplet U/S 2	1.15	322	1.270	14.35	1018	12.5	7.81	*	*	*	*	Slight Injector Face Overheating
9 1-25	C #1	Triplet U/S 2	1.15	197	7.878	14.5	980	8.5	5.99	*	*	*	*	Slight Injector Face Overheating
10 1-26	C #1	Triplet U/S 2	1.0	559	1.954	13.58	1222	21.3	13.1	*	*	*	*	Injector Face Overheated
11 2-2	C #1	Fan U/S 1	0.6	352	1.270	14.76	1144	14.2	2.0	*	*	*	*	No Hardware Damage
12 2-2	C #1	Fan U/S 1	1.0	353	1.239	14.16	954	14.75	2.12	*	*	*	*	No Hardware Damage
13 2-5	C #1	Fan U/S 1	0.7	484	1.769	14.49	1266	17.4	3.44	*	*	*	*	No Hardware Damage
14 2-5	C #1	Fan U/S 1	1.25	509	1.759	14.61	1162	18.4	3.21	*	*	*	*	No Hardware Damage
15 2-5	C #1	Fan U/S 1	0.75	643	2.233	13.88	1344	19.55	3.34	*	*	*	*	No Hardware Damage
16 2-7	C #1	Fan U/S 1	3.0	627	2.216	14.15	1127	21.97	4.46	*	*	*	*	No Hardware Damage; Instru- mentation Difficulty
17 2-7	C #1	Fan U/S 1	1.4	655	2.250	13.5	1433	22.9	3.73	*	*	*	*	No Hardware Damage; Low Mixture Ratio
18 2-10	K	Fan U/S 1	2.0	260	0.760	7.9	1285		3.20	*	*	*	*	No Hardware Damage; Low Mixture Ratio
19 2-10	K	Fan U/S 1	2.0	256	0.760	9.5	1310	11.5	1.52	*	*	*	*	

*Instrumentation difficulty

CONFIDENTIAL

CONFIDENTIAL

TABLE 14

(Continued)

Test Date, Chamber No.	Chamber Segment	Injector	Test Duration, seconds	Chamber Pressure, psia	Injector Flow, lb/sec	Mixture Ratio, o/f	Fuel Injection Temperature, R	Throat Heat Flux, Btu/sq in.-sec	Injector-End Heat Flux, Btu/sq in.-sec	Characteristic Velocity (From Chamber Pressure), ft/sec	Corrected Characteristic Velocity Efficiency, percent	From Chamber Pressure	From Throat	Momentary Ratio $\frac{\dot{V}_0}{\dot{V}_g}$	$\frac{\dot{V}_0}{\dot{V}_g} \times 10^3$	Remarks
20 2-10	K	Fan U/N 1	2.0	355	1.2143	13.80	1319	14.2	2.97	8000	96.3	97.9	4.08	4.268	4.268	No Hardware Damage
21 2-10	K	Fan U/N 1	2.0	506	1.727	13.6	1356	17.6	2.64	8050	95.9	98.17	2.80	4.385	4.385	No Hardware Damage
22 2-10	K	Fan U/N 1	1.8	645	2.086	12.9	1446	20.35	3.4	8160	99.3	101.4	2.62	3.88	3.88	Slight Fuel Trapezoid Melting
23 2-13	K	Fan U/N 1	1.0	638	2.165	13.6	524	17.1	9.45	8075	97.2	100.6	0.855	11.438	11.438	Injector Face Overheating
24 2-16	K	Fan U/N 1	19.0	355	1.1492	13.16	1432	11.07	3.22	8467	101.4	104.3	4.45	4.125	4.125	No Additional Hardware Damage
25 2-16	K	Fan U/N 1	9.0	236	0.7670	14.60	1371	10.9	1.91	8415	105.2	106.0	5.65	4.807	4.807	No Additional Hardware Damage
26 2-23	G _c #2	Fan U/N 1	3.5	65	0.248*	14.7	1128	5.64	3.75	**	**	**	**	**	**	No Additional Hardware Damage; Instrumentation Difficulty**
27 2-23	G _c #2	Fan U/N 1	9.0	65	0.248*	14.7	1243	6.1	4.14	**	**	**	**	**	**	Injector Face Overheating; Instrumentation Difficulty**
28 3-1	G _c #2	Triplet U/N 3	0.7	368	1.280	14.40	1240	15.4	1.67	8005	96.7	99.0	4.27	5.001	5.001	No Hardware Damage
29 3-1	G _c #2	Triplet U/N 3	2.3	371	1.296	14.60	1380	16.3	2.21	7961	96.0	98.3	4.4	2.877	2.877	No Hardware Damage
30 3-1	G _c #2	Triplet U/N 3	7.0	374	1.304	14.90	1467	16.71	3.47	7970	96.2	99.4	4.56	2.738	2.738	No Hardware Damage
31 3-5	G _c #2	Triplet U/N 3	0.7	611	2.170	13.91	1360	22.5	5.5	7823	95.78	96.0	2.90	2.50	2.50	No Hardware Damage; Slight Oxidizer Strip Overheating
32 3-5	G _c #2	Triplet U/N 3	0.1	—	—	—	1330	—	—	—	—	—	—	—	—	Chamber Burnout Due to Lack of Water Coolant, No Injector Damage
33 3-8	G _c #1	Triplet U/N 3	1.2	361	1.278	14.28	1160	15.2	2.3	7952	97.13	97.16	3.88	3.28	3.28	No Hardware Damage
34 3-8	G _c #1	Triplet U/N 3	15.0	375.6	1.264	14.15	1452	16.92	2.41	8257	99.1	102.19	5.38	2.65	2.65	No Additional Hardware Damage
35 3-8	G _c #1	Triplet U/N 3	2.6	515.9	1.772	13.84	1310	20.4	3.65	8090	96.2	98.68	3.45	2.67	2.67	Slight Additional Oxidizer Strip Overheating
36 3-12	G _c #1	Triplet U/N 3	0.7	513.2	1.765	14.11	1285	19.9	4.27	8075	96.3	98.58	3.16	2.85	2.85	No Additional Hardware Damage

*Estimated
**Instrumentation difficulty

CONFIDENTIAL

CONFIDENTIAL

TABLE 14
(Concluded)

Test Date, No. 1968	Chamber Segment	Injector	Test Duration, seconds	Chamber Pressure, psia	Injector Flow, lb/sec	Mixture Ratio, o/f	Fuel Injection Temperature, °F	Throat Heat Flux Btu/sq in.-sec	Injector-End Heat Flux Btu/sq in.-sec	Characteristic Velocity (From Chamber Pressure), ft/sec	Corrected Characteristic Velocity Efficiency, Percent From Chamber Pressure	From Throat	Momentum Ratio $\frac{V_o}{V_{th}}$	$\frac{V_o}{V_{th}} \times 10^3$	Remarks
37 3-12	G _c #1	Triplet U/N 3	0.5	—	—	—	1175	—	—	—	—	—	—	—	Injector Overheating and Strip Fatigue Failure; Instrumentation Difficulty
38 3-25	G _c #1	Fan U/N 2	0.7	382.5	1.402	16.02	1145	17	1.4	8260	98.2	99.76	5.4	3.12	No Hardware Damage
39 3-27	G _c #1	Fan U/N 2	2.6	377.6	1.292	14.69	1324	18.3	1.01	8018	98.4	99.45	6.4	2.66	No Hardware Damage
40 3-27	G _c #1	Fan U/N 2	10.0	385.6	1.449	16.67	1160	18.2	1.48	8163	97.2	99.74	6.2	2.62	No Hardware Damage
41 3-29	G _c #1	Fan U/N 2	1.5	520.4	1.757	14.39	1340	21.35	2.14	8218	97.9	100.36	4.17	2.80	No Hardware Damage
42 3-29	G _c #1	Fan U/N 2	10.0	525.8	1.792	14.33	1423	21.4	2.49	8268	97.9	100.56	2.07	2.66	No Hardware Damage
43 3-29	G _c #1	Fan U/N 2	1.5	634.8	2.2042	14.39	1342	24.8	2.92	8243	97.4	100.52	3.38	2.76	No Hardware Damage
44 4-3	G _c #1	Fan U/N 2	9.2	661	2.1996	13.70	1493	25.1	3.53	8329	98.3	103.54	4.10	2.25	Slight Fuel and Oxidizer Trapsold Melting
45 4-3	G _c #1	Fan U/N 2	3.0	220.8	0.7874	14.94	1269	12.6	0.81	*	*	*	*	*	No Additional Hardware Damage; Oxidizer Contamination
46 4-3	G _c #1	Fan U/N 2	8.0	222.2	0.792	15.16	1362	13.3	0.93	*	*	*	*	*	No Additional Hardware Damage; Oxidizer Contamination
47 4-3	G _c #1	Fan U/N 2	18.5	207.9	0.7642	13.92	1449	13.2	0.93	*	*	*	*	*	No Additional Hardware Damage; Oxidizer Contamination
48 4-3	G _c #1	Fan U/N 2	19.0	150.9	0.4783	12.94	1405	8.5	1.9	*	*	*	*	*	No Additional Hardware Damage; Oxidizer Contamination
49 4-3	G _c #1	Fan U/N 2	8.3	94.6	0.3611	14.63	1269	7.2	1.63	*	*	*	*	*	No Additional Hardware Damage; Oxidizer Contamination
50 4-3	G _c #1	Fan U/N 2	4.0	72.5	0.3041	14.1	1027	6.0	1.63	*	*	*	*	*	No Additional Hardware Damage; Oxidizer Contamination
51 4-30	5TWC	Fan U/N 2	0.300	439	1.295	8.6	1482	—	—	—	—	—	—	—	Thrust Chamber and Injector Damage

*Oxidizer contamination

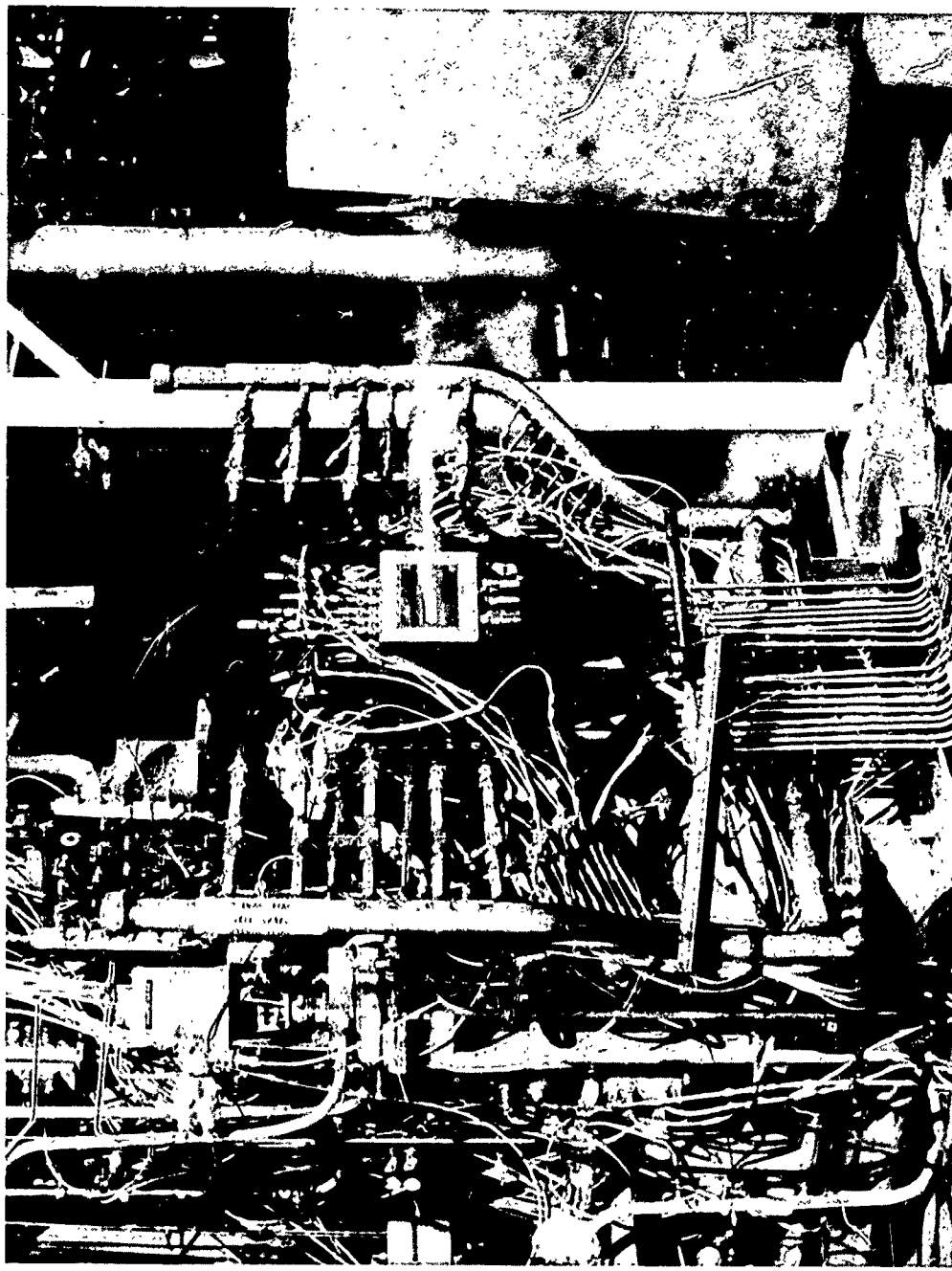


Figure 68. 5-Inch Solid-Wall Thrust Chamber Segment
at Victor Test Stand

CONFIDENTIAL

2. Evaluation of injector/chamber contour c^* performance
3. Evaluation of the chamber wall heat transfer characteristics

(U) All tests were satisfactory, and all test objectives were met. Slight erosion of several fuel trapezoids (face extensions required to maintain proper orifice L/D) occurred. The overall injector condition was excellent, and there was no evidence of face overheating or thermal fatigue failure of the strips. Test 017 was accomplished at the maximum nominal design point of chamber pressure, fuel inlet temperature, and mixture ratio.

(U) Low-frequency chamber pressure oscillations, approximately 3 Hz, were noted on the longer duration tests. The oscillations were apparent in the chamber pressure, fuel injection pressure, and oxidizer injection pressure measurements. It was determined that the oxidizer injection pressure oscillations had the greatest magnitude and caused oscillations in chamber pressure and fuel injection pressure.

(U) A combined heat transfer and hydrodynamic analysis was conducted to determine the cause of the oscillations and provide design criteria to circumvent the problem. A total quantitative solution could not be obtained, although the following qualitative conclusions were drawn;

1. The oxidizer was undergoing a phase change, liquid to two phase, in the subcritical and supercritical pressure regime.
2. Unstable film boiling and temperature stratification of the oxidizer were occurring in the feed passages behind the injector face.
3. The oxidizer conditions in the feed passages combined with the existing heat flux were evaluated against criteria established (Ref. 2).

(U) The criteria established in Ref. 2 defines stable and unstable flow regimes as a function of heat flux and coolant parameters. This criteria has been used and verified during the design and test of liquid

CONFIDENTIAL

oxygen and liquid hydrogen heat exchangers at Rocketdyne. Application of this criteria to the oxidizer injection conditions indicated that unstable film boiling existed in the feed passages behind the impinging fan injector face.

(U) Design modifications, based on this criteria, were incorporated in the second fan injector and subsequent injectors.

(2) Tests 018 through 025

(U) The test hardware consisted of the impinging fan injector, U/N 1, and the K-contour, solid-wall thrust chamber. The primary test objectives were the same as tests 011 through 017.

(C) Tests 020 through 025 were satisfactory, and all test objectives were obtained. Because of the low-frequency chamber pressure oscillations which occurred previously, test 023 was conducted to evaluate the effect of hydrogen injection temperature on the oxidizer injector flow instability. The use of ambient hydrogen did result in the cessation of chamber pressure oscillations, but a high injector face heat flux due to low hydrogen injection velocity was encountered and resulted in overheating of the injector face.

(3) Tests 026 and 027

(C) The test hardware consisted of the impinging fan injector, U/N 1, and the G_c contour, solid-wall thrust chamber, U/N 2. The primary test objectives were the same as tests 011 through 025, with the tests to be conducted at the minimum design chamber pressure (approximately 70 psia).

(C) Test 026 was a satisfactory 3.5 second test. Test 027 was terminated by the test observer after 9.0 seconds because of exhaust flame pattern

CONFIDENTIAL

color changes. Posttest inspection revealed injector face overheating and erosion. Although face overheating was realized, thermal fatigue of the injector strips was not evident.

(U) Analysis indicated failure due to higher than design face heat flux. Additional discussion is presented in the subsequent Test Analysis section.

(4) Tests 028 through 032

(U) The test hardware assembly consisted of the modified triplet injector, U/N 3, and the G_c , U/N 2, solid-wall thrust chamber. The test objectives were:

1. Injector face heat transfer and cooling capability
2. Injector-chamber contour c^* performance capability
3. Evaluation of the injector-chamber contour heat transfer characteristics

(U) Tests 028 through 031 were satisfactory and without incident.

(C) Test 032 was scheduled for a relatively long duration at 650 psia chamber pressure. The test was terminated by the test observer during transition to mainstage because of exhaust flame discoloration. Post-test inspection revealed chamber throat region overheating and erosion. Investigation revealed the cause of failure to be lack of thrust chamber coolant water. The coolant water had been inadvertently stopped just prior to automatic sequence start.

(U) A review of all operating procedures, safety interlocks, etc., was conducted, and required changes were immediately instituted to prevent a recurrence of the incident.

CONFIDENTIAL

(5) Tests 033 through 037

(U) Tests 033 through 037 were a continuation of the modified triplet (U/N 3) evaluation using the G_c , U/N 1 thrust chamber. Tests 033 through 036 were satisfactory and of the programmed durations.

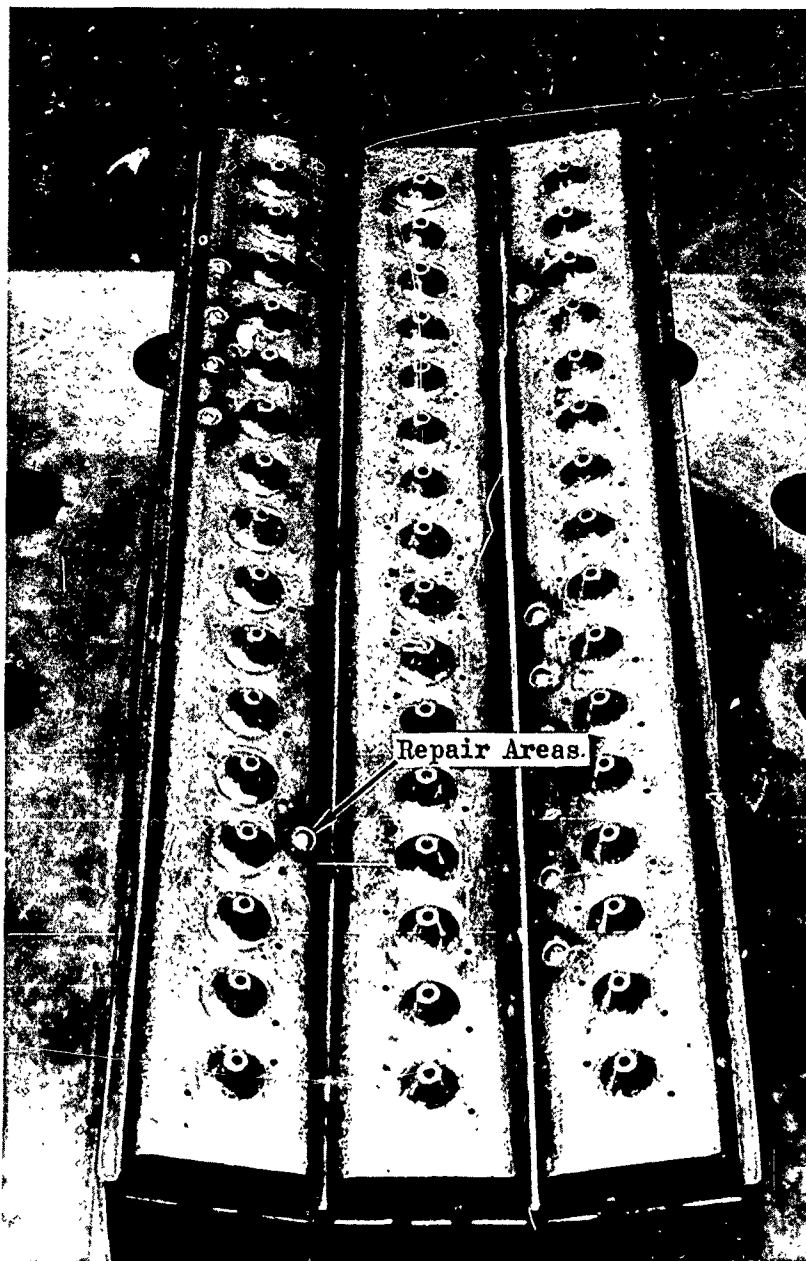
(C) Test 037 was terminated by the test observer during transition to mainstage because of exhaust flame discoloration. Posttest inspection revealed apparent fatigue failure of an injector oxidizer strip because of localized overheating. Oxidizer feed passage restrictions consisting of braze alloy were considered to be the cause of the local overheating.

(U) During previous initial water-flow checkout tests it was determined that there were restrictions due to braze flow in the oxidizer feed passages immediately behind the injector face. This problem was resolved by electrical discharge machine drilling of auxiliary feed passages. This necessitated drilling through the injector strip face to achieve these repairs. These holes were subsequently plugged by electron beam welding after necessary repairs were made. The twelve repair areas are shown in Fig. 69. A satisfactory water flow check was completed following the repair.

(6) Tests 038 through 043

(U) The test hardware assembly consisted of the modified fan injector (U/N 2) and the G_c (U/N 1) solid-wall thrust chamber. The tests were satisfactory and were of programmed duration. Test objectives were met; however, the throat heat transfer rates were slightly higher than on previous tests. It appeared that the numerous thermal cycles experienced by the G_c , U/N 1, thrust chamber had led to a degeneration of the chamber wall in the throat region. This degeneration consists of slight waviness of the wall and surface roughness. The throat region was repeatedly polished for satisfactory removal of the roughness, but

CONFIDENTIAL



1EH42-2/29/68-C1A

Figure 69. 5-Inch Triplet Injector U/N 3 With Repair

CONFIDENTIAL

CONFIDENTIAL

the waviness condition (yielding of the thin walls in line with coolant passages) could not be corrected without a significant delay in the test program. The injector received only slight flame polishing and there was no evidence of serious face overheating or deterioration.

(7) Tests 043 through 050

(U) The test hardware assembly consisted of the modified fan injector (U/N 2) and the G_c (U/N 1) solid-wall thrust chamber. The tests were satisfactory and were of programmed duration. Characteristic velocity performance at the lower chamber pressures was unusually low (tests 045 through 050).

(C) An immediate chemical analysis of the fluorine in the gas bottles was performed, and 6 percent by weight of air was found in the fluorine. Because of the fluorine contamination and an inability to fix the absolute level of contamination during the test, the performance computed for tests 045 through 050 is not considered to be an accurate prediction of the injector performance at the low chamber pressure operating points. A discussion of injector face heat transfer and performance is provided in subsequent paragraphs.

b. 5-INCH TUBULAR-WALL THRUST CHAMBER SEGMENT TEST

(C) The test hardware assembly consisted of the modified fan injector (U/N 2) and the 5-inch tubular wall throat chamber (Test 051). The segment chamber assembly with the coolant circuit illustrated is shown in Fig. 70. The initial test, following coolant system blowdowns, was scheduled for 1-second duration as a checkout test. The test was terminated prematurely because of damage to the thrust chamber and injector. The test was completed at the end of the report period; the failure analysis has not been completed. The complete results of this analysis will be presented in the next quarterly report.

CONFIDENTIAL

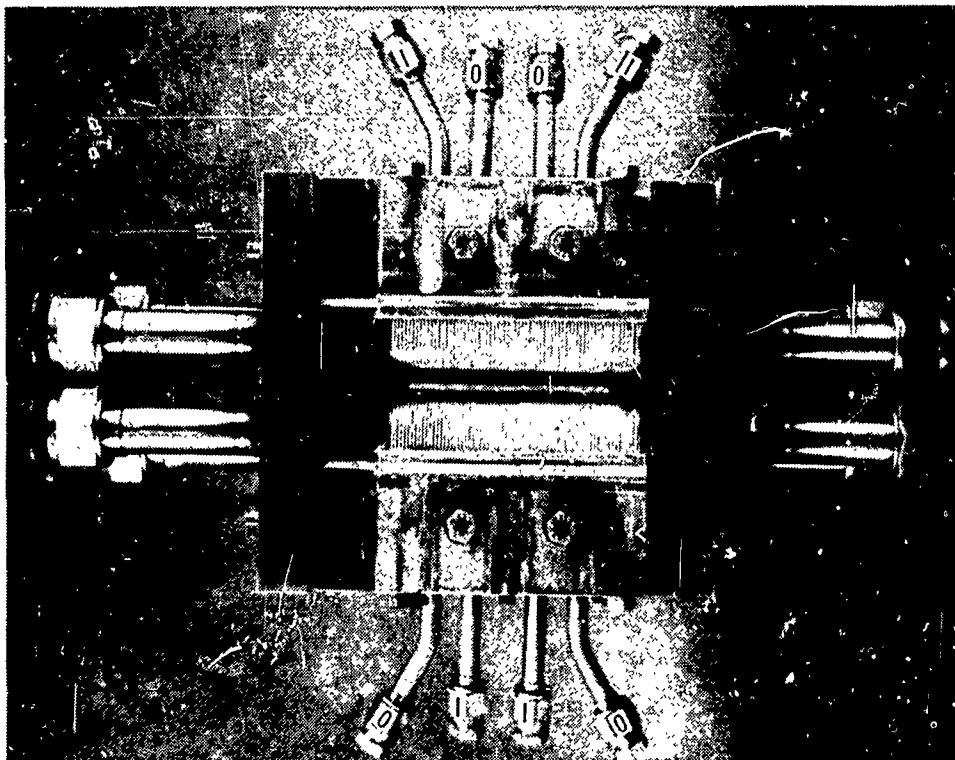
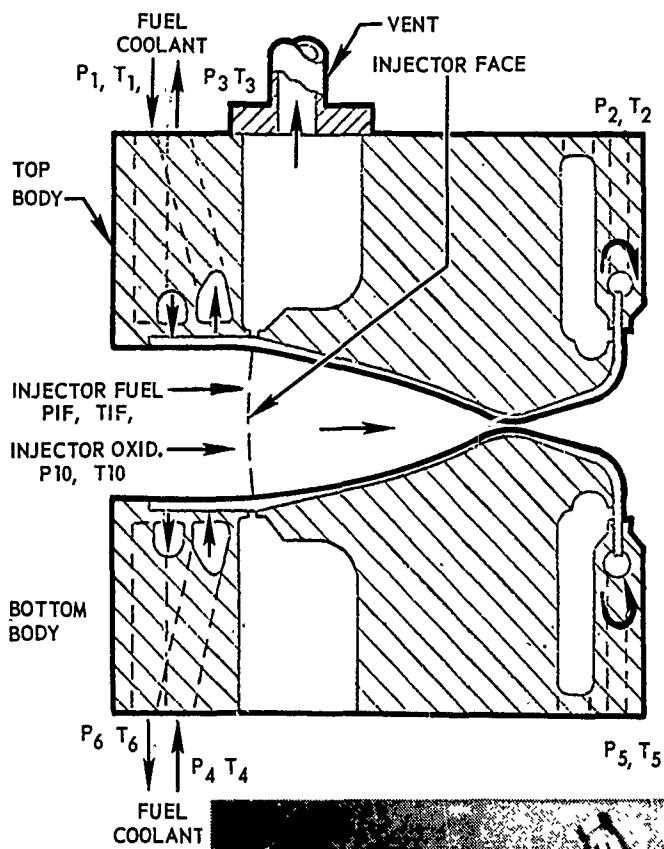


Figure 70. 5-Inch Tubular-Wall Thrust Chamber Segment

CONFIDENTIAL

CONFIDENTIAL

(U) High-frequency chamber pressure transducers, Kistler Type 614A4, were used on tests 010 through 050 to aid in the identification of any high-frequency acoustic oscillations that might be occurring in the combustion chamber. An examination of this data has indicated that no significant oscillations of this type have been encountered.

c. THRUST CHAMBER SEGMENT TEST SUMMARY

(U) Three copper, water-cooled, 5-inch segment thrust chambers have been tested. Six injectors have been fabricated; five of which have been test fired.

(C) The No. 1 G_c contour segment, 3.5-inches from injector face to throat, has been fired successfully on 32 tests. The overall condition of the chamber remains excellent; however, repeated thermal cycles have initiated slight yielding of the copper wall in the throat region.

(C) The No. 2 G_c contour chamber segment was test fired for a total of seven tests and 24-seconds mainstage duration. Comparison of chamber heat flux and performance with No. 1 chamber segment indicated no difference between the two segments.

(C) The K-contour, solid-wall thrust chamber, 5-inches from injector face to throat, was used successfully for nine test firings without sustaining any damage. The heat transfer results were used as a basis for a comparison of tubular wall thrust chamber designs having either a 3.5- or 5.0-inch length injector face-to-throat. The results of the analysis indicate that the use of the K contour would be less desirable with respect to cooling inlet pressure requirements and tube gas-side wall temperatures in the inner body up-pass due to the increased enthalpy in the coolant. The heat flux distribution in the two types of chambers is very similar in the throat region, but the K contour has more surface area in the combustion zone and provides more coolant temperature rise. A comparison of the measured heat flux distribution in the two chambers is shown in Fig. 71.

CONFIDENTIAL

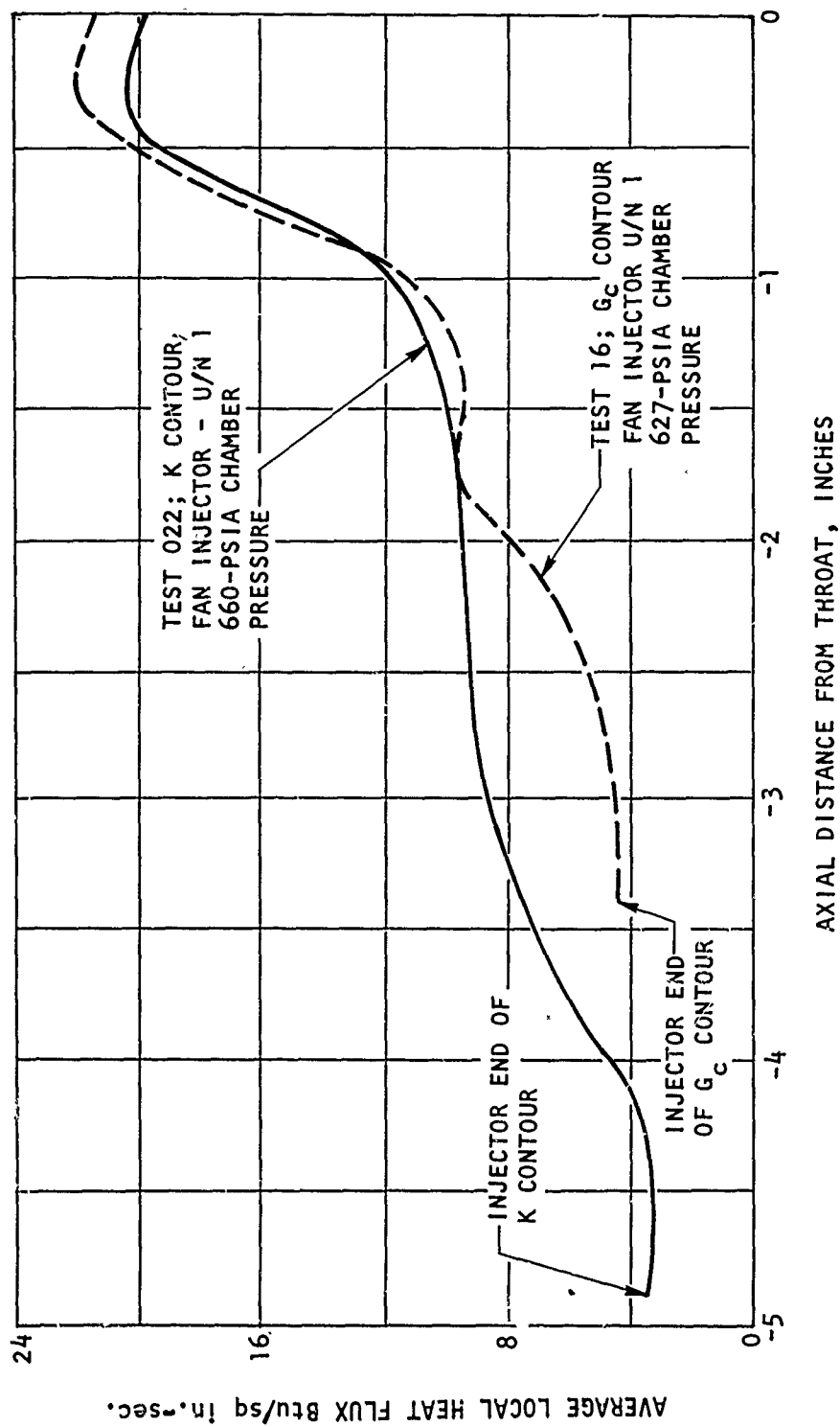


Figure 71. Heat Flux Distribution Measured in Contour K and G_c Contour Solid-Wall Thrust Chambers

CONFIDENTIAL

CONFIDENTIAL

(C) The second fan injector (U/N 2) was used successfully on 13 solid-wall segment test firings which covered the complete chamber pressure design range of 661 to 72 psia. The condition of the injector following these tests was good as shown in Fig. 72.

d. INJECTOR FACE HEAT FLUX DATA ANALYSIS

(C) Initial 5-inch segment triplet injector evaluations revealed deficiencies in the injector face cooling capabilities (mainly the oxidizer strips) under the face heat flux conditions to which the injector was subjected. There were essentially two problems:

1. The heat flux was higher than predicted, particularly when the oxidizer became two phase.
2. The face cooling design was marginal.

(C) Some of the remedial techniques to overcome the problem were detailed in the first quarterly report. These techniques were successful in all instances, except in the low chamber pressure range (150 psig and lower).

(C) It was found that the injector mechanics (relationship of propellant phase, mixing length, injection angle, etc.) and resultant face heat flux were primarily a function of the fluorine condition, e.g., liquid two-phase, saturated vapor, etc. Injector operation in the low chamber pressure region resulted in higher than predicted face heat flux due to a change in basic injector mechanics that was self-sustaining and progressive. The increased face heat flux resulted in less dense fluorine injection, which in turn resulted in an increased face heat flux, and the cycle continued until a true gas-gas injection mechanism existed.

(C) To evaluate the condition of the fluorine injected into the chamber, a thermodynamic analysis was performed using the face heat flux as the source of an enthalpy change. As the pressure drop in the injector is

CONFIDENTIAL

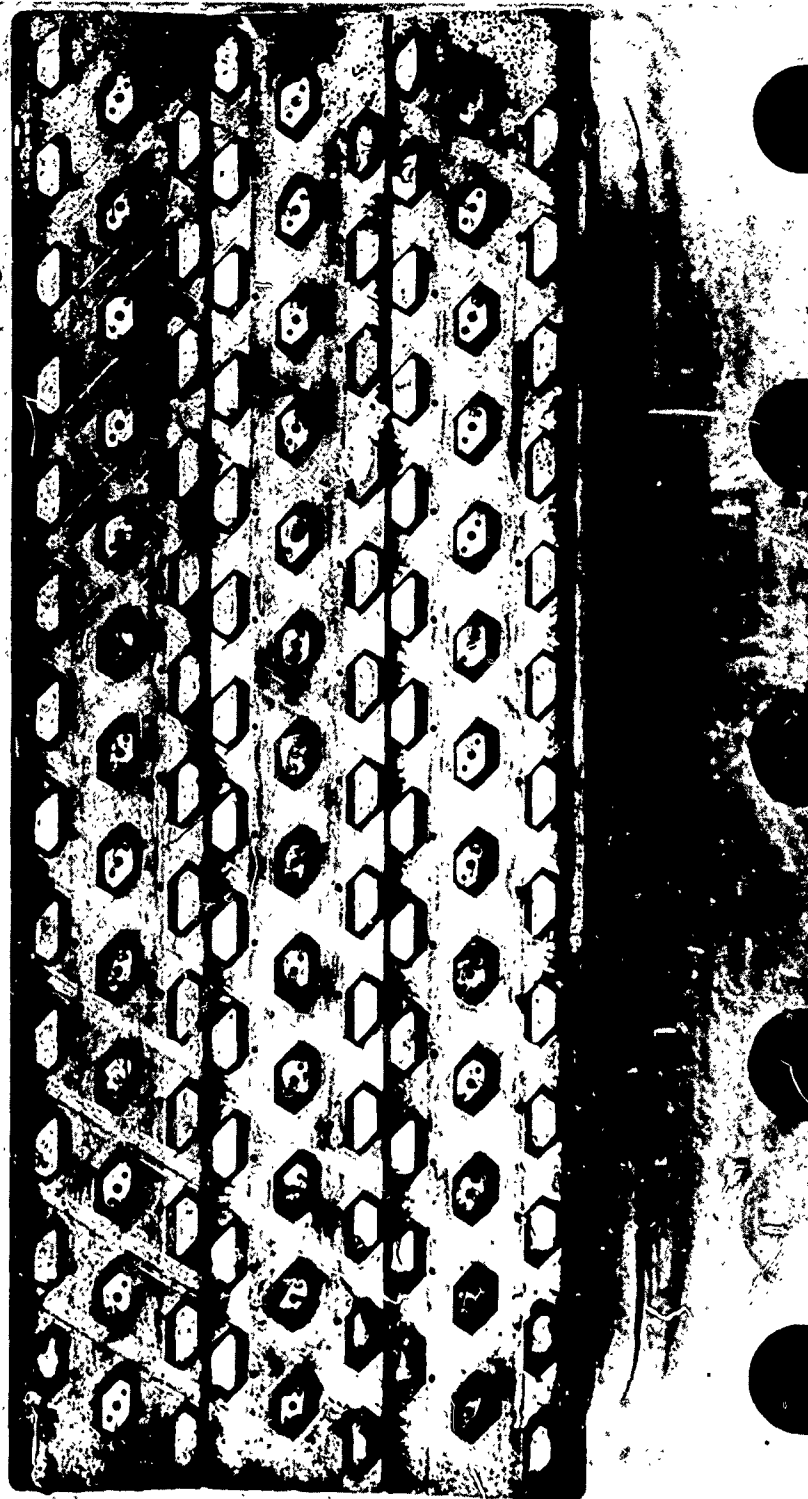


Figure 72. Fan Injector U/N 2 After Test 50 (93 Seconds Accumulated
During 13 Tests at Chamber Pressures of 72 to 661 psia)

CONFIDENTIAL

CONFIDENTIAL

primarily through the orifices, the properties of the fluorine as it reaches the orifices can be found assuming a constant pressure process. This is only an approximation, because the face heat flux is measured at the wall and the actual face area cooled by the fluorine is not exactly known. If this area is assumed to be $2/3$ of the face (hydrogen cools $1/3$), the change in enthalpy can be calculated, and the fluorine quality entering the orifice can be determined. Figure 68 shows the face heat flux necessary to effect the vaporization process as a function of chamber pressure (oxidizer flow). Also plotted is the heat flux measured for the fan injector U/N 2 during testing. As shown, the test data curve is discontinuous near the point of saturated liquid fluorine injection (tests 46 and 47). This indicates higher face heat flux with two-phase fluorine than with liquid. The discontinuity is attributed to a basic change in injector mechanics.

(U) A curve that designates the maximum allowable heat flux as a function of chamber pressure is also depicted in Fig. 73. The values derived from this curve were used for test redline values.

(C) The fan injector fluorine orifice pressure drop (U/N 2) as a function of flowrate is shown in Fig. 74. The change in slope as a result of operation in the two-phase flow region can be seen.

e. INJECTOR PERFORMANCE

(C) Forty-one 5-inch segment tests were conducted during this second quarterly period. Operating levels and corrected performance data are presented in Table 14 for the tests which were considered suitable for performance determination. Calculation of performance based on thrust, however, was not made for tests which were conducted at chamber pressure below 200 psia. This was necessitated by nozzle flow separation which occurred at these operating levels. Figure 75 presents the corrected c^* efficiency vs chamber pressure for the U/N 2 fan injector as calculated from the chamber pressure and thrust measurements.

CONFIDENTIAL

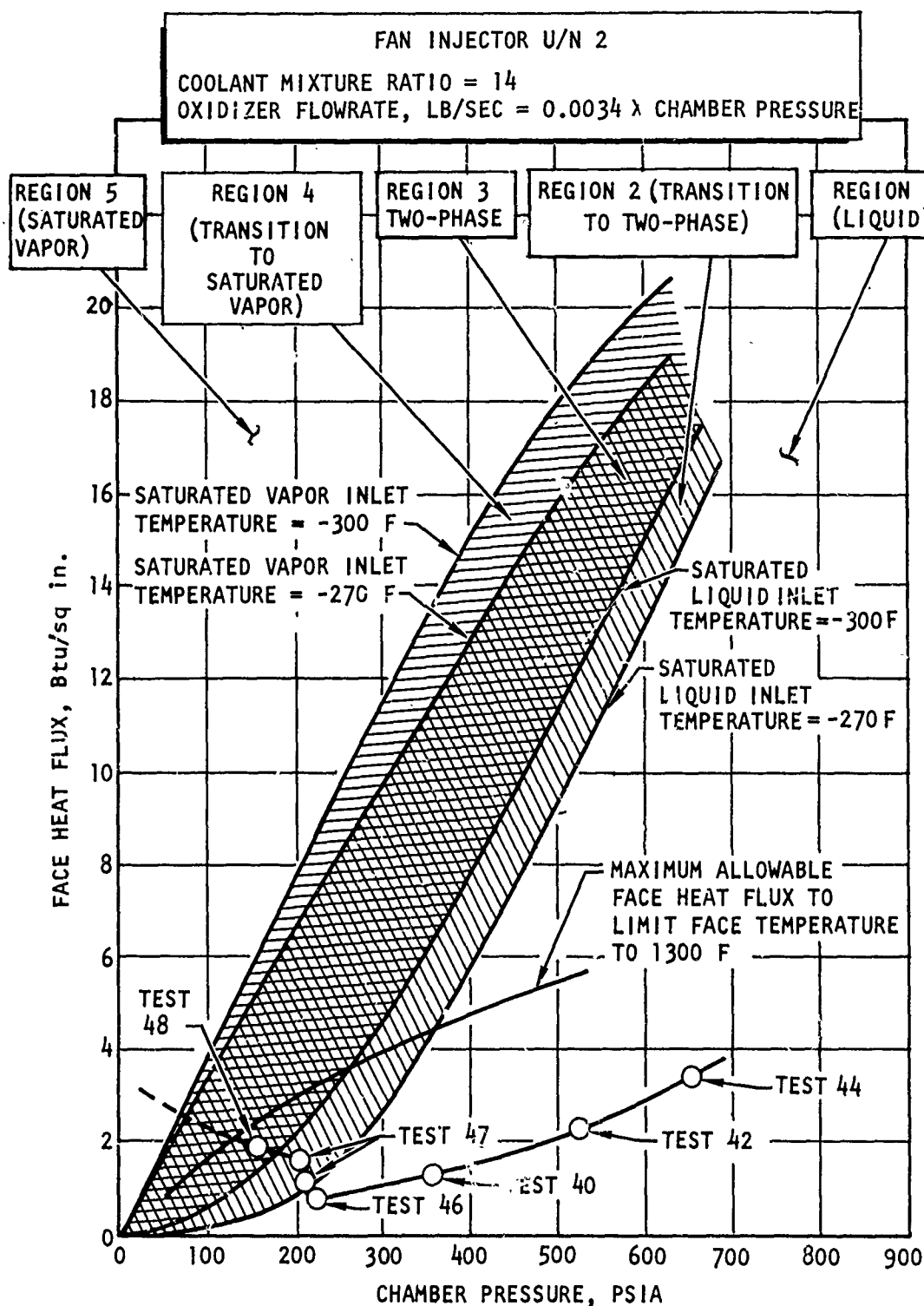


Figure 73. Heat Flux vs Chamber Pressure Showing Quality of Fluorine Injected on a Bulk Basis

CONFIDENTIAL

CONFIDENTIAL

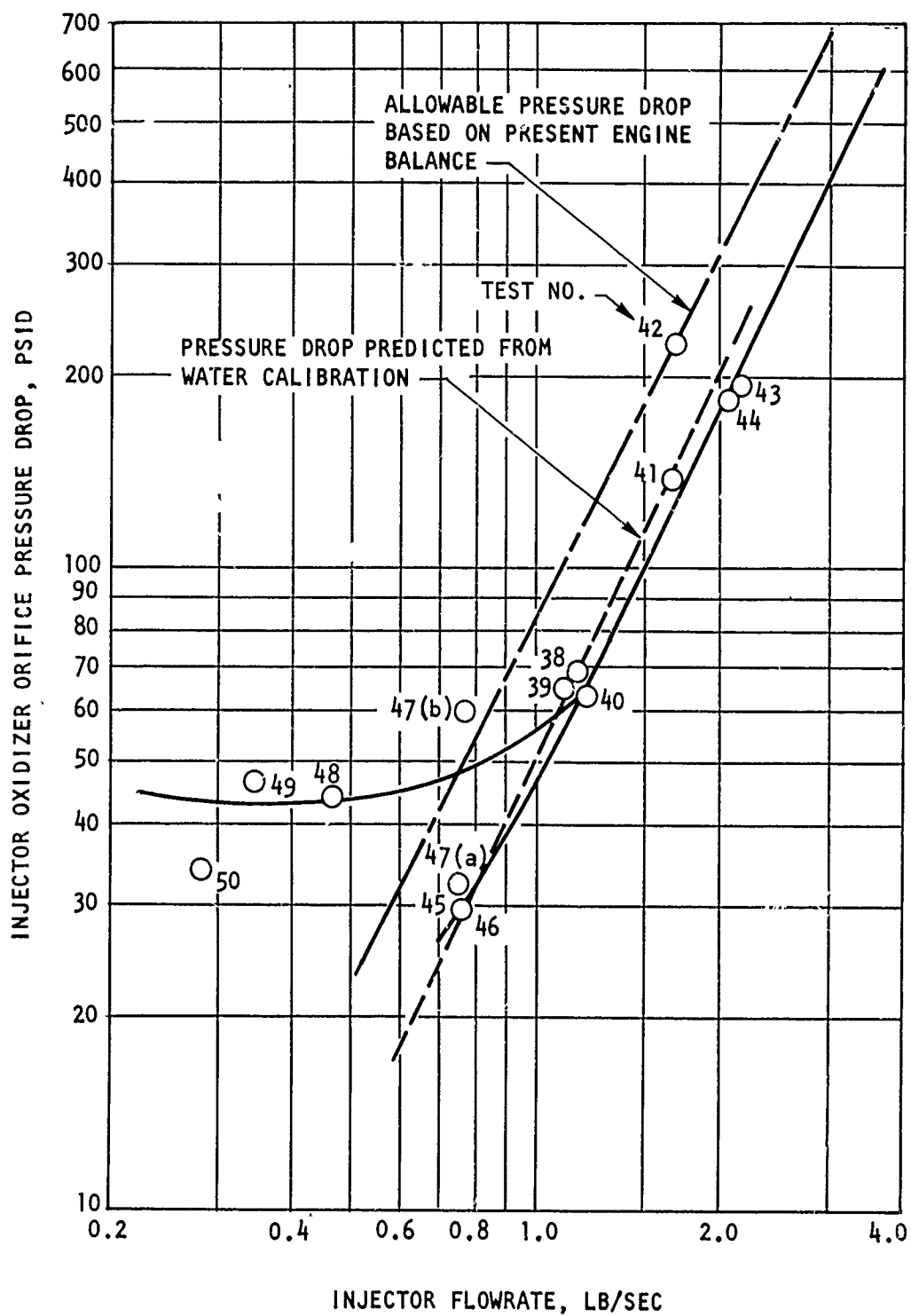


Figure 74. 5-Inch Fan Injector Orifice Pressure Drop vs Flowrate
(U/N 2)

CONFIDENTIAL

CONFIDENTIAL

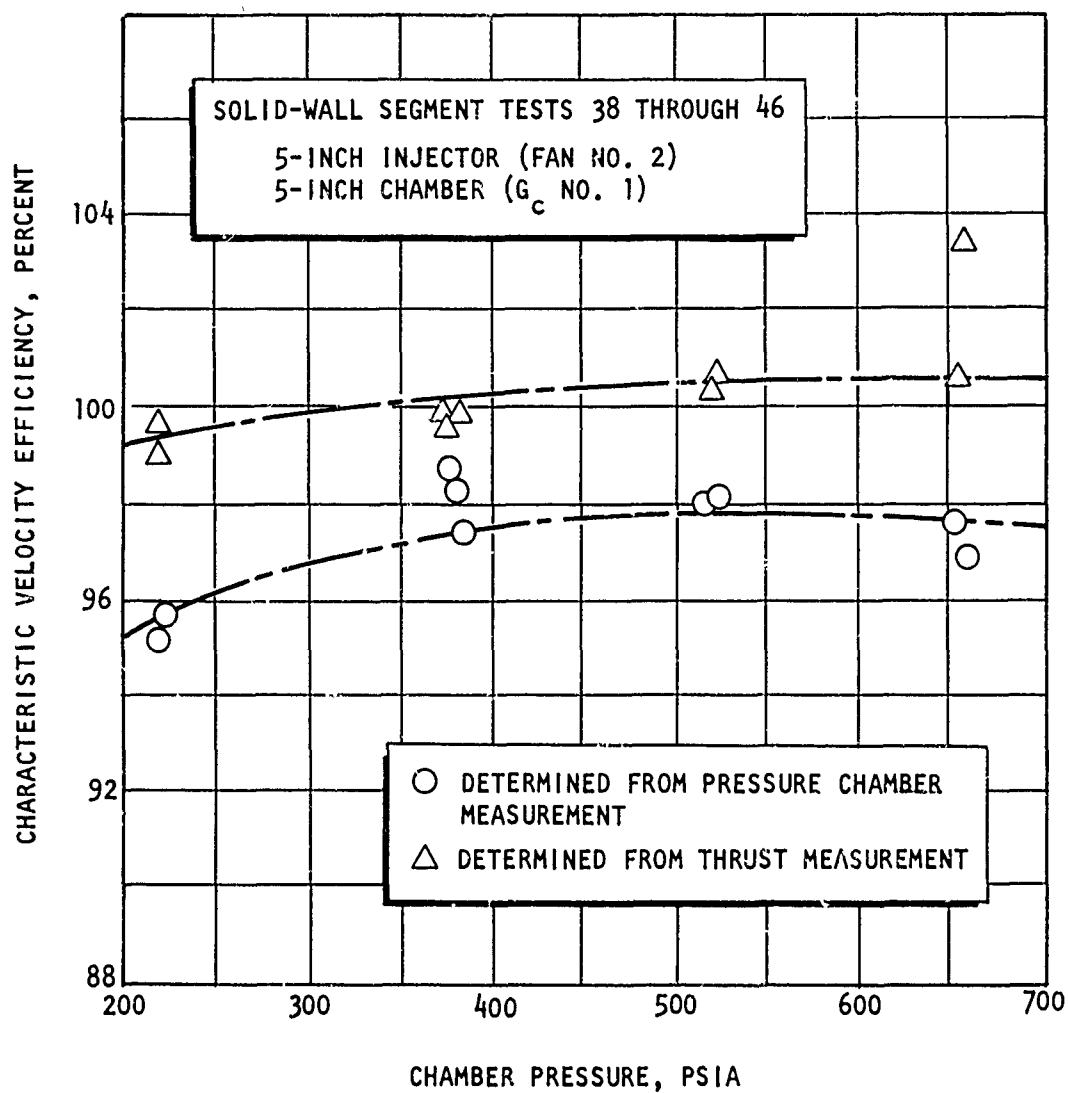


Figure 75. Performance During Solid-Wall Segment Tests 38 Through 46

CONFIDENTIAL

(U) There is an apparent variation in the performance values as determined by the two methods. At this time, there is no reason to favor or disfavor either of the methods of calculating combustion efficiency. Both methods require analytically determined correction factors. The calculation of the combustion efficiency based on chamber pressure requires a correction factor to account for the thermal shrinkage of the solid-wall segment throat. This correction, which can be a significant effect, can not be experimentally verified.

(U) The measured thrust values must also be corrected for nozzle thrust coefficient corrections (drag, kinetics, divergence). These specific values have not been verified experimentally. However, related experimental programs have provided a high degree of confidence in the analytical methods of predicting nozzle corrections. All of the experimental and analytical corrections and methods used in the reduction of the test data have been reviewed and compared with the values obtained in previous similar test programs.

(U) Correlation of the data with such parameters as injection momentum ratios and mixture ratio divided by fuel velocity was investigated. These parameters are shown in Table 14. There is a trend of increasing c^* efficiency with decreasing values of injection momentum ratio ($\dot{w}_o V_o / \dot{w}_f V_f$) and mixture ratio over fuel velocity ($\dot{w}_o / \dot{w}_f V_f$). This was determined to be primarily caused by the fuel injection velocities. High fuel injection velocities resulted in improved performance. Variations in chamber pressure and injection temperature resulted in variations in fuel injection density. Chamber pressure and mixture ratio differences also influenced propellant flowrates. All of these factors affect fuel injection velocity for a specific injector. Basic injector design differences and injector orifice size also affect injection velocity. The uncertainty in oxidizer phase at injection may have also produced some of the data scatter. Previous testing indicated that fuel velocity was a much more influential performance parameter than oxidizer velocity. For this reason, the parameter ($\dot{w}_o / \dot{w}_f V_f$) was postulated as a superior correlating parameter to pure

CONFIDENTIAL

momentum flux ratio. The c^* efficiency is plotted in Fig. 76 against this parameter $[(\dot{w}_o/\dot{w}_f)/V_f = MR_c/V_f]$.

(U) In Fig. 76 the dashed curve indicates the location of the best fit through the corrected performance data from previous injector test data of contract AF04(611)-11617. The comparison with the new data is relatively good. The implications of Fig. 76 are that the injectors are operating approximately to form, and that high performance is to be expected with higher fuel velocity.

(U) Figure 75 shows the corrected c^* efficiency based on chamber pressure plotted against the operating level of chamber pressure for the fan injector, U/N 2. Although there is an apparent drop off of performance with pressure, it may not be actually occurring. The various factors which could add to the drop in performance include throat area uncertainty at the lower chamber pressures, propellant contamination, and lack of uniformity of calibration of the oxidizer cavitating venturries.

(C) The overall conclusion with respect to the performance (η_{c^*}) of the modified fan injector (U/N 2) is that it obtains approximately 98 percent of full shifting (equilibrium) performance over much of its operating range. The performance at the low chamber pressure range has not yet been adequately investigated.

f. CHAMBER WALL HEAT TRANSFER

(U) The segment heat transfer test data results were presented earlier in the report in the Task I Thrust Chamber Analysis and Design section because of the close relationship of these data to that activity.

4. TURBOPUMP BEARING AND SEAL PROGRAM

(C) The design layout of the bearing and seal tester was completed (Fig. 77). The tester consists of a commercial supercharger turbine

CONFIDENTIAL

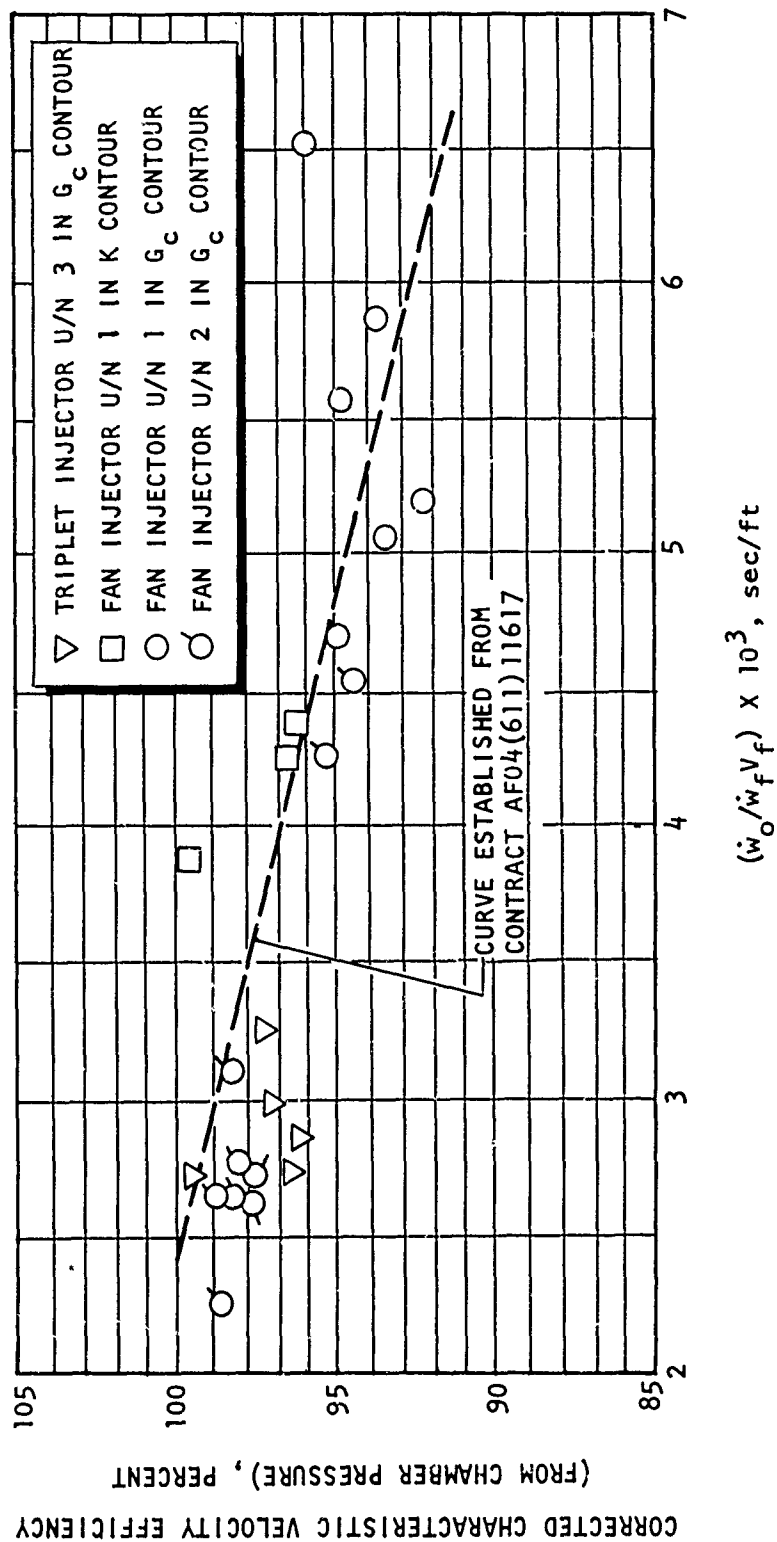


Figure 76. Characteristic Velocity Efficiency vs Oxidizer Flowrate
Divided by Fuel Momentum Flux

CONFIDENTIAL

CONFIDENTIAL

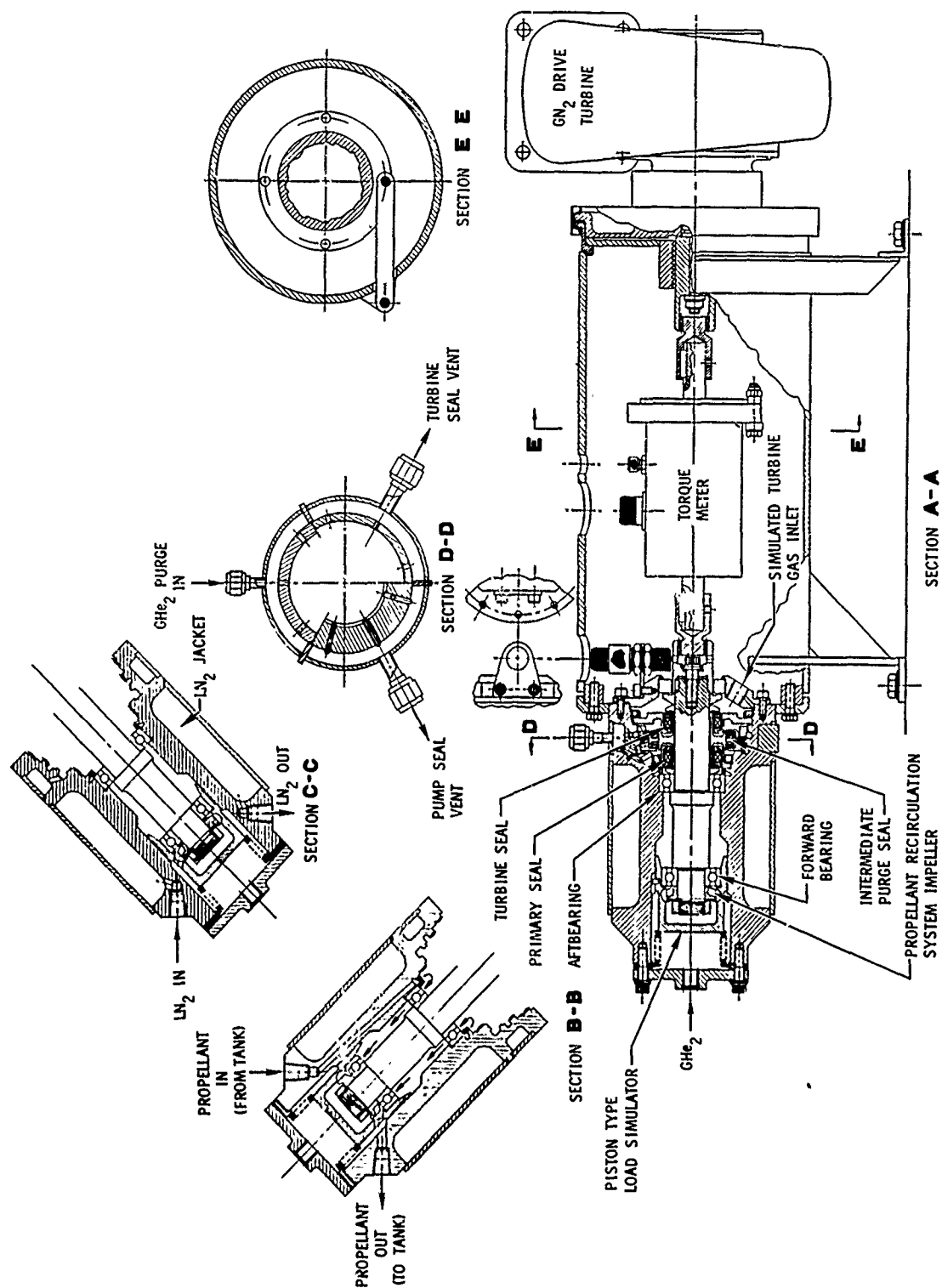


Figure 77. Oxidizer Bearing and Seal Tester Design

CONFIDENTIAL

CONFIDENTIAL

coupled to the bearings and seal shaft through a torque meter. The tester is designed to pass liquid fluorine from the tank into the oxidizer seal area, then forward through both bearings to a set of small inducer blades mounted on the shaft, then out of the tester and back to the tank. The inducer blades compress the oxidizer sufficiently to discharge it back into the run tank. With this design, it is possible to eliminate the use of an oxidizer catch tank and at the same time increase the test duration capability.

(U) Axial load on the bearings is applied by pneumatic pressure (gaseous nitrogen) introduced at the forward end of the shaft and is transmitted to the bearings through a sleeve. Isolation of the gaseous nitrogen and liquid fluorine is accomplished by use of a stainless steel bellows assembly.

(U) Turbine gas pressure is to be simulated with gaseous nitrogen introduced into the cavity aft of the turbine gas seal. Thermal conditioning of the tester is to be accomplished with an liquid nitrogen jacket which encloses the forward end of the assembly.

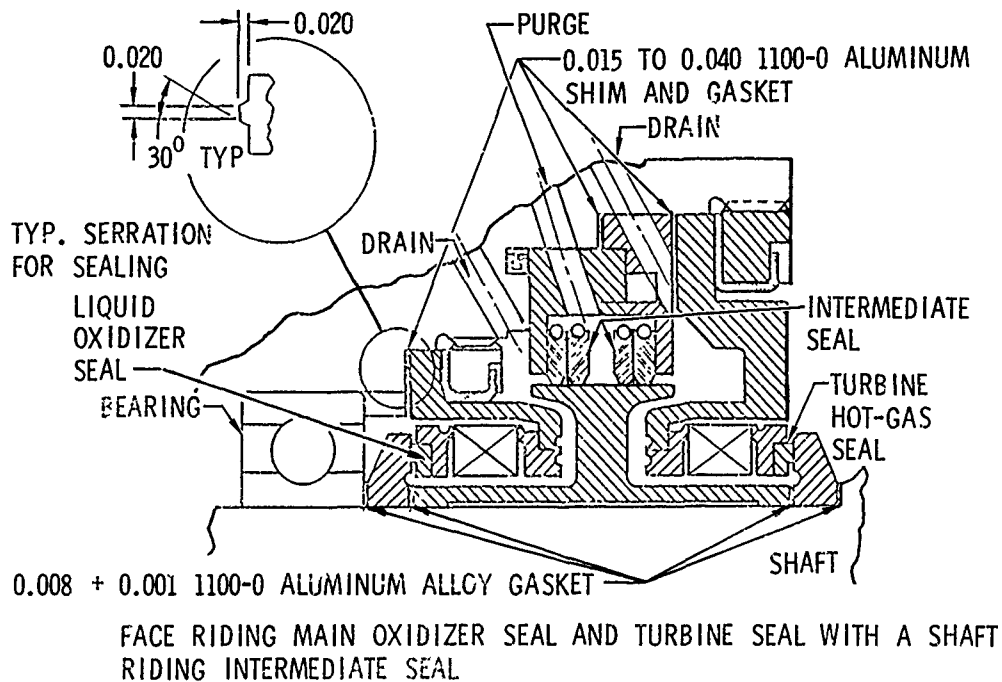
(U) Appropriate purge ports have been included to provide the means for effecting a pneumatic dam at the intermediate seal.

(U) Two seals which are to be tested were shown in the first quarterly report. Some modifications have been made to these designs (Fig. 78) and a third configuration (Fig. 79) is being considered. This configuration replaces the shaft-riding intermediate seal with a gas face seal. In this configuration, the purge gas is directed into the immediate area of the primary seals and provides more positive scavenging of any seal leakage.

(U) The seal assembly, comprised of two face-riding primary seals and the shaft-riding intermediate seal, has been selected as the primary seal package. The other two designs are considered as backups.

CONFIDENTIAL

PRIMARY CONFIGURATION



ALTERNATE CONFIGURATION

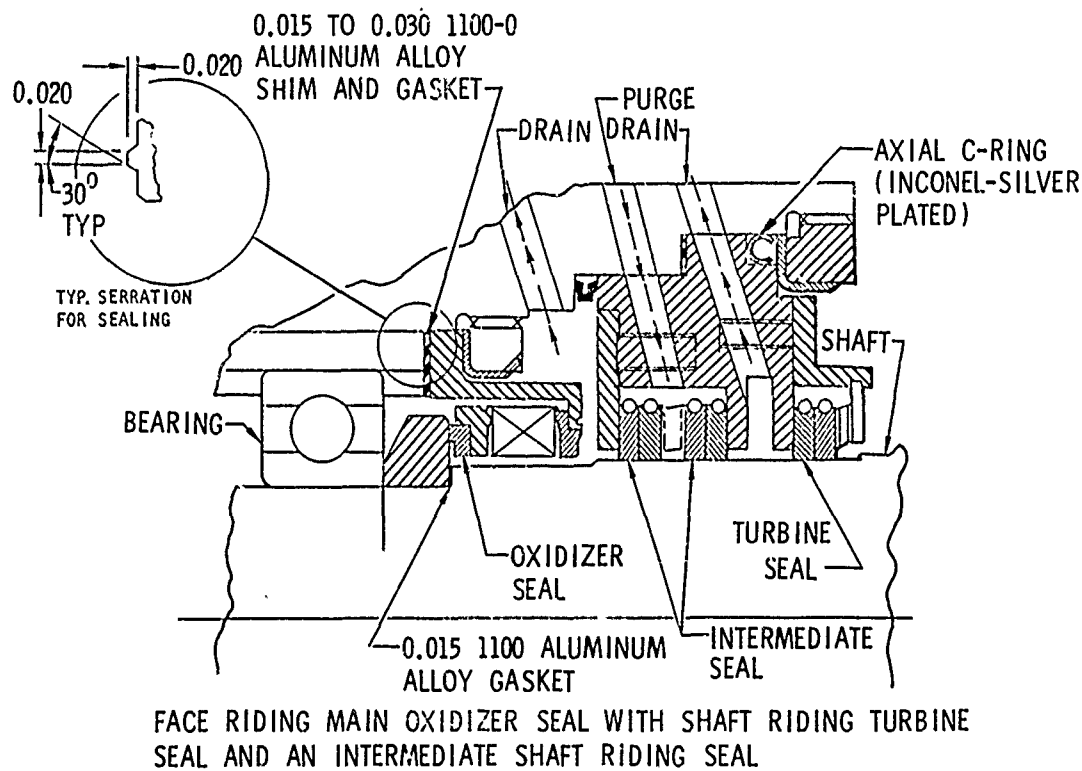


Figure 78. Oxidizer Turbopump Seal Designs

CONFIDENTIAL

CONFIDENTIAL

FACE-RIDING OXIDIZER AND TURBINE SEALS,
GAS FACE INTERMEDIATE SEAL

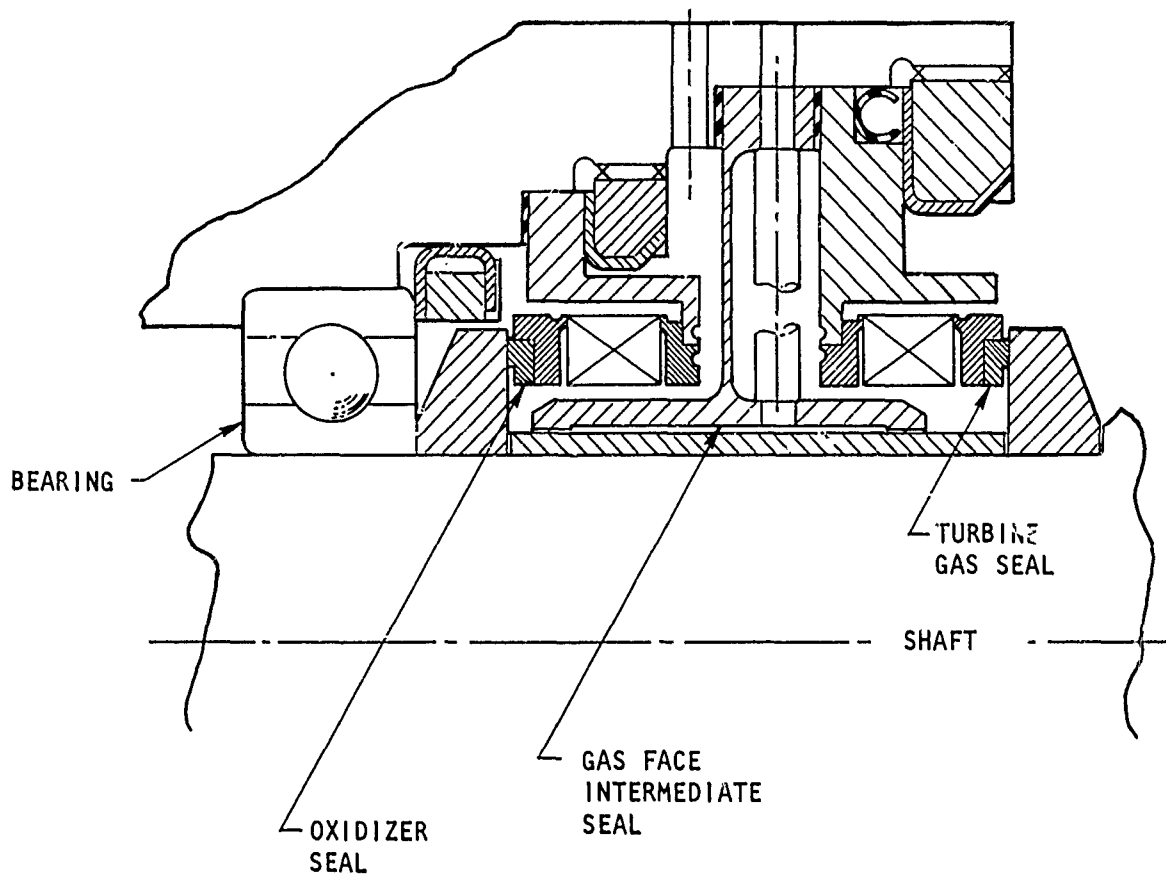


Figure 79. Main Engine Oxidizer Pump Turbine Seal Design
(Second Alternate)

CONFIDENTIAL

(U) Effort in the next report period is to be concentrated on detailed design of the tester. A complete package is to be designed to house the tester so that facility connections can be made by connecting pneumatic and control lines to a panel on the tester package. With this approach, it will be possible to perform a complete checkout of the assembly in the engineering laboratory prior to installing it in the NFL test facility.

5. FACILITY OPERATION AND PREPARATION

(U) Facility activity during this report period consisted of continuing operation of the Victor test stand for the 5-inch segment testing and the design modification of Rocketdyne's Nevada Field Laboratory (NFL) site B-4A in preparation for full-thrust chamber and turbopump bearings and seals test programs.

a. VICTOR TEST STAND

(U) Testing of the 5-inch thrust chamber/injector segments continued during this report period at the Victor test stand. The following paragraphs present the problems which were encountered in the operation and the corresponding solutions.

(1) Oxidizer Lines

(U) It is important to keep the oxidizer, that is delivered to the test stand engine, at a uniform temperature. Changes in propellant temperature during a run will complicate flowrate calculations because of density transients. This occurred in several hot firings on Victor test stand. A warm "slug" of oxidizer built up in a section of unchilled line, and after approximately 2 seconds of run duration this warm slug of oxidizer reached the thrust chamber segment and affected the oxidizer flowmeters, oxidizer injection pressure, and chamber pressure. During system analysis,

CONFIDENTIAL

it was concluded that this warm slug of oxidizer formed in the oxidizer tank shutoff valve, which was only partially chilled, and in the run tank dip tube, which was not chilled. This condition was slightly improved by completely jacketing the valve; however, the tank dip tube could not be economically modified. For this reason, it was decided that a large volume liquid nitrogen jacketed run line, placed downstream of these undesirable heat sinks, would eliminate the warm oxidizer problem. This new line extended the steady-temperature run duration from 1 to 5 seconds, and was put to use after test 040.

(2) Oxidizer Injector Pressure Surges

(U) Some of the run data exhibited oxidizer injection pressure surges which occurred soon after oxidizer main valve opening as shown in Fig. 80. To avoid possible hardware damage, a reduction in this surge was desirable. The magnitude of the pressure surge depended on the starting conditions.

(C) Previously, the oxidizer line from main valve to injector was chilled with liquid nitrogen, and then primed with liquid nitrogen just before oxidizer main valve opening. To attenuate the oxidizer pressure surge in the injector at starting, the run operating procedure was changed. To force out the liquid nitrogen used to chill the injector, a 2-second helium purge was introduced in the oxidizer main line between the stand oxidizer main valve and injector. This provided a cavity for the liquid fluorine test to fill during startup in order to avoid liquid fluorine ramming. This was initiated after test 037.

(3) Oxidizer Flowmeters

(U) To improve the measurement precision, 0.50-inch flowmeters have been used since test 008 instead of the low rps 1-inch meters originally selected for the program. However, these small flowmeters are more susceptible to failure because of the size of the bearings and the low turbine inertia. Any two-phase flow through these flowmeters can overspin the turbine and damage the bearings and/or turbine blades.

CONFIDENTIAL

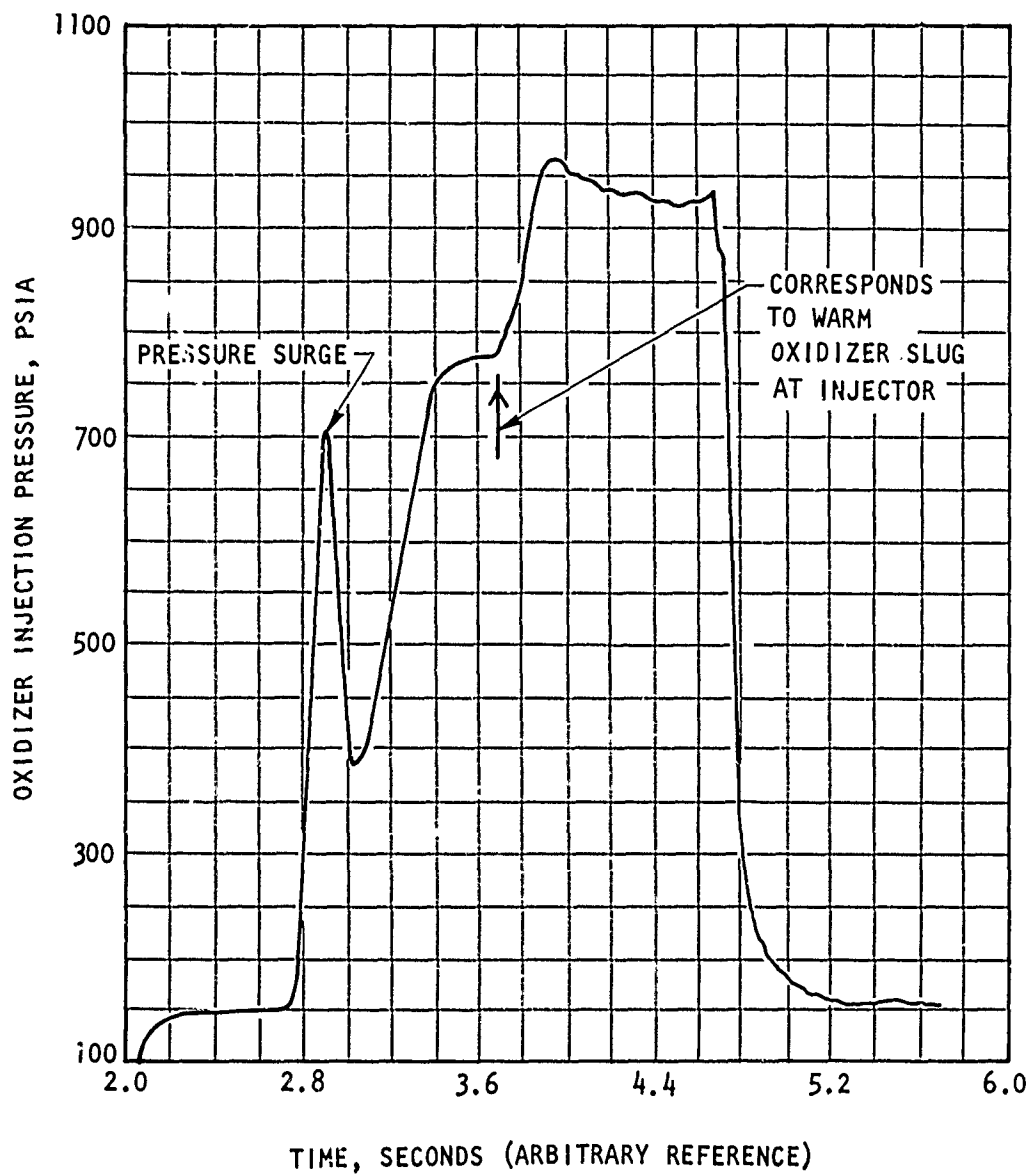


Figure 80. Oxidizer Injection Pressure During Start of Test 36

CONFIDENTIAL

(U) During prerun oxidizer line priming, some two-phase flow and flow-meter overspinning has occurred, and postrun recalibrations were performed on these flowmeters when possible. A cavitating venturi in the oxidizer line provides a backup oxidizer flow measurement. Precision flow calibrations are presently being made on all cavitating venturies used in these tests.

(4) Propellant Impurity

(U) During tests 047 through 050, it was suspected from the performance data that either one or both of the propellants used was contaminated. Samples were taken of the propellants in storage following test 050. The results of these samples analysis are shown in Table 15. For comparison purposes, analysis of previous samples of the propellants is shown. It was found that the posttest sample of (test 050) oxidizer contained 6.8 percent (by weight) air. Because the majority of the air content is nitrogen, the presence of this air percentage could have a significant effect on the injector performance. The fuel purity was found to be satisfactory. There was no way of determining the actual content of the oxidizer used during the individual tests in question as no samples were taken during the test period. It has been the practice to sample the delivered oxidizer on a spot basis only. The frequency of these spot checks depends on the rate of use and uniformity of delivery source.

(U) It is possible that the impurity content on the tests in question was not the same, and it is also possible that some preferential sampling occurred which may not be completely representative of the total delivered oxidizer.

(U) Because the oxidizer storage system is maintained at pressures above atmospheric pressure, it was concluded that the air was received in the oxidizer as delivered. All storage bottled suspected of contamination were removed from the system.

CONFIDENTIAL

TABLE 15
CHEMICAL ANALYSIS OF FLUORINE AND HYDROGEN
AT VICTOR TEST STAND

Date	Chemical	Content, weight percent
18 January 1968 (Fluorine)	F ₂	97.7
	HF	0.49
	CO ₂	0.01
	Air	0.82
	He	1.0
	CF ₄ , SF ₆ , ClF ₅	Trace
4 April 1968 (Fluorine, for Tests 044 Through 046)	F ₂	97.9
	He	1.1
	Air	0.6
	SF ₄	0.1
	HF	0.2
	CF ₄	0.1
	CO ₂	0.01
17 April 1968 (Fluorine, Following Test 050)	F ₂	92.5
	Air	6.8
	He	0.2
	CO ₂	0.1
	CF ₂	Trace
2 January 1968 (Hydrogen)	Ar	<0.5 ppm
	O ₂	0.7 ppm
	N ₂	3.0 ppm
	CO	None Detected
	CO ₂	None Detected
	CH ₄	None Detected
Purity >99.999-Percent H ₂ by Volume		
18 April 1968 (Hydrogen)	Ar	<0.5 ppm
	O ₂	0.5 ppm
	N ₂	1.3 ppm
	CO	None Detected
	CO ₂	<0.5 ppm
	CH ₄	None Detected
Purity >99.999-Percent H ₂ by Volume		

CONFIDENTIAL

(5) New Gaseous Fluorine Storage Facility

(C) It has been the practice to purchase gaseous fluorine and store it in "K" bottles. As each of these bottles hold 4 to 6 pounds of fluorine, a considerable amount of material handling was required. A plan was put into effect on 27 April 1968 to buy bulk liquid fluorine, convert it to gas, and store it in high-pressure vessels capable of holding 1000 pounds of fluorine. A schematic of the high-pressure gaseous fluorine storage facility is shown in Fig. 81.

(6) Hydrogen Heat Exchanger

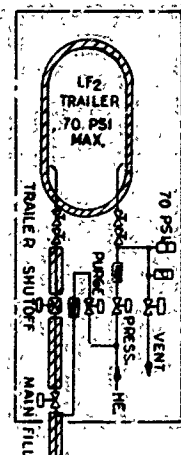
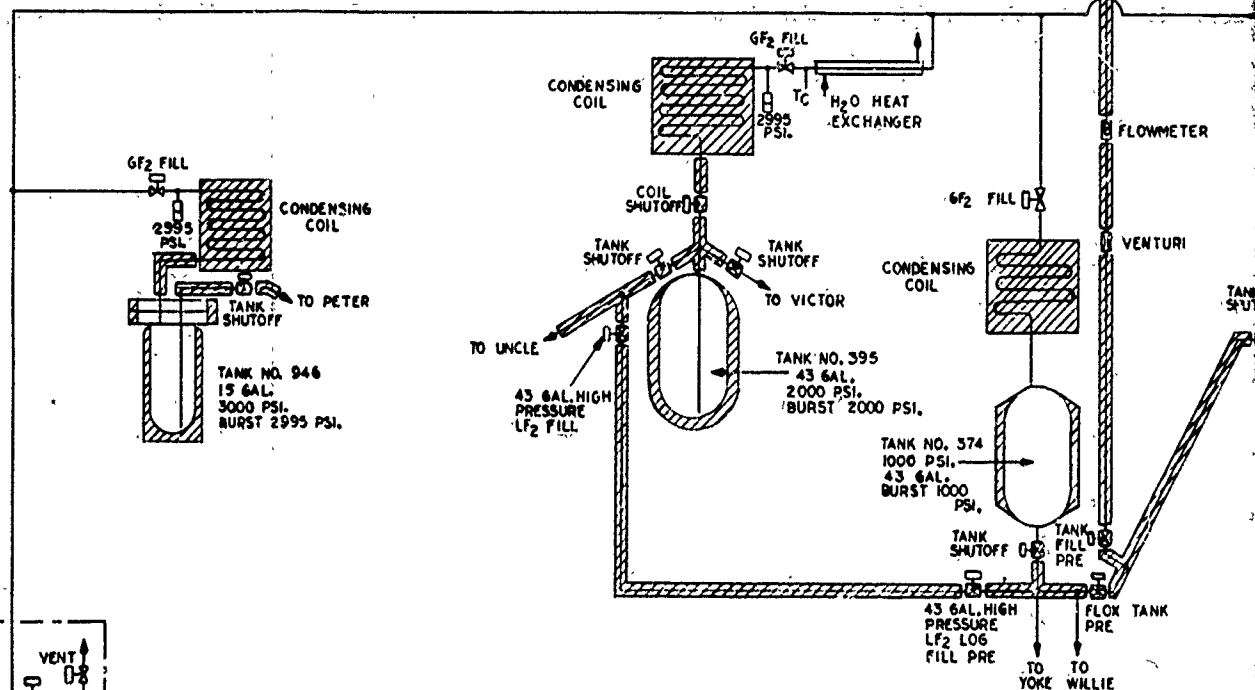
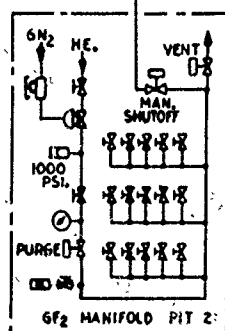
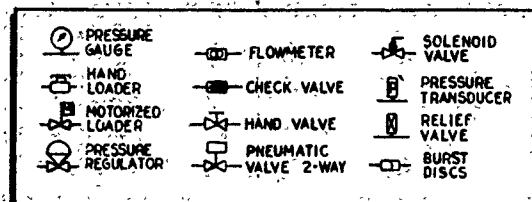
(C) For the thrust chamber segment test program, 1000 F hydrogen, which simulates the injector fuel temperature used in an actual regeneratively cooled tube wall engine, must be delivered to the solid wall segment injector. Thus, a high-pressure/high-temperature gas-powered hydrogen heater was designed and fabricated from 321 stainless steel (first quarterly report).

(U) Because 321 stainless steel has only moderate resistance to hydrogen embrittlement, it is necessary to rebuild the heat exchanger every 25 to 30 runs. This was accomplished during this report period after tests 026 and 050.

b. NEVADA FIELD LABORATORY TEST FACILITY DESIGN MODIFICATION

(U) Design of modification of the NFL test site for the AMPT program was 25 percent completed during this quarterly period. The design utilizes existing facility equipment (e.g., valves, vessels, pumps, etc.) located either at NFL or at other Rocketdyne facilities. However, to meet the requirements of the AMPT program, modifications to some of the equipment is necessary. To avert a possible program interference problem,

CONFIDENTIAL



FLUORINE TRANSFER AND STORAGE FACILITY AT PROPULSION



176

CONFIDENTIAL

2

and at the same time facilitate program flexibility, it was decided to include the turbopump bearings and seal test facility at the B-4A test stand instead of test stand B-3A where it was originally scheduled for installation.

(1) Oxidizer System

(U) The run tank identified for use at the B-4A test stand is a 360-gallon 2000-psi, liquid nitrogen jacketed tank. The modification design was completed and the contract was awarded. Significant design modifications of the tank include the addition of a liquid nitrogen jacket, a jacketed dip tube, and enclosure of the tank in a polyurethane insulation jacket. The requirement of the jacket on the dip tube was the result of an investigation during the segment test program at Victor test stand which revealed the probable source of warm slugs of oxidizer to be the uninsulated dip tube in the Victor test stand run tank.

(U) The storage tank to be used at NFL, test stand B-4A is to be a 525-gallon liquid nitrogen jacketed tank presently located at NFL test stand B-3A. The tank requires no internal modifications.

(2) Fuel System

(U) The modification design of the fuel run tank was completed and the contract was awarded for modifications. The tank is a 1000-gallon, vacuum-jacketed vessel rated for 3000 psi service.

(U) Significant design modifications include the addition of Perlite in the vacuum jacket, the addition of polyurethane insulation around the tank and inlet and outlet ducting, and modifications to the inlet and outlet flanges.

(U) The fuel storage tank is a 28,000-gallon, vacuum-jacketed dewar. This tank requires no modifications.

(3) Altitude Facility Design

(U) The use of the altitude simulator facility for the AMPS engine requires that the facility be tailored to the AMPS engine size and flowrates. The design provides for a water-jacketed diffuser insert to be installed on tracks inside the existing diffuser section. This will provide access to the diffuser for inspection and repairs. The existing water system is to be modified to provide control for proper cooling flowrates for the variable thrust operation. The design configuration of the diffuser has been finalized and detailed design was initiated.

(4) Thrust Measuring System

(U) A conceptual design was completed of the thrust measuring system for the main engine thrust chamber. The design includes provisions for measuring angular misalignment and thrust vector displacement in addition to measuring total axial thrust. Because the firing attitude of the thrust chamber is horizontal, the "side" load cells will serve the dual purpose of supporting the thrust mount and thrust chamber.

CONFIDENTIAL

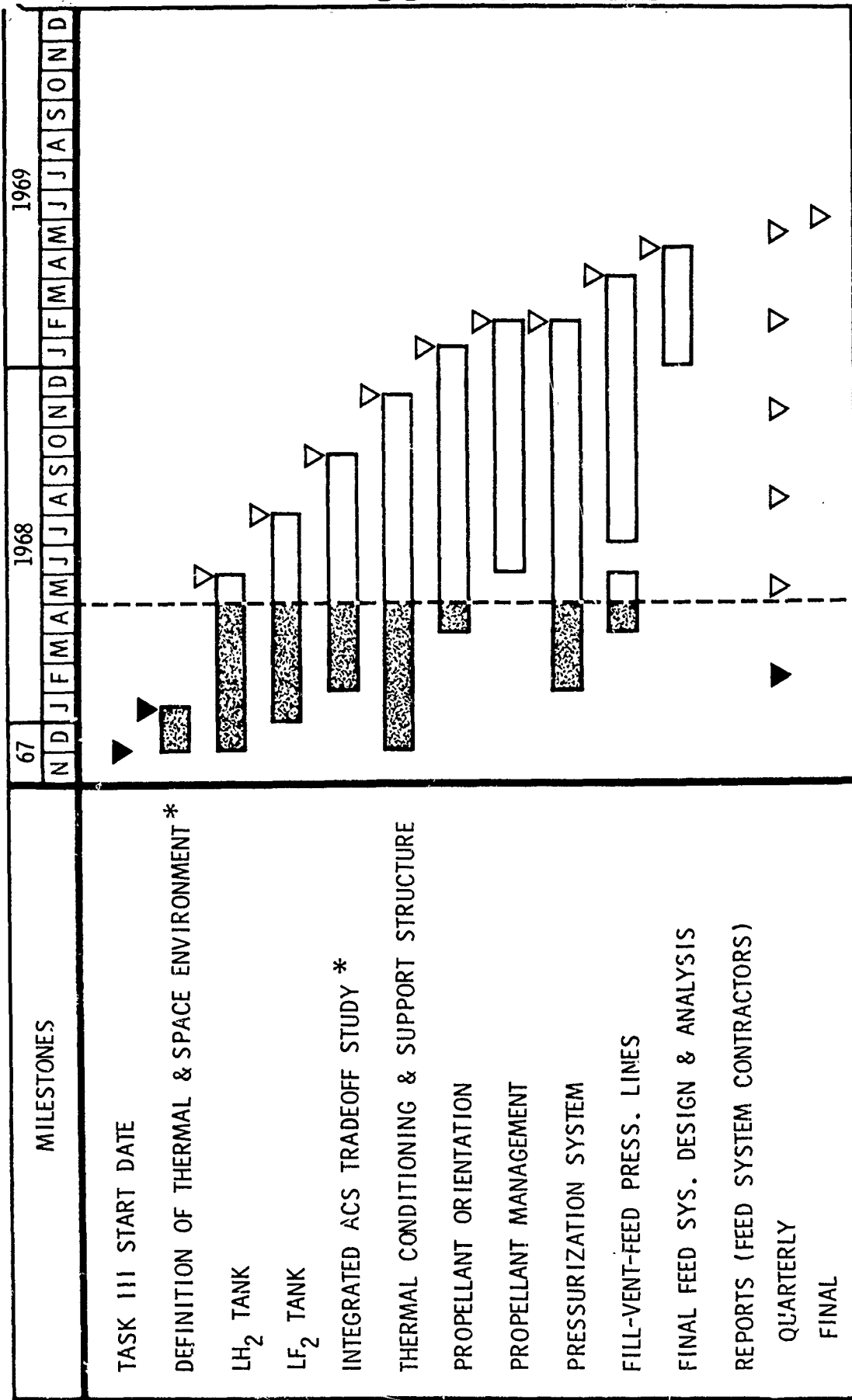
TASK III, PROPELLANT FEED SYSTEM ANALYSIS AND DESIGN

- (C) This task provides for analysis and design of the propellant feed system to be integrated with the advanced engine design resulting from Tasks I and II. The status of high-energy LF_2/LH_2 propulsion technology is to be assessed, and a definitive high-energy propellant feed system will be optimized and designed for maximum system ΔV .
- (U) This task is being conducted by two selected subcontractors: General Dynamics/Convair and Lockheed Missiles and Space Company. The start date for both subcontractors was 4 December 1967, which was approximately 1 month later than start of the overall program by Rocketdyne. Both subcontractors are scheduled to complete their technical efforts on 1 May 1969. The Task III schedule is shown in Fig. 82, with each of the subtasks listed.
- (C) The propellant feed system analysis includes those attitude control system considerations necessary to ensure operational suitability of the total propulsion system. The basic attitude control system being considered during all design studies is the independent Compound A/MHF-5 system reported in AFRPL-TR-65-252. As a separate subtask (Fig. 82), the impact of an integrated gaseous F_2/H_2 attitude control system on the optimized propellant feed system design will be investigated.
- (U) The first subtask (Fig. 82), Definition of Thermal and Space Environments, was completed during the first quarterly period and are reported in report AFRPL-TR-68-17. These data provided the environmental analysis and design criteria for conducting the subsequent configuration subtasks.
- (U) The major emphases by both subcontractors during the subject report period was on the propellant tank subtasks and the thermal conditioning and support structure subtask. Propellant tank shape optimizations were accomplished and tank material selections were made. Outer structural shroud designs were defined, and candidate materials and types of construction were evaluated. Insulation optimization analyses continued with insulation type,

location, number of layers, etc. being analyzed. Work also progressed on the pressurization subsystem optimization and configuration definition.

- (U) During the quarterly period work was also started on the propellant orientation, fill-vent-feed and pressurization lines, and integrated attitude control system subtasks.
- (U) The detail results of the Task III effort accomplished by Convair and Lockheed during the second quarterly report period is presented in Appendixes I and II, respectively.

CONFIDENTIAL



* AFRPL REVIEW & APPROVAL

GRP-4 CONFIDENTIAL

Figure 82. Task III Schedule

181/182
CONFIDENTIAL

ROCKWELL
A DIVISION OF NORTH AMERICAN ROCKWELL CORPORATION
6033 CANOGA AVENUE, CANOGA PARK, CALIFORNIA 91304

CONFIDENTIAL

REFERENCES

1. AFRPL-TR-68-17, Advanced Maneuvering Propulsion Technology Program, (First Quarterly Report), February 1968, CONFIDENTIAL.
2. LA 3543, Thermal-Acoustic Oscillations Induced By Forced Convection Heating of Dense Hydrogen, Los Alamos Scientific Laboratory Report, Rodney S. Thurston.
3. RPL-TDR-64-120, Analysis of an Optimum Thrust Modulated Propulsion System for Use in a Space Maneuvering Vehicle, The Bell Aerosystems Company, Vol. 1 through 3, Contract No. AF04(611)-8163, June 1964, CONFIDENTIAL.
4. AFRPL-TR-65, Maneuvering Satellite Propulsion System Optimizations Study, Rocketdyne, Vol. II, Contract AF04(611)-10745, April 1966, CONFIDENTIAL.

APPENDIX I, CONVAIR TASK III RESULTS
FOR SECOND QUARTERLY PERIOD

CONFIDENTIAL

TABLE OF CONTENTS

Section	Page
1 LH ₂ AND LF ₂ PROPELLANT TANKS	1-1
1.1 Introduction.	1-1
1.2 Selected Tank Configuration	1-1
1.3 Evaluation Factors	1-3
1.3.1 System Weight.	1-3
1.3.1.1 Design Assumptions	1-5
1.3.1.2 One-Piece Bulkheads, Cold Allowables	1-7
1.3.1.3 One-Piece Bulkheads, Room Temperature Allowables	1-12
1.3.1.4 Final Configuration Comparisons.	1-17
1.3.2 Meteoroid Protection Requirements.	1-21
1.3.2.1 Evaluation Factors.	1-21
1.3.2.2 Method of Analysis.	1-24
1.3.3 Selection Criteria.	1-33
1.3.3.1 Compatibility with Propellant	1-33
1.3.3.2 Fabrication	1-33
1.3.3.3 Weld Seams	1-34
1.3.3.4 Toughness.	1-34
1.3.3.5 Interface Seals and Dissimilar Metals Problems	1-34
1.3.3.6 Cost.	1-34
1.4 Structural Material Evaluation	1-34
1.4.1 Candidate Materials	1-34
1.4.2 Strength-to-Density Ratios.	1-35
1.4.3 Compatibility of Candidate Materials in Fluorine.	1-36
1.4.4 Material Characteristics	1-36
1.4.4.1 Alloy 718	1-36
1.4.4.2 301-3/4 H Stainless Steel.	1-37
1.4.4.3 Ti-5Al-2.5 Sn (ELI)	1-37
1.4.4.4 Aluminum Alloys	1-38

CONFIDENTIAL

CONFIDENTIAL

TABLE OF CONTENTS (Continued)

Section	Page
1.5 LH ₂ and LF ₂ Tank Manufacturing	1-39
1.5.1 Elliptical Dome Forming	1-39
1.5.1.1 Selected Forming Method.	1-39
1.5.1.2 Other Forming Methods Evaluated	1-40
1.5.2 Elliptical Dome Machining.	1-41
1.5.3 Elliptical Dome Heat Treat	1-41
1.5.4 Elliptical Dome Chem-Milling	1-41
1.5.5 Tank Welding	1-42
2 THERMAL CONDITIONING AND SUPPORT STRUCTURE (TASK 2).	2-1
2.1 Introduction.	2-1
2.2 Superinsulation Optimization	2-3
2.2.1 Design	2-3
2.2.1.1 Tank Mounted Insulation System.	2-5
2.2.1.2 Alternate Considerations-Tank Mounted Insulation System	2-17
2.2.1.3 Shroud Mounted Insulation Sys- tem	2-21
2.2.1.4 Alternate Considerations.	2-33
2.2.1.5 Blanket Joint Design	2-34
2.2.1.6 Pressure Loads Due to Rapid Evacuation	2-48
2.2.1.7 Weights Analysis	2-53
2.2.2 Insulation System Thermal Performance	2-53
2.2.2.1 Candidate Insulation Systems	2-53
2.2.2.2 Assumptions	2-61
2.2.2.3 Insulation Configurations and Resulting Propellant Tank Heat Transfer	2-61
2.2.2.4 Thermal Analytical Parameters	2-66
2.2.2.5 Basis for Maximum Space Heat- ing Assumptions.	2-79
2.2.3 Performance Trade-Offs	2-81
2.2.4 Insulation Thickness Optimization	2-86

CONFIDENTIAL

TABLE OF CONTENTS (Continued)

Section		Page
	2.2.4.1 Shroud Mounted Insulation System	2-90
	2.2.4.2 Tank Mounted Insulation System	2-90
	2.2.4.3 Comparative Performance	2-91
2.2.5	Ground Thermal Performance	2-94
2.2.6	Selection Criteria.	2-94
	2.2.6.1 Ground Hold Capability	2-95
	2.2.6.2 Component Fabrication and Assembly	2-95
	2.2.6.3 Insulation Compression Effects.	2-95
	2.2.6.4 Structural Considerations	2-96
	2.2.6.5 Insulation Preconditioning	2-96
	2.2.6.6 Venting Through the Super-insulation	2-96
	2.2.6.7 Inspection and Checkout	2-96
	2.2.6.8 Cost.	2-96
	2.2.6.9 Boost Phase Heating Effects.	2-97
	2.2.6.10 Test Conditions	2-97
	2.2.6.11 Incorporation of Vent Free Fluorine System.	2-97
2.3	Support Structures	2-97
2.3.1	Outer Structural Shell	2-97
	2.3.1.1 Structural Configuration Comparisons	2-98
	2.3.1.2 Analysis Procedure	2-99
	2.3.1.3 Design Calculations	2-109
	2.3.1.4 Weights Analysis	2-112
2.3.2	Support Struts	2-114
	2.3.2.1 LF ₂ Tank Struts.	2-114
	2.3.2.2 LH ₂ Tank Struts.	2-114
3	INTEGRATED ATTITUDE CONTROL SYSTEM (IACS) STUDY	3-1
3.1	Introduction.	3-1
3.2	Design Parameters	3-1

CONFIDENTIAL

UNCLASSIFIED

TABLE OF CONTENTS (Continued)

Section	Page
4	PROPELLANT ORIENTATION 4-1
4.1	Introduction. 4-1
4.2	Capillary Devices. 4-1
5	PRESSURIZATION SYSTEM 5-1
5.1	Introduction. 5-1
5.2	Mission Requirements 5-1
5.3	Tank Pressure Requirements. 5-3
5.3.1	System Pressure Drop 5-4
5.3.1.1	Inertia Pressure Loss. 5-4
5.3.1.2	Friction Line Loss. 5-6
5.3.1.3	Maximum System Pressure Drop 5-7
5.3.1.4	Static Head Due to Acceleration 5-7
5.3.1.5	System Total Pressure Drop Characteristics 5-13
5.3.2	Inert Weights 5-13
5.3.2.1	Line Weights. 5-13
5.3.2.2	Residual Weights 5-13
5.3.3	Selected Line Size 5-13
5.4	Candidate Pressurization Schemes 5-16
5.4.1	Ambient Helium 5-16
5.4.2	Cold Helium 5-16
5.4.3	Supercritical Helium. 5-16
5.4.4	Hot Hydrogen 5-16
5.4.5	Main Tank Injection 5-18
5.5	Thermodynamic Pressurization Models 5-18
6	REFERENCES. 6-1

UNCLASSIFIED

UNCLASSIFIED

LIST OF FIGURES

Figure		Page
1-1	Propellant Tank Design (Tasks 2 and 3)	1-2
1-2	Tank Configuration Selection Evaluation	1-4
1-3	Equatorial Butt Weld at the Tangent Line	1-7
1-4	Oxidizer Tank Weight versus a/b	1-8
1-5	Fuel Tank Weight versus a/b	1-9
1-6	System Weight versus Oxidizer Tank a/b	1-11
1-7	Oxidizer Tank Weight versus a/b	1-13
1-8	Fuel Tank Weight versus a/b	1-14
1-9	System Weight versus Oxidizer Tank a/b	1-15
1-10	Oxidizer Tank Weight versus a/b	1-19
1-11	Fuel Tank Weight versus a/b	1-20
1-12	Tank Wall Thickness Required for Meteoroid Protec- tion	1-23
1-13	AMPS Structural Shroud	1-27
1-14	Yearly Sporadic Meteor Flux	1-29
2-1	Thermal Conditioning and Support Structure	2-2
2-2	Superinsulation Optimization	2-4
2-3	AMPS Tank Mounted Insulation System.	2-6
2-4	Blanket Gore Interconnection	2-7
2-5	Insulation Wrapping	2-10
2-6	Typical Chill Plate Penetration	2-10
2-7	Tank Assembly Procedure.	2-12
2-8	Fuel Tank Support Pin Location	2-13
2-9	Support Pin Load	2-14
2-10	Insulation Reinforcement	2-16
2-11	Blanket Attachment Bonds	2-19
2-12	Aluminized One Mil Mylar Face Sheets	2-20
2-13	Tape-reinforced One Mil Mylar Face Sheets.	2-20
2-14	AMPS Shroud Mounted Insulation System	2-22
2-15	Twin Pin Fastener Assembly	2-24
2-16	Blanket Support Pins.	2-24
2-17	Blanket Support Pin Detail.	2-25
2-18	Completed Drop Cord Installation	2-25
2-19	Side Wall Blanket Overlap	2-26
2-20	Drop Cord Attachment Assembly.	2-26
2-21	Blanket Position and Interconnection	2-27
2-22	Inboard Blanket Layer	2-28

UNCLASSIFIED

UNCLASSIFIED

LIST OF FIGURES (Continued)

Figure		Page
2-23	Adapter Ring Attachment	2-28
2-24	Side Wall Insulation Access Opening	2-29
2-25	Blanket Support Pin Load	2-30
2-26	Blanket Face Sheet Load	2-31
2-27	Scrim Base Load Conditions	2-32
2-28	Cylinder Radius and Hoop Load	2-33
2-29	Side Wall Attachment with Fiberglass Pins	2-34
2-30	Spot Bonded Blankets with Pressure Sensitive Tape	2-35
2-31	Spot Bonded Blankets with Velcro Tape	2-36
2-32	Velcro Tape Attachment	2-36
2-33	Single Pin Blanket Attachment with Velcro Tape	2-37
2-34	Snap Pin Blanket with Dacron Lacing	2-38
2-35	Laced Blanket with Velcro Tape	2-40
2-36	Fiberglass Twin Pin Fastener	2-41
2-37	Gore Line Fasteners.	2-42
2-38	Weight Breakdown - Gore Line Fastener	2-44
2-39	Typical Test Specimen	2-45
2-40	Test Result Summary	2-46
2-41	Tear-Out Test Setup.	2-47
2-42	Side Wall Batten	2-49
2-43	Propellant Tank Equator	2-51
2-44	Four Blanket Installation	2-51
2-45	Detailed Weights Analysis	2-54
2-46	Insulation System Weight versus Number of Layers	2-55
2-47	Insulation Comparison - NRC-2, Dimplar and Superfloc	2-57
2-48	Compressions and Recovery Test Results.	2-59
2-49	Propellant Tank Heat Transfer - Space Conditions.	2-62
2-50	Propellant Tank Heat Transfer - Space Conditions.	2-63
2-51	Propellant Tank Heat Transfer - Ground Conditions	2-64
2-52	Propellant Tank Heat Transfer - Ground Conditions	2-65
2-53	Typical AMPS Superinsulation Lay-Up.	2-67
2-54	AMPS Superinsulation Optimization Analysis.	2-68
2-55	Emittance of Superfloc Mylar Sheets	2-70
2-56	Overall Radiative Exchange Factor Between Parallel Shields With the Same Area but Different Emittance	2-71
2-57	Dimensionless Function $f(\delta/t)$ for Computation of Super- insulation Seam Heat Leak.	2-73
2-58	Local Strut Temperature Determination	2-75
2-59	Single Strut Heat Transfer Rates.	2-76
2-60	Single Strut Heat Transfer.	2-77

UNCLASSIFIED

CONFIDENTIAL

LIST OF FIGURES (Continued)

Figure		Page
2-61	AMPS Vehicle Tank Strut Configuration	2-78
2-62	Cylindrically Configured Shroud-Tank Combinations . .	2-79
2-63	AMPS Performance Penalties: Mission Number 1 . . .	2-82
2-64	AMPS Performance Penalties: Mission Number 2 . . .	2-83
2-65	AMPS Performance Penalties: Mission Number 3 . . .	2-84
2-66	AMPS Fuel Tank Inert Weight Variance	2-87
2-67	Shroud Mounted Insulation 14 Day Mission	2-88
2-68	Tank Mounted Insulation 14 Day Mission	2-89
2-69	Insulation System Weight versus Heat Transfer to Pro- pellant Tanks	2-92
2-70	Insulation System Weight Compression - Equal Heat Input, versus Equal Layers	2-93
2-71	Titan IIIC (0,1,2)/AMPS Bending Moments and Axial Loads.	2-101
2-72	Titan III Design Flutter Boundaries.	2-103
2-73	Axial Loaded Cylinder Correlation Factors	2-105
2-74	Z Factors for Axial Loaded Cylinders	2-108
3-1	Integrated Attitude Control System - Single Combustor .	3-2
3-2	Advanced Attitude Control System Schematic (Single Combustor).	3-3
3-3	Integrated Attitude Control System (IACS) Study. . . .	3-4
4-1	Propellant Orientation (Task 6)	4-2
4-2	A Propellant Orientation Concept	4-3
5-1	Pressurization System Study (Task 8)	5-2
5-2	LF ₂ 3.0 Inch Line System Start Transient Pressure Drop	5-5
5-3	LH ₂ 2.5 Inch Line System Start Transient Pressure Drop	5-8
5-4	LF ₂ Feed Line Maximum Pressure Drop versus Line Diameter	5-9
5-5	LH ₂ Feed Line Maximum Pressure Drop versus Line Diameter	5-10
5-6	gph Head versus Time Oxidizer Duct	5-11
5-7	LF ₂ Propellant Feed System - Total System Pressure Drop During Start Transient - First Burn.	5-12
5-8	Propellant Line Weight versus Diameter	5-14
5-9	Propellant Residuals versus Line Diameter	5-15

CONFIDENTIAL

CONFIDENTIAL

LIST OF FIGURES (Continued)

Figure		Page
5-10	Helium Storage Weights.	5-17
5-11	Outflow Pressurization Hydrogen Collapse Factor . . .	5-19
5-12	Outflow Pressurization Oxygen Collapse Factor. . . .	5-20
5-13	Ullage Mixing	5-21

LIST OF TABLES

Table		Page
1-1	Optimum Configuration Weighting Factors	1-5
1-2	Ultimate and Yield Allowables	1-6
1-3	Oxidizer and Fuel Tank Combination	1-10
1-4	Tank Material Combinations and Weights	1-10
1-5	Tank Material Combinations and Weights	1-16
1-6	Wall Gages for Meteoroid Requirement	1-16
1-7	Adjusted System Weight and Tank Configuration. . . .	1-17
1-8	Final System Weight Comparison	1-18
1-9	Tank Combination Weight Penalties	1-21
1-10	Design Meteoroid Mass as a Function of Space Resid- ence	1-30
1-11	Material Thickness Equation Values	1-31
1-12	Single Wall Thicknesses for Non-Penetration Require- ments.	1-31
1-13	Tank Wall Thicknesses for Meteoroid Requirements . . .	1-32
1-14	Yield and Tensile Strength-to-Density Ratios	1-35
2-1	Candidate Systems	2-56
2-2	Insulation Spacer Weight Comparison	2-60
2-3	Superinsulation and Ground Operation Insulation Con- figurations	2-61
2-4	Performance Basis (14-Day Mission)	2-85
2-5	Comparative Mission Performance	2-91
2-6	Comparative Shell Weights.	2-98
2-7	Required Dimensions, Station 110	2-100

CONFIDENTIAL

UNCLASSIFIED

LIST OF TABLES (Continued)

Table		Page
2-8	Properties of Materials.	2-110
2-9	Ring-Stiffened Monocoque Structures	2-111
2-10	AMPS Shell Structure	2-113
3-1	Vehicle Operating Conditions and AACS Requirements .	3-5
3-2	List of IACS Information Received from BAC	3-7
5-1	Fourteen Day Missions and Performance	5-3
5-2	System Maximum Pressure Drop	5-13

UNCLASSIFIED

CONFIDENTIAL

SUMMARY

(U) This report presents the work conducted during the second quarter on Task III of the Advanced Maneuvering Propulsion System (AMPS) program.

(U) Two major portions of the task were accomplished. The propellant tank material and shape were determined and the optimum insulation system was defined. This allowed the establishment of the basic system configuration which can now be used for subsequent subsystem investigations (Illustration on page xiii).

(C) Each propellant tank is constructed from 2219 T81 aluminum with one piece bulkheads. The hydrogen tank is spherical while the fluorine tank has a bulkhead ratio of 1.2. The tanks are suspended with fiberglass support struts from a skin stringer 2024-T86 aluminum conical structural shroud.

(C) The superinsulation is mounted on the propellant tanks with the hydrogen tank requiring 45 layers and the fluorine tank requiring 32 layers. The degradation in ideal ΔV capability due to the insulation weight and hydrogen boil-off is approximately 2.5 percent for the most sensitive mission which is the 90 percent burn on the first day and 10 percent burn on the last day.

(U) The main selection criterion in arriving at the tank and insulation configuration is maximum vehicle performance in terms of ΔV capability, but there were many other factors evaluated prior to the final selection.

(U) During this reporting period there were three other tasks initiated: the integrated attitude control system study, the pressurization system study, and the propellant orientation study.

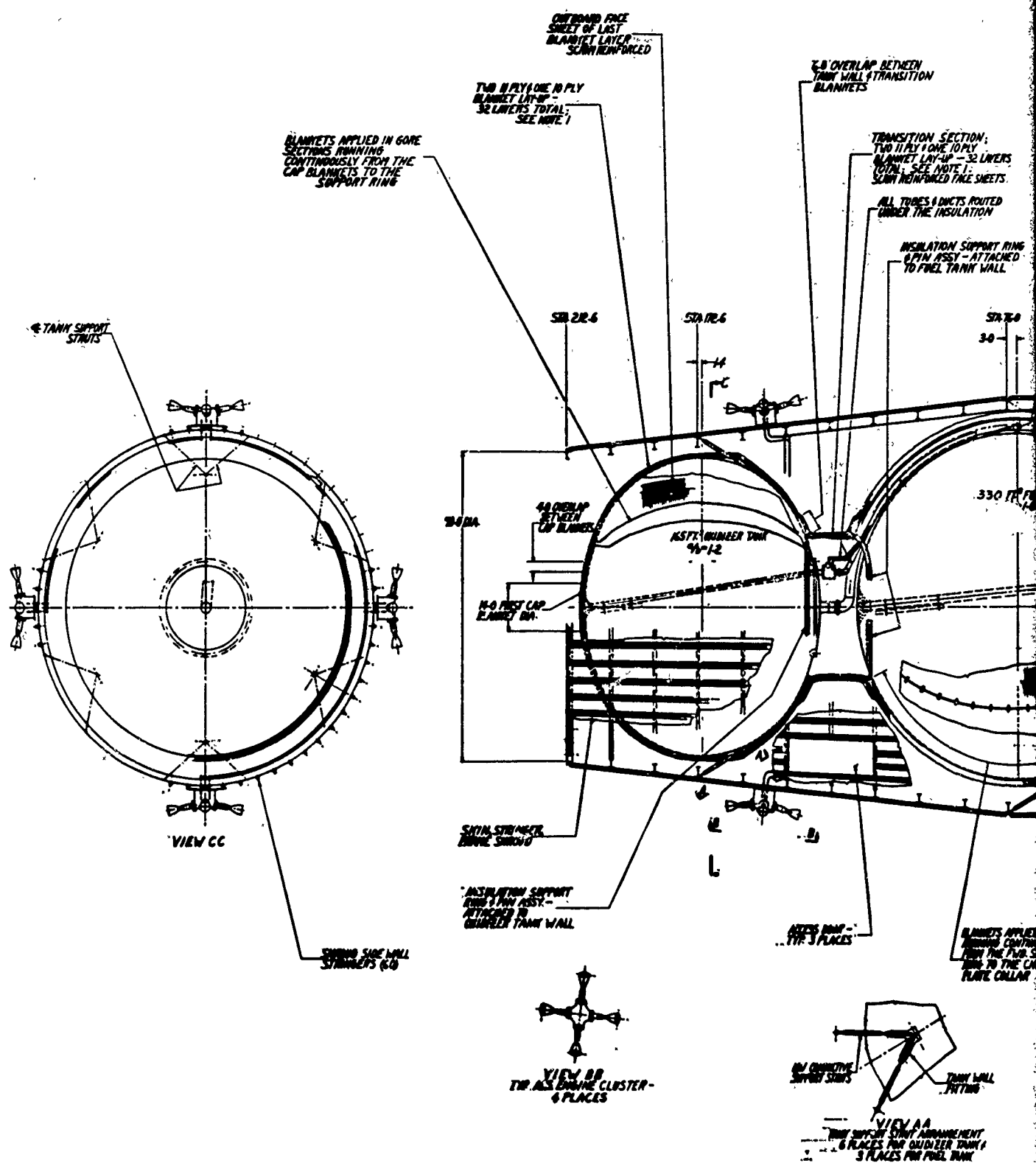
(U) The basic data for the integrated ACS study was obtained from Bell Aerospace Company. The initial task in this area is concerned with evaluating the vehicle compartment temperature extremes with respect to the IACS and to determine the heat load from the ACS pumps to the cryogenic liquids.

(U) The propellant orientation study was initiated at the end of this quarter, with the preliminary effort concerned with reviewing a broad range of concepts.

(U) The pressurization system task also began the last month of this quarter with the initial analytical work centered on qualitative comparison of different concepts, consideration of the most severe mission combinations, and evaluation of various thermodynamic models. A system pressure drop analysis was conducted to determine propellant feed line sizes and pressure drops, and consequently to establish tank pressure requirements.

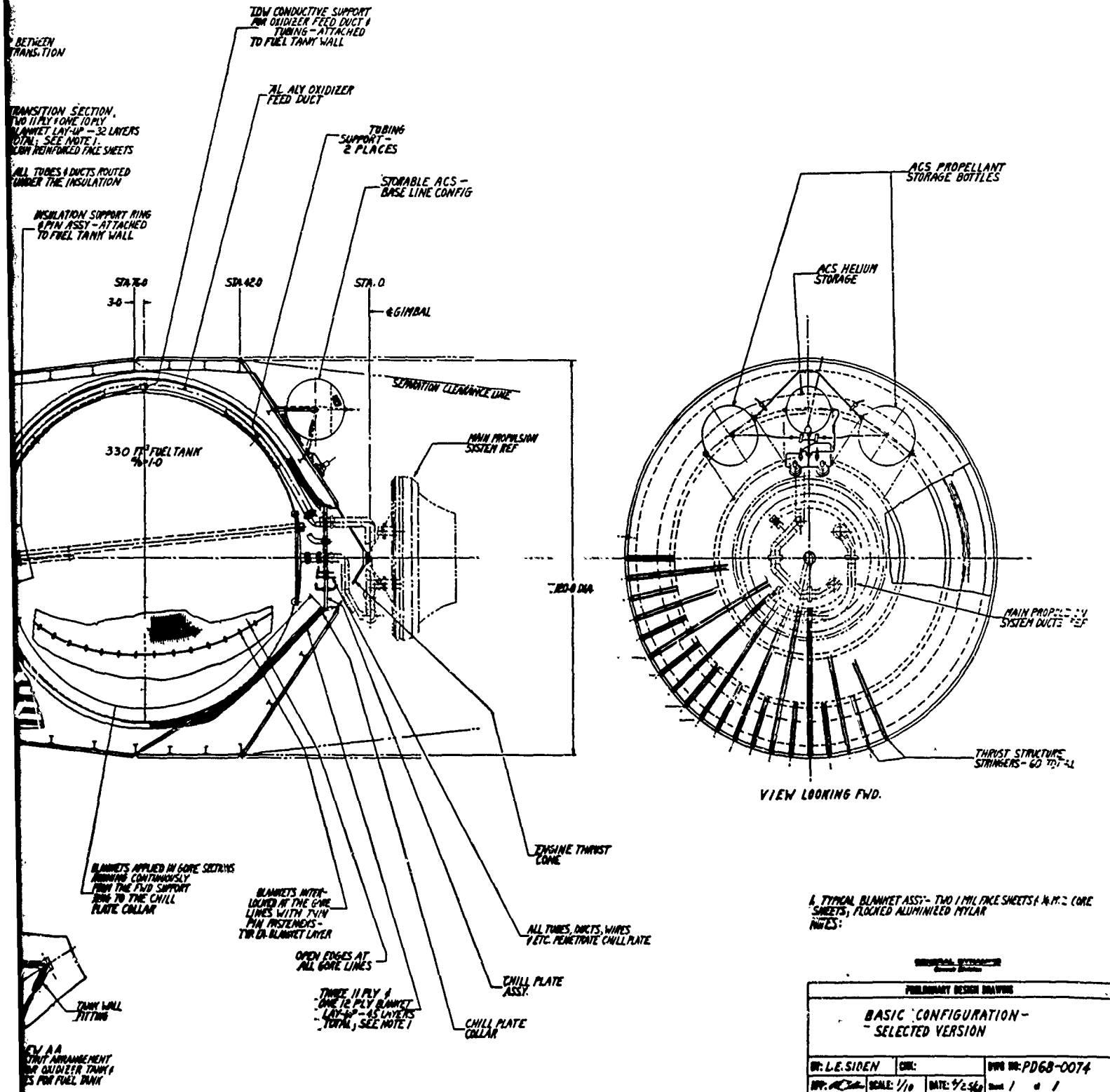
CONFIDENTIAL

CONFIDENTIAL



CONF

CONFIDENTIAL



ORIGINAL SPECIFICATION			
PRELIMINARY DESIGN DRAWING			
BASIC CONFIGURATION - SELECTED VERSION			
DR: L.E. SIDEN	CHK:	DWG NO: PD68-0074	
APP: [Signature]	SCALE: 1/10	DATE: 9-2-68	Sheet 1 of 1

(C) Basic Configuration - Selected Version

CONFIDENTIAL

CONFIDENTIAL

SECTION 1

LH₂ AND LF₂ PROPELLANT TANKS (C)

1.1 INTRODUCTION

(U) The initial requirement in the design of the propellant tanks is the selection of the optimum tank materials and tank shape. In order to accomplish this a preliminary sizing study was conducted to establish the tank volumes. A detailed tradeoff study was then conducted to determine the optimum tank material and shape using minimum system weight as the main criterion, but considering many other factors.

(U) Following the selection of the optimum tank combination a flight configuration drawing will be evolved using the results of the superinsulation optimization study and the structural shell study. This will allow the iteration of the system weight and sizing, combined with the latest estimates of subsystem weight. The tanks for the ground test article can then be designed. As system requirements are modified during the course of the study the tank drawings will be updated.

(U) The effort conducted during the second quarter of the study was concerned with the tank optimization and is described in detail in the following discussion. The design of the tanks for the ground test article will be conducted during the next quarter. A simple time-oriented flow diagram of this task is given in Figure 1-1, with the shaded areas representing the tasks completed.

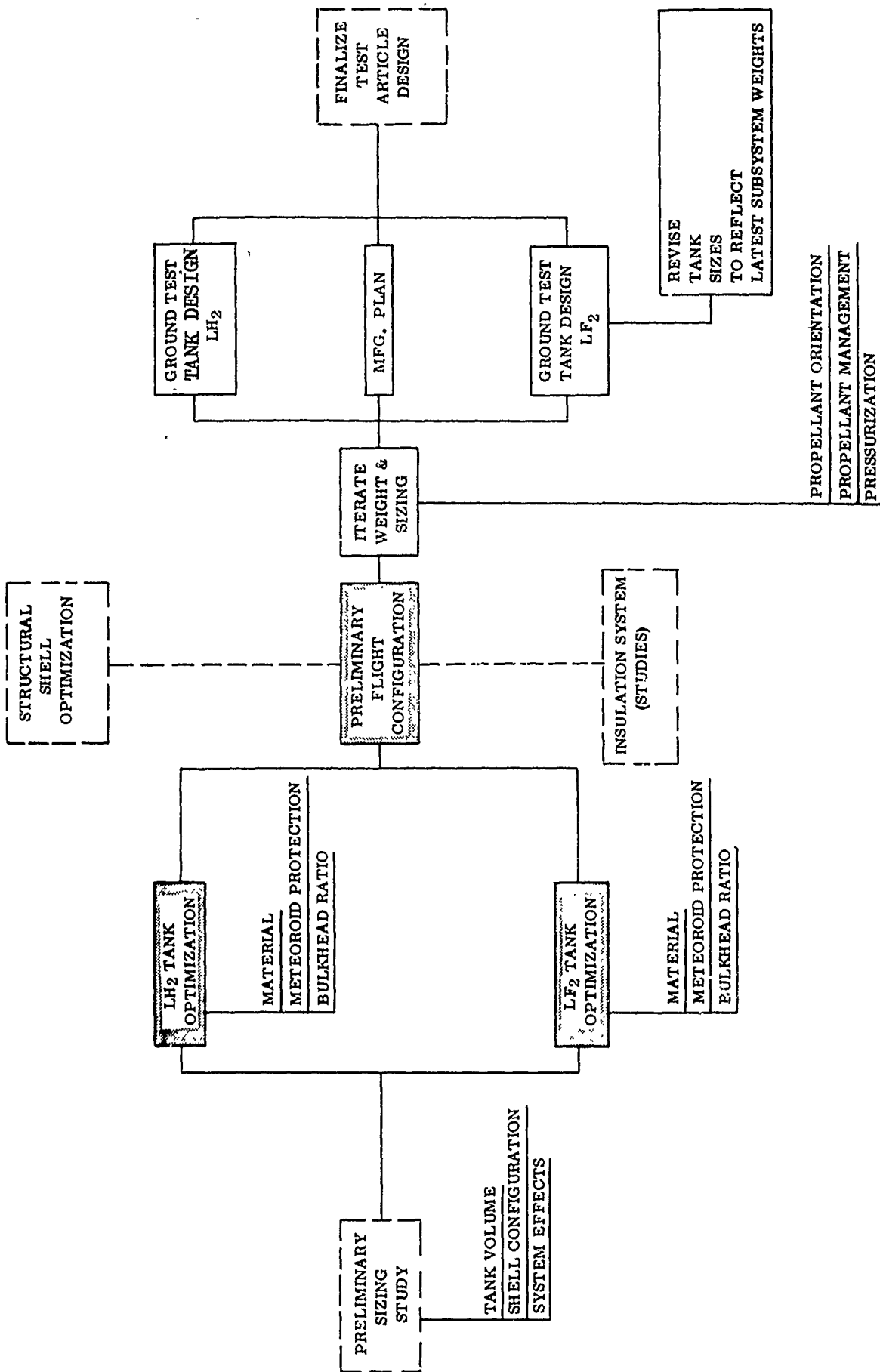
1.2 SELECTED TANK CONFIGURATION

(U) Previous studies have shown that the optimum AMPS type vehicle configuration consists of the two propellant tanks suspended from an outer structural shroud. The basic factors that remained to be established were the optimum tank material and tank bulkhead ratio.

(C) The selection of the optimum vehicle structural configuration has been completed during this quarter, resulting in a conical outer shroud with a spherical LH₂ tank (skin gage 0.0408) and a LF₂ tank (skin gage 0.0491) with a bulkhead ratio of 1.2. The tanks are constructed of 2219-T81 aluminum with one-piece bulkheads. Different tank combinations were considered varying both material and bulkhead ratio. Six basic combinations were evaluated as follows:

CONFIDENTIAL

CONFIDENTIAL



(C) Figure 1-1. Propellant Tank Design

CONFIDENTIAL

CONFIDENTIAL

(C)	<u>LF₂ Tank</u>	<u>LH₂ Tank</u>
(1)	301-3/4 H CRES	301-3/4 H CRES
(2)	718 Annealed and aged Ni base alloy	718 Annealed and aged Ni base alloy
(3)	2219-T81 aluminum	2219-T81 aluminum
(4)	2219-T81 aluminum	Titanium 5Al-2.5 Sn ELI
(5)	718 Ni base alloy annealed and aged	Titanium 5Al-2.5 Sn ELI
(6)	Titanium 5Al-2.5 Sn ELI	Titanium 5Al-2.5 Sn ELI

(C) For each combination the system variable weight was calculated as a function of tank bulkhead ratio. The variable weight included tank weights (LF₂ and LH₂), shroud weight, and propellant residuals. This allowed the selection of optimum tank bulkhead ratios for each combination using weight as the comparison criteria. The optimum combinations (i. e., bulkhead ratio) for each of the above six cases were then compared considering many factors, with weight being the most significant. From this comparison a final selection was made, with the above described aluminum tank combination resulting in the optimum system shown in Figure 1-2. In each of the columns the rating to the left of the slash refers to the LF₂ tank and to the right of the slash refers to the LH₂ tank.

(U) The tank combination that ranked second was an aluminum fluorine tank with a bulkhead ratio of 1.2 and titanium fuel tank with a bulkhead ratio of 1.1.

1.3 EVALUATION FACTORS

(U) The factors considered in establishing the optimum configuration were weighted as shown in Table 1-1.

(U) The establishment of a weighting value for these evaluation factors is obviously subjective. These values were derived based on General Dynamics Convair's (GDC) experience with cryogenic upper stage vehicle work and on the requirement for maximum stage ΔV without compromising the extended space residence capability.

(U) 1.3.1 SYSTEM WEIGHT. The most significant factor, by far, of all the selection criteria is the weight, since the available ideal ΔV is a direct function of this item. Consequently, it was weighted with a 45 percent importance rating, which is 4-1/2 times as much as any other item.

CONFIDENTIAL

CONFIDENTIAL

MATERIAL ALLOWABLES & TANK GAGES FOR COMBINATIONS SHOWN

MATERIAL	OXIDIZER TANK			FUEL TANK			GAGE REQ'D FOR METEOROID PROTECTION		WELD JOINT EFFICIENCY
	F_{tu} 75°F	F_{ty} 75°F	GAGE	F_{tu} 75°F	F_{ty} 75°F	GAGE			
301-3/4 H	169,000	120,000	.0181	169,000	120,000	.0170	.0157	14 DAYS	60%
2219-T81	60,000	44,000	.0491	60,000	44,000	.0408	.0304		50%
718-20% CW AGED	190,000	180,000	.0156	190,000	180,000	.0158	.0150		60%
TITANIUM 5AL-2.5 Sn ELI	100,000	90,000	.0270	100,000	90,000	.0255	.0227		90%
718 (A) AGED	180,000	150,000	.0163	180,000	150,000	.0150	.0150		60%

OPTIMUM TANK COMBINATION

OXIDIZER	FUEL	SYSTEM WEIGHT / RATING	COMPA- TIBI- LITY WITH PRO- PELLANT	METEOROID PROTECTION		FABRICATION WELDABILITY		
				SPACE RESID. MARGIN	RATING	FUSION WELDS	FUSION WELD REPAIRS	TIG SPOT WELDS
301-3/4 H a/b = 1.2	301-3/4 H a/b = 1.1	849.9 / .50	1.0/1.0	8/4	.577/.595	1.0/1.0	1.0/1.0	1.0/1.0
718 (A) AGED a/b = 1.3	718 (A) AGED a/b = 1.1	817.6 / .763	0.9/1.0	4/0	.54/0	0.7/0.7	0.7/0.7	0.7/0.7
2219-T81 a/b = 1.2	2219-T81 a/b = 1.0	804.2 / .872	0.9/1.0	52/21	1.0/1.0	0.7/0.7	1.0/1.0	0.5/0.5
2219-T81 a/b = 1.2	Ti-5AL-2.5 Sn ELI a/b = 1.1	790.3 / .985	0.9/1.0	52/5.5	1.0/.631	0.7/0.6	1.0/0.1	0.5/0.5
718-20% CW AGED a/b = 1.3	Ti-5AL-2.5 Sn ELI a/b = 1.1	788.5/1.0	0.9/1.0	2/5.5	.52/.631	0.7/0.6	0.7/0.1	0.7/0.7
Ti-5AL-2.5 Sn ELI a/b = 1.2	Ti-5AL-2.5 Sn ELI a/b = 1.1	776.9	NO/1.0					
RATING FACTORS →		45%			5%	4%	4%	1%

NOTE: ONE PC. BHDS FOR 2219-T81 TANKS.
GORE CONSTRUCTED BHDS. FOR 718, 301 & TITANIUM TANKS.

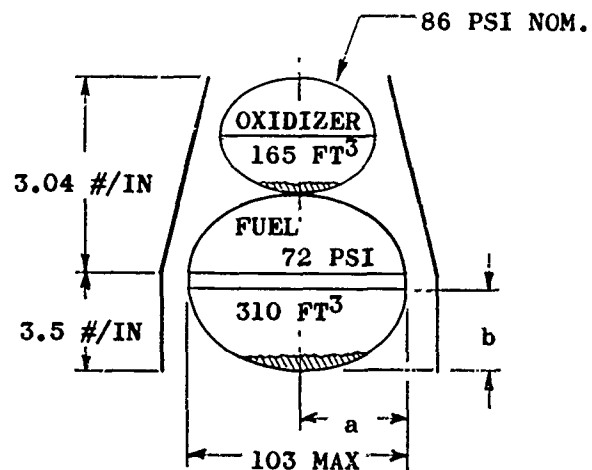
CONFIDENTIAL

CONFIDENTIAL

SYSTEM WT. = TANKS + RESIDUALS + SHROUD WT.

REQ'D METEOROID PROTECTION		WELD JOINT EFFICIENCY
14 DAYS		60%
		50%
		60%
		90%
		60%

OXIDIZER
TANK
RATING → **X/X** ← FUEL
TANK
RATING



FABRICATION WELDABILITY					WELD SEAM		FRACTURE TOUGHNESS		*		COST	TOTAL RATING %
N	FUSION WELD REPAIRS	TIG SPOT WELDS	RESIST SPOT WELDS	FORM- ABILITY	LENGTH INCHES	RATING	BASE METAL	JOINTS	INTER- FACE SEALS	DIS-SIM METALS ELECTRO CORRO.		
0	1.0/1.0	1.0/1.0	1.0/1.0	1.0/1.0	2533/3414	0/0	1.0/0.5	1.0/0.3	.8/1.0	.8/1.0	1.0/1.0	66.18
7	0.7/0.7	0.7/0.7	0.7/0.7	0.9/0.9	2030/2794	.2/.182	1.0/1.0	1.0/1.0	.8/1.0	.8/1.0	0.8/0.8	76.78
7	1.0/1.0	0.5/0.5	0.9/0.9	0.8/0.8	273/316	.89/.907	1.0/0.9	1.0/0.9	1.0/0.8	1.0/0.8	0.9/0.9	88.07
6	1.0/0.1	0.5/0.5	0.9/0.9	0.8/0.3	273/2794	.89/.182	1.0/0.9	1.0/0.9	1.0/0.8	1.0/1.0	0.9/0.5	84.03
6	0.7/0.1	0.7/0.5	0.7/0.9	0.9/0.3	2030/2794	.2/.182	1.0/0.9	1.0/0.9	.8/0.8	.8/1.0	0.7/0.5	80.48
												NOT COMPA- TIBLE
	4%	1%	1%	10%		5%	5%	8%	1%	1%	10%	

RATING 0.5 TO 1.0 (0.5 POOR & 1.0 BEST) FOR
METEOROID PROTECTION & SYSTEM WEIGHT

RATING 0.0 TO 1.0 (0.0 POOR & 1.0 BEST) FOR ALL OTHERS

*ALUMINUM DUCTS FOR OXIDIZER TANKS & CRES OR MONEL FOR FUEL TANKS.

Figure 1-2. Tank Configuration Selection Evaluation

CONFIDENTIAL

2

CONFIDENTIAL

(U) TABLE 1.1. OPTIMUM CONFIGURATION WEIGHTING FACTORS

Factor	Weight (percent)
Weight	45%
Formability	10%
Cost	10%
Meteoroid Protection Margin	5%
Length of Weld Seams	5%
Toughness (base material)	5%
Toughness (weld joints)	8%
Fusion Welds	4%
Fusion Weld Repairs	4%
TIG Spotwelds	1%
Resistance Spotwelds	1%
Interface Sealing	1%
Dissimilar Metal Problems	1%

(U) The assumptions and procedures employed in calculating the tank wall gages, weld zone gages, shroud weights, and residuals were reported in detail in the first quarterly progress report. The analysis was expanded to cover the following materials:

301 - 3/4 H steel
718 nickel base alloy (annealed + aged)
Titanium (annealed) 5Al-2.5 Sn ELI

(C) 1.3.1.1 Design Assumptions. The following assumptions were used as a basis for calculating the system weights:

(C) a. Tank Volumes

LF₂: 165 ft³

LH₂: 310 ft³

(U) b. Design Factors

1.25 × operating pressure - stressed to F_{tu}

1.00 × operating pressure - stressed to F_{ty}

Wall gages were checked for both conditions and the maximum value was chosen. These design factors have been accepted by the Air Force and NASA.

CONFIDENTIAL

CONFIDENTIAL

(U) c. Weld Efficiencies

301 60 percent yield
718 60 percent ultimate
Titanium 90 percent yield
2219 50 percent yield

In order to obtain a 100 percent joint efficiency it becomes necessary to provide a weld "land" (a built-up area) or to use a doubler. This results in additional weight in the weld areas as a one-inch wide heat zone is considered on each side of the weld.

(U) d. Ultimate and Yield Allowables. The ultimate and yield allowables shown in Table 1-2 were used:

(U) TABLE 1-2. ULTIMATE AND YIELD ALLOWABLES

	-320° F		-200° F		Room Temp.	
	F _{tu}	F _{ty}	F _{tu}	F _{ty}	F _{tu}	F _{ty}
301-3/4 H	250, 000	135, 000	227, 000	124, 000	169, 000	120, 000
2219-T81	74, 500	52, 800	66, 000	48, 400	60, 000	44, 000
718 Annealed (aged)	247, 000	133, 000	228, 000	180, 000	180, 000	150, 000
718 (20% cold worked)					190, 000	180, 000
Ti 5Al-2.5 Sn ELI	180, 000	168, 000	152, 000	144, 000	100, 000	90, 000
Ti 6Al-4V	205, 000	200, 000				

Two Titanium alloys were considered: 5Al-2.5 Sn ELI and 6Al-4V. The 5Al-2.5 Sn ELI material was selected over the 6Al-4V in the final analysis due to its superior notch sensitivity properties at low temperatures.

(C) e. Outer Shroud Weights. The outer shroud weights were assumed to be 3.5 lb/in. for the cylindrical section and 3.04 lb/in. for the tapered section.

(U) f. Residual Weights. The residual weights were based on 12 inch baffles at the tank outlet, assuming no start baskets. These weight calculations were reported in the previous quarterly report. The residual weights without start baskets are used for the comparison criterion since the selection of a propellant orientation device remains to be accomplished.

CONFIDENTIAL

CONFIDENTIAL

(C) g. Tank Diameters. The tank diameters were limited to 103 inches to allow sufficient clearance between the outer shell and the propellant tanks; considering shell frames, superinsulation, and propellant feed lines. This imposed no problem on the LF_2 tank since at all a/b considered the major axis was less than 103 inches; however, because of the larger size of the LH_2 tank, a cylindrical section is required when the a/b is between 1.05 and 1.1.

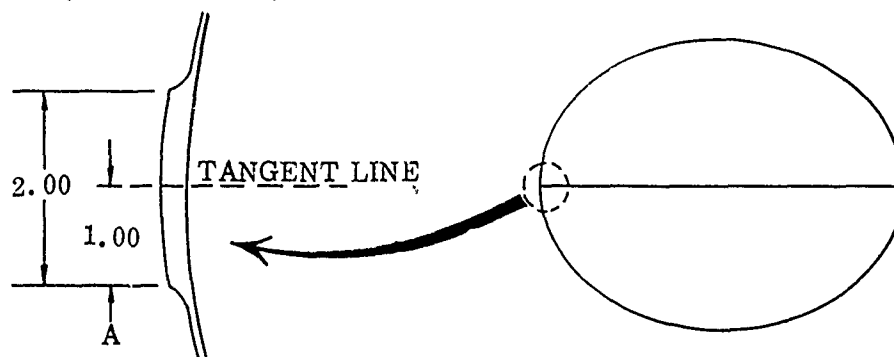
(C) h. Tank Operating Pressures. The tank operating pressures are as follows:

LF_2 tank forward shell - 83 psia

LF_2 tank aft shell - 86 psia

LH_2 tank - 72 psia

(C) 1.3.1.2 One-Piece Bulkheads, Cold Allowables. In order to obtain a minimum weight, optimum system it was first assumed that all tanks could be constructed of one-piece bulkheads using the cold allowable temperatures. The cold allowables are based on material temperatures being maintained within approximately $100^\circ F$ of the propellant temperatures (i. e., $-200^\circ F$ for F_2 tank, $-320^\circ F$ for H_2 tank). One-piece, constant gage bulkheads were assumed using a single two-inch wide equatorial butt weld at the tangent line. (See Figure 1-3).



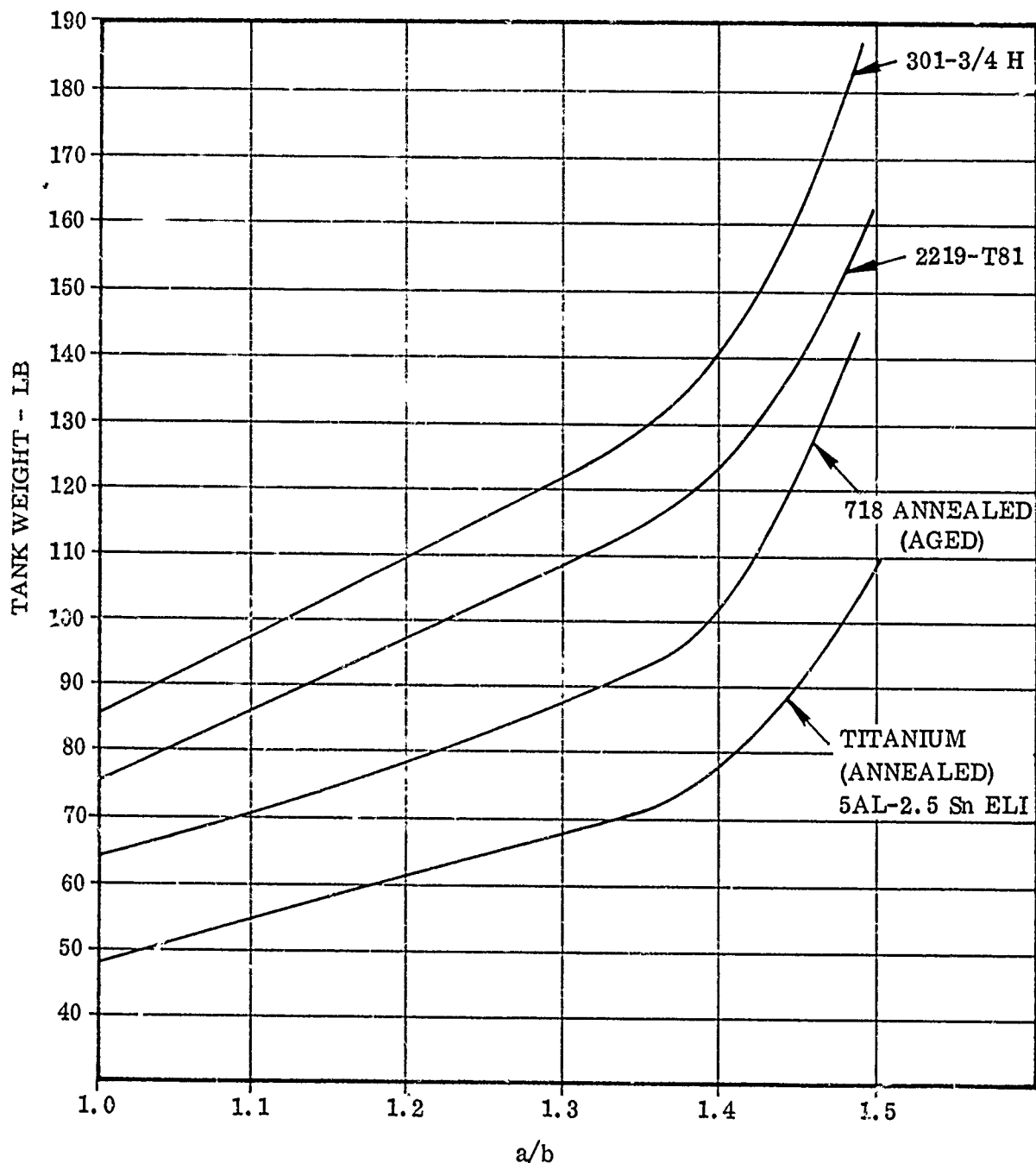
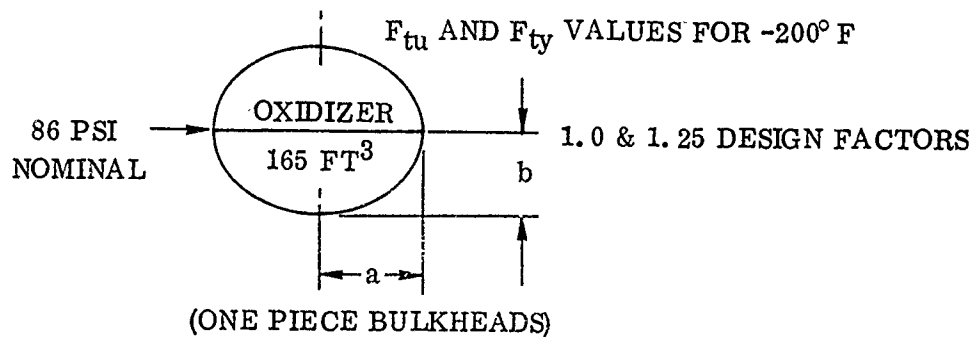
(U) Figure 1-3. Equatorial Butt Weld at the Tangent Line

(U) Tank weights versus a/b ratios were plotted for each material as shown in Figures 1-4 and 1-5.

(U) The oxidizer and fuel tanks were coupled as shown in Table 1-3 and the system weight (tank weights + residual weights + outer shroud weight) was calculated for each combination.

CONFIDENTIAL

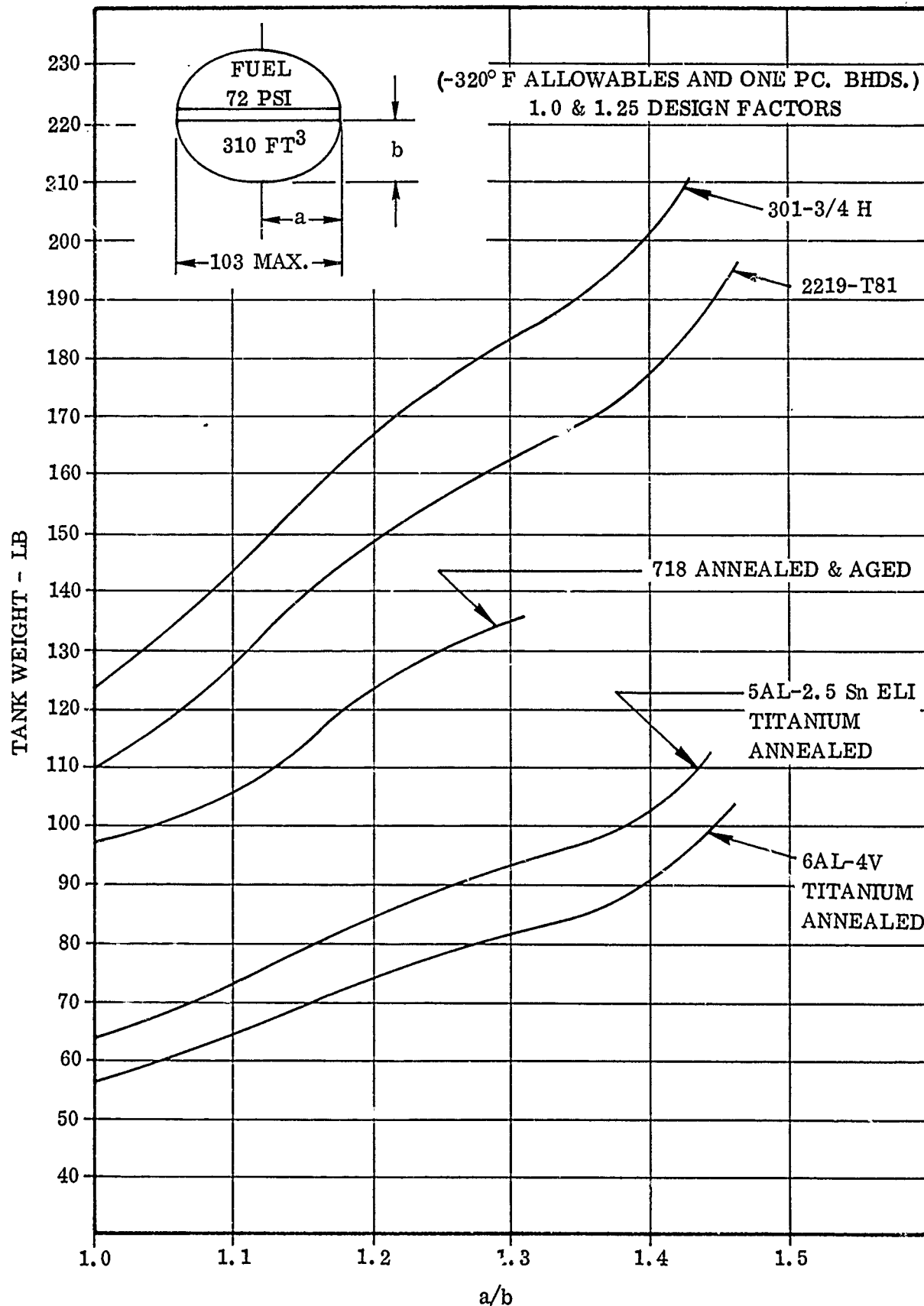
CONFIDENTIAL



(C) Figure 1-4. Oxidizer Tank Weight versus a/b

CONFIDENTIAL

CONFIDENTIAL



(C) Figure 1-5. Fuel Tank Weight versus a/b (-320° F Allowables and One-Piece Bulkheads)

CONFIDENTIAL

CONFIDENTIAL

(C) TABLE 1-3. OXIDIZER AND FUEL TANK COMBINATION

Fuel Tank a/b	Oxidizer Tank a/b	Fuel Tank a/b	Oxidizer Tank a/b
1.0 1.1 1.2 1.38	1.0	1.0 1.1 1.2 1.38	1.3
1.0 1.1 1.2 1.38	1.2	1.0 1.1 1.2 1.38	1.38

(C) Since each combination of LF_2 tank a/b and LH_2 tank a/b has a unique value of propellant residual and shroud length (ergo weight) the total system weight can be presented as a function of tank a/b combination. Figure 1-6 shows a plot of this for the aluminum tank combination. A similar calculation was made for each of the proposed material combinations. The optimum point can then be taken for each tank material combination, and these points are as shown in Table 1-4.

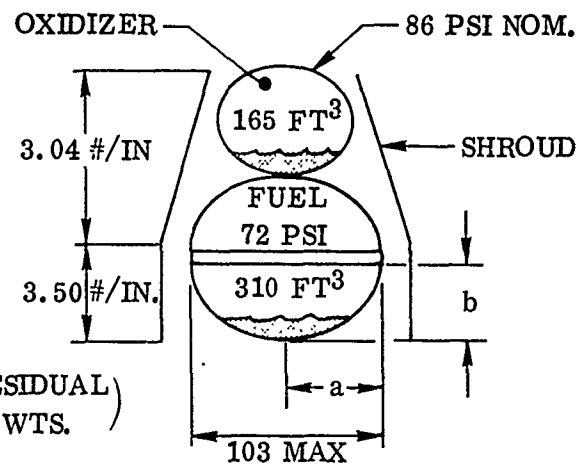
(C) TABLE 1-4. TANK MATERIAL COMBINATIONS
AND WEIGHTS (COLD ALLOWABLES)

Tank Combination for Optimum System Weight		System Weight (lb)	Tank Wall Gage	
LF_2	LH_2		LF_2	LH_2
301-3/4 H a/b = 1.2	301-3/4 H a/b = 1.0	799.06	0.0174	0.0134
2219-T81 a/b = 1.2	2219-T81 a/b = 1.0	772.45	0.0447	0.0340
718 (A) Aged a/b = 1.3	718 (A) Aged a/b = 1.1	733.3	0.0132	0.0106
2219-T81 a/b = 1.2	Ti5Al-2.5 Sn ELI a/b = 1.1	720.95	0.0447	0.0142
718 (A) Aged a/b = 1.3	Ti5Al-2.5 Sn ELI a/b = 1.1	700.9	0.0132	0.0142
Ti5Al-2.5 Sn ELI a/b = 1.38	Ti5Al-2.5 Sn ELI a/b = 1.1	680.8	0.0214	0.0142

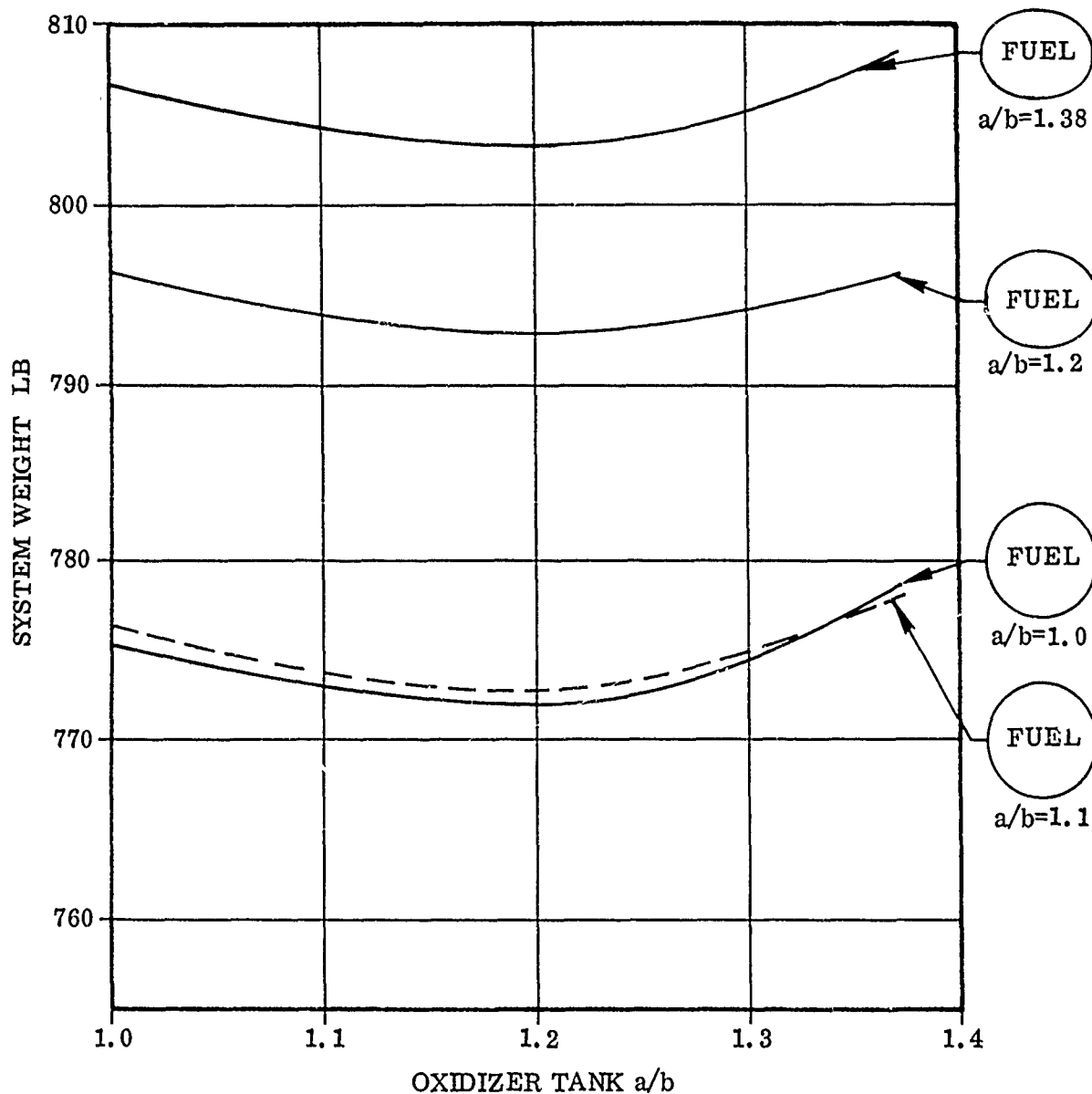
CONFIDENTIAL

CONFIDENTIAL

SINGLE PC. BHDS
ALLOWABLES BASED ON
-200° F FOR OXIDIZER TANK
-320° F FOR FUEL TANK
2219-T81 TANKS



$$\left(\begin{matrix} \text{SYSTEM} \\ \text{WT.} \end{matrix} \right) = \left(\begin{matrix} \text{SHROUD} \\ \text{WT.} \end{matrix} \right) + \left(\begin{matrix} \text{TANK} \\ \text{WTS.} \end{matrix} \right) + \left(\begin{matrix} \text{RESIDUAL} \\ \text{WTS.} \end{matrix} \right)$$



(C) Figure 1-6. System Weight versus Oxidizer Tank a/b

CONFIDENTIAL

CONFIDENTIAL

(C) These weights represent the optimum combination of tanks for the various materials. A titanium LF_2 tank was considered to establish the weight advantage of such a system if it could be used; however, it is ruled out for this application because of compatibility problems with LF_2 .

(U) It can be seen from Figure 1-6 that the system weight is quite flat as a function of a/b ratio, which means that factors other than weight could affect the final selection. This is also true for the other tank combinations.

(U) Although minimum weight is achieved with low temperature allowables, in reality this is often not a practical design basis. If low temperature allowables are used, this means that at no time during checkout and test can the tanks be exposed to operating pressures under ambient conditions. This becomes even more critical when it is considered that the pressurization system has not yet been established and may use warm temperature pressurant. For these reasons it has been decided to base the tank weights on room temperature allowables even though some weight penalty is incurred. If, in the future, it is decided that low temperature allowables can be practically employed, the tank weights can be reduced accordingly.

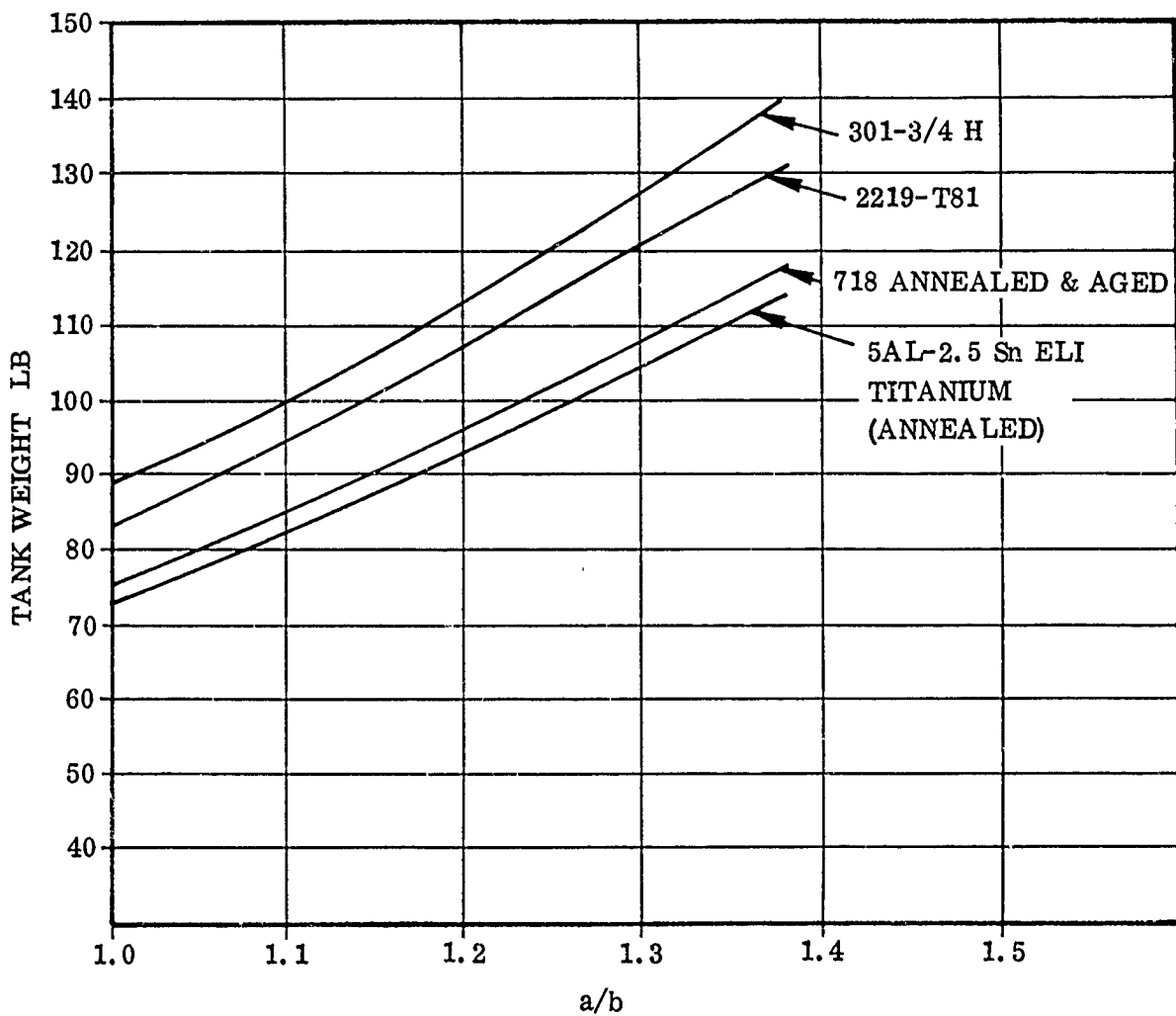
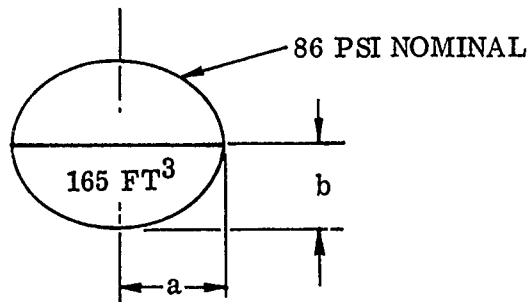
(U) 1.3.1.3 One-Piece Bulkheads, Room Temperature Allowables. The same method of analysis was employed as for the cold allowables, but in this case room temperature allowables were utilized for calculating the propellant tank weights. The results are shown in Figures 1-7 and 1-8. These tank weights were then again coupled with the shell and residual weights and the typical results are shown in Figure 1-9 for the aluminum tanks. The optimum points for the various tank combinations are shown in Table 1-5.

(C) It can be noted that the change of stress allowables from the cold condition to the ambient condition kept the system ranking the same with the exception of the changing of position of the 718 tank combination with the combination of 2219 LF_2 tank and titanium LH_2 tank; however, the weight spread from top to bottom is significantly reduced. Using the cold allowables, the difference from the lightest combination to the heaviest was 118 pounds, while using room allowables reduces the spread to 45 pounds. The titanium, in particular, has a significant difference in room temperature allowables and cold allowables.

(C) The tank weights so far calculated have been determined with tank wall gages based on the assumed operating pressures; however, one of the ground rules of the study was to provide meteoroid protection resulting in a probability of 0.995 that there would be no tank penetration for a 14 day space residence time. In order to accommodate this, some of the tank wall gages had to be increased. A detailed discussion of the meteoroid protection requirement is given in Section 1.3.2. In summary, the wall gages needed for the meteoroid protection are given in Table 1-6.

CONFIDENTIAL

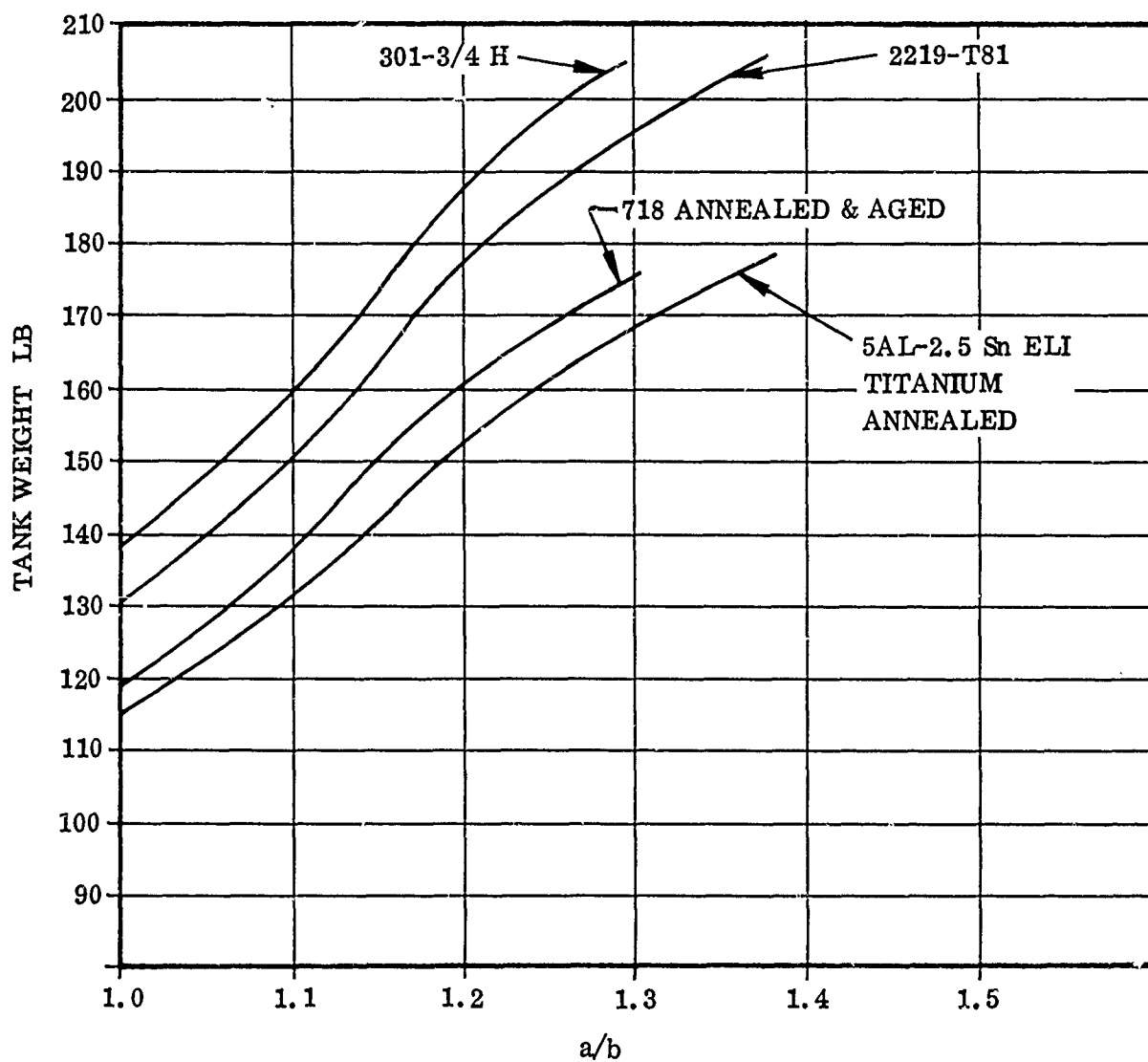
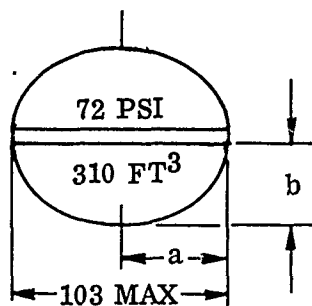
CONFIDENTIAL



(C) Figure 1-7. Oxidizer Tank Weight versus a/b (Room Temperature Allowables and One-Piece Bulkheads)

CONFIDENTIAL

CONFIDENTIAL



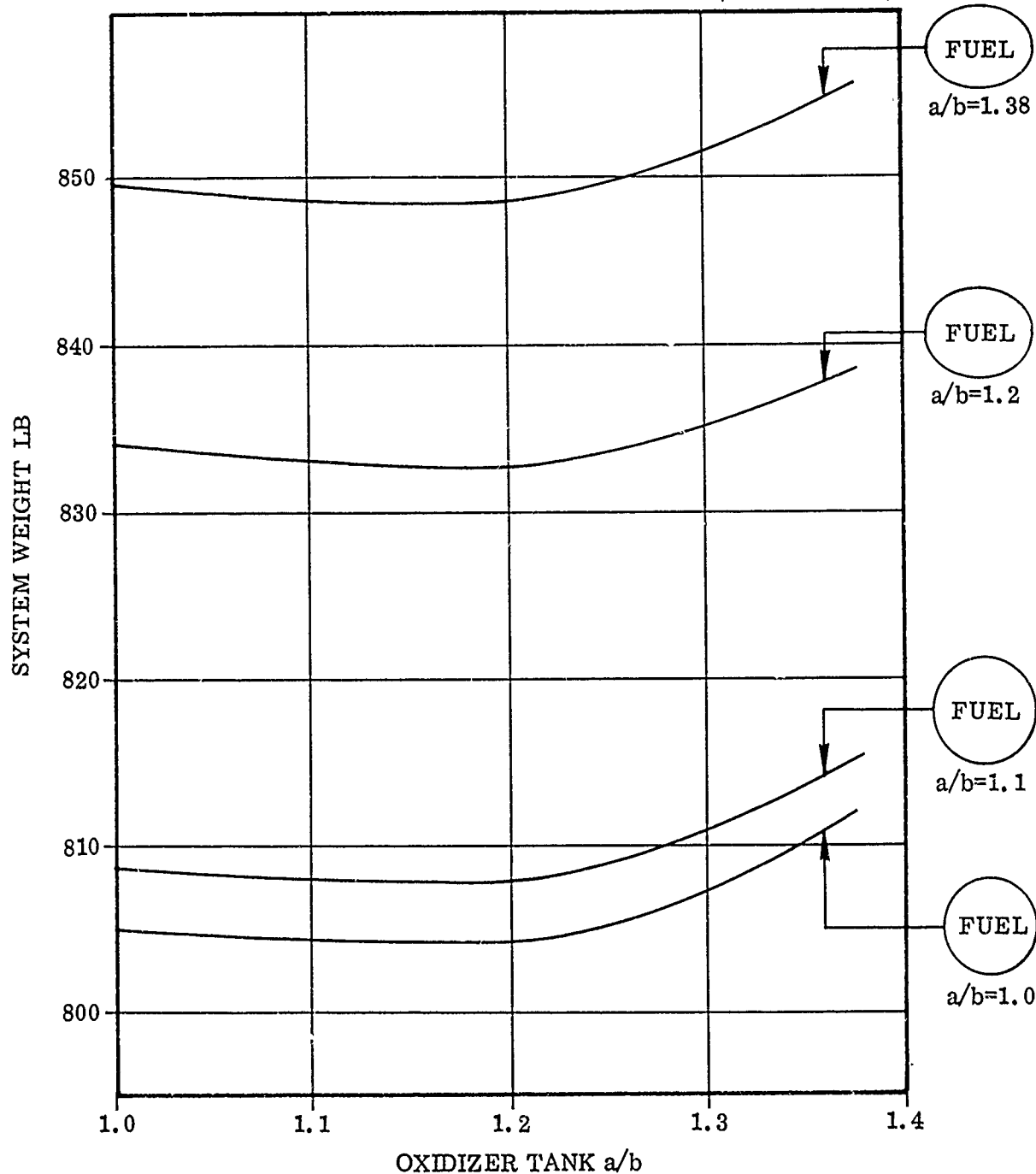
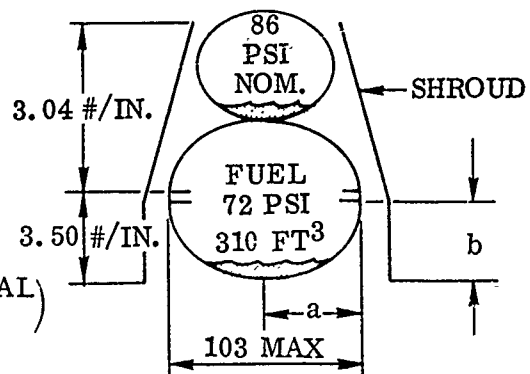
(C) Figure 1-8. Fuel Tank Weight versus a/b (Room Temperature Allowables and One-Piece Bulkheads)

CONFIDENTIAL

CONFIDENTIAL

SINGLE PC. BHDS
ROOM TEMP. ALLOWABLES
2219-T81 TANKS

$$\left(\begin{matrix} \text{SYSTEM} \\ \text{WT.} \end{matrix} \right) = \left(\begin{matrix} \text{SHROUD} \\ \text{WT.} \end{matrix} \right) + \left(\begin{matrix} \text{TANK} \\ \text{WT.} \end{matrix} \right) + \left(\begin{matrix} \text{RESIDUAL} \\ \text{WT.} \end{matrix} \right)$$



(C) Figure 1-9. System Weight versus Oxidizer Tank a/b (Room Temperature Allowables)

CONFIDENTIAL

CONFIDENTIAL

(C) TABLE 1-5. TANK MATERIAL COMBINATIONS AND WEIGHTS (AMBIENT ALLOWABLES)

Tank Combination for Optimum System Weight		System Weight (lb)	Tank Gage	
LF ₂	LH ₂		LF ₂	LH ₂
301-3/4 H a/b = 1.2	301-3/4 H a/b = 1.0	817.85	0.0181	0.0150
2219-T81 a/b = 1.2	2219-T81 a/b = 1.0	804.26	0.0491	0.0408
2219-T81 a/b = 1.2	Ti5Al-2.5 Sn ELI a/b = 1.0	787.87	0.0491	0.0225
718 (A) Aged a/b = 1.2	718 (A) Aged a/b = 1.1	777.29	0.0146	0.0138
718 (A) Aged a/b = 1.2	Ti5Al-2.5 Sn ELI a/b = 1.0	775.11	0.0146	0.0225
Ti5Al-2.5 Sn ELI a/b = 1.2	Ti5Al-2.5 Sn ELI a/b = 1.0	772.8	0.0270	0.0225

(C) TABLE 1-6. WALL GAGES FOR METEOROID REQUIREMENT

Material	Wall Gage
301-3/4 H	0.0157
2219-T81	0.0304
718	0.0150
Titanium	0.0227

(C) Comparing these values with the wall gages in Table 1-5, it can be seen that certain tanks fail to meet these values. In order to assure the probability of no penetration, it is necessary to increase the tank wall gage. Since the optimization curves (Figure 1-9) show very small weight penalty in going to higher a/b ratios, this becomes a practical way to meet the meteoroid protection requirements because a higher tank a/b results in thicker tank walls. The exception to this is the 718 LH₂ tank, since a flatter bulkhead begins to lengthen the cylindrical section appreciably. In this case it is optimum to merely increase the skin gage at the same bulkhead ratio.

CONFIDENTIAL

CONFIDENTIAL

(C) Adjusting the tank a/b ratios to provide the required wall thickness, we obtain the system weight versus tank configuration shown in Table 1-7.

(C) TABLE 1-7. ADJUSTED SYSTEM WEIGHT AND TANK CONFIGURATION

Tank Combination		System Weight (lb)	Tank Skin Gages	
LF ₂	LH ₂		LF ₂	LH ₂
301-3/4 H a/b = 1.2	301-3/4 H a/b = 1.1	822.62	0.0181	0.0170
718 (A) Aged a/b = 1.3	718 (A) Aged a/b = 1.1	792.48	0.0163	0.0150
2219-T81 a/b = 1.2	2219-T81 a/b = 1.0	804.26	0.0491	0.0408
2219-T81 a/b = 1.2	Ti 5Al-2.5 Sn ELI a/b = 1.1	788.17	0.0491	0.0255
718 (A) Aged a/b = 1.3	Ti 5Al-2.5 Sn ELI a/b = 1.1	777.53	0.0163	0.0255
Ti 5Al-2.5 Sn ELI a/b = 1.2	Ti 5Al-2.5 Sn ELI a/b = 1.1	773.1	0.0270	0.0255

(U) It can be seen that accommodation for the meteoroid requirement has caused the largest weight increase in the 718 tanks. Most of the other system weights remain relatively unaffected because of the near zero slope of the weight versus a/b ratio curve. The aluminum tank combination required no change in configuration since it already had sufficient tank wall thickness. The system weights shown in Table 1-7 represent the weights obtainable with one-piece bulkhead construction using room temperature allowable stress values and considering the meteoroid protection requirements. One further item required consideration: actual construction of one-piece bulkhead tanks.

(C) 1.3.1.4 Final Configuration Comparisons. Current available mill sheet widths are 36 inches for 301 steel and 48 inches for 718 and titanium; therefore, an additional weight analysis for 301, 718, and titanium was performed assuming gore constructed bulkheads and room temperature allowables. The 2219-T81 can be obtained in sufficient sheet size to form one-piece bulkheads. All gore elements were considered butt welded using 2-inch weld zone widths. The gore sections required per bulkhead are:

CONFIDENTIAL

CONFIDENTIAL

(C)	<u>LF₂ Tank</u>	<u>LH₂ Tank</u>
301	9	10
718	7	8
Titanium	7	8

Plots of tank weights versus a/b ratios for each material using gores are shown in Figure 1-10 for the LF₂ tank and in Figure 1-11 for the LH₂ tank. The resulting system weights are shown in Table 1-8.

(C) TABLE 1-8. FINAL SYSTEM WEIGHT COMPARISON

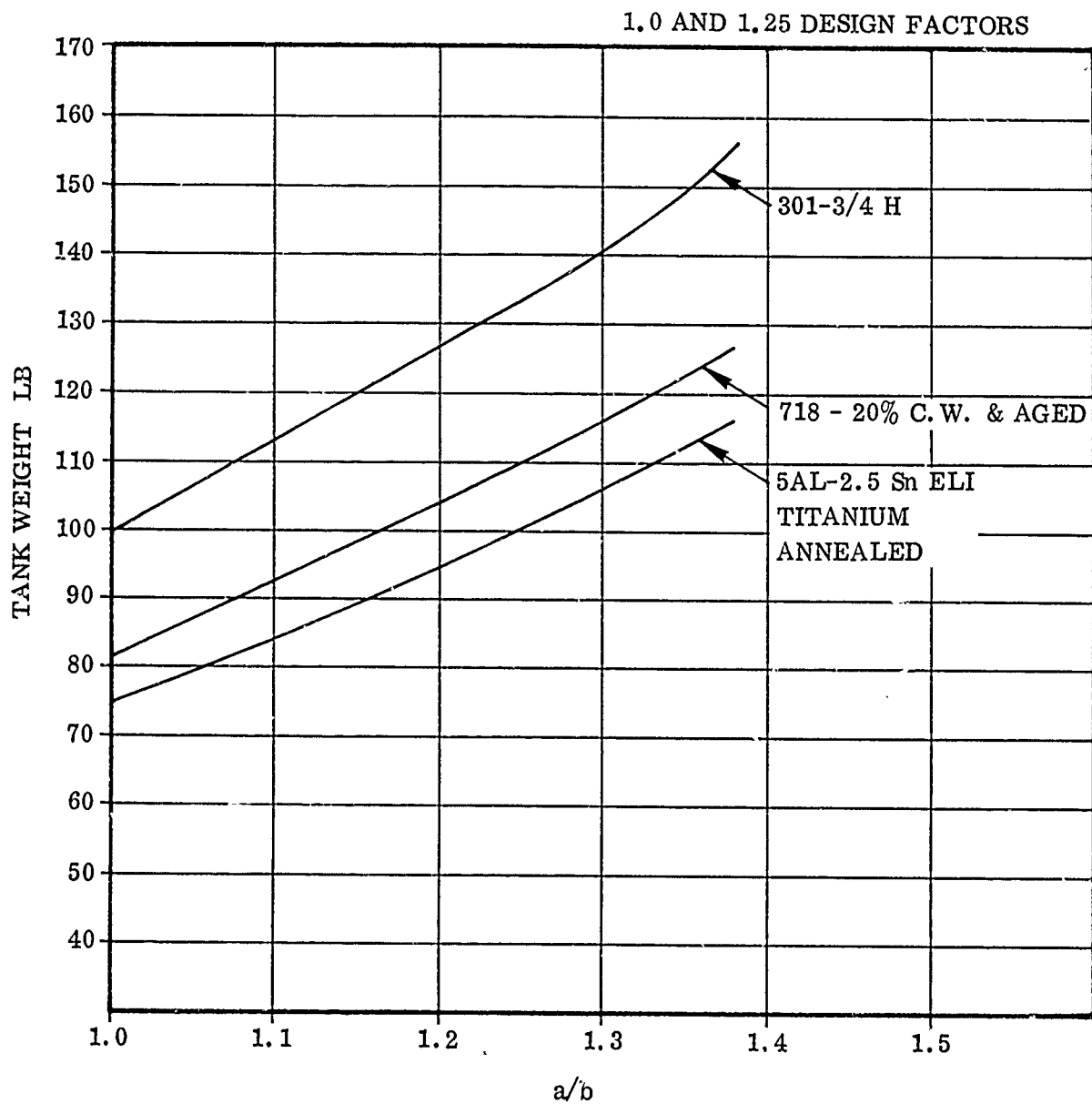
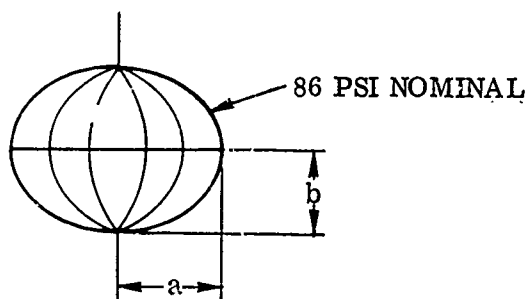
Tank Combination		System Weight (lb)
LF ₂	LH ₂	
301-3/4 H a/b = 1.2	301-3/4 H a/b = 1.1	849.93
718 (A) Aged a/b = 1.3	718 (A) Aged a/b = 1.0	817.63
2219-T81 a/b = 1.2	2219-T81 a/b = 1.1	804.26
2219-T81 a/b = 1.2	Ti 5Al-2.5 Sn ELI a/b = 1.1	790.35
718 (20% c.w.) a/b = 1.3	Ti 5Al-2.5 Sn ELI a/b = 1.1	788.5
Ti 5Al-2.5 Sn ELI a/b = 1.2	Ti 5Al-2.5 Sn ELI a/b = 1.1	776.92

(C) All the above bulkheads are constructed of welded gores with the exception of the aluminum tanks. There is very little weight penalty incurred in the titanium tanks when using gores because of the high weld efficiencies obtainable; however, the 301 and 718 tanks are noticeably heavier because of the relatively poor weld efficiencies (60 percent for both 301 and 718).

(C) The rating of each system is given in Figure 1-2, which summarizes all the evaluation factors. Each combination is rated on a 0 to 1 basis with 1 being best and 0 worse. Since the total weight difference is only 61.4 pounds, or of the order of 8 percent of the minimum weight system, the rating was based from 0.5 to 1. It was felt that a zero rating for any combination would be unreasonable. The weight of the system including the titanium fluorine tank, was not considered because of compatibility problems.

CONFIDENTIAL

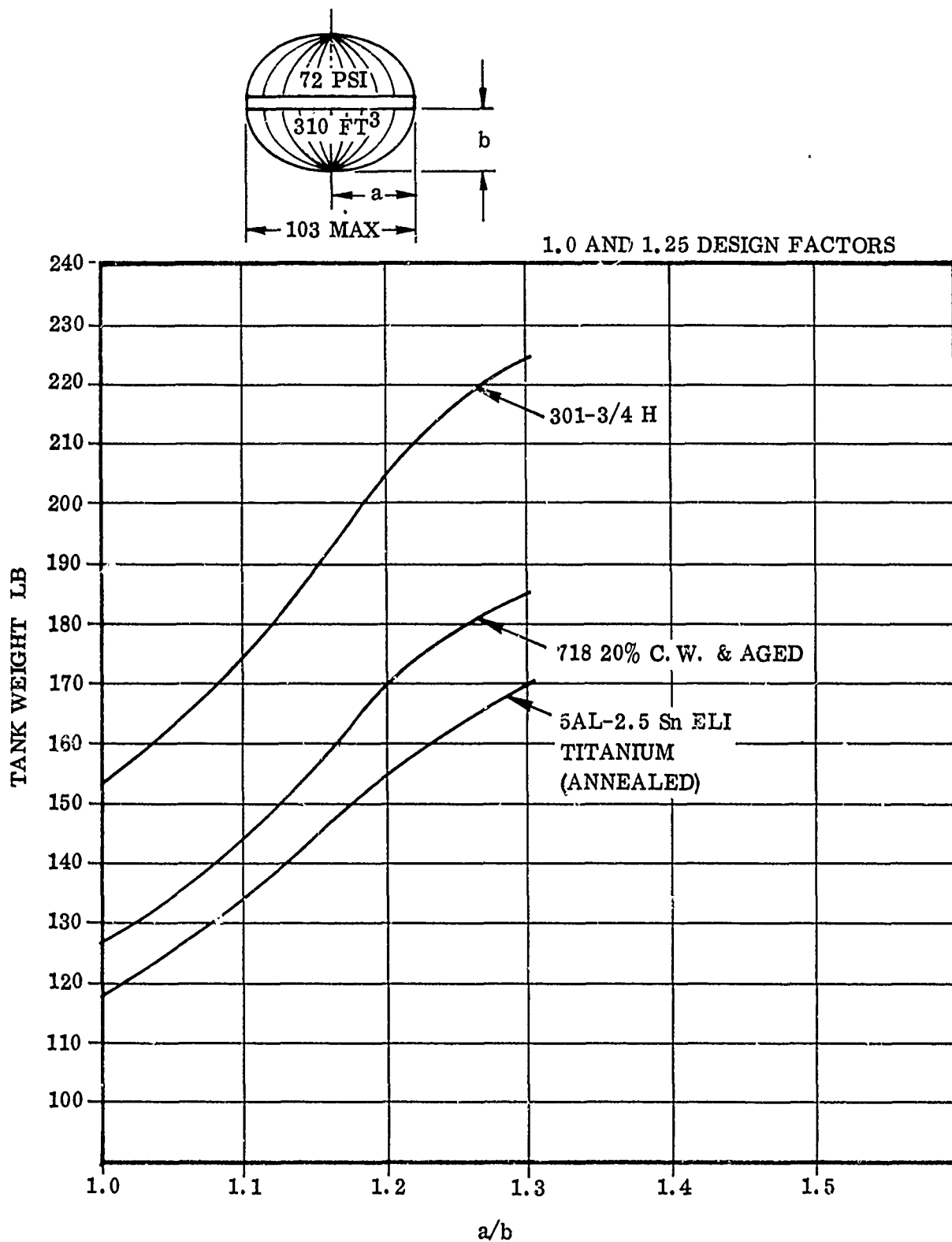
CONFIDENTIAL



(C) Figure 1-10. Oxidizer Tank Weight versus a/b (Room Temperature Allowables - Gore Constructed Bulkheads)

CONFIDENTIAL

CONFIDENTIAL



(C) Figure 1-11. Fuel Tank Weight versus a/b (Room Temperature Allowables - Gore Constructed Bulkheads)

CONFIDENTIAL

CONFIDENTIAL

(C) The rating is therefore equal to

$$1 - \left[\frac{\text{Weight of system to be rated} - \text{minimum weight system}}{\text{Maximum weight system} - \text{minimum weight system}} \right] \times 0.5$$

The rating for the 2219-T81 combination is, for example,

$$1.0 - \left[\frac{804.2 - 788.5}{849.93 - 788.5} \right] \times 0.5 = 0.872$$

(C) 1.3.2 METEOROID PROTECTION REQUIREMENTS. The propellant feed system must be designed such that the probability of no propellant tank penetration by meteoroids shall be 0.995 for a 14 day space residence time. The analysis assumes a double wall protection system utilizing the structural shroud as the outer shield and the propellant tank walls as the inner shield.

(U) 1.3.2.1 Evaluation Factors. There are two factors which are affected by the meteoroid protection requirements. The first is system weight, since the selection of certain tank bulkhead combinations was dictated by the meteoroid protection requirements rather than by the stress levels resulting from tank pressure. The tank wall gages required are noted in Section 1.3.1.3; however, the weight penalty incurred by the necessity to meet the meteoroid requirements was in most cases insignificant. The penalties for the various tank combinations were as shown in Table 1-9.

(C) TABLE 1-9. TANK COMBINATION WEIGHT PENALTIES

LF ₂	LH ₂	Weight
718 A (Aged)	718 A (Aged)	15.24
301-3/4 H	301-3/4 H	4.77
718 A (Aged)	Ti 5Al-2.5 Sn ELI	2.42
Ti 5Al-2.5 Sn ELI	Ti 5Al-2.5 Sn ELI	0.3
2219-T81	Ti 5Al-2.5 Sn ELI	0.3
2219-T81	2219-T81	—

No change was required in the aluminum tank configuration since the tank wall thickness needed to meet the pressure requirements was sufficient to provide adequate meteoroid protection. With these adjusted weight figures all systems provide the required thickness.

CONFIDENTIAL

CONFIDENTIAL

(C) The second factor affected by meteoroid requirements is the space residence capability. For a given system design, the longer the vehicle is in orbit the more probable it is that a meteoroid penetration may occur. Consequently, for a given probability of no penetration the tank wall thickness requirement increases with increased mission duration. The required tank wall thickness as a function of days in orbit is given in Figure 1-12, assuming a probability of 0.995 for no penetration.

(C) Although all the subject systems meet the meteoroid protection requirement some have excess capability, particularly the aluminum tank combination. The aluminum LF₂ tank has a required skin gage of 0.0491 inch while the LH₂ tank has a skin gage of 0.0408, as dictated by tank pressure requirements. These give space residence capabilities of 66 days for the LF₂ tank and 35 days for the LH₂ tank which result in "space residency margin" of 52 and 21 days, respectively. These values become meaningful when extended space residence margin is evaluated. Depending on the mission and/or tank material, it becomes necessary to increase the tank skin gage or decrease the probability of no penetration as space residence time increases.

(C) A weighting factor of only 5 percent was used for this criteria since, as noted before, every system has been designed to meet the minimum requirement, and where necessary, has already been penalized in the weight column. The space residency margin represents the capability of the system to extend its stay time; or conversely, it can be interpreted as a margin of safety for the 14 day mission.

(C) Ratings were established per the following relations

$$1.0 - \left[\frac{\text{System with maximum margin} - \text{Margin of system to be rated}}{\text{System with maximum margin}} \right] \times 0.5$$

(C) For example

The rating for the 301-3/4 H oxidizer tank is

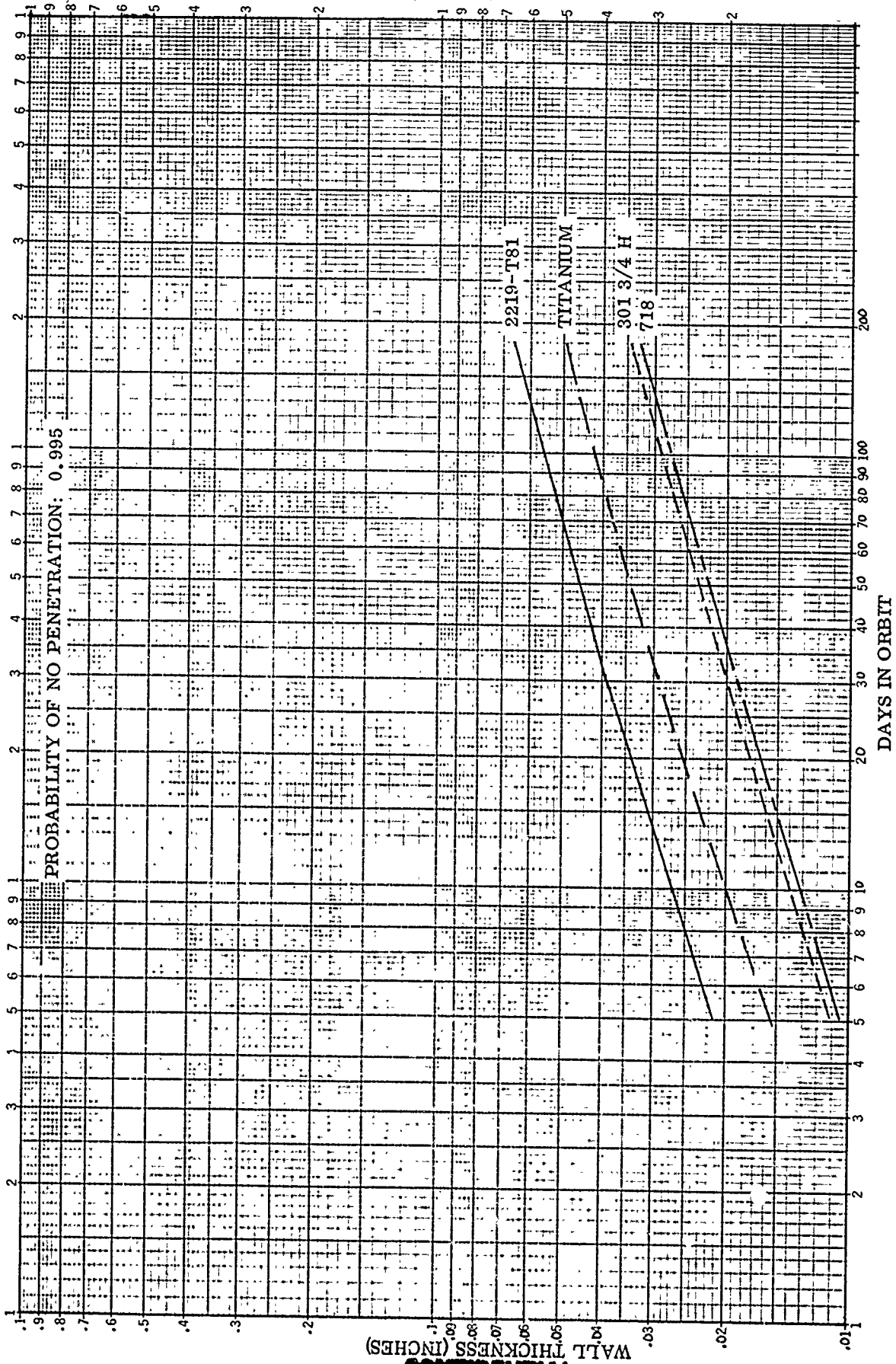
$$1.0 - \frac{52 - 8}{52} \times 0.5 = 1.0 - \frac{44}{52} \times 0.5 = 0.577$$

The rating for the fuel tank is

$$1.0 - \frac{21 - 4}{21} \times 0.5 = 1.0 - (0.405) = 0.595$$

CONFIDENTIAL

CONFIDENTIAL



CONFIDENTIAL

(C) Figure 1-12. Tank Wall Thickness Required for Meteoroid Protection

CONFIDENTIAL

(I') Although the absolute values of tank wall thickness may change as more information on meteoroid flux rates becomes available, the basic trend is indicated by the rating sheet. The quantitative values may be altered but the qualitative rating should remain essentially the same.

(C) 1.3.2.2 Method of Analysis. A basic ground rule of the AMPES study is that the probability of no propellant tank penetrations by meteoroids shall be 0.995 for a 14 day space residence time. In order to calculate the tank wall thicknesses required to meet this probability, the meteoroid environment from Reference 1 was used and the basic method of calculation follows from that suggested in Reference 2.

(U) The probability of sustaining an impact by a meteoroid is equal to the time in orbit divided by the frequency of impact by a meteoroid.

$$P_{\text{impact}} = \frac{\tau}{\theta} \quad (1)$$

where

τ = time in orbit

θ = frequency of impact (days/particle impact)

The frequency of impact, θ , is the inverse of the average rate of meteoroids of mass m or larger.

$$n_0 = \frac{1}{\theta} = \text{particles/day}$$

The meteoroid flux rate is generally given in terms of particles/day per unit area or

$$N = \text{particles/day} - M^2$$

The total number of particles impacting on a given area is therefore NA , and the frequency of impact is

$$\theta = \frac{1}{NA} \quad (2)$$

The probability of impact can now be expressed as

$$P_{\text{impact}} = \tau NA \quad (3)$$

There are other factors which must be considered when calculating the meteoroid impact probability, and these are discussed below.

CONFIDENTIAL

CONFIDENTIAL

- (U) a. Stream Meteoroids and Sporadic Meteoroids. Sporadic meteoroid impingement can occur from any direction and therefore requires that the entire exposed surface area of the object in question be considered. The stream meteoroids may last from a few hours to many days. As noted in Reference 1, a simplifying assumption can be made for preliminary design studies by accounting for the stream meteoroids by increasing the sporadic flux by a factor of 1.4. This, then, requires using only the sporadic flux rate in Equation 3, which now becomes,

$$P_{\text{impact}} = \tau NA (1.4) \quad (4)$$

- (U) b. Shielding Factor. The shielding factor (S_F) pertains to shielding effects resulting from bodies in proximity to the object of interest, and is equal to $(1 - \xi)$.

$$A_C = (1 - \xi) A \text{ (Reference 1)}$$

where

A = area of vehicle

A_C = effective area

$$\xi = \text{viewing loss} = \frac{1 - \cos \theta}{2}$$

$$\sin \theta = R/(R+H)$$

R = radius of shielding body

H = distance from shielding body

- (C) In the AMPS case, the only shielding considered is that resulting from the earth although there are small secondary effects from the engine, attitude control bottles, etc.

Therefore

$$\sin \theta = \frac{3959}{3959 + 115} = 0.9717$$

$$\theta = 76^\circ 21'$$

$$\cos \theta = 0.23599$$

$$\xi = \frac{1 - 0.23599}{2} = \frac{0.76401}{2} = 0.382$$

$$S_F = (1 - \xi) = 0.618$$

CONFIDENTIAL

CONFIDENTIAL

- (C) This shielding factor modifies the area, as noted above, by a factor of 0.618. The impact probability equation now becomes

$$P_{\text{impact}} = \tau N (0.618) A (1.4)$$

The probability of no impact is equal to

$$1 - P_{\text{impact}}, \text{ or}$$

$$P_{\text{ni}} = 1 - P_{\text{impact}}$$

$$P_{\text{impact}} = 1 - P_{\text{ni}}$$

$$1 - P_{\text{ni}} = \tau N (0.618) A (1.4)$$

$$N = \frac{1 - P_{\text{ni}}}{(0.865) A \tau} \quad (5)$$

- (C) c. Surface Area. The exposed surface area consists of the lateral area of the structural shroud and the thrust cone. The forward bulkhead of the AMPS is assumed to be adequately shielded by the payload. The surface area of the shroud (shown typically in Figure 1-13) is 391 ft². An additional area of 90 ft² results from the thrust cone, giving a total area of 480 ft². The outer structure is of skin stringer construction with hat sections running axially along the outer shroud. The hat sections, coupled with the basic skin, effectively result in a double wall shield which reduces the affected area from the total area exposed to meteoroid impingement. It is estimated that the area reduction resulting from the frames and stringers is of the order of 20 percent. The effective area then exposed to meteoroids is 0.8 (480) = 384 ft². The criteria used for flux rates is based on area in terms of square meters and the corresponding value for exposed area is

$$A_s = 35.67 \text{ M}^2$$

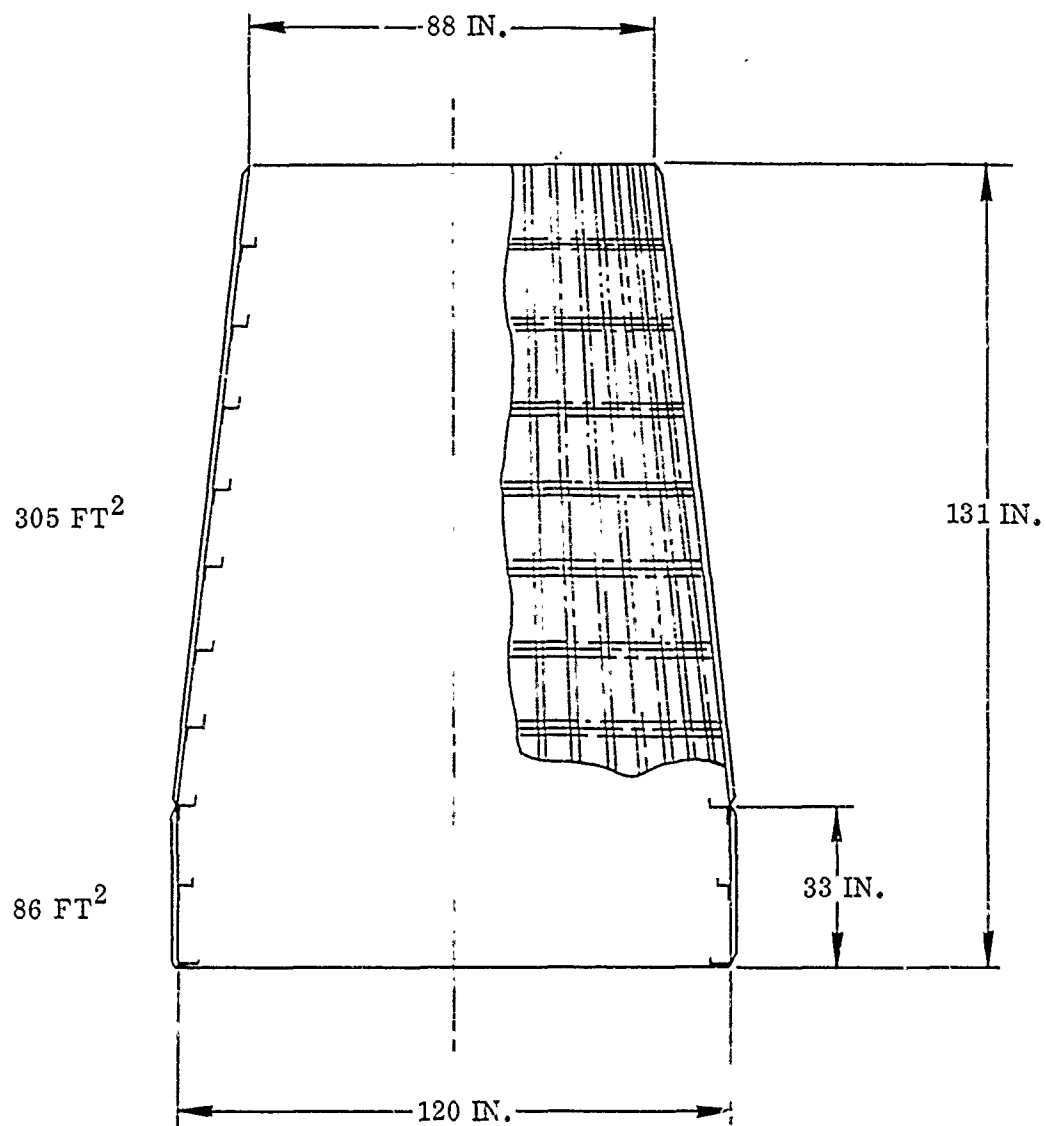
The flux rate for an AMPS type vehicle can now be expressed as

$$N = \frac{1 - P_{\text{ni}}}{30.85 \tau} \frac{\text{Particles}}{\text{Sec M}^2} \quad (6)$$

- (U) d. Allowable Flux Rate (in seconds). The allowable flux rate can be found from Equation 6 as a function of probability of no impact and time in orbit. The flux rate versus mass of meteoroid is given by

CONFIDENTIAL

CONFIDENTIAL



(C) Figure 1-13. AMPS Structural Shroud

CONFIDENTIAL

CONFIDENTIAL

$$(U) \quad \log N = -1.00 \log m + \log S - 13.60 \text{ (Reference 1)} \quad (7)$$
$$10^{-8} \leq m \leq 10^{-2.15}$$

where

N = number of impacts of mass m or greater per square meter per second

m = mass in grams

S = seasonal variation

log = log base 10

If we design a protective system to exclude all impacts below mass m, the only impacts of interest would be those of mass m or greater, which are given as a function of N. Therefore, the allowable flux rate can be expressed as a probability of no penetration $P(x = 0)$ if we design the system to withstand meteoroids of mass m or lower, as given by Equation 7 (i.e., the probability of no penetration is equal to the probability of no impact by meteoroids of mass m or greater). The flux equation can then be expressed as

$$N = \frac{1 - P(x = 0)}{30.58 \tau}$$

(C) For a 14 day mission ($\tau = 12.096 \times 10^5$ sec) and a $P(x = 0) = 0.995$

$$N = 1.339 \times 10^{-10} \text{ particles/meter}^2 - \text{sec} \quad (8)$$

(U) e. Design Mass of Meteoroids. The design mass of a meteoroid for our conditions and assumed probability can now be expressed by Equation 7 as follows

$$-\log m = \log N - \log S + 13.60$$

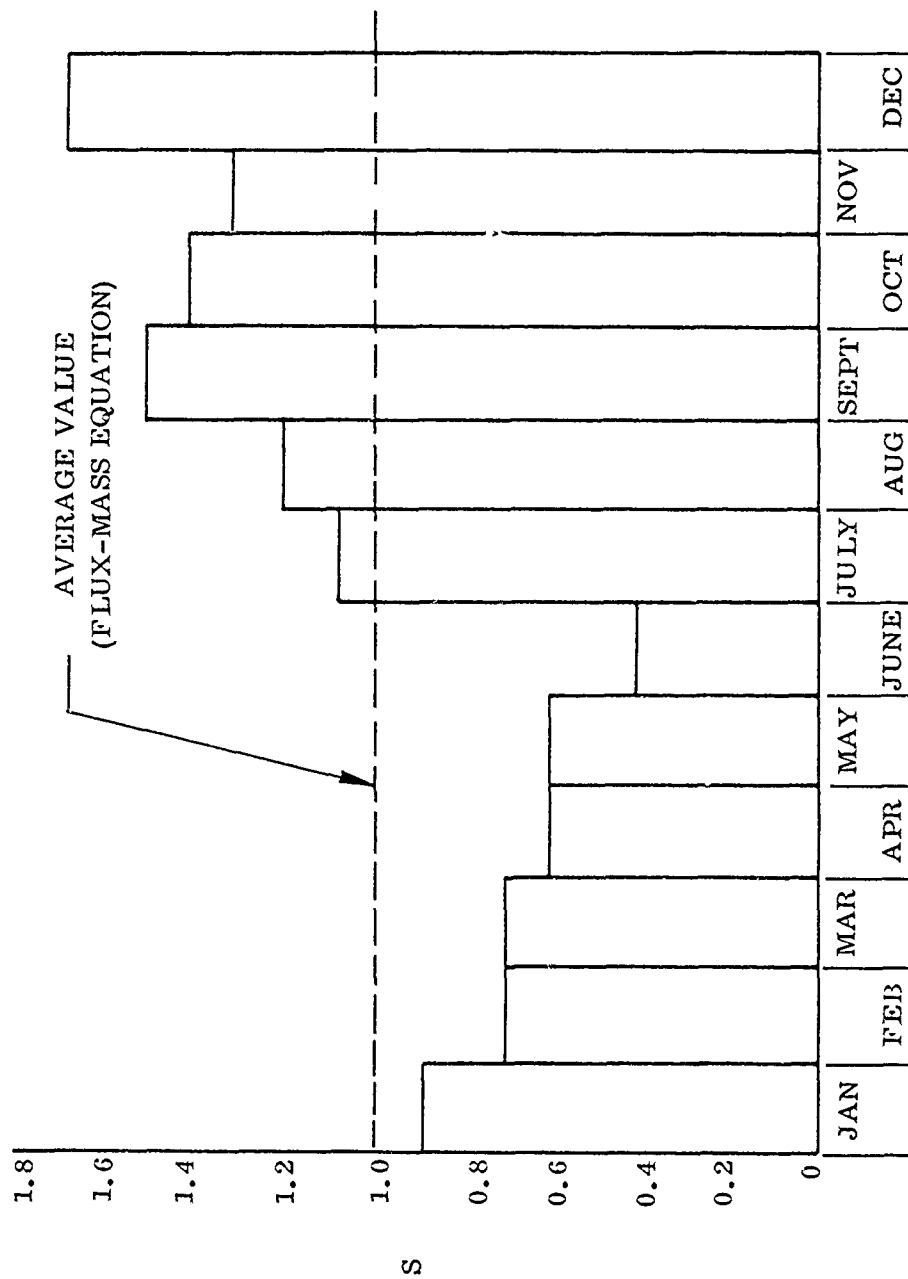
$$= \log N/S + 13.60$$

The variation of flux rate during a yearly period(s), assuming December launch, is shown in Figure 1-14. For a mission of 30 days or less, the value of 1.7 will be used. For missions of longer duration, the appropriate average value will be used assuming a launch date which gives the maximum S value.

The design meteoroid mass as a function of space residence is given in Table 1-10.

CONFIDENTIAL

CONFIDENTIAL



(C) Figure 1-14. Yearly Sporadic Meteor Flux

CONFIDENTIAL

UNCLASSIFIED

TABLE 1-10. DESIGN METEOROID MASS AS A FUNCTION OF SPACE RESIDENCE

Time (days)	N	S	m (grams)
5	3.75×10^{-10}	1.7	1.139×10^{-4}
14	1.339×10^{-10}	1.7	3.2×10^{-4}
30	0.624×10^{-10}	1.7	6.85×10^{-4}
60	0.312×10^{-10}	1.525	12.3×10^{-4}
180	0.104×10^{-10}	1.38	33.4×10^{-4}

It can be noted that the meteoroid masses all fall within the range for which the flux equation is valid (i. e. , $10^{-8} \leq m \leq 10^{-2.15}$).

- f. Protective System Design. The equation for the required thickness to prevent meteoroid penetration is taken from Reference 2.

$$t = 222 \left(\frac{m}{E_T \rho_T} \right)^{1/3}$$

where

t is the thickness in inches of a single plate required to prevent penetration

m is the meteoroid mass in grams

E_T is the Youngs modules of wall material, psi

ρ_T is the density of the wall material, lb/in.³

This equation is applicable for a meteoroid velocity of 30 km/sec and a density of 0.5 gm/cc which are values consistent with the flux rate model of Reference 2. The materials considered for the propellant tanks are: 2219 T81 Al Aly, 301-3/4 hard, Titanium 5Al-2 1/2 Sn ELI, 718 inconel annealed and aged. The values of $E_T \rho_T$ which were used are shown in Table 1-11.

UNCLASSIFIED

UNCLASSIFIED

TABLE 1-11. MATERIAL THICKNESS EQUATION VALUES

	$E_T \rho_T$	$(E_T \rho_T)^{1/3}$
2219	1.02×10^6	100.7
718	8.59×10^6	204.5
301	7.54×10^6	196
Ti	2.48×10^6	135.2

Consequently, the equations for single wall thickness required to meet the "no penetration" requirement are, for the specific materials

$$\begin{aligned}
 t(2219-T81) &= 2.20 (m)^{1/3} \\
 t(718) &= 1.085 (m)^{1/3} \\
 t(301) &= 1.133 (m)^{1/3} \\
 t(T_1) &= 1.642 (m)^{1/3}
 \end{aligned}$$

The corresponding single wall thicknesses to meet the required probability of no penetration are given as a function of space residence time in Table 1-12.

TABLE 1-12. SINGLE WALL THICKNESSES FOR NON-PENETRATION REQUIREMENTS

Time (Days)	$m^{1/3}$	t inches			
		2219	718	301	Ti
5	0.0483	0.106	0.0524	0.055	0.079
14	0.0684	0.150	0.074	0.0775	0.112
30	0.0881	0.194	0.0956	0.1	0.145
60	0.107	0.235	0.116	0.121	0.176
180	0.1492	0.328	0.162	0.169	0.245

- g. Double Wall Protection. It can be noted that the values required to provide single wall protection result in wall thicknesses that are excessively large. A double plate wall is far more effective than that provided by a single plate, as shown by the following equation

$$\bar{t} = 0.27 t \quad (\text{Reference 2})$$

UNCLASSIFIED

UNCLASSIFIED

TABLE 1-10. DESIGN METEOROID MASS AS A FUNCTION OF SPACE RESIDENCE

Time (days)	N	S	m (grams)
5	3.75×10^{-10}	1.7	1.139×10^{-4}
14	1.339×10^{-10}	1.7	3.2×10^{-4}
30	0.624×10^{-10}	1.7	6.85×10^{-4}
60	0.312×10^{-10}	1.525	12.3×10^{-4}
180	0.104×10^{-10}	1.38	33.4×10^{-4}

It can be noted that the meteoroid masses all fall within the range for which the flux equation is valid (i. e., $10^{-8} \leq m \leq 10^{-2.15}$).

- f. Protective System Design. The equation for the required thickness to prevent meteoroid penetration is taken from Reference 2.

$$t = 222 \left(\frac{m}{E_T \rho_T} \right)^{1/3}$$

where

t is the thickness in inches of a single plate required to prevent penetration

m is the meteoroid mass in grams

E_T is the Youngs modules of wall material, psi

ρ_T is the density of the wall material, lb/in.³

This equation is applicable for a meteoroid velocity of 30 km/sec and a density of 0.5 gm/cc which are values consistent with the flux rate model of Reference 2. The materials considered for the propellant tanks are: 2219 T81 Al Aly, 301-3/4 hard, Titanium 5Al-2 1/2 Sn ELI, 718 inconel annealed and aged. The values of $E_T \rho_T$ which were used are shown in Table 1-11.

UNCLASSIFIED

UNCLASSIFIED

TABLE 1-11. MATERIAL THICKNESS EQUATION VALUES

	$E_T \rho_T$	$(E_T \rho_T)^{1/3}$
2219	1.02×10^6	100.7
718	8.59×10^6	204.5
301	7.54×10^6	196
Ti	2.48×10^6	135.2

Consequently, the equations for single wall thickness required to meet the "no penetration" requirement are, for the specific materials

$$\begin{aligned}
 t(2219\text{-T81}) &= 2.20 (m)^{1/3} \\
 t(718) &= 1.085 (m)^{1/3} \\
 t(301) &= 1.133 (m)^{1/3} \\
 t(T_1) &= 1.642 (m)^{1/3}
 \end{aligned}$$

The corresponding single wall thicknesses to meet the required probability of no penetration are given as a function of space residence time in Table 1-12.

TABLE 1-12. SINGLE WALL THICKNESSES FOR NON-PENETRATION REQUIREMENTS

Time (Days)	$m^{1/3}$	t inches			
		2219	718	301	Ti
5	0.0483	0.106	0.0524	0.055	0.079
14	0.0684	0.150	0.074	0.0775	0.112
30	0.0881	0.194	0.0956	0.1	0.145
60	0.107	0.235	0.116	0.121	0.176
180	0.1492	0.328	0.162	0.169	0.245

- g. Double Wall Protection. It can be noted that the values required to provide single wall protection result in wall thicknesses that are excessively large. A double plate wall is far more effective than that provided by a single plate, as shown by the following equation

$$\bar{t} = 0.27 t \quad (\text{Reference 2})$$

UNCLASSIFIED

CONFIDENTIAL

(U) where

\bar{t} is the total required thickness in inches to prevent complete penetration of a double plate wall

t is the required thickness for single plate protection

(U) The constant 0.27 is an effectiveness factor for two plates spaced two inches apart with no filler between plates.

(U) The configuration of the AMPS results in double plate protection with the outer shell being the outer plate and the propellant tank wall being the inner plate. The separation distance is somewhat larger than two inches and it is felt that the use of this coefficient will be conservative. The source data (Reference 2) does not list effectiveness factors for plates placed further than two inches, but the value increases to 0.5 as the distance is reduced to one inch.

(U) It is further stated that the thickness of the outer plate should be from 0.15 to 0.25 of the total thickness required.

(U) h. Required Tank Thickness. Using the criteria in g above, it can be assumed that the tank wall thickness must be equal to $0.75 \bar{t}$.

$$\bar{t} = 0.27 t$$

$$t_t = (0.75)(0.27)t = 0.2025 t$$

where

t_t = tank wall thickness

t = required single wall thickness

(C) The values of tank wall thickness required to meet meteoroid requirements, as a function of time are shown in Table 1-13 and plotted in Figure 1-12.

(U) TABLE 1-13. TANK WALL THICKNESSES FOR METEOROID REQUIREMENTS

Time (Days)	2219	718	301	T_i
5	0.0215	0.0106	0.0111	0.0156
14	0.0304	0.015	0.0157	0.0227
30	0.0393	0.0194	0.0202	0.0294
60	0.0476	0.0235	0.0245	0.0356
180	0.066	0.0328	0.034	0.0496

CONFIDENTIAL

CONFIDENTIAL

(C) The outer shell is composed of aluminum skin with a minimum thickness of 0.030. The required outer shell thickness (assuming 0.25 \bar{t}) would be approximately 0.022 for the 180 day space residence case, which is still below the design requirement. Consequently, in all cases the excess thickness of the outer shell represents a design safety factor. The exact margin cannot be calculated since the effectiveness of the excess thickness is not known, so for these calculations it will be assumed to represent a margin of safety (albeit undefined).

(U) The tank wall thicknesses shown in Figure 1-12 will be used for design purposes.

(U) 1.3.3 SELECTION CRITERIA. There are many factors that must be considered when selecting the optimum tank configuration. Although system weight is the most critical parameter, other items may have a significant effect on the practicality of a particular material combination. These were listed in Section 1.3 and a discussion of the relative importance of the criteria is given below. A discussion of the material characteristics is given in Section 1.4.

(C) 1.3.3.1 Compatibility with Propellant. This item was considered as a "go" "no go" factor rather than one that has a quantitative rating factor. All materials considered are compatible with fluorine with the exception of titanium. Consequently, the combination with the titanium fluorine tank was not evaluated beyond the compatibility column (see Figure 1-2). The weight of the system was calculated to obtain a point for the lightest system, considering no other factors.

(C) 1.3.3.2 Fabrication

(C) a. Weldability. Weldability as defined in this evaluation included two principal criteria: (1) the ability to produce sound welds during fabrication and, (2) satisfactory performance of the weldments for the intended service, e.g., strength, ductility, toughness, and corrosion resistance of the weld joints. The ability to easily repair a weld is also considered an important factor, as the possible scrapping of a complete tank assembly because of a poor weld is to be avoided at all costs.

(U) b. Formability. The formability of the material is simply the ability to easily form the bulkheads. This is based on all bulkheads being made from gore sections with the exception of the 2219 aluminum. The 301 is rated highest here because of the extensive experience GDC has had with the construction of 301 gore bulkheads.

CONFIDENTIAL

CONFIDENTIAL

(C) 1.3.3.3 Weld Seams. The length of a weld seam is a qualitative figure of merit, particularly with respect to the possible leakage areas. The aluminum tanks have the least length of weld seam because of the one-piece bulkhead. The seam lengths shown include both the girth weld and gore section welds. The ratings are based on 1.0 for zero weld seam and 0.0 for the maximum weld seam length. For example, the 301 combination rating having the longest weld seam is rated 0.0. The aluminum tank combination rating is found from

LF₂ tank:

$$1 - \frac{273}{2533} = 1 - 0.108 = 0.892$$

LH₂ tank:

$$1 - \frac{316}{3414} = 1 - 0.0925 = 0.907$$

(U) 1.3.3.4 Toughness. Notch toughness defines the ability of a material to plastically deform locally in the presence of stress-raisers without cracking, and is usually associated with the resistance of a material to fracture initiation. Fracture toughness, on the other hand, describes the resistance to unstable crack propagation, low-ductility, or brittle fracture in the presence of a crack.

(U) 1.3.3.5 Interface Seals and Dissimilar Metals Problems. A dissimilar metal situation arises between the propellant tanks and the propellant feed lines. This is not a significant item and can be handled adequately with proper design; however, it is felt to be an item that should be considered. The present system has an aluminum feed line connected to the LF₂ tank (for thermal reasons) and a CRES or monel line connected to the fuel tank.

(U) 1.3.3.6 Cost. The cost of the various tank combinations includes the total cost of the tank fabrication. Included are such items as material development, fabrication, and assembly.

1.4 STRUCTURAL MATERIAL EVALUATION

(C) 1.4.1 CANDIDATE MATERIALS. The selection of candidate structural materials for fluorine and hydrogen tankage systems on the AMPS program was limited to those alloys known to have a satisfactory history of past performance as a structural material in similar applications or known to possess a desirable combination of material characteristics to provide reliable lightweight tankage compatible with the environmental conditions. The candidate materials evaluated for this application included:

- a. Inconel 718, annealed and aged
- b. Inconel 718, 20 percent cold rolled and aged

CONFIDENTIAL

UNCLASSIFIED

- c. 301-3/4 H stainless steel
- d. 2014-T6 aluminum alloy
- e. 2219-T81 aluminum alloy
- f. 2021-T81 aluminum alloy
- g. Titanium 5Al-2.5 Sn alloy, ELI grade

Each of the candidate materials was evaluated with respect to strength-to-density ratio based upon room temperature allowables, adequate toughness of the base material and welds for structural application at cryogenic temperature, space residency, compatibility with propellants, corrosion resistance, and fabricability. Evaluation of the characteristics included the ability of the materials to be readily formed, machined, heat treated, chemically milled, and welded.

1.4.2 STRENGTH-TO-DENSITY RATIOS. Since the major portion of the structural weight is dependent upon the yield and ultimate tensile strength-to-density ratios at room temperature, these values were compared for all materials listed above and are presented in Table 1-14.

TABLE 1-14. YIELD AND TENSILE STRENGTH-TO-DENSITY RATIOS

Alloy and Condition	F_{tu} ksi	$F_{tu}/\rho \times 10^{-3}$ in.	F_{ty} ksi	$F_{ty}/\rho \times 10^{-3}$ in.
Ti-5Al-2.5 Sn (ELI)	100	680	90	555
2014-T6	66	655	58	575
718-20%CR+AGE	190	640	170	575
2021-T81	66	640	58	565
718-ANN.+AGE	180	605	150	505
2219-T81	60	590	44	430
301-3/4 H	169	590	120	420

The ultimate tensile and yield strengths for all materials listed above represent either statistically-based material allowables or guaranteed minimum values, except for the 20 percent cold rolled and age 718 alloy which represent tentative minima established from GDC test results. As noted in Section 1.3 the F_{ty} originally used for this material for the optimization study was 180,000. Subsequent information has reduced this to the above quoted 170,000. Based upon strength-to-density ratios only, the best candidate materials for lightweight tankage are the Ti-5Al-2.5 Sn (ELI), 2014-T6, and 718-20 percent CR+aged alloys. The 2219-T81 aluminum alloy has a lower strength-to-density ratio; however, it possesses other significant qualities discussed in Section 1.4.4.

UNCLASSIFIED

CONFIDENTIAL

(C) 1.4.3 COMPATIBILITY OF CANDIDATE MATERIALS IN FLUORINE. All candidate materials, with the exception of the Ti-5Al-2.5 Sn (ELI) alloy, are considered to be compatible with gaseous or liquid fluorine. A number of materials generally classified as stainless steels, copper-bearing aluminum alloys, and age hardenable nickel-base alloys have been used successfully and are recommended for major components in fluorine systems (Reference 16). Titanium and its alloys, however, are not recommended for use in either fluorine or oxygen systems due to their shock sensitive characteristics and the violent oxidation reaction which occurs when clean un-oxidized surfaces are subjected to impact or undergo cracking or fracture while in contact with these oxidizers in either the gaseous or liquid state (References 16 and 17). This, therefore, precludes the use of titanium for a fluorine tankage system.

(C) Extensive tests were conducted both at GDC and the Marshall Space Flight Center to study the reactivity of titanium in gaseous and liquid oxygen, (References 18, 19, and 20). These tests involved the puncturing of pressurized diaphragms, fracturing of weld joints by static and cyclic tensile loads, simulated micrometeoroid penetration tests, and the detonation of explosive charges in the vicinity of thin titanium sheet in the presence of liquid and gaseous oxygen. The tests have demonstrated the marked tendency of titanium to undergo violent deflagration and combustion in the oxygen environments. Although not substantiated by tests, it would be expected that the reaction of titanium with fluorine under similar test conditions would be reasonably comparable to the titanium-oxygen reactivity.

(C) The compatibility of various materials in liquid fluorine was investigated in 1963 by GDC to determine the feasibility of using fluorine-type propellants (F_2 , OF_2 , and FLOX mixtures) in the Atlas system (Reference 21). One of the materials tested during this investigation included the 301 stainless steel which is being considered as a candidate material on the AMPS program. Test specimens made from 301XH sheet containing spotwelds and fusion welds were stressed to > 50 percent of the yield strength and immersed in liquid fluorine for 200 hours. From tests conducted on each sample before and after immersion, it was concluded that 301XH stainless steel was compatible with liquid fluorine in both the welded and unwelded conditions. Nickel base alloys such as Inconel 718 would be expected to be equally compatible with liquid fluorine and fluorine-oxygen mixtures.

(U) 1.4.4 MATERIAL CHARACTERISTICS

(U) 1.4.4.1 Alloy 718. This age hardenable nickel-base alloy was originally developed for use at high temperature; however, extensive tests conducted by GDC on alloy 718 thin sheet materials, cold rolled from 0 to 30 percent and subsequently double aged, have indicated that this alloy possesses high strength-to-density ratios combined with excellent low temperature fracture toughness characteristics of both base material and fusion or resistance welds. (References 22, 23, 24, 25, 26, and 27). In addition to the above desirable properties, alloy 718 has outstanding corrosion resistance, excellent formability, and weldability. The material is readily weldable in either the annealed or age-hardened condition and has the capability of being easily repair-welded.

CONFIDENTIAL

CONFIDENTIAL

(U) In general, unlike in other precipitation hardenable nickel-base alloys, weld cracking is not a problem in alloy 718 unless the restraint on the weld is excessive. This characteristic of excellent weldability is attributed to the sluggish response of the alloy to thermal treatment. Tests conducted by GDC have indicated that alloy 718 in the annealed or 20 percent cold rolled condition can be readily formed into bulkhead gores and then readily welded either prior to or after aging. The toughness of the base material, fusion welds, and resistance welds was considered satisfactory down to -423° F (Reference 28).

(C) 1.4.4.2 301-3/4 H Stainless Steel. The primary reason for considering cold-rolled 301 stainless steel sheet for the liquid fluorine tank (B. P. -306° F) is because of the extensive experience GDC has had with this material in the production of over 550 Atlas and Space Launch Vehicle (SLV) missiles. These missiles use liquid oxygen (B. P. -297° F) and RP-1 as propellants. Both the fuel and liquid oxygen tanks of these missiles are made of type 301 stainless steel sheet, ranging in thickness from 0.010 to approximately 0.060 inch, cold rolled to the 1/2 hard, 3/4 hard, and extra hard tempers. The 1/2 and 3/4 hard tempers are used for parts that are stretch-formed and welded into bulkheads and domes. All the production and inspection problems arising from forming, cleaning, handling, welding, and sizing have been resolved. In addition, there is a large amount of mechanical property data available from both full size tank tests and laboratory specimen tests at room and liquid nitrogen (-320° F) temperature. These tests include the tensile properties of the base metal, and the static strength and the fatigue resistance of complex spot and fusion welded joints (References 33 through 37).

(C) The main reason for considering cold-rolled 301 stainless steel for the liquid hydrogen tank (B. P. -423° F) is because of its successful application in the Centaur vehicle. Extensive testing of various heats of 301XH (0-71004) containing complex spot and fusion welded joints revealed that the joints in certain heats of material manifested brittle behavior at -423° F (References 39 through 45). As a consequence, all coils of type 301XH are qualified by weld joint fatigue tests at -423° F prior to selection for use on a production Centaur vehicle. In addition, 301-1/2 hard bulkheads are produced by chemically milling and butt-welding only, eliminating the low fatigue strength spot welded splice. These two modifications have resulted in cold-rolled type 301 CRES liquid hydrogen tank structures that have operated and flown satisfactorily and which demonstrate high reliability.

(C) 1.4.4.3 Ti-5Al-2.5 Sn (ELI). The high chemical reactivity of this alloy in thin gage sheet with both gaseous and liquid fluorine precludes its use for fluorine tanks and associated hardware; however, this ELI (Extra Low Impurity) grade is presently the only titanium alloy which has been recommended or considered for use in liquid hydrogen tankage systems. This particular grade of titanium was developed cooperatively by TMCA and GDC. Work at GDC showed that when the interstitial impurity elements (carbon, nitrogen, hydrogen, oxygen, and iron) were kept to a low level, the Ti-5Al-2.5 Sn alloy retained a very high level of ductility and resistance to brittle

CONFIDENTIAL

CONFIDENTIAL

(C) fracture in both the base metal and weld joints down to -423°F (Reference 14). Extensive tests have been conducted at GDC on this alloy and grade, in thick sheet stock, over a temperature range from 75°F down to -423°F . It has been concluded that Ti-5Al-2.5 Sn (ELI) possesses an excellent combination of strength, ductility, brittle fracture resistance, and fatigue resistance in both the base material and the weld joints (References 25, 27, 29, 30, 31, and 32). Furthermore, this alloy will exhibit excellent general and stress corrosion cracking resistance for this hydrogen tankage system in which the environmental conditions are well defined. In addition to the above mentioned desirable material characteristics, the Ti-5Al-2.5 Sn alloy is not heat treatable and, unlike the other candidate materials, is not dependent upon an aging cycle, cold work, or a combination of both to develop the minimum strength levels shown in Section 1.4.2. This is a significant advantage since the material will be procured, fabricated, and used in the annealed condition; and will produce weld joint efficiencies approaching 100 percent, thereby eliminating or minimizing the need for weld lands.

(C) The use of Ti-5Al-2.5 Sn (ELI) for large diameter liquid hydrogen tankage when compared to other likely candidate materials has certain disadvantages or problem areas which must be resolved by further investigation, or fully evaluated, before any compromise can be made. These disadvantages include:

- (C) a. The larger the component the greater the risk that embrittlement of the base material or welds due to oxygen or hydrogen contamination will result during various phases of fabrication. This is particularly true for oxygen contamination during the final stages of processing a finished or semi-finished part. Oxygen contamination, unlike hydrogen or titanium hydride contamination, cannot be removed by heat treatment.
- (C) b. The most serious disadvantage of welded titanium tanks is the next to impossible task of consistently producing satisfactory and reliable weld repairs. Small or short length weld repairs along with multiple repairs are extremely difficult to make without oxygen contamination of the weld. The result is an embrittled weld lacking adequate ductility or toughness, which is unacceptable at liquid hydrogen temperature.
- (C) c. A potential problem area which is under investigation is the possibility of sensitivity of this material to hydrogen embrittlement when a freshly exposed surface is exposed to extremely pure hydrogen.

(C) 1.4.4.4 Aluminum Alloys. Three high strength age-hardenable aluminum alloys of the 2000 series were selected as candidate materials for use in both liquid fluorine and liquid hydrogen tankage systems. These alloys included 2014-T6, 2219-T81, and 2021-T81 and each is considered an excellent choice for service down to -423°F based upon good strength, ductility, and notch toughness of both base materials and their weldments. (References 26, 27, 45, 46, and 47).

CONFIDENTIAL

UNCLASSIFIED

Although the 2219-T81 is of lower strength than the other two candidate alloys, its selection as the best aluminum material was based upon excellent fracture toughness characteristics, ease of welding, ease of weld repair, and the high resistance to stress corrosion cracking of both notched and unnotched welds in either the as-welded or welded and aged condition. In addition, the excellent stress corrosion cracking resistance of the 2219-T81 alloy in the short transverse direction makes this material an ideal choice for application requiring the machining of parts from plate or from hand forgings. The 2014-T6 aluminum alloy has the highest strength-to-weight ratios; however, problems associated with poor weldability, susceptibility to cracking in welds, and the difficulty in making sound repair welds are all considered significant disadvantages and grounds for eliminating this alloy as a candidate material. Furthermore, the 2014-T6 alloy exhibits a very low stress corrosion cracking threshold level in the short transverse direction (approximately 7 ksi) and would, therefore, be a poor material choice where parts must be machined from thick product forms. In all welded conditions the 2014-T6 alloy is also susceptible to stress corrosion cracking at the edge of the weld bead, whereas, 2219-T81 has been found to be resistant to stress corrosion cracking regardless of the condition or temper of the weldment.

The 2021-T81 is a relatively new alloy specifically designed for cryogenic temperatures and possesses excellent weldability combined with excellent strength, ductility, and fracture toughness down to -423° F. Although this alloy has strength-to-density ratios near the 2014-T6 level, and possesses promising material characteristics for welded cryogenic structures, it was eliminated from consideration due to limited technical data or history on past performance as a cryogenic structural material.

1.5 LH₂ and LF₂ TANK MANUFACTURING

To achieve the primary objectives of the AMP3 program; that is, to maximize ΔV capability of the system; it is necessary that a design and subsequent fabrication technique be employed that assures the production of the lightest weight tankage system which satisfies all other mission constraints such as space residency, micro-meteoroid penetration, zero leakage, cryogenic propellants, etc. Numerous tradeoff studies discussed in earlier sections of this report conclude that propellant tanks constructed from two dome sections; each fabricated from a single piece of material, welded together with a single girth weld; offer the greatest possibility of meeting the primary objective while satisfying all mission constraints. This section is devoted to a brief discussion of the manufacturing techniques considered and recommended by GDC for tankage system fabrication.

1.5.1 ELLIPTICAL DOME FORMING

1.5.1.1 Selected Forming Method. GDC recommends the single-piece dome sections formed from 2219-T351 aluminum material by the hot spin forming method. The dome sections will be spun formed on a 144-inch Liefeld spinning lathe. Material

UNCLASSIFIED

UNCLASSIFIED

blanks will be heated with oxygen-butane torches. During the forming sequence, temperatures will be controlled and recorded with Thermodot recording pyrometers. GDC has found that heat is necessary to reduce the forming pressures required to form 2219 in the solution heat-treated and stretched (T351) condition. This condition is available only from the mill. A maximum time of two hours at a maximum temperature of 350° F will be required to hot spin form the domes. A normal artificial aging treatment (350° F for 18 hours) will be employed after the machining operation to ensure that all portions of the dome are in the fully aged condition. No adverse effects will be experienced in meeting the minimum mechanical properties or achieving maximum corrosion resistance of the artificially aged (T81) domes due to the thermal exposure and work hardening of this copper-bearing aluminum alloy during the spinning operation.

The selection of the spin forming process by GDC has been made on the basis of previous successes by this method on domes of equal or greater diameters, availability of existing equipment, low cost for limited quantity production tooling, and low unit cost for finished dome.

1.5.1.2 Other Forming Methods Evaluated

- a. Explosive Forming. A wide variety of bulkheads and dome ends have been formed from the 2219-T31 aluminum alloy by use of the explosive forming technique up to 37 inches in diameter size. Experience to date has shown considerable difficulty in control of dome contours, due to placement and size of the "shape charge" used during the explosive forming process. Machining of large dies required for explosive forming is very costly, and when a die exceeds the capacities of standard machining equipment, the cost increases greatly. Die handling at the rather isolated explosive forming area also contributes to additional cost. To date, GDC sees no practical application of this forming method to the fabrication of dome sections for the AMPS tankage system and would see no justification for pursuing a costly, high risk development program to satisfy program requirements.
- b. Bulge Forming. This involves the use of liquid under pressure to bulge-form metal into specific configurations. A metal blank or a pre form is located on a tool base and sealed at the periphery with a clamping ring or the flange of a shell die, and liquid under pressure is fed through an opening in the tool base to act as a liquid punch. GDC has obtained excellent results in bulge forming thin gauge (0.050 inch) 2219 aluminum in the annealed condition. To form 2219-T31 material, GDC's experience has shown it would be necessary to apply heat at the time of bulge forming. Costs of facilities required to pump large volumes of hot fluids under high pressure for forming large domes are excessively high for limited quantity hardware production. It is felt that "hot bulge forming" dome sections is completely

UNCLASSIFIED

UNCLASSIFIED

feasible, but for limited production runs it offers no advantages over spin forming, and because of cost is not recommended.

- c. Double Action Draw Forming. This method combines the techniques of draw forming and hydraulic bulge forming. Fabrication of 2219-T31 aluminum domes has been achieved by this method; however, equipment and tooling costs are high compared to costs for the spin forming method.

1.5.2 ELLIPTICAL DOME MACHINING. After final spinning to contour, a tracer controlled machine cut will be taken over the outer surface of the dome. It should be noted that during machining a local re-rolling operation may be required to bring the part back to contour, due to stress relief from machining.

Thickness tolerance will be held to ± 0.015 inch, which allows for a final chem-mill to thickness after aging. Thickness will be ultrasonically measured using an ultrasonic thickness gauge. For purposes of measuring and documenting thickness variations, the domes will be divided into eight sections. A template will be prepared for one section, with hole cutouts that will permit readings to be taken on 20 concentric bands at approximately 3-inch centers in each section. Index marks and thickness readings will be identified on the surface of each dome. High spots will be outlined with squares, low spots will be outlined with triangles to highlight thickness variations.

1.5.3 ELLIPTICAL DOME HEAT TREAT. Dome ends will be run through a complete aging cycle following finish machining and inspection of the bulkheads. No credit will be given to the additional amount of work hardening from the hot spin operation. The aging cycle will consist of heating the dome in an aging oven, certified by GDC Quality Control for aluminum, to a temperature of 350° F, and holding it at that temperature for a period of 18 hours. This will result in a final material condition of T-81. Tensile test coupons cut from excess material on the spun dome will be aged concurrently with the domes. These coupons will be tested to verify the final material condition.

1.5.4 ELLIPTICAL DOME CHEM-MILLING. Selective masking and etching will be used to machine the various pads, doublers, and weld lands into the finish formed bulkhead. Chem-milling will be performed with material in the aged condition to avoid excessive surface roughness and variation in dissolution rates associated with this alloy when it is not etched in the aged condition. The grid pattern of thickness measurements marked on the surface of the domes following final spinning and machining operations will be used as the starting point for chem-milling. Final thickness will be measured ultrasonically after chem-mill, and will be documented in the same manner as the measurements after forming. The etched pattern will be inspected and controlled by master shell templates.

UNCLASSIFIED

UNCLASSIFIED

1.5.5 TANK WELDING. All liquid hydrogen tank welds will be standard II or better, per MIL-R045774 specification. Automatic Tungsten Inert Gas (TIG) dc straight polarity welding equipment will be used with 2319 filler wire and helium gas backup on all major tank welds. Tank weld beads will be removed to improve the fatigue and strength properties of the welded joint. Dye penetrant and radiographic inspection will be conducted on all welds to detect unacceptable surface and internal weld defects. Weld joints will also undergo a helium leak test after completion of each weld.

UNCLASSIFIED

CONFIDENTIAL

SECTION 2

THERMAL CONDITIONING AND SUPPORT STRUCTURE (TASK 2)

2.1 INTRODUCTION

(C) The thermal conditioning and support structure subtask is concerned with establishing an optimum insulation system which provides maximum performance for a 14-day space residence mission. This subtask is also concerned with defining the support structure (outer shell and tank supports) which minimizes heat leak and system inert weight.

(U) A simplified flow schematic of the major tasks is presented in Figure 2-1. The requirement for the initial tasks was to establish a basic configuration which could be used as a basis for the ground test article design. The various subtasks then feed into the test article design as the program progresses. An integrated thermal analysis will then be conducted on the overall system prior to incorporating the results in the final design of the test article.

(U) The first two tasks (shown shaded in Figure 2-1), superinsulation optimization and support structure design, have been essentially completed during this reporting period. The only remaining item from these tasks is the design drawing of the structural shell. The configuration has been defined and a stress analysis has been completed.

(U) During the next quarter all remaining tasks will be initiated except for the analysis of the effects of extended space residence and ground hold capability.

(C) The optimization of the superinsulation system resulted in the selection of tank mounted Superfloc superinsulation having 45 layers on the hydrogen tank and 32 layers on the fluorine tank. The main criterion of this selection was ΔV , although many other factors were evaluated prior to the selection of the tank mounted insulation.

(U) In this document, the discussions dealing with superinsulation optimization present the detailed background information used to arrive at the selected configuration. This information is divided into six sections. Section 2.2.1 discusses the various design approaches and considerations for both tank mounted and shroud mounted systems; including blanket construction, installation procedures, fastening methods, and loads analysis. Section 2.2.2 discusses different candidate insulation systems, basic superinsulation performance, penetration effects, and the resulting heat leaks into the propellant tanks as a function of layer thickness for both the tank mounted and shroud mounted cases. Section 2.2.3 discusses the performance trade-off effects in terms of ΔV penalty as a function of propellant boiloff and inert weight. Section 2.2.4 presents the results of the trade-off analysis comparing both the tank mounted and shroud

CONFIDENTIAL

CONFIDENTIAL

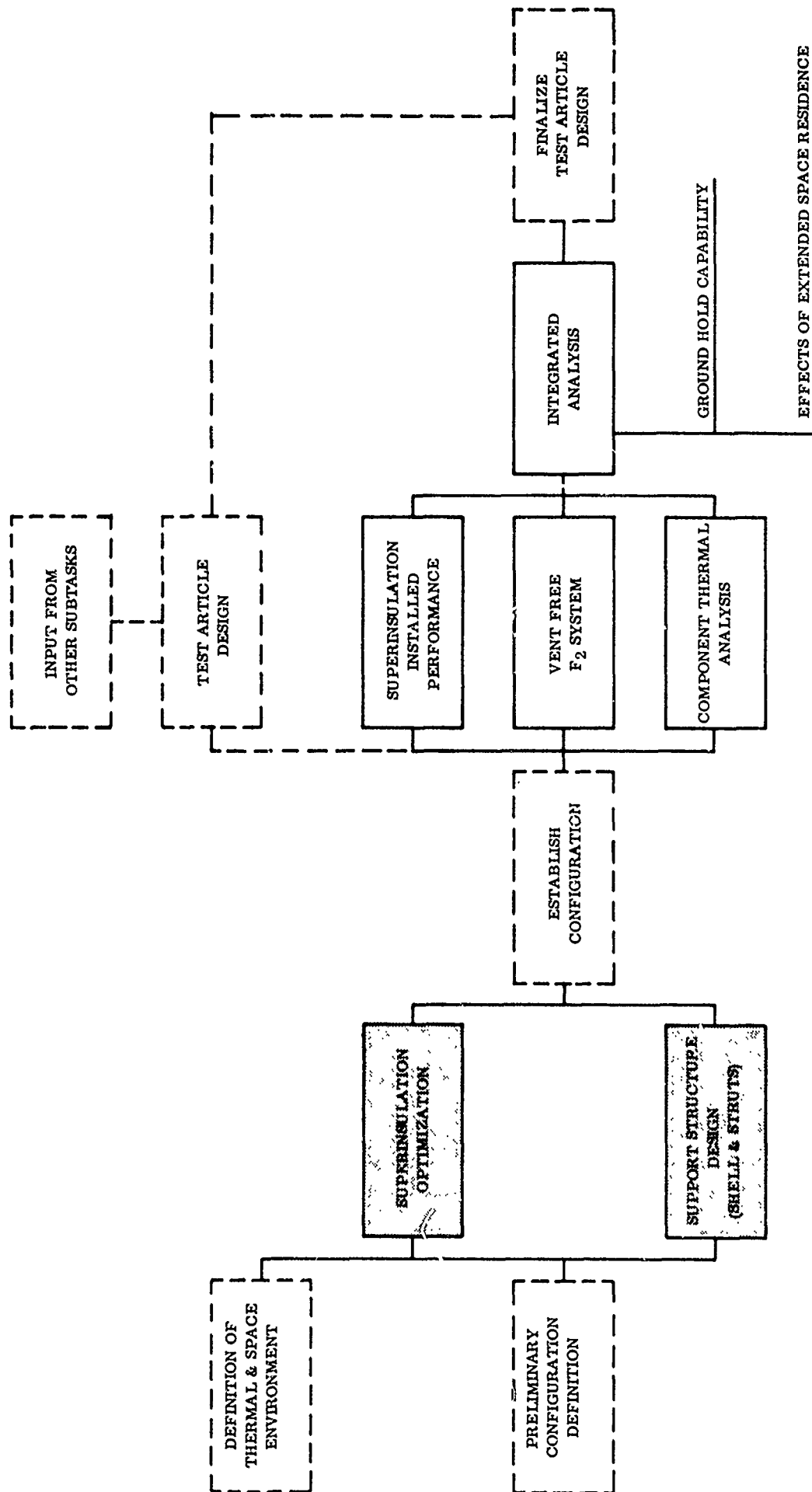


Figure 2-1. Thermal Conditioning and Support Structure

CONFIDENTIAL

CONFIDENTIAL

mounted system using ΔV penalty as the performance criterion. Section 2.2.5 discusses some considerations for ground environmental control. Section 2.2.6 qualitatively discusses all the other factors that led to the selection of the tank mounted insulation system.

(U) The discussion dealing with the support structure is divided into two sections: Section 2.3.1, dealing with the optimization of the structural shroud, and Section 2.3.2, dealing with the support struts.

2.2 SUPERINSULATION OPTIMIZATION

(C) A detailed trade-off study to determine the optimum thickness (number of layers) and location (tank or shroud mounted) of the superinsulation resulted in the selection of tank mounted Superfloc superinsulation, with 45 layers on the hydrogen tank and 32 layers on the fluorine tank. This system results in maximum vehicle performance while affording other advantages over the shroud mounted system.

(C) The insulation is installed in gore section blankets with the blankets interconnected by fiberglass twin pin fasteners. The fluorine tank installation consists of 3 blankets, 2 of which contain 11 layers and the third 10 layers. The hydrogen tank installation consists of 4 blankets, three containing 11 layers and one containing 12 layers.

(U) The blankets are composed of 1/4 mil flocked, aluminized mylar (Superfloc) with the two face sheets being 1 mil. The entire outer face sheet of the outer blanket consists of scrim reinforced mylar to provide additional strength to the lay-up.

(C) The ΔV penalty incurred as a result of insulation system weight and propellant boiloff for the most sensitive mission (90 percent burn the first day and 10 percent burn the last day) is approximately 550 ft/sec, or 2.5 percent of the initial velocity increment available. This assumes that all heat into the tanks results in propellant boiloff and that none is absorbed in raising the bulk temperature of the propellant. Absorbing some of the heat in the propellant would result in less performance penalty.

(U) The various factors that went into the insulation optimization study are shown in Figure 2-2.

(U) 2.2.1 DESIGN. Two basic design configurations were considered, one having the superinsulation mounted on the tanks and the other having the superinsulation mounted on the structural shell. In order to evaluate the relative advantages of each system it was necessary to establish a realistic installation which is representative of one that could be used and would approach an optimum configuration for the subject application. This required not only an evaluation of the basic superinsulation, but also evaluation of methods of attachment, joint design, structural estimates, evacuation pressure loads, and other design considerations.

CONFIDENTIAL

UNCLASSIFIED

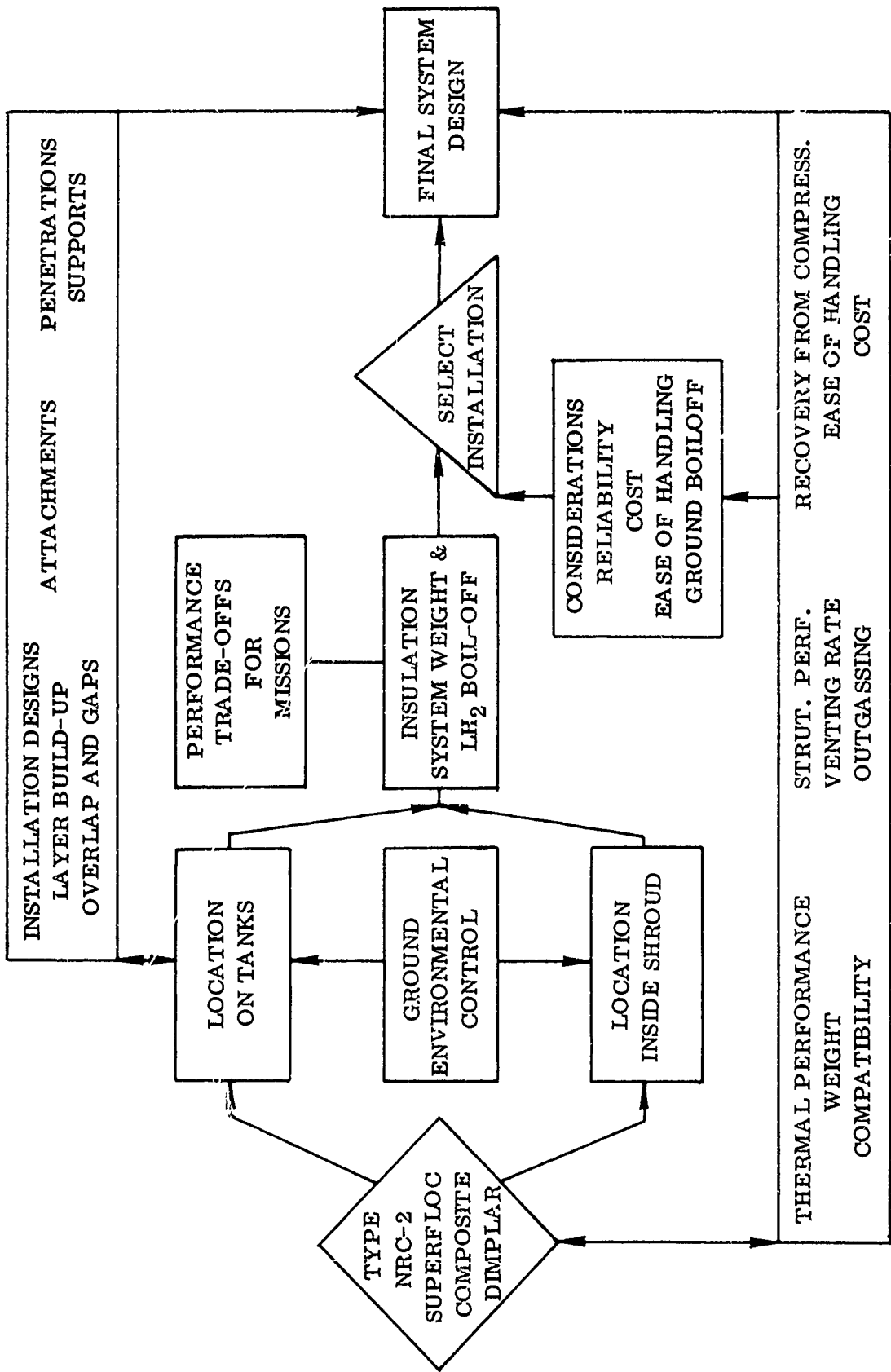


Figure 2-2. Superinsulation Optimization

UNCLASSIFIED

CONFIDENTIAL

(U) Sections 2.2.1.1 and 2.2.1.2 of this design discussion are concerned with the tank mounted insulation system, describing the selected system and also describing some alternate concepts. The drawing of the selected system (See Figure 2-3.) can be considered as a working drawing showing some concepts which were finally discarded. A structural estimate is included to assure that the superinsulation system is capable of withstanding the various loads that occur.

(U) The shroud mounted insulation system is discussed in Sections 2.2.1.3 and 2.2.1.4, in the same manner as for the tank mounted installation.

(U) Section 2.2.1.5 discusses the various concepts that can be utilized to join the gore blankets at the seams; including spot bonds, pins, and tape. Some test results evaluating the tear-out strength of mylar are also included.

(U) Section 2.2.1.6 discusses the maximum pressure loads that can be encountered during ascent, and the method of analysis used to arrive at the results.

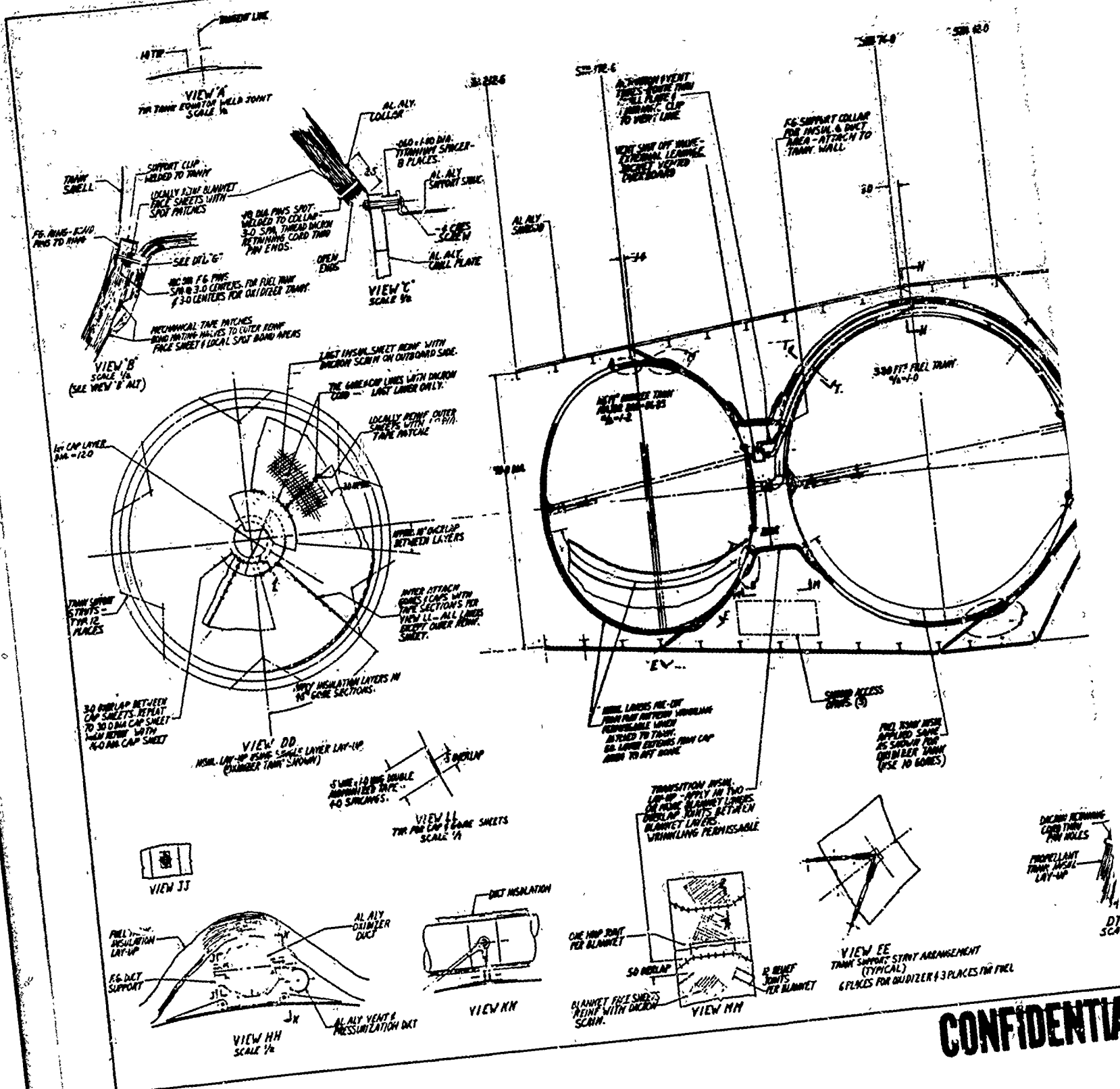
(U) Section 2.2.1.7 gives a detailed weights analysis of the selected systems and presents the relationship of weight as a function of the number of layers of superinsulation.

(C) 2.2.1.1 Tank Mounted Insulation System. The preferred tank mounted insulation system consists of a forward insulation lay-up on the oxidizer tank, an aft lay-up on the fuel tank, a transition or neck section between the two tanks, and an aft chill plate assembly. The chill plate is essentially a flux interceptor through which all ducting and lines pass to the outside of the shroud. The plate is cooled by the vented hydrogen and serves to effectively eliminate the heat leak through the penetrations. The ducts, tubes, wiring, and chill plate assemblies are attached to the fuel tank; the insulation applied over the complete assembly (LH₂ and LF₂ tanks) prior to installing into the shroud. A discussion of the installation procedure is given in this section. Each insulation lay-up is independently supported which in turn minimizes compression on the layers at the forward region of the oxidizer tank during acceleration. The completed system is a continuous insulation envelope surrounding both tanks and terminating at the aft chill plate. The low conductive tank support struts are the only penetrations through this envelope.

(U) a. Oxidizer Tank Insulation Lay-up (Reference: Figure 2-3). The oxidizer tank insulation is installed in blanket gore sections extending continuously from the forward cap section to the aft attachment pins. Each blanket is prefabricated using 1/4 mil core sheets and 1 mil outer face sheets (10 sheets total). The layers are interconnected by engagement of reinforced blanket holes with pins (View "a" alternate in Figure 2-3). This prevents interply shifting, provides attachment points, and facilitates handling. (See Figure 2-4.)

CONFIDENTIAL

CONFIDENTIAL



CONFIDENTIAL

UNCLASSIFIED

a. Oxidizer Tank Insulation Lay-up (Continued)

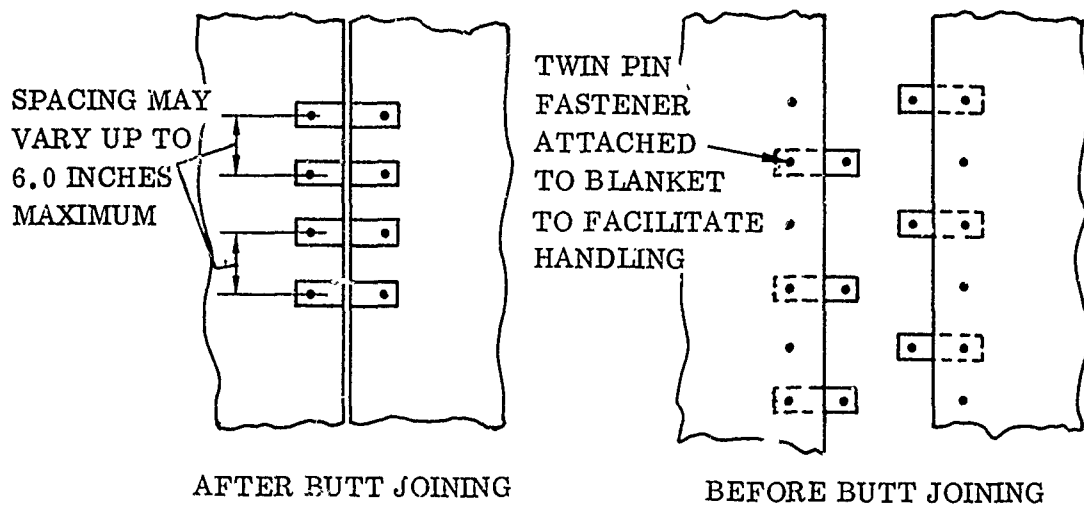


Figure 2-4. Blanket Gore Interconnection

The pins are fiberglass fittings which are simply engaged with the blanket holes. A retainer strip is then engaged with the pin ends, and the assembly is locked by installing a retaining assembly over the top of the pins, connecting them. A detailed discussion of attachment methods is given in Section 2.2.1.3.

Holes punched through the layers are equipped with local spot reinforcement patches for resisting tear-out from the pins. The forward cap blankets are circular in shape and are fabricated in the same manner as described for the gore sections. The cap blanket diameters are varied from approximately 14 to 32 inches to permit overlaps between butt joints. A 40 inch diameter zone on the aft end of the oxidizer tank is equipped with a fiberglass ring containing pins for attaching the blankets. This ring is riveted or bolted to aluminum clips which in turn are welded to the tank shell or local chem-milled zones.

A fiberglass fairing is bonded to the tank shell at each support zone. (See Views P and M in Figure 2-3.) This fairing positions the insulation lay-up away from the attachment area and allows a gradual transition of the layers over the support areas without excessive wrinkling.

A typical blanket layer installation is made by positioning a 14 inch diameter cap blanket on the forward end of the tank. A gore blanket is then butted to the cap blanket and connected using twin pin fasteners. The aft end of the blanket is then slipped over the retaining pins and held in position by temporary plastic or rubber grommets placed over the pin ends. The succeeding gore sections are installed in the same manner completing the first blanket layer. The gore line butt joints between the blankets are connected with the twin fasteners.

UNCLASSIFIED

UNCLASSIFIED

a. Oxidizer Tank Insulation Lay-up (Continued)

A second blanket layer applied using a cap section diameter larger than that used in the first lay-up. This provides an overlap at the butt joints. (See View DD in Figure 2-3.) The gores are positioned approximately 10 degrees from the previous layer location, providing an overlap between gore lines. The aft end of the gore blankets is then engaged with the retainer pins by removing the temporary grommets at each pin and replacing them after the layers are in place. These procedures are repeated until the required blanket build-up is completed. When installing the last layer, the temporary pin grommets are replaced by connecting the permanent connection across the pin ends.

The outboard face sheet of the last blanket assemblies is bonded integrally with a dacron scrim reinforcement. When the blankets are connected at the gore and cap joints, this reinforced outer layer forms a high strength outer shroud for retaining the overall insulation lay-up.

- b. Transition or Neck Section Insulation Lay-up. This area is installed after all plumbing connections are completed. The pins attached to the oxidizer and fuel tanks for support of the gore blankets are extended in length to accommodate the transition blankets. (See View B in Figure 2-3.) A typical transition blanket is a single-piece, prefabricated flat pattern assembly of sufficient width to overlap the tank insulation and extend completely around the neck zone. The face sheets are scrim reinforced and the core is composed of 1/4 mil layers which are connected (using twin pins) at the edges with the face sheets. Holes are punched through the blanket layers approximately 3 inches from the edge and spaced on 6 inch centers for receiving the support pins. The face sheets are reinforced at these holes to prevent tear-out. The blanket is locally split near the edges at 12 places to allow overlaps with the tank lay-ups. A typical installation consists of engaging the holes in the blanket with the support pins on the tanks, and retaining it with dacron cord looped through holes in the pins. The edges of the blanket are then engaged with the scrim reinforced outer layers of the oxidizer and fuel tanks by hand pressing the mechanical tape patches against a mating patch which is bonded to the outer reinforced tank insulation layer. (See View B in Figure 2-3.) The ends of the blanket (See View MM in Figure 2-3.) are attached using a fiberglass twin pin fitting shown in View RR of Figure 2-3. This installation procedure is repeated for the number of required blanket layers. Procedures are changed slightly when installing the final outboard layer. The pin ends are equipped with a fiberglass washer bonded to a mechanical tape section per detail G of Figure 2-3. The blanket construction is altered slightly by replacing the open holes (formerly used for pin engagement) with local mechanical tape patches bonded to the reinforced face sheet. Blanket installation then consists of engaging the mechanical tape patches. The blanket ends are attached using the twin pin fasteners per View RR of Figure 2-3. This final blanket layer therefore provides a complete cover for the pin ends.

UNCLASSIFIED

UNCLASSIFIED

- c. Fuel Tank Insulation Lay-up. The fuel tank insulation is applied in the same manner as described for the oxidizer tank except cap sections are not required and more gores are used. The gore elements are engaged with the support pins located at the forward end of the tank and retained with dacron cord looped through the pin ends. The aft ends are engaged with the pins on the chill plate collar and retained in the same manner. (See View C of Figure 2-3.) The retainer pins on the chill plate collar are positioned inboard. A temporary fixture is therefore required when installing the blankets. This fixture simulates the chill plate collar interfaces except the pins are positioned outboard and the assembly can be removed in sections. After completion of the lay-up, the fixture is removed in sections and the chill plate collar pins are engaged with the insulation holes. To prevent interlayer shifting, temporary clothes-pin type clamps are attached to the lay-up between pins before removing the fixture. Fiberglass fairings are provided at each tank support fitting to position the insulation away from the attachment area and to minimize the profile discontinuities. An additional fiberglass fairing type collar is attached to the tank wall at the plumbing area. This fairing spans over the plumbing forming a base for the insulation and is part of the forward pin attachment zone. Insulation blankets which cover the plumbing area are fabricated over-size to allow for the local profile change. The blankets lay directly over the plumbing components.
- d. Feed Line Insulation and Supports. The aluminum alloy oxidizer feed line is supported from the fuel tank wall at one area (See View HH of Figure 2-3.) using a fiberglass support yoke which engages with sockets in the duct wall. The insulation is applied to the duct in single layers by simple circumferential wrapping and retaining with local $1/2 \times 1$ inch tape pieces. (See Figure 2-5, A.) The ends of the insulation layers are overlapped approximately $1/2$ inch before taping. The width of each wrap is limited to approximately 24 inches so that the duct can be covered without unusual wrinkling. Each 24 inch length sheet is overlapped approximately 2 inches with the adjacent sheet. (See Figure 2-5, B.) All joints are staggered approximately 2 inches between layers. Shifting between layers is avoided by hand punching one 0.30 diameter hole at each end of a typical 24 inch length sheet and placing a tape piece over the hole and applying thumb pressure. One layer is therefore adhered to the next layer by the exposed adhesive section at the hole. (See Figure 2-5, C.)

Another method suggests spiral wrapping the line with approximately 10 inch wide insulation strips with 2 inch overlaps. Local tape patches are placed over the seams while wrapping.

UNCLASSIFIED

UNCLASSIFIED

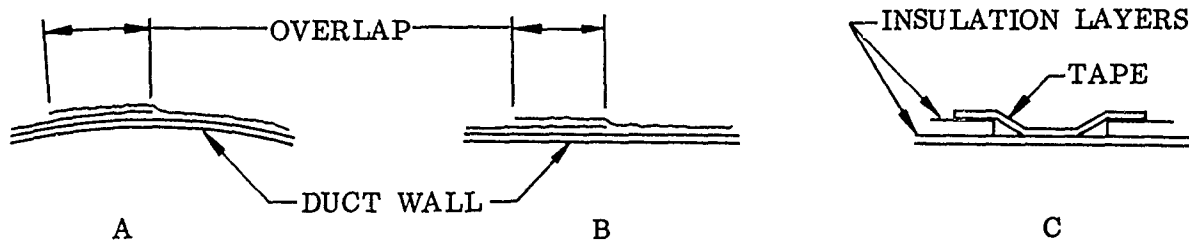


Figure 2-5. Insulation Wrapping

- e. Vent Ducting. The aluminum vent duct is supported from the fuel tank wall at three points. One attachment is integral with the oxidizer duct support (See View HH of Figure 2-3.) and two attachments are made using fiberglass fairlead type brackets equipped with CRES retaining bands and cap sections. (See Views TT and UU of Figure 2-3.) The vent duct is not insulated since a valve is used near the tank interface. Miscellaneous sensing tubes and wiring are supported by marriage clipping to the vent duct. Plumbing connections which are inside the insulation are welded where possible. Flanged joints incorporate seal arrangements such that cavities between seals can be vented overboard. Valves are completely enveloped with brazed or welded sheet metal type shrouds which are vented overboard.
- f. Chill Plate Installation. The chill plate is an aluminum alloy sandwich type circular flat plate structure composed of two face sheets separated by a ribbed core. The assembly serves as a support for the plumbing and provides internal flow passages for cooling vent gas. The plate is fabricated in two 180 degree halves to allow assembly with the plumbing lines. A typical duct attachment is shown in Figure 2-6.

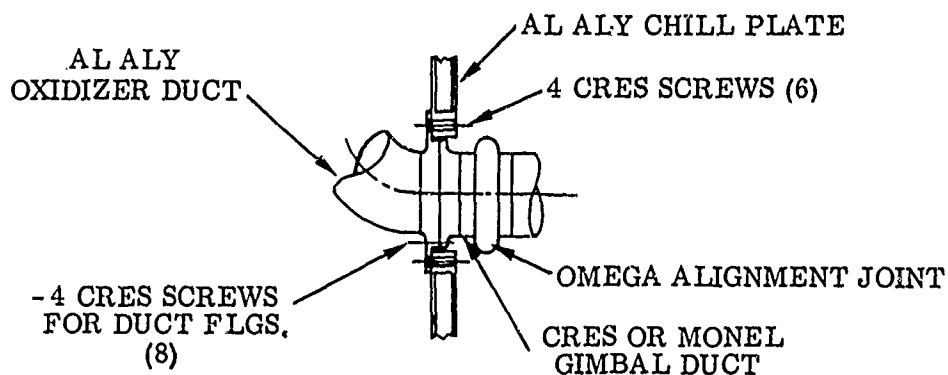


Figure 2-6. Typical Chill Plate Penetration

UNCLASSIFIED

CONFIDENTIAL

(U) f. Chill Plate Installation (Continued)

(U) Installation consists of connecting the chill plate to the plumbing line flanges; engaging the engine thrust cone using titanium tubular spacers (See View C of Figure 2-3.) and bolting the collar, chill plate and thrust cone together. (See inboard view on Figure 2-3.) The collar is provided with nut plates at the inboard side. The assembly is then completed by riveting the shroud thrust structure to the engine thrust cone.

(U) The chill plate is equipped with a removable aluminum collar containing support pins for the fuel tank insulation. During the insulation assembly, the collar is disconnected from the chill plate and supported by a fixture. All plumbing line ends are left hanging within the perimeter of the chill plate collar. Access to the chill plate collar pins is therefore through the areas bordered by the plumbing lines and the collar.

(U) g. Assembly Procedure. The tanks are temporarily coupled together, plumbed and insulated prior to installing in the shroud. This is accomplished by insulating the oxidizer tank (except for the aft 40 inch diameter zone) and cutting support strut openings in the lay-up. (See Figure 2-7A.) Similarly the fuel tank, complete with plumbing and chill plate collar, is insulated (Figure 2-7B.) The insulated tanks are then suspended in a tubular fixture using the flight support struts. (See Figure 2-7C.) This fixture is designed to fit inside of the flight shroud and incorporates features for dismantling in small sections. The plumbing connections between tanks and the insulation transition section are next completed. This assembly (with fixture) is inserted into the shroud (Figure 2-7D). The tanks are supported from the shroud by disconnecting the struts from the fixture (one at a time) and re-connecting to the shroud frame fittings (Figure 2-7E). The fixture is removed in sections through the access openings and the aft end. The assembly is then completed by installing the chill plate, engine thrust cone, and thrust structure per the previous discussions.

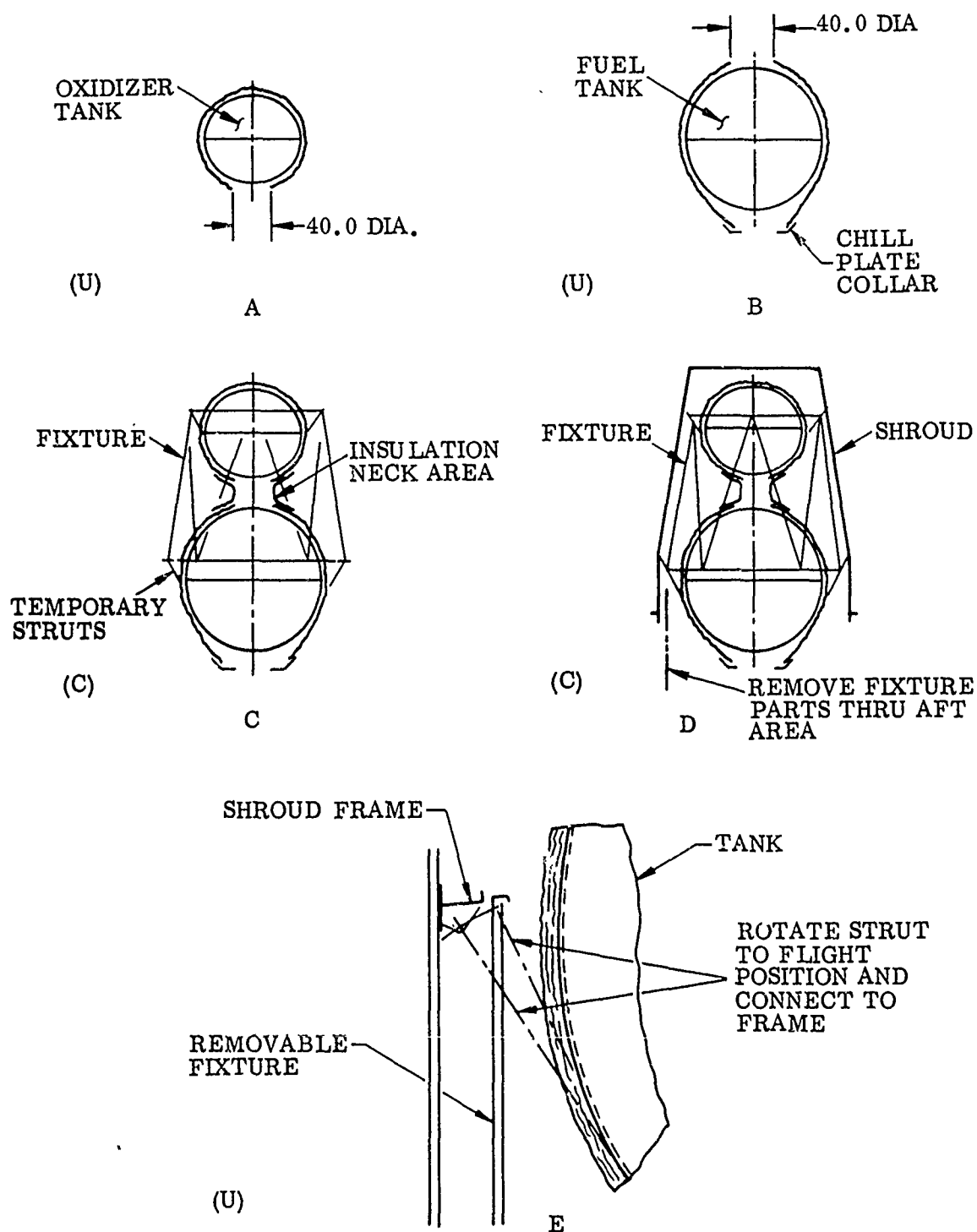
(U) h. Insulation Structural Estimate. A superinsulation lay-up is inherently a non-precision assembly. Small material gages, multiple layers, low stiffness, tolerances, and flat patterns applied over double curvature surfaces are some typical contributing items. Accurate predictions of load distributions between layers and at the attachments are questionable; therefore, the following conservative assumptions were made in estimating the structural integrity of the system:

(C) (1) 0.10 psi pressure differential across the blanket assembly during evacuation (Reference: Section 2.2.1.6)

(U) (2) Primary loads are reacted by the blanket face sheets only. The 1/4 mil core sheets would react only those loads necessary to prevent interlayer shifting.

CONFIDENTIAL

CONFIDENTIAL



(C) Figure 2-7. Tank Assembly Procedure

CONFIDENTIAL

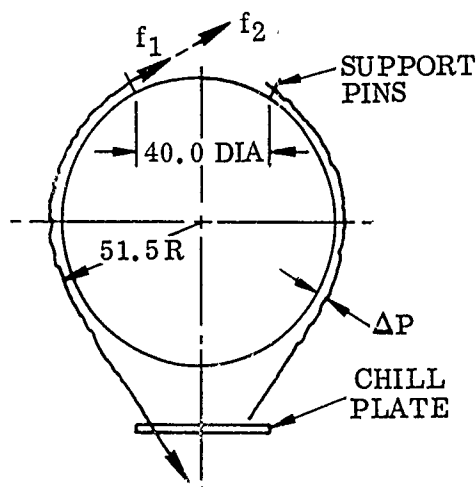
CONFIDENTIAL

(C) h. Insulation Structural Estimate (Continued)

(3) Seven g's aft acceleration

(4) Loads due to inertia and pressure differential occur simultaneously.

(U) The support pins located on the forward end of the fuel tank (See Figure 2-8.) react inertia loads due to the insulation weight and loads due to the 0.10 psi ΔP across the lay-up. Hoop forces from the transition section are neglected since each of these blankets is scrim reinforced and assembled into a continuous cylindrical configuration.



(U) Figure 2-8. Fuel Tank Support Pin Location

(C) The meridional and hoop forces for a sphere are $\frac{PR}{2} = f_1$

For 0.10 psi and a 51.5 inch radius,

$$f_1 = \frac{0.10 \times 51.5}{2} = 2.575 \text{ lb/in. (See Figure 2-8.)}$$

$$\begin{aligned} \left(\begin{array}{l} \text{Insulation} \\ \text{Weight Acting} \\ \text{On The Pins} \end{array} \right) &= \left(\begin{array}{l} \text{Basic} \\ \text{Lay-Up} \\ \text{Weight} \end{array} \right) + \left(\begin{array}{l} \text{Weight of} \\ \text{Gore Line} \\ \text{Fasteners} \end{array} \right) \\ &= 32.17 + 5.75 \\ &= 37.92 \text{ lb} \end{aligned}$$

f_2 = load due to insulation weight in lb/in. (g factor = 7.0)

$$\text{Therefore } f_2 = \frac{37.92 \times 7.0}{\pi \times 40.0}$$

= 2.11 lb/in. at the 40.0 diameter zone.

F = total load per pin.

CONFIDENTIAL

CONFIDENTIAL

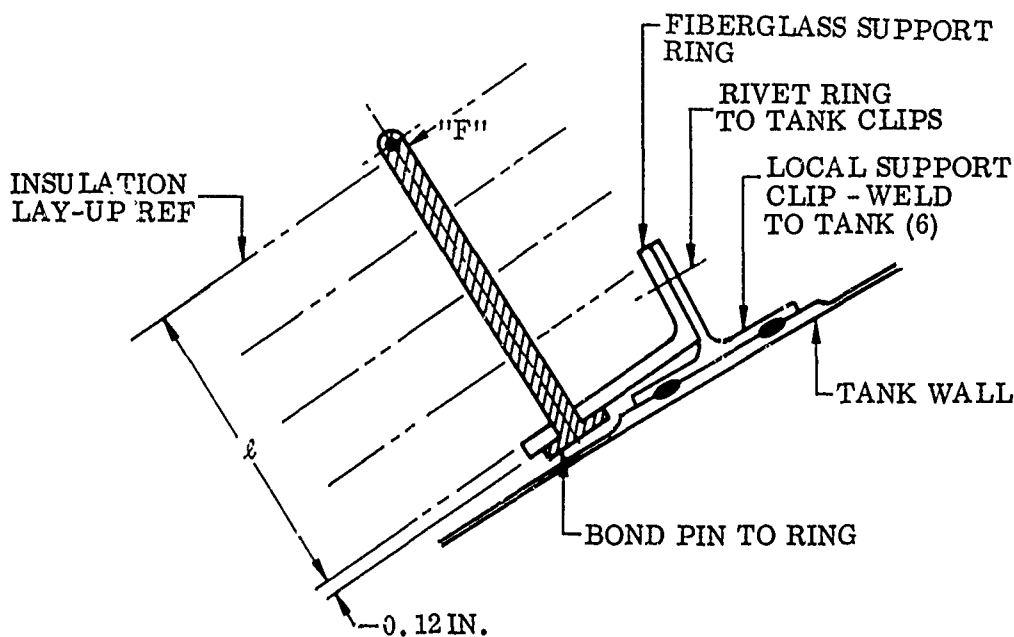
(C) h. Insulation Structural Estimate (Continued)

(C) Therefore assuming a three inch pin spacing at the 40.0 inch diameter zone,

$$\begin{aligned} F &= (f_1 + f_2) (3.0) \\ &= (2.575 + 2.11)(3.0) \\ &= 14.05 \text{ lb/pin} \end{aligned}$$

Referring to Figure 2-9, the load F is conservatively assumed to act as a single load on the pin end. Considering the pin as a cantilever beam, the maximum moment "M" = F × ℓ

$$\begin{aligned} &= 14.05 \times 2.0 \\ &= 28.1 \text{ in.-lb} \end{aligned}$$



(C) Figure 2-9. Support Pin Load

The 2.0 value for "ℓ" assumes the transition section lay-up per View B of Figure 2-3. If the lay-up per View B alternate of Figure 2-3 is used, the pin length increases to 2.8, with "M" increasing to 39.3 in.-lb. For this analysis, the 39.3 in.-lb value for "M" will be used. The moment of inertia for the cross section $I = \frac{\pi (r)^4}{4}$ where r = pin radius assuming a 0.18 pin diameter,

$$I = \frac{\pi (0.09)^4}{4} = 0.0000515 \text{ in.}^4$$

$$\text{Bending stress } S_b = \frac{Mr}{I} = \frac{39.3 \times 0.09}{0.0000515} = 68,700 \text{ psi}$$

CONFIDENTIAL

CONFIDENTIAL

(C) h. Insulation Structural Estimate (Continued)

An $F_{tu} = 100,000$ psi for fiberglass is obtainable.

Assuming a 1.0 inch wide strip through the support ring (See Figure 2-9),

$$I = \frac{1.0 (0.12)^3}{12} = 0.000144 \text{ in.}^4$$

$$\text{Therefore the bending stress} = \frac{39.3 \times 0.06}{0.000144} = 16,400 \text{ psi}$$

$$\text{Pin shear stress} = \frac{14.05}{0.785 (0.18)^2} = 552 \text{ psi}$$

$$\text{The load per face sheet } F_f = \frac{F}{n}$$

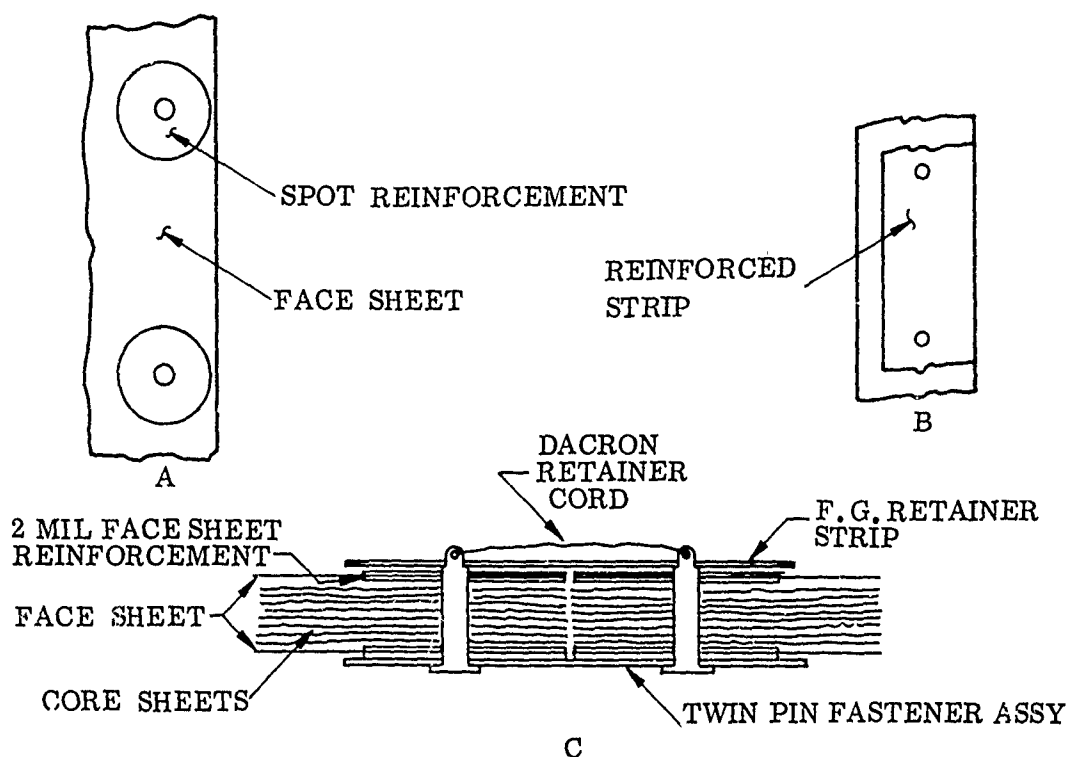
Where n = number of face sheets

$$\text{Therefore } F_f = \frac{14.05}{8} = 1.755 \text{ lb.}$$

- (U) GDC tests indicate a minimum tear-out strength of 2.5 pounds for a single reinforcement. (See Figure 2-40 in Section 2.2.1.5.) Due to unknowns associated with load distribution, perfection of attachment holes, etc., dual reinforcement such as shown for specimens Nos. 1, 2 and 3 in Figure 2-40 are recommended.
- (U) It may be desirable in the final design to replace the spot type reinforcements shown in Figure 2-10, A, with a continuous reinforcing band shown in Figure 2-10, B. This would distribute the load more uniformly into the face sheet areas between pins.
- (U) The blankets are held together at the gore lines with twin pin fiberglass fasteners as shown in Figure 2-10, C. This arrangement is similar to a bicycle chain link. The meridional or hoop loads at the gore lines are basically due to the 0.10 psi ΔP . Assuming that the outer blanket only reacts this load and a six inch maximum spacing between fasteners, the load per face sheet hole equals
- $$\frac{2.575 \times 6}{2} = 7.72 \text{ lb}$$
- (U) Assuming that the last outboard blanket reacts the loads from ΔP , the basic face sheet stress = $\frac{2.575}{0.001 \times 2} = 1,287 \text{ psi}$

CONFIDENTIAL

CONFIDENTIAL



(C) Figure 2-10. Insulation Reinforcement

(C) h. Insulation Structural Estimate (Continued)

- (U) The 1/4 mil core sheets must resist inertia loads at the pins to prevent interlayer shifting. The weight of 32 core sheets is 16.70 pounds; therefore the load per core sheet per pin at the forward support ring:

$$f_c = \frac{16.70 \times 7}{42 \times 32} = 0.087 \text{ lb, where } 42 = \text{the number of support pins. GDC}$$

tests show a 0.562 pound minimum tear-out strength for unreinforced 1/4 mil sheets.

- (U) Mylar film is obtainable with an $F_{tu} = 21,000$ psi. The outboard face sheet of the last blanket layer is integrally reinforced with dacron scrim to form a high strength retaining shroud around the completed insulation lay-up. Reinforced mylar films are obtainable with strengths up to 275 pounds per inch of width in both warp and fill directions. The Schjeldahl Corporation manufactures an X-850 laminate composed of 1/4 mil aluminized mylar, 0.6 oz/yd² dacron scrim, and 1/2 mil aluminized mylar, bonded together with a thermoplastic polyester adhesive. A tensile strength of 58 pound/inch (warp direction) and 45 pound/inch (fill direction) is quoted. Hook tear strength is 110 pounds maximum. It therefore appears that the environmental loads are well within the capabilities of the materials considered.

CONFIDENTIAL

UNCLASSIFIED

2.2.1.2 Alternate Considerations - Tank Mounted Insulation System. There are numerous ways in which a superinsulation system may be installed on a propulsion system and the selected version represents what is presently determined to be the optimum for present application. Other systems and methods were considered and are discussed below. The actual attachment methods (i.e., pins, cords, etc.) are a separate subject and are discussed in detail in Section 2.2.1.3.

In general, the following items should be used as ground rules when evaluating insulation systems:

- (1) Insulation must yield maximum thermal characteristics.
- (2) Insulation assembly on a tank should be rapid with a minimum of skilled labor and special handling required.
- (3) Insulation must remain affixed to the tank and undamaged during rapid evacuation.
- (4) Insulation assembly should be designed to minimize outgassing in vacuum.
- (5) Insulation should be easily repaired if damaged.

- a. Insulation Layer Buildup. The two basic considerations in superinsulation lay-up is whether to use individual layers or multi-layer assemblies (i.e., blankets). An alternate arrangement is shown where the insulation is applied in single 1/4 mil layer elements. Installation procedures are the same as shown for the blanket layer approach except the gore and cap elements are overlapped approximately 1/2 inch and interconnected with 1/2 x 1 inch sections of tape at 4.0 inch spacing. This joint overlap reduces the need for precision cutting and positioning of the elements and prevents the tape elements from adhering to the previous layer. The last ply (1 to 2 mil gage) of the single layer lay-up is integrally bonded with dacron scrim; butt-jointed at the gore and cap lines; and laced at approximately 3.0 inch intervals with dacron cord which forms an integral external shroud for the complete lay-up.

To preserve the thermodynamic properties, the handling of superinsulation should be kept to a minimum. Touching the surface with bare hands, for example, can alter the surface characteristics.

Compared to a blanket lay-up approach, the single layer application requires more handling and therefore more chances of damage to the surfaces. The blanket application, however, provides more exposed open butt joints between layers which may prove to be a thermal disadvantage. Relative to venting problems, the blanket application appears to provide less resistance to flow than the single layer approach, since all edges are open at the butt joints and overlaps occur only between blanket layers rather than between plies.

UNCLASSIFIED

UNCLASSIFIED

a. Insulation Layer Buildup (Continued)

The advantages of single layer buildup and blanket buildup can be summarized as follows:

(1) Encapsulation with individual layer buildup

Advantages: (a) Thermally excellent

Disadvantages: (a) Extreme installation and handling difficulty

(b) Possible venting problems

(c) Repairs very difficult

(2) Encapsulation with blankets

Advantages: (a) Ease of installation

(b) Edges provide venting area

(c) Repairable

Disadvantages: (a) Not as efficient thermally

A third system may be considered, which is the tape wound insulation (Good-year System). The major advantage of this system is the machine installation procedure; however, the disadvantages are:

(1) Repairs very difficult

(2) Possible venting problems.

It does not appear that this system offers significant advantage to warrant further consideration.

Based on the known advantages and disadvantages, it appears that the blanket configuration offers the best solution for insulating a tank. The thermal inefficiency may possibly become negligible by use of proper blanket edge and joint design.

- b. Blanket Design. Once it is established that the insulation will be installed in blanket sections, the methods of blanket assembly must be considered. The ellipsoidal tank shape imposes compound curvature requirements on the blanket assemblies. These can be satisfied by either forming the blankets in the shape of the bulkheads or making cap and gore sections. The formed shapes eliminate joints and have obvious installation advantages; however, the state of the art in mylar forming is presently not developed to the desired extent. Stretch forming and vacuum forming are insufficient since mylar's "memory" will eventually return it to a flat sheet. It is possible to stretch form or vacuum form in an oven such that a permanent set takes place;

UNCLASSIFIED

UNCLASSIFIED

b. Blanket Design (Continued)

however, even under these conditions the optical properties of the aluminized sheet may be altered considerably.

The built up shapes using cap and gore sections are easily manufactured, although perhaps not as easily installed; however, they appear to offer a reasonable solution to the installation problems.

Figure 2-11, A, shows an alternate blanket construction which employs interlayer spot bonds for preventing shifting between plys. These local areas also provide high strength attachment points since all layers (including the face sheets) are integrally bonded. To facilitate venting, the blanket edges between spots are open. Attachments at the blanket butt joints (See Figure 2-11, B.) are made by looping a cord section through the holes in the spot bonds. Compared to the plain hole construction, spot bonds offer convenient

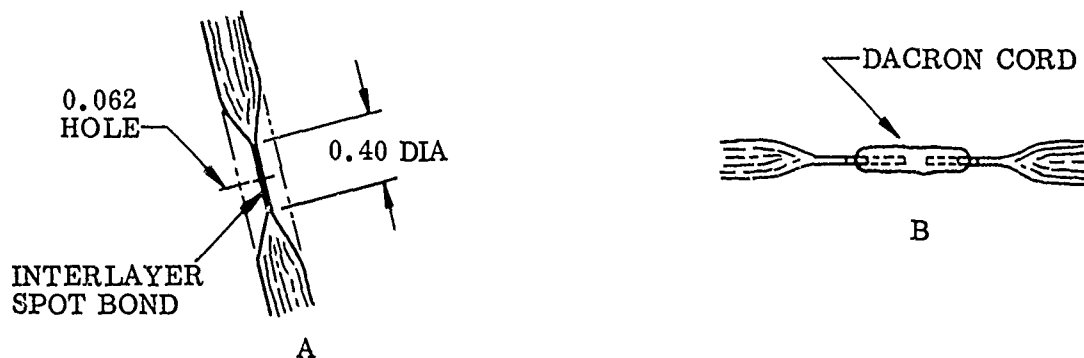


Figure 2-11. Blanket Attachment Bonds

blanket handling during installation since pins and temporary retaining devices are not required. There are, however, some thermal disadvantages. In addition to locally short circuiting the blanket layers, these spot bonds cause blanket compression in a varying degree at a circular zone surrounding the bond. The magnitude of this zone (from no blanket compression at the outer perimeter to the bond) may approach 10 times the basic spot bond diameter depending upon the number of blanket layers and bond diameter.

- c. Blanket Reinforcement and Retention. The insulation must be so designed that venting and flight loads do not permanently deform nor degrade the insulation. To accomplish this, extra structural membranes and blanket retention devices may be required.

UNCLASSIFIED

UNCLASSIFIED

c. Blanket Reinforcement and Retention (Continued)

Following is a list and brief discussion of different concepts considered.

(1) Aluminized One Mil Mylar Face Sheets (Figure 2-12).

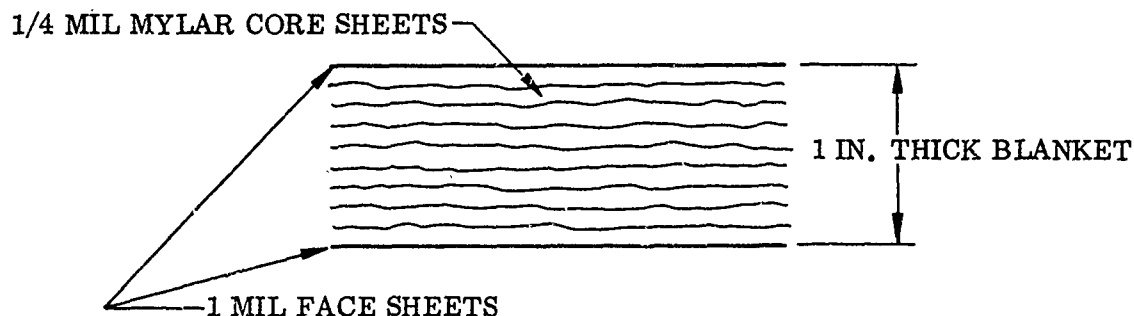


Figure 2-12. Aluminized One Mil Mylar Face Sheets

A one mil face sheet will carry considerable load but is very tear sensitive, particularly if pin type connections, with holes through the blanket, are used. Blankets should be considerably easier to handle with the one mil face sheets, compared with the 1/4 mil mylar layers.

(2) Tape Reinforced One Mil Mylar Face Sheets (Figure 2-13).

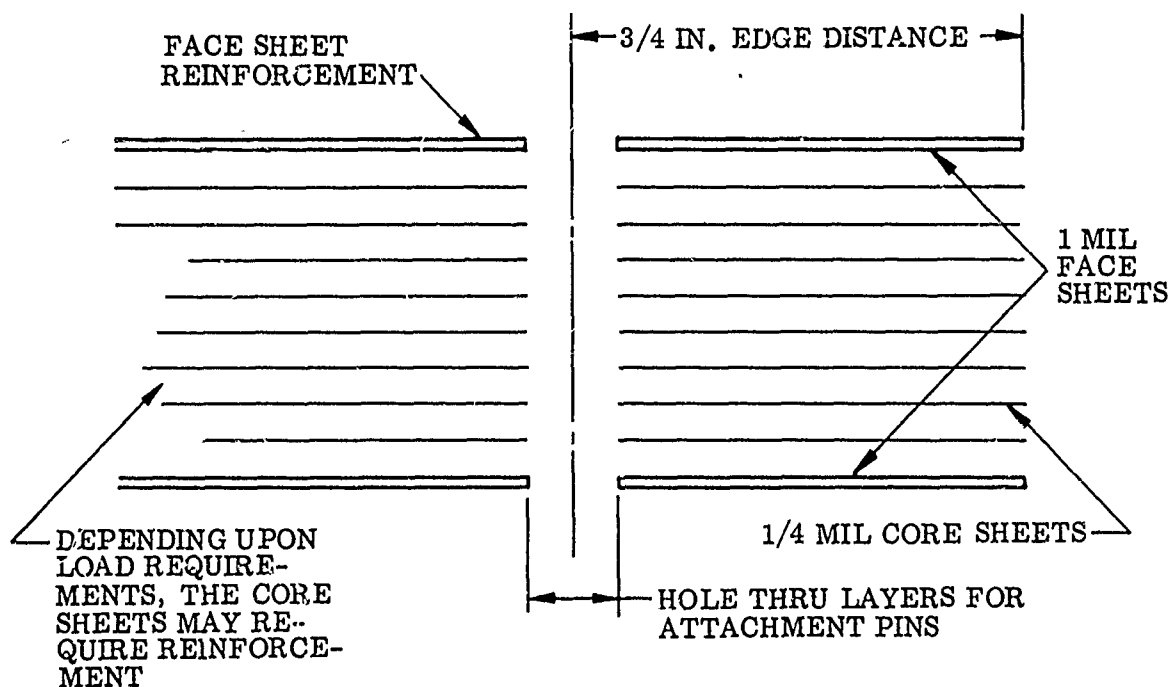


Figure 2-13. Tape-reinforced One Mil Mylar Face Sheets

UNCLASSIFIED

UNCLASSIFIED

c. Blanket Reinforcement and Retention (Continued)

Addition of the tape reinforcement will increase the face sheet tear resistance considerably. The tape addition will increase blanket manufacturing cost, and if pressure sensitive tape is used it will increase the outgassing.

- (3) **Scrim Reinforced Mylar Face Sheets.** The scrim reinforced face sheets consist of 1/4 or 1/2 mil, double aluminized mylar with dacron scrim bonded to it, instead of a thicker mylar face sheet.

Advantages: (a) Light weight
(b) Excellent tear resistance

Disadvantages: (a) Scrim degrades cap sheet emittance
(b) Thin face sheeted blankets will not handle as well as blankets with thick facings
(c) Bonding adhesive could outgas.

- (4) **Kapton One Mil Face Sheets.** Kapton is stronger than mylar but is considerably more expensive and difficult to metalize. Its use would probably eliminate any need to add tape reinforcement.

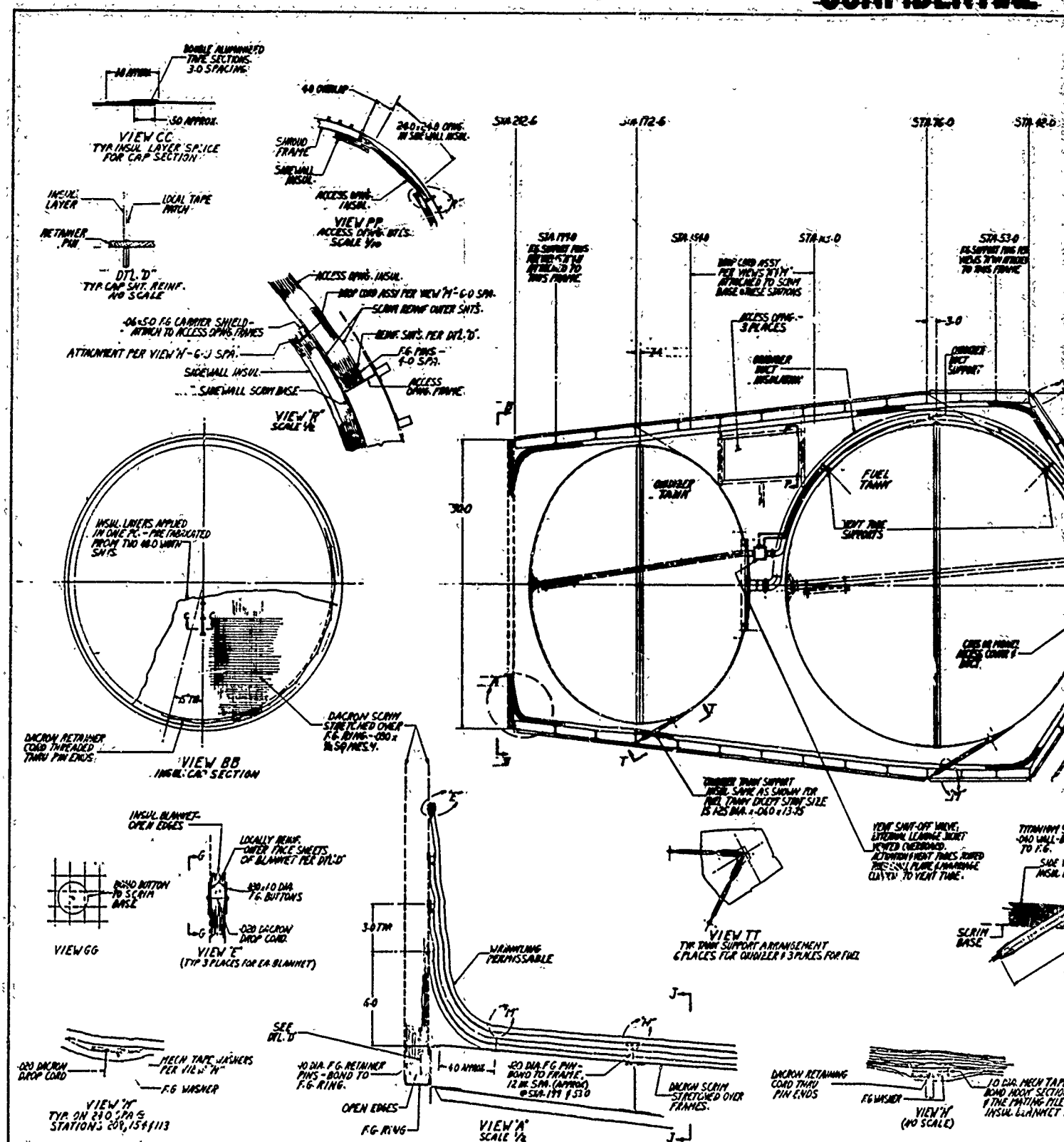
- (5) **Insulation Encapsulation Net.** The net completely surrounds and retains the entire insulation buildup. During boost the insulation on the front of the forward tank will be compressed and the aft insulation will part from the tank slightly. After orbital insertion the insulation will recover to its original thickness. The main function of the net is to distribute venting forces and prevent local failure of the insulation. Properly designed face sheets and blanket joints should provide the same function.

The selected version as stated earlier, was (2), the tape reinforced, one mil mylar face sheets.

2.2.1.3 Shroud Mounted Insulation System (Reference: Figure 2-14). The preferred shroud mounted insulation arrangement consists of a forward lay-up or "cap section", a shroud lay-up or "side wall", a thrust structure lay-up or "aft wall", and a chill plate assembly. The oxidizer and fuel tanks are installed (using low conductive struts) after the cap and side walls are completed. Ducts, tubes, and wiring are attached to the fuel tank prior to the installation. The aft wall and chill plate are assembled before installing the engine thrust structure. Access openings for connection and checkout of plumbing and wiring are provided through the shroud and the side wall insulation. These openings incorporate features for closing the insulation system before installing the external shroud access door. The cap, side wall, and aft wall sections are equipped with a dacron scrim base which is part of the insulation support arrangement. The complete system is a continuous insulation envelope surrounding both tanks and terminating at the chill plate. All plumbing and wiring is routed through the chill plate. The tank supports and the access openings are the only penetrations through this envelope.

UNCLASSIFIED

CONFIDENTIAL



UNCLASSIFIED

- a. Forward Cap Section Lay-up. The forward cap section consists of a low conductive ring with scrim stretched over the forward and aft faces forming a tennis racket type support. The insulation layers are sandwiched between the two scrim layers. (See Views A and BB of Figure 2-14.) The ring has a channel shaped cross section and contains retainer pins bonded to one leg. The scrim is attached to both legs of the channel by bonding or riveting. Either attachment method requires a hem type reinforcement at the edges.

The completed buildup is a flat circular sandwich with two scrim faces and a superinsulation core. All insulation layers are flocked with the edges at the periphery left open for venting. Before installing the insulation sheets, the ends of the side wall lay-up are attached to the scrim base. (See Views A, E, and GG of Figure 2-14.)

A typical insulation layer may be a single circular piece or it may be made from two or more flocked mylar strips overlapped and taped together at intervals (See Views BB and CC of Figure 2-14.) A one or multiple piece construction depends upon available material widths. Venting advantages may be offered in a multiple piece construction; however, the seams between layers should be staggered. The edges of each sheet may be strengthened at the holes with mylar spot patches or a continuous hem type reinforcement for resisting tear-out (See Detail D of Figure 2-14.) For large pin spacings, the mylar spot patches may prove more effective.

- b. Side Wall Insulation Lay-up. The outer shroud is a skin stringer frame type structure with the frames protruding at the inboard side. The superinsulation lay-up must cover these frames and incorporate supports to resist loads due to acceleration, venting, and acoustics. To assist in these supports, a high strength scrim is stretched from the forward to the aft end and attached by bonding or riveting (See View A of Figure 2-14.) to the frames. The scrim is hemmed and reinforced at the attachments to prevent tear-out. This approach provides a support base for the insulation buildup and retains the blanket positions during venting. Also, intermittent secondary supports can be applied without direct attachments to the frames.

The insulation is applied in blanket sections running continuously from the forward cap section to the aft chill plate. This simplifies installation, promotes venting between the blanket layers, and provides a uniform load distribution to the primary support pins. A typical blanket assembly is shown in Detail K of Figure 2-14. This assembly consists of two, one mil mylar face sheets sandwiched with eight 1/4 mil core sheets. All layers are flocked. Holes are punched (through all layers) at the edges of the assembly for receiving support pins and fasteners. To prevent interlayer shifting during assembly, temporary pins are inserted through the holes and retained with plastic or rubber grommets inserted over the pin ends. A second arrangement may be employed by installing one end of the gore line twin pin fastener into alternate holes of the blankets (See Figure 2-15) and retain

UNCLASSIFIED

CONFIDENTIAL

(U) b. Side Wall Insulation Lay-up (Continued)

temporarily with a dacron cord or a grommet. At assembly, the temporary retainers are removed, the pins engaged one at a time, and permanently retained. The spacing between fasteners provides sufficient clearances for this operation. Temporary clothes pin type clamps suggest a third method of holding the layers together during assembly; however, the clamping force necessary to assure no interlayer shift may cause permanent compression in local areas with possible thermal degradation. The arrangement shown in Figure 2-15 is recommended

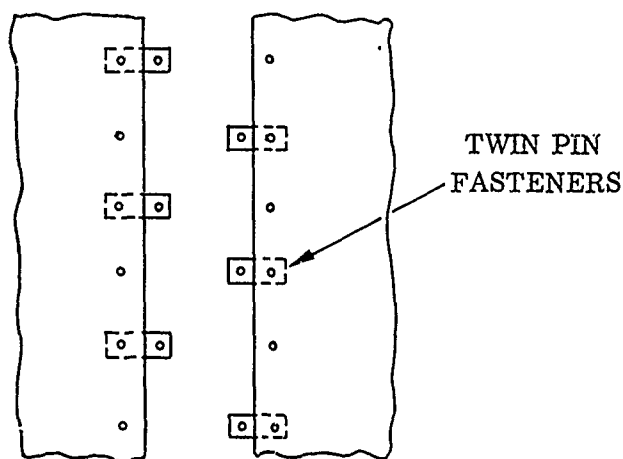


Figure 2-15. Twin Pin Fastener Assembly

- (C) The total weight of the side wall blankets is approximately 63.0 pounds. Assuming an acceleration of 7 g's, a pound load of 441 acting aft must be supported. This is accomplished by using low conductive pins bonded or riveted to the forward frame of the shroud. (See Figure 2-16.)

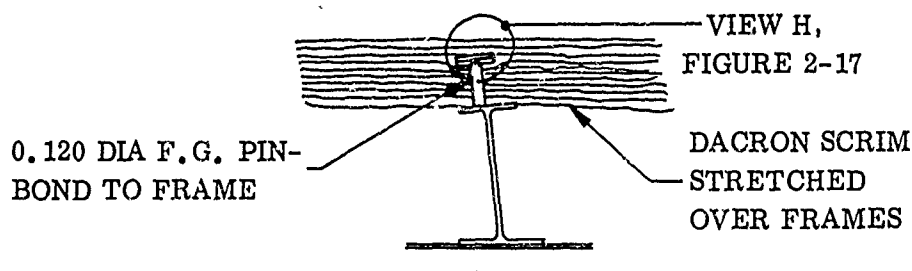


Figure 2-16. Blanket Support Pins

The ends of these pins are equipped with a washer containing a mechanical tape hook or pile section. (See Figure 2-17, View H.) The washer is retained by inserting a cord section through a hole provided in the pin. This mechanical tape section provides support for the last inboard blanket layer

CONFIDENTIAL

CONFIDENTIAL

(U) b. Side Wall Insulation Lay-up (Continued)

- (C) which covers the pin ends. To accommodate loads acting forward and inboard, a second row of support pins is installed at the aft frame (Station 53.0), Reference drawing. The blankets are therefore supported at the forward and aft regions by supports attached directly to the shroud structure.

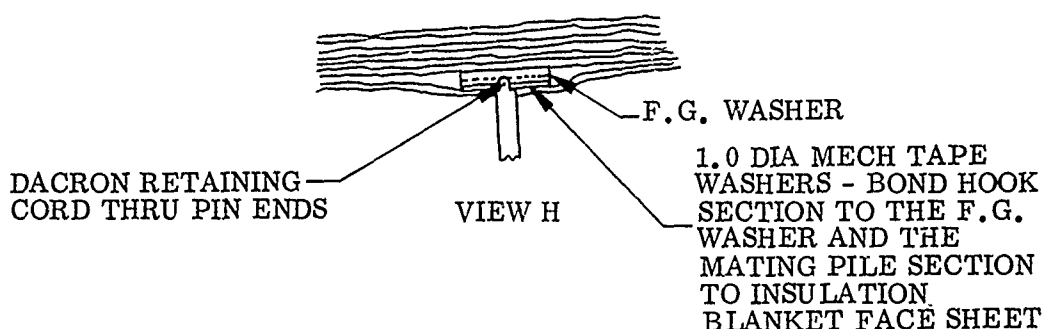


Figure 2-17. Blanket Support Pin Detail

- (U) The tapered configuration of the shroud, loads acting inboard and outboard, and possible horizontal positioning of the shroud during assembly require secondary blanket supports. The purpose of these supports is to hold the blanket assemblies against the dacron scrim base with minimum influence to primary load distributions. They are not intended to react forward and aft loads. A typical secondary attachment is shown in Views A and M of Figure 2-14, and in Figure 2-18. The drop cord fastener consists of two fiberglass washers interconnected with a dacron cord section. One washer (with the cord attached) is bonded to the dacron scrim based. The opposite washer is attached after the cord is engaged with the reinforced holes in the blanket layers. A tool is required to install these drop cords since access is from the inboard side only. The tool is a simple small plastic tube. After the washer is bonded to the scrim base, the drop cord is threaded through the tube and knotted for retainment. After the blankets are engaged, the tube and cord are pinched locally while the knotted end is cut off. The tube is then withdrawn, the inboard washer installed, and the end knotted to retain the washer. (See Figure 2-18.)

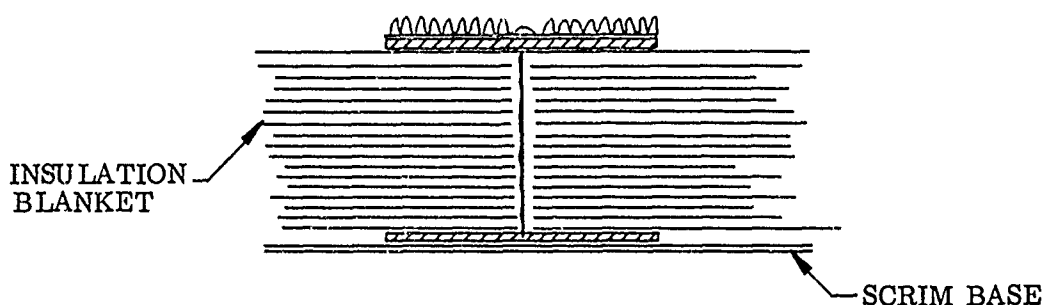


Figure 2-18. Completed Drop Cord Installation

CONFIDENTIAL

UNCLASSIFIED

b. Side Wall Insulation Lay-up (Continued)

The side wall blankets overlap the forward section as shown in Figure 2-19.

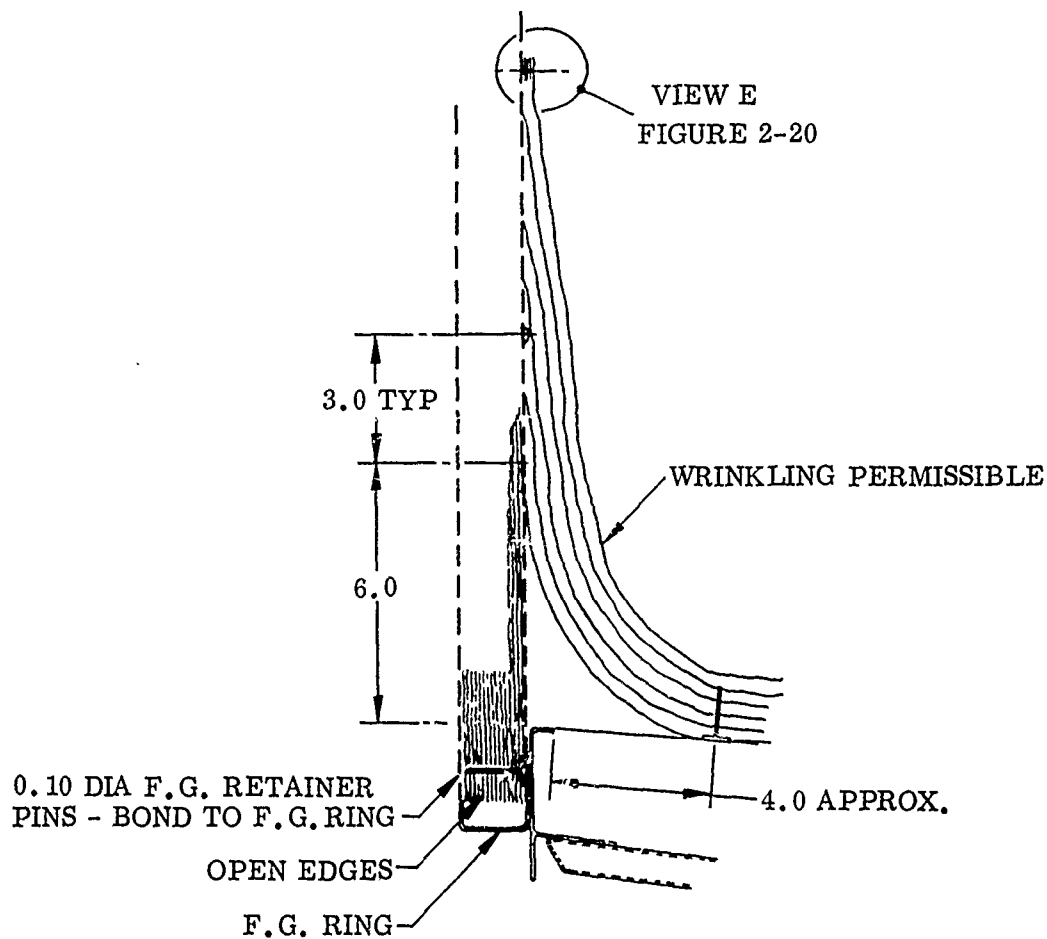


Figure 2-19. Side Wall Blanket Overlap

This overlap is accomplished by attaching the blanket ends to the cap section scrim base using drop cord assemblies as shown in Figure 2-20.

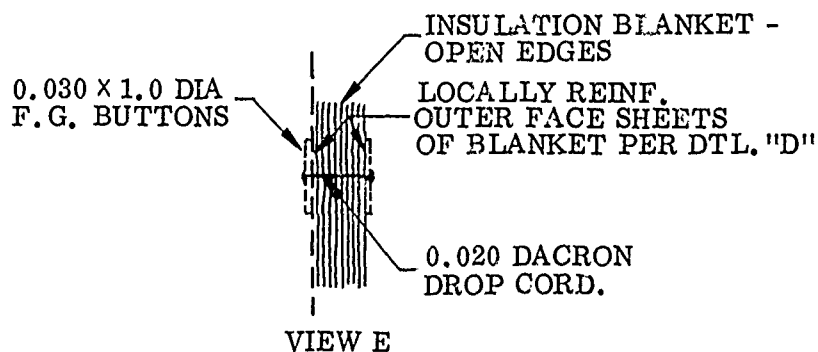


Figure 2-20. Drop Cord Attachment Assembly

UNCLASSIFIED

UNCLASSIFIED

b. Side Wall Insulation Lay-up (Continued)

Compared to the side wall area, the drop cords in this region are simpler to install due to greater accessibility. Each blanket layer overlaps the preceding drop cord installation by approximately 3.0 inches. Since the blankets are not preformed, wrinkling will occur in the corner area. During acceleration, some sagging of the blankets will occur between the drop cords positioned in the cap section and the drop cords located 4.0 inches aft of the forward frame. This is permissible since the blankets are interfastened at the butt joints which prevents development of large openings.

The side wall lay-up is accomplished before installing the propellant tanks. A vertical position for the shroud is suggested for this installation.

- c. Aft Wall Insulation Lay-up. The aft wall lay-up consists of engaging the free hanging ends of the side wall blankets with the chill plate collar pins and interconnecting the blankets at the butt joints. A scrim base similar to that used on the side wall is also provided. Since the chill plate collar pins are oriented inboard, an assembly fixture similar to that described for the tank mounted system is recommended. Starting with the side wall inboard layer, the blankets are positioned (one at a time) to engage with the fixture pins, and are temporarily retained. (See Figure 2-21A.) The blankets are interconnected at the gore line butt joints using the twin pin fasteners as shown in Figure 2-21B.

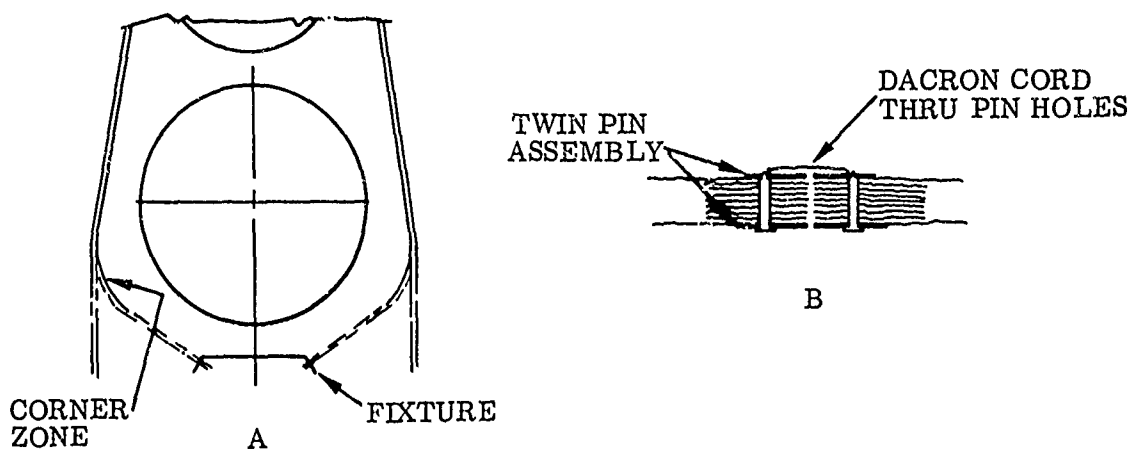


Figure 2-21. Blanket Position and Interconnection

The above procedures are repeated for the remaining layers. A properly installed blanket should span loosely from the shroud frame to the fixture. A blanket under tension will cause severe distortion and local compression of the layers at the corner zone shown in Figure 2-21A. The chill plate collar is installed next, and the fixture is removed per the procedures earlier outlined for the tank mounted system.

UNCLASSIFIED

UNCLASSIFIED

c. Aft Wall Insulation Lay-up (Continued)

A second method is available which requires no pin fixture. All holes in the aft ends of the blanket are equipped with temporary plastic pins. Starting with the first inboard layer, three gore line fasteners are installed at one butt joint. This three-fastener installation is repeated for the remaining seven butt joints. The inboard blanket layer is then in the position described in Figure 2-22A. The three-fastener assembly is next repeated until all butt joints are completed and the blankets assume the position shown in Figure 2-22B.

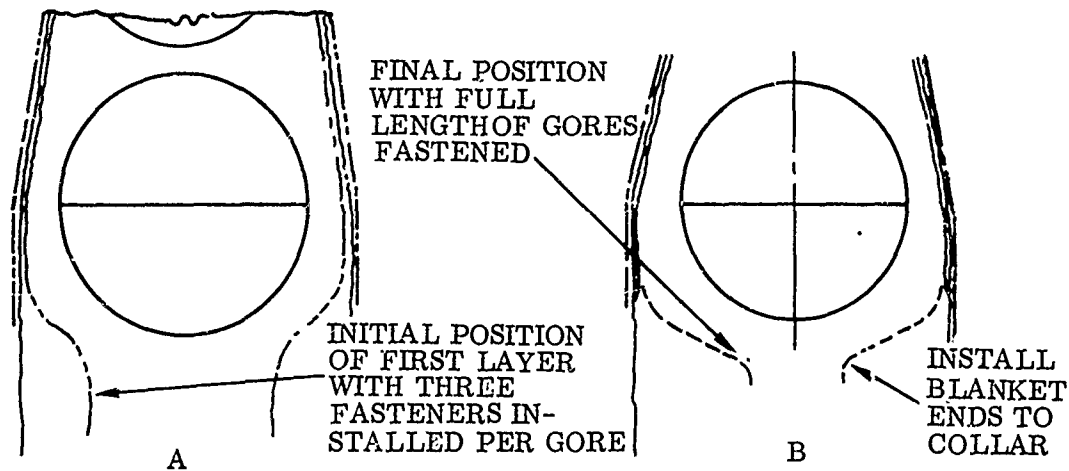


Figure 2-22. Inboard Blanket Layer

This procedure is used for all remaining blanket layers. The chill plate collar is next positioned and held by an assembly fixture. The plastic pins in the blanket ends are carefully removed (one at a time) and the layers engaged and retained with the chill plate collar. This second method requires more skill compared to the first approach.

The aft wall requires a scrim base to support the insulation over the thrust structure frames and for retainment during acceleration loads and venting. This is provided by riveting an adapter ring to the shroud frame. (See Figure 2-23.) Scrim is then stretched from this ring to the chill plate collar and

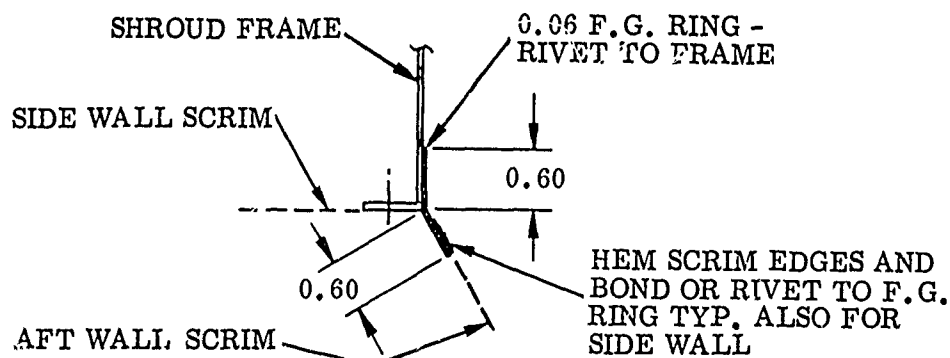


Figure 2-23. Adapter Ring Attachment

UNCLASSIFIED

UNCLASSIFIED

c. Aft Wall Insulation Lay-up (Continued)

attached by riveting or bonding. The edges are hem reinforced to prevent tear-out. The scrim base is therefore positioned such that the thrust structure frames will be near or in contact with the scrim surface. Under load, the blanket layers bear against the scrim base which in turn contacts the structural frames.

d. Access Through Side Wall Insulation. Access through the side wall insulation is accomplished by riveting or bonding a low conductive insulation carrier shield to the periphery of the opening (See Figure 2-24.), permitting an overlap between the side wall lay-up and the access opening insulation.

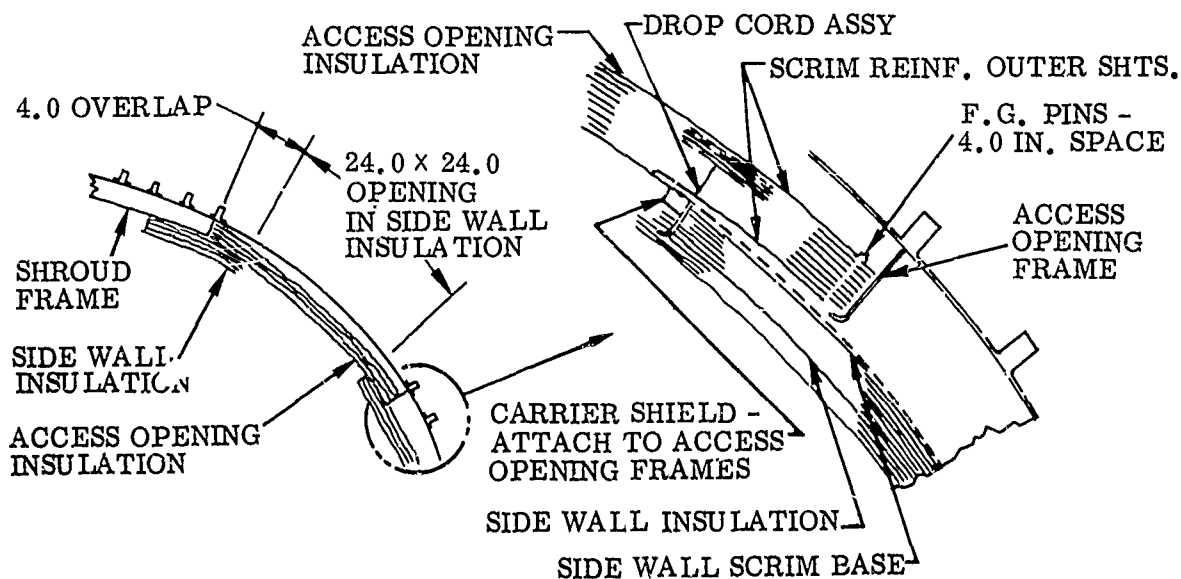


Figure 2-24. Side Wall Insulation Access Opening

The inboard perimeter of this shield is equipped with support pins similar to those used for the side wall. The ends of the pins are covered with the last inboard blanket layer by engaging the mechanical tape patches.

Support pins are bonded or riveted to the primary frame of the access opening at the outboard side. These pins support the insulator layers which close the access opening. Drop cords are used at the inner perimeter of the opening to keep the closing insulation layers against the carrier shield, as shown in Figure 2-24. The closure insulation lay-up may be applied as blanket or individual layers. All support pin holes are reinforced. Installation simply consists of engaging 30 layers with the support pins and drop cords. These layers are retained temporarily at the support pins while the drop cord installations are completed. The last 10 layers are then engaged with the pins and permanently retained by installing dacron cord through the pin ends. The access cover door is installed after completion of the insulation.

UNCLASSIFIED

CONFIDENTIAL

- (U) e. Assembly Procedure. The assembly procedure for installing the tanks into the shroud is similar to that described for the tank mounted insulation system except the struts are disconnected from the fixture and tank (one at a time); inserted through the opening in the side wall insulation; and reconnected to the shroud frame and tank.
- (C) f. Insulation Structural Estimate (Forward Primary Support Pins). The total side wall blanket weight = 63.2 pounds. A portion of this weight is reacted by the aft wall supports. For this analysis, the 63.2 pounds will be considered acting upon the forward support pins and the side wall slope will be neglected.

Assuming 7 g's acceleration, four support pins per blanket, and eight blankets,

$$F = \frac{63.2 \times 7}{4 \times 8} = 13.8 \text{ lb per pin (See Figure 2-25A)}$$

"F" is conservatively assumed as a concentrated load at the pin end (See Figure 2-25B.) Using a minimum pin diameter = 0.180,

$$I_{\text{pin}} = \frac{\pi (0.09)^4}{4} = 0.0000515 \text{ in.}^4$$

$$\text{The bending moment } M = 13.8 \times 1.6 = 22.1 \text{ in.-lb}$$

$$\text{Therefore the bending stress } S_b = \frac{22.1 \times 0.09}{0.0000515} = 38,700 \text{ psi.}$$

$F_{tu} = 100,000$ psi for fiberglass is obtainable.

$$\text{The shear stress } S_s = \frac{13.8}{0.785 (0.18)^2} = 543.0 \text{ psi}$$

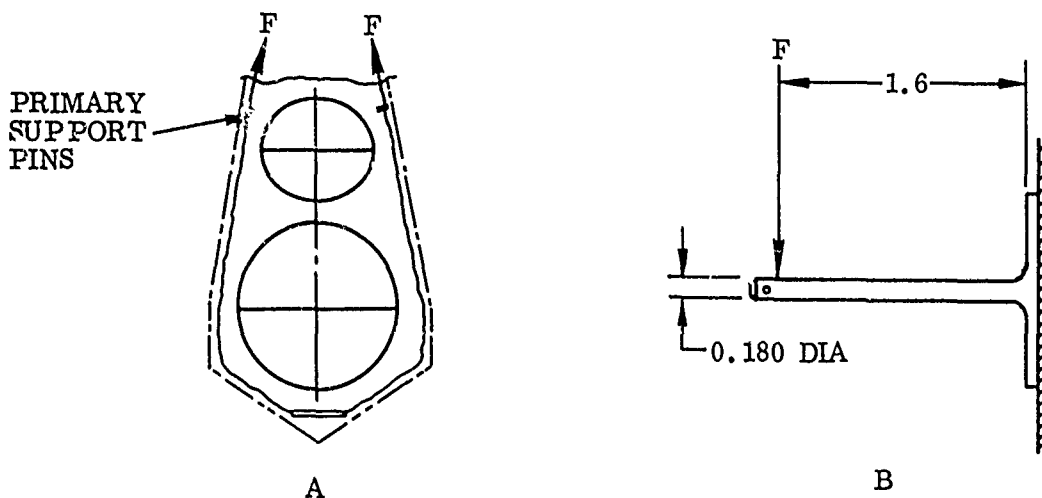


Figure 2-25. Blanket Support Pin Load

CONFIDENTIAL

CONFIDENTIAL

(C) f. Insulation Structural Estimate (Forward Primary Support Pins) (Continued)

Assuming that the blanket face sheets deliver the load "F"; the load per face sheet per pin

$$f_f = \frac{F}{n}$$

Where n = number of face sheets.

Using two face sheets per blanket and 4 blanket layers,

$$n = 2 \times 4 = 8$$

Therefore $f_f = \frac{13.8}{8} = 1.720$ lb (See Figure 2-26.)

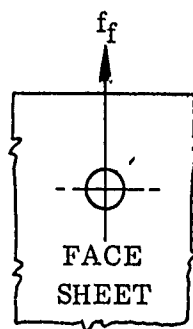


Figure 2-26. Blanket Face Sheet Load

(U) From GDC tests, the minimum tear-out load for a 1/4 mil sheet reinforced on one side is 2.5 pounds. For reinforcements on two sides the minimum load recorded was 7.75 pounds.

(U) The 1/4 mil core sheets must resist inertia loads at the pins to prevent interlayer shifting. The weight of 32 core sheets is 34.2 pounds; therefore, the load per core sheet per support pin

$$f = \frac{34.2 \times 7}{4 \times 8 \times 32} = 0.234 \text{ lb}$$

(U) From CDC tests, the minimum tear-out load for a 1/4 mil sheet with no reinforcement was recorded at 0.562 pound. Perfect support holes with no edge disturbances for all layers cannot be feasibly achieved. Also the test data and detail knowledge of loads due to vibration, acoustics, distribution, and etc. is limited; therefore, it is recommended that the core sheets be reinforced on one side giving an approximate tear-out strength of 2.5 pounds. Also, a dual reinforcement should be applied to the face sheets which would yield a 7.75 pound tear-out strength.

CONFIDENTIAL

CONFIDENTIAL

(C) f. Insulation Structural Estimate (Forward Primary Support Pins) (Continued)

- (U) Blanket lengths and attachment locations are controlled such that all blanket assemblies will be in a slack or loose condition between the primary support pins. This allows the blanket lay-up to compress freely (when exposed to a pressure differential) and bear upon the scrim base without additional reactions at the end support pins; therefore, the scrim base must be capable of the load conditions shown in Figure 2-27. For estimating, a 13.0 inch diameter diaphragm without flexure stiffness is assumed between frames. This diaphragm is uniformly loaded and the edges held.

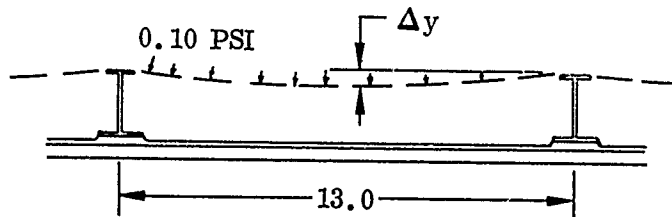


Figure 2-27. Scrim Base Load Conditions

- (U) From formulas by R.J. Roark (4th Edition, p 247) for stress and strain

$$\Delta y = 0.662 \quad a \left[\frac{w a}{E t} \right]^{1/3}$$

where Δy = maximum deflection at center of diaphragm (inches)

a = radius of diaphragm (inches)

w = unit applied load = 0.10 psi

E = modulus of elasticity = 550,000 for dacron

t = diaphragm thickness = 0.015 inch (effective)

This is conservative.

$$\text{Therefore } \Delta y = 0.662 (6.5) \left[\frac{(0.10)(6.5)}{(550,000)(0.015)} \right]^{1/3} = 0.1842 \text{ in.}$$

Using Δy , the radius of an equivalent cylinder is determined using the properties of a circle

$$r = \frac{C^2 + 4 h^2}{8 h}$$

- (U) where C = length of cord = 13.0 inches

$$h = \Delta y$$

r = radius of circle (inches)

CONFIDENTIAL

CONFIDENTIAL

(C) f. Insulation Structural Estimate (Forward Primary Support Pins) (Continued)

(U) Therefore $r = \frac{(13)^2 + 4(0.1842)^2}{8(0.1842)} = 115 \text{ inches (See Figure 2-28A)}$

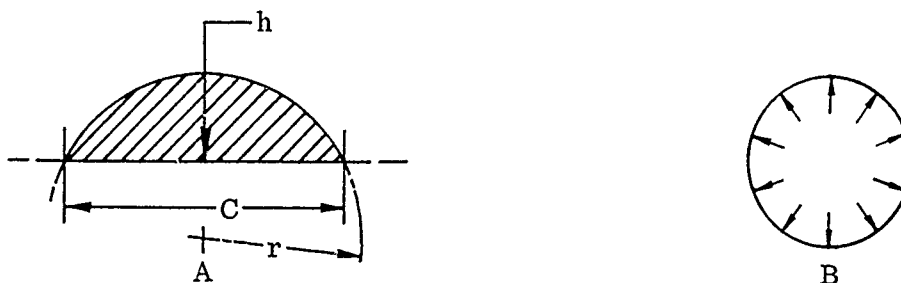


Figure 2-28. Cylinder Radius and Hoop Load

The hoop membrane stress for a cylinder $= \frac{wR}{t}$; therefore the membrane load $= (0.10)(115) = 11.5 \text{ lb/in.}$

The hoop load (in plane of frames) using the maximum shroud radius $= (0.10)(60) = 6.0 \text{ lb/in. (See Figure 2-28B.)}$

Approximate preload due to stretching scrim over frames $= 4.0 \text{ lb/in.}$

A scrim capable of 45 lb/in. was included in the weight analysis.

(U) 2.2.1.4 Alternate Considerations. The general comments regarding alternatives in terms of layer construction, etc., that were discussed in the tank mounted insulation system also pertain here; however, the one major area that differs is the side wall attachments. Two alternate concepts of side wall attachment are discussed below.

(U) The first alternate method uses fiberglass pins bonded at each frame. (See Figure 2-29A.) The pin cross section is less than the primary load pins since inboard-outboard loads are resisted only. The pin engages all blanket layers with a continuous retainer cord installed through the ends. The danger of local blanket compression is eliminated since retainment is controlled by the fixed distance between the cord and the pin base. This method, however, can present load distribution difficulties. It is intended to react the aft load at the forward row of primary support pins only; therefore the clearance between hole and pin must be sufficient to assure that no appreciable forward and aft loads are reacted. This clearance contributes to thermal degradation, and local insulation cover patches may be required. (See Figure 2-29B.)

(U) A second alternate suggests designing all pins for the prime forward and aft loads. Standard clearance between pins and holes would be used; therefore the load distribution would be affected by location and hole size tolerances. The pin diameters in this case would be larger than for the previous alternative. Due to the present thermal requirements, the use of drop cords is assumed.

CONFIDENTIAL

UNCLASSIFIED

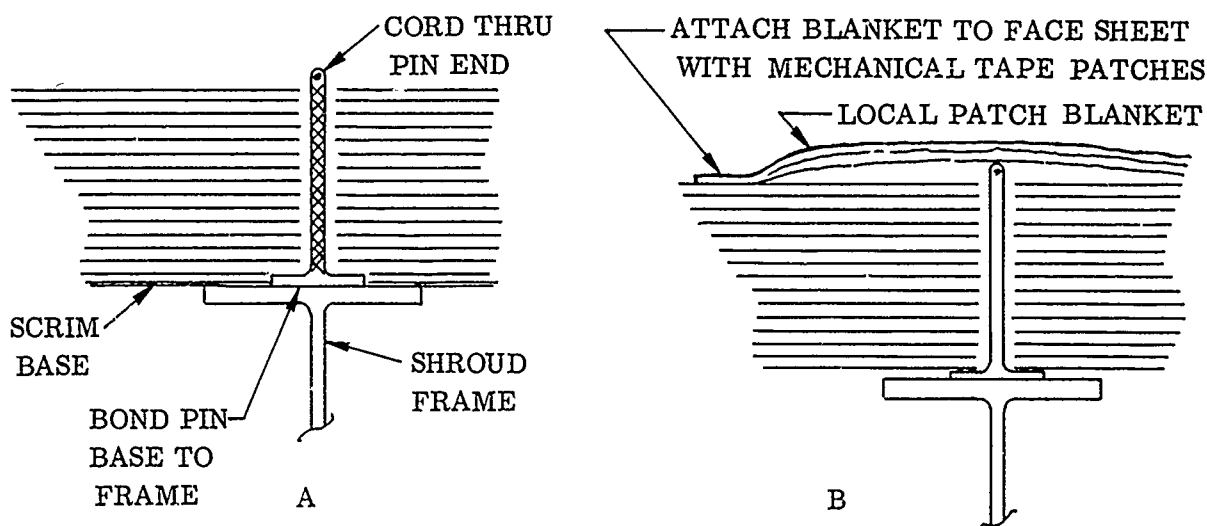


Figure 2-29. Side Wall Attachment with Fiberglass Pins

2.2.1.5 Blanket Joint Design. The individual blanket assemblies must be adequately connected to each other while providing proper flow area between blankets and at the gore lines to allow adequate venting and outgassing. Some of the other characteristics desirable of fasteners are as follows:

- (1) Ease of installation
- (2) Insensitive to mechanic dexterities
- (3) Use of non-outgassing materials
- (4) Minimum disturbance to blanket layers during installation
- (5) Capability of withstanding flight loads
- (6) Retaining devices positive and easy to inspect
- (7) Overall simplicity
- (8) Positive and accurate positioning of blanket edges.

The method finally selected for the gore line fastener is referred to as the "twin pin fastener". This consists of two fiberglass pins bonded to a fiberglass base strip. After the pins are engaged with the blanket a retainer strip is installed over the upper end of the pins, locking the pin ends into position. A dacron cord locks the strip to the pins. Blanket retainment is positive on both sides since the two strips act as washers overlapping the engagement holes. There are numerous other methods that can be employed as gore line fasteners, and the advantages and disadvantages of each are discussed below.

a. Spot Bonded Blankets Interconnected by Pressure Sensitive Tape. (See Figure 2-30.)

Each blanket is spot bonded around its periphery at equal spacings by the use of a thermoplastic tape, such as Schjeldahl GT 100 tape, between each layer

UNCLASSIFIED

UNCLASSIFIED

a. Spot Bonded Blankets Interconnected by Pressure Sensitive Tape (Continued)

of superfloc in the bond area. Each blanket is attached to the adjoining one with pressure sensitive tape.

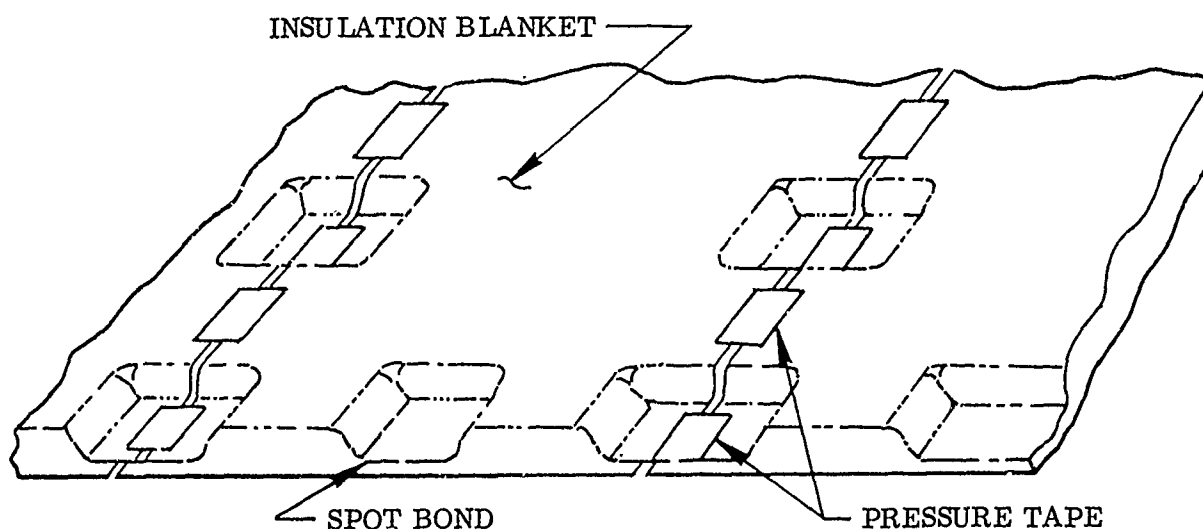


Figure 2-30. Spot Bonded Blankets with Pressure Sensitive Tape

- | | |
|----------------|---|
| Advantages: | (a) Spot bonding creates a stable blanket |
| | (b) Blankets are easily installed |
| Disadvantages: | (a) Spot bonds are thermal shorts |
| | (b) Labor per spot bond very high |
| | (c) Pressure sensitive tape may be structurally inadequate |
| | (d) Pressure sensitive tape adhesive outgasses considerably |
| | (e) Difficulty exists in applying enough pressure to tape over a thick insulation buildup |
| | (f) Blanket gap not fixed. |

b. Spot Bonded Blankets Interconnected by Thermoplastic Tape. Same method as in a., except thermoplastic tape is used instead of the pressure sensitive tape to interconnect the individual blankets. Comparing this to the pressure sensitive tape method:

UNCLASSIFIED

UNCLASSIFIED

b. Spot Bonded Blankets Interconnected by Thermoplastic Tape (Continued)

- (1) Blankets are more difficult to install
- (2) Same difficulty exists in applying pressure to the tape over a thick insulation buildup
- (3) Bond between tape and superfloc is seriously degraded by insulation wrinkling beneath the thermoplastic tape
- (4) Outgassing problem of pressure sensitive tape is eliminated.

c. Spot Bonded Blankets Interconnected by Velcro Tape. (See Figures 2-31 and 2-32.)

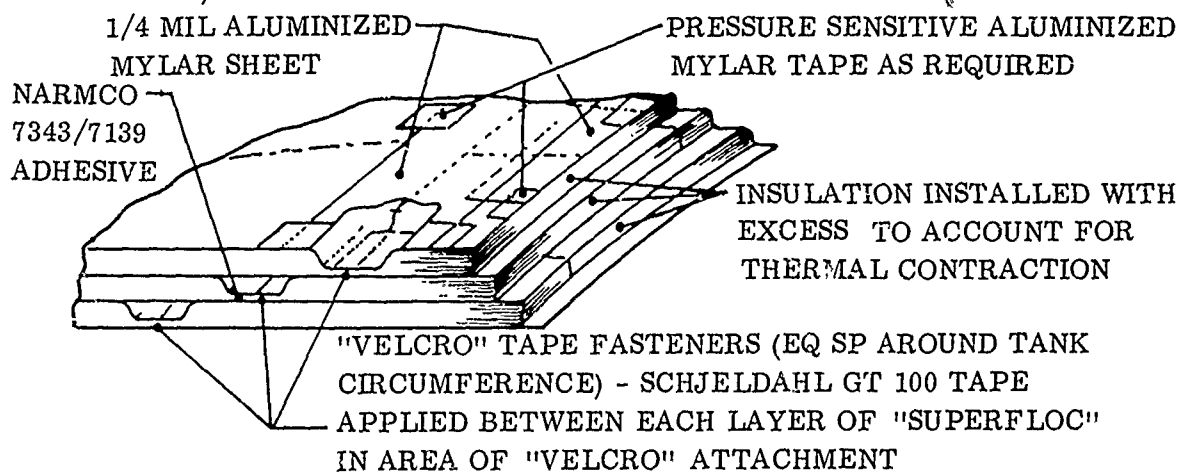


Figure 2-31. Spot Bonded Blankets with Velcro Tape

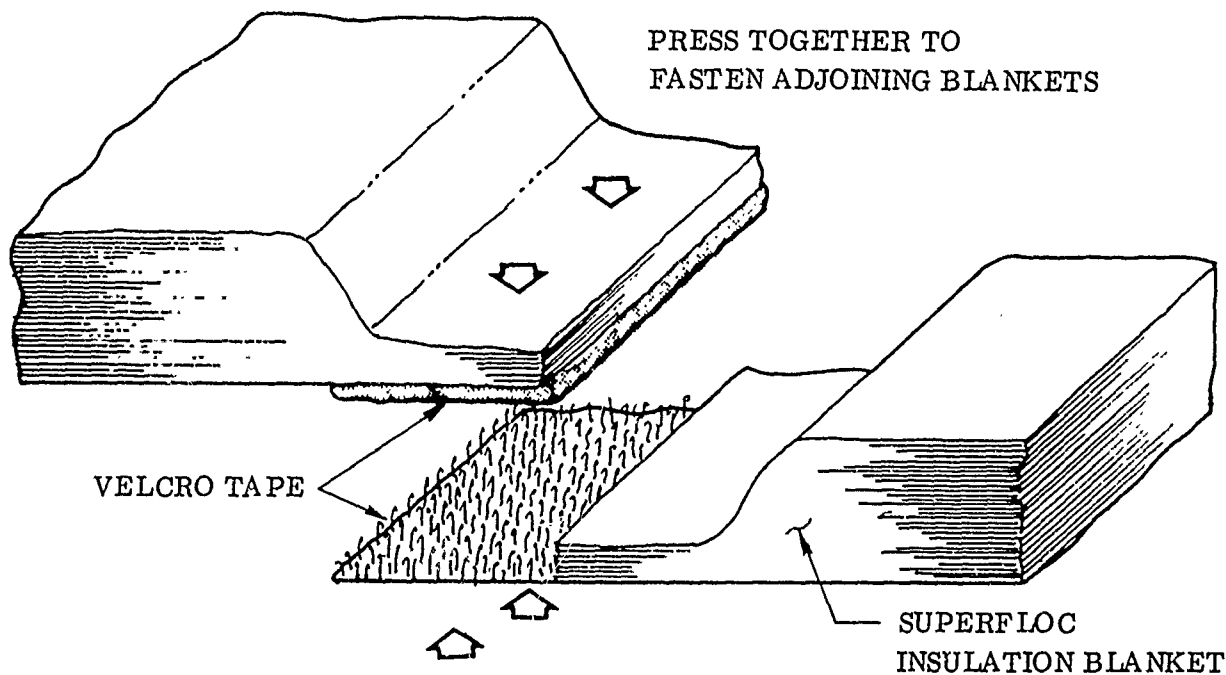


Figure 2-32. Velcro Tape Attachment

UNCLASSIFIED

UNCLASSIFIED

c. Spot Bonded Blankets Interconnected by Velcro Tape (Continued)

- Advantages:
- (a) Spot bonding creates a stable blanket
 - (b) Blankets extremely easy to install
 - (c) Very little pressure required for proper blanket interconnection

- Disadvantages:
- (a) Spot bonds are thermal shorts
 - (b) Labor per spot bond very high
 - (c) Some pressure sensitive tape may be required to retain blanket edges between spot bonds
 - (d) Blanket gap can vary,

d. Single Pin Blanket Attachment Interconnected by Velcro Tape. (See Figure 2-33.)

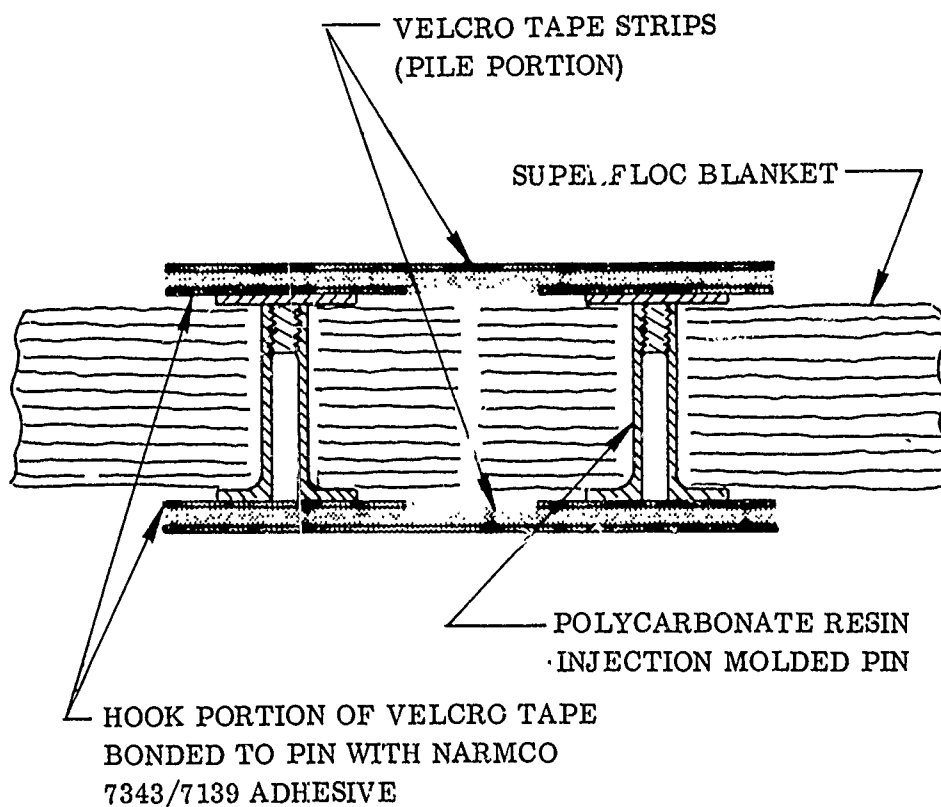


Figure 2-33. Single Pin Blanket Attachment with Velcro Tape

UNCLASSIFIED

UNCLASSIFIED

d. Single Pin Blanket Attachment with Velcro Tape (Continued)

- Advantages:
- (a) Low thermal degradation caused by pins
 - (b) No tolerance problem
 - (c) Individual blankets are stable and edges are positioned
 - (d) Blankets handle easily since the bonded velcro hook tape can be used for tool pickup
 - (e) Tank installation very simple.

- Disadvantages:
- (a) An excessive number of pins per blanket may be required for flight loading
 - (b) Blanket gap not fixed
 - (c) System is fairly heavy

e. Snap Pin Blanket Attachment Interconnected by Dacron Lacing. (See Figure 2-34.)

In comparison with the concept in d, above, this system has fewer components and is light; but it is more difficult and takes more time to install insulation blankets on a tank. Unequal lace tension could lead to an undesirable load distribution.

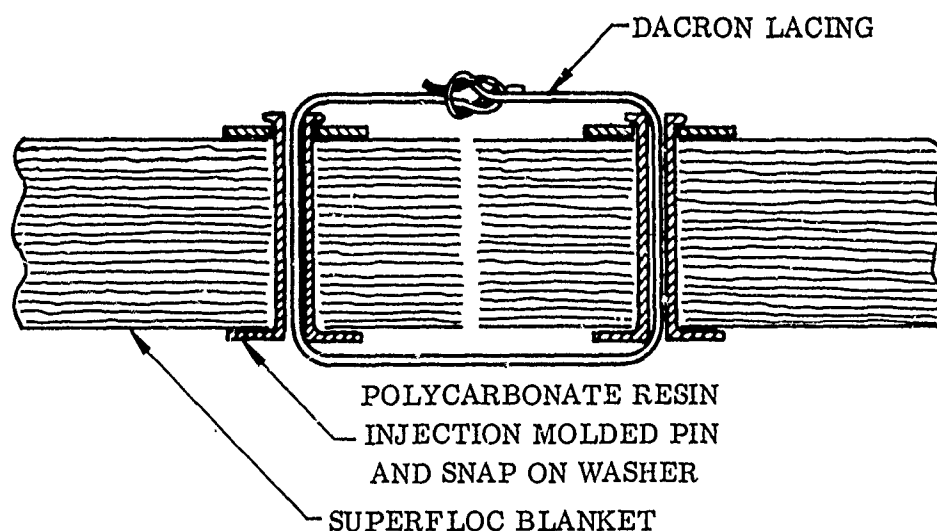


Figure 2-34. Snap Pin Blanket with Dacron Lacing

UNCLASSIFIED

UNCLASSIFIED

- f. Laced Blanket Attachment Interconnected by Velcro Tape. (See Figure 2-35.) All blanket joints in this concept could be taped 100 percent. Vent holes, as shown in Figure 2-35, could be included in the tape to permit utilization of the butt joint venting.

- Advantages:
- (a) Complete lacing of blanket edges will give large blanket load carrying capability
 - (b) 100 percent taped blanket joints are aesthetically pleasing
 - (c) No tolerance problem
 - (d) Blankets handle easily since the laced-on velcro tape can be used for tool pickup
 - (e) Tank installation very simple.
- Disadvantages:
- (a) Lacing blanket edges during manufacturing time consuming
 - (b) Lacing may tend to cut superfloc
 - (c) Large amount of velcro tape (made of nylon) causes outgassing.

This concept would be very attractive if the lacing could be installed by machine.

- g. Fiberglass Twin Pin Fastener. (See Figure 2-36.)

- Advantages:
- (a) Pins cause little blanket thermal degradation
 - (b) Low outgassing
 - (c) Handling of spot bond tape pieces eliminated
 - (d) Positive blanket gap.
- Disadvantages:
- (a) An excessive number of pins per blanket may be required for flight loading
 - (b) Considerable dexterity required to tie cord or install snap ring device.

As was discussed previously, the twin pin fastener was selected for this application; however, there are various methods of constructing these fasteners.

UNCLASSIFIED

UNCLASSIFIED

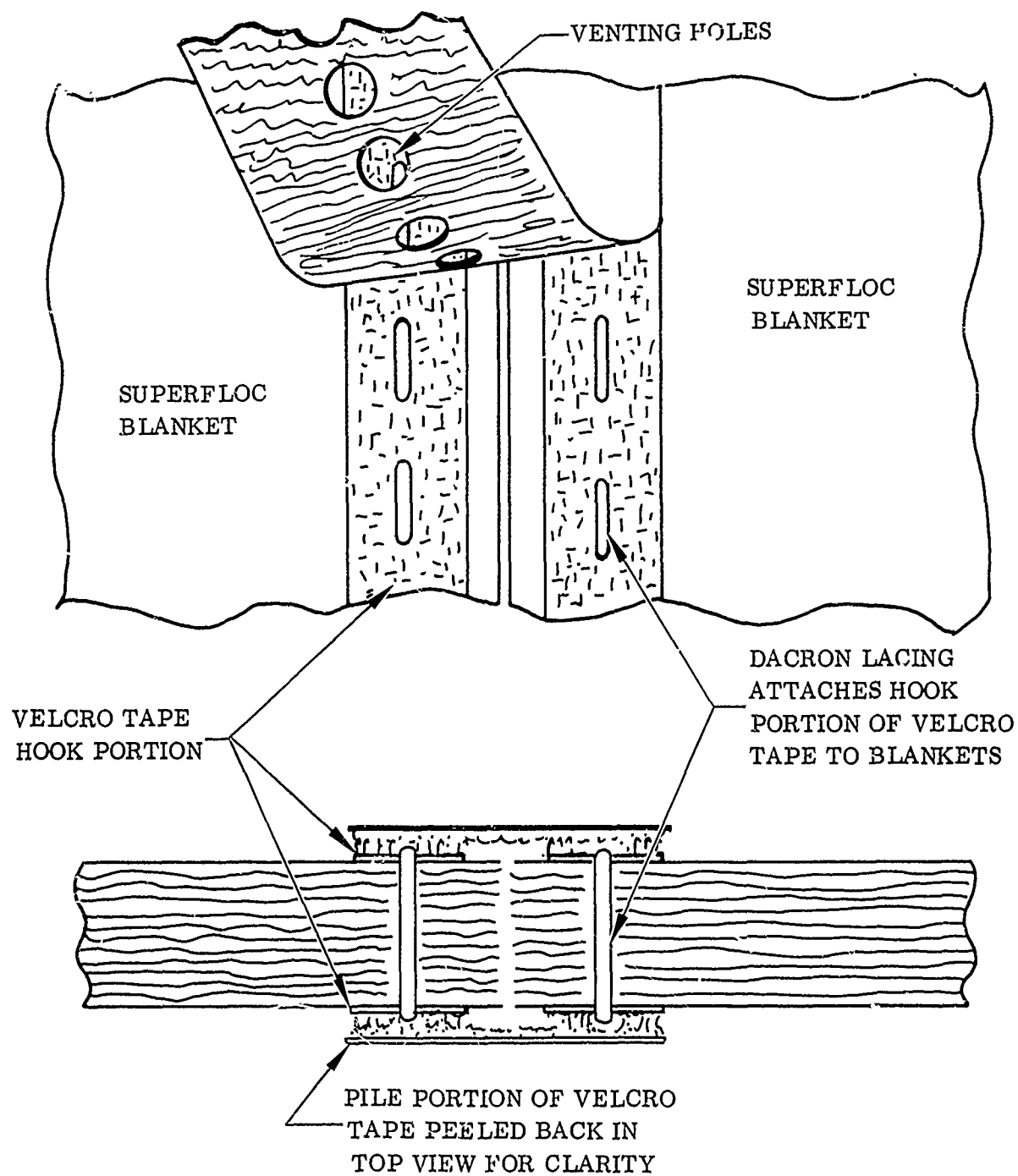


Figure 2-35. Laced Blanket with Velcro Tape

UNCLASSIFIED

UNCLASSIFIED

g. Fiberglass Twin Pin Fastener (Continued)

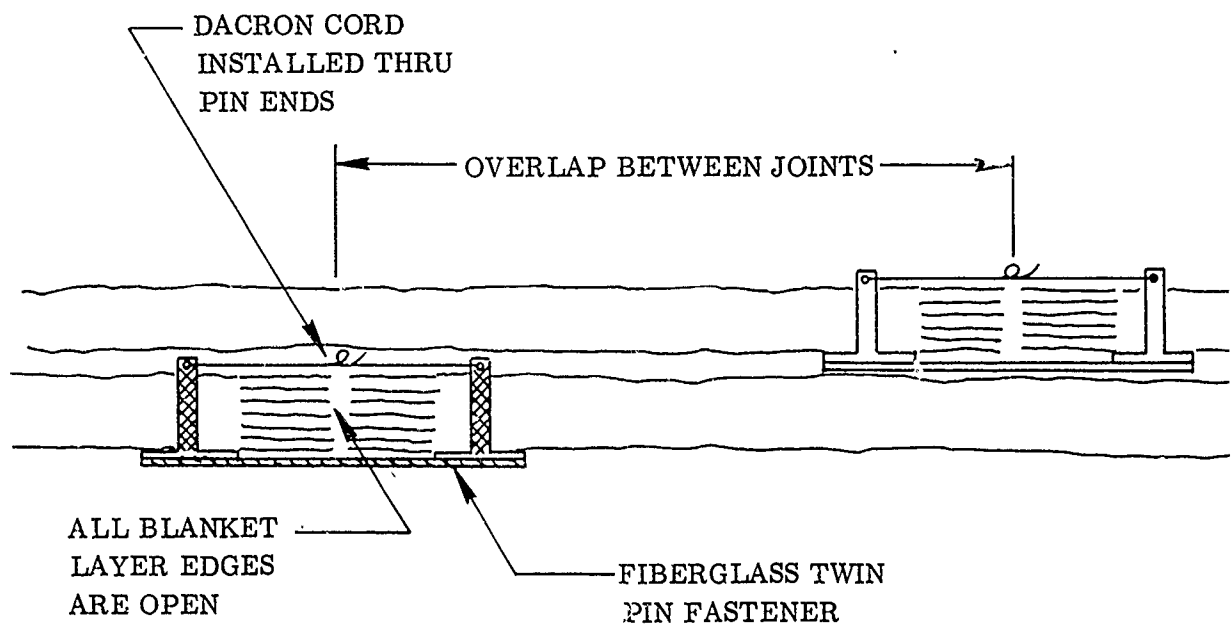


Figure 2-36. Fiberglass Twin Pin Fastener

Some twin pin types under consideration at GDC are shown in Figure 2-37. Case I in Figure 2-37 employs a fiberglass base strip with two holes equipped with pins. The fiberglass pins have circular bases which bond to the base strip. After the pins are engaged with the blanket, a dacron cord is looped through holes provided in the ends of the pins, and ties. This cord serves as the locking and retainment device. Case I meets the majority of the requirements. Exceptions are sensitivity to mechanic dexterity and inspection difficulties. The use of a cord is sensitive to mechanic dexterities. A loosely installed cord can place the pins and the base strip under unfavorable loading during flight; however, this could be overcome by adding weight.

A cord installed under tension may over-stress the pins. Inspection difficulties could develop in defining a loose or a tight cord. With an improperly installed cord, the capability of withstanding flight loads becomes questionable. Blanket retainment is positive on the base side since this strip acts as a washer overlapping the holes in the blanket. Retainment may be only partial on the cord side since the face sheet (and neighboring plys) could slip over the pin end and onto the cord under cycling loads. The cord would still retain the layers but the small diameter may cut through or start a tear in the face sheet reinforcement.

UNCLASSIFIED

UNCLASSIFIED

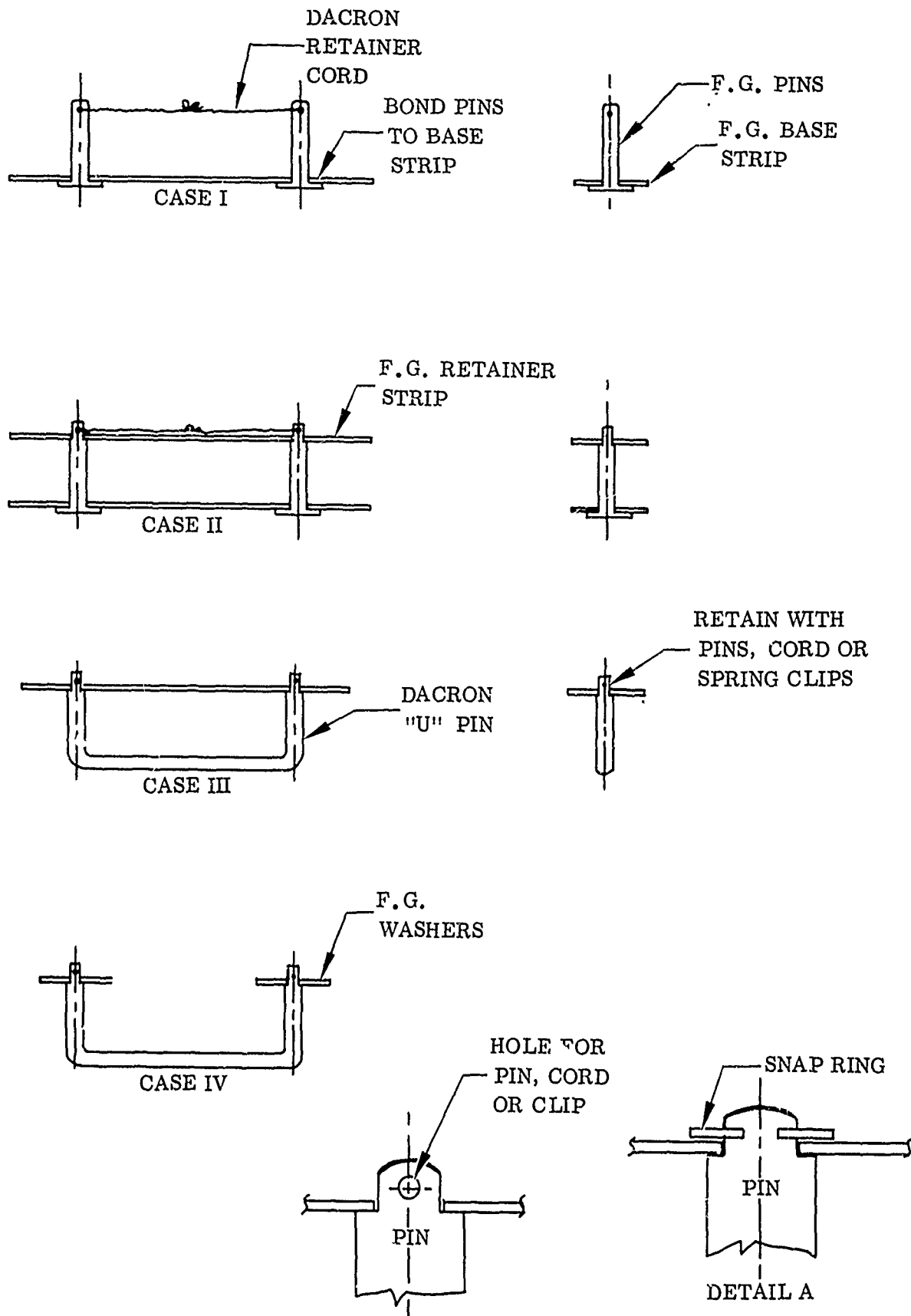


Figure 2-37. Gore Line Fasteners

UNCLASSIFIED

UNCLASSIFIED

g. Fiberglass Twin Pin Fastener (Continued)

Case II is similar to Case I except the pin ends incorporate an end shoulder for receiving a retainer strip. This strip is identical to the base component except for the hole sizes. The use of a retainer strip locks the pin ends into position and divorces the pin load condition from the cord tension. A loose or tight cord locks the strip to the pins. Blanket retainment is positive on both sides since the two strips act as washers overlapping the engagement holes. Depending on load requirements, Case II may provide a weight penalty due to the additional component.

Case III reduces the number of components and simplifies the overall configuration. The pins and base section are moulded into a single "U" shaped clip. The ends of the clip are engaged with a strip similar to that shown for Case II. This strip can be retained with a cord or with individual cotter type lock pins. Retainment of the blanket face sheet is not positive at the base side since the sheet could slip over this member in a manner similar to that described for the cord in Case I. The possibility of starting a fracture in the face sheet reinforcement is reduced, however, since the cross section of the base is larger than that of the cord.

Case IV employs the same configuration as Case III except the retainer strip has been replaced with two washers. This provides a weight saving but places the assembly at a load disadvantage since the ends are not tied together to form a complete chain type link. The individual washers provide good blanket face sheet retainment. Retainment at the base section, however, is limited per the discussions under Case III.

Fasteners for retaining items to pins, shafts, etc., are commercially available in almost unlimited configurations. Common types are cotter keys, snap rings, hair pin type spring clips, push-on grommets, push-on snaps, and screw collars. Detail A in Figure 2-37 shows a possible arrangement which employs a snap ring. When considering minimum disturbance to the insulation layers, it appears reasonable to avoid push on type retainers. These types could cause damage to blankets under the twin pin assembly due to the force required for engagement. A plier type tool may be used for this purpose; however, this is another tool requirement which may or may not be used properly. Also, removal may cause injury to the insulation since the twin pin assembly must be firmly held to disengage the snaps which have a sudden release action. Inspection may be difficult due to the engagement of small close tolerance parts. The push on type fastener is easily profiled for avoiding sharp exposed edges.

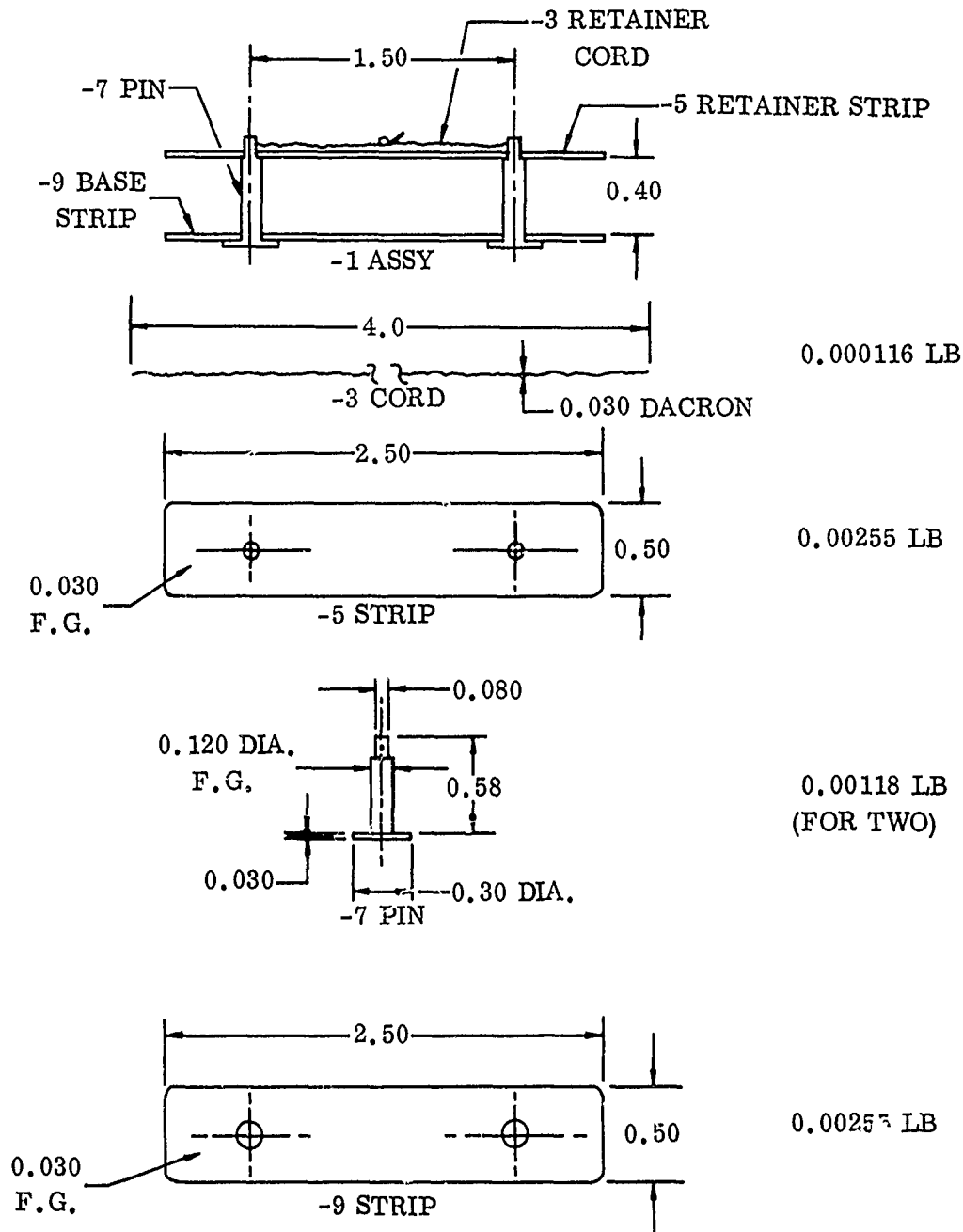
Snap ring fasteners avoid the push pull actions but due to their small circular shapes are difficult to handle and easily lost. Usually tools are required to facilitate handling, installation and removal. This type is inherently absent of protruding edges which may cause damage to the insulation. The use of pins (hair pin spring types) or cords inserted through holes is favored since

UNCLASSIFIED

UNCLASSIFIED

g. Fiberglass Twin Pin Fastener (Continued)

the engagement is easy to inspect, positive, and more adaptable to handling without special tools. The cord offers the advantages of installing or removing without a load, and the absence of stiff protruding edges. Spring clips or pins on the other hand relieve the requirement of tying knots but will have the tendency to expose sharp edges. Case II is the selected pin because of the large number of pins required. Detailed weight analysis was conducted on this pin and is shown in Figure 2-38.



TOTAL WEIGHT FOR -1 ASSY = 0.006396 LB

Figure 2-38. Weight Breakdown - Gore Line Fastener

UNCLASSIFIED

UNCLASSIFIED

- h. Tear-Out Tests. Tear-out tests were conducted on twelve specimens using 1/4 mil double aluminized mylar sheets reinforced at the attachment holes. A typical specimen configuration is shown in Figure 2-39. Eight specimens were reinforced at the holes with No.850 PAU V5200 Scotch Brand aluminized mylar tape. Two specimens were reinforced with No.810 Scotch Brand Magic Transparent tape. Two additional specimens were tested with no reinforcement. Figure 2-40 shows the reinforcement configuration for each specimen.

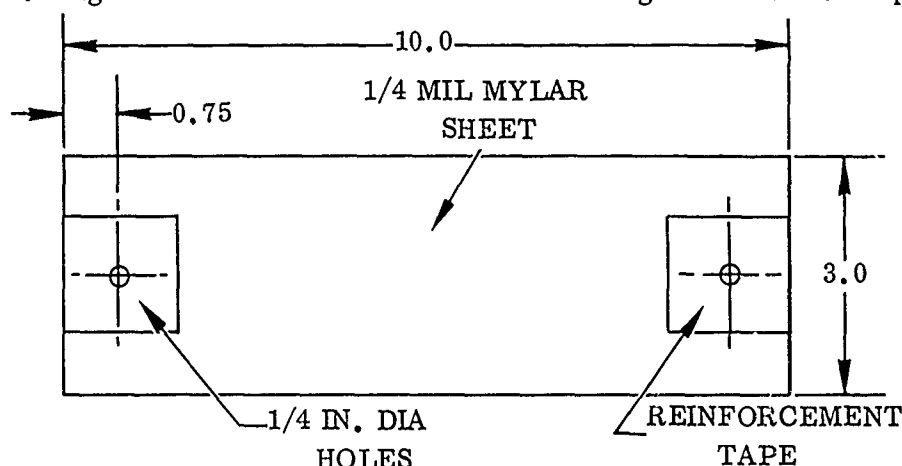


Figure 2-39. Typical Test Specimen

No special procedures were used in applying the reinforcement tapes. The patches were manually cut and applied at room temperature. Due to thin material gauges and dexterity limits, small air pockets and wrinkles between tape and base sheet were present in all specimens.

One 1/4 inch diameter hole at a 3/4 inch edge distance (See Figure 2-39.) was cut at each end of the specimen using a common hand paper punch. The specimens were sandwiched between two sheets of heavy bond paper when punched. This served as a back-up resulting in clean cut holes. The test was conducted at 72° F using the test set-up shown in Figure 2-41. The results of these tests are tabulated in Figure 2-40. All loads were slowly applied such that the progressive yielding and elongation at the holes could be visually monitored.

Scattering of failure loads was experienced due to the inherent variations in materials, edge distance tolerances, and the tape application. Specimens 1, 2, and 3 were reinforced on both sides of the basic sheet. Specimen 1 was initially loaded to the limit of a 5 pound scale. A higher limit scale was then used for the second loading which resulted in a 11.5 pound failure load. Tear-out load was not achieved for specimen 2 since the basic face sheet failed at 7.75 pounds. Specimen 3 achieved an 8.50 pound failure load.

UNCLASSIFIED

CONFIDENTIAL

TEST SPECIMEN NUMBER	REINFORCEMENT CONFIGURATION	TYPE OF REINF. TAPE	LOAD @ FAILURE LBS.	TYPE OF FAILURE	LOAD @ WHICH HOLE ELONGATION STARTED	COMMENTS
1		#850 PAU V5200 SCOTCH BRAND ALUMINIZED MYLAR TAPE	11.50	DUAL TEAR OUT	APPROX. 1.0 LB	LOADED INITIALLY TO 5.0 LB. RELOADED TO FAILURE
2			7.75	NONE		BASIC SHEET FAILED
3			8.50			
4			4.38			
5			3.00			
6			4.75			
7		#810 SCOTCH BRAND MAGIC TRANSPARENT TAPE	0.562		NOT DETECTABLE	
8			0.625	SINGLE TEAR OUT		
9		#850 PAU V5200 SCOTCH BRAND ALUMINIZED MYLAR TAPE	2.75		APPROX. 1.0 LB	
10			2.88			
11		#850 PAU V5200 SCOTCH BRAND ALUMINIZED MYLAR TAPE	8.5	NONE	APPROX. 1.0 LB	BASIC SHEET FAILED
12			2.5	SINGLE TEAR OUT		

(C) Figure 2-40. Test Result Summary

CONFIDENTIAL

UNCLASSIFIED

h. Tear-Out Tests (Continued)

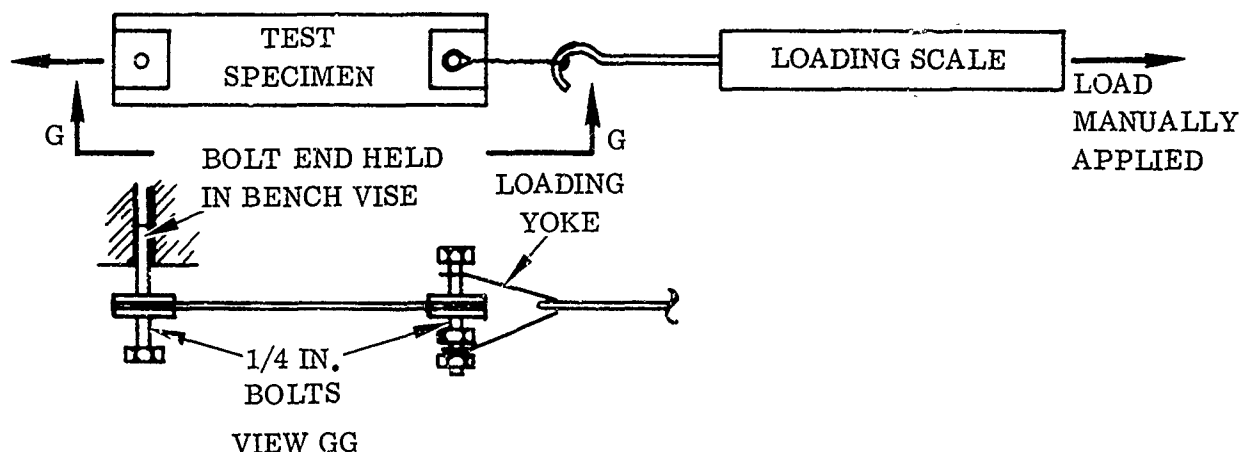


Figure 2-41. Tear-Out Test Setup

Specimens 4, 5, and 6 were reinforced with tape patches on one side only. (See Figure 2-40.) Failure loads ranging from 3.00 pounds for specimen 5 to 4.75 pounds for specimen 6 were recorded.

A typical blanket construction is two 1 mil face sheets with 1/4 mill core sheets. Assuming that the face sheets resist the loads due to venting, the core sheets must resist their own inertia loads to prevent interlayer shifting. From a manufacturing viewpoint, it would be desirable to eliminate the reinforcements on the core sheets; therefore, specimens 7 and 8 were tested without reinforcements and failure loads recorded at 0.562 and 0.625 pound respectively.

Specimens 9 and 10 were reinforced with No. 810 Scotch Brand Magic Transparent tape to obtain comparative data between conventional and specialized materials. Failure loads of 2.75 and 2.88 pounds, respectively, were recorded.

To effectively transmit loads between pins without excessive wrinkling and yielding of the base sheet, it may be desirable to substitute the local spot patches for a continuous reinforcement tape strip. Therefore specimens 11 and 12 were tested with a continuous mylar tape strip and loads were recorded at 8.5 and 2.5 pounds, respectively. Specimen 11 was taped on both sides and specimen 12 on one side only. (See Figure 2-40.) The 8.5 pound load for specimen 11 was due to basic sheet failure.

Except for specimen 1, all failures were the single tear-out type. (See Figure 2-40.) Specimen 1 failed along two planes. All failures were preceded by a local buckling along the edge of the hole and general elongation of the hole (approximately $1.5 \times$ the basic hole diameter). The combination of edge buckling and hole elongation created small tears along the edge of the holes from which failure propagated rapidly. Pronounced hole elongation and

UNCLASSIFIED

UNCLASSIFIED

h. Tear-Out Tests (Continued)

edge buckling were observed at approximately 1 pound loading for all specimens except 7 and 8 which were not detected due to the low failure loads. Final design requirements will be influenced by venting, inertia, vibration, acoustic loads, temperature, and the rate of load application. Depending upon the magnitude of these requirements, a broad range of reinforcement strengths are obtainable by using dacron scrims integrally bonded to the tape sections.

2.2.1.6 Pressure Loads Due to Rapid Evacuation. As the ambient pressure is decreased about an insulated tank, the gas residing in the insulation causes a pressure differential across the batten. The resulting stresses may be large enough to rupture the insulation. In order to scale the stress, it is necessary to determine the interstitial gas pressure as a function of length and time throughout the batten. It is also necessary to determine the maximum pressure across the battens to assure that the insulation attachment method is sufficiently strong to preclude insulation tear-out or failure of the supports.

The actual problem of the pressure calculation involves a knowledge of the interaction between pressure differential and batten deformation. A solution would be complex and unnecessary, since a knowledge of the maximum stress is sufficient to determine if the insulation will fail; therefore, the pressure differential is calculated as a function of time, assuming that the insulation does not deform.

The calculation of interstitial gas pressure requires a knowledge of the flow resistance. This is to be determined experimentally for each type of insulation as a function of layer density. At the present time, the only available data are given in Reference 12 which is applicable to NRC-2 insulation. The value for Superfloc will be established later this year; however, it is felt that the flow resistance of Superfloc should be lower than NRC-2, resulting in a conservative analysis for this phase of the study.

The following assumptions were made concerning the gas flow:

- (1) The gas flow is analagous to continuum flow in a porous medium
- (2) The flow is one-dimensional and isothermal
- (3) The gas is perfect with constant fluid properties.

- a. Method of Analysis. The blankets are assumed to be shaped with a sufficiently large radius such that the flow is similar to that in a flat batten. It is also assumed that one end is sealed. This end would be the middle of a batten having two open ends. A sketch of this batten is shown in Figure 2-42. With the above assumptions, a mathematical model may be derived which predicts the pressure histories at all points in the insulation. The mass flow rate is given by the equation:

UNCLASSIFIED

UNCLASSIFIED

a. Method of Analysis (Continued)

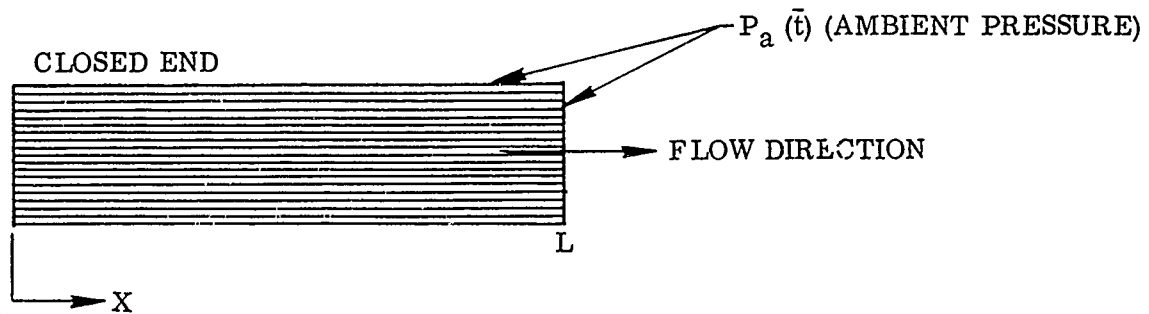


Figure 2-42. Side Wall Batten

$$\dot{m} = -\frac{K}{\mu} \rho \frac{\partial p}{\partial x} \frac{\text{lbm}}{\text{sec}}$$

where

$$\mu = \text{gas viscosity} \frac{\text{lbf-sec}}{\text{sq ft}}$$

K = permeability of the medium, sq ft

NOTE: K is a function of the layer density, the frequency of perforations, and any flow restrictions such as exit spacing. For this calculation, the data from Reference 12 was used.

If a mass balance is performed on a differential control element in the insulation, the following equations result:

$$\dot{m}_{in} - \dot{m}_{out} = \frac{\partial p}{\partial t} dx$$

$$-\frac{K}{\mu} \rho \frac{\partial p}{\partial x} + \frac{K}{\mu} \rho \frac{\partial p}{\partial x} + \frac{K}{\mu} \frac{\partial}{\partial x} \left(\rho \frac{\partial p}{\partial x} \right) dx = \frac{\partial p}{\partial t} dx$$

$$\frac{K}{\mu} \frac{\partial}{\partial x} \left(\rho \frac{\partial p}{\partial x} \right) = \frac{\partial p}{\partial t}$$

Since the gas is assumed perfect, its equation of state may be written

$$\rho = \frac{p}{RT}$$

Substituting, and noting that the flow is isothermal

UNCLASSIFIED

UNCLASSIFIED

a. Method of Analysis (Continued)

$$\frac{1}{RT} \frac{\partial p}{\partial t} = \frac{K}{\mu} \frac{\partial}{\partial x} \left(\frac{p}{RT} \frac{\partial p}{\partial x} \right)$$

$$\frac{\mu}{K} \frac{\partial p}{\partial t} = \frac{\partial}{\partial x} \left(p \frac{\partial p}{\partial x} \right) = p \frac{\partial^2 p}{\partial x^2} + \left(\frac{\partial p}{\partial x} \right)^2 \quad (1)$$

The following boundary and initial conditions are imposed on equation 1 to complete the mathematical model:

<u>Boundary Conditions</u>	<u>Initial Condition</u>
$p(L, t) = p_a(t)$	$p(x, 0) = p_0$

(2)

$$\frac{\partial p}{\partial x}(0, t) = 0$$

where

$x = 0$ is the closed end of the batten, or the middle if both ends are open

$x = L$ is the open end of the batten

$p_a(t)$ is the ambient pressure

p_0 is the initial pressure

Equation 1, with boundary and initial conditions equation 2, completes the statement of the mathematical model for the batten.

A numerical method is employed for the solution of the above boundary value problem and a digital computer program is utilized. If more than one batten layer is used, the inside battens do not experience an ambient pressure decay; therefore, the pressure in the inside battens must be calculated using a different boundary value problem.

The calculation used to determine the pressure for this application was based on the maximum flow path of the gore section (assuming tank mounted insulation). This maximum length occurs at the equator of the propellant tanks as shown in Figure 2-43.

The gores of the oxidizer tank were used since the higher interstitial temperatures (assumed average temperature of 330° R) result in higher viscosity (10^{-5} lb/ft-sec), and consequently, lower vent rates. It was also assumed that the venting medium was helium. The total flow length used was 1.4 ft. Although the circumference of the tank is greater than that of the oxidizer tank, there are more gore sections and the flow path length is comparable.

UNCLASSIFIED

UNCLASSIFIED

a. Method of Analysis (Continued)

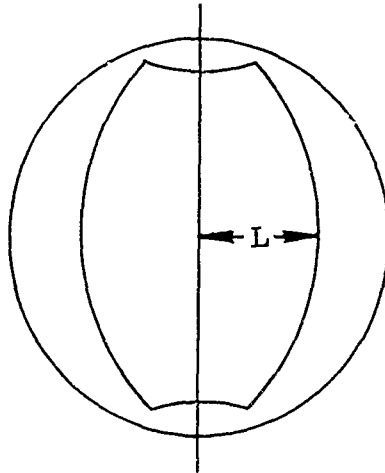
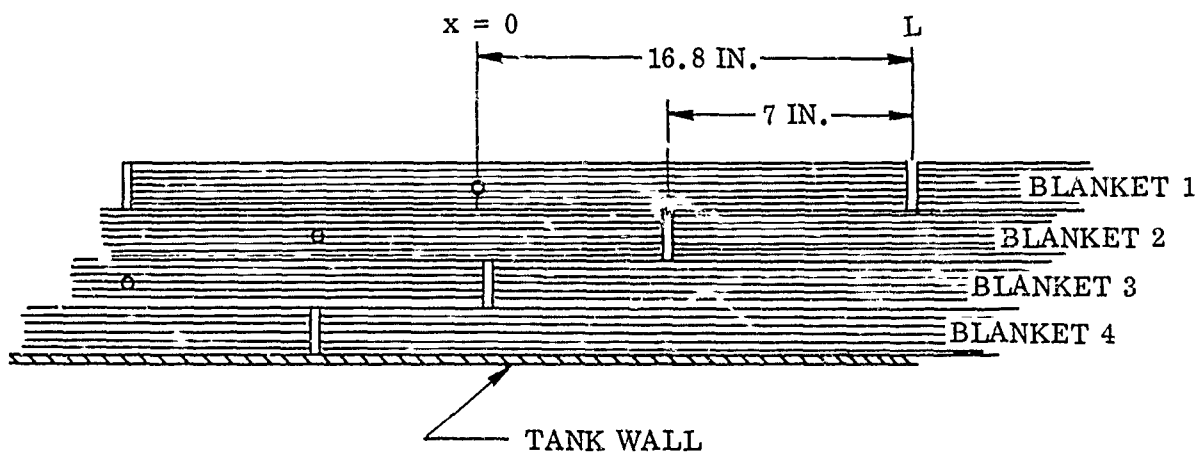


Figure 2-43. Propellant Tank Equator

A typical lay-up of 4 battens was assumed with each batten having an overlap of 7 inches (10 degrees) between succeeding battens. Refer to Figure 2-44 for the configuration of a typical multiple batten system.



($x = 0$); CENTER OF BLANKET
(EQUAL FLOW PATH DISTANCE TO EDGE)

$x = L$; EDGE OR SEAM OF EACH BLANKET

Figure 2-44. Four Blanket Installation

UNCLASSIFIED

CONFIDENTIAL

(U) a. Method of Analysis (Continued)

The pressure in layer 1 may be calculated from the solution to equation 1 with boundary and initial conditions equation 2, since the gas exits at $x = 16.8$ and $p(16.8, t)$; however, the gas in layer 2 exits at $x_1 = 9.8$, and the pressure at this is $p_1(9.8, t)$. Therefore, the pressure in layer 2 may be calculated from equation 1 with the following boundary and initial calculations:

<u>Boundary Conditions</u>	<u>Initial Conditions</u>	
$p_2(L, t) = p_1(9.8, t)$	$p_2(x, 0) = p_0$	(3)
$\frac{\partial p_2}{\partial x}(0, t) = 0$		

Similarly, the pressure in layer 3 may be calculated from equation 1 with the following boundary and initial conditions:

<u>Boundary Conditions</u>	<u>Initial Conditions</u>	
$\frac{\partial p_3}{\partial x}(0, t) = 0$	$p_3(x, 0) = p_0$	(4)
$p_3(L, t) = p_2(9.8, t)$		

The pressure in the last layer next to the tank may be calculated with the following boundary and initial conditions:

<u>Boundary Conditions</u>	<u>Initial Conditions</u>	
$\frac{\partial p_4}{\partial x}(0, t) = 0$	$p_4(x, 0) = p_0$	
$p_4(L, t) = p_3(9.8, t)$		

- (C) b. Maximum Pressure Load. The pressure history of each batten during boost was then calculated to determine the maximum ΔP that would occur across the total lay-up (40 layers). The maximum ΔP occurs from the middle of the inside batten to ambient pressure at 76 seconds after launch and is equal to 2.263 lb/ft² or 0.0157 psi. A design value of 0.1 psi was used in estimating the insulation structural loads, allowing sufficient design margin.

- (U) Although the flow path lengths for the shroud mounted insulation are greater (24 inches), the use of 0.1 psi should here also allow reasonable margin for the slower vent rate.

CONFIDENTIAL

CONFIDENTIAL

(C) b. Maximum Pressure Load (Continued)

(U) It should be noted that this calculation was performed only to provide structural loading estimates for rapid evacuation during boost. The out-gassing and venting rates while in the free molecular flow regime will be conducted later in the program to assure adequate flow area and determine the effect on the selected thermal conditioning system.

(U) The rapid evacuation analysis was conducted at this time to assure adequate support for the systems.

(U) 2.2.1.7 Weights Analysis. A detailed parts list was generated for the complete insulation system and a weight analysis was conducted. The detailed weight analysis is for 40 layers of superfloc based on the selected tank mounted and shroud mounted systems previously described. The parts list includes miscellaneous items such as rivets, hem reinforcements at the scrim edges, dacron cord, bolts, spacers, pins, spot reinforcement patches, clips, and allowances for adhesives. Figure 2-45 presents the summary of this effort. The weight of the complete system as a function of number of layers of superinsulation is shown in Figure 2-46.

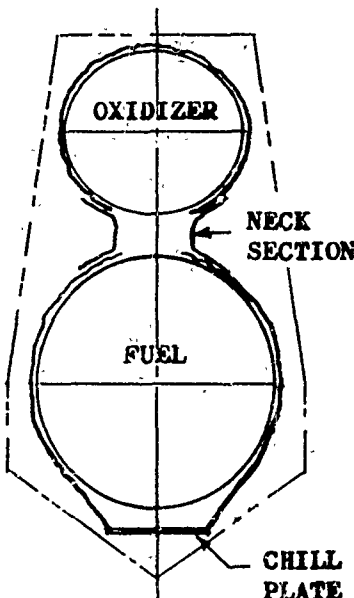




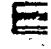






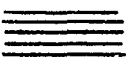



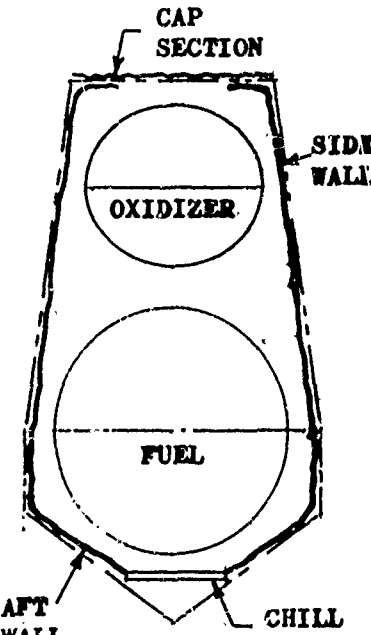

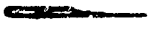





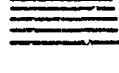

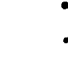





(U) 2.2.2 INSULATION SYSTEM THERMAL PERFORMANCE. In order to establish the heat leak into the propellant tanks as a function of insulation thickness and location it was first necessary to evaluate different types of superinsulation, and the effect of penetrations, seam gaps, fasteners, and struts.

(U) Candidate insulation systems were evaluated, including Dimplar, NRC-2, Superfloc, and a composite type. The performance of Superfloc was then used in conjunction with data for seams, pins and struts to establish the heat leak into each installation as a function of the number of layers.

(U) 2.2.2.1 Candidate Insulation Systems. There have been extensive laboratory tests and model demonstrations of superinsulations but as yet there have been no flight vehicle applications. Practical manufacturing, installations and handling requirements must be considered while ensuring optimum flight performance and reasonable ground heat-transfer. Table 2-1 shows five promising basic candidate systems for the AMPS program, with ratings based on thermal performance (ρk factors), strength, out-gassing capability, purge/vent, and ease of application. The ρk data are based on a temperature range of 540 to 140°R. The lowest ρk value is indicated for Convair's Superfloc insulation. Following in ρk performance are the crinkled double aluminized mylar with tissue glass spacers (composite type), and National Research Corporation's NRC-2. It is anticipated that the performance of a new Superfloc configuration with reduced tuft sizes (0.050 inch diameter) and increased tuft spacings (1/2 inch) will exceed those shown in Table 2-1. The earlier type of Superfloc consisted of 0.090 inch diameter tufts and 3/8 inch spacing. Figure 2-47 presents some additional data comparing Superfloc, NRC and Dimplar.

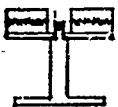
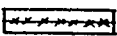
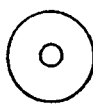

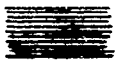
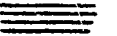

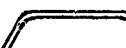
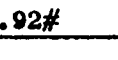
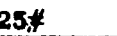
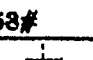
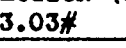


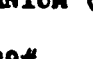

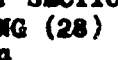


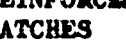




CONFIDENTIAL

CONFIDENT

 <p>TANK MOUNTED INSULATION (40 LAYERS)</p>	 <p>TANK SUPPORT FAIRINGS (9) F.G.</p> <p>10.58#</p>	 <p>TANK CLIPS FOR INSUL. SUPPORT (12) AL ALY.</p> <p>.167#</p>	 <p>TANK CHEM MILLED ZONES FOR INSUL. SUPPORT CLIPS.</p> <p>.116#</p>	 <p>INSUL. SUPPORT RING WITH PINS F.G. (2)</p> <p>3.00#</p>	 <p>SUPPO WITH TAPE (84)</p> <p>.64</p>
	 <p>DACRON CORD</p> <p>.01#</p>	 <p>FAIRING FOR INSUL. SUPPORT OVER DUCTS F.G. (1)</p> <p>.30#</p>	 <p>SUPPORT CLIP FOR FAIRING (4) AL ALY.</p> <p>.06#</p>	 <p>RIVETS FOR INSUL. SUPPORT ATTACHMENTS AL ALY.</p> <p>.07#</p>	 <p>1/4 M SUPER FOR O TANK</p> <p>10.92</p>
	 <p>1/4 MIL SUPERFLOC FOR FUEL TANK (32)</p> <p>16.70#</p>	 <p>1 MIL SUPERFLOC FACE SHEETS FOR FUEL TANK (8)</p> <p>14.20#</p>	 <p>DACRON SCRIM</p> <p>2.38#</p>	 <p>CHILL PLATE COLLAR AL ALY.</p> <p>2.40#</p>	 <p>CHILL COLLA AL AL</p> <p>.19</p>
 <p>SHEROUD MOUNTED INSULATION (40 LAYERS)</p>	 <p>DACRON SCRIM</p> <p>6.64#</p>	 <p>HEM REINFORCEMENTS FOR SCRIM F.G.</p> <p>1.68#</p>	 <p>RIVETS FOR ATTACHING SCRIM & ACCESSORIES AL ALY.</p> <p>.44#</p>	 <p>FWD. CAP RING (1) F.G.</p> <p>8.55#</p>	 <p>PINS CAP S RING F.G.</p> <p>.07</p>
	 <p>1/4 MIL SUPERFLOC FOR FWD CAP SECTION (40)</p> <p>4.07#</p>	 <p>1/4 MIL SUPERFLOC FOR SIDE AFT WALLS (32)</p> <p>34.2#</p>	 <p>1 MIL SUPERFLOC FACE SHEETS FOR AFT & SIDE WALLS (8)</p> <p>29.0#</p>	 <p>1/4 MIL SUPERFLOC FOR OXIDIZER DUCT (6)</p> <p>.15#</p>	 <p>DROP BUTTO FWD A & ACC (150)</p> <p>.60</p>
	 <p>AFT WALL SCRIM ATTACHMENT RING (1) F.G.</p> <p>1.77#</p>	 <p>ACCESS DOOR INSUL CARRIER (3) F.G.</p> <p>8.06#</p>	 <p>TWIN PIN FASTENER FOR SIDE & AFT WALL (840) F.G.</p> <p>5.37#</p>	 <p>CHILL PLATE COLLAR AL ALY.</p> <p>2.40#</p>	 <p>CHILL COLLA AL AL</p> <p>.19</p>

CONFIDENT

CONFIDENTIAL

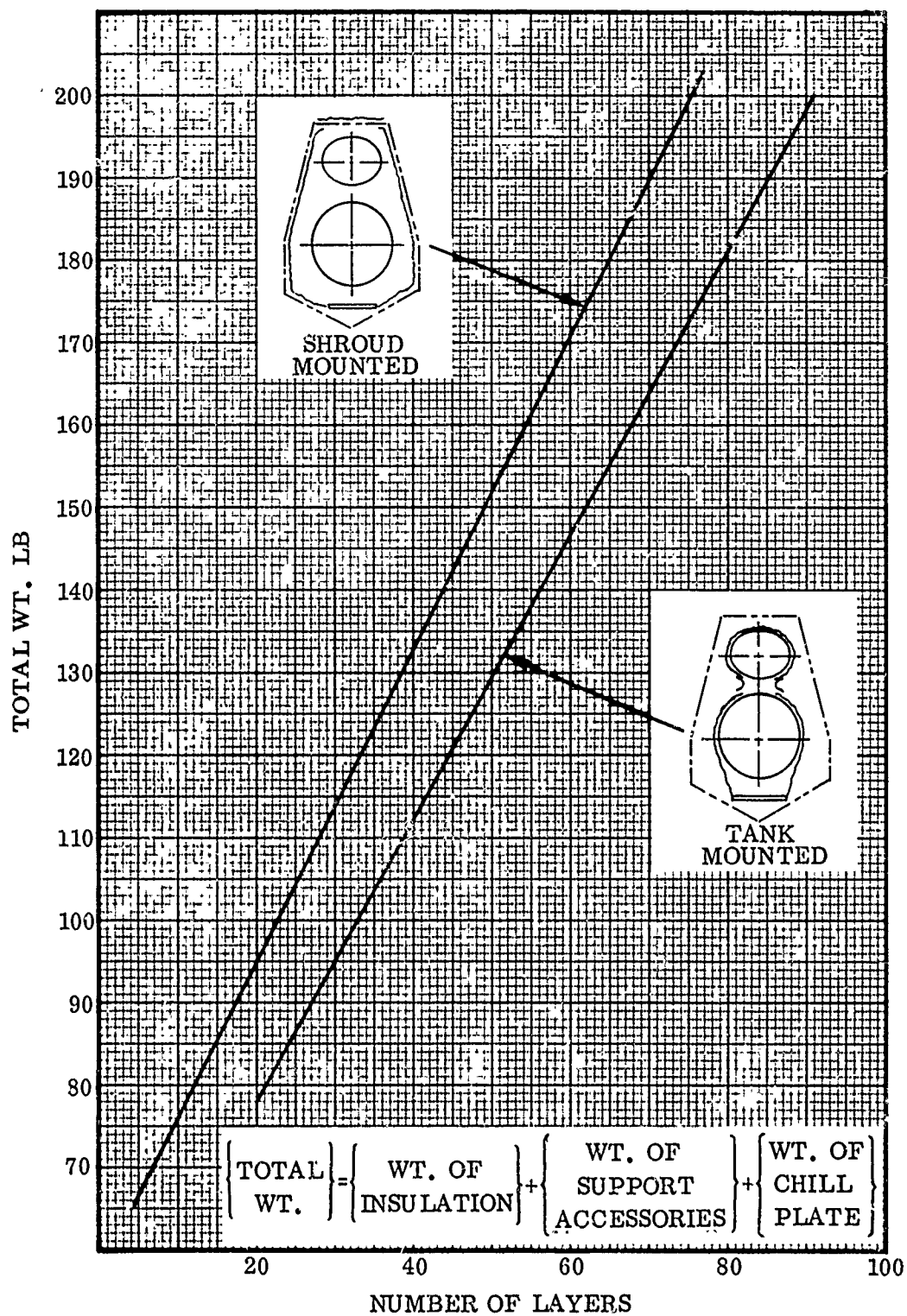
 SUPPORT PIN WITH PINS (2)	 MECH. TAPE PATCHES (84)	 MYLAR (2 MIL) REINFORCEMENT PATCHES	 TWIN PIN GORE LINE FASTENERS F.G. (1270)	WT = 107.43 5% CONTINGENCIES = 5.37 TOTAL = 112.80#
 SUPPORT PIN WITH PINS (2)	 MECH. TAPE PATCHES (84)	 MYLAR (2 MIL) REINFORCEMENT PATCHES	 TWIN PIN GORE LINE FASTENERS F.G. (1270)	
 SUPPORT PIN WITH PINS (2)	 MECH. TAPE PATCHES (84)	 MYLAR (2 MIL) REINFORCEMENT PATCHES	 TWIN PIN GORE LINE FASTENERS F.G. (1270)	
 SUPPORT PIN WITH PINS (2)	 MECH. TAPE PATCHES (84)	 MYLAR (2 MIL) REINFORCEMENT PATCHES	 TWIN PIN GORE LINE FASTENERS F.G. (1270)	WT = 126.12 5% CONTINGENCIES = 6.3 TOTAL = 132.42#
 SUPPORT PIN WITH PINS (2)	 MECH. TAPE PATCHES (84)	 MYLAR (2 MIL) REINFORCEMENT PATCHES	 TWIN PIN GORE LINE FASTENERS F.G. (1270)	
 SUPPORT PIN WITH PINS (2)	 MECH. TAPE PATCHES (84)	 MYLAR (2 MIL) REINFORCEMENT PATCHES	 TWIN PIN GORE LINE FASTENERS F.G. (1270)	

(C) Figure 2-45. Detailed Weights Analysis
2-54 Appendix I

CONFIDENTIAL

2

CONFIDENTIAL



(C) Figure 2-46. Insulation System Weight versus Number of Layers

CONFIDENTIAL

UNCLASSIFIED

TABLE 2-1. CANDIDATE SYSTEMS

Candidate System						
Insulation Type	Shield	Spacer	540-140° R ρ K Btu-lb/ Hr Ft 4 °R	Strength	Purge/ Vent	Application
Composite	1/4 MIL Mylar AMA	Crinkling and Tissue Glass	2.3*	Spacer Delicate	Poor	Fair
Dimplar	1/2 MIL Mylar AMA	Dimpled	13.0	Very Good	Excellent	Good
NRC-2	1/4 MIL Mylar AM	Crinkling	2.3*	Good	Fair	Fair
ADL	1/4 MIL Mylar AMA	Silk Netting	3.5*	Excellent (Net Support)	Fair	Good
Convair (Superfloc)	1/4 MIL Mylar AMA	Dacron Flock Tufts 3/8 in. Spaced	2.05*	Gcod	Excellent	Good

UNCLASSIFIED

*REF.: Investigation regarding development of a High Performance Insulation System
 NAS8-20758, 2nd Quarterly Progress Report
 10 December 1967

UNCLASSIFIED

1. IDEAL SHIELD ($\epsilon = 0.03$)
2. CONVAIR SUPERFLOC DENIER 3-1/2 IN.
SPACED DACRON TUFTS
3. CONVAIR SUPERFLOC DENIER 3-3/8 IN.
SPACED DACRON TUFTS
4. NRC-2 (NATIONAL RESEARCH CORP.
DATA)
5. NRC-2 (CONVAIR TEST DATA)
6. DIMPLAR

$$T_H = 535^\circ \text{R}$$

$$T_C = 140^\circ \text{R}$$

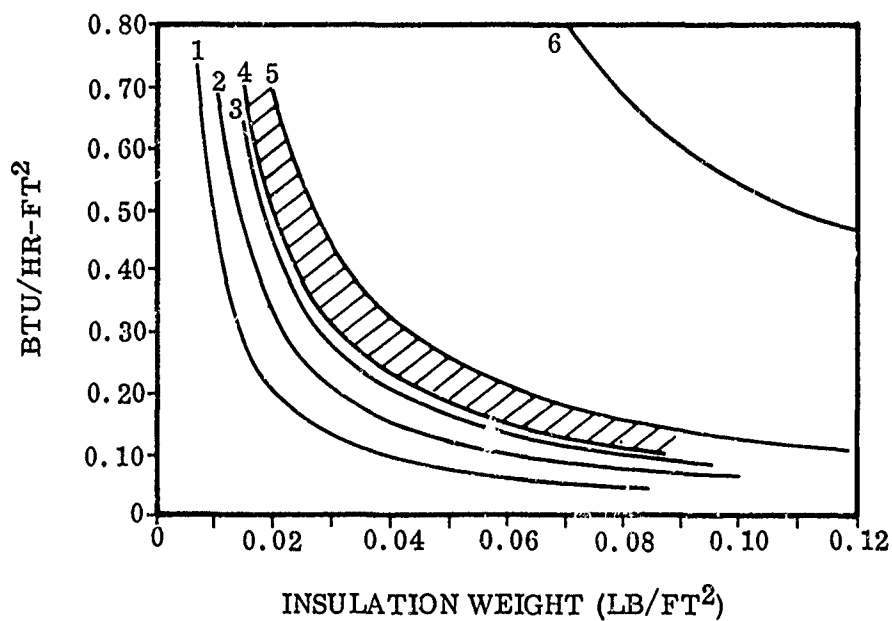


Figure 2-47. Insulation Comparison - NRC-2, Dimplar and Superfloc

UNCLASSIFIED

UNCLASSIFIED

Of primary importance for the selection of the basic insulation system is the spacer material. The important factors are conductivity, strength, density control, and weight. Promising spacers are the tissue glass and dacron flock tufts, with crinkling (NRC-2) also considered an acceptable method.

The conductive path through the spacer material is difficult to evaluate, but conduction can be minimized by proper design. In the case of superfloc the fine fibers effectively reduce conduction heat transfer between layers. Heat flow is further impeded when the contact areas between the individual fibers approach point contact. When superinsulation is compressed, the point contacts deform, decreasing the contact resistance between the layers. The degree of recovery is a strong indication of deterioration of thermal properties resulting from boost loads; therefore, to determine the relative spring back, two of the candidate systems, NRC-2 and Superfloc, were tested during a dead weight compression test (References 14 and 15).

The recovery of NRC-2 was 85 percent (Reference 14). The recovery of the Superfloc (Reference 15) was between 76.8 and 93.6 (See Figure 2-48.) for the configuration with 1/2 inch tuft spacing to the configuration with 1/4 inch tuft spacing, respectively. The high percentage of recovery for both insulations indicates that both methods of spacing promise to withstand mechanical compressions and high 'g' forces during vehicle boost without excessive deterioration of thermal performance. The recovery of the tissue glass spacer of the composite insulation will be tested shortly.

As far as strength of spacer materials is concerned, the tissue glass is the weakest material among the candidates. There is some doubt that this material is sufficiently strong to withstand acceleration and acoustic vibration loads during vehicle boost and to take the evacuation stresses due to the rapid changes in ambient pressure.

Insulation density control greatly influences the thermal performances, and based on test experience at Convair, the spacer material controls the density of all the candidates. The density of Superfloc is the easiest to control, followed by the tissue glass, the silk netting, and the dimpling. The crinkling method is the weakest method to control the density. The weight of the candidate insulation spacers compare in the order shown in Table 2-2.

The strengths of the candidate systems under consideration are dictated by the strengths of the radiation shields and spacer materials. All radiation shields are metallized fibers of excellent tensile strength. The factor which influences the stability of the insulation system most is the spacer. Silk netting gives excellent support to an insulation system while tissue glass spacers are delicate and may shatter under cryogenic temperature during boost.

UNCLASSIFIED

UNCLASSIFIED

TEST NO.	TEST SPACING (IN)	LENGTH (IN)	DENIER	SIMULATED LOAD (GM/FT ²)	NO. OF LAYERS	INITIAL	LOADED	REMOVED	PERCENTAGE COMPRESSION	PERCENTAGE RECOVERY
1	3/8	0.04	3	1296	200	4.981	1.891	4.050	62.0	81.0
2	1/4	0.04	3	1591	200	6.526	2.979	6.110	54.4	93.6
3	3/8	0.04	15	1550	200	4.850	2.084	4.280	57.0	88.4
4	3/8	0.08	15	1494	200	7.190	2.015	6.308	72.0	87.9
5	1/2	0.04	3	1133	200	3.02	0.829	2.320	72.6	76.8

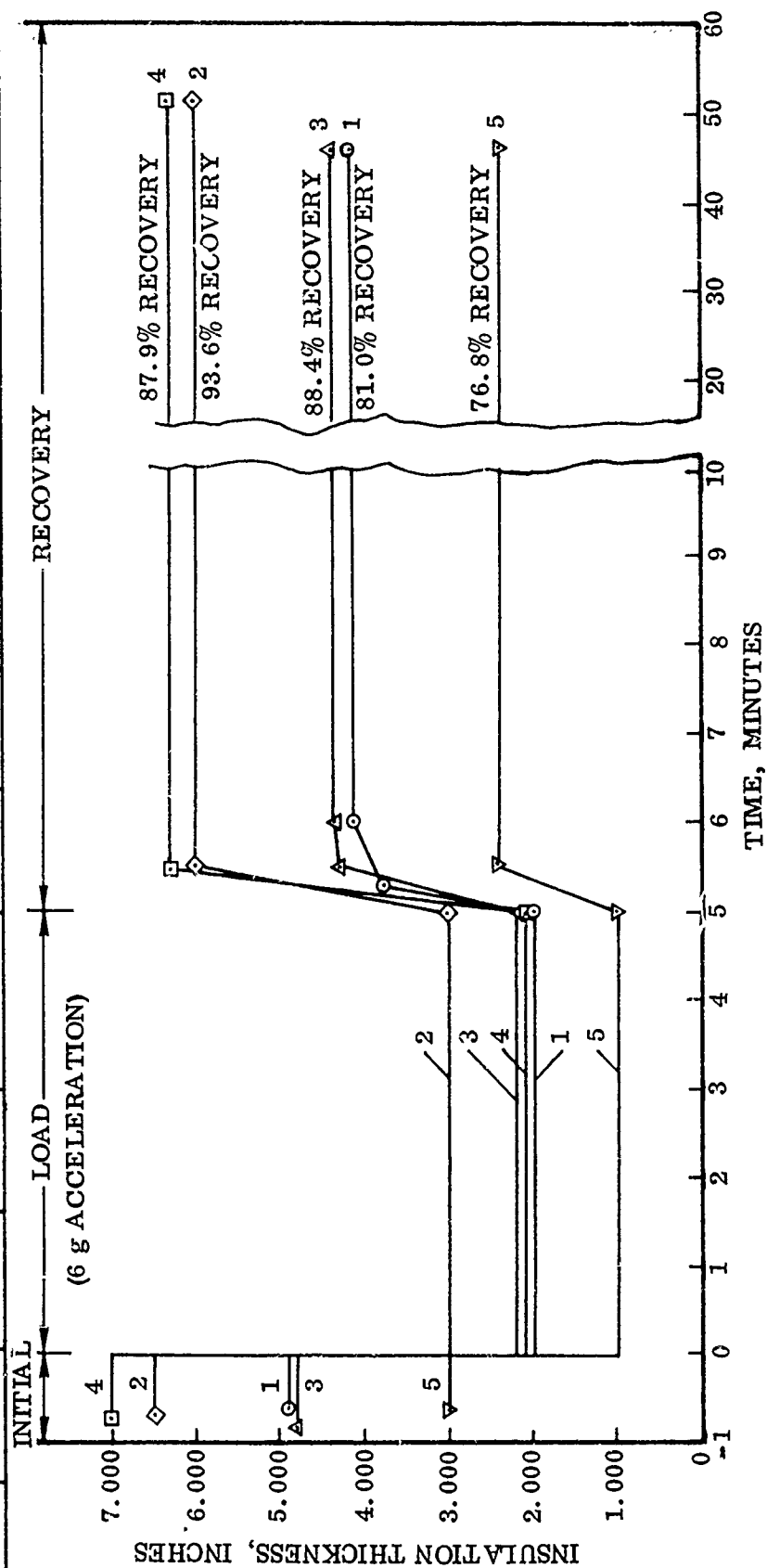


Figure 2-48. Compressions and Recovery Test Results

UNCLASSIFIED

UNCLASSIFIED

TABLE 2-2. INSULATION SPACER WEIGHT COMPARISON

		Spacer	Shield + Spacer lb/ft ² - Layer	Reference Number
1	NRC-2 (Crinkling)	0.0001 lb/ft ² -layer	0.0019	15
2	Dacron Fibers + Adhesive (New Superfloc Conf.) 1/2 in. SP-3D	0.00027	0.00207	15
3	Dacron Fibers + Adhesive 3/8 in. SP-3D Superfloc	0.00058	0.00238	15
4	Borosilicate Glass Fiber (Tissue Glass)	0.00080		
	For Crinkling	0.00010		
	Total	0.0090	0.00270	14,15
5	Silk Netting	0.0014	0.00320	14
6	Dimplar (Heavy Radia- tion Shields Required to Produce Dimpling)	0.0056	0.00740	3

The last factor to consider is the actual application of the insulation system to the cryogenic tank. It was mentioned before that density control is a very important consideration. Superfloc, the silk netting insulation, and the tissue glass insulation are easy to apply, while NRC-2 is harder to control.

It should be noted that the tissue glass spacer insulation, when mounted in blankets effectively loses one reflective shield in each blanket because the top shield of one blanket is in direct contact with the bottom shield of the adjacent blanket. Thus for the AMPS insulation design using four blankets, four effective radiation shields are lost.

The evaluation of candidate superinsulation systems is a continually evolving process and it would be premature to select one system over another at this time; however, the thermal performance of Superfloc and the composite type appear to be preferred and similar, and the use of one of these in the insulation optimization study will not result in an irrevocable decision. As the program progresses and more information is established for the various superinsulations, the selection criteria can be reviewed to assure the use of the proper insulation system. For the purpose of the selection of insulation location and thickness, the performance of Convair Superfloc has been chosen.

UNCLASSIFIED

CONFIDENTIAL

(C) 2.2.2.2 Assumptions. Thermal analyses of the shroud mounted and tank mounted insulation systems were based on the following assumptions:

- a. Ground operation was assumed to occur in a convective heat transfer environment sufficient to maintain an external shroud temperature of 100°F.
- b. Maximum incident space heating was assumed to correspond to a circular, polar orbit, and a 6:00 am or 6:00 pm launch on 26 April, 17 August, 30 October, or 13 February. The following incident heat rates for a payload-earthward oriented, conical-shroud vehicle are the orbital-averaged, surface-averaged values employed in the analysis:
 - (1) Solar Radiation, 138 Btu/hr-ft²
 - (2) Earth Thermal Radiation, 27.5 Btu/hr-ft²
 - (3) Earth Albedo Radiation, 4.3 Btu/hr-ft²
 - (4) Orbital Aerodynamic Heating, 11.6 Btu/hr-ft²
- c. The conical shroud external surfaces were assumed to be provided with a white thermal control coating having solar absorptivity and emissivity values of 0.30 and 0.85, respectively.
- d. The combined effect of assumptions b. and c. result in a shroud temperature of 480°R, which was assumed constant throughout the analysis for maximum heating space environmental conditions.
- e. The superinsulation (Superfloc) natural layer density was assumed to be 30 layers/inch.
- f. Ground environment inner shroud conditioning gas (GN₂/GHe) inlet temperatures were assumed to be 460°R. Shroud internal convective heat transfer was predicated on respective GN₂ and GHe flow rates of 800 lb/hr and 40 lb/hr.

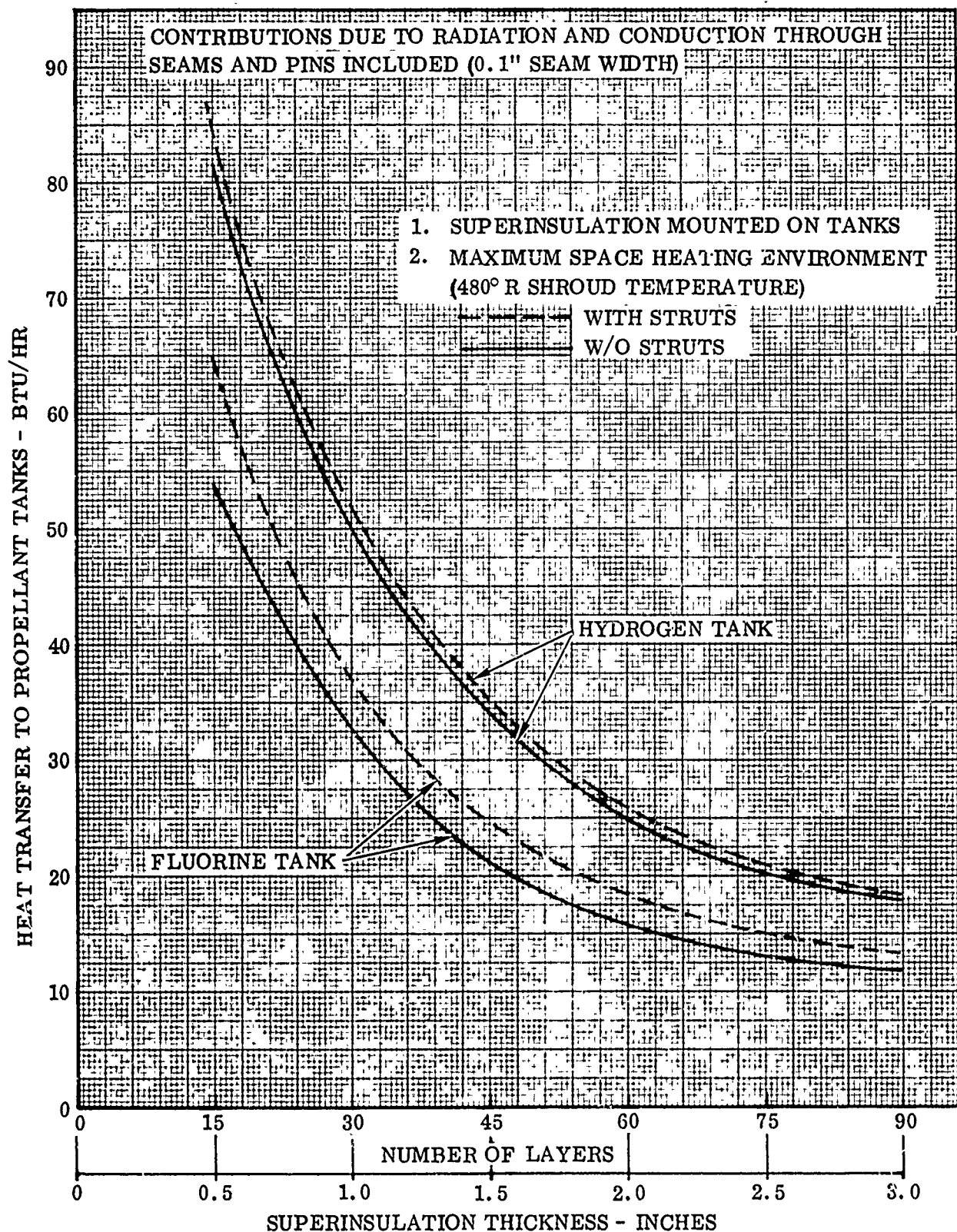
(U) 2.2.2.3 Insulation Configurations and Resulting Propellant Tank Heat Transfer. Parametric thermal analyses were performed in which alternate configurations of propellant tank insulation were evaluated. Respective superinsulation (Superfloc) and ground operation insulation configurations are summarized in Table 2-3, together with notation of the figures in which the corresponding resulting heat rates are presented.

(U) TABLE 2-3. SUPERINSULATION AND GROUND OPERATION INSULATION CONFIGURATIONS

Superfloc Installation	Ground Operation Thermal Control Provision	Predicted Tank Heat Rates	
		Space	Ground
Tank-mounted	Foam on tanks, GN ₂ purge	Figure 2-49	Figure 2-51
Tank-mounted	GHe purge	Figure 2-49	Figure 2-51
Shroud-mounted	Foam on tanks, GN ₂ purge	Figure 2-50	Figure 2-52
Shroud-mounted	Perforated blanket on tanks, GHe purge	—	Figure 2-52

CONFIDENTIAL

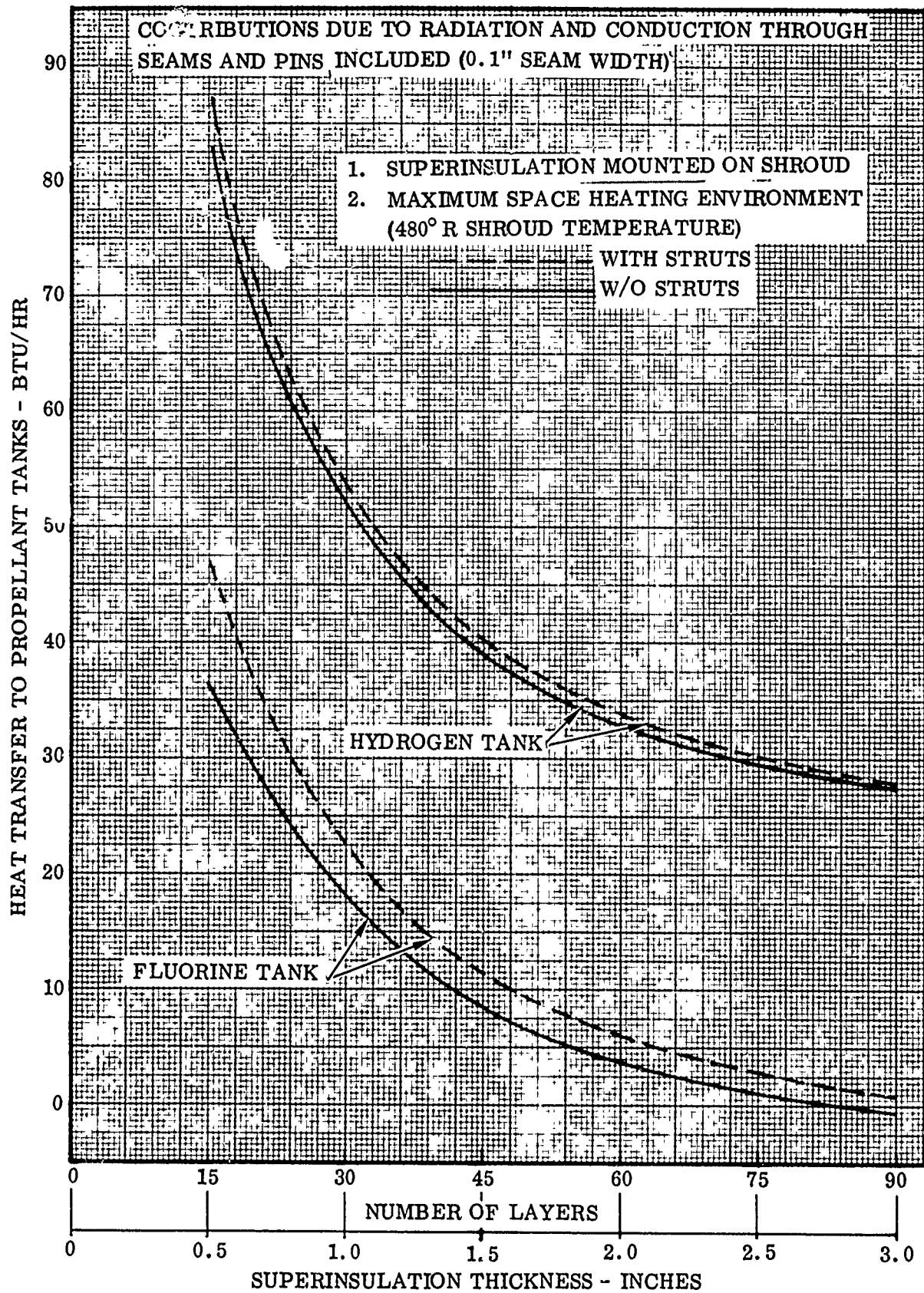
CONFIDENTIAL



(C) Figure 2-49. Propellant Tank Heat Transfer - Space Conditions
(Tank-Mounted Insulation)

CONFIDENTIAL

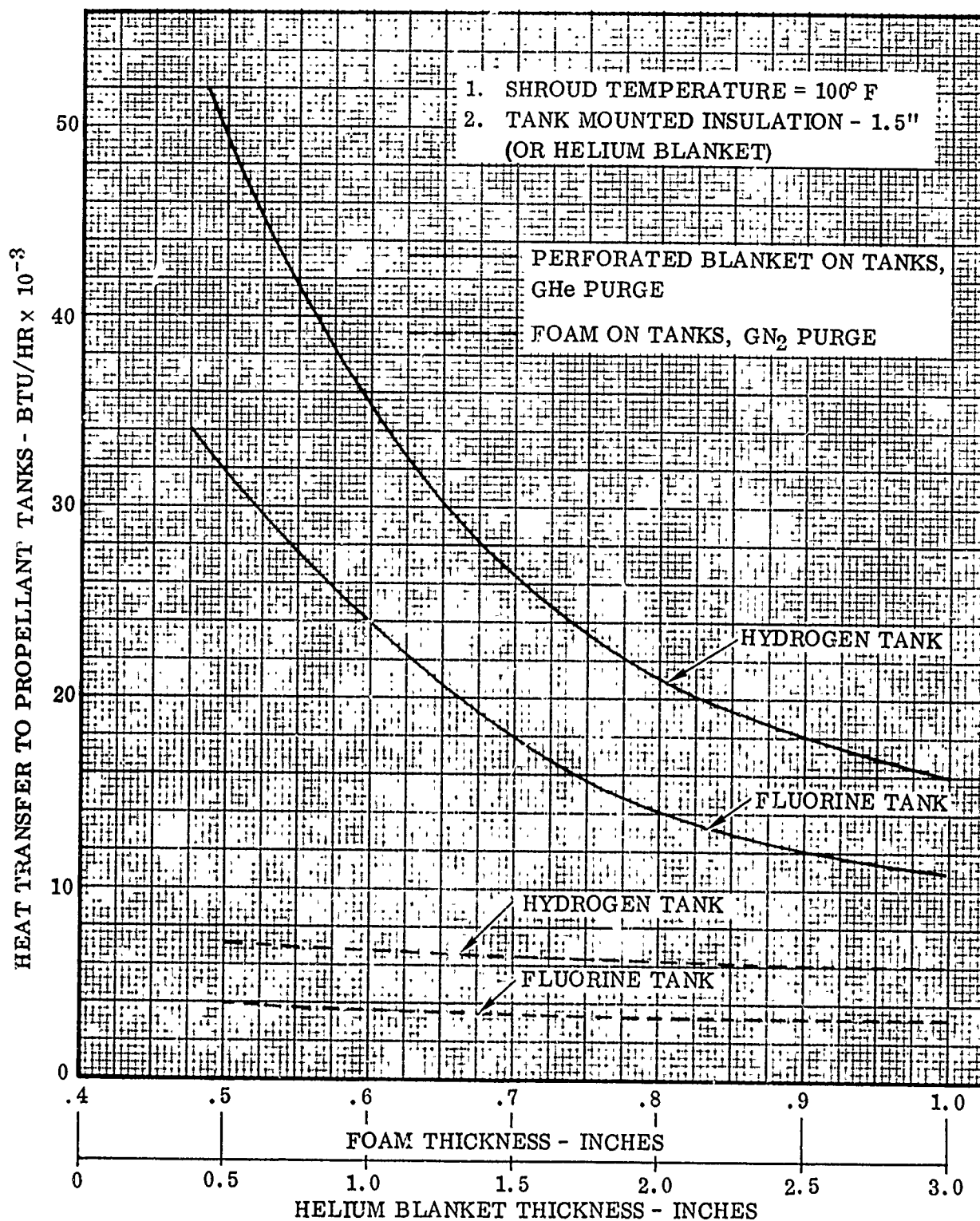
CONFIDENTIAL



(C) Figure 2-50. Propellant Tank Heat Transfer - Space Conditions (Shroud-Mounted Insulation)

CONFIDENTIAL

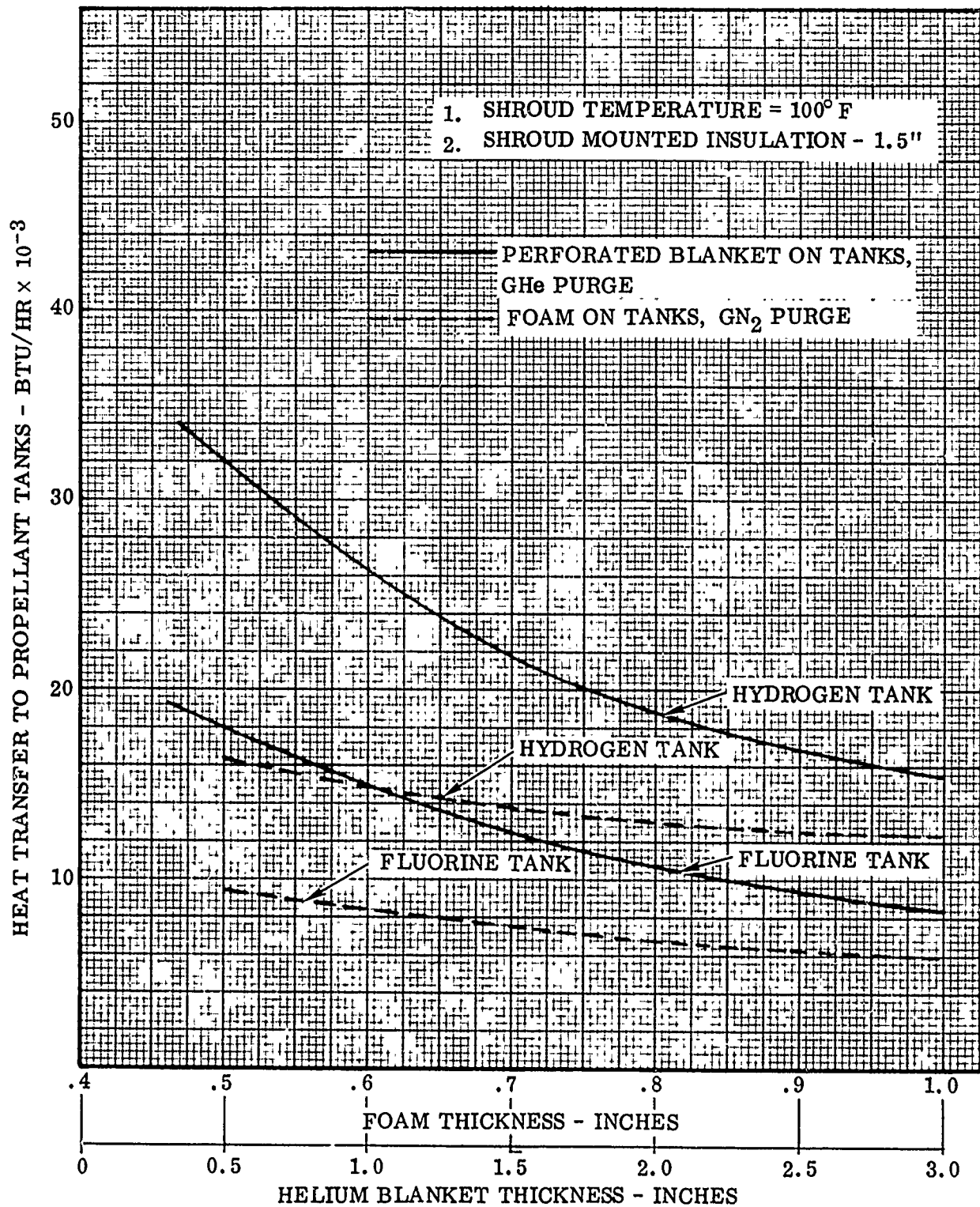
CONFIDENTIAL



(C) Figure 2-51. Propellant Tank Heat Transfer - Ground Conditions
(Tank-Mounted Insulation)

CONFIDENTIAL

CONFIDENTIAL



(C) Figure 2-52. Propellant Tank Heat Transfer - Ground Conditions
(Shroud-Mounted Insulation)

CONFIDENTIAL

CONFIDENTIAL

2.2.2.4 Thermal Analytical Parameters. The Superfloc was assumed throughout the analyses to be installed in three-blanket layers, and the insulation thickness was varied by varying the number of Superfloc layers per blanket. The shroud radiation properties of assumption c. correspond to the approximate values for currently available white paints after exposure to the high temperatures associated with boost phase aerodynamic heating. The superinsulation was assumed to be filled with conditioning gas during ground operation, and gaseous conduction was assumed to be the dominant mode of heat transfer within the insulation. In the analyses of configurations having shroud mounted superinsulation, a nominal insulation thickness of 1.5 inches was assumed for all ground performance applications. For these analyses, the shroud insulation thickness was not a thermally critical parameter affecting ground thermal control.

- a. Superfloc Performance. Superfloc effective conductance was evaluated as a composite of four separate, parallel contributing terms representing: (1) interlayer radiation, (2) radiation along gaps occurring at the juncture of insulation blankets, (3) conduction through the Superfloc tufts, and (4) conduction through the blanket mounting pins. The respective expressions, as derived in the following discussion and presented in Figure 2-53 were treated analytically as parallel heat paths; and lateral (normal to the heat-flow direction) temperature equilization was assumed to occur at the inner and outer surfaces of each blanket. Figure 2-54 presents a typical simplified thermal network in which the analytical expressions of Figure 2-53 were employed to generate the resultant propellant tank heating rates.

- (1) Radiation through Superfloc. Radiation through n parallel surfaces, each with equal areas, is computed by the expression

$$Q_r = \frac{F A \sigma (T_h^4 - T_c^4)}{(n - 1)} \quad (5)$$

where T_h and T_c are the temperatures of the hot and cold bounding layers respectively, and A is the mean area.

For cases where the surface emittances are constant,

$$F = (1/\epsilon_1 + 1/\epsilon_2 - 1)^{-1} \quad (6)$$

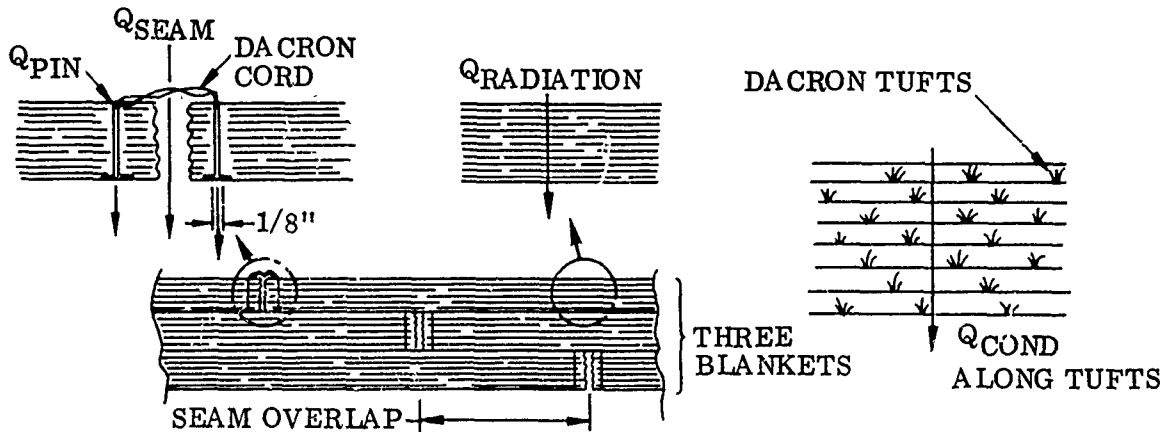
where ϵ_2 and ϵ_1 are the emittances of the aluminized mylar sheets with and without flocked tufts, respectively. In general, ϵ decreases with temperature. To determine an effective value of F for Superfloc, where the temperature gradient through the layers is not linear, equation 6 can be used if ϵ_1 and ϵ_2 are evaluated at an appropriate temperature. From test data for 15 layers of Superfloc, the mean temperature, T^* , is determined to be

$$T^* = 0.7 (T_h - T_c) + T_c \quad (7)$$

Extension of this relationship to $n > 15$ is assumed to be valid since the temperature profiles are assumed to be similar for $n > 15$.

CONFIDENTIAL

UNCLASSIFIED



$$Q_{RADIATION} = \frac{A\sigma}{\left(\frac{1}{\epsilon_1} + \frac{1}{\epsilon_2} - 1\right)(n-1)} (T_h^4 - T_c^4)$$

$$Q_{COND ALONG TUFTS} = (A/t) (3.32 \times 10^{-6}) (T_h - T_c)$$

$$Q_{SEAM} = t l f \sigma (T_h^4 - T_c^4)$$

$$Q_{PIN} = (k A_{pin}/t) (T_h - T_c)$$

(REF:

WHERE: A = AREA OF BLANKET (FT²)

n = NUMBER OF SUPERFLOCK LAYERS

t = BLANKET THICKNESS (FT)

l = TOTAL LENGTH OF SEAMS PER BLANKET (FT)

f = DIMENSIONLESS FUNCTION (GAP WIDTH TO DEPTH RATIO) FOR SUPERINSULATION SEAM HEAT LEAK

A_{PIN} = TOTAL CROSS SECTIONAL ATTACHMENT PIN AREA

k = FIBERGLASS ATTACHMENT PIN THERMAL CONDUCTIVITY (0.13 BTU/HR-FT-°R)

σ = STEFAN-BOLTZMANN'S CONSTANT, 0.1713 × 10⁻⁸ BTU/HR-FT²-°R⁴

ε = SUPERINSULATION LAYER EMITTANCE

SUBSCRIPTS

1 = SMOOTH SIDE OF SUPERINSULATION LAYER

2 = FLOCKED SIDE OF SUPERINSULATION LAYER

h = OUTER INSULATION LAYER

c = INNER INSULATION LAYER

Figure 2-53. Typical AMPS Superinsulation Lay-Up

UNCLASSIFIED

CONFIDENTIAL

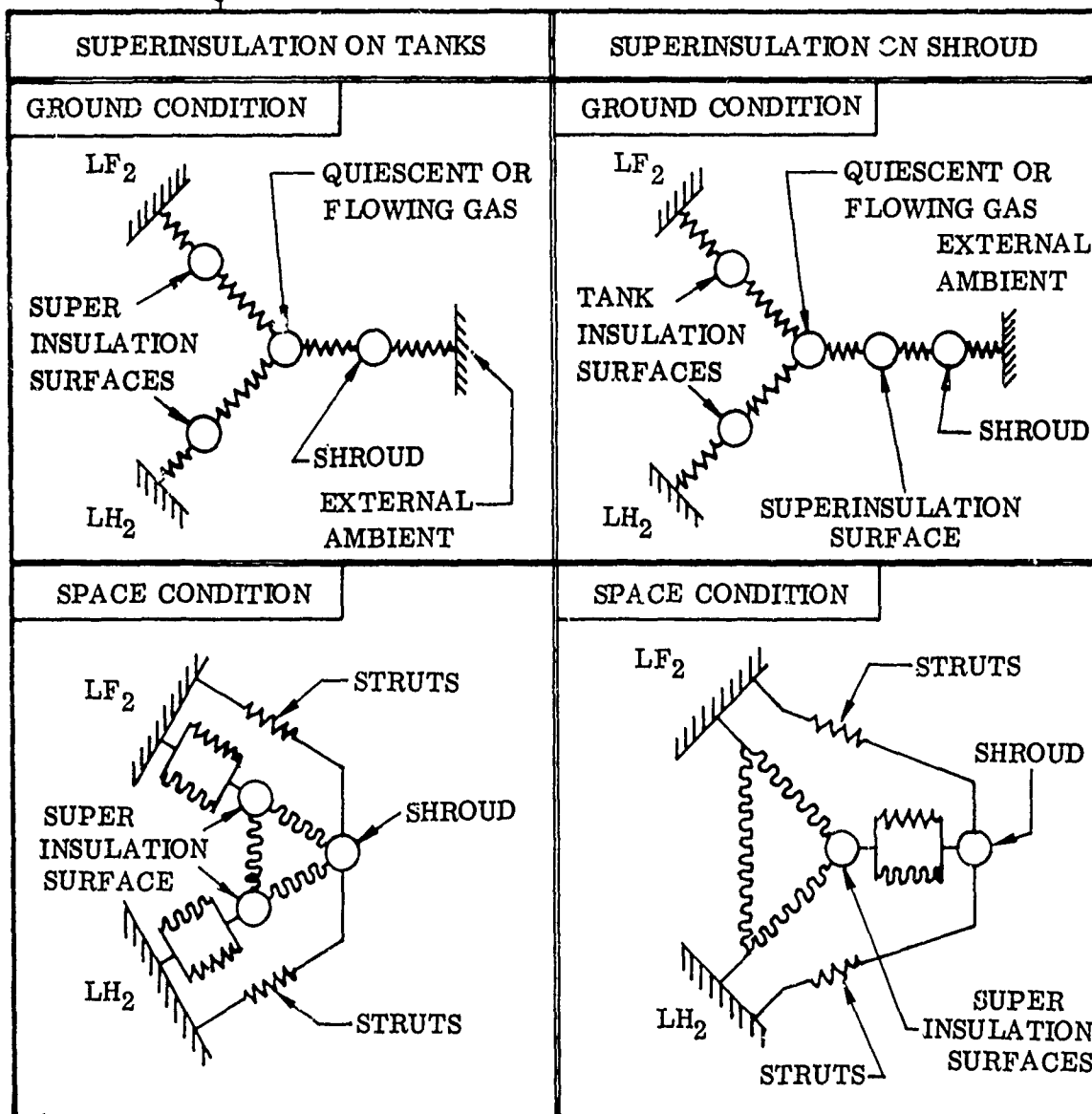
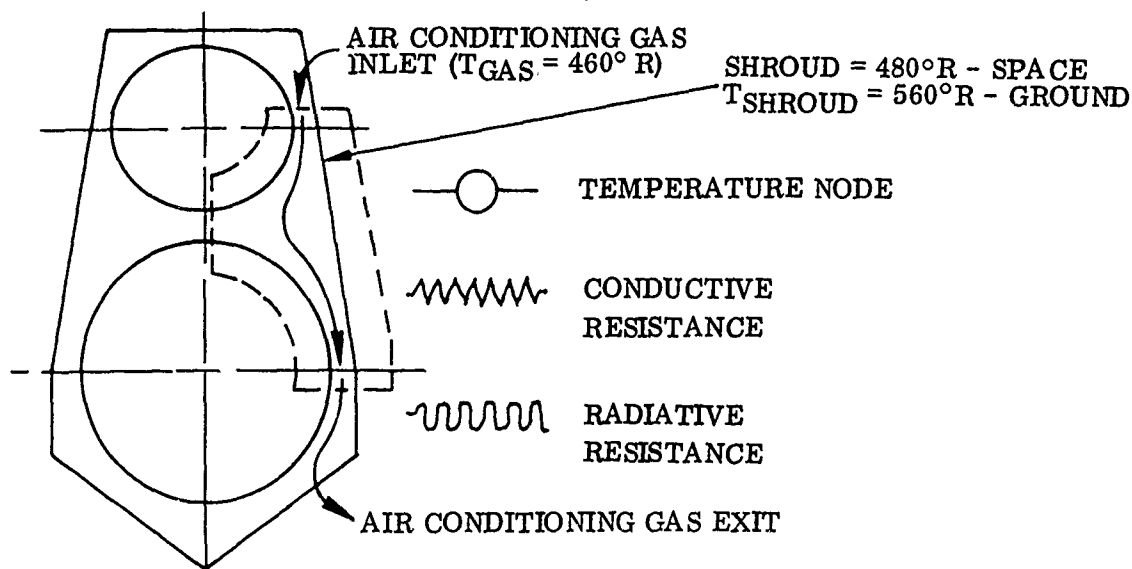


Figure 2-54. AMPS Superinsulation Optimization Analysis

CONFIDENTIAL

UNCLASSIFIED

a. Superfloc Performance (Continued)

(1) (Continued)

Reference 5 suggests an expression for determination of ϵ_2 knowing ϵ_1 , based on the ratio of unflocked aluminized mylar area to the tuft area (A_o/A_t):

$$\epsilon = \frac{A_t}{A_o} \epsilon_t + \frac{A_o - A_t}{A_o} \epsilon_1 \quad (8)$$

where the emittance of the Dacron tufts, ϵ_t , is assumed to be 1.0.

Test data for ϵ_1 together with equation 6 provide ϵ values for both sides of the mylar sheet which are plotted in Figure 2-55 as a function of sheet temperature. The function F is plotted, using equation 7, in Figure 2-56 as a function of T_h and T_c .

Incorporating the Superfloc density of 360 layers per foot, and expressing equation 1 as a resistance, we have

$$R_r = \frac{(T_h - T_c) (360 t - 1)}{A \sigma (T_h^4 - T_c^4)} \quad (9)$$

where R is in hr-°R/Btu, t is the thickness of the insulation blanket in feet, and A is the total area in ft².

(2) Conduction Through Superfloc Tufts. Reference 5 presents values of Q/A which are higher than can be explained by equation 5. The difference, assuming negligible residual gas conduction, must be due to thermal conduction through the Dacron tufts and other conductive heat paths. To express such a conduction phenomenon in usable form, it is necessary to determine a conductance which, when multiplied by the insulation-bounding temperature difference, and divided by the insulation blanket thickness, yields the desired difference between Q/A values. This conductance can be supposed to be dependent only upon temperature, as long as the Superfloc density remains 30 layers per inch. The temperature dependence can be represented by the thermal conductivity variation with temperature of Dacron, but unfortunately this information is currently unavailable. The conductance, determined to be 3.32×10^{-6} Btu/hr-ft-°R is therefore considered to be constant. This assumption is conservative.

No data are available concerning the performance of Superfloc at densities different than 30 layers per inch.

UNCLASSIFIED

UNCLASSIFIED

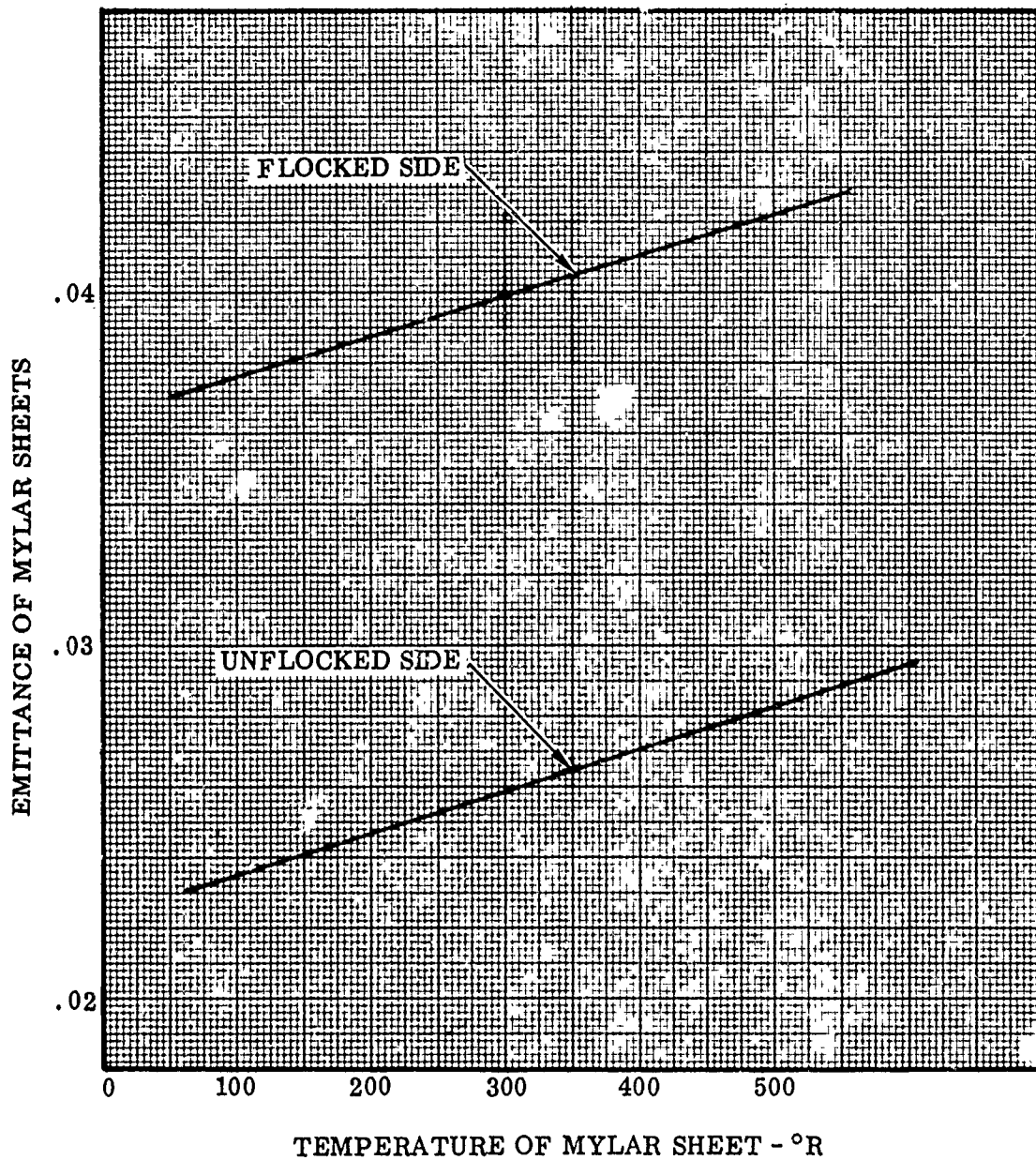


Figure 2-55. Emittance of Superfloc Mylar Sheets

UNCLASSIFIED

UNCLASSIFIED

$$F = \frac{1}{\frac{1}{\epsilon_1} + \frac{1}{\epsilon_2} - 1}$$

ϵ_1 AND ϵ_2 ARE EVALUATED AT T_* .

WHERE $T_* = (T_{HOT} - T_{COLD}) 0.7 + T_{COLD}$

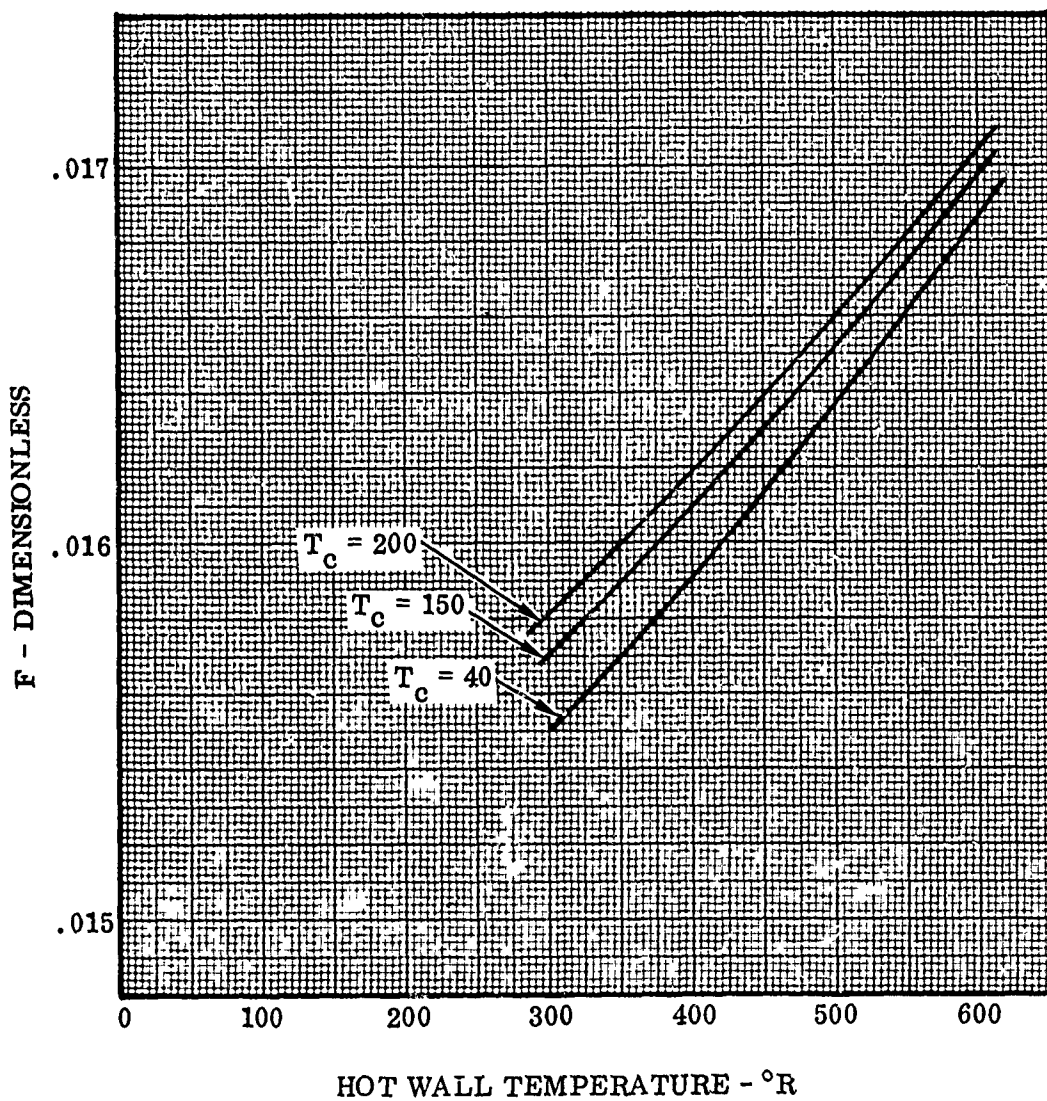


Figure 2-56. Overall Radiative Exchange Factor Between Parallel Shields With the Same Area but Different Emittance

UNCLASSIFIED

UNCLASSIFIED

a. Superfloc Performance (Continued)

(2) (Continued)

The equivalent resistance for conduction is

$$R_c = \frac{t}{A (3.32 \times 10^{-6})} \quad (10)$$

where R_c is in $\text{hr-}^\circ\text{R/Btu}$, t is in feet, and A is the total area in square feet. Since the heat paths represented by equations 9 and 10 are parallel, the resistances must be combined in this way.

- b. Seams and Pinned Connections. When Superfloc blanket edges are brought together to form a seam, radiation heat transfer occurs in the gap. This situation is analyzed in Reference 6. The resulting equation for tuft seams is

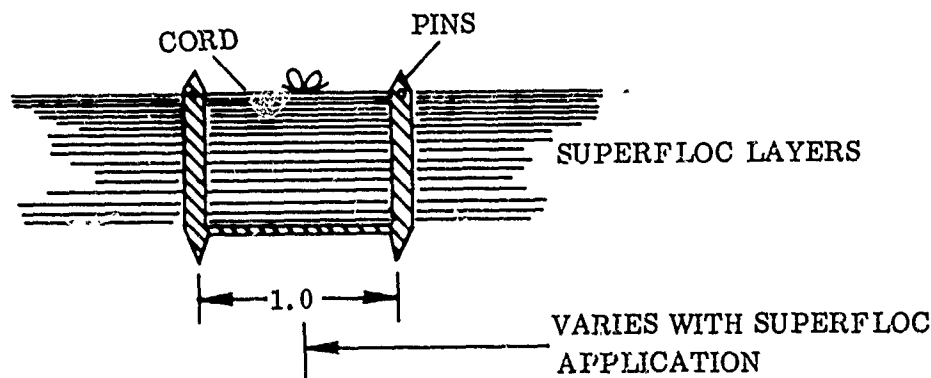
$$\frac{Q_s}{l} = t f \sigma (T_h^4 - T_c^4) \quad (11)$$

where Q_s/l is in $\text{Btu/hr per foot of seam}$, t is the seam depth in feet, and f is a dimensionless function of the butted joint width to depth ratio, δ/t , plotted in Figure 2-57. Written as a resistance, equation 11 is

$$R_s = \frac{T_h - T_c}{l t f \sigma (T_h^4 - T_c^4)} \quad (12)$$

where R_s is in $^\circ\text{R-hr/Btu}$.

Associated with the seams are fiberglass pins, occurring in pairs one inch apart, which hold the blankets together. The effect of these pins on tank heat transfer depends, in part, on the contact between the pins and the Superfloc layers.



UNCLASSIFIED

UNCLASSIFIED

$$q_c = t \sigma f (T_1^4 - T_2^4) - \text{BTU/HR (PER FOOT OF SEAM)}$$

WHERE t = THICKNESS OF BUTTED INSULATION BLANKETS (FT).

NOTE: THIS IS TO BE ADDED TO THE NORMAL S.I. HEAT TRANSFER.

REFERENCE: A.D. LITTLE REPORT 65008-00-04, OCT. 1964, "LIQUID PROPELLANT LOSSES DURING FLIGHT"

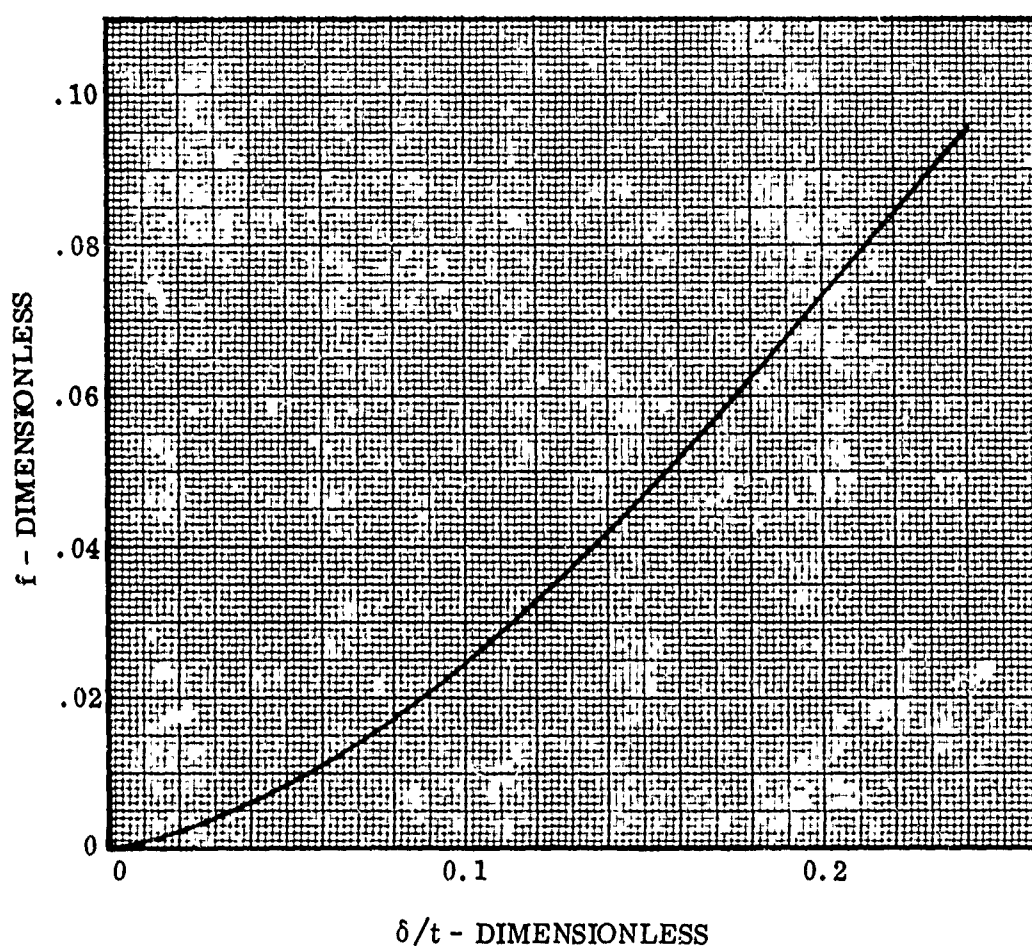


Figure 2-57. Dimensionless Function f (δ/t) for Computation of Superinsulation Seam Heat Leak

UNCLASSIFIED

UNCLASSIFIED

b. Seams and Pinned Connections (Continued)

For zero pin and layer contact, the pin temperature will not significantly affect the Superfloc, and heat transfer will occur solely by conduction through the pins. In this case the pin ends can be assumed to take on the temperature of the bounding layers.

When there is good contact between the pins and the layers, local heat transfer will occur because the conductance down the 0.1 inch diameter fiberglass pin and the conductance along the 1/4 mil aluminized mylar layers are the same order of magnitude. Heat will be conducted to the pins because at any given location the local layer temperature will always be higher than the local pin temperature, for equivalent bounding temperatures. A situation will then develop where the Superfloc layers close to the pins are cooler than the same layers at a great distance. A decrease in Superfloc heat transfer will result, offsetting to some degree the additional heating introduced to the pins from the adjacent layers. Lateral temperature equalization was assumed for this study (zero pin/layer contact).

As a first approximation it may be assumed, therefore, that with or without good layer to pin contact, the contribution to tank heating due to the pins is just conduction through the fiberglass pins. Because of poor contact at the pin ends, the ΔT across the pins may not be as great as the ΔT across the Superfloc blanket. It is conservative however, to consider it so.

Pin heat conduction can be computed using the following relation:

$$Q_p = \frac{k A_p (T_h - T_c)}{t} \quad (13)$$

where Q_p is in Btu/hr, A_p is the cross-sectional area of both pins, and t is the insulation thickness, or pin length. T_h and T_c are the hot and cold external Superfloc layer temperatures. The resistance is

$$R_p = \frac{t}{A_p k} \quad (14)$$

where R_p is in hr-°R/Btu.

- c. Struts (Tank Supports). AMPS tank struts, as currently designed, are tubular fiberglass members, attached directly to the shroud and the tanks. For tank mounted superinsulation there is approximately 5.0 inches of fiberglass strut next to the propellant tanks that is shielded from radiation from the shroud and outer superinsulation layer. In this length, very little heat transfer occurs at the strut surface, and the temperature gradient is linear.

The local strut temperature at the intersection of the strut and the outer layer of superinsulation can be determined by a fin analysis where radiation from the shroud occurs between $x = 0$ and $x = \ell$ in the model shown in Figure 2-58.

UNCLASSIFIED

CONFIDENTIAL

(U) c. Struts (Tank Supports) (Continued)

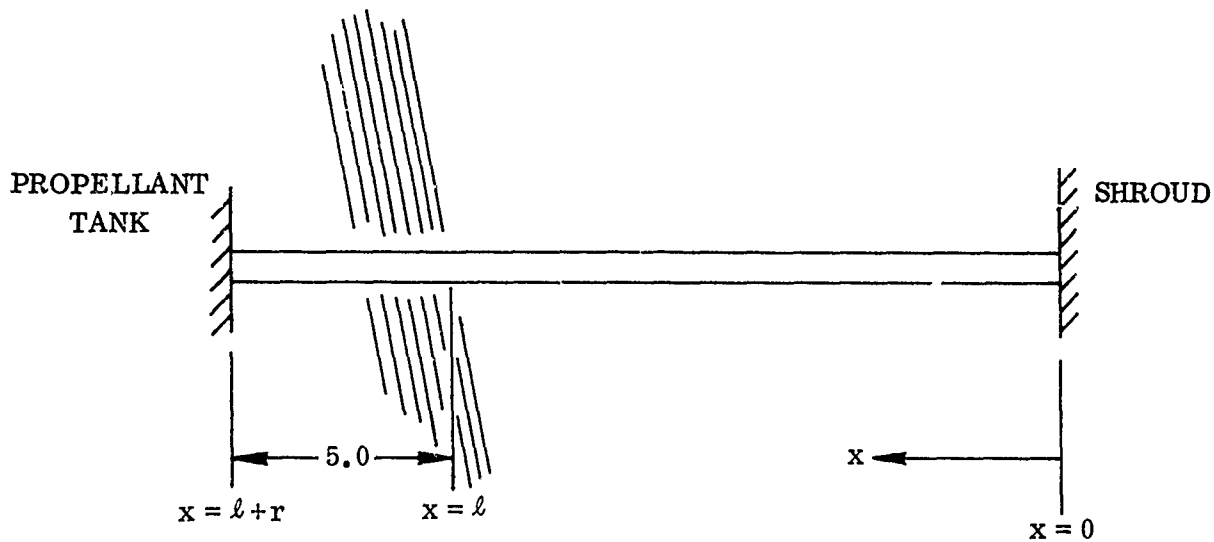


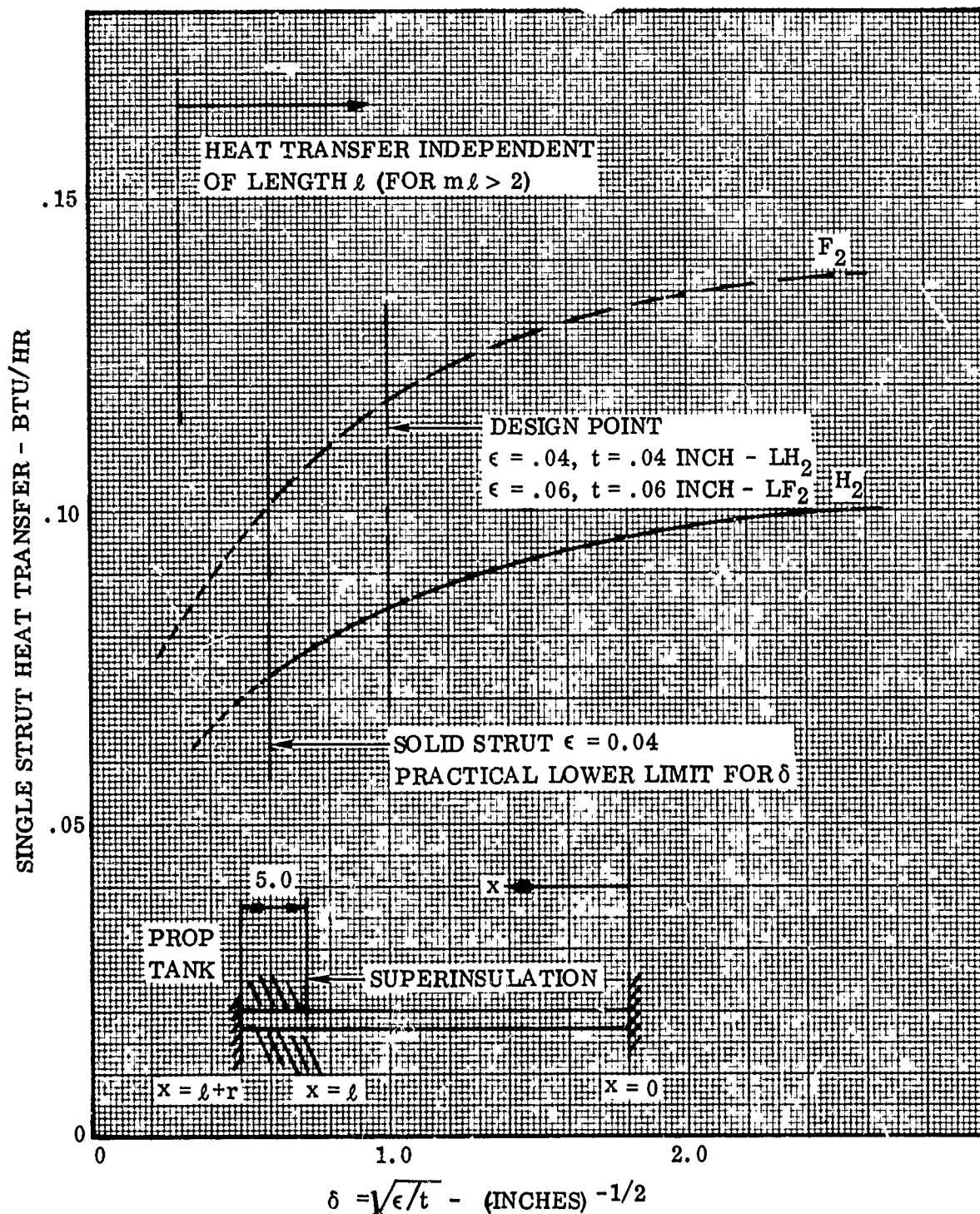
Figure 2-58. Local Strut Temperature Determination

- (C) Knowing T_ℓ , the temperature of the strut at $x = \ell$, strut heat transfer is easily computed and is shown in Figure 2-59. The value of T_ℓ depends on the radiation absorbed at the strut surface, a function of the surface area and emittance. Figure 2-59 is developed for constant mean thermal conductivity of fiberglass of 0.13 Btu/hr-ft-°R and constant cross-sectional area. The areas are based upon design configurations of 1.0 inch diameter and 0.04 inch wall thickness for the H₂ struts, and 1.25 inch diameter with 0.06 inch wall thickness for the F₂ struts.
- (U) Figure 2-60 shows the effect of insulating the strut. In the limit of a large number of layers, heat transfer is inversely proportional to the total length of the strut. Cooling of the struts with boiled-off propellant vapor is currently under investigation, but does not appear warranted for this application.
- (U) The above numbers are representative of the values that can be achieved on a given installation; however, for this analysis the strut heat leaks were determined by conservatively assuming the maximum temperature potential to occur across a strut length; as in Figure 2-61; corresponding to the strut section actually contained within the penetrated insulation blankets. The additional propellant tank heat leak due to the struts is shown on Figures 2-49 and 2-50.

CONFIDENTIAL

CONFIDENTIAL

CONSTANT CROSS SECTIONAL AREA SINGLE STRUT WRAPPING

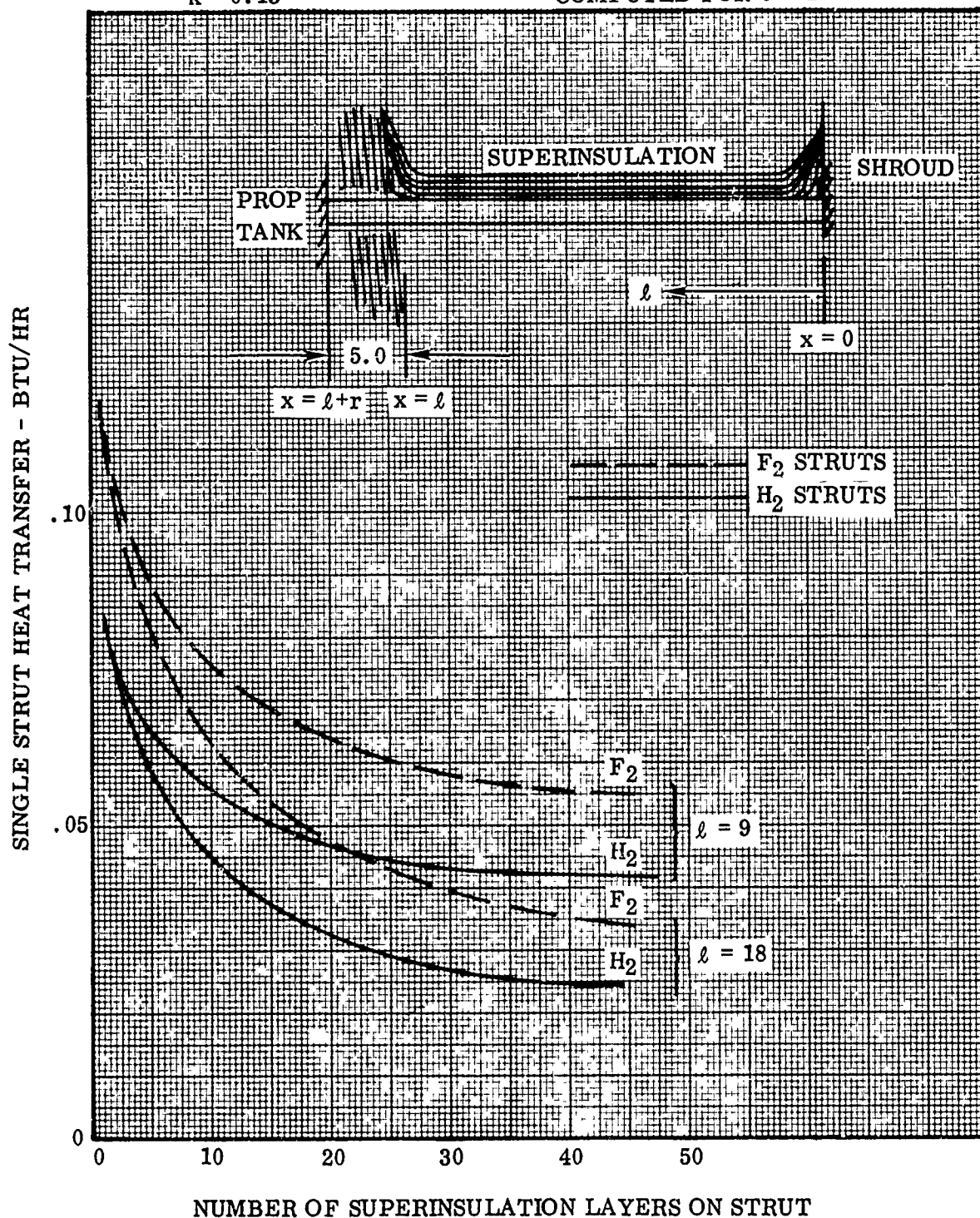


(C) Figure 2-59. Single Strut Heat Transfer Rates

CONFIDENTIAL

CONFIDENTIAL

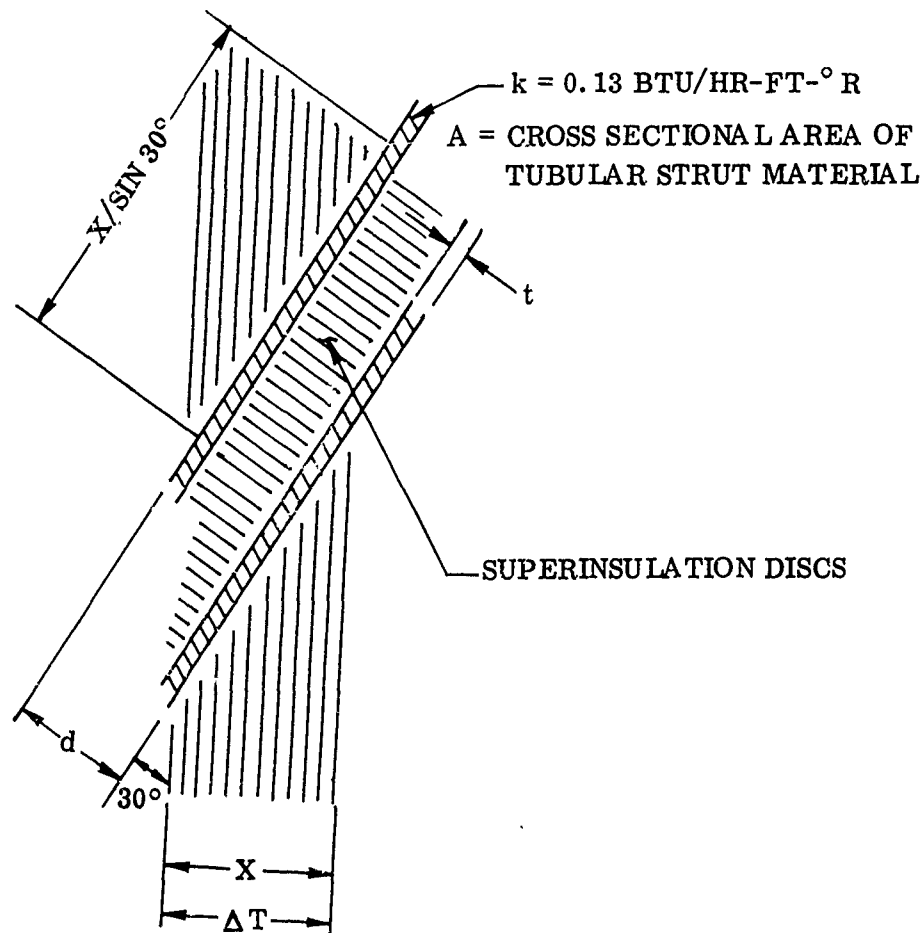
SUPERINSULATION APPLIED TO STRUT
SURFACE, CONSTANT CROSS SECTIONAL AREA
FIBERGLASS
 $k = 0.13$
VALUES AT $n = 1$
COMPUTED FOR $\delta = 1$



(C) Figure 2-60. Single Strut Heat Transfer

CONFIDENTIAL

CONFIDENTIAL



$$Q_{\text{STRUT}} = \frac{kA}{2X} \Delta T$$

STRUT PHYSICAL PARAMETERS

	LF ₂	LH ₂
d	1.25 IN.	1.00 IN.
t	0.06 IN.	0.04 IN.
ΔT	330°R	440°R
k	0.13 $\frac{\text{BTU}}{\text{HR-FT-}^\circ\text{R}}$	0.13 $\frac{\text{BTU}}{\text{HR-FT-}^\circ\text{R}}$

STRUT HEAT TRANSFER RATE

NUMBER OF TANK SI LAYERS	LH ₂ BTU/HR	LF ₂ BTU/HR
20	2.39	6.72
40	1.195	3.36
60	0.797	2.24
80	0.597	1.68

(C) Figure 2-61. AMPS Vehicle Tank Strut Configuration

CONFIDENTIAL

UNCLASSIFIED

2.2.2.5 Basis for Maximum Space Heating Assumptions. The surface-averaging assumptions, when used in conjunction with the shroud external surface radiation properties, lead to the incident heat rate values of assumption b. The resulting shroud temperatures would tend to maximize heat transfer from the shroud to the propellant tanks. This fact can be demonstrated by means of an idealized comparison of hypothetical, geometrically identical segments of cylindrically-configured shroud-tank combinations shown in Figure 2-62A and B.

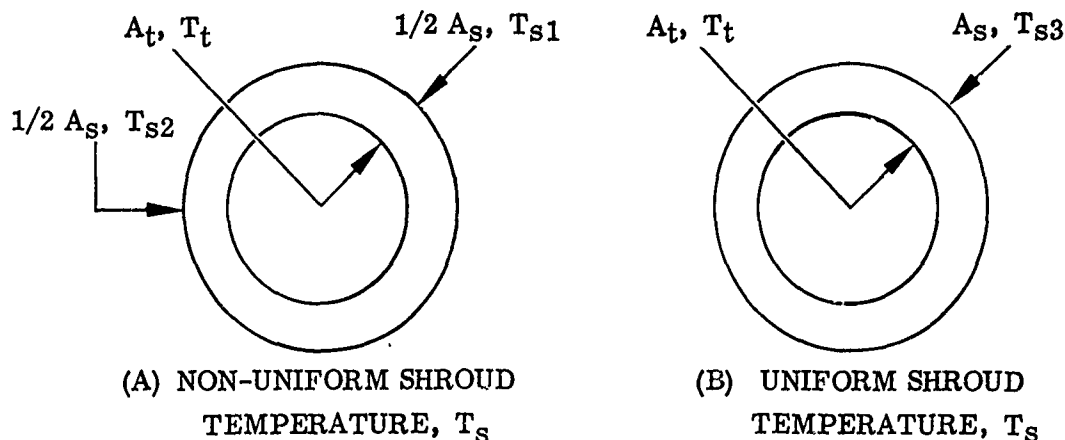


Figure 2-62. Cylindrically Configured Shroud-Tank Combinations

Let it be assumed that the volumetric envelopes of configurations (A) and (B) in Figure 2-62, are subjected to identical incident space heating rates, and that the respective interior/exterior emissivity and exterior solar absorptivity values are assumed to be identical. Since shroud temperatures must reside at or near conditions of thermal equilibrium (realistic for the AMPS application), it is readily seen that for equivalent reradiation to deep space, the following correspondence applies:

$$\frac{T_{s1}^4 + T_{s2}^4}{2} = T_{s3}^4 \quad (1)$$

If shroud-to-tank heat transfer is limited to the radiative mode in terms of shroud area (A_s), tank area (A_t), the identical radiation exchange factors ($\mathfrak{F}_{1t} = \mathfrak{F}_{2t} = \mathfrak{F}_{3t}$), and the Stefan-Boltzmann constant (σ); it follows that the shroud-tank heat transfer (Q_{tr}) for configuration (A)

$$(Q_{tr})_a = \sigma \mathfrak{F}_{1t} \frac{A_s}{2} (T_{s1}^4 - T_t^4) + \sigma \mathfrak{F}_{2t} \frac{A_s}{2} (T_{s2}^4 - T_t^4) \quad (2)$$

is equivalent to the corresponding shroud-tank heat transfer for configuration (B),

$$(Q_{tr})_b = \sigma \mathfrak{F}_{3t} A_s (T_{s3}^4 - T_t^4) \quad (3)$$

UNCLASSIFIED

UNCLASSIFIED

This is true because the fourth-power temperature equivalence of equation 1 applies. Total radiation heat transfer from shroud to tank is thus quantitatively independent of shroud temperature distribution, so long as total incident space heating remains unaltered.

Conductive heat transfer from shroud to tank in configurations A and B of Figure 2-62 would be related linearly to conductive resistances (R_{st} assumed identical for the two configurations), and to the respective skin temperatures. Since the constraint of equation 1 remains, the heat conduction for configuration A,

$$(Q_{tc})_a = \frac{\frac{T_{s1} + T_{s2}}{2} - T_t}{R_{st}} \quad (4)$$

is not equivalent to the heat conduction for configuration B:

$$(Q_{tc})_b = \frac{T_{s3} - T_t}{R_{st}} = \frac{\left(\frac{T_{s1}^4 + T_{s2}^4}{2}\right)^{1/4} - T_t}{R_{st}} \quad (5)$$

If it is postulated that in configuration A, T_{s2} can be related to T_{s1} , such that

$$T_{s2} = n T_{s1} \quad (6)$$

A comparative evaluation of the respective conduction heat rates can be expressed as

$$(Q_{tc})_b - (Q_{tc})_a = \frac{T_{s1}}{R_{st}} \left[\left(\frac{1 + n^4}{2} \right)^{1/4} - \frac{1 + n}{2} \right] \quad (7)$$

It is seen that subject to the constraints of equation 1, heat conduction in configuration B exceeds the heat conduction in configuration A for all values of $n \neq 1$ (equation 7). Employment of the uniform shroud temperature distribution of 480°R thus assures maximum propellant tank heat transfer rates.

UNCLASSIFIED

CONFIDENTIAL

(C) 2.2.3 PERFORMANCE TRADE-OFFS. In order to evaluate the performance of the AMPS as a function of the insulation system, a study was conducted to provide information on the in-orbit performance loss (in terms of ΔV) as a function of the rate of fuel (LH_2) boiloff and a change in the gross inert weight of the AMPS vehicle. It was assumed that no fluorine boiloff occurs and that the LH_2 boiloff is adequately predictable to exclude the possibility of excess LF_2 residual. This would be accomplished by some initial loading of excess hydrogen coupled with a propellant utilization system.

(C) Figures 2-63 through 2-65 illustrate the results of this study for the following three missions that exemplify the range of the AMPS capabilities:

- a. Mission number 1. A single burn, utilizing all of the remaining impulse propellants, after a 14-day, in-orbit residency period
- b. Mission number 2. A single burn preceding the 14-day residency requirement utilizing 90 percent of the impulse propellants, with a second burn using all of the impulse propellants remaining after the 14-day coast
- c. Mission number 3. 31 burns of equal impulsive magnitude distributed evenly over the 14-day, in-orbit residency period, i.e., a single burn every 10.8 hours, approximately.

(U) The performance-penalty calculations were referenced to the nominal, ideal velocity increment available for the various missions. The specific impulse of the engine and the vehicle mass ratio, in conjunction with the logarithmic rocket equation, were used for the nominal and the off-nominal cases to yield the respective performance penalties. Table 2-4 shows a list of the basic performance data used for the nominal performance capabilities of the AMPS vehicle, as obtained from Reference 7.

(C) The nominal in-orbit performance capability (initial incremental velocity available) of the AMPS vehicle, based on the data in Table 2-4, for the various missions are as follows:

<u>MISSION</u>	<u>ΔV CAPABILITY</u>
No. 1	22,435 fps
No. 2	21,958
No. 3	22,080

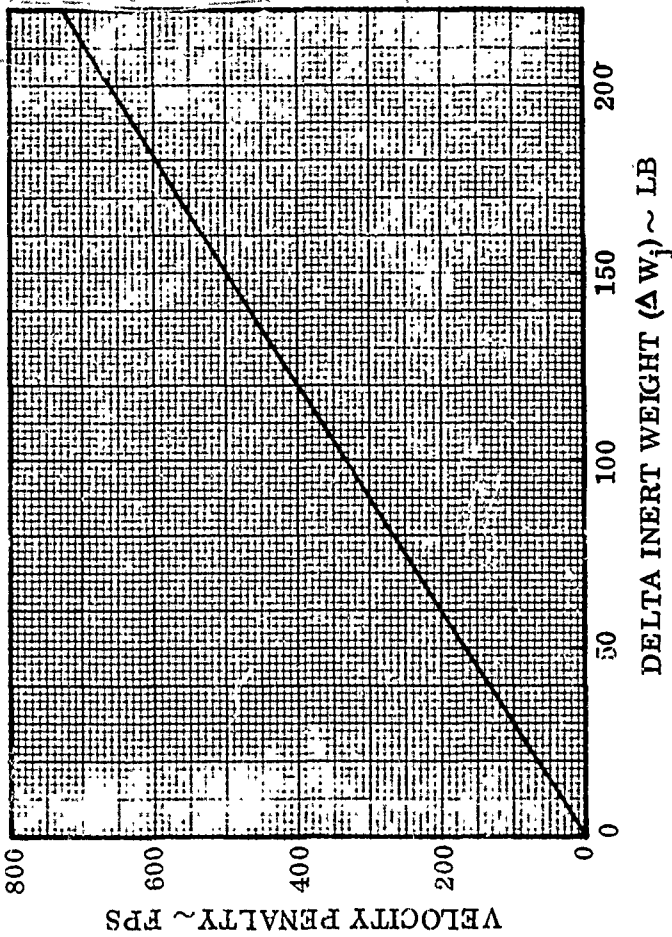
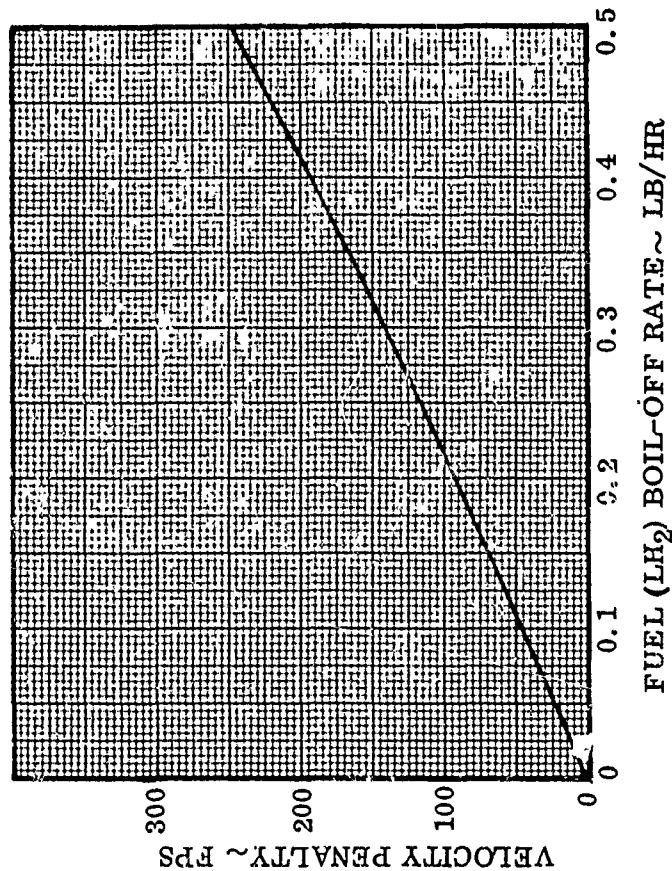
The difference in the ideal ΔV of the three missions is a result of the usage of the reaction control propellants which are assumed to be used at a constant rate throughout the 14-day mission.

CONFIDENTIAL

CONFIDENTIAL

MISSION: SINGLE BURN AFTER 14 DAY (336 HR) ORBIT COAST

- NOTES: 1. ORBIT START AMPS GROSS WEIGHT 20,000 LB
2. 2,000 LB PAYLOAD
3. SPECIFIC IMPULSE 460 SEC
4. BURN MIXTURE RATIO (OXIDIZER/FUEL) 12.1
5. ZERO OXIDIZER BOIL-OFF AND RESIDUALS



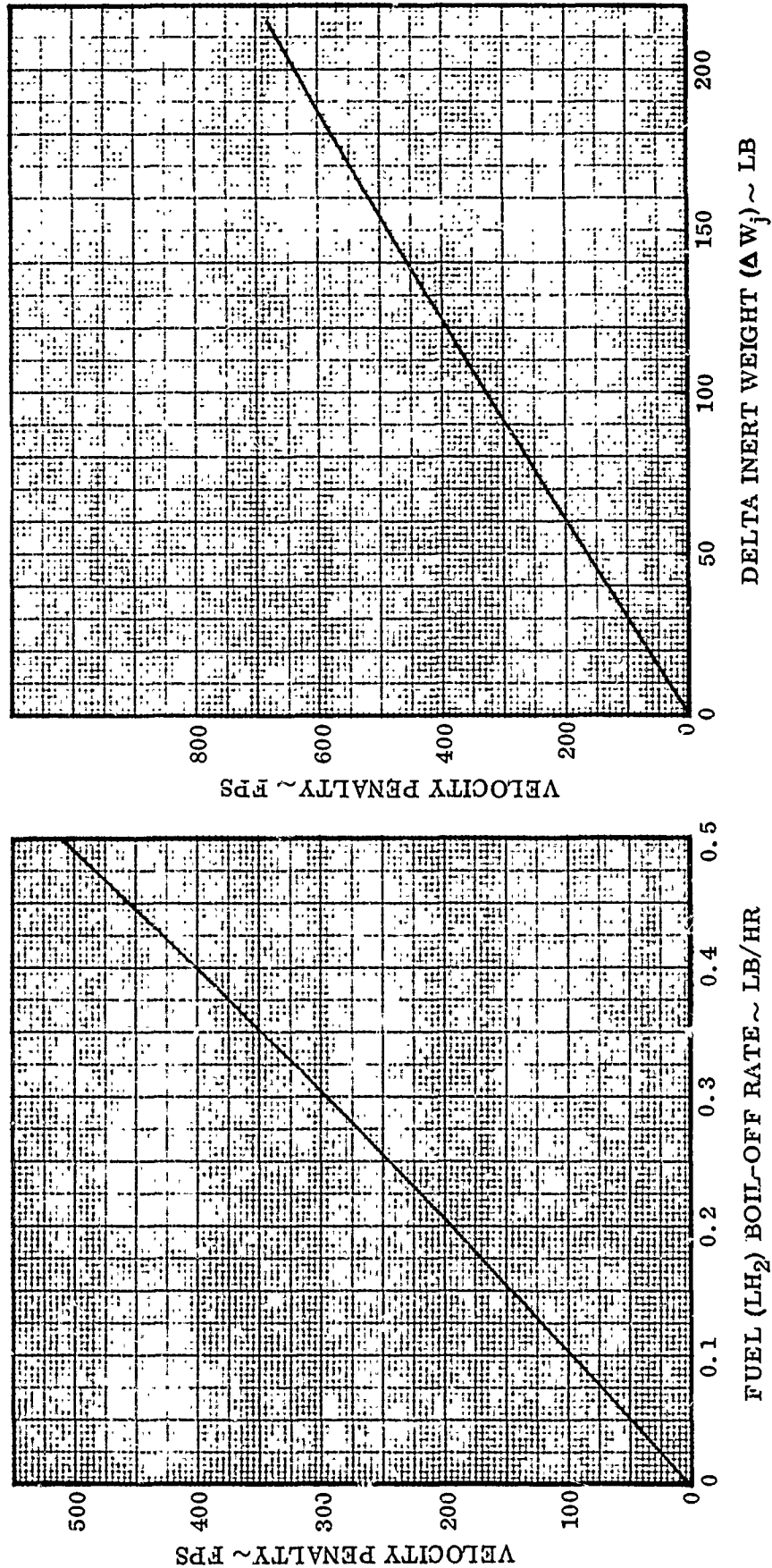
(C) Figure 2-63. AMPS Performance Penalties: Mission Number 1

CONFIDENTIAL

CONFIDENTIAL

MISSION: 90 PERCENT BURN - 14 DAY (336 HR) ORBIT COAST - 10 PERCENT BURN

- NOTES: 1. ORBIT START AMPS GROSS WEIGHT 20,000 LB
2. 2,000 LB PAYLOAD
3. SPECIFIC IMPULSE 460 SEC
4. BURN MIXTURE RATIO (OXIDIZER/FUEL) 12:1
5. ZERO OXIDIZER BOIL-OFF AND RESIDUALS



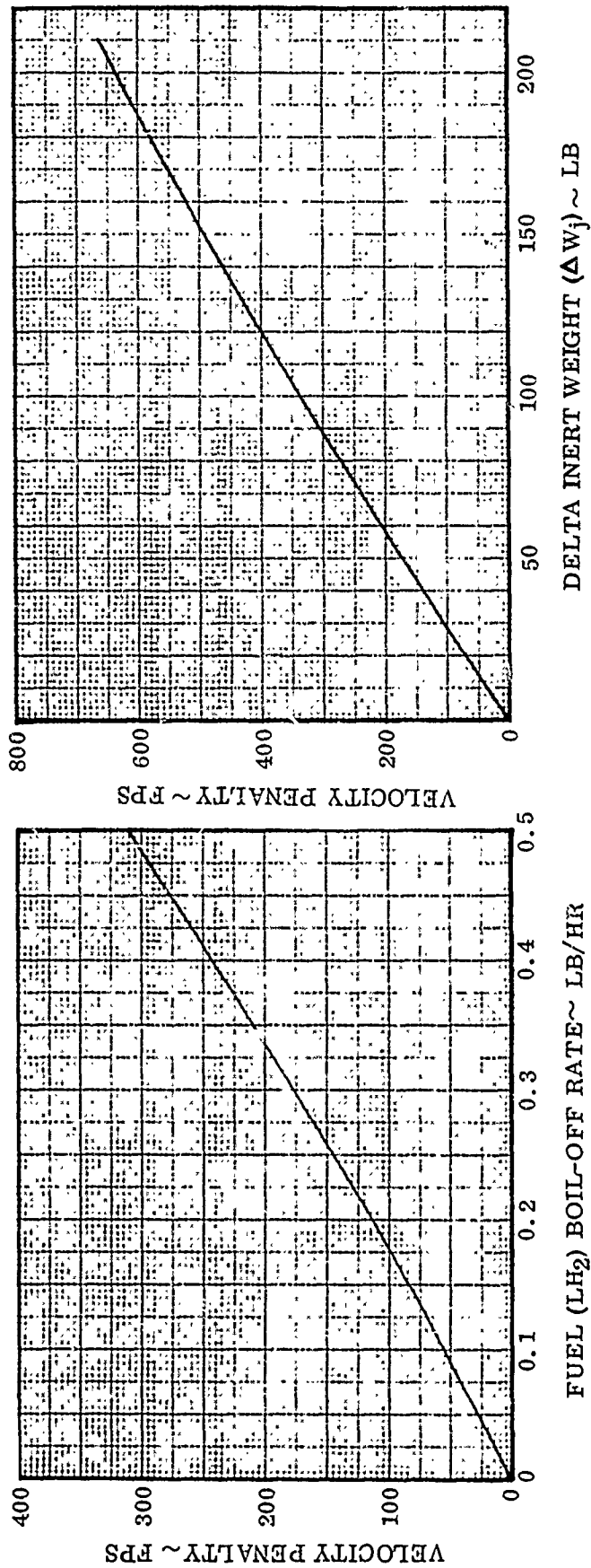
(C) Figure 2-64. AMPS Performance Penalties: Mission Number 2

CONFIDENTIAL

CONFIDENTIAL

MISSION: 31 EQUAL BURNS DURING 14 DAY ORBIT RESIDENCY
(1 BURN EVERY 10.8 HRS)

- NOTES: 1. ORBIT START AMPS GROSS WEIGHT 20,000 LB
2. 2,000 LB PAYLOAD
3. SPECIFIC IMPULSE 460 SEC
4. BURN MIXTURE RATIO (OXIDIZER/FUEL) 12:1
5. ZERO OXIDIZER BOIL-OFF AND RESIDUALS



(C) Figure 2-65. AMPS Performance Penalties: Mission Number 3

CONFIDENTIAL

CONFIDENTIAL

(C) TABLE 2-4. PERFORMANCE BASIS (14-DAY MISSION)

<u>Propulsion:</u>	
Propellants	
Fuel	LH ₂
Oxidizer	LF ₂
Burn Mixture Ratio (constant)	
Oxidizer/Fuel	12:1
Specific Impulse (constant)	460 sec
<u>Weights: (in pounds)</u>	
Propellants (usable)	
Fuel	1, 184
Oxidizer	14, 209
Stage Inert (total wet)	2, 332
Reaction Control System (RCS)	275
Propellant	
Payload	2, 000
Gross Weight (constant)	20, 000

(C) As seen in the performance basis listed above, the burn mixture ratio was assumed to be invariant throughout this analysis, and hence the specific impulse is kept at the constant value of 460 seconds. Once fuel boiloff is considered, oxidizer residuals remain as unused quantities. For example, for every pound of LH₂ that boils off, 12 pounds of potentially usable LF₂ remains. This causes excessive penalties to overall performance, therefore the constraint that no usable oxidizer propellants are to remain, was added and used throughout this study. To realize this constraint and to remain within the ground rules of a constant burn mixture ratio and gross weight vehicle in orbit, the following method was used to determine the performance penalties due to fuel boiloff:

- Step 1 Select a total fuel boiloff amount for the mission.
- Step 2 Bias the fuel tank (by adding to the fuel tank) by the amount of fuel boiloff to keep the burn mixture ratio at 12:1 (oxidizer/fuel) and decrease the usable oxidizer proportionally to keep the gross weight at 20, 000 pounds.

CONFIDENTIAL

CONFIDENTIAL

(C) Step 3 Enlarge the fuel tank to handle the extra propellant proportional to the volume of this "biasing" fuel. This, of course, increases the stage inert weight.

Step 4 Decrease the amount of usable oxidizer by the amount of increase in the stage inert weight due to Step 3 above, in order to keep the gross weight of the vehicle at 20,000 pounds.

Step 5 Note that Steps 2 and 4 above, in conjunction with the constant mixture ratio constraint, cause a residual fuel to now exist. Therefore, assume that the resulting fuel residual is also boiled off and add this amount to the original selected in Step 1 above.

Step 6 Iterate the above five steps until a specified tolerance on the various parameters is met.

(U) Figure 2-66 was utilized for the variation of stage inert weight with additional LH₂ tanking (Step 3 of the above method). It is noted that by decreasing the amount of usable oxidizer (in Steps 2 and 4), any corresponding decrease in oxidizer tank size was assumed to be negligible in this study.

(C) The results of the above methodology are shown in Figures 2-63 through 2-65 for the three missions, by describing the incremental velocity penalty* as a function of the fuel boiloff rate in pound/hour during the 14-day orbit residency period. Due to the number of calculations required, Reference 8 was used for the performance tradeoffs of Mission 3 (Figure 2-65) per the same methodology described above.

(U) Through an analysis similar to the one described above, the performance penalties due to a change in the gross (wet) inert weight of the AMPS vehicle may be calculated. These results are also summarized for the various missions examined.

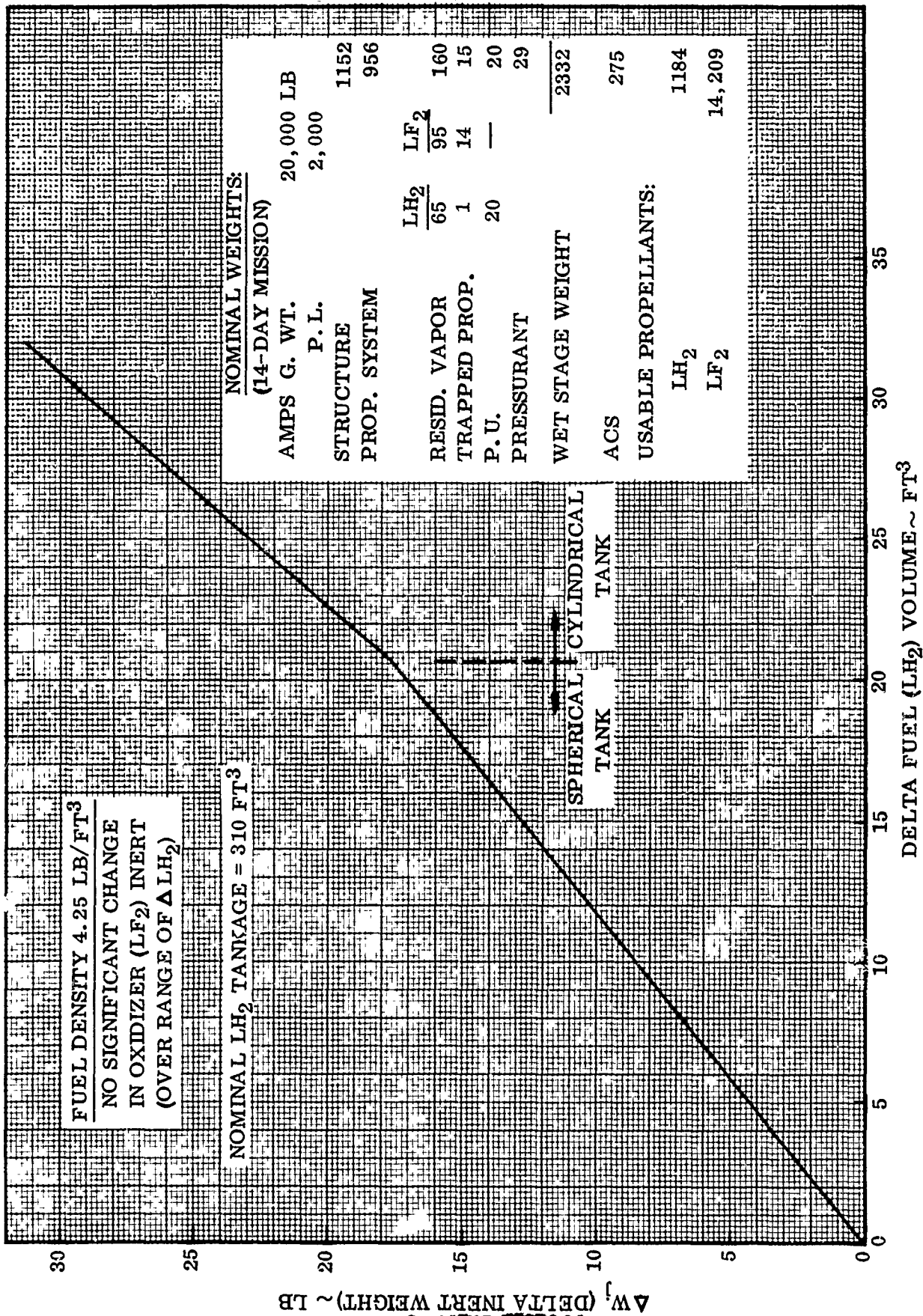
(U) Although this study was based on a specific AMPS vehicle design, it is felt that small changes in such parameters as the nominal propellant loadings and the structural weights will not significantly affect the final results of this analysis. Significant changes in these parameters (larger than about ± 10 percent), however, may warrant reinvestigation of the results of this report.

(C) 2.2.4 INSULATION THICKNESS OPTIMIZATION. The results of the weights analysis and the thermal performance analysis were combined with the performance tradeoff factors to establish ΔV penalty as a function of type of mission, location of superinsulation (tank or shroud), and number of layers of insulation. The results are shown in Figures 2-67 and 2-68 for a 14-day mission duration. The ΔV penalty is referenced from the initial incremental velocity available from Section 2.2.3.

*As referenced to the nominal ΔV 's listed herein.

CONFIDENTIAL

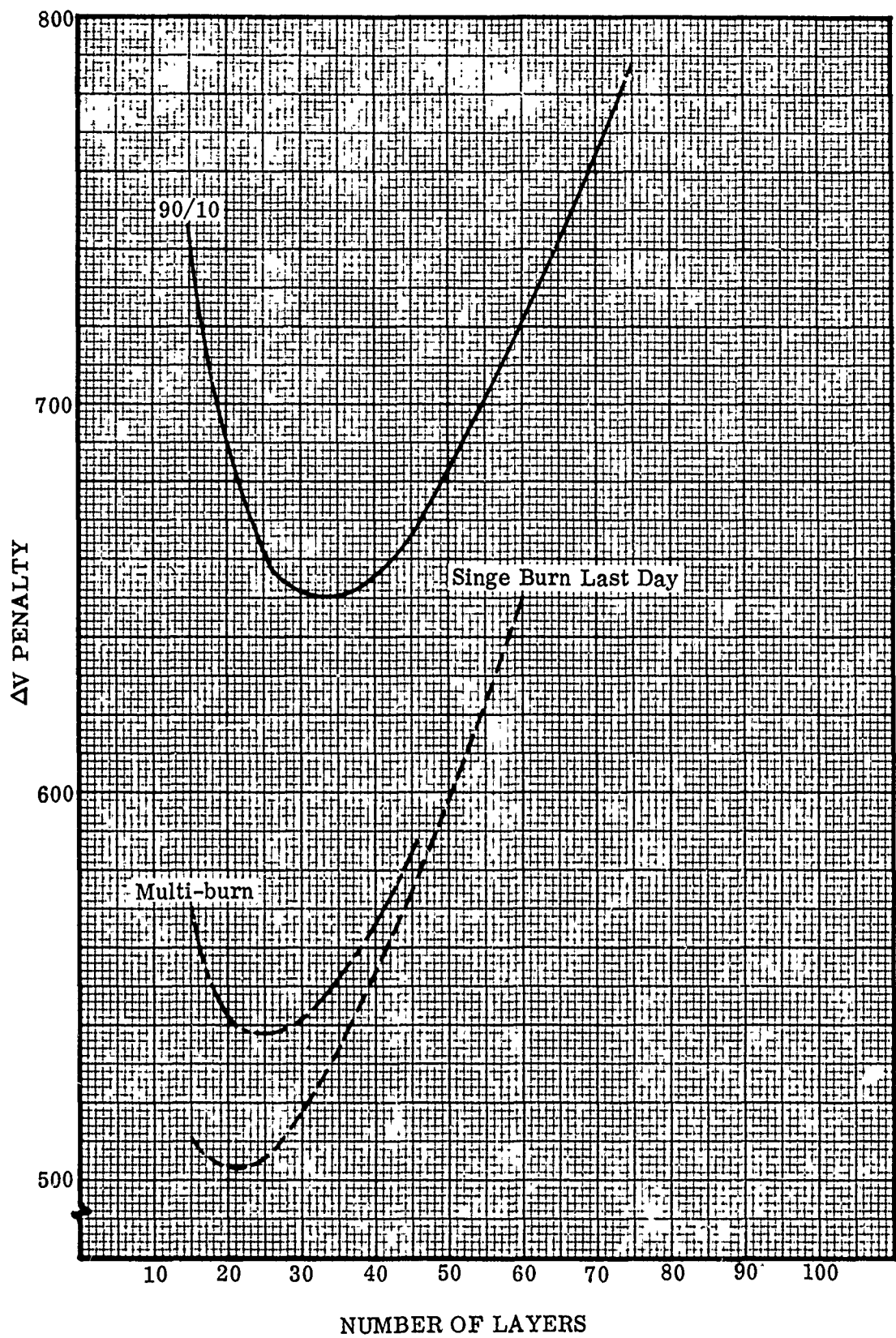
CONFIDENTIAL



(C) Figure 2-66. AMPS Fuel Tank Inert Weight Variance

CONFIDENTIAL

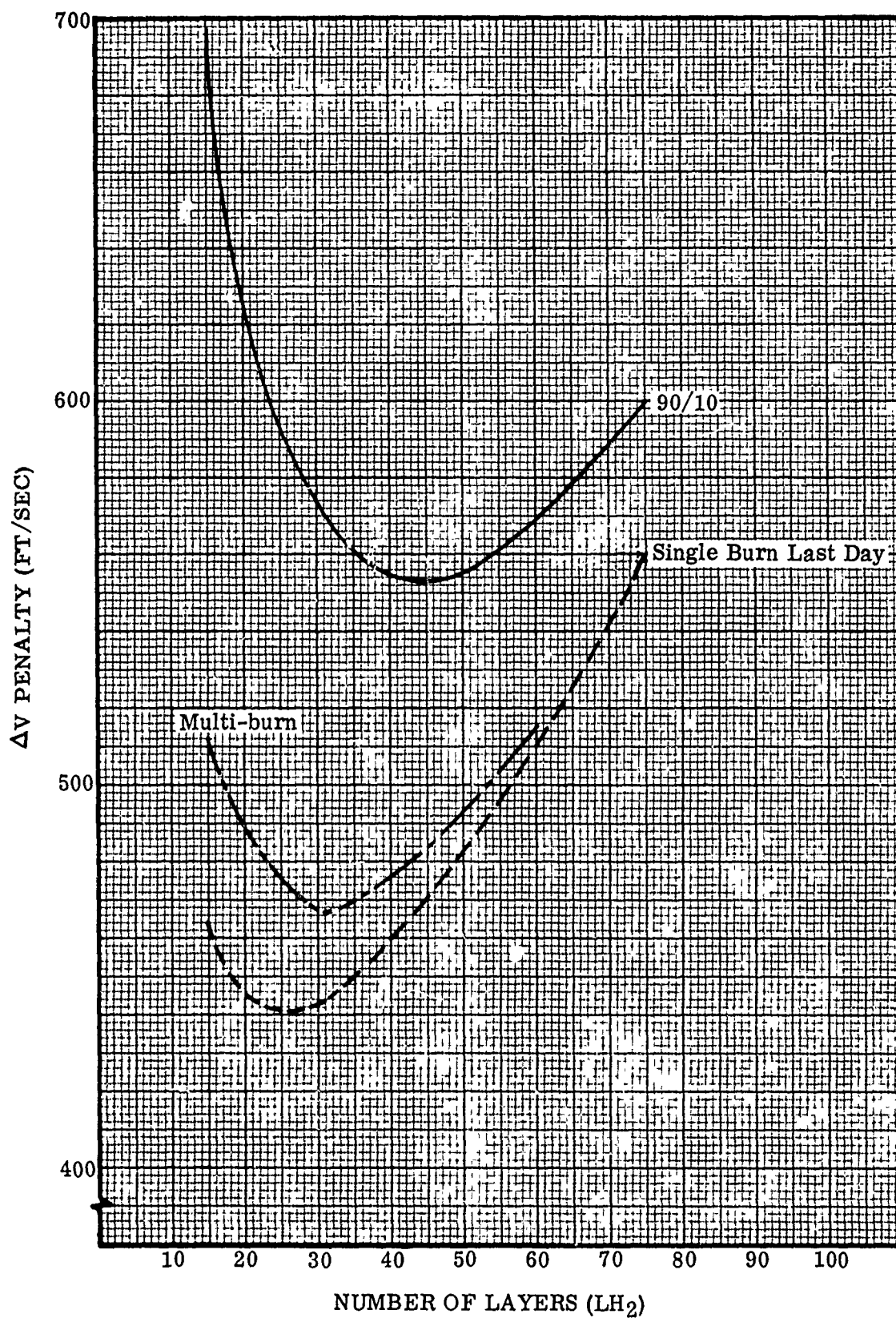
CONFIDENTIAL



(C) Figure 2-67. Shroud Mounted Insulation 14 Day Mission

CONFIDENTIAL

CONFIDENTIAL



(C) Figure 2-68. Tank Mounted Insulation 14 Day Mission

CONFIDENTIAL

CONFIDENTIAL

(C) 2.2.4.1 Shroud Mounted Insulation System. Figure 2-67 shows the results of the thickness optimization study for the shroud mounted insulation system. The optimum number of layers for the various missions specified is as follows:

<u>Mission</u>	<u>Number of Layers</u>
90/10	33
Single burn last day	21
Multi-burn equally spaced	24

As would be expected, as the mission becomes more severe from a LH₂ boiloff point of view, (i.e., 90/10 mission) the optimum number of layers increases. This is due to the fact that the sensitivity to thermal performance becomes greater, while the sensitivity to inert weight increase is essentially unaffected by type of mission.

(C) 2.2.4.2 Tank Mounted Insulation System. The weights used for the tank mounted insulation system are based on equal heat leak to the LF₂ and LH₂ tank rather than equal number of layers on each tank. It can be shown that the relationship between heat absorbed and mass of propellant lost by boiloff is:

$$\dot{Q}_t = \dot{m}g \left[\frac{e_g}{(\epsilon - 1)} + h_g - e_L \frac{\epsilon}{\epsilon - 1} \right]$$

where

$$\epsilon = \rho_L / \rho_v$$

$\dot{m}g$ = vent mass flow rate lb/hr

\dot{Q}_t = total tank heating BTU/hr

h_g = enthalpy of vent gas BTU/lb

e_g = internal energy of ullage vapor BTU/lb

e_L = internal energy of tank liquid BTU/lb

ρ_L = density of liquid lb/ft³

ρ_v = density of ullage vapor lb/ft³

For saturated hydrogen at 46 psia, the above relationship results in

$$\dot{m}g = 0.00536 \dot{Q}_t$$

CONFIDENTIAL

CONFIDENTIAL

(C) The optimum design point will be to have LF_2 heating rates equal to the cooling capacity of the hydrogen ventage. This would result in a maximum allowable heating rate to the fluorine tank of $1.2 Q_{H_2}$. To allow some design margin the fluorine tank insulation thickness is based on allowing equal heat transfer to that of the hydrogen tank (i.e., $Q_{LH_2} = Q_{LF_2}$). The resulting system weight is shown in Figures 2-69 and 2-70. Figure 2-70 shows the difference in insulation system weight when basing it on equal heat leak rather than equal number of layers. The resulting ΔV penalty as a function of layers on the LH_2 tank is shown in Figure 2-68. The minimum ΔV penalty occurs with the following number of layers:

Mission	LH_2 Layers	LF_2 Layers
90/10	48	35
Single burn last day	27	18
Multi-burn - equally spaced	30	20

(C) 2.2.4.3 Comparative Performance. The difference in tank mounted and shroud mounted performance for the various missions at their optimum points is summarized in Table 2-5.

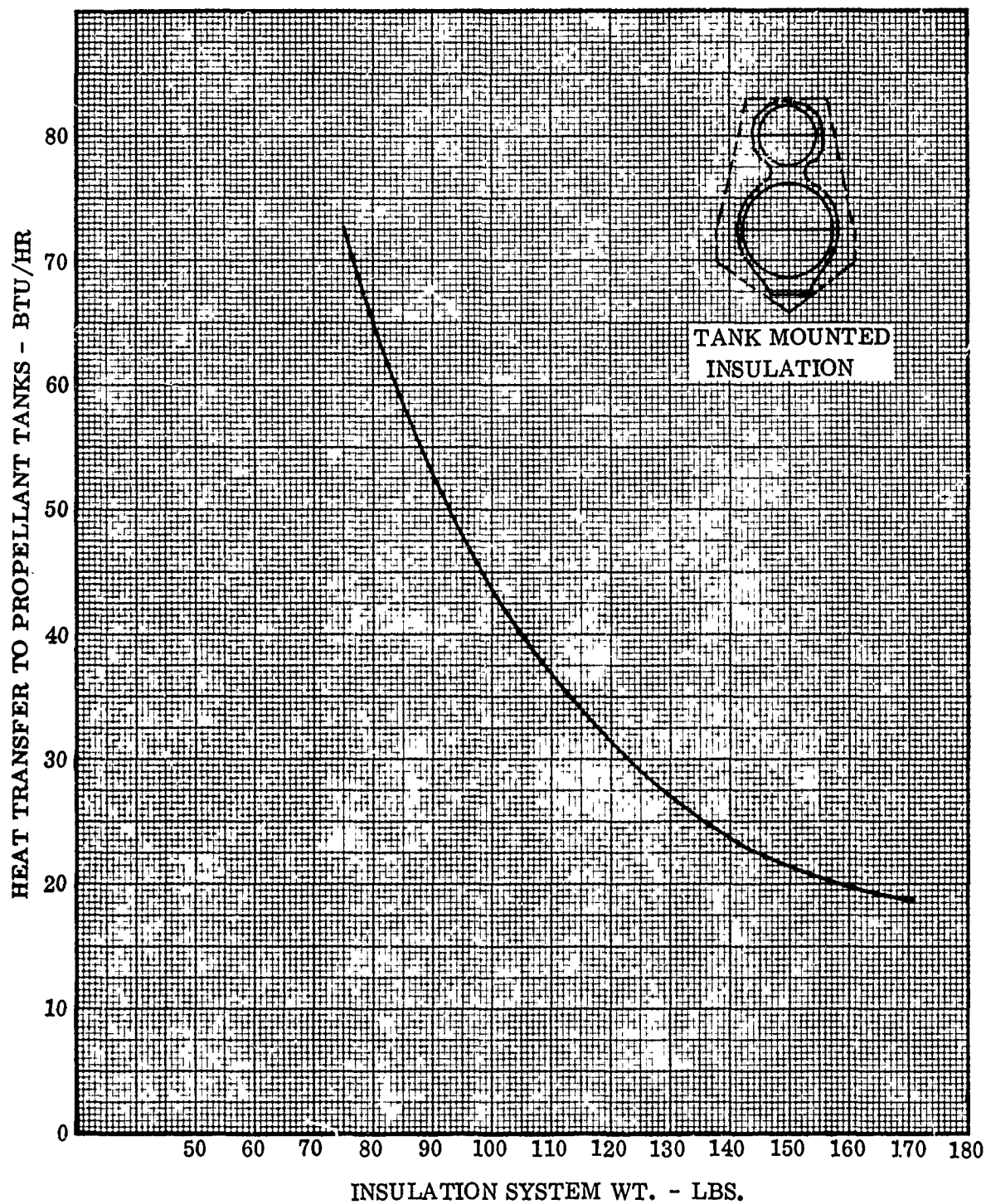
TABLE 2-5. COMPARATIVE MISSION PERFORMANCE

Mission	Velocity Penalty		
	Tank Mounted	Shroud Mounted	Difference
90/10	553	651	98
Single burn last day	442	503	61
Multi-burn	466	538	72

(C) These performance differences are not particularly significant, representing less than 0.5 percent of the total available ΔV ; however, as mission duration increases the spread in performance between the two installation techniques also increases. A calculation was made to determine the difference for a 42 day space residence time to obtain an indication of the performance penalties as a function of time in orbit. The extended residence was limited to 42 days rather than 180 days to allow the use of the performance tradeoff factors calculated for the 14-day mission. The difference in performance penalty for the 90/10 mission increased from the 98 ft/sec for the 14-day mission to approximately 180 ft/sec for the 45-day mission. The significant factor is that the performance advantage of the tank mounted insulation system increases with increased mission duration.

CONFIDENTIAL

CONFIDENTIAL

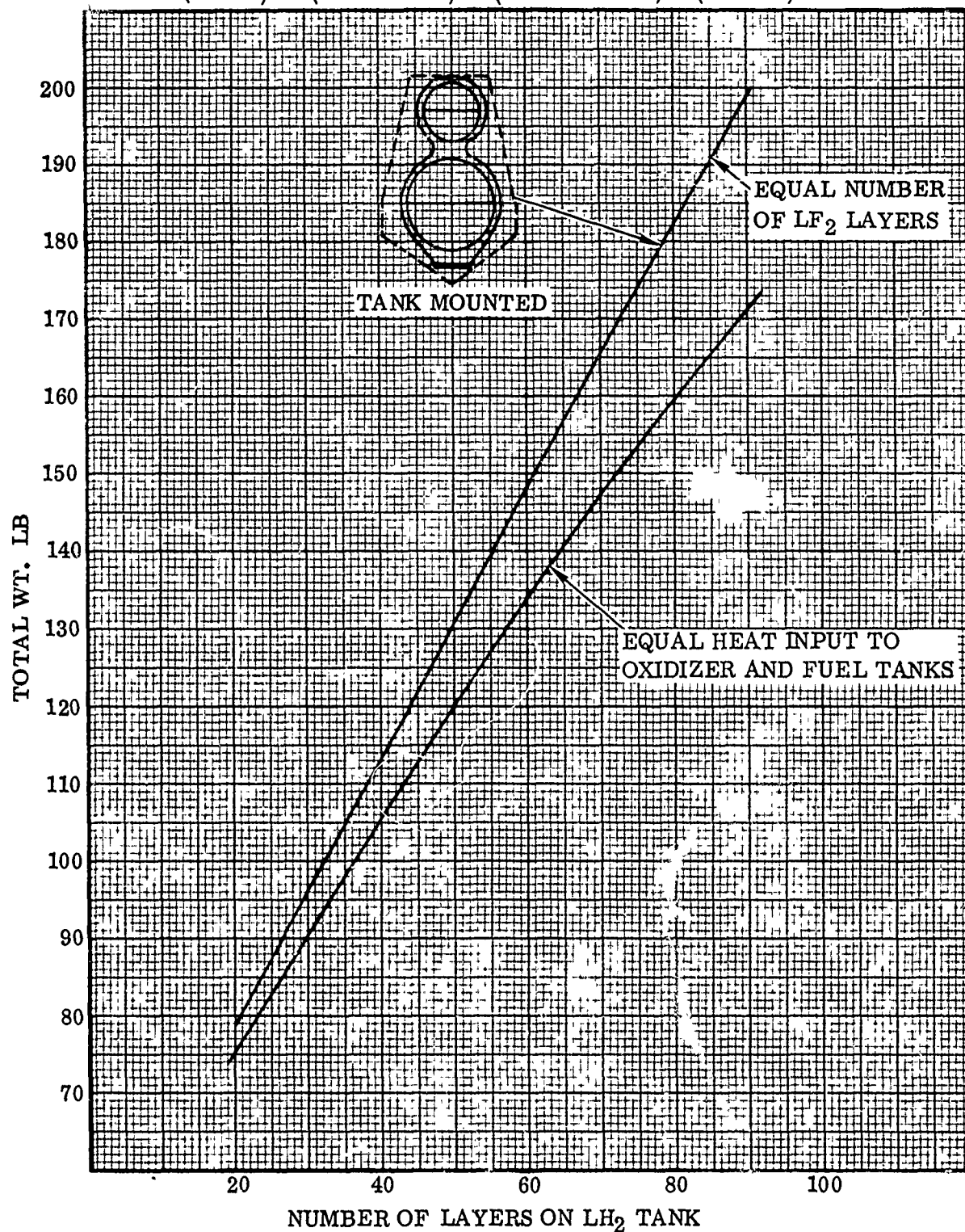


(C) Figure 2-69. Insulation System Weight versus Heat Transfer to Propellant Tanks

CONFIDENTIAL

CONFIDENTIAL

$$\left(\begin{matrix} \text{TOTAL} \\ \text{WT.} \end{matrix} \right) = \left(\begin{matrix} \text{WT. OF} \\ \text{INSULATION} \end{matrix} \right) + \left(\begin{matrix} \text{WT. OF} \\ \text{SUPPORT} \\ \text{ACCESSORIES} \end{matrix} \right) + \left(\begin{matrix} \text{WT. OF} \\ \text{CHILL} \\ \text{PLATE} \end{matrix} \right)$$



(C) Figure 2-70. Insulation System Weight Comparison - Equal Heat Input versus Equal Layers

CONFIDENTIAL

CONFIDENTIAL

(U) It should be noted that the performance calculations represent "worse case" conditions and are presented to allow relative selection criteria. There may be advantages gained by letting the bulk propellant absorb some portion of the heat input by increasing its temperature rather than continually boiling off. Although the performance of the tank mounted insulation systems is greater than for the shroud mounted system the ΔV differences in themselves are not overpowering.

(U) 2.2.5 GROUND THERMAL PERFORMANCE. Internal shroud conditioning with GN_2 leads to a requirement for careful installation of closed-cell foam on all LH_2 tank surfaces, ducts, and vent lines. While properly maintained foam is a superior insulation, local cracks or discontinuities in the insulation will permit formation and runoff of liquid nitrogen. Tank surface/foam interfaces tend to deteriorate progressively with added tanking cycles. The rigid insulation application requirements can be relaxed if an internal helium environment is employed for shroud conditioning, since no helium liquefaction can occur; however, any non-vacuum tank insulation will then tend to approach the conductive characteristics of gaseous helium because of the helium permeability characteristics of most materials. A realistic limiting insulation characteristic would thus correspond to heat conduction through a layer of entrapped helium. An insulating layer of helium can be maintained by application of a multi-layer blanket of crinkled mylar, dimplax, or Superfloc, in which the inter-layer dimension is too small to sustain convective heat transfer. A one-inch material lay-up of Superfloc (30 layers) would assure helium interlayer Grashof-Prandtl characteristics which preclude the possibility of free convection. The lay-up thickness can be varied to provide the degree of insulation desired. Application need not conform to the carefully-fitted requirements normally associated with foam insulations since liquefaction is not a problem. The blanket can be fastened or constrained by any convenient method.

(C) The heating rates with 1.5 inch helium blanket on the LH_2 tank are 22,000 BTU/hr for the shroud mounted insulation and 26,400 BTU/hr for the tank mounted insulation systems. This is of the order of 116 and 139 lb/hr boiloff for the two cases, respectively. This is felt to be a reasonable ground hold boiloff rate for hydrogen. The method is therefore tentatively selected as the ground hold conditioning system.

(U) 2.2.6 SELECTION CRITERIA. The selection of the superinsulation location is based on many factors other than ΔV penalty, although this is the major contributing item in the evaluation criteria. The other items considered in arriving at the optimum configuration were:

Ground Hold Capability

Component Fabrication and Assembly

Insulation Compression Effects

CONFIDENTIAL

UNCLASSIFIED

Structural Considerations

Insulation Preconditioning

Venting through the Superinsulation

Interlayer Venting and Outgassing

Inspection and Checkout

Cost

Boost Heating Problems

Ground Test Conditions

Incorporation of Vent Free Fluorine System

These items were all evaluated qualitatively to determine the relative advantages of the two installations.

2.2.6.1 Ground Hold Capability. The simplicity of the mylar bag concept to minimize ground heat transfer appears, at this time, to be quite attractive. Using this approach the tank mounted insulation system already provides the necessary requirements with the approximate 1.5 inch of insulation. The shroud mounted installation requires additional mylar blankets around the propellant tanks, which will add inert weight, although some additional benefit will be derived for space thermal performance. In summary, it can be stated that the tank mounted installation provides a simpler system for ground hold conditions, while incurring no additional weight penalty.

2.2.6.2 Component Fabrication and Assembly. Both systems are built up from basically the same blanket concept and there does not appear to be a significant difference in the blanket assembly. The shroud mounted installation requires a cap section while the tank mounted requires a transition neck section; however, it should be easier to install the shroud mounted blankets as there are no compound curvatures involved as in the tank mounted case. The insulation mounted on the tanks will have more wrinkles and may require more care during the actual assembly. The shroud mounted system should have a slight advantage in this area, although by assembling the complete insulation system on the tanks (and neck section) prior to assembling the tanks into the shroud should minimize this advantage.

2.2.6.3 Insulation Compression Effects. The compressive effects on the superinsulation during the boost phase will be greater on the tank mounted insulation than on the shroud mounted because of the direction of force applied. The insulation mounted on the side wall will have virtually no compression during boost while that mounted on

UNCLASSIFIED

UNCLASSIFIED

the forward bulkhead of the propellant tanks will be compressed by the "g" forces; however, the compression recovery of a superinsulation such as Superfloc should result in very little performance degradation.

2.2.6.4 Structural Considerations. On the tank mounted installation the loads causing outboard forces place the scrim reinforced face sheets in tension. Forces acting inboard compress the lay-up against the tank wall. Therefore the lay-up is restricted between the scrim layer and the tank wall. On the shroud mounted installation the scrim base supporting the insulation acts as a flexible membrane spanning between frames. The lay-up therefore is free to move depending on the flexibility of the scrim base. The forward flat cap section acts as a large unsupported membrane which may require additional support if unpredictable loads develop. The tank mounted insulation system appears less sensitive to acoustic and vibration loads.

2.2.6.5 Insulation Preconditioning. Some preconditioning of the insulation system may be required to minimize outgassing. Once the insulation is preconditioned (e.g., warm helium purge, etc.) it appears easier to control the environment of the tank mounted insulation compared with controlling the shroud mounted environment. This is primarily a function of the distance of the insulation from the ambient air interface (i.e., the structural shell).

2.2.6.6 Venting Through the Superinsulation. During ascent, the gas trapped beneath the insulation must be vented to prevent excessive pressure loads across the blanket lay-ups. The amount of gas required to be vented for the shroud mounted case is that included in the total volume of the shroud. The amount required for venting in the case of the tank mounted insulation is that trapped between the layers and the tank and the volume encompassed by the transition neck section. Because of the lower required volumetric flowrate the tank mounted system would be preferred.

2.2.6.7 Inspection and Checkout. Some systems and components other than propellant tanks may be located within the structural shell. In order to inspect and checkout such items it is necessary, in the case of the shroud mounted system, to penetrate the insulation system. Proper access doors must be provided. There is also, however, a disadvantage with the tank mounted section if the item of interest must be reached through the neck section. This could involve a valve, P.U. probe, etc. In this case, the transition neck section must be removed. It does not appear that either of the two systems enjoy a distinct advantage in this area.

2.2.6.8 Cost. Although more layers of superinsulation are required for the tank mounted case, for basic thermal performance the shroud mounted case requires additional insulation for ground hold conditions. The cost of material, assembly, and installation should be comparable for both systems.

UNCLASSIFIED

CONFIDENTIAL

(U) 2.2.6.9 Boost Phase Heating Effects. It has been previously shown in the first quarterly report that the structural shroud frame temperature may approach 350° F. The insulation mounted on the tanks should not be significantly affected by this temperature because of their remote location. The shroud mounted insulation is separated from the frames by only the scrim base thickness, and is therefore more susceptible to this temperature environment. At 330° to 350° F the basic characteristics of the mylar are not changed, but some structural degradation can be expected.

(U) 2.2.6.10 Test Conditions. The shroud mounted insulation system offers a higher degree of safety for the test conditions because of the remote location of the insulation lay-up from the fluorine tank; however, the requirement for ground insulation will again put insulation in close proximity to the fluorine tank. If this ground insulation were removed during simulated altitude testing for safety considerations, it could affect the validity of the test results.

(C) 2.2.6.11 Incorporation of Vent Free Fluorine System. The tank mounted insulation system allows more flexibility in establishing the proper operation of the vent free fluorine system by allowing the thickness of insulation (and consequently the heating rates) to be varied independently on the LH₂ and LF₂ tanks. The shroud mounted insulation system results in a unique heating rate to the LF₂ tank for each heating rate of the LH₂ tank.

(U) After thoroughly evaluating the above criteria the decision was made to install the insulation on the propellant tanks rather than on the shroud.

2.3 SUPPORT STRUCTURES

(C) The support structures consist of the outer structural shell and the tank support struts. The outer shell is of 2024 T-86 aluminum skin stringer construction. There are 60 hat section stringers (0.035 inch thickness) riveted to the skin of the shell structure. These stringers are stabilized by rings spaced 11 to 14 inches apart. The basic skin thickness is 0.030 inch.

(U) The support struts for the propellant tanks are constructed of fiberglass because of its high strength to thermal conductivity ratio.

(U) A tradeoff study was conducted on various structural configurations, and the aluminum skin stringer was chosen to be optimum for this application. The basic characteristics and dimensions of the shell have been defined, and during the next quarter the shell drawings will be generated.

(U) 2.3.1 OUTER STRUCTURAL SHELL. The selection of the outer structural shell is based on minimum system weight. In order to determine which system results in

CONFIDENTIAL

UNCLASSIFIED

maximum performance a tradeoff analysis was conducted considering different materials and different types of construction. It should be noted that the results of the tradeoff study are theoretical minimum weights which give a relative ranking of the various configurations. In all cases the actual values of a detailed design would be heavier. The aluminum skin stringer was shown to be preferred based on the tradeoff study. A detailed weights analysis was then conducted on the shroud to arrive at a practical system weight.

2.3.1.1 Structural Configuration Comparisons. Various structural configurations are compared for the outer shell; honeycomb sandwich, skin and stringers, ring-stiffened monocoque, and Jaffee metal. Typical structural alloys of titanium and magnesium, and a typical composite such as fiberglass are considered for each type of construction. The comparative weights are calculated on the basis of "ideal" considerations for strength only, with no adjustment for manufacturing or thermal problems. Realistic structures will be heavier in all cases because of minimum gage considerations; manufacturing advantages of using constant thicknesses rather than tapering skin thicknesses; and thermal considerations. The analysis, however, is intended to provide accurate comparisons of weights required for structural purposes. Where non-optimum structures are used because of manufacturing or thermal considerations, the theoretical weights provide a basis for estimating tradeoff penalties.

The results of the shell analysis are shown in Table 2-6.

TABLE 2-6. COMPARATIVE SHELL WEIGHTS

	Titanium	Aluminum	Magnesium	Fiberglass
Honeycomb Sandwich	256	256	256	313
Skin-Stringer	324	277*	254	257
Monocoque	986	773	602	665
Jaffee Metal	430	—	—	—
*Recommended for thermal reasons and practical considerations.				

The weights shown are minimum structural weights required for the cylinder between Stations 42 and 76, and the conical frustrum between Stations 76 and 212.6. The total exposed area is 401 square feet; and the weights are obtained by designing a typical cross-section at Station 110, obtaining the weight per square foot, and multiplying by 401. The weights of the tank support rings, end connections, and other members are therefore assumed equal for all shell materials and designs. This comparison may

UNCLASSIFIED

UNCLASSIFIED

be biased slightly in favor of honeycomb sandwich structures, since connections to honeycomb are more difficult than connections to monocoque or sheet-stringer structures, and the additional fitting weight will partially offset the weight advantage shown for sandwich construction. The sandwiches are also more expensive and difficult to fabricate and inspect, and subject to unreliability if the bond joint becomes overheated. The sheet-stringer structure is therefore recommended.

Detailed dimensions of the candidate structures are shown in Table 2-7. All cross-sections are for a typical Station 110, where the radius is 56.25 inches and the loads are a mean value. The increased weight per square foot aft of this station balances the decreased weight at forward stations where loads are smaller. Minimum gage problems are not considered, as ideal weights for strength are being compared. Considering an aluminum alloy as the preferred material, the skin gages are 0.010 for honeycomb face sheets, 0.020 for sheet stringer, and 0.125 for full monocoque. All but the full monocoque will probably require ablative coatings to prevent overheating during boost. The practical skin stringer would therefore have about 0.030 skin instead of the 0.020 ideal value, but the stringers and frames could be reduced slightly, and the total weight increase would be less than 20 percent for a 50 percent increase in skin gage. It is more efficient to dissipate heat in an ablative coating such as "Thermolag", than to provide structure as heat sink, since a pound of thermolag will dissipate many times the BTUs that a pound of structure will absorb; however, the maximum structural loads are imposed before heating occurs, and the structure consequently has high permissible temperatures. The external surface requires a finish which will provide good emissivity during space residence, and the ablative coatings are probably less efficient in this respect.

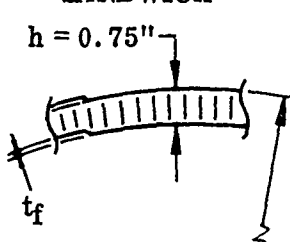
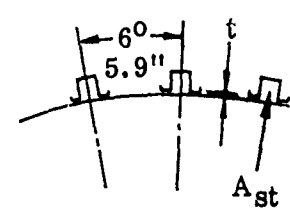
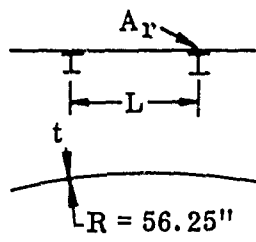
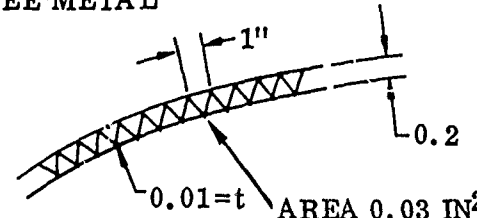
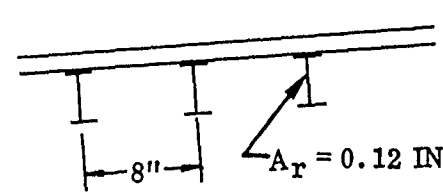
The sheet-stringer structures have been extensively used for years in conventional airplanes. For subsonic airplanes, it is most efficient to use the minimum skin gage required for shear flow and normal loading, and concentrate as large a proportion of the material in stiffeners as feasible. For the AMPs shell structure, the minimum skin gage and the stiffener spacing are determined by skin panel flutter conditions during boost. These are calculated from theoretical curves for unpressurized flat panels; and the skin weights become a function of $W/\sqrt[3]{E}$ for different materials with the same stiffener spacing, where W is the material density in lb/in^3 and E is the modulus of elasticity. Most of the buckling characteristics also depend on $W/\sqrt[3]{E}$ or W/\sqrt{E} . The metal alloys compared all have the same ratio of W/E , but the total structural weight, depending on $W/\sqrt[3]{E}$, is less for magnesium than for aluminum, and less for aluminum than for titanium. Magnesium is considered less desirable than aluminum for corrosion and thermal properties.

2.3.1.2 Analysis Procedure. The tentative loads and dimensions for the AMPs shell are shown in Figure 2-71. The typical cross-section at Station 110 has a loading and size which is estimated to require an average weight per square foot. The limit loads at this station are 66,000 pounds axial compression, 1,900,000 inch-pounds

UNCLASSIFIED

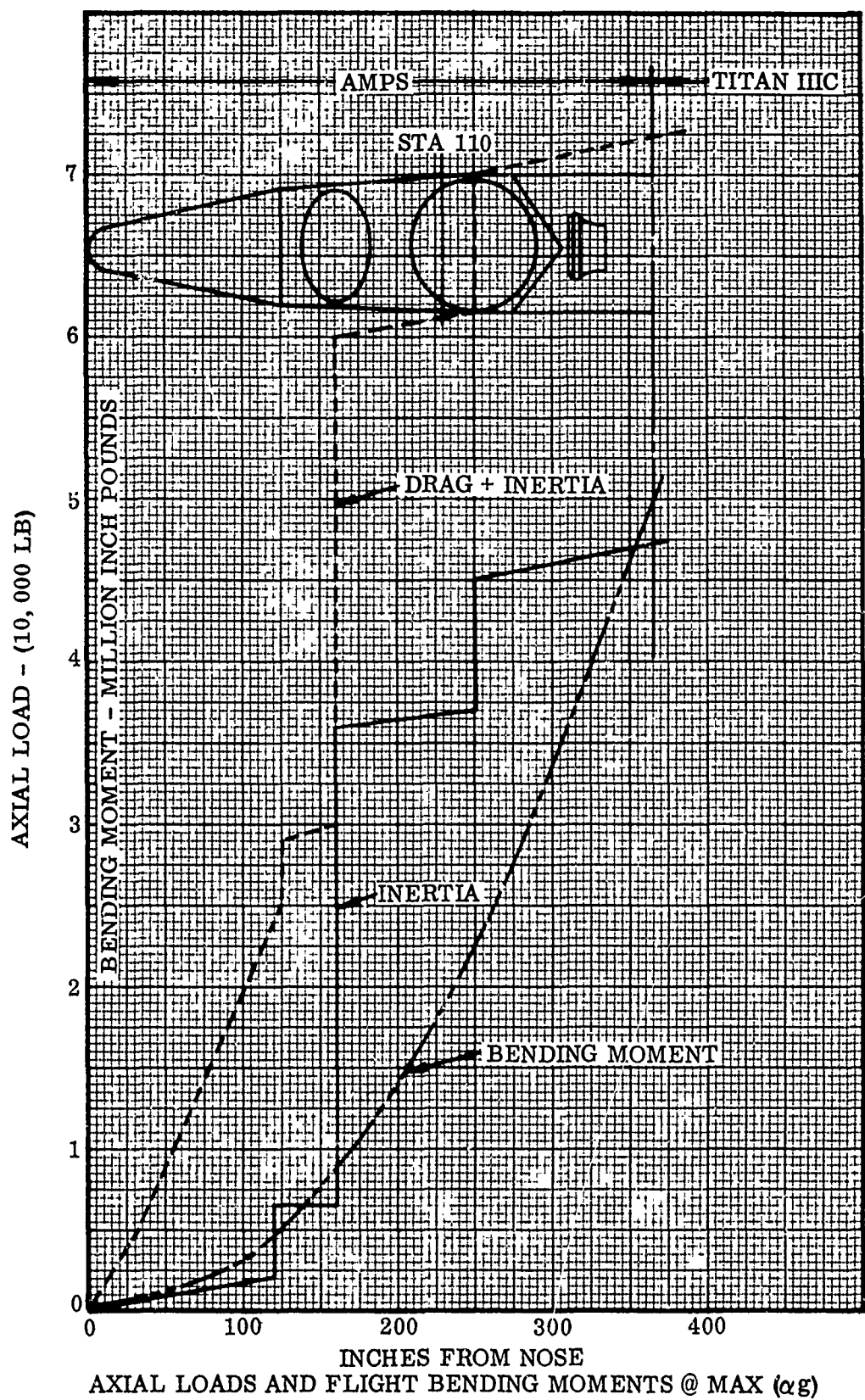
UNCLASSIFIED

(U) TABLE 2-7. REQUIRED DIMENSIONS, STATION 110

<div> <p>HONEYCOMB SANDWICH</p>  <p>h = 0.75"</p> <p>R = 56.25"</p> <p>CORE 4 LB/FT³</p> <p>ADHESIVE 0.10LB/FT²</p> </div>		Titanium	Aluminum	Magnesium	Fiberglass
		W= 0.165	W= 0.10	W= 0.065	W= 0.06
Face Sheet Thickness, t_f		0.0061	0.010	0.0154	0.025
Equivalent Thickness, \bar{t}		0.027	0.044	0.068	0.090
WT/FT ²		0.638	0.638	0.638	0.780
<div> <p>SKIN-STRINGER</p>  <p>60°</p> <p>5.9"</p> <p>A_{st}</p> </div>	Skin Thickness t	0.017	0.020	0.023	0.027
	Stringer Area A _{st}	0.054	0.090	0.135	0.150
	Ring Area A _r	0.108	0.176	0.272	0.294
	Ring Spacing L	13.8"	13.8	13.8	13.8
	$\bar{t} = t + \frac{A_{st}}{5.9} + \frac{A_r}{L}$	0.034	0.048	0.066	0.074
	WT/FT ²	0.809	0.692	0.616	0.640
<div> <p>MONOCOQUE</p>  <p>A_r</p> <p>L</p> <p>t</p> <p>R = 56.25"</p> </div>	Skin Thickness t	0.094	0.125	0.15	0.18
	Ring Area A _r	0.174	0.123	0.138	0.182
	Ring Spacing L	8.0	13.8	13.8	13.8
	$\bar{t} = t + A_r/L$	0.103	0.134	0.160	0.193
	WT/FT ²	2.46	1.93	1.50	1.66
<div> <p>JAFFEE METAL</p>  <p>1"</p> <p>0.2</p> <p>0.01=t</p> <p>AREA 0.03 IN²</p> </div> <div>  <p>8"</p> <p>A_r = 0.12 IN²</p> </div> <div> <p>$\bar{t} = 0.03 + 0.12/8 = 0.045$</p> <p>WT/FT² = 1.07</p> </div>					

UNCLASSIFIED

CONFIDENTIAL



(C) Figure 2-71. Titan IIC (0, 1, 2)/AMPS Bending Moments and Axial Loads

CONFIDENTIAL

UNCLASSIFIED

bending moment, and 2.5 psi external crushing pressure. These loading conditions allow for a 99 percent launch availability during an αq of 6,000 which is considerably higher than the AMPS αq of 4,200 established as part of the design criteria during Task I. Ultimate loads are 1.25 times limit loads. The loads per inch are calculated as follows, for ultimate conditions:

Compression

$$N_{\phi_1} = \frac{1.25 P}{2 \pi R} = \frac{1.25 \times 66,000}{353} = 234 \text{ lb/in.} \quad (1)$$

Bending

$$N_{\phi_2} = \frac{1.25 M}{\pi R^2} = \frac{1.25 \times 1,900,000}{9,960} = 238 \text{ lb/in.} \quad (2)$$

Lateral Pressure

$$N_{\theta} = 1.25 pR = 1.25 \times 2.5 \times 56.25 = 176 \text{ lb/in.} \quad (3)$$

For allowable values $N_{\phi_{a1}}$, $N_{\phi_{a2}}$, and N_{θ_a} the stress ratios are as follows:

$$R_1 + R_2 + R_3 = \frac{N_{\phi_1}}{N_{\phi_{a1}}} + \frac{N_{\phi_2}}{N_{\phi_{a2}}} + \frac{N_{\theta}}{N_{\theta_a}} \leq 1.0 \quad (4)$$

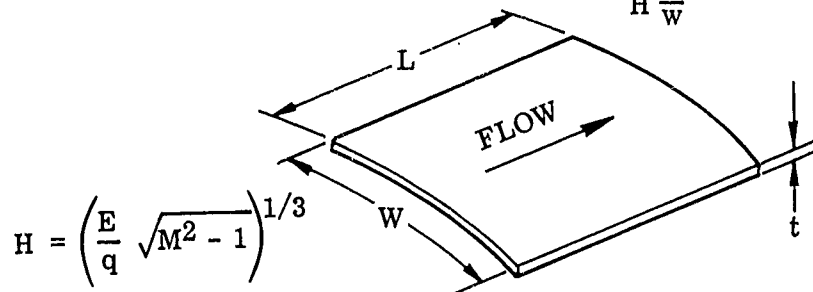
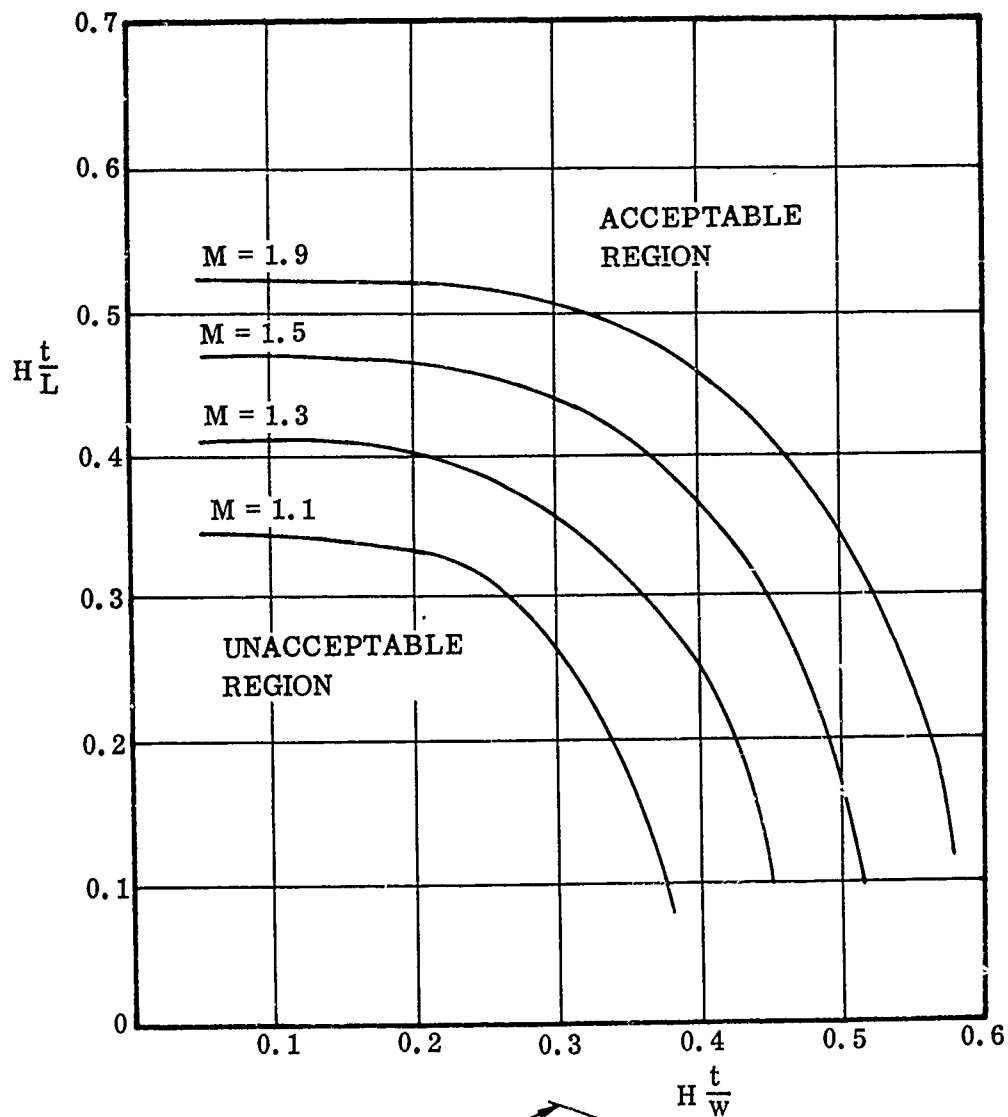
The margin of safety is obtained from this.

$$\text{M.S.} = \frac{1}{R_1 + R_2 + R_3} - 1 \quad (5)$$

The skin panel flutter conditions are calculated from Figure 2-72. This figure defines the design conditions used for the Titan III payload fairing, as specified in RFP No. FO4697-67-R0101. For a typical value of $q = 6.5$ psi at $M = 1.5$, the value of H is $0.556 \sqrt{3E}$. For aluminum panels with $L = 13.8$ inches and $W = 4.7$ inches, a thickness t of 0.020 inch is required. For other materials, the thickness is inversely proportional to $\sqrt{3E}$, and the skin gages shown in Table 2-7 for skin-stringer construction; 0.017, 0.023, and 0.027 for titanium, magnesium, and fiberglass, respectively are obtained from this relation. The honeycomb and full monocoque structures have no skin panel flutter problems.

UNCLASSIFIED

UNCLASSIFIED



$$H = \left(\frac{E}{q} \sqrt{M^2 - 1} \right)^{1/3}$$

E = Mod. of Elasticity

q = Dynamic Pressure

M = Mach Number

$$AR = \frac{W}{L}$$

Figure 2-72. Titan III Design Flutter Boundaries

UNCLASSIFIED

UNCLASSIFIED

The allowable loads for shells are obtained by methods of NASA SP-8007, "Buckling of Thin-Walled Circular Cylinders" (Reference 9), with modifications described in GDC Report No. GDC-BNZ68-015, "Vacuum Shell Selection" (Reference 10). The allowable values of N_{ϕ_a} and N_{θ_a} are calculated independently, and combined according to Equations 4 and 5.

The honeycomb structure is thick enough to require no internal rings or stringers, whereas, Jaffee metal must be supported by rings of about 8-inch spacing. If the Jaffee metal had the required 0.75 inch thickness to omit the rings, the corrugations would be too widely spaced to support the skin adequately, for the thin gages which are optimum. The honeycomb must have a cell size of about 0.2 inch to support face sheets of 0.010-inch gage. Since the honeycomb requires no support rings, the cylinder length is used as 96.6 inches, the distance between tank support rings. The frustum is analyzed as a cylinder of 56.25-inch radius.

The allowable axial load for a long cylinder is $0.605 \gamma E t^2/R$, where γ is a correlation factor obtained empirically. Values of γ are shown in Figure 2-73 (from Reference 9) as a function of R/t . For an isotropic sandwich with flexural stiffness $EA h^2/4$ instead of $EA t^2/12$, the equivalent t is $\sqrt{3} h$. The correlation factor γ from Figure 2-73 is obtained as a function of $R/(h\sqrt{3})$ in place of R/t . The theoretical buckling load ($\sqrt{4KD}$) is also increased by the factor of $\sqrt{3}$.

$$N_{\phi_a} = 0.605 \sqrt{3} \gamma E 2t_f h/R$$

$$N_{\phi_a} = 2.09 \gamma E t_f h/R \quad \left[\text{for } \frac{\gamma L^2}{Rh} > 7 \right] \quad (6)$$

The total depth between centers of face sheets is h , and the face sheets each have thicknesses t_f .

A moderately long cylinder has a crushing strength from lateral pressure as follows:

$$N_{\theta_a} = \frac{0.926 \sqrt{\gamma} E t^{2.5}}{L R^{0.5}} \quad \left[\text{for } \frac{\gamma L^2}{Rt} > 200 \right] \quad (7)$$

The correlation factor γ , is about 0.9, or experimental values are above 0.95 times theoretical buckling values. For sandwiches, Equation 7 becomes

$$N_{\theta_a} = \frac{4 E t_f h^{1.5}}{L \sqrt{R}} \quad \left[\text{for } \frac{\gamma L^2}{Rh} > 300 \right] \quad (8)$$

UNCLASSIFIED

UNCLASSIFIED

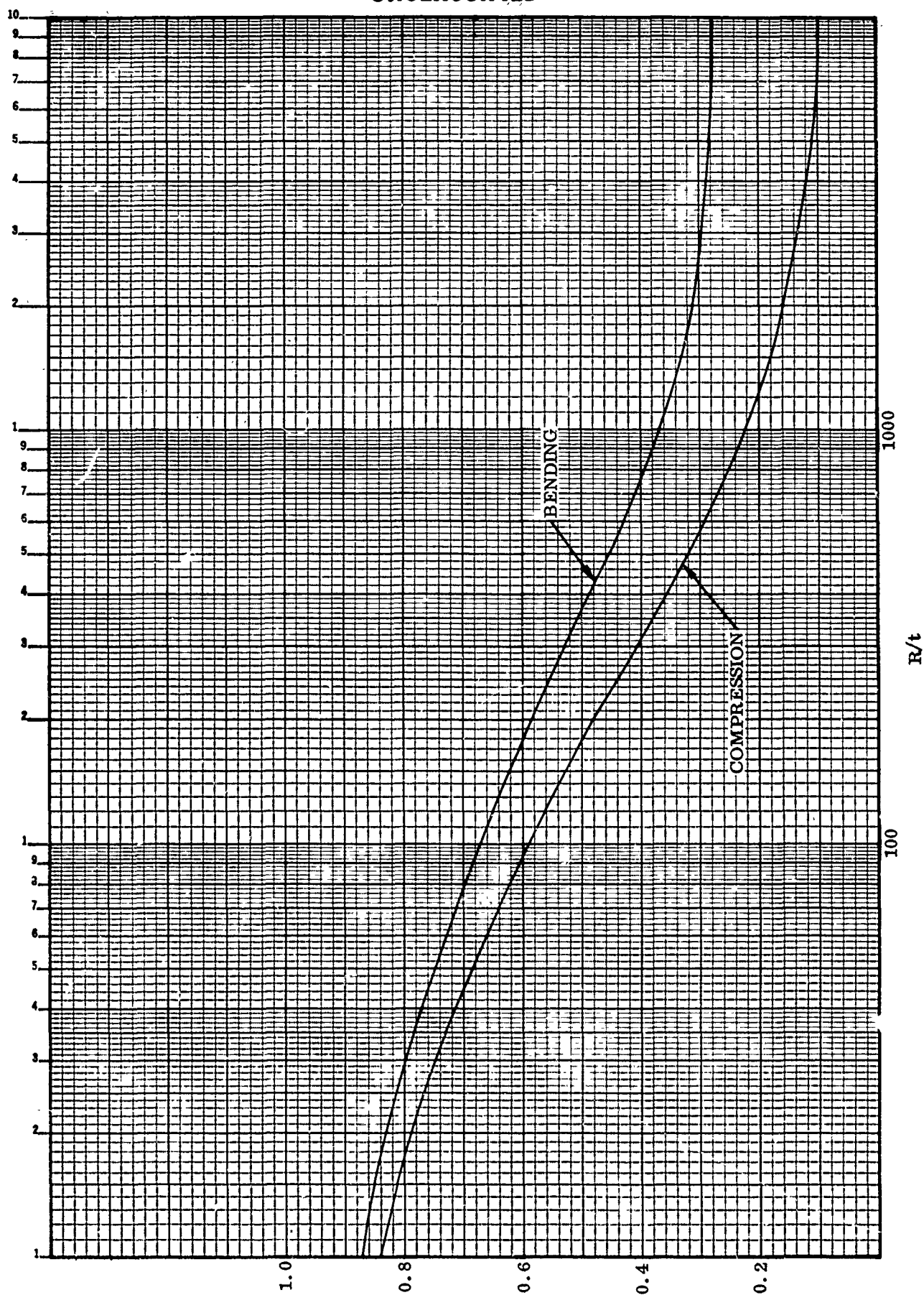


Figure 2-73. Axial Loaded Cylinder Correlation Factors

UNCLASSIFIED

UNCLASSIFIED

The resistance to lateral pressure depends primarily on the flexural stiffness in the hoop direction and the extensional stiffness in the axial direction.

For full monocoque structures, the allowable axial loads are obtained from the equation

$$N_{\phi} = 0.605 \gamma E t^2 / R \quad \left[\text{for } \frac{\gamma L^2}{Rt} > 4 \right] \quad (9)$$

with γ obtained from Figure 2-73. Practical thicknesses are not adequate to resist hoop compression for a length, L , of 96 inches (Equation 8). It is necessary to provide rings to reduce the unsupported length. For all materials except titanium, the rings are spaced at 13.8 inches, dividing the length of 96.6 inches into seven spaces. For titanium, a ring spacing of 8 inches is shown in Table 2-7. The rings do not affect the axial strength, since the wavelength of wrinkles is much smaller than the ring spacing. The rings provide flexural stiffness in the hoop direction. Substituting $\gamma = 0.9$ into Equation 7,

$$N_{\theta a} = \frac{0.878 E t^{2.5}}{L R^{0.5}} \quad \left[\text{for } \frac{\gamma L^2}{Rt} > 200 \right] \quad (10)$$

The thickness effect is primarily the result of bending stiffness in the hoop direction. For a long cylinder of length L_0 , hoop stiffness is provided by rings at spacing L , with moment of inertia I_r , or $I_2 = I_r/L$ per unit length. Equation 10 is modified as follows, from theory and tests.

$$N_{\theta a} = \frac{0.875 (I_2/I_1)^{0.75} E t^{2.5}}{L_0 R^{0.5}} \quad (11)$$

For hoop stiffness to resist the same pressure as the short length between rings, Equations 10 and 11 may be equated, using $I_1 = t^3/12$.

$$\frac{I_2}{I_1} = \left(\frac{L_0}{L} \right)^{4/3}$$
$$I_r = I_2 L = (L_0/L)^{4/3} (L t^3/12) \quad (12)$$

This defines the required ring stiffness. A shape factor is assumed for approximating ring weights.

$$A_r = 0.6 \sqrt{I_r} \quad (13)$$

UNCLASSIFIED

UNCLASSIFIED

From these assumptions, the rings are lighter with a few widely spaced rings, than with more rings at closer spacing.

The foregoing equations for allowable buckling loads are applicable to cylinders of moderate length. For short cylinders, the curvature effect is smaller, and the cylinder walls act as narrow flat plates with width equal to the cylinder length. The behavior is a function of the curvature, and the buckling loads are defined as follows:

$$N_{\theta} = K_y \frac{\pi^2 E I_1}{L^2 (1 - \mu^2)} = 0.905 K_y E t^3 / L^2 \quad (14)$$

$$N_{\phi} = \frac{\pi^2 E I_1}{L^2 (1 - \mu^2)} = 0.905 K_x E t^3 / L^2 \quad (15)$$

The terms K_x and K_y are functions of the curvature parameter, Z .

$$Z = \frac{L^2}{Rt} \sqrt{1 - \mu^2} = 0.954 L^2 / Rt \quad (16)$$

Equations 14, 15, and 16 correspond to Equations 7 and 9 when the cylinder is moderately long. The terms K_x and K_y are read from Figure 2-74 as functions of γZ . From Figure 2-74, the values of K_x plot as straight lines for γZ greater than 3 or 4, and have the equation,

$$K_x = 0.702 \gamma Z \quad (\gamma Z > 4) \quad (17)$$

Equations 15, 16, and 17 yield Equation 9. It is easier to use Equation 9 in the applicable range, but necessary to use Equations 15 and 16 with Figures 2-73 and 2-74 when γZ is less than 3. For orthotropic structures, the axial strength depends on the extensional stiffness in the hoop direction and the flexural stiffness in the axial direction. For long cylinders, the modification is as follows:

$$N_x = 2.09 \gamma \frac{E}{R} \sqrt{I_1 t_2} \quad (18)$$

where t_2 is the area per unit length resisting hoop stresses and I_1 is the moment of inertia of a longitudinal beam of unit width. For ring-stiffened monocoque cylinders, $I_1 = t^3/12$. For short cylinders with orthotropic properties, the values are as follows:

UNCLASSIFIED

UNCLASSIFIED

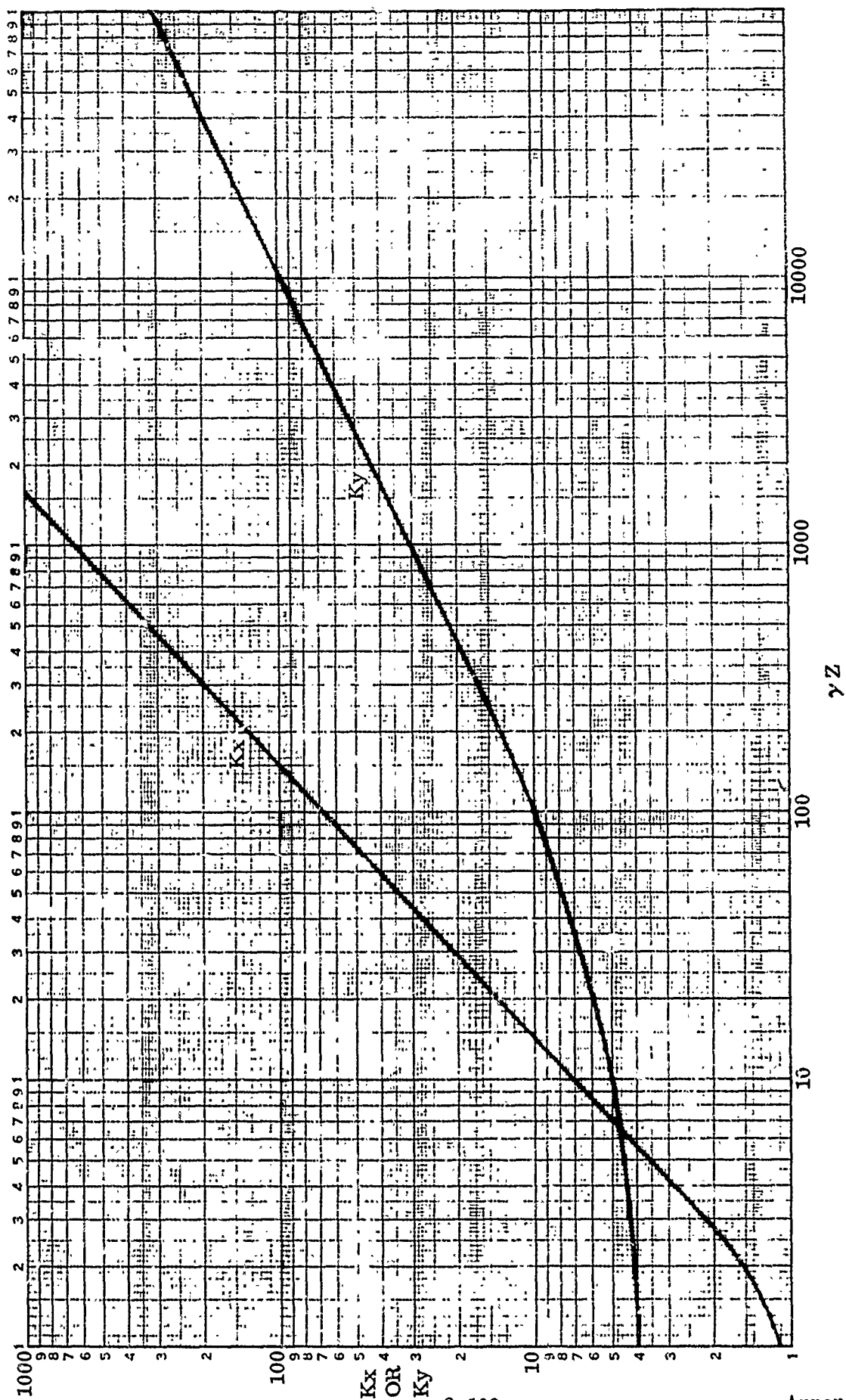


Figure 2-74. Z Factors for Axial Loaded Cylinders

UNCLASSIFIED

UNCLASSIFIED

$$Z_x = 0.954 L^2 / (R \sqrt{12 I_1 / t_2}) \quad (19)$$

$$N_x = 10.86 K_x E I_1 / L^2 \quad (20)$$

$$\text{In Figure 2-73, use } R / \sqrt{12 I_1 / t_2} \text{ for } R/t \quad (21)$$

For short cylinders resisting lateral load, the curve of K_y in Figure 2-74 is non-linear for $Z < 200$. It is necessary to use the curves instead of Equations 10 and 11. The linear portion is defined by the equation,

$$K_y = 1.04 \sqrt{\gamma Z_y} \quad [\gamma Z > 200] \quad (22)$$

With $\gamma = 0.9$, Equations 22, 16, and 14 yield Equation 10. For orthotropic cylinders, the lateral pressure capability depends on I_2 and t_1 . For $\gamma = 0.9$ and $\mu = 0.3$,

$$\gamma Z_y = 0.248 L^2 \sqrt{I_2^3 t_1 / (I_1^2 R)} \quad (23)$$

Equations 14, 22, and 23 yield the following:

$$N_\theta = pR = 5.65 E \sqrt[4]{I_2^3 t_1 / (L \sqrt{R})} \quad (\text{for } Z > 200) \quad (24)$$

Equation 24 yields Equation 11, with $I_1 = t_1^3 / 12$.

Sheet-stringer structures are efficient for axial loading, but depend on the rings for resisting crushing loads. The skin resists very little hoop compression, and the stringers act as beam-columns in transferring lateral pressure to the rings. The rings must resist the radial stringer reactions by hoop compression, and must be stiff enough to resist buckling. The stringers act in the short column range and have compression strength of the order of the yield strength of the material, which is higher than the allowable stress in monocoque skins. Since methods of analysis are conventional, only the resulting design is presented.

2.3.1.3 Design Calculations. The four materials were chosen for comparison in order to obtain approximate weight effects of various parameters. The three metals were chosen with exactly the same ratio of w/E in order to compare the density effects. The composite material is selected arbitrarily, and assumed isotropic. The properties are assumed as shown in Table 2-8.

For equal tension stiffness, the fiberglass would be 50 percent heavier than the other materials. For buckling applications, or panel flutter criteria, in which the weight varies inversely as the cube root of E ($w/\sqrt[3]{E}$) the fiberglass is lighter than everything but magnesium. No yield or ultimate strength values is shown, since it is assumed that the material has compressive yield strength comparable to the other properties.

UNCLASSIFIED

UNCLASSIFIED

TABLE 2-8. PROPERTIES OF MATERIALS

	Titanium	Aluminum	Magnesium	Fiberglass
Elastic Modulus E (psi)	16.5×10^6	10×10^6	6.5×10^6	4×10^6
Material Density w (lb/in. ³)	0.165	0.100	0.065	0.060
w/E	10^{-8}	10^{-8}	10^{-8}	1.5×10^{-8}
$w/\sqrt[3]{E}$	6.48×10^{-4}	4.65×10^{-4}	3.5×10^{-4}	3.8×10^{-4}

The honeycomb sandwich shells are analyzed by Equations 6 and 8. In each equation, the strength is proportional to $E t_f h$. All of the metals have equal weights when the sandwich depth, h , is the same and when the face skin thickness, t_f , varies inversely with E . The optimum proportions for this type of sandwich occur when the core weight is equal to the face skin weight. The proportions shown in Table 2-7, with a 0.75 inch core thickness of 4 lb/ft³, give a core weight of 0.25 lb/ft² for a face skin weight of 0.288 lb/ft². This is close to the optimum value, and keeps the skins thicker for fabrication purposes. The ultimate compressive stress of 24,000 psi for aluminum is below the yield stress, and the skins will not wrinkle with cell sizes of about 0.30 inch. Smaller cells are desirable to permit some fabrication tolerance.

The metal honeycomb was the same weight for all materials but the fiberglass faces are about 50 percent heavier, (ratio of w/E) and the total sandwich about 25 percent heavier.

The sheet-stringer structure was analysed for aluminum, and the skin weight ratioed as $w/\sqrt[3]{E}$, according to the panel flutter requirement. The stringers and frames were assumed to have the same weight for all materials, since allowable column stresses are not specified for the alloys. This appears realistic, although slightly biased in favor of the denser materials. The low density materials probably have a slight advantage for rings and stringers.

The ring-stiffened monocoque analysis is shown in Table 2-9. The structure is inefficient from strength-weight considerations, but illustrates the analysis procedure for Jaffee metal and other possible types of structures.

The Jaffee metal structure is analyzed as an orthotropic structure with the flexural stiffness and extensional stiffness both varying. The analysis is a cut-and-try procedure, using both curves of Figure 2-74, whereas, the full monocoque structure acted in the long-cylinder range for axial loads. The optimization of Jaffee metal involves the sandwich thickness and sheet gages, as well as the ring spacing

UNCLASSIFIED

UNCLASSIFIED

(U) TABLE 2-9. RING-STIFFENED MONOCOQUE STRUCTURES

	Titanium	Aluminum	Magnesium	Fiberglass
Shell Radius, R (in.)	56.25	56.25	56.25	56.25
Skin Thickness, t (in.)	0.044	0.125	0.15	0.15
Ring Spacing, L (in.)	8.0	13.8	13.8	13.8
Ratio R/t	598	450	375	312
Correlation Factor Comp. γ (Figure 2-73)	0.306	0.35	0.375	0.43
Compression Allowable $N_{\phi a1}$ (Eq. 9) (lb/in)	477	588	590	600
Correlation Factor Bending, γ (Figure 2-73)	0.433	0.47	0.49	0.54
Bending Allowable $N_{\phi a2}$ (Eq. 10)	680	790	774	755
Curvature Parameter $\gamma Z = 0.86 L^2/Rt$	10.4	24	20	16.7
Lateral Pressure Coefficient K_y (Figure 2-74)	5.1	6.3	5.9	57
Allowable Hoop Compression $N_{\phi a}$ (Eq. 14) (lb/in)	1040	580	615	630
Stress Ratios				
Compression $N_{\phi 1}/N_{\phi a1} = R_1$	0.49	0.40	0.40	0.39
Bending $N_{\phi 2}/N_{\phi a2} = R_2$	0.35	0.30	0.31	0.32
Hoop $N_{\theta}/N_{\theta a} = R_3$	0.17	0.30	0.29	0.28
Combined Stress Ratios ΣR (Eq. 4)	1.01	1.00	1.00	0.99
Required Ring Stiffness I (Eq. 12) (in ⁴)	0.0152	0.031	0.0536	0.0925
Ring Area $0.6 I_r$ (Eq. 13) (in ²)	0.074	0.123	0.138	0.182
Effective Thickness $\bar{t} = t + A_r/L$ (in.)	0.1033	0.134	0.16	0.193
Weight/ft ² = $\bar{t} \omega \times 144$ (lb)	2.46	1.93	1.50	1.66
Total Weight, (401 sq. ft.) lb.	986	773	602	665

UNCLASSIFIED

CONFIDENTIAL

(U) and stiffness. The range of variables could vary from unstiffened proportions similar to the honeycomb with thickness of about 0.75 inch to thinner sandwiches similar to the full monocoque. Another possibility would be to use sheet-stringer construction with Jaffee metal having circumferential corrugations; however, the proposed configuration is believed efficient for the present loading.

(C) 2.3.1.4 Weights Analysis. The structural comparisons give relative weights required to resist applied loads and panel flutter conditions. All of these configurations probably require ablative paint to prevent overheating. Since the ablative paint may reduce the thermal efficiency of the surface, thicker gages are recommended to provide more heat sink. A sheet-stringer aluminum alloy structure, with skin thickness about 0.030, is probably required for a practical design. Increasing the skin from the 0.020 required for strength to the 0.030 gage, adds about 66 pounds total weight. The stringer construction for the practical case was assumed to be 0.035 which would result in an additional 45 pounds.

(U) The honeycomb structures would be overheated at outer bond lines, unless protected by a considerable thickness of ablative paint. The connection, detail weight, manufacturing cost, and potential bonding reliability provide further problems for a honeycomb design.

(U) The Jaffee metal structure has the disadvantage of heavy connections, high cost, and thick gages; however, the material and the bonding will withstand much higher temperatures than honeycomb sandwiches. Thermal protection might be possible by venting boiloff gases through the corrugations. Structural considerations, however, still favor the aluminum sheet-stringer structure.

(C) The detailed weights analysis of the aluminum skin stringer is given in Table 2-10. It can be noted that a practical realistic weight of about 490 pounds (excluding thrust structure) is realized compared to the theoretical minimum of 277. This increase is due to practical minimum skin gage limitations, end rings, tank support rings, support ring fittings, rivets, and small contingency factors.

(C) The shroud weight in pounds per inch is 3.12 for the straight section and 2.72 for the tapered section. The figures originally used in the tank optimization study were 3.5 for the straight section and 3.04 for the tapered. The lighter weight for the shroud would tend to drive the propellant tanks to a more optimum structural configuration; however, the selection has already been made to make the LH₂ tank spherical. By making the LF₂ tank spherical the shroud length would be reduced by approximately 6 inches. Using the new weight figure of 2.72 pounds per inch in lieu of 3.04, the weight differential between a bulkhead ratio of 1.2 and 1.0 would be reduced by only two pounds; therefore, the original tank optimization, based on 3.04 and 3.5 pounds, respectively, is valid.

CONFIDENTIAL

CONFIDENTIAL

(C) TABLE 2-10. AMPS SHELL STRUCTURE

<u>WEIGHT SUMMARY</u>	
Forward Conical Section	382.9 lb
Skins	140.7
Stringers (30)	125.0
Forward Ring	6.4
LF ₂ Tank Support Ring	19.5
Support Ring Fittings (12)	6.5
LH ₂ Tank Support Ring (1/2)	9.7
Intermediate Rings (8)	60.6
Rivets, Contingency	14.5
	<u>382.9</u>
L = 138.5 inches	
$\frac{W}{L} = \frac{382.9}{138.5 \text{ inches}} = 2.76 \text{ lb/inch}$	
Cylindrical Section	106.2 lb
Skins	38.5
Stringers (60)	30.7
LH ₂ Tank Support Ring (1/2)	9.7
Aft Ring	19.3
Tank Support Fittings (6)	4.0
Rivets, Contingency	4.0
	<u>106.2</u>
L = 34 inches	
$\frac{W}{L} = \frac{106.2}{34} = 3.12 \text{ lb/inch}$	
Aft Conical Section	85.6 lb
Skins	38.8
Stringers (60/30)	33.0
Intermediate Rings (2)	10.8
Rivets, Contingency	3.0
	<u>85.6</u>
L = 31.5 inches	
$\frac{W}{L} = \frac{85.6}{31.5} = 2.72 \text{ lb/inch}$	
Thrust Cone Forging	14.0 lb
TOTAL SHELL	588.7 lb

CONFIDENTIAL

CONFIDENTIAL

2.3.2 SUPPORT STRUTS

(C) 2.3.2.1 LF₂ Tank Struts. The LF₂ tank is supported by 12 fiberglass support struts. (See View M of Figure 2-3 in Section 2.2.1.1). The primary function of the struts is to provide stable propellant tank attachment to the shell during transportation and flight, while providing a minimum heat transfer path from the shell to the tank. Fiberglass is used as the structural material since it has the highest strength to thermal conductivity ratio available of all the normally used metals and structural plastic composites.

(C) It is highly desirable from a load distribution and analytical standpoint to use the struts entirely as tension or compression members. For this reason, spherical rod ends are used at both ends for attachment to the tank and shell. By employing opposite thread hands on the rod ends, the strut is an infinitely adjustable turnbuckle which is used to provide an even load distribution among the struts. Since the struts are axially loaded, the glass fabric used is a unidirectional weave with the longitudinal filaments laid parallel to the strut axis. Based on 100,000 psi axial fiberglass allowables, and using flight loading for a 20,000-pound vehicle, the fluorine tank requires 12 struts with a 1.25-inch outside diameter and a 0.06-inch wall thickness. The struts are attached in pairs at 60-degree increments to the propellant tank and singly connected in 30-degree increments to the shroud structure.

(U) The transfer of the load from the tubular fiberglass body of the strut to the rod end is accomplished through a tapered titanium insert. The glass is molded over this insert and retained by a sleeve which acts in hoop tension to react the insert's wedging action. Both the insert and titanium sleeve are bonded to the fiberglass. Compressive loads are transferred directly to the tube by a raised lip on the end of the insert. The strut material has good resistance to thermal conduction, but a direct radiation path exists down the inside of the tube from insert to insert. To eliminate this heat path, discs of superinsulation are inserted into the tube. A locknut for safety wiring is provided on the shell rod end of the strut to prevent strut rotation after the proper length is determined during installation.

(C) 2.3.2.2 LH₂ Tank Struts. The function and general construction of the LH₂ tank struts are identical to that of the fluorine tank strut. (See View P of Figure 2-3 in Section 2.2.1.1). Since the hydrogen tank loads are considerably less than those for the fluorine tank, fewer struts are necessary.

(U) Six struts with a 1.00-inch outside diameter and a 0.04-inch wall thickness were required. The struts are attached in pairs at 120-degree increments to the propellant tank and singly connected to the outer structural shroud.

CONFIDENTIAL

CONFIDENTIAL

2.3.2 SUPPORT STRUTS

(C) 2.3.2.1 LF₂ Tank Struts. The LF₂ tank is supported by 12 fiberglass support struts. (See View M of Figure 2-3 in Section 2.2.1.1). The primary function of the struts is to provide stable propellant tank attachment to the shell during transportation and flight, while providing a minimum heat transfer path from the shell to the tank. Fiberglass is used as the structural material since it has the highest strength to thermal conductivity ratio available of all the normally used metals and structural plastic composites.

(C) It is highly desirable from a load distribution and analytical standpoint to use the struts entirely as tension or compression members. For this reason, spherical rod ends are used at both ends for attachment to the tank and shell. By employing opposite thread hands on the rod ends, the strut is an infinitely adjustable turnbuckle which is used to provide an even load distribution among the struts. Since the struts are axially loaded, the glass fabric used is a unidirectional weave with the longitudinal filaments laid parallel to the strut axis. Based on 100,000 psi axial fiberglass allowances, and using flight loading for a 20,000-pound vehicle, the fluorine tank requires 12 struts with a 1.25-inch outside diameter and a 0.06-inch wall thickness. The struts are attached in pairs at 60-degree increments to the propellant tank and singly connected in 30-degree increments to the shroud structure.

(U) The transfer of the load from the tubular fiberglass body of the strut to the rod end is accomplished through a tapered titanium insert. The glass is molded over this insert and retained by a sleeve which acts in hoop tension to react the insert's wedging action. Both the insert and titanium sleeve are bonded to the fiberglass. Compressive loads are transferred directly to the tube by a raised lip on the end of the insert. The strut material has good resistance to thermal conduction, but a direct radiation path exists down the inside of the tube from insert to insert. To eliminate this heat path, discs of superinsulation are inserted into the tube. A locknut for safety wiring is provided on the shell rod end of the strut to prevent strut rotation after the proper length is determined during installation.

(C) 2.3.2.2 LH₂ Tank Struts. The function and general construction of the LH₂ tank struts are identical to that of the fluorine tank strut. (See View P of Figure 2-3 in Section 2.2.1.1). Since the hydrogen tank loads are considerably less than those for the fluorine tank, fewer struts are necessary.

(U) Six struts with a 1.00-inch outside diameter and a 0.04-inch wall thickness were required. The struts are attached in pairs at 120-degree increments to the propellant tank and singly connected to the outer structural shroud.

CONFIDENTIAL

UNCLASSIFIED

SECTION 3

INTEGRATED ATTITUDE CONTROL SYSTEM (IACS) STUDY

3.1 INTRODUCTION

The purpose of this subtask is to investigate the impact of an integrated gaseous attitude control system upon the optimized propellant feed system design. For this impact investigation, use is made of the analysis and test results from Contract AF04(611)-10818. The latest data on this ACS system were obtained from Bell Aerosystems on 21 March 1968. Agreement to use this data in the sub-contract task was then obtained and the primary system (single combustor) was installed on the selected vehicle concept drawing, with alternate locations for pumps and other components (Figure 3-1). A schematic of the single combustor system is shown in Figure 3-2. Analytical work is now underway to (1) evaluate the vehicle compartment temperature extremes with the IACS installations, and (2) determine the heat load from the pumps to the cryogenic liquids, considering actuation efficiencies and other effects. Following this, several feed system supply configurations will be evaluated to determine liquid availability to the pumps. NPSP ranges will also be determined at this time.

A study to evaluate the recommended location of the thrusters will be performed, considering mission requirements and dynamic response. A finalized recommended system will be defined and the propellant feed supply system configuration will be selected. The conceptual design will be evaluated for control, sequencing, and check-out operations, and the pumps and transfer lines will be evaluated for heat transfer effects.

A weights study of the selected system will be performed.

The selected system will then be compared to the baseline storable propellant system to determine its relative advantages or disadvantages, considering performance, weight, reliability, and complexity.

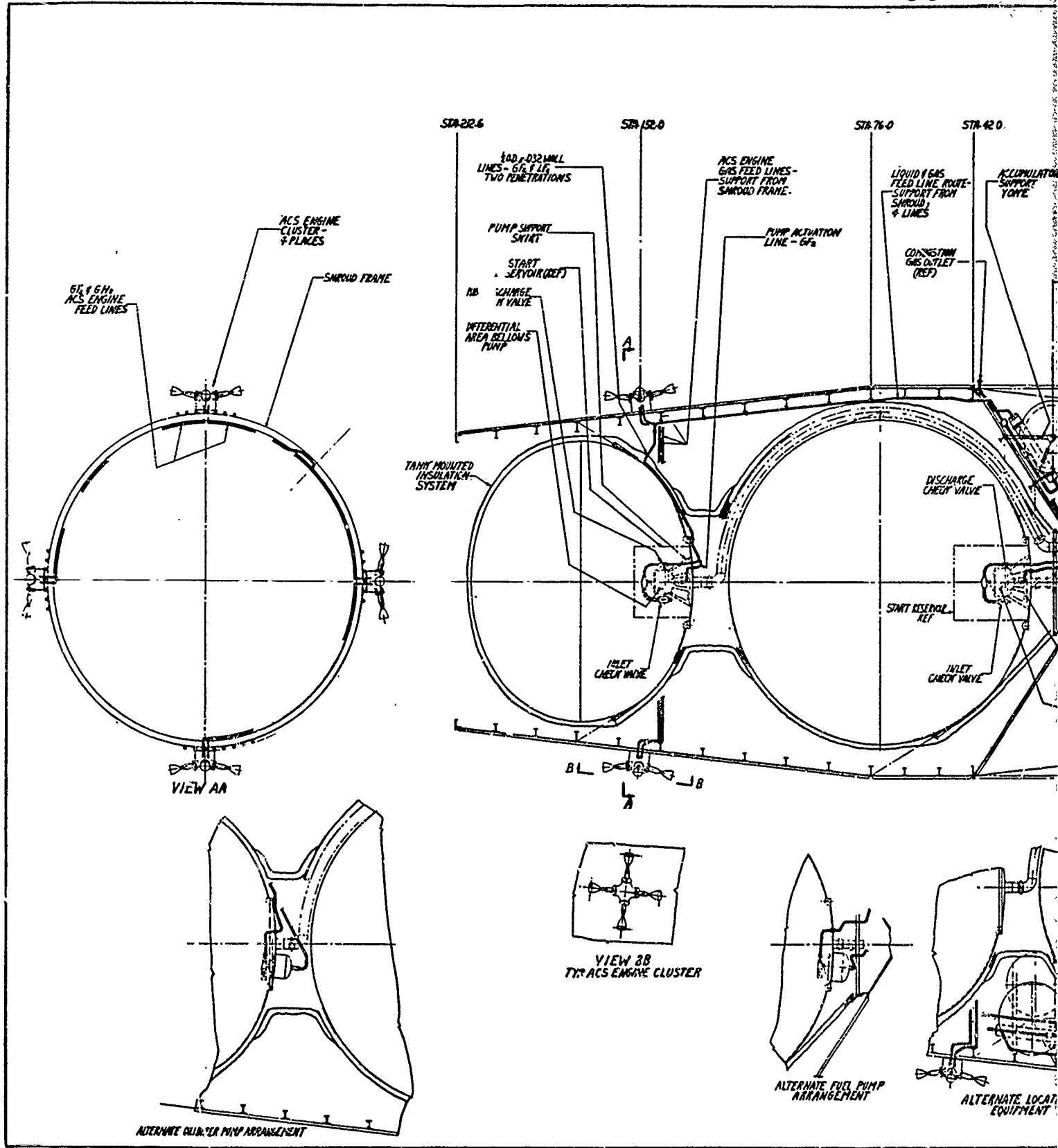
Finally, the results of Bell Aerosystems current program will be used to update the study. Figure 3-3 shows the integrated attitude control system study plan.

3.2 DESIGN PARAMETERS

The design parameters that Bell Aerosystems Company is using as the basis for the integrated attitude control system design are shown in Table 3-1. Convair proposes to utilize the data for the AACS requirements (item II) just as they are.

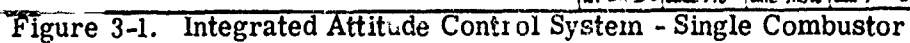
UNCLASSIFIED

CONFIDENTIAL



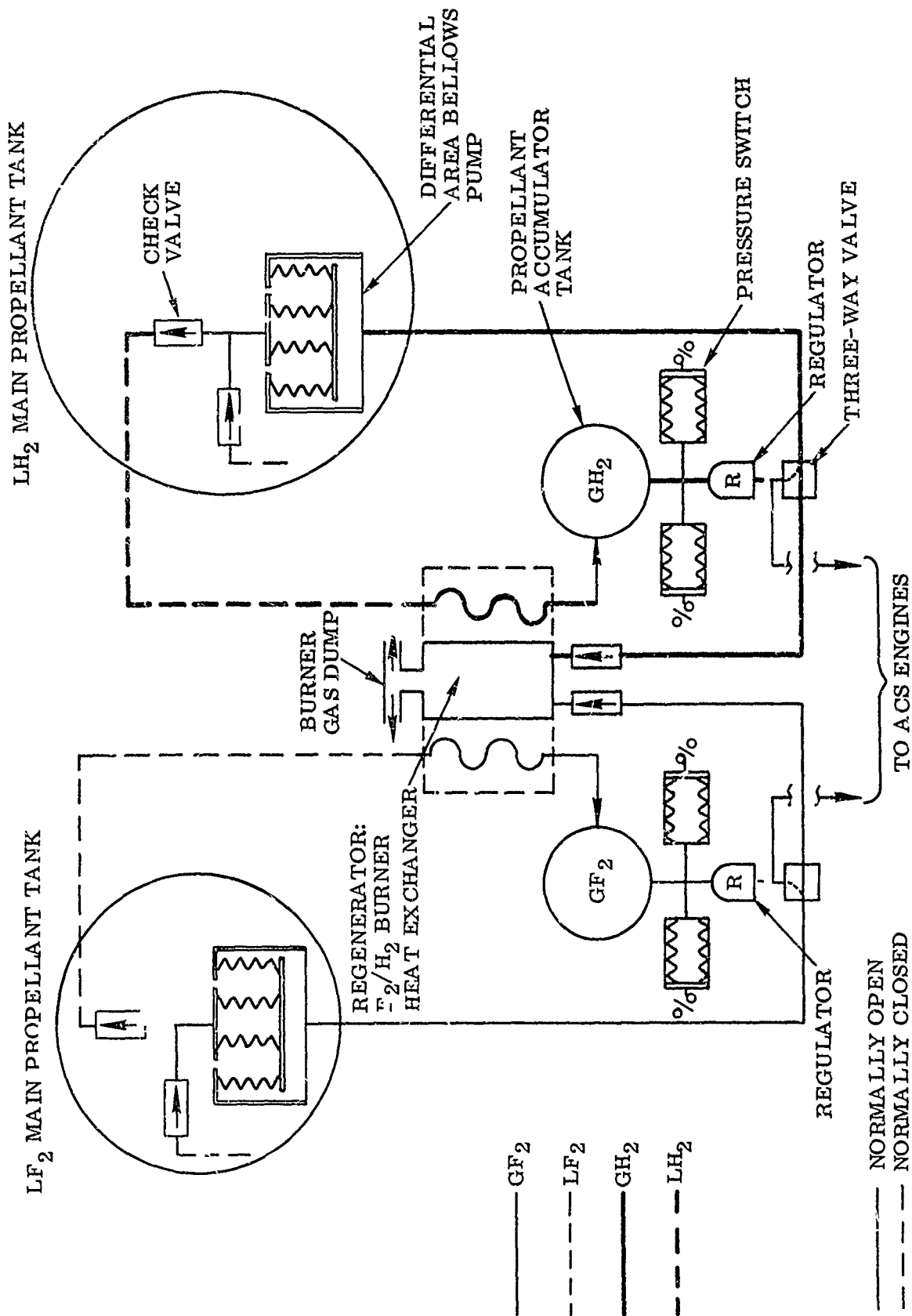
CONFIDENTIAL

CONFIDENTIAL



2

CONFIDENTIAL



(C) Figure 3-2. Advanced Attitude Control System Schematic (Single Combustor)

CONFIDENTIAL

UNCLASSIFIED

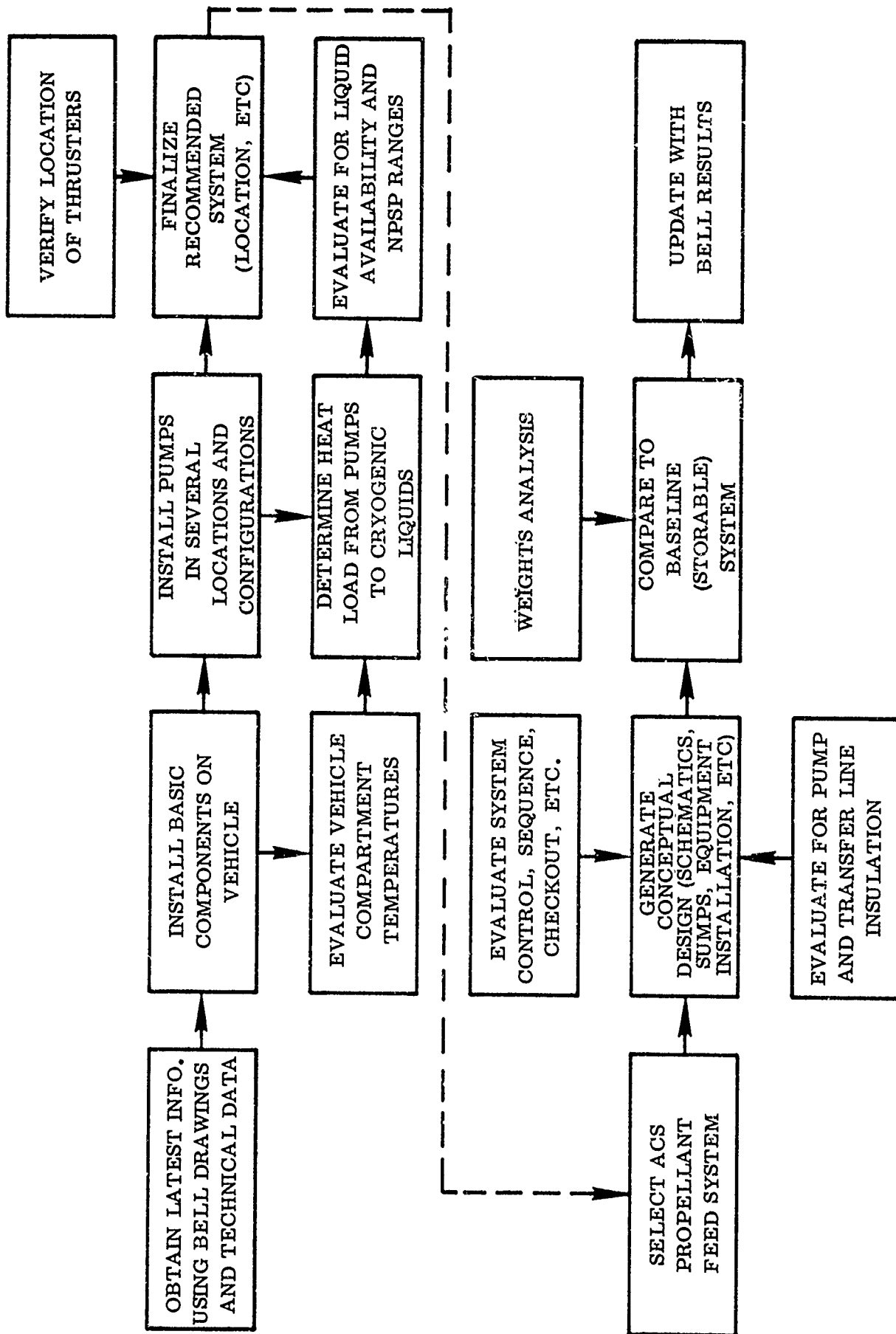


Figure 3-3. Integrated Attitude Control System (IACS) Study

UNCLASSIFIED

CONFIDENTIAL

(C) TABLE 3-1. VEHICLE OPERATING CONDITIONS AND AACS REQUIREMENTS

	Fuel	Oxidizer
I. <u>Main Feed System</u>		
(a) Nominal regulated tank pressure (main engine firing), psia	70	70
(b) Maximum regulator lock-up pressure (prior to engine restart), psia	70	70
(c) Maximum vent pressure, psia	71.5	N. A.
(d) Maximum tank pressure during coast, psia	45.8	52.7
(e) Maximum vapor pressure during coast, psia	41.9	13.4
(f) Maximum propellant saturation temperature, °R	44.0	151.5 (100% Purity)
(g) Minimum propellant saturation temperature, °R	37	144 (Bell Selection)
(h) Propellant vapor pressure at (g), psia	16.0	8.1
(i) Total tank pressure at (g)	19.9	47.9
(j) Main tank volumes, ft ³	281.5	164.0
(k) Loaded propellant weight, lb.	1124.2	14,614.8
(l) Propellant loading temperature, °R	37	144 (Bell Selection)
(m) Outage (end of mission), lb.		
(n) Mixture Ratio (O/F)		
1. Loaded		13:1
2. Engine		13:1
(o) Propellant Density (lb/ft ³)		
1. Minimum	4.10 at 44°R	94.5 at 152°R
2. Maximum	4.42 at 37°R	96.4 at 144°R
(p) Vehicle ambient temperature, °R		400
(q) Vehicle nominal temperature, °R		400

CONFIDENTIAL

CONFIDENTIAL

(C) TABLE 3-1. VEHICLE OPERATING CONDITIONS AND AACS REQUIREMENTS
(CONTINUED)

	Fuel	Oxidizer
II. <u>AACS Requirements</u>		
(a) Number of thrusters	16	
(b) Thrust (each), lb	16	
(c) Approx. total impulse, lb-sec	85,100	
1. Roll control (main engine on)	2,050	
2. Rotation (3-180° maneuvers)	1,410	
3. Target inspection (ten targets)		
(i) Rotation	18,800	
(ii) Translation	60,000	
(iii) Station keeping	58	
4. Limit cycle operation		
(i) Roll axes	2,420	
(ii) Pitch and yaw axes	388	

(C) The data describing the characteristics of the Main Feed System (item I), however, will be revised to reflect the latest system characteristics as they are defined during the course of the study. Most of the parameters have not as yet been finalized for the AMPS study. Two items which must be revised are the vehicle and engine mixture ratio, and the vehicle nominal temperature. The present engine mixture ratio is 12:1 and the initial loaded mixture ratio is 10.56:1. The vehicle shroud temperature is 480°R rather than the quoted 400°R. The other items appear to be representative although, as mentioned previously, the exact values remain to be established.

(U) A list of all information received so far from BAC is shown in Table 3-2.

CONFIDENTIAL

UNCLASSIFIED

TABLE 3-2. LIST OF IACS INFORMATION RECEIVED FROM BAC

1. AMPS/AACS Integration (list)
2. IACS follow on (schedule)
3. Vehicle operating conditions and AACS requirements (including duty cycle)
4. Single combustor system schematics (2)
5. Single combustor system replenishment pump design point and operating conditions
6. Flow characteristics of selected design point
7. Single combustor system accumulator design points
8. System pressure schedule
9. Single combustor system dry weight
10. Heat exchanger design parameters
11. Performance curve (1)
12. (Alternate) dual combustor system schematics (2)
13. Dual combustor system replenishment pump design point and operating conditions
14. Dual combustor system accumulator design points
15. Single combustor system line sizes and routing
16. (Alternate) dual combustor system line sizes and routing
17. Predicted single combustor system pumping cycle flow characteristics (2 curves)
18. Drawing-flight type 3-way valve
19. Drawing - fuel pump
20. Drawing - oxidizer pump
21. Drawing - gas regenerator - single pass (favored)
22. Drawing - double pass individual gas regenerator
23. Drawing - multiple pass gas regenerator (alternate)

UNCLASSIFIED

3-7/3-8

Appendix I

UNCLASSIFIED

SECTION 4

PROPELLANT ORIENTATION

4.1 INTRODUCTION

A propellant orientation system will be designed for AMPS for the purpose of achieving a quick restart capability. This system will position and contain liquid continuously at the propellant tank outlets in order that it be available to the engine upon demand.

Work on the propellant orientation system was just beginning at the end of this quarter. During the next report period a broad range of concepts will be reviewed including capillary devices, dielectrophoresis, bladders, settling motors and start tanks with diaphragms. The influence of other systems on the orientation system, particularly pressurization, vent free fluorine and integrated ACS will be assessed as these systems are more clearly defined. Mission requirements will be analyzed to establish critical operational parameters.

System effects on the AMPS performance, and mission limitations due to an orientation system installation will be evaluated. Burnout residuals must be carefully considered and minimized during the course of the system selection evaluation. Propellant must be supplied not only until full thrust is obtained, but also until propellants have resettled in the main tank. Limits of allowable vapor ingestion during this restart period must be assessed. Also, care must be taken that the related systems not be seriously perturbed. A work plan for this study is outlined in Figure 4-1.

4.2 CAPILLARY DEVICES

To date, a major portion of the propellant orientation effort has been directed at capillary control devices. A capillary device is a container, constructed of mesh or perforated plates, which relies on the interfacial properties of propellants to retain liquids in zero or low adverse g fields. Significant success has been achieved with positive liquid control of non-cryogenic fluids for both bulk positioning and engine feed. The possibility of utilizing these devices for control of cryogenic propellants presents one major additional difficulty, that of propellant heating. In spite of the rapid advances being made in superinsulated systems, propellant heating cannot be ignored for the extended durations of AMP's orbital coast. Thus a capillary device, or start basket, must be designed to isolate the contained propellants from excessive heating in order to minimize the amount of vapor generated. Furthermore, precautions must be taken to permit as much vapor as possible to escape the start basket.

UNCLASSIFIED

UNCLASSIFIED

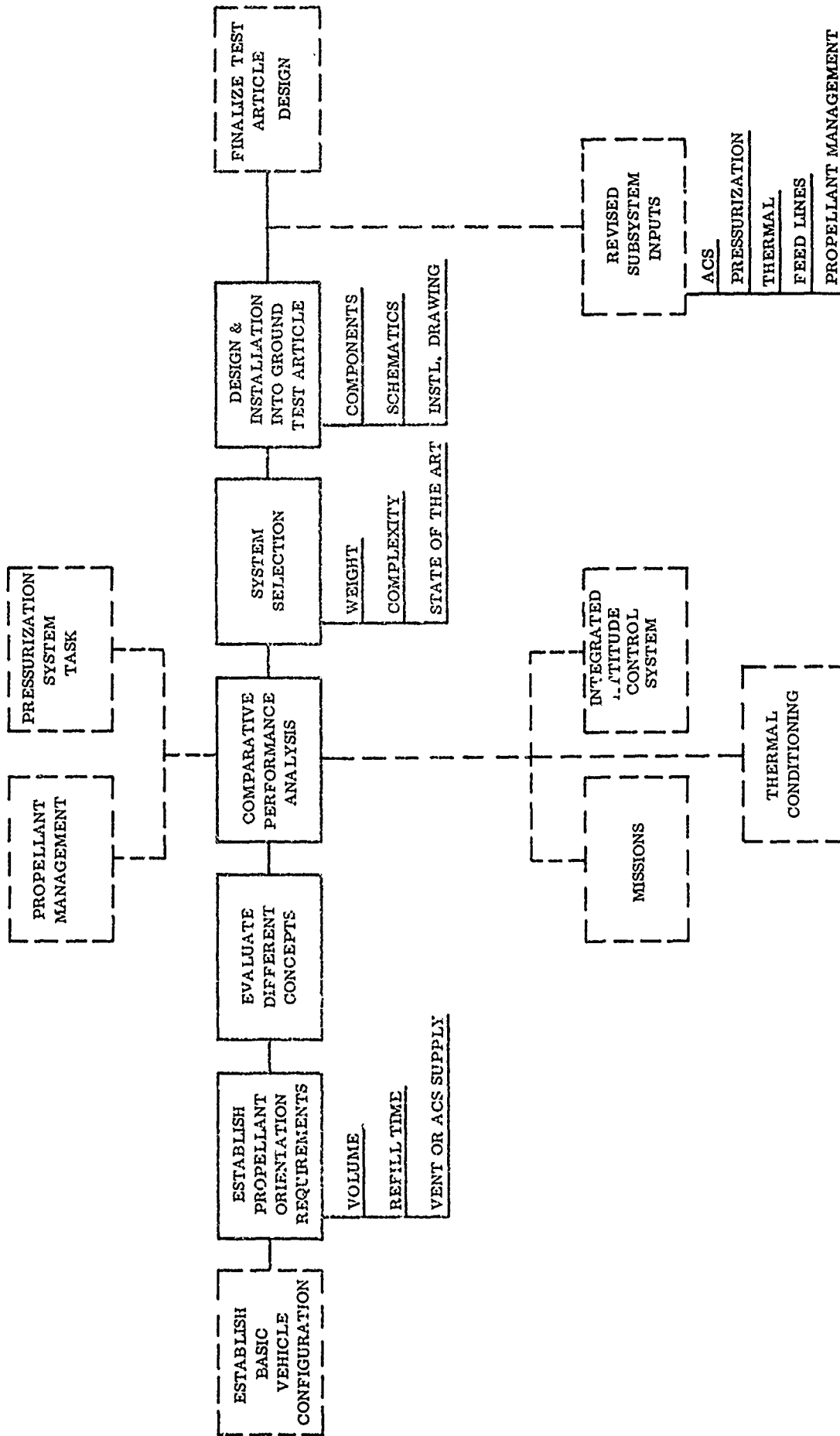


Figure 4-1. Propellant Orientation

UNCLASSIFIED

UNCLASSIFIED

One concept to be evaluated incorporates a heat flux interceptor screen as the method of separating the boil-off from the contained liquid propellant. This screen is shown in Figure 4-2 covering approximately one half of the wetted propellant tank area.

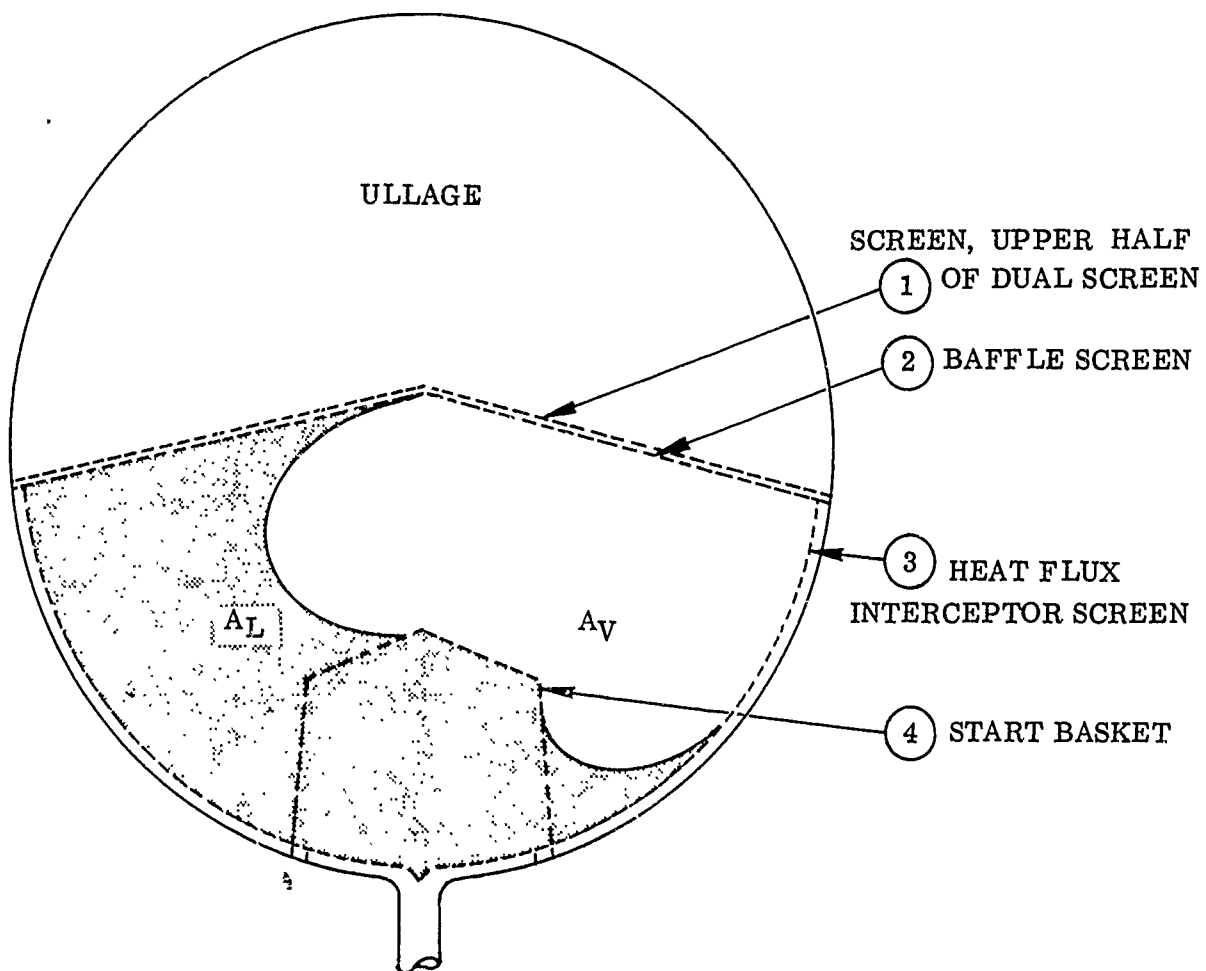


Figure 4-2. A Propellant Orientation Concept

UNCLASSIFIED

UNCLASSIFIED

The worst case situation occurs when the propellant level is below the dual screen/baffle, (1)/(2). This portion of the tank is bounded by a heat flux interceptor screen, (3), which is adjacent to the tank wall and separated from it by a small gap. The start basket, (4), will initially be completely liquid filled. The area enclosed by (2) and (3) contains mostly liquid A_L and some vapor A_V . The gap between (3) and the tank wall initially contains liquid. As very low g levels are encountered, screens (1), (2), and (3) become or stay wetted and prevent gas from entering region A. As heat enters through the tank walls, vaporization of the liquid in the gap occurs and drives a small amount of liquid from the gap through the larger mesh dual screen into the ullage. Additional heating will create a complete vapor boundary in the tank wall to screen gap. Further heat input is intercepted by the wetted screen, (3). Vaporization occurs on the outside of the screen and the gas migrates to the ullage. The liquid being vaporized must be replaced by gas so the gas volume, A_V , slowly increases. The start basket, (4), is enclosed by a smaller mesh screen than (1), (2), or (3) and thus retains its original amount of all liquid. The ullage space consists of all vapor except for the very small liquid loss due to clearing the screen wall gap.

The propellant feed device is a single screen start basket which has the primary function of retaining a supply of vapor free cryogenic propellant for use at engine start. The basket is designed so that boil-off migrating from the warm propellant feed line will be channeled around the basket along the gap leading to the ullage. This passage may be tapered toward the ullage to encourage vapor motion at zero g. The surface tension forces of the start basket fluid/screen interface are sufficient to preclude any vapor break-through during low adverse g conditions, thereby maintaining a liquid filled start basket. When propellant demand occurs, there may be a small amount of vapor ingested before 100 percent liquid is made available to the engine.

At post orbital injection engine shutdown, severe sloshing can occur, with resulting propellant velocities exceeding the retention capability of the screens. To minimize liquid passing through the screens, baffles may be built into the baffle screen, (2), to deflect liquid flow.

The capillary propellant orientation concept discussed above is only one of several which will be examined. Comparisons will be made among several approaches, including dielectrophoresis. Analysis of system operating parameters will continue through the next quarter.

UNCLASSIFIED

CONFIDENTIAL

SECTION 5

PRESSURIZATION SYSTEM

5.1 INTRODUCTION

(U) The AMPS pressurization system study was started in the quarter being reported here. The early phase of this study is concerned with the definition of mission requirements, system ground rules, thermodynamic models, and selection of a group of pressurization schemes for conducting trade-off studies. Following the trade-off studies an operational analysis will be conducted of the selected propellant tank pressurization systems for the most severe AMPS mission to determine the characteristics required to allow system sizing and provide vapor residuals. Finally, system component design studies will be conducted to size hardware and establish component operating criteria. Figure 5-1 shows the selected pressurization system optimization study work plan.

5.2 MISSION REQUIREMENTS

(U) The AMPS system must accommodate a broad range of possible missions requiring different pressurization cycles and pressurant usage. One type of pressurization system is probably not optimum for all possible missions. It is clear, however, that the selected system must be sized to provide sufficient pressurant for the maximum usage mission. This mission will be defined during the next quarter.

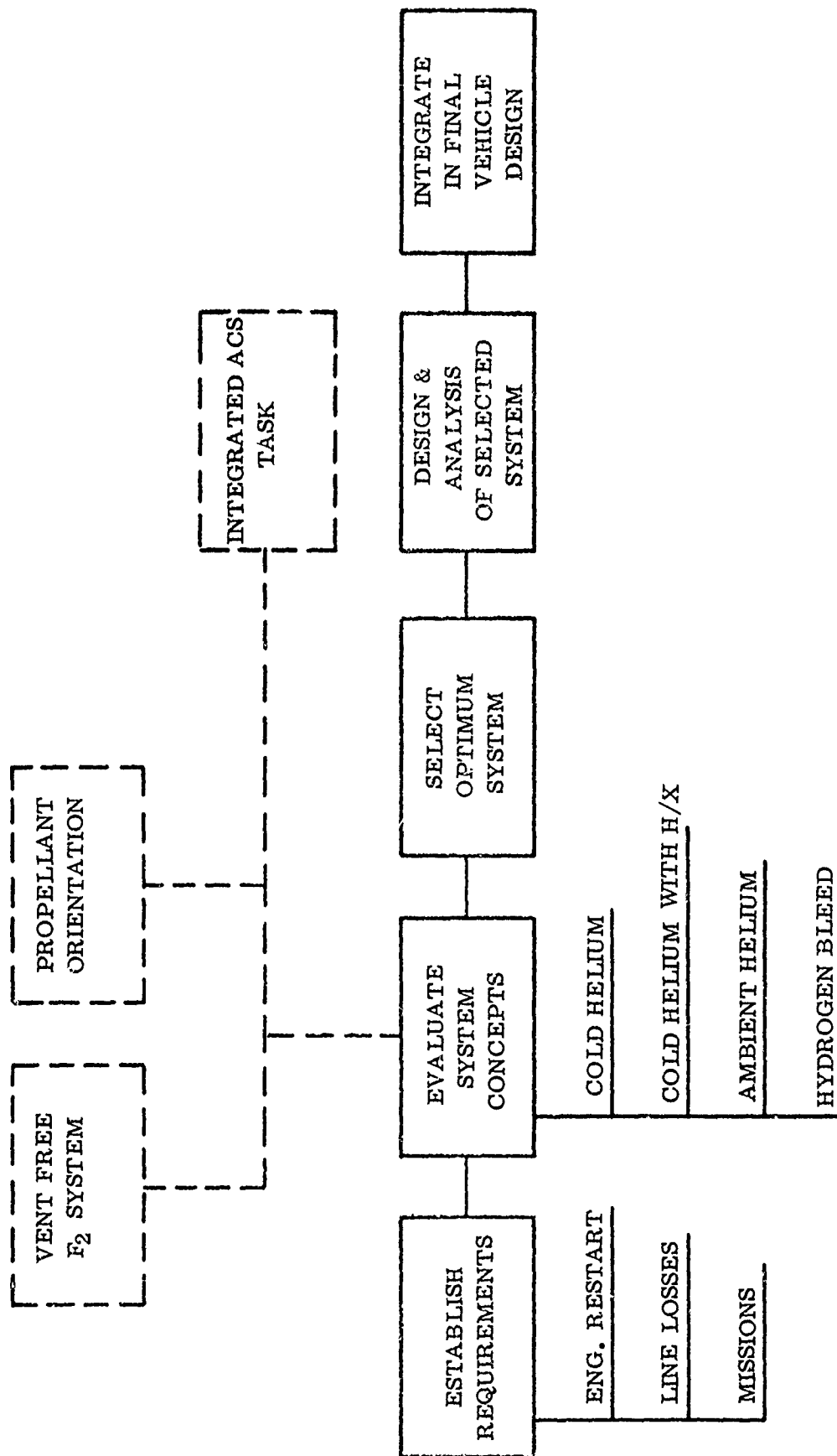
(C) There is an additional major requirement: quick response to an engine restart command. In general, the requirement imposed on the vehicle is that events preparatory to an engine start be minimized. Thus the ideal pressurization system would maintain the propellant tank in a continuous state of readiness by providing the engine start NPSP requirements at all times. It may not be possible to achieve instant response, but quick restart on AMPS will strongly influence design of the entire system.

(C) Propellant tank venting conditions and requirements will also influence the selection of a pressurization system. First, a ground rule has been established that the fluorine tank will not be vented during a mission. Tank venting can be avoided by some combination of insulation and heat exchange with hydrogen ventage to chill the fluorine tank. This condition may favor a pressurization scheme where NPSP is continually maintained throughout a mission because helium will not be vented overboard. The decision must await the results of the Fluorine Vent Free System study to determine the feasibility of such a scheme.

(C) Hydrogen tank venting will be necessary to maintain tank pressure within prescribed limits. If advantageous, however, it would be possible to impose a ground

CONFIDENTIAL

CONFIDENTIAL



5-2

Appendix I

Figure 5-1. Pressurization System Study

CONFIDENTIAL

CONFIDENTIAL

rule of liquid venting only through a heat exchanger system. This would also interrelate with the propellant orientation system. This condition would be equivalent to a non-venting fluorine tank where a pressurization system is concerned.

(C) The schemes selected for evaluation will be checked against the above requirements. Those which show promise will be evaluated in greater detail by checking performance for any or all of the 14 day missions shown in Table 5-1.

(C) TABLE 5-1. FOURTEEN DAY MISSIONS AND PERFORMANCE

Mission	First Day	14th Day
90/10	1 burn	1 burn
90/10	27 burns	4 burn
100	1 burn	—
100	—	1 burn
100	31 equal burns over 14 day period	

A rating system will be established to compare the various pressurization schemes on the basis of weight, complexity, cost and reliability. These factors will then be weighed against the quick restart requirement, if a compromise must be made.

5.3 TANK PRESSURE REQUIREMENTS

(U) The tank pressurization requirements are set by the minimum pressures required by the engine pumps to assure proper operation and preclude cavitation.

(C) The engine inlet pressures used to determine the tank pressurization requirements are:

	<u>Oxidizer</u>	<u>Fuel</u>
Minimum required pump inlet NPSH (ft)	37	55
Main engine inlet pressure (psia)	55.0	65.0

(U) In order to meet these requirements at the engine inlet it is necessary to provide a tank pressure sufficient to overcome the losses in the propellant lines. The total pressure requirement at the pump inlet can be provided by propellant vapor pressure but the NPSH represents a requirement above the vapor pressure of the subject propellants.

CONFIDENTIAL

CONFIDENTIAL

(U) 5.3.1 SYSTEM PRESSURE DROP. The pressure drop in the propellant feed system is composed of three separate items: friction loss, inertia loss, and positive pressure provided by the static head of the fluid above the pump inlets. These can be represented as:

$$\Delta P_{\text{total}} = \Delta P_{\text{inertia}} + \Delta P_{\text{friction}} - \Delta P_{\text{static head}}$$

Inertia is a factor only during the start transient of the engine. During steady state this drops out.

(U) 5.3.1.1 Inertia Pressure Loss. There is a pressure loss encountered when accelerating a fluid column which is equal to:

$$\Delta P = (\ddot{\omega}) (L/A) 1/g$$

where

$\ddot{\omega}$ = flow acceleration - lb/sec²

L = column length

A = flow cross sectional area

g = 32.2 ft/sec²

(U) The flow acceleration is set by the flow demand characteristics of the engine turbopump and is effectively the slope of the flow rate versus time curve. The acceleration loss for any specific configuration is then proportional to the length of the feed line divided by its cross sectional area.

(C) Using the present length of feed lines (225 in. for the LF₂ line and 84 in. for the LH₂ line) the inertia loss can be calculated from the following relationship:

$$\Delta P_{\text{LF}_2} = 0.741 \ddot{\omega}/D^2$$

$$\Delta P_{\text{LH}_2} = 0.276 \ddot{\omega}/D^2$$

where

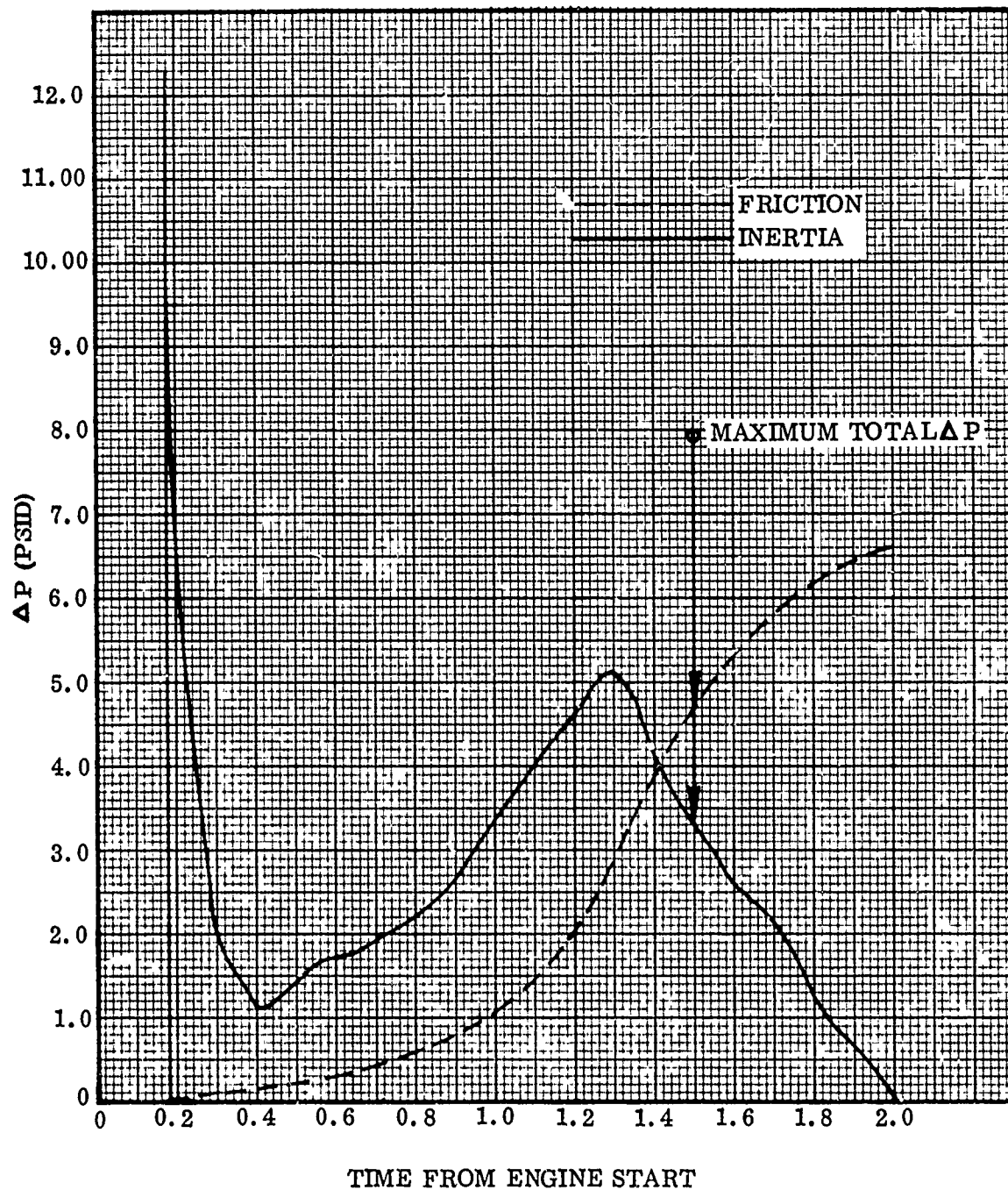
$\ddot{\omega}$ = flow acceleration in lb/sec²

D = diameter of the feed line

The flow acceleration ($\ddot{\omega}$) is obtained from the engine start transient flow rate curves. The inertia loss for a 3-inch line diameter for the fluorine system is shown in Figure 5-2. The loss for other diameter lines can be found by simply ratioing the square of the diameters. It can be noted that there is an initial steep slope of the flow rate curve from zero flow.

CONFIDENTIAL

CONFIDENTIAL



(C) Figure 5-2. LF₂ 3.0 Inch Line System Start Transient Pressure Drop

CONFIDENTIAL

CONFIDENTIAL

(U) The question arises as to whether this is a realistic requirement to impose on the propellant feed system. The major problem occurring during the start transient is the necessity to provide sufficient NPSP to prevent pump cavitation. The required pump NPSP is a steady state value, and a dimensionless parameter often used to evaluate cavitation limits is suction specific speed,

$$S_s = \frac{NQ^{1/2}}{(Hg)^{3/4}}$$

where

N = pump speed (rad/sec)

Q = volumetric flowrate (ft³/sec)

H = minimum inlet head required to suppress cavitation (ft)

g = 32.2 ft/sec²

If the flow through the pump does not deviate exceedingly far from normal, it can be assumed that suction specific speed remains a constant; which in effect says

$$H = \text{const } N^{4/3} Q^{2/3}$$

(U) Since the maximum system pressure drop in the start transient occurs prior to the time flow or pump speed are up to rated values, the NPSP requirements should be less than those during steady state; however, since the flow conditions during the start transient may be quite far from "normal" the scaling laws may not adequately describe the situation. For this analysis the steady state NPSP requirement is used throughout the start transient.

(C) During the initial part of the flow, transient cavitation is not considered to be a problem because of the extremely low pump speed; consequently, the initial flow spike is ignored and the pressure drop calculations for the LF₂ are based on flow conditions subsequent to 0.2 seconds.

(C) Figure 5-3 shows a curve for the LH₂ feed line for a 2.5 inch diameter line which is similar to the curve for the 3.0 inch line.

(C) 5.3.1.2 Friction Line Loss. The friction line loss relationships for the two propellant feed lines are:

$$\text{For LF}_2, \Delta P_F = 0.440 \frac{\dot{W}^2}{D^5}$$

$$\text{For LH}_2, \Delta P_F = 7.15 \frac{\dot{W}^2}{D^5}$$

CONFIDENTIAL

CONFIDENTIAL

(C) These functions are based on each line having three flex joints and three 90° elbows. The line loss during the start transient in the 3.0 inch LF₂ line is plotted in Figure 5-2, and for the 2.5 inch LH₂ line in Figure 5-3.

(C) 5.3.1.3 Maximum System Pressure Drop. The friction pressure loss and inertia pressure loss were added during the start transient to establish the maximum line ΔP . These values are plotted versus line diameter in Figures 5-4 and 5-5 for the LF₂ and LH₂ feed lines, respectively. It can be noted that the start transient loss is always greater than the steady state friction loss for the LF₂ system, while in the case of the LH₂ system, because of the short propellant line and low value of flow acceleration, the steady state ΔP establishes the maximum ΔP at all line sizes.

(C) 5.3.1.4 Static Head Due to Acceleration. A positive pressure is provided by the static head of the fluid above the pump inlets, which is a function of both the fluid level and the acceleration of the vehicle. Because of the low density of LH₂ and the relatively short head available (aft mounted tank), the effects of ρgh on the fuel feed system are ignored; however, these effects are appreciable in the fluorine system. The pressure available from static head in the LF₂ system is equal to:

$$\Delta P = 0.644 T/W \times H$$

where

$$\Delta P = \text{psid}$$

$$T = \text{thrust (lbf)}$$

$$W = \text{weight (lbm)}$$

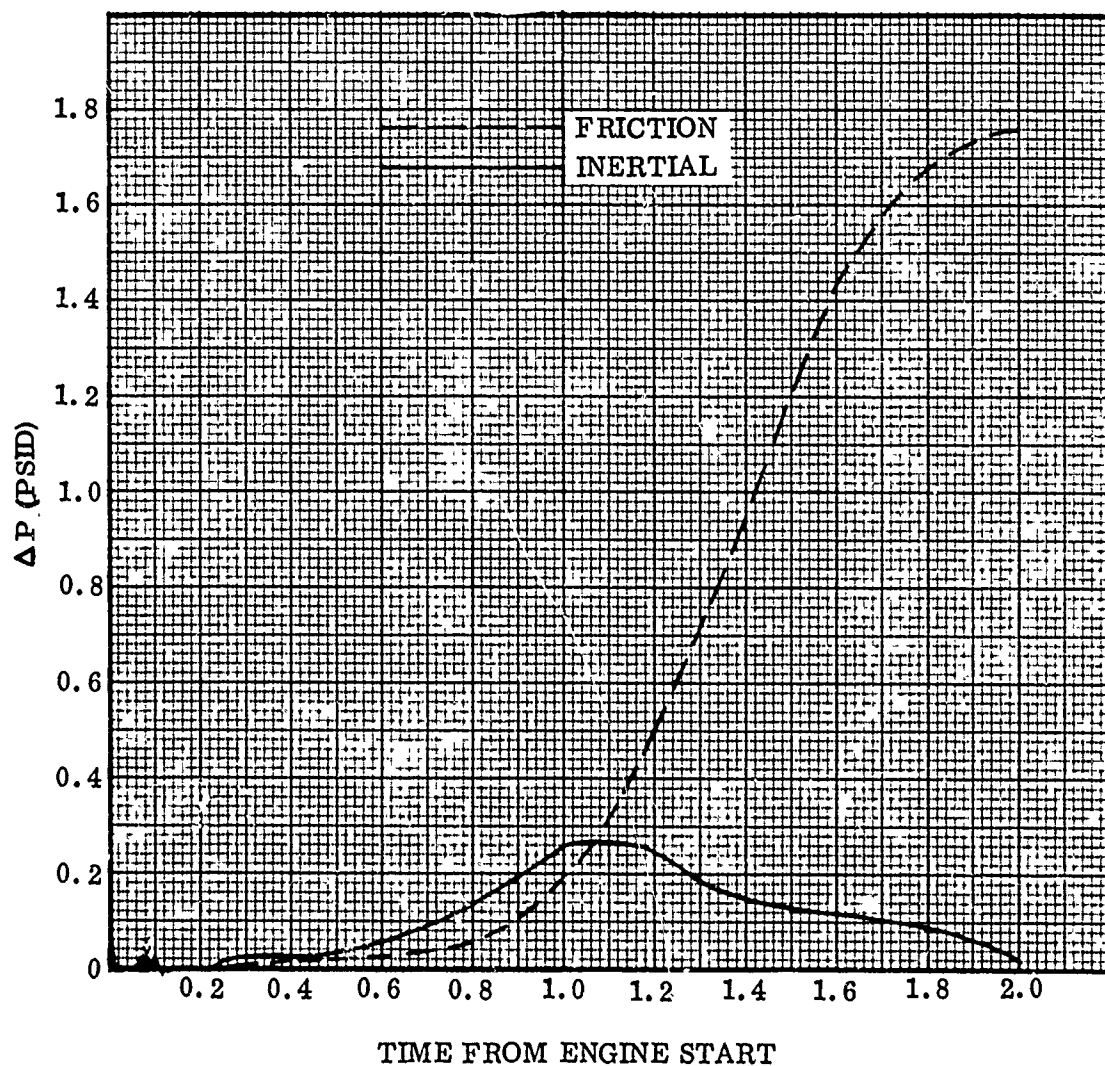
$$H = \text{height of liquid above pump inlet}$$

The additional pressure available at the pump inlet for the first and last burn of a 31 burn mission is shown in Figure 5-6, assuming full engine thrust.

(U) The main effect that this pressure has during the LF₂ start transient is to move the time of maximum ΔP to the initiation of flow where the ρgh is zero and the pressure drop is due essentially to inertia loss. This is true except in the case of the 2 inch line where the maximum ΔP occurs at the steady state condition. The maximum ΔP occurring during the start transient is shown in Figure 5-7. It should be noted that at line sizes of 2.5 inches and above the steady state ΔP is made up by ρgh head, requiring no positive pressurization in the propellant tanks. This calculation was done for full thrust conditions; however, if the thrust is decreased (i. e., throttling) the pressure drop, which is a function of $(\dot{W})^2$, will decrease faster than the ρgh head which is a linear function of thrust and consequently almost a linear function of W . The ρgh should, therefore, be sufficient at all thrust levels to compensate for system pressure drop during steady state operation.

CONFIDENTIAL

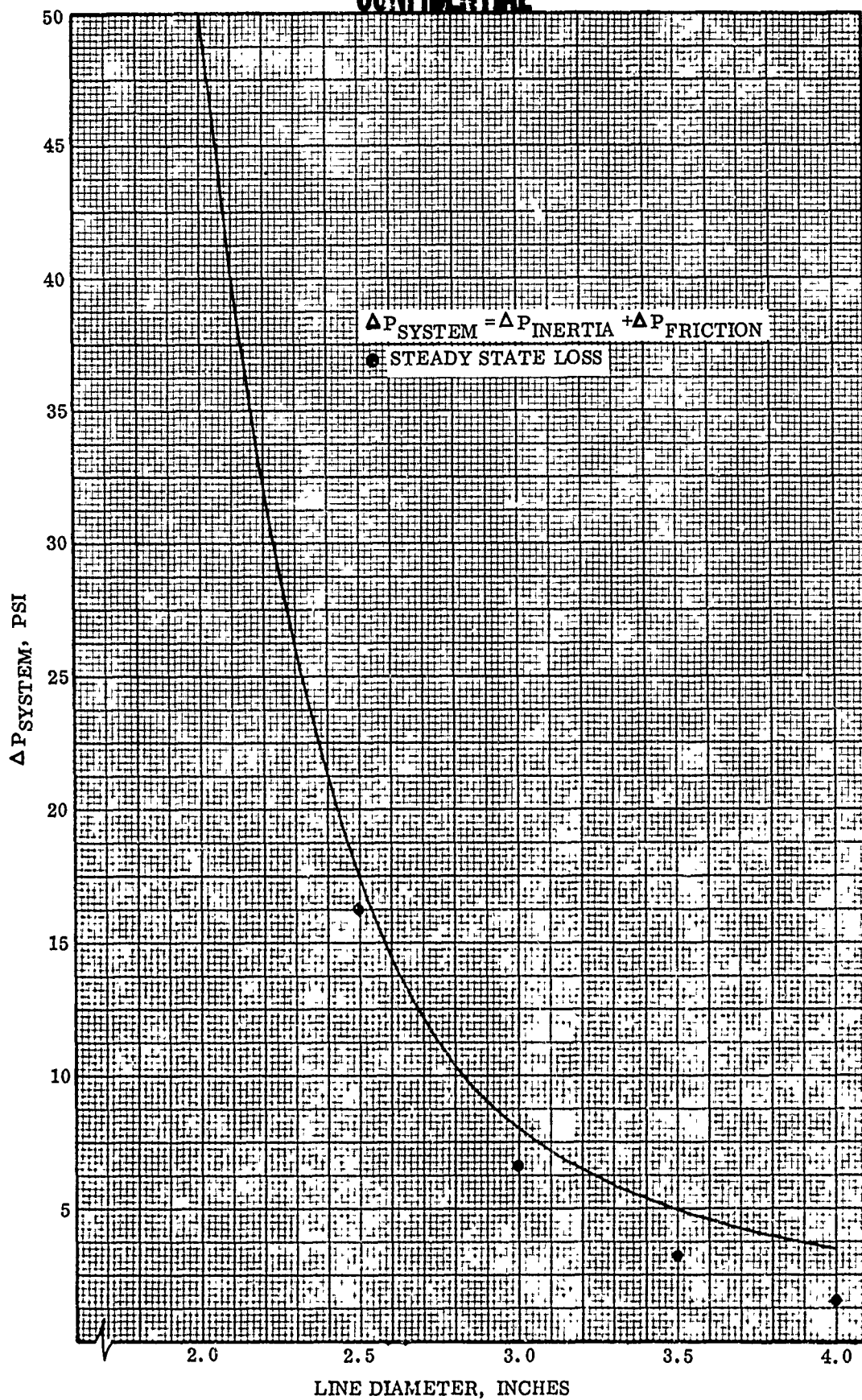
CONFIDENTIAL



(C) Figure 5-3. LH_2 2.5 Inch Line System Start Transient Pressure Drop

CONFIDENTIAL

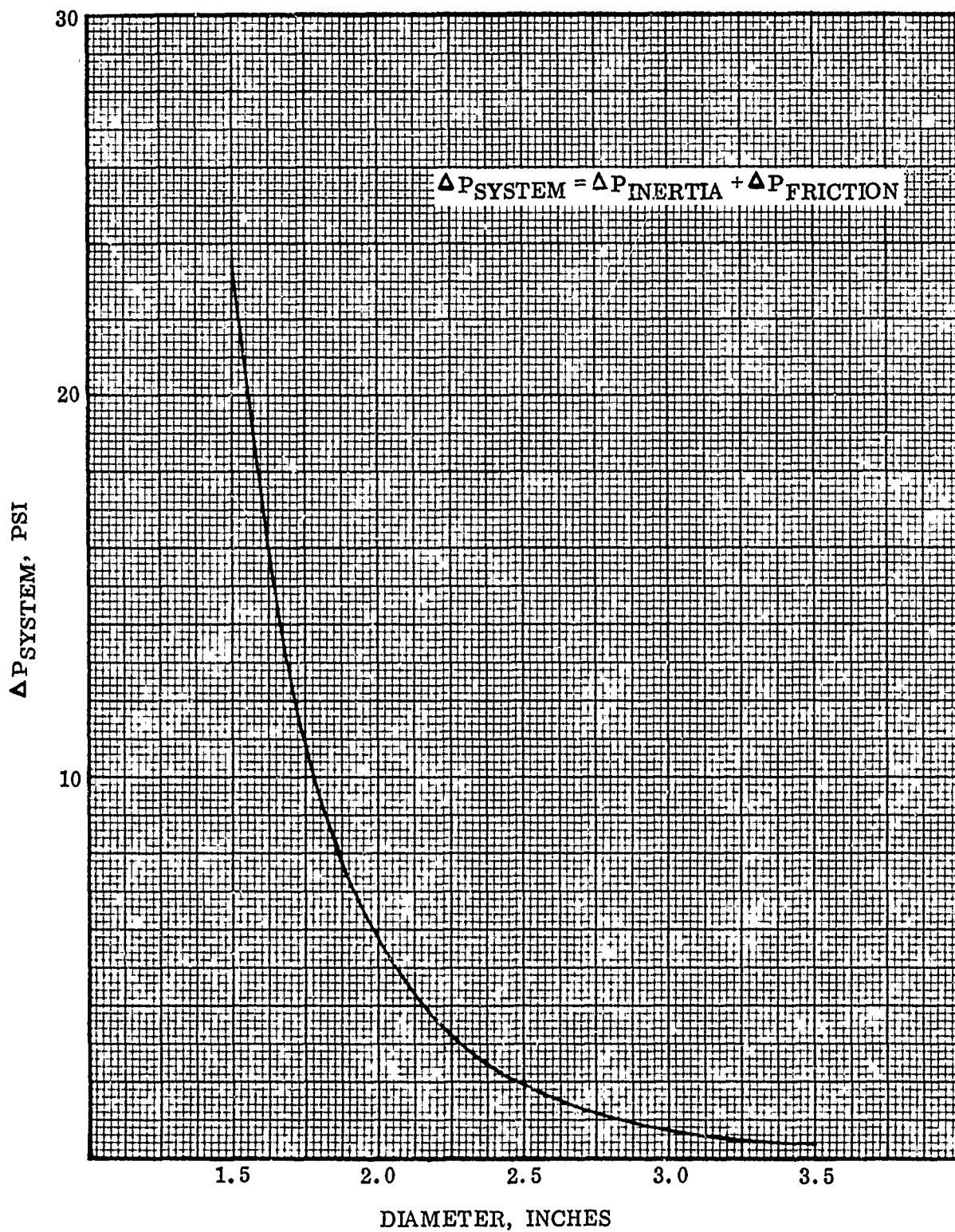
CONFIDENTIAL



(C) Figure 5-4. LF_2 Feed Line Maximum Pressure Drop versus Line Diameter

CONFIDENTIAL

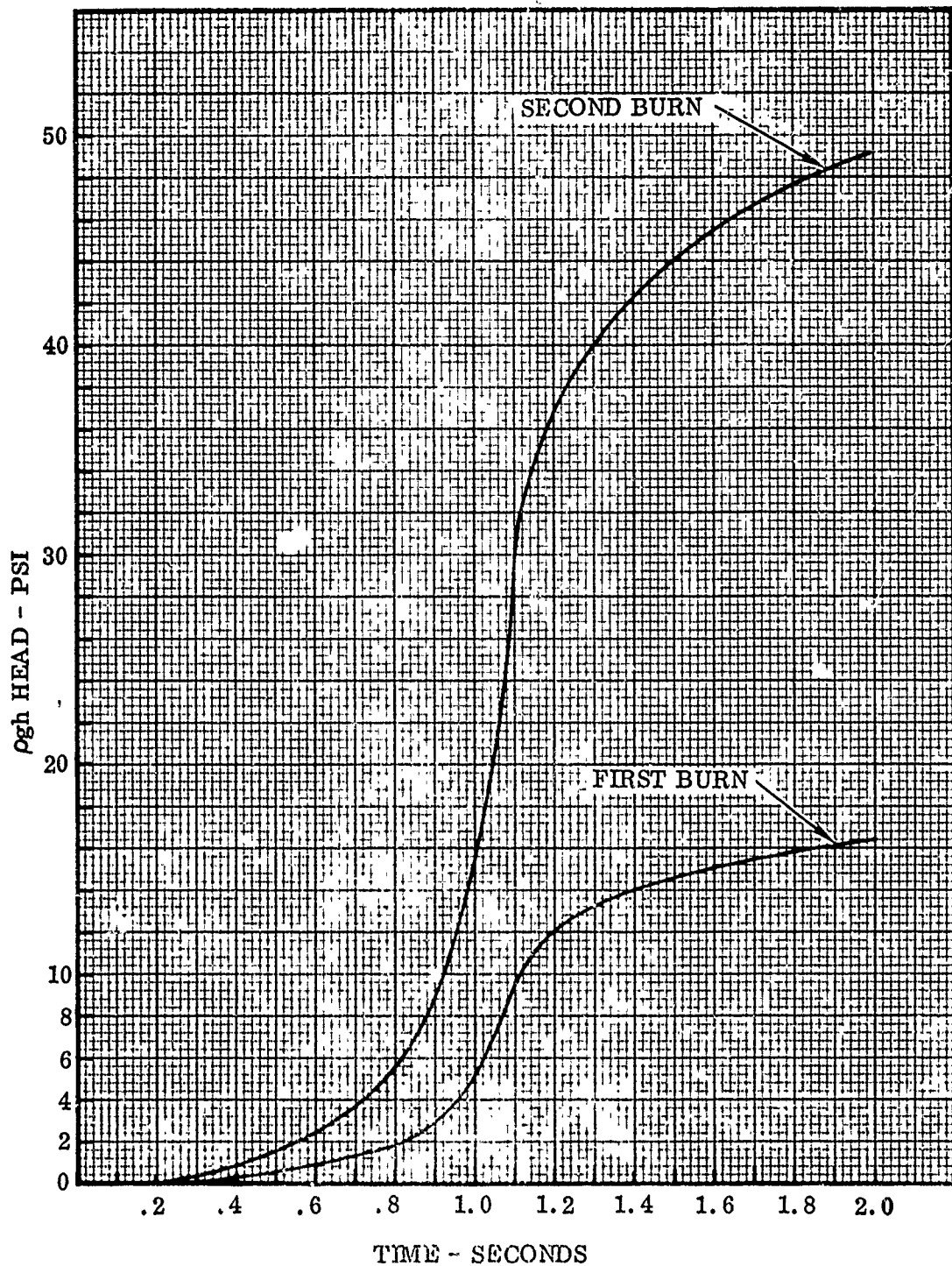
CONFIDENTIAL



(C) Figure 5-5. LH_2 Feed Line Maximum Pressure Drop versus Line Diameter

CONFIDENTIAL

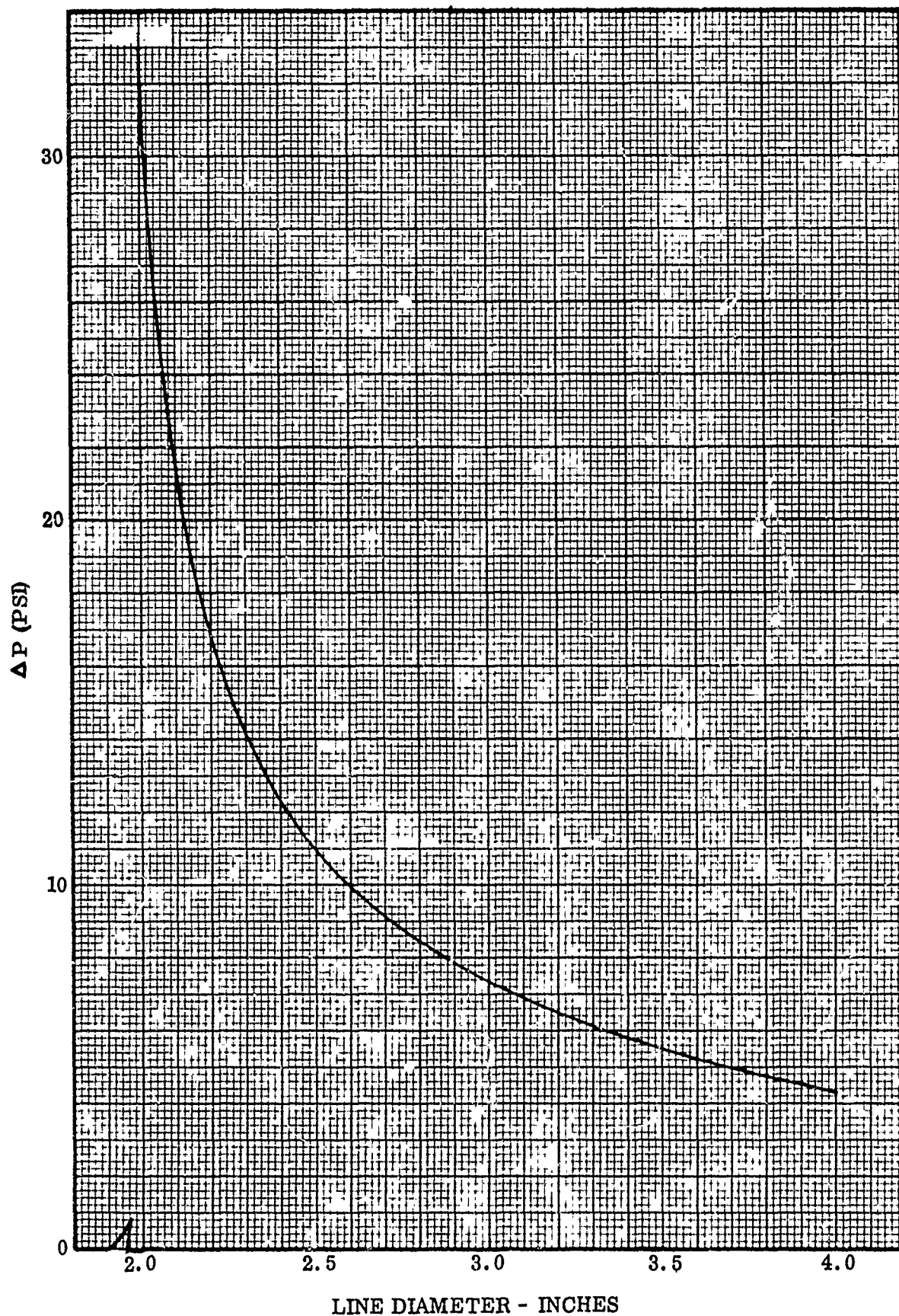
CONFIDENTIAL



(C) Figure 5-6. ρgh Head versus Time Oxidizer Duct

CONFIDENTIAL

CONFIDENTIAL



(C) Figure 5-7. LF_2 Propellant Feed System - System Total Pressure Drop During Start Transient - First Burn

CONFIDENTIAL

CONFIDENTIAL

(C) 5.3.1.5 System Total Pressure Drop Characteristics. The system maximum pressure drop including inertia, friction, and ρgh effects can be summarized for various line diameters as shown in Table 5-2.

(C) TABLE 5-2. SYSTEM MAXIMUM PRESSURE DROP

Line Diameter	Start	LF ₂ Steady State	Start	LH ₂ * Steady State
1.5"			25	23.5
2.0"	17.02	33.1	5.57	5.57
2.5"	10.84	0	1.83	1.83
3.0"	7.5	-9.7	0.735	0.735
3.5"	5.4	-13.3	0.34	0.34
4.0"	4.2	-14.8		
*Not including ρgh effects				

The negative sign for the LF₂ pressure drop indicates that the ρgh is higher than the friction losses, resulting in a positive pressure at the pump inlet.

(U) 5.3.2 INERT WEIGHTS.

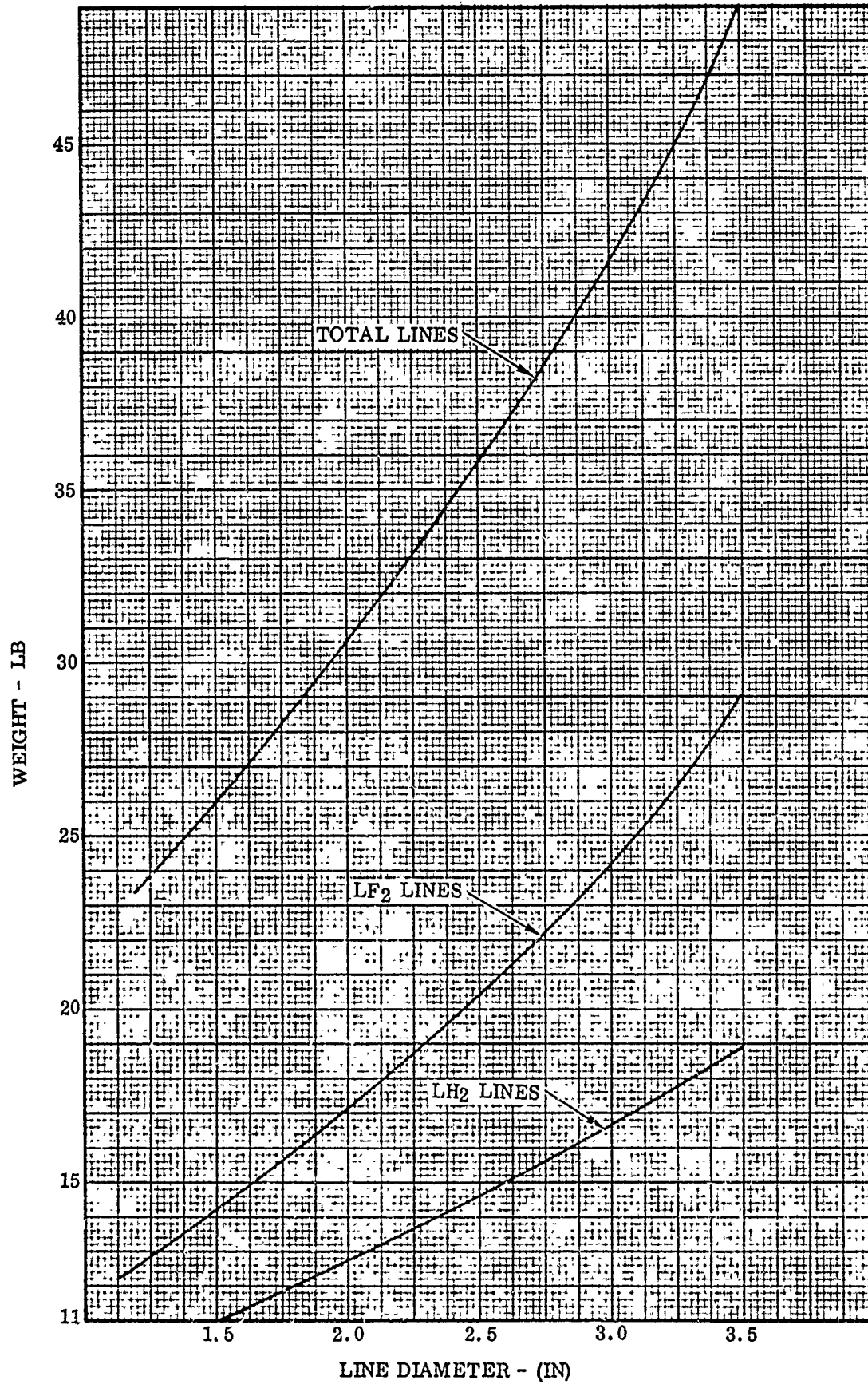
(U) 5.3.2.1 Line Weights. The line weights are also a function of line diameter and must be considered when establishing the line size. Figure 5-8 shows the weight of the propellant lines as a function of diameter.

(C) 5.3.2.2 Residual Weights. The propellant line residuals are shown in Figure 5-9. The LF₂ residuals are based on utilizing the propellants down the line until the liquid head level is 6 feet above the pump inlet. The exact minimum level that can be attained is dependent on the tank pressure, the line pressure drop, and the burnout thrust to weight ratio. This figure is felt to be representative of the level that can be attained near burnout, although the actual level will be determined after the design is finalized. The curve gives an indication of the increase in residual propellants as a function of line diameter. For multi-burn missions some of this propellant will be lost each burn, and in fact, the hydrogen in the line will probably be vented after each burn.

(C) 5.3.3 SELECTED LINE SIZE. Based on the system pressure drop, line weights, and liquid residuals, the preliminary line sizes chosen are 3 inches for the LF₂ system and 2.5 inches for the LH₂ system, with the corresponding pressure drops at full thrust.

CONFIDENTIAL

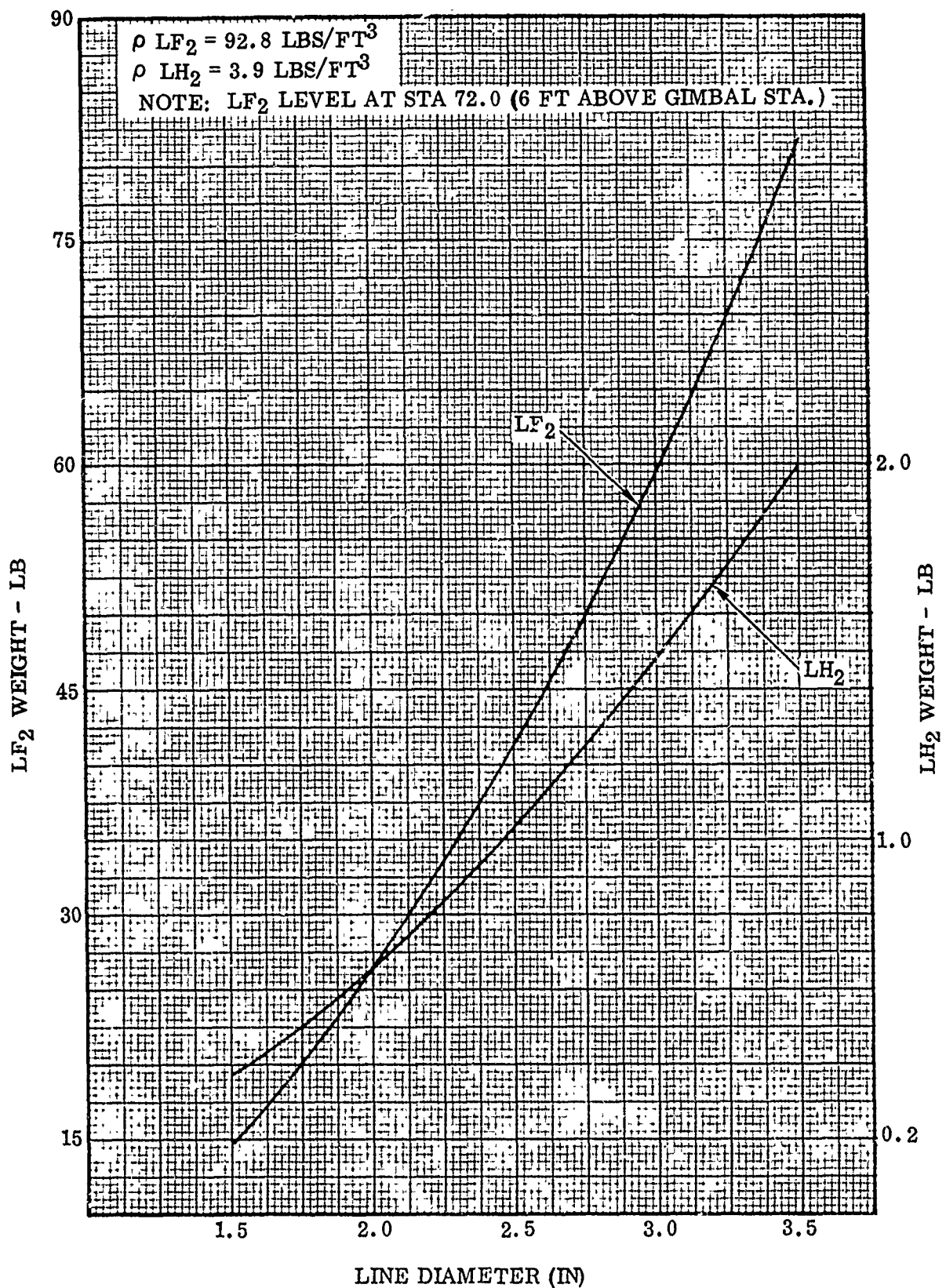
CONFIDENTIAL



(C) Figure 5-8. Propellant Line Weight versus Diameter

CONFIDENTIAL

CONFIDENTIAL



(C) Figure 5-9. Propellant Residuals versus Line Diameter

CONFIDENTIAL

CONFIDENTIAL

(C)		<u>Start</u>	<u>Steady State</u>
	LF ₂ (psid)	7.5* (7.94)	-9.7* (6.6)
	LH ₂ (psid)	1.8	1.8

*Includes ρgh effects for a first burn condition - the numbers in parenthesis show the pressure drops excluding these effects.

As the program progresses and pressurization system weights are established, the line size selection will be reviewed to determine the effect of pressure drop on system weight and to verify that the correct line size has been assumed to assure minimum system weight.

5.4 CANDIDATE PRESSURIZATION SCHEMES

(U) The schemes to be considered in the trade-off study to select the optimum system for the AMPS mission are listed below. Each concept may serve the entire pressurization system, or various combinations may be used for repressurization and outflow of the two propellant tanks.

(U) 5.4.1 AMBIENT HELIUM. This is the "standard system", but it necessitates heavy, space consuming storage bottles. For one-burn missions, helium consumption is less than it would be with cold helium.

(C) 5.4.2 COLD HELIUM. It is more efficient to store helium at LH₂ temperature: titanium spheres for storing helium at 40°R require 1/5 the bottle weight required for storing helium at 540°F (See Figure 5-10.); however, residual helium in the bottle could be a major penalty on single burn. Residuals become smaller for multiple burn missions as additional time is available for warming helium back to 40° R. System complexity increases as heater systems are added to the bottle and/or prestart supply. For a single burn mission, residuals can be minimized by return of warm H₂ to the H₂ tank helium bottle, and return of warm helium to the F₂ tank helium bottle to increase temperatures to 40° R.

(U) 5.4.3 SUPERCRITICAL HELIUM. This technique achieves very high helium densities (greater than 10 lb/ft³) by loading at extremely low temperatures (approximately 12°R) and supercritical pressures (approximately 500 psia) (Reference 11). Elaborate GSE, including liquid helium supply, is required; plus airborne heat exchangers. For a cryogenic vehicle such as AMPS the complexity of this novel approach may be undesirable. Furthermore, even if stored in a vacuum jacketed, super-insulated bottle, helium could warm excessively during a long coast, necessitating vent losses.

(C) 5.4.4 HOT HYDROGEN. Propellant vapor to pressurize the tank can originate from main engine bleeds or from auxiliary pump and heat exchanger systems. Due to its light weight, gaseous hydrogen is preferred over helium for fuel tank pressurization.

CONFIDENTIAL

CONFIDENTIAL

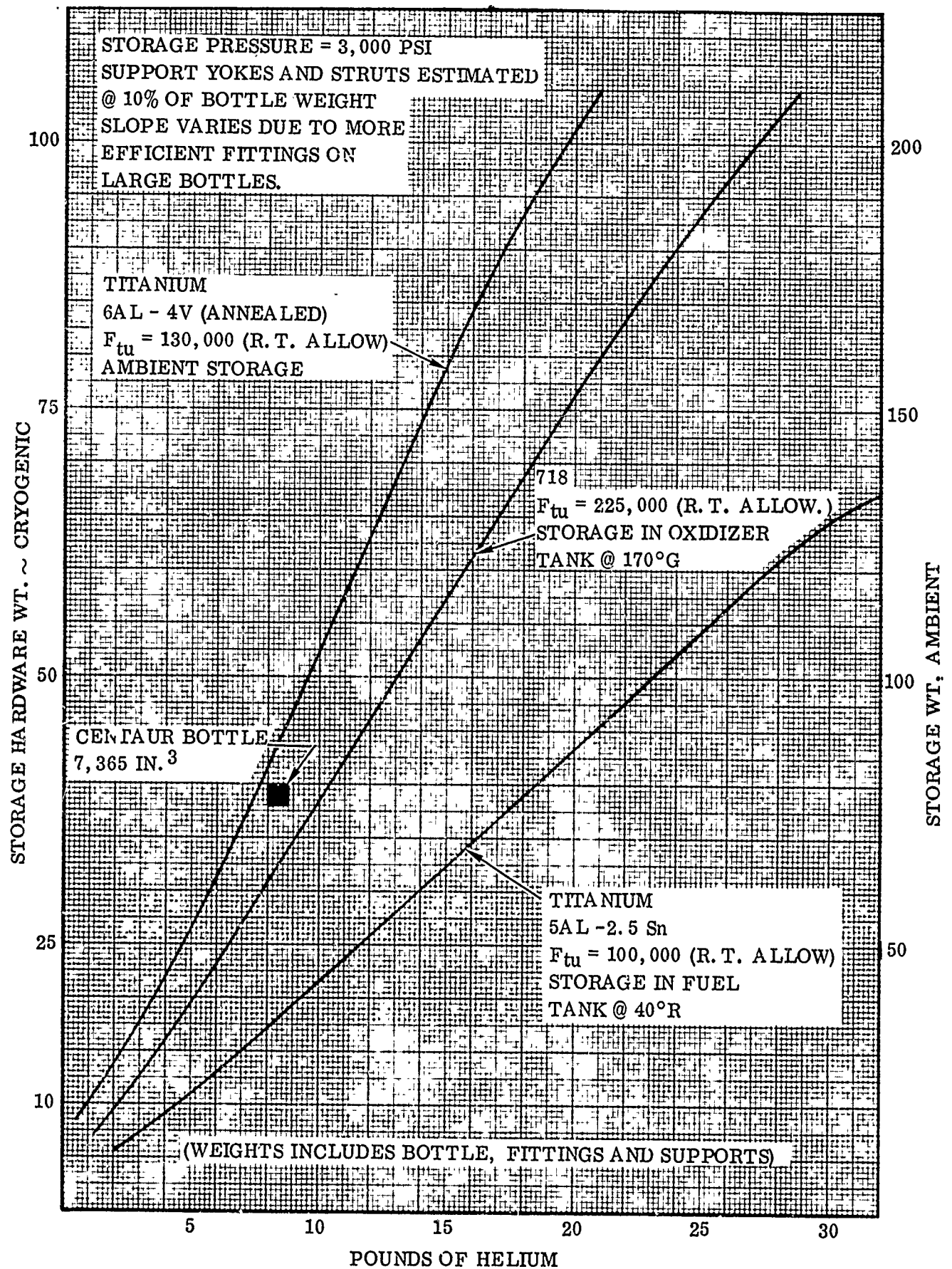


Figure 5-10. Helium Storage Weights

CONFIDENTIAL

CONFIDENTIAL

(C) There is no advantage to pressurizing the oxidizer tank with fluorine gas since the propellant vapor should be minimized to save weight.

(C) 5.4.5 MAIN TANK INJECTION. Some success has been achieved in creating tank pressure by spraying a hypergolic fluid into the ullage. Report AFRPL-TR-65-64 gives some Martin-Marietta test results. A similar technique burns solid or liquid propellants in a separate gas generator, then exhausts the products into the main tank ullage. These schemes raise serious problems in compatibility of combustion or reaction products with the vehicle propellants. HF, the principal product of main propellant injections on AMPS, would freeze and sink in hydrogen. Molecular weight of such pressurants is high. The systems are largely experimental, not flight proven.

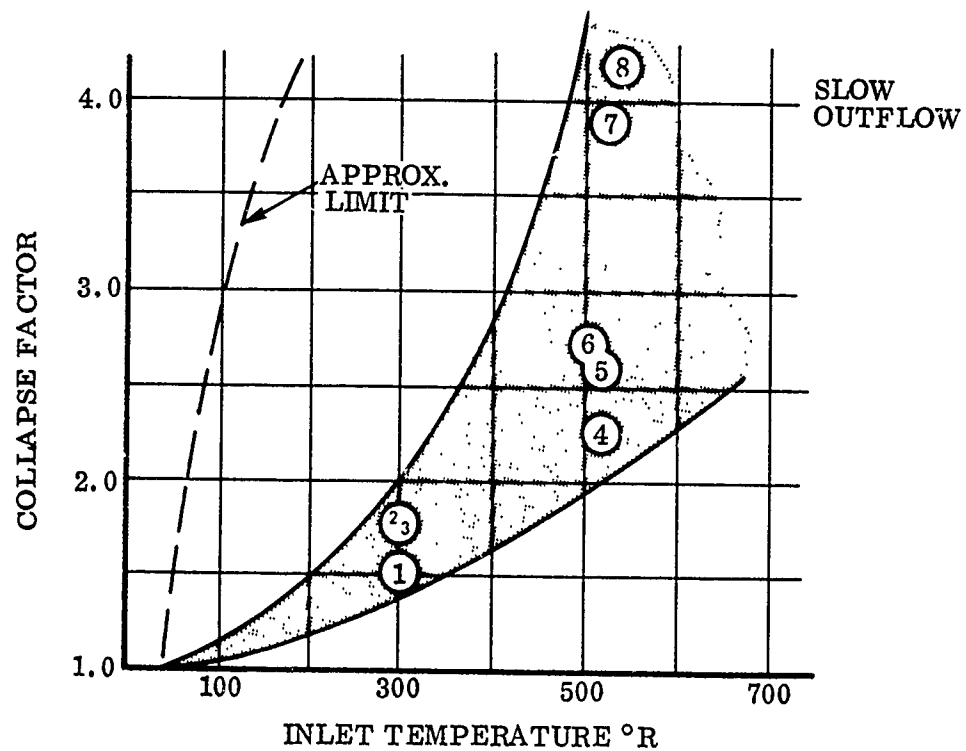
5.5 THERMODYNAMIC PRESSURIZATION MODELS

(U) Uncertainties in ullage mixing or stratification, thermal losses to the tank walls, and heat and mass transfer at the liquid surface all grossly effect pressurant requirements. These thermal processes are influenced by tank shape (long cylinder versus sphere), diffuser effectiveness, propellant location, wall material and mass, and vehicle/propellant agitation or disturbances. Figures 5-11 and 5-12 show collapse factors obtained from several tests conducted in a one-g environment. Collapse factor is the amount of pressurant actually required compared to the amount which would be required in an adiabatic process. These curves illustrate the large variations in available data. Even larger variations are expected for AMPS because of the uncertainty regarding fluid conditions, orientation, g-level, and mission history.

(U) In light of all the unknowns or uncertainties related to variables affecting pressurant requirements, it appears preferable to bracket the limits of pressurant usage rather than perfect a thermodynamic model that relies on collapse factors. Furthermore, this approach may result in similar total system weight (hardware plus residual). To illustrate, Figure 5-13 shows helium system weights and GO_2 residuals for Centaur, plotted against percent ullage mixing. It is interesting to note that while the individual weights vary greatly, their sum is nearly constant. Therefore, during the next quarter an investigation will be conducted to determine if the use of bracketing analyses (perfect mixing and no mixing for the case of a helium pressurant) is justified for the pressurized system study.

CONFIDENTIAL

UNCLASSIFIED



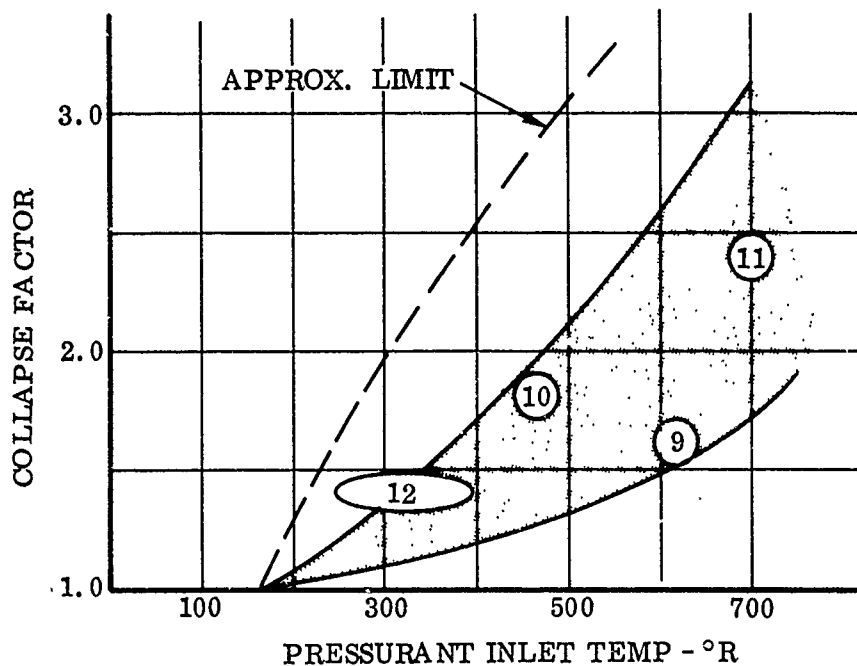
Test Data										
Vol		Wall	Propel	Press	T _{IN} ° R	psia	Drain Time-Sec	Disturb	Press Consum	Ref
1	70 ft ³	0.090 CRES	LH ₂	GH ₂	300	47	95	0.5 cps	2.47 #	1
2	70 ft ³	0.090 CRES	↑	He	300	46	99	0.5 cps	5.79 #	1
3	70 ft ³	0.090 CRES		GH ₂	300	46	105	Sud slosh	2.88 #	1
4	70 ft ³	0.090 CRES		GH ₂	520	48	103	0.5 cps	2.13 #	1
5	23 ft ³	0.3 CRES		GH ₂	517	58	107	none	1.24 #	2
6	25 ft ³	0.3 CRES	↓	He	505	56	100	none	2.63 #	2
7	22 ft ³	0.3 CRES		GH ₂	512	56	302	none	1.76 #	2
8	23 ft ³	0.3 CRES		LH ₂	He	532	58	337	none	4.09 #

- "Analysis of the Pressurization Gas Required for an Evaporating Propellant Pressurization System, E. F. Cox and J. W. Tatum, Lockheed, Georgia, 1961 Cryogenic Engineering Conference Paper Vol. 7 F-6.
- "Gas Requirements in Pressurized Transfer LH₂", D. F. Gluck and J. F. Kline, LeRC, 1961 Cryogenic Engineering Conference Paper Vol. 7 F-5.

Figure 5-11. Outflow Pressurization Hydrogen Collapse Factor

UNCLASSIFIED

UNCLASSIFIED



Test Data										
	Vol	Wall	Propel	Press	T _{IN} °R	psia	Drain Time-Sec	Disturb	Press Consum	Ref
9	1350 ft ³	3/8 CRES	LO ₂	GO ₂	620	72	70	none	750#	1
10	2.2 ft ³	1/8 Al	LN ₂	He	460	50	117	none	0.14#	1
11	2700 ft ³	0.04 CRES	LO ₂	He	700	25	120	flight	30#	2
12	1263 ft ³	Al	LO ₂	He	240 to 400	45	1300	flight	94#	3

1. "Experiences with Pressurized Discharge of LO₂ from Large Flight Vehicle Propellant Tanks", H. E. Nein and R. R. Head, MSFC, Presented at 1961 Cryogenic Engineering Conference Paper F-7, Volume #7 Advances in Cryogenic Engineering.
2. AE61-0596, "Thermal Analysis of Atlas 55D Ullage", 23 June 1961.
3. MPR - SAT - FE - 64-17, SA-5 Flight Data

Figure 5-12. Outflow Pressurization Oxygen Collapse Factor

UNCLASSIFIED

UNCLASSIFIED

CENTAUR LO₂ TANK OUTFLOW PRESSURIZATION STUDY

CONDITIONS: 403 FT³ LO₂ TANK, INITIALLY SATURATED LO₂ AT 26 PSIA, FINAL PRESS 35 PSIA

ASSUMPTION: AMBIENT HELIUM BOTTLE WEIGHT = 11 LB/LB of He

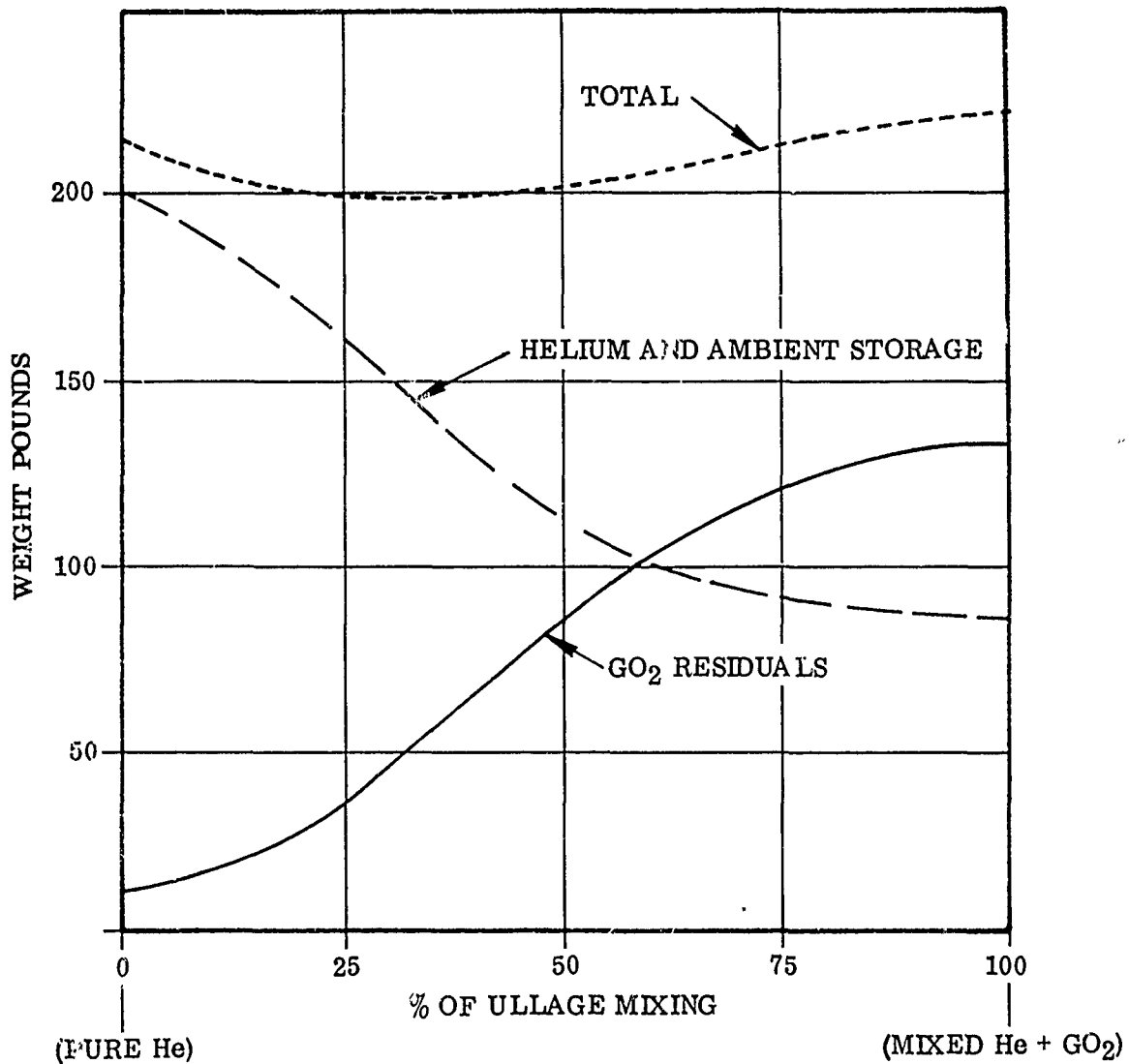


Figure 5-13. Ullage Mixing

UNCLASSIFIED

UNCLASSIFIED

SECTION 6

REFERENCES

1. "Design Standards Bulletin," Serial Number DS-21, Revision A, NASA Manned Spacecraft Center.
2. "Aerospace Meteoroid Environment and Penetration Criterion," Aerospace Corporation, Contract Number AF04(695)-269, 17 August 1964.
3. "System Effects on Propellant Storage and Vehicle Performance - Douglas Aircraft First Quarterly Progress Report," Douglas Report SM-47918, 3 May - 23 July 1965.
4. "Investigation of a Light Weight Self-Evacuating Prefabricated Multi-Layer Insulation System for Cryogenic Propulsion Stages," Union Carbide, Linde Division NAS3-6289.
5. K. E. Leonhard, et al, "Development of a New Superinsulation for Cryogenic Space Tankage," ASME Aviation and Space Division Conference, June 1968.
6. "Liquid Propellant Losses During Space Flight," A. D. Little, Inc., Report Number 65008-00-04, October 1964.
7. "Advanced Maneuvering Propulsion System (AMPS) Quarterly Progress Report (U)," General Dynamics Convair Division, GDC-BNZ68-013, 9 February 1968. Confidential.
8. R. E. Drowns, "Performance Program (With Duty Cycle Capability) for a Maneuvering Satellite System," General Dynamics Convair Division, Aeroballistics Technical Note TN-65-AC-02, (also System Development Technical Memorandum Number 148), 26 April 1965.
9. "Buckling of Thin-Walled Circular Cylinders," NASA SP-8007, September 1965.
10. "Vacuum Shell Selection," Convair Report Number GDC-BNZ68-015.
11. J. S. Tyler, "Cryogenic Storage of Helium for Propellant Tank Pressurization," (Airesearch), Conference on Propellant Tank Pressurization and Stratification at MSFC, 20 January 1965.
12. "Analytical and Experimental Studies of Gas Flow through Multi-Layer Insulation," LMSC-A742593-V, August 1965.

UNCLASSIFIED

UNCLASSIFIED

REFERENCES (Continued)

13. "Investigation Regarding Development of a High Performance Insulation System." NAS8-20768 2nd Quarterly Progress Report, 10 December 1967.
14. "Superinsulation Research and Structural Integration Program," GDA-ERR-AN-650, December 1964.
15. "Superinsulation Research and Development Program," GDC-ERR-AN-1201, December 1967.
16. Aerospace Fluid Component Designers' Handbook, Volume II, Revision B; Technical Documentary Report Number RPL-TDR-64-25, March 1967.
17. "Fluorine System Handbook," NASA CR-72064, DAC-59074 by Advanced Propulsion Staff "Douglas," Contract NASW-1351, July 1967.
18. J. E. Chafey, W. E. Witzell, and W. G. Scheck, "Titanium - Oxygen Reactivity Study," General Dynamics/Astronautics Report Number AE62-0674, for NASA under Contract NAS8-2664, July 1962.
19. W. A. Riehl, C. F. Key, and J. B. Gayle, "Reactivity of Titanium with Oxygen," Marshall Space Flight Center Report MTP-P and WE-M-62-13, November 1962.
20. J. L. Christian, J. E. Chafey, A. Hurlich, J. F. Watson, and W. E. Witzell, "Compatibility of Metals and Cryogenic Liquids, Metal Progress, Volume 83, Number 4, April 1963.
21. S. A. Yalof, A. H. Bleich, A. F. Hooper, and R. W. Tryon, "Compatibility of Atlas Materials With Fluorine Propellants," Convair Report ERR-AN-64-483, July 1964.
22. J. L. Christian, "Evaluation of Materials and Test Methods at Cryogenic Temperatures," GD/A Report ERR-AN-400, December 1963.
23. J. L. Christian, "Mechanical Properties of High Strength Sheet Materials at Cryogenic Temperatures," GD/A Report ERR-AN-255, November 1962.
24. J. L. Christian, "Effects of Chemistry and Processing on the Mechanical Properties of Engineering Alloys at Cryogenic Temperatures, Materials Science and Technology for Advanced Applications, Volume II, Proceedings of the 1964 Golden Gate Metals Conference, American Society for Metals.

UNCLASSIFIED

UNCLASSIFIED

REFERENCES (Continued)

25. J. L. Christian and J. R. Kerr, "Selection of Optimum Materials for Use in Liquid-Hydrogen Fueled Aerospace Vehicles," Aeronautical Systems Division, Technical Documentary Report Number ASD-TDR-63-798.
26. J. L. Christian, C. T. Yand, and W. E. Witzell, "Physical and Mechanical Properties of Pressure Vessel Materials for Application in a Cryogenic Environment," Part III, ASD-TDR62-258, December 1964.
27. W. E. Witzell, "Fracture Data for Materials at Cryogenic Temperatures," Technical Report AFML-TR-67-257, November 1967.
28. L. D. Girton, "Evaluation of Sheet Alloy 718 for Formed and Welded Missile Parts," GD/A-ERR-AN-656, December 1964.
29. J. L. Christian, "Determination of the Effect of Oxygen Content on the Mechanical Properties of Ti-5Al-2.5Sn Alloy at Room and Cryogenic Temperatures," General Dynamics/Astronautics Report Number MRG-266, October 1961.
30. J. L. Christian, A. Hurlich, J. E. Chafey, and J. F. Watson, Mechanical Properties of Titanium-5Al-2.5Sn Alloy at Room and Cryogenic Temperatures, submitted to AIME for publication.
31. J. L. Christian and J. E. Chafey, "Determination of the Effect of Iron and Oxygen Contents on the Mechanical Properties of Titanium-5Al-2.5Sn Alloy Sheet at Liquid Hydrogen Temperature (-423° F)," General Dynamics/Astronautics Report Number MRG 262, October 1961.
32. J. L. Christian, "Physical and Mechanical Properties of Pressure Vessel Materials for Application in a Cryogenic Environment," General Dynamics/Astronautics Report Number ASD-TDR-62-258, for USAF under Contract AF33(616)-7719, March 1962.
33. D. J. Ferris, "Investigation of Spotwelding Type 301 Stainless Steel," Convair Engineering Test Laboratory Report 9437, 19 April 1957.
34. R. J. Barlow and O. Bobbitt, "Spotweld Heli-Arc, Material Efficiency Tests, Model 7," Convair Report 57-511(7E-951), 10 September 1958.
35. D. H. Love and Lindeneau, "Comparison Fatigue Tests of Welded Joints in 301 and 301(N), Model 7," Convair Report, 10 October 1958.

UNCLASSIFIED

APPENDIX II, LOCKHEED TASK III RESULTS
FOR SECOND QUARTERLY PERIOD

UNCLASSIFIED

REFERENCES (Continued)

47. J. L. Christian and A. Hurlich, "Physical and Mechanical Properties of Pressure Vessel Materials for Application in a Cryogenic Environment," ASD-TDR-62-258, Part II, April 1963.
48. W. E. Witzell and C. J. Krapp, "Flow Enlargement Characteristics of Welded 2219-T81 Aluminum Alloy," NASA-CR-72288, April 1968.
49. "Cryogenic Insulation Development," Convair Division of General Dynamics Report GDC-DDB67-007, Contract NAS8-18021, January 1968.

UNCLASSIFIED

6-5/6-6

Appendix I

APPENDIX II, LOCKHEED TASK III RESULTS
FOR SECOND QUARTERLY PERIOD

CONTENTS

Section	Page
FOREWORD	iii
ABSTRACT	v
ILLUSTRATIONS	ix
TABLES	xiii
PROGRAM HIGHLIGHTS	1
SUBTASK 1 - DEFINITION OF THERMAL AND SPACE ENVIRONMENTS	5
Maximum $q\alpha$	5
Maximum Orbital Acceleration Levels	6
Meteoroid Environment	6
SUBTASKS 2 AND 3 - LH ₂ AND LF ₂ TANK DESIGN AND ANALYSES	8
Tank Material Section	9
Manufacturing Analyses	19
Vented LH ₂ Tank Selection	21
Configuration Optimization Studies	25
SUBTASK 4 - ATTITUDE CONTROL SYSTEM INTEGRATION STUDY	69
SUBTASK 5 - THERMAL CONDITIONING AND SUPPORT STRUCTURE	74
Screening Analyses of Shell Structures	74
Screening Analyses of Tank Support Systems	83
Screening Analyses of Insulation Composites	87
Thermal Design Data for Configuration Selection Parametric Studies	95
SUBTASK 6 - PROPELLANT ORIENTATION	99
SUBTASK 7 - PROPELLANT MANAGEMENT SYSTEM	105
SUBTASK 8 - PRESSURIZATION SYSTEM	107
Screening Analyses	108
Parametric Pressurization Data for Selected Concept	143

Section	Page
SUBTASK 9 - FILL, VENT, AND FEED PRESSURIZATION LINES STUDY	145
SUBTASK 10 - FINAL FEED SYSTEM DESIGN	147
FUTURE ACTIVITIES	149
REFERENCES	151
ENCLOSURE A - PRESSURIZATION ANALYSIS	A-1

ILLUSTRATIONS

Figure		Page
1	Configuration Selection Optimization Studies (C)	3
1-1	Maximum Vehicle Acceleration Level in Orbit as a Function of Vehicle Burnout Weight and Percent Propellants Remaining (C)	7
2-1	Fracture Toughness of Aluminum Alloys (C)	11
2-2	Fracture Toughness vs. Temperature of Aluminum and Titanium Alloys (C)	12
2-3	LH ₂ Tank Weight as a Function of Pressure and Tank Materials (C)	14
2-4	LF ₂ Tank Weight as a Function of Pressure and Tank Materials (C)	15
2-5	Mechanical Properties Comparison of Aluminum Alloys (C)	16
2-6	Shear Forming 60-in.-Diameter 2021 Aluminum Tank	
2-7	Configuration Selection Optimization Studies (C)	27
2-8	Conical/Cylindrical and Cylindrical Shells (C)	29
2-9	Cylindrical Shell Weight as a Function of Axial Line Load	31
2-10	Cylindrical Shell Weight Per Inch of Shell Length as a Function of Axial Line Load	32
2-11	Liquid Hydrogen Tank Configurations (C)	41
2-12	LH ₂ Tank Parametric Weights, 290 ft ³ Volume (C)	42
2-13	LH ₂ Tank Parametric Weights, 306 ft ³ Volume (C)	43
2-14	LH ₂ Tank Parametric Weights, 320 ft ³ Volume (C)	44
2-15	LH ₂ Tank Parametric Weights, 340 ft ³ Volume (C)	45
2-16	Liquid Fluorine Tank Configurations (C)	46
2-17	LF ₂ Tank Parametric Weights, 150 ft ³ Volume (C)	47
2-18	LF ₂ Tank Parametric Weights, 156 ft ³ Volume (C)	48
2-19	LF ₂ Tank Parametric Weights, 160 ft ³ Volume (C)	49

CONFIDENTIAL

LMSC-680959

Figure		Page
2-20	LF ₂ Tank Parametric Weights, 170 ft ³ Volume (C)	50
2-21	LH ₂ Tank Insulation Weight as a Function of Heat Flux (C)	57
2-22	LF ₂ Tank Insulation Weight as a Function of Heat Flux (C)	58
2-23	Helium Requirements for LH ₂ Tank, Duty Cycle No. 4 (C)	59
2-24	Helium Requirements for LF ₂ Tank; Duty Cycle No. 4 (320° R Expulsion) (C)	60
2-25	Pressurization System Weight Scaling Equation (C)	62
2-26	Helium Bottle Weight as a Function of Usable Helium Weight (C)	63
2-27	Hydrogen Vented for 14-Day Mission as a Function of Ambient Heat Rate (C)	65
2-28	Residual GH ₂ Parametric Data, Duty Cycle No. 4 (C)	67
2-29	Residual Fluorine Gas Parametric Data, Duty Cycle No. 4 (C)	68
4-1	Tank Configurations Examined in the Attitude Control Study (C)	70
4-2	Sump Centrifugal Acceleration Levels as a Function of ACS Thruster Burn Time (C)	73
5-1	Integrally Stiffened Cylinder Configurations (C)	75
5-2	Maximum Shell Temperatures and Heat Fluxes with Vehicle Axis Tangent to the Earth's Surface	81
5-3	Maximum Shell Temperatures and Heat Fluxes with Vehicle Axis Normal to the Earth's Surface	82
5-4	Ranking of LH ₂ Tank Support Systems (C)	85
5-5	Ranking of LF ₂ Tank Support Systems (C)	86
5-6	Measured Conductivities of Promising Multilayer Composites	88
5-7	Density-Thermal Conductivity Ranking of Insulation Composites (C)	91
5-8	Effect of Comprehensive Load on Insulation Heat Rates for the LH ₂ Tank (C)	93

CONFIDENTIAL

LOCKHEED MISSILES & SPACE COMPANY

Figure		Page
5-9	Effect of Compressive Load on Insulation Heat Rates for the LF_2 Tank (C)	94
6-1	Preliminary Estimate of LH_2 Propellants to be Trapped by the Orientation System for Restart (C)	101
6-2	Preliminary Estimate of LF_2 Propellants to be Trapped by the Orientation System for Restart (C)	102
8-1	Acceleration Stability Levels of Contained Propellants Vs. Electrode Voltage and Electrode Configuration (Dielectrophoretic Device) (C)	112
8-2	Comparative Weight Penalty- Pressurization System 1, Duty Cycle 4 (C)	116
8-3	Comparative Weight Penalties for Systems 2a and 2b (C)	117
8-4	Comparative Weight Penalties for Systems 3a Through 3d (C)	119
8-5	Pressurization System Weight Comparison for Vented and Nonvented Systems (C)	121
8-6	Normalized Weight Penalty Comparison of the Pressurization Systems (C)	124
8-7	Selected Pressurization System Schematic (C)	125
8-8	Hydrogen Tank Pressure Histories, Duty Cycle 3, $37^\circ R$ Helium Prepressurization (C)	127
8-9	Fluorine Tank Pressure Histories, Duty Cycle 3, $154^\circ R$ Helium Prepressurization (C)	129
8-10	Effect of Pressure and Low Temperature Allowables on LH_2 Tank Weight (C)	131
8-11	Effect of Pressure and Low-Temperature Allowables on LF_2 Tank Weight (C)	132
8-12	Effect of Volume and Low Temperature Allowables on LH_2 Tank Weight (C)	133
8-13	Helium Storage Volume Required as a Function of Helium Mass and Storage Pressure (C)	135
8-14	Pressurant Bottle Weight as a Function of Volume, Tank Shape, and Material Allowables (at 3,500 psi) (C)	136

CONFIDENTIAL

LMSC-680959

Figure		Page
8-15	Pressurant Bottle Weight as a Function of GHe Weight, Tank Shape, and Material Allowables (at 3,500 psia) (C)	137
8-16	Bottle Size as a Function of Volume (C)	138
8-17	Helium Bottle Pressure Optimization (C)	140
8-18	Pressurant Bottle Weight as a Function of Volume and Material Allowables at 1,250 psia (C)	141
8-19	Effect of Final Blowdown Pressure on Optimum Storage Pressure and System Weight (C)	142
9-1	Liquid Fluorine Feed-Line Pressure Drop as a Function of Line Diameter (C)	146

CONFIDENTIAL

LOCKHEED MISSILES & SPACE COMPANY

TABLES

Table		Page
2-1	Materials Considered for Propellant Tanks	9
2-2	Vented Vs. Nonvented Tanks - A Weight Summary Comparison of Affected Parameters (C)	23
2-3	Assumptions Used for Calculation of LH ₂ and LF ₂ Tank Weights as a Function of a/b Ratio (C)	35
5-1	Candidate Shell Material Properties (C)	77
5-2	Minimum Practical Layer Density (C)	89
5-3	Relative Ranking of Insulation on the Basis of Effective Conductivity (C)	90
5-4	Relative Ranking of Insulation on the Basis of ρk Product (C)	90
5-5	Relative Rankings of Insulation on the Basis of Heat Flow With 6.2-g Compressive Load (C)	92
5-6	Relative Ranking of Insulation Based on Composite Characteristics $\rho k [(Q_o + \Delta Q)/Q_o]$ (C)	95
5-7	As-Installed Tank Insulation Thermal Performance (C)	97
8-1	Pressurization Systems Investigated (C)	109
8-2	Duty Cycles (C)	110
8-3	Assumptions or Input Data Used in the Pressurization System Screening Analyses (C)	111

PROGRAM HIGHLIGHTS

(C) The Phase I systems analysis and preliminary design effort can be performed in various ways. Lockheed has elected to perform the work in three steps or phases. The first is a preliminary screening wherein data on materials, propellant tanks, support structures, insulation, vent-free fluorine systems, propellant orientation systems, pressurization systems, etc., are gathered, sifted, analyzed, and narrowed to the most suitable elements for use in this program. This involves a thorough literature survey and detailed discussions with various organizations on tank forming methods, flight reliability of pressurization systems, and so on. It also involves reliance on certain Lockheed development activities for answers to key technical questions. For example, Lockheed has recommended, later in this quarterly report, the selection of 2021-T62 aluminum alloy for the propellant tanks. This would not be possible without extensive concurrent development which included the fabrication and thorough testing of two 2021 aluminum propellant tanks.

(U) The screening analyses and support development is followed by an analytical optimization study. The optimization study has as its input the results obtained from the screening phase and the environmental constraints jointly established by Rocketdyne, Lockheed, and GD/Convair in Subtask 1. The optimization study is divided into workable parts and is computerized. The optimization technique employed for Subtasks 2 and 3, for example, is shown schematically in Fig. 1. This optimization study will define the optimum tankage and vehicle outer shell configurations. Similar parametric studies are conducted for the following subsystems:

- Thermal Conditioning
- Propellant Orientation, including Attitude Control Inputs
- Propellant Management
- Pressurization System

CONFIDENTIAL

LMSC-680959

(U) The third step in this process is to perform the detail design of each subsystem and component which is then integrated into the entire vehicle design. A final system integration is performed, the output of which forms the ultimate product of Phase I.

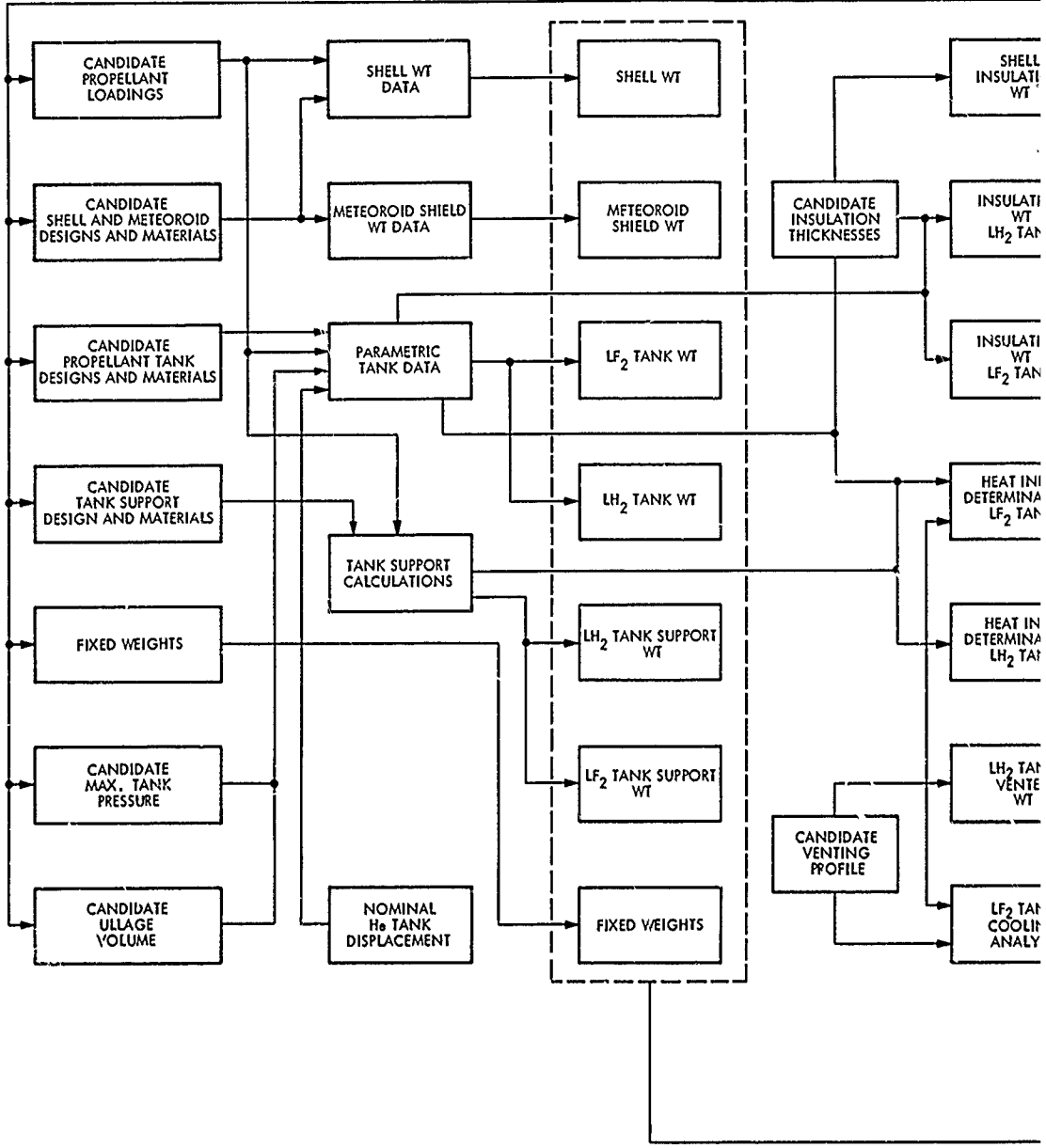
(C) During this quarter, a number of goals were reached. The screening and optimization studies resulted in the following selections:

- The tank material recommended for both the LH₂ tank and the LF₂ tank is 2021-T62 aluminum alloy. 2219-T87 aluminum alloy, using the same weld wire and similar fabrication techniques, is recommended as backup material.
- The tank support systems have been narrowed to a fiberglass filament-wound 4-point support system for the LH₂ tank and to a titanium/stacked-washer 4-point support system for the LF₂ tank.
- The pressurization system emerging from the screening and optimization analyses is one where pressurizing helium is stored at 37°R in the LH₂ tank. It is used at 37°R for prepressurizing the hydrogen tank and at 154°R for prepressurizing the LF₂ tank; warm gaseous hydrogen is the expulsion gas in the hydrogen tank and gaseous helium is the expulsion gas in the LF₂ tank. Optimization of the expulsion temperatures remains to be done.

(U) Details of the analyses to substantiate these recommendations are presented in this report, along with progress in other areas, under their respective subtask headings.

CONFIDENTIAL

LOCKHEED MISSILES & SPACE COMPANY



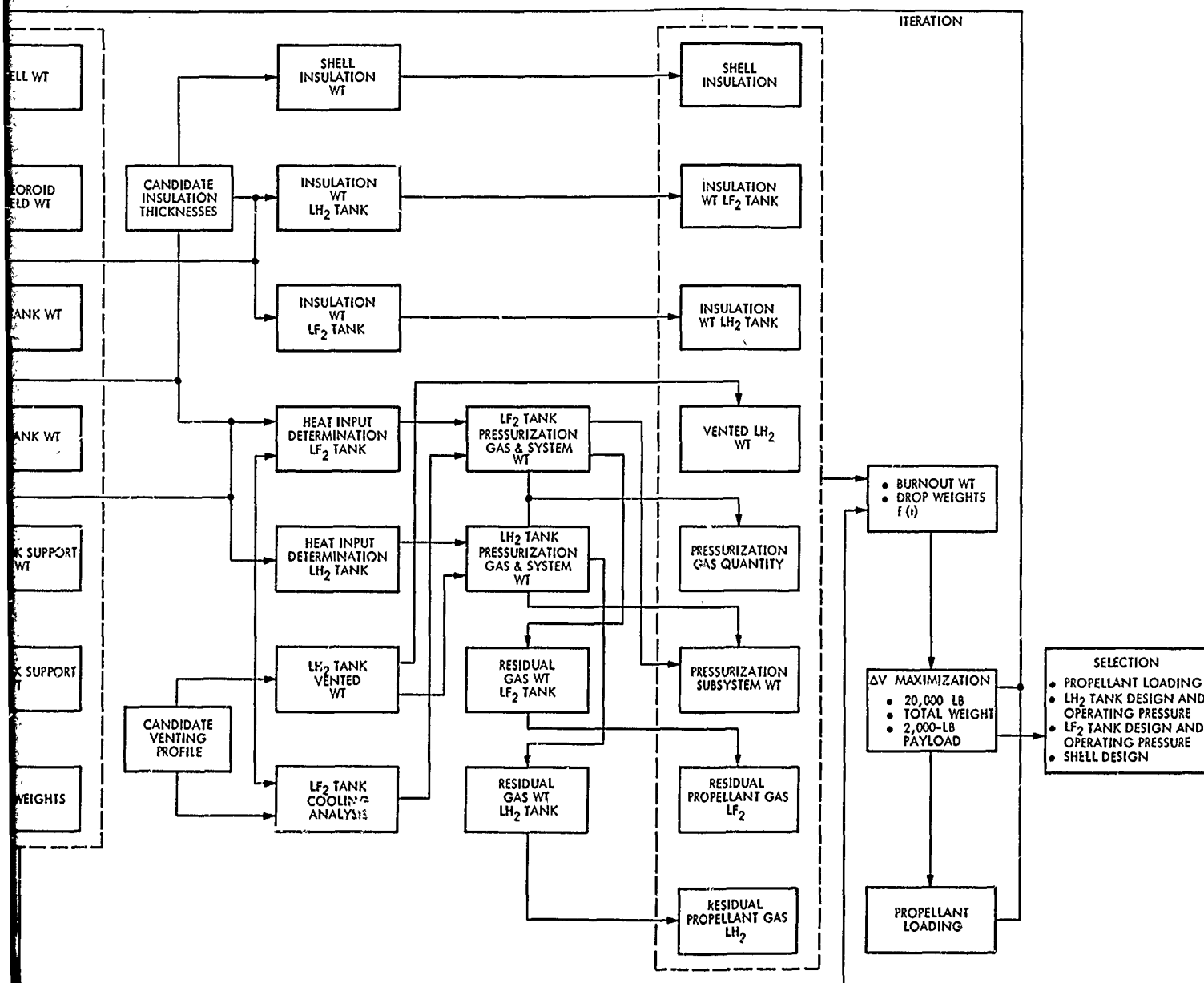


Fig. 1 Configuration Selection Optimization Studies (C)

CONFIDENTIAL

LMSC-680959

SUBTASK 1 - DEFINITION OF THERMAL AND SPACE ENVIRONMENTS

(U) This task was completed during the first quarter. However, from time to time it appears prudent to evaluate the established environmental constraints as work progresses. Where warranted by new input, Lockheed will recommend modification of existing or addition of new environmental constraints.

MAXIMUM $q\alpha$

(C) In the previous work on environments, maximum $q\alpha$ values defined by Lockheed and GD/Convair did not include thrust dispersions and wind loads. These data were obtained subsequently from the Martin-Marietta Company. Reference 1 defines the maximum $q\alpha$ value of 4200 psf-deg for a Titan IIC launch from the Eastern Test Range into a highly elliptical orbit. The wind data used in these trajectories were taken from NASA Document TND-610. Individual values of q , α , time of maximum $q\alpha$, and axial and lateral accelerations are shown below.

**RECOMMENDED VALUES FOR TRAJECTORY AT
MAXIMUM $q\alpha$ WITH DISPERSIONS**

Time after launch:	60 sec
q :	800 lb/ft ²
α :	5.25 deg
Max $q\alpha$	4200 psf-deg .
N (axial):	2.0 g
N (lateral):	± 0.2 g

CONFIDENTIAL

CONFIDENTIAL

LMSC-680959

(This page is unclassified.)

MAXIMUM ORBITAL ACCELERATION LEVELS

(U) The maximum acceleration level of the vehicle in orbit as a function of propellant used and burnout weight is shown in Fig. 1-1. The effect of this environment on vehicle design is described in the applicable subtasks.

METEOROID ENVIRONMENT

(U) The meteoroid environment criteria presently being used is given in Aerospace Meteoroid Environment and Penetration Criteria, TOR-269(4560-40)-2, V. C. Frost.

(U) This document is currently being revised, but Mr. Frost has stated that the revisions will not be published until the last half of this year.

(U) In discussions with the Rocketdyne Program Manager and Assistant Program Manager about the meteoroid environment criteria, it was agreed that the best criteria now available is the meteoroid flux criteria given in Space Environment Criteria Guidelines for Use in Space Vehicle Development, NASA MSFC Document TMX-53521, 1 Feb 1967, and the meteoroid penetration criteria given in the referenced Aerospace Corporation document. The criteria referenced in these two documents will be used by Lockheed in all future analyses under this contract where the meteoroid environment influences analytical or design work.

CONFIDENTIAL

LOCKHEED MISSILES & SPACE COMPANY

CONFIDENTIAL

LMSC-680959

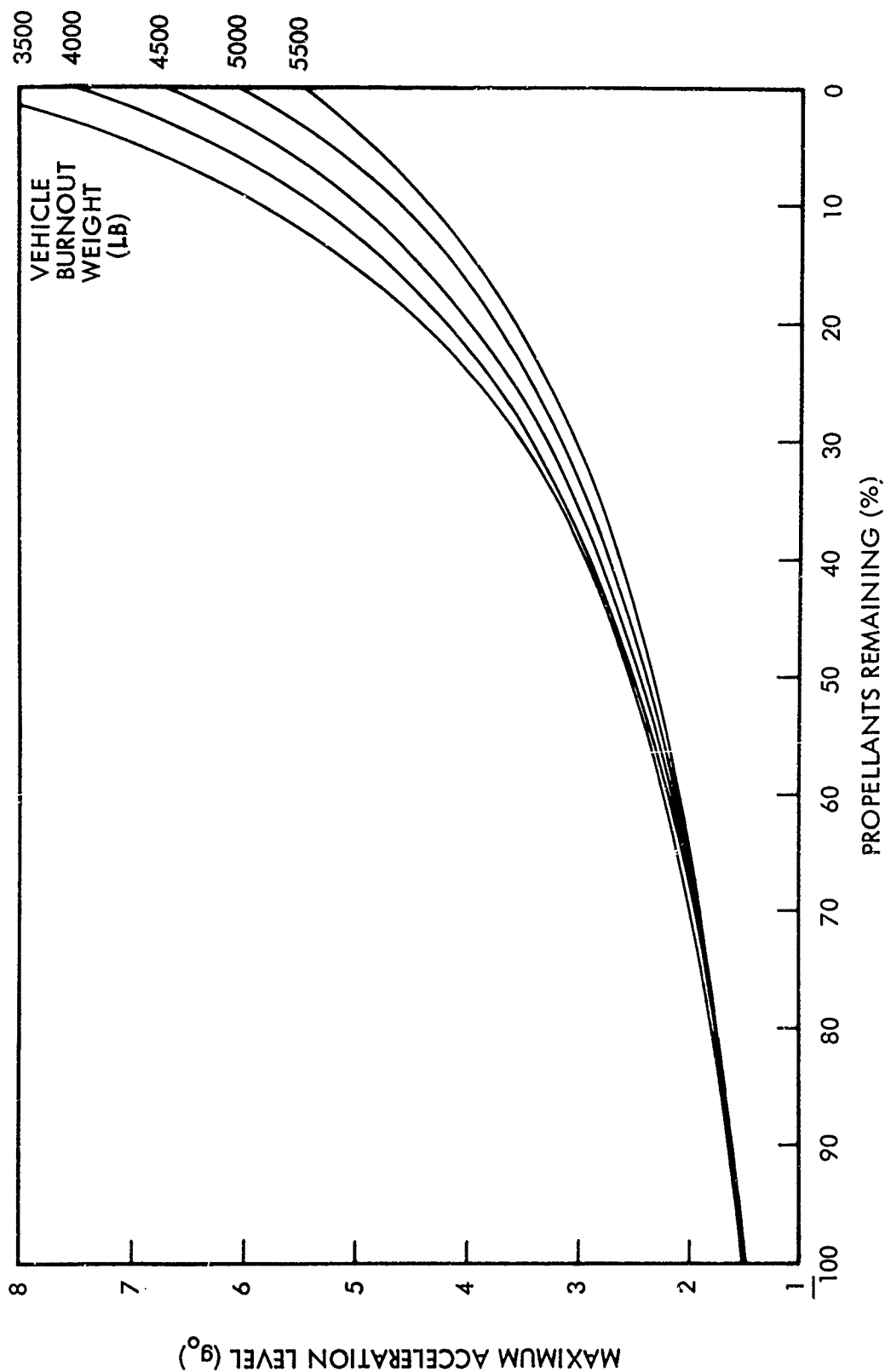


Fig. 1-1 Maximum Vehicle Acceleration Level in Orbit as a Function of Vehicle Burnout Weight and Percent Propellants Remaining (C)

CONFIDENTIAL

LOCKHEED MISSILES & SPACE COMPANY

CONFIDENTIAL

LMSC-680959

(This page unclassified)

SUBTASKS 2 AND 3 - LH₂ AND LF₂ TANK DESIGN AND ANALYSES

(U) Because of close interrelationship between analyses performed on Subtasks 2 and 3, these subtasks are presented together to provide a better understanding of the work performed.

(U) The overall program approach used in Subtasks 2 and 3 is presented below to illustrate how the work performed to date fits into this plan. Following this synopsis, details on work performed this quarter are given.

(U) The approach that Lockheed has elected to follow can be divided into three steps or phases. The first is a screening phase, wherein many tank and outer shell materials, configurations, manufacturing techniques, tooling limitations, quality, and cost factors were examined and compared. The purpose of these screening analyses is to evaluate on a comparative basis those elements which affect the AMPS vehicle design, to establish realistic bases for the optimization studies which are to follow, and to narrow the input data in a sound manner so that the optimization studies may be limited to a reasonable scope.

(U) The second step in the Lockheed approach is to use the data derived from the screening analyses in an optimization study, wherein tank configurations, materials, shell configuration, etc., can be selected with confidence that the correct selections have been made. The optimization study being conducted in this second phase is shown schematically in Fig. 1, p. 2.

(U) The third step is the design phase, where the precise design of the propellant tanks, their access openings, fill/drain fittings, pressurization line fittings, electrical feedthroughs, seals, etc., are determined.

CONFIDENTIAL

LOCKHEED MISSILES & SPACE COMPANY

CONFIDENTIAL

LMSC-680959

(This page is unclassified.)

TANK MATERIAL SELECTION

(U) The screening analyses conducted in support of Subtasks 2 and 3 resulted in the selection of tank materials.

(U) Materials which exhibit characteristics most suitable for cryogenic tankage should be carefully investigated prior to the start of the optimization study. The most significant design criteria for evaluating candidate materials are:

- High strength-to-weight ratio
- Compatibility with designated cryogens
- Reliable welding characteristics
- Superior forming characteristics
- High fracture toughness characteristics

The materials which were considered for the propellant tankage are enumerated in Table 2-1.

Table 2-1

MATERIALS CONSIDERED FOR PROPELLANT TANKS

Aluminum Alloys

6061-T6

2014-T6

2219-T87

2021-T62

Titanium Alloys

5Al 2.5 Sn (ELI grade)

6Al 4V (ELI grade)

Stainless Steel

301 N (Hydrogen tank only)

304 L

Inconel

718

Appendix II

CONFIDENTIAL

LOCKHEED MISSILES & SPACE COMPANY

CONFIDENTIAL

LMSC-680959

Aluminum Alloys

(C) The 6061-T6 aluminum alloy was eliminated as a candidate material because its tensile properties are approximately 30 percent less than 2021-T62 and 2219-T87 alloys. Additionally, storage tests have shown that hydrogen permeates 6061 aluminum alloy. It is suspected that the leaks occur due to passage of hydrogen molecules through the relatively coarse interstitial passages. Repetitive tests with gases fail to show evidence of leakage at room temperatures, so it is concluded that the slight leakage is a temperature-related phenomenon.

(C) The yield strength of 2014-T6 compares favorably to 2219-T87 and 2021-T62 at cryogenic temperatures. The weld tensile strength of 2014-T6 at 37° R is 70,000 psi compared to 73,000 psi for 2219-T87. This alloy is inferior to 2219-T87, however, in fracture toughness capability. Figure 2-1 shows the relative fracture toughness of 2219-T87 and 2014-T6 at 37° R.

(C) This curve shows that, for a given crack configuration, 2014-T6 alloy will propagate at a stress level of approximately 10,000 psi lower than 2219-T87 alloy. Figure 2-2 shows that 2014-T6 aluminum is also inferior to 2219-T87 aluminum in plane-strain fracture toughness. Thus, a tank designed on the basis of 2014-T6 fracture toughness characteristics will be heavier than tanks made of 2219-T87 or 2021-T62.

(C) The 2219-T87 alloy is superior to either 6061-T6 or 2014-T6 in weld tensile strength at cryogenic temperatures, in fracture toughness capability, and in demonstrated weldability. Lockheed has fabricated a number of 2219-T87 cryogenic tanks (spherical and elliptical) and has succeeded in reducing the weld repair to zero in the last two tanks fabricated. This has not been demonstrated either in 6061-T6 or 2014-T6 weldments, even though a great number of propellant tanks are being constructed from these materials. 2219-T87 has repeatedly demonstrated no leakage of cryogen under long-duration cyclic testing and is very resistant to handling damage.

CONFIDENTIAL

LOCKHEED MISSILES & SPACE COMPANY

CONFIDENTIAL

LMSC-680959

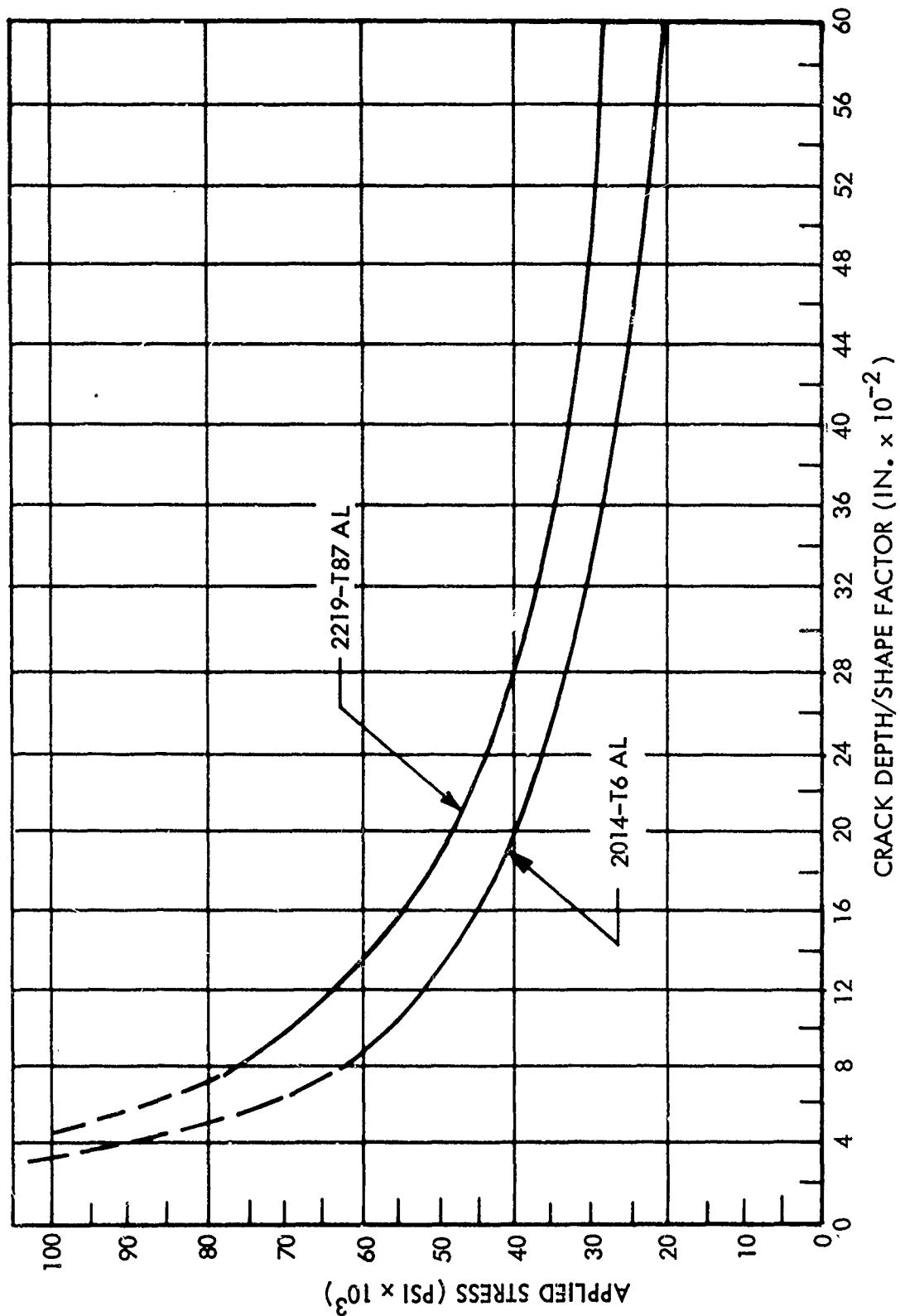


Fig. 2-1 Fracture Toughness of Aluminum Alloys (C)

CONFIDENTIAL

LOCKHEED MISSILES & SPACE COMPANY

CONFIDENTIAL

LMSC-680959

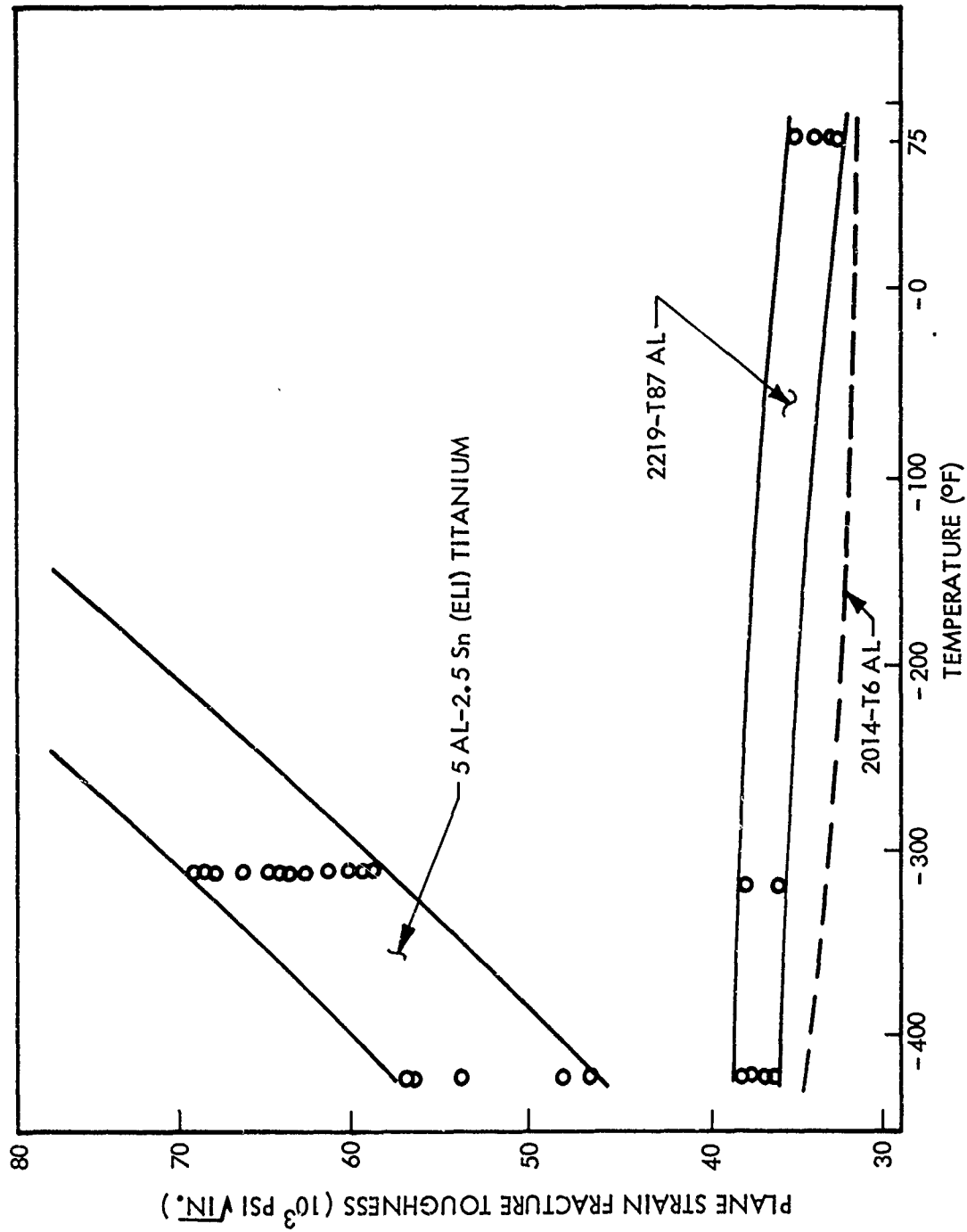


Fig. 2-2 Fracture Toughness vs. Temperature of Aluminum and Titanium Alloys (C)

CONFIDENTIAL

LOCKHEED MISSILES & SPACE COMPANY

(C) Figures 2-3 and 2-4 show that 2021-T62 possesses the highest strength-to-weight ratio of all the aluminum alloys considered. The weights shown in Figs. 2-3 and 2-4 are predicated on ellipsoidal tank configurations having an a/b ratio of 1.4 to 1. The weights, of course, vary as a function of the a/b ratio, but the relative ranking for the materials remain the same. Considerable research has been conducted by Lockheed and Alcoa exploiting the mechanical properties, forming characteristics, and welding procedures for 2021 aluminum. The mechanical properties obtained by both Alcoa and Lockheed are tabulated in Fig. 2-5.

(C) The 2021-T62 alloy exhibits improved mechanical properties for both parent metal and weldments compared to 2219-T87. At this time, there are insufficient data to plot the fracture toughness of 2021-T62 at cryogenic temperatures. However, limited experimental test data have shown that 2021-T62 compares favorably with 2219-T87 in the notch/unnotched tensile ratio values. It is anticipated that the curve profile for 2021-T62 would be essentially the same as that shown in Fig. 2-1 for 2219-T87 aluminum alloy. Additional tests are planned to verify the fracture toughness of 2021-T62 aluminum alloy. The weldability of the two alloys 2219-T87 and 2021-T62 appears to be the same based on fabrication of two 2021 tanks and several 2219 tanks. The same weld wire (2319) is used for both materials.

Titanium Alloys

(C) Figure 2-5 shows that the fracture toughness of the titanium alloys decreases rapidly as temperature decreases. Because of this phenomenon the material thickness must be increased to overcome the problem of flaw propagation, and this produces a weight increase in the tank membrane. This factor alone, however, is not sufficient to completely negate other benefits manifested by this material. In service, however, the phenomenon of titanium-hydrogen incompatibility under certain conditions is prevalent. Subsequent to this discovery, considerable experimentation was conducted by Beech Aircraft and the Battelle Memorial Institute to determine the cause and a possible remedy for preventing future failures. Although the exact mechanics of failure are not clear,

CONFIDENTIAL

LMSC-680959

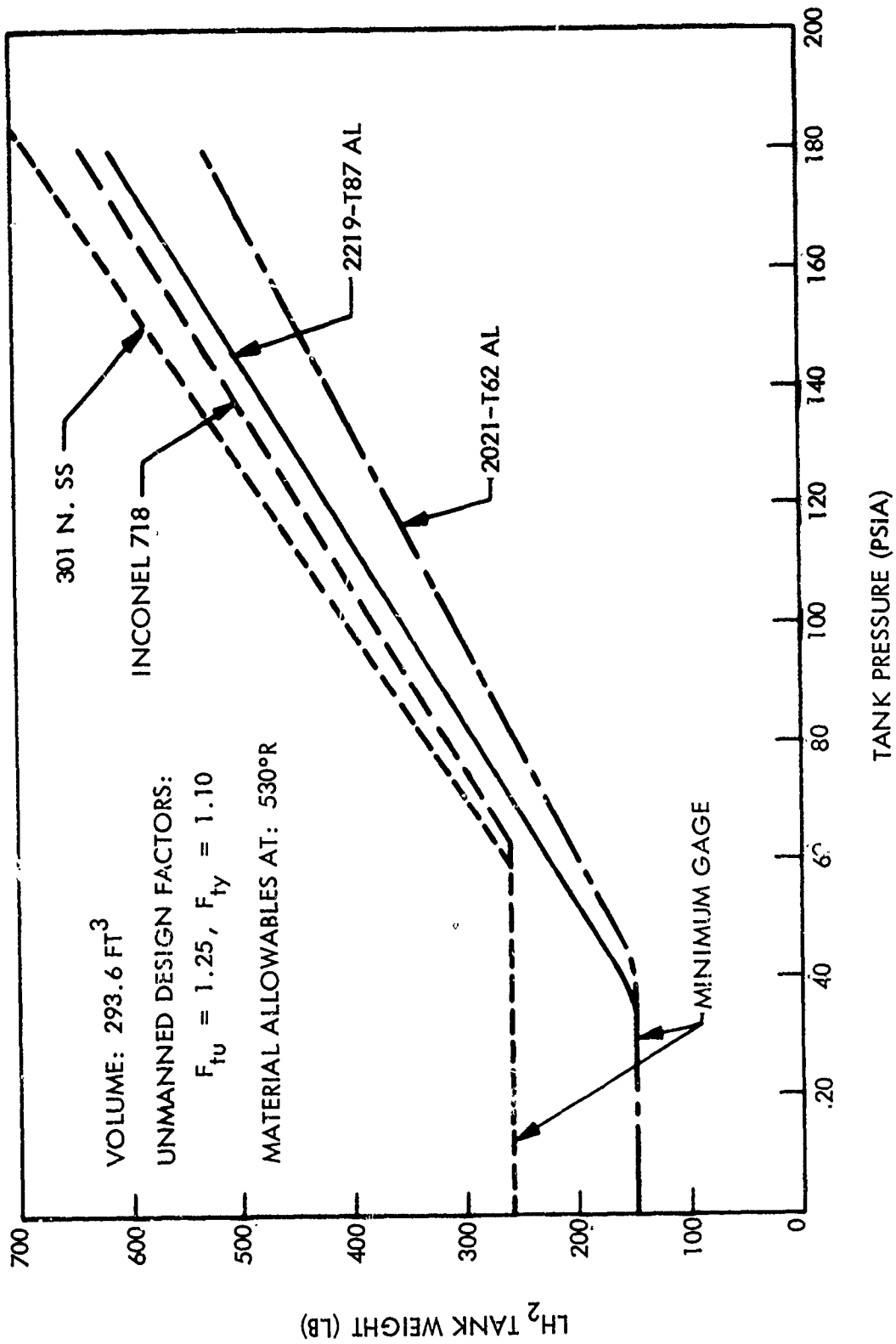


Fig. 2-3 LH₂ Tank Weight as a Function of Pressure and Tank Materials (C)

CONFIDENTIAL

LOCKHEED MISSILES & SPACE COMPANY

CONFIDENTIAL

LMSC-680959

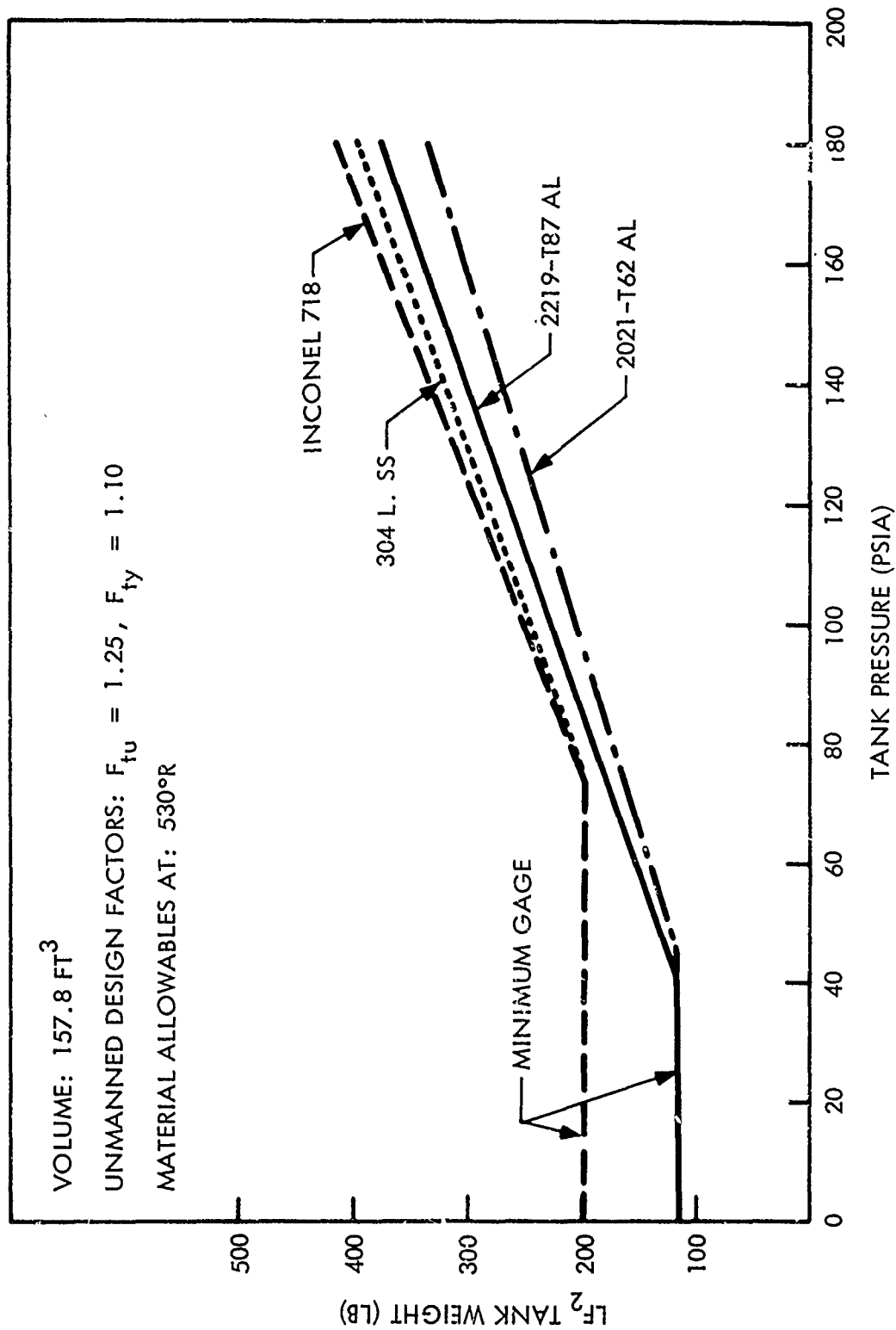


Fig. 2-4 LF₂ Tank Weight as a Function of Pressure and Tank Materials (C)

CONFIDENTIAL

LOCKHEED MISSILES & SPACE COMPANY

CONFIDENTIAL

LMSC-680959

MECHANICAL PROPERTY	2219-T87 ALUMINUM		2021-T62 ALUMINUM	
	ALCOA GREEN LETTER	LOCKHEED EXPERIENCE (110-IN. TANK)	ALCOA	LOCKHEED EXPERIENCE (60-IN. TANK)
<u>PARENT METAL</u>				
TENSILE ULTIMATE (PSI)	68,000	69,500	73,000 TO 79,000	63,000
TENSILE YIELD (PSI)	56,000	55,000	61,000 TO 69,000	58,300
ELONGATION (% IN 2 IN.)	10	9.5	9 TO 11	10
<u>WELDMENTS</u>				
TENSILE ULTIMATE (PSI)	41,000	37,900	40,000 TO 51,000	50,800
TENSILE YIELD (PSI)	30,000	33,900	26,000 TO 44,000	44,100
ELONGATION (% IN 2 IN.)	3	5	1.5 TO 3	2.2

Fig. 2-5 Mechanical Properties Comparison of Aluminum Alloys (C)

CONFIDENTIAL

LOCKHEED MISSILES & SPACE COMPANY

hydride scaling and subsequent spalling of the material during the thermal and pressure cycling of the tankage are contributing factors. For these reasons, titanium alloys were eliminated as candidate materials for the liquid hydrogen tank. Its higher cost, compatibility problems, and lack of weight advantage make it unattractive for the fluorine tank.

Stainless Steels

(C) The 301 N stainless steel alloy was considered for the liquid hydrogen tank only, since the higher carbon content in the alloy may make it incompatible with liquid fluorine. Figure 2-3 shows that this material is the heaviest of all candidate materials considered.

(C) The 304 L stainless steel alloy was selected as the most appropriate austenitic steel for the liquid fluorine tank. Figure 2-4 shows that the tank weight for this material is heavier than both aluminum alloy material candidates.

Inconel

(C) Inconel 718 has good forming characteristics as well as excellent welding capability. Weld-joint efficiency approaches 100 percent. However, the maximum size flat sheet that is available in the cold-rolled condition is not large enough for forming the shells, so that the bulkheads must be fabricated in gore sections. This condition somewhat offsets the desirable features of this material, because the additional welds increase costs. Figure 2-3 shows that the liquid hydrogen tankage fabricated of Inconel 718 is heavier than 2219-T87 and 2021-T62 aluminum alloys. Figure 2-4 shows that the liquid fluorine tankage fabricated of Inconel 718 is the heaviest of all.

Selected Material

(C) Of the candidate materials which are available for fabricating the liquid hydrogen and liquid fluorine tanks 2021-T62 shows promise of producing the lightest weight tankage. Present experimental data being produced by Lockheed indicate that this

CONFIDENTIAL

LMSC-680959

aluminum alloy possesses all characteristics essential to light-weight cryogenic spacecraft tankage. Lockheed is currently conducting intensive research to exploit and establish the mechanical properties, fracture toughness, forming characteristics, and welding procedures for 2021 in various tank configurations as shown in Fig. 2-6.

Lockheed recommends 2021-T62 as the tankage material to be used in the AMPS vehicle, with 2219-T87 as a backup. Both materials will require the same tooling and processes; therefore, the change from 2021-T62 to 2219-T87, in case of need, can be effected easily.

MANUFACTURING ANALYSES

(C) Manufacturing analyses were conducted for the selected aluminum alloy 2021-T62 and the backup material 2219-T87. These analyses are required at this time to provide realistic data for the parametric tank configuration and design studies.

Depth Limitations on 2219 Forming

(U) To achieve T87 properties with 2219 aluminum alloy, it is necessary to start with 2219-T351 plate, cold work during forming so as to achieve the T37 condition, and then age the formed half-shells to T87 condition. Since the material must be cold worked from its T351 condition into a T37 condition, heat treating cannot be used during the forming process. To date this forming process has limited the depth of 2219-T87 half-shells to approximately $\sqrt{2}$:1 ellipsoids. This depth may be extended somewhat by the use of a contoured Y-ring. The limitations on the Y-ring width are sizes of forgings which can be fabricated with the desired properties and machining problems encountered as the Y-ring size increases. Lockheed has formed half shells from 2219 of the following sizes: 41.5-in. hemisphere; 46-in. hemisphere; 60-in. hemisphere; 110-in. ellipsoids. The hemispheres did not reach T87 properties, but ranged from T6 to T8 in temper. It was concluded that 2219-T87 hemispheres exceeding 60-in. diameter cannot be formed, and those smaller will require substantial development. The 2219-T62 hemispheres can be formed, because the material can be heat treated during forming, but the ultimate tensile strength of 2219-T62 is 10,000 psi less than 2219-T87, and the yield is 16,000 psi less.

CONFIDENTIAL

LOCKHEED MISSILES & SPACE COMPANY

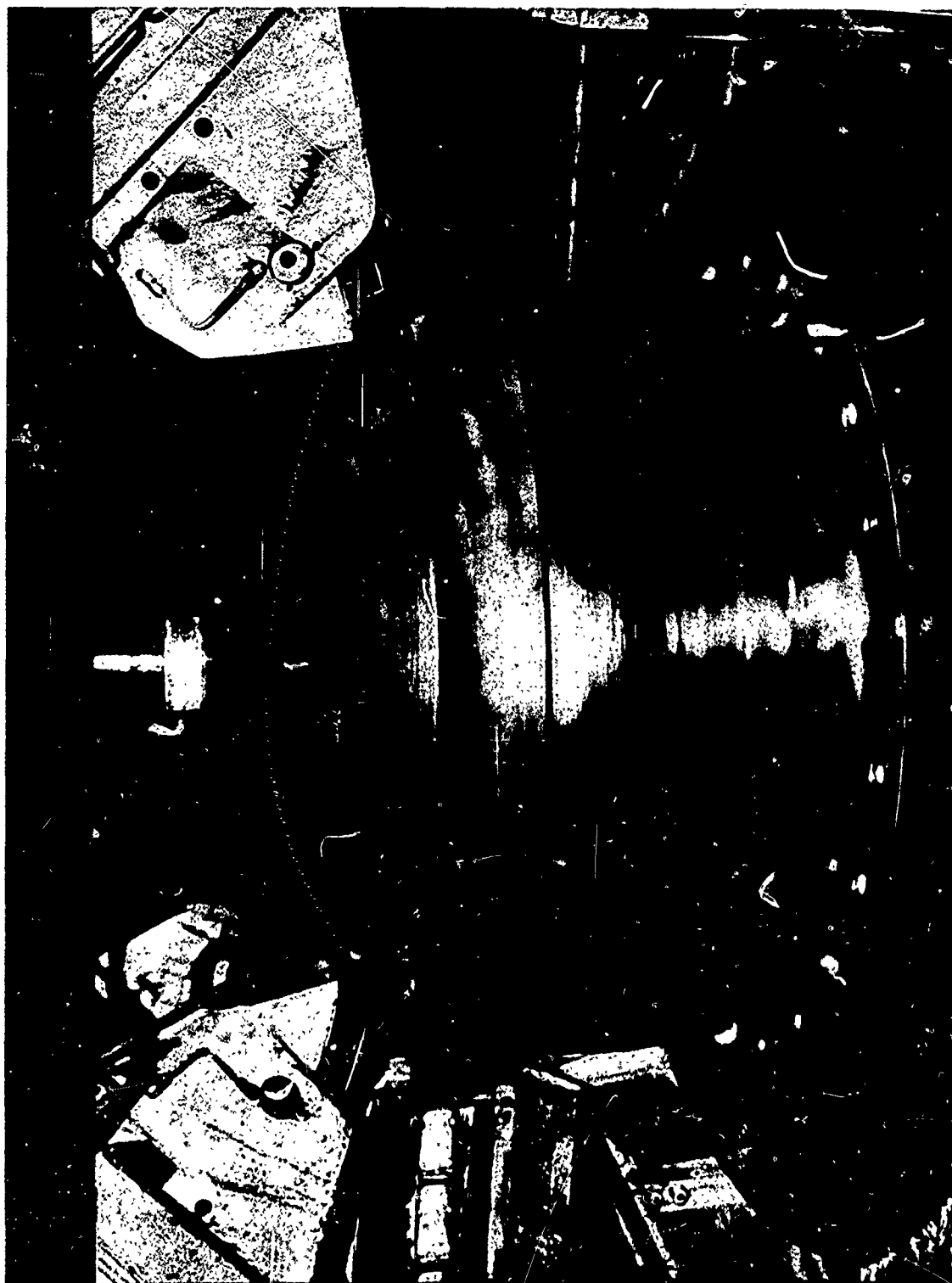


Fig. 2-6 Shear Forming 60-in.-Diameter 2021 Aluminum Tank

Depth Limitations on 2021 Forming

(U) Lockheed has now made more than a dozen 60-in. hemispheres from 2021 aluminum alloy. Two tanks with Y-ring girth sections have been fabricated and tested. In addition, numerous smaller development parts have been tested. The T62 condition apparently cannot be reached in this forming process. However, the process used has been compared with previous 2219 alloy fabrication. The conclusion is drawn that annealed 2021 plate can be formed by the double-action draw process on the 8,000-ton Birdsboro press at the Lockheed California Company in a manner similar to the 110-in. tank half shells. By re-annealing the 2021 during the forming process it is considered that the T62 condition in hemispheres can be reached.

Width of Material

(U) Both 2219 and 2021 aluminum alloys are now available in 140-in. widths. This is the widest stock available and can be obtained in thicknesses of interest to this program (1/8 and 1/4-in. thick). However, using the double-action draw process, this size of initial sheet cannot be formed into a hemisphere large enough for the LH₂ tank for the AMPS vehicle. The upper limit to hemispherical forming by this technique would be approximately the LF₂ tank size. Industry has, in the past, exerted considerable effort in bulge-forming 2219 aluminum. The power required was excessively high and compression waves were set up in the material. No way to eliminate this has been found; the bulge forming technique has been largely discontinued, although Lockheed uses it as an adjunct to double-action draw forming on its 8,000-ton Birdsboro press.

(U) This technique should be somewhat easier to employ with 2021 aluminum. The conclusion is that hemispherical tank half shells having the desired T62 or T87 properties for 2021 and 2219, respectively, cannot be formed for the LH₂ tank. The sheet size and depth limitations indicate a maximum depth of $\sqrt{2}$:1 and a maximum diameter of 110-in. are possible with the available tooling and starting material. Therefore, a hemispherical tank for LH₂ would necessarily be constructed of gore panels, with their

CONFIDENTIAL

LMSC-680959

additional tooling, forming, and welding costs. It is also concluded that it might be possible to fabricate a hemispherical LF_2 tank from 2021 and achieve the T62 properties, though this will certainly advance the state-of-the-art considerably. The 2219-T87 properties are now obtainable only up to approximately $\sqrt{2}$:1 half shells for either tank.

Progress on 2219 and 2021 Aluminum Welding

(U) The strength of 2219 and 2021 welds can be increased by post-weld aging. However, tank distortion may occur during aging and must be considered before the full benefits of the aging procedure can be realized. The following recent Lockheed test results are indicative of the improvement in 2219 weld strength which could be achieved by post-weld aging:

Item	Ultimate Tensile Strength (psi)	Yield Tensile Strength (psi)	Elongation (percent in 2 in.)
2219-T351 Parent Material (0.250 plate)	56,300	42,500	23.0
Unaged Welds	39,900 to 41,600	22,900 to 24,600	5.5 to 6.5
Aged Welds (18 hr at 350° F)	46,100 to 47,300	35,200 to 36,300	2.5 to 3.0

The 2021 utilizes the same weld wire (2319), and its strength improvement through post-weld aging is similar to that given above.

VENTED LH_2 TANK SELECTION

(C) The screening analyses conducted in support of Subtasks 2 and 3 resulted in the selection of the vented LH_2 tank concept.

CONFIDENTIAL

LOCKHEED MISSILES & SPACE COMPANY

CONFIDENTIAL

LMSC-680959

(C) A weight comparison of vented vs. nonvented tank operation was made based on work performed in Subtasks 2, 3, and 8, and in related studies on other affected systems. This comparison is shown in Table 2-2. The term "vented" refers to a vented LH_2 tank and a cooled, nonvented LF_2 tank, and the term "nonvented" means that neither tank is vented. The "nonvented" concept is feasible from a technical standpoint as demonstrated by Lockheed in an inhouse 110-in. tank demonstration test. This tank, equipped with flight-type insulation, tank supports, fill/drain line, pressurization and venting lines, etc., was tested in the Cryogenic Vehicle Flight Simulator located at the Lockheed Santa Cruz Test Base. This system showed that a liquid-hydrogen tank of the AMPS vehicle size can be used in space in a nonvented mode up to 200 days while still maintaining pressure at less than 70 psi in the tank. Selection of the vented mode was based on system performance.

(C) The pressurization system selected contributed greatly to the selection of the vented mode. The pressurization analyses established tank pressures, residual-gas weights, GH_2 boiloff weight, and pressurant hardware weights. The selected system for this comparison (see Subtask 8) provides the lightest-weight system for vented and nonvented tanks. As described in Subtask 8, the expulsion temperatures have yet to be optimized but higher expulsion temperatures penalize the nonvented LH_2 tank more than the vented tank due to higher tank pressures and residual-gas weights. Consequently, the weight difference between the systems will increase as the expulsion temperature is increased. Tank weights were based on 140° R material allowables for the LH_2 tank because 140° R hydrogen expulsion gas is the warmest gas used. Helium expulsion gas at 153° R in the LF_2 tank allowed use of low-temperature allowables. An emergency vent system was placed on the nonvented tanks which were of the same design as those of the vented system. During normal operation, this system is nonoperational. The vented system is operated using power from H_2/O_2 fuel cells. Weight of the fuel cell hardware is not included, because other vehicle systems will also require electrical power, and the FCS will supply all the vehicle requirements.

(C) The vented system is based on the assumption that LH_2 is drawn from the propellant orientation device for controlling tank pressure. Because pressurization studies show that venting helium overboard incurs a substantial weight penalty, a positive

CONFIDENTIAL

LOCKHEED MISSILES & SPACE COMPANY

CONFIDENTIAL

LMSC-60959

Table 2-2

VENTED VS. NONVENTED TANKS A WEIGHT SUMMARY COMPARISON OF AFFECTED PARAMETERS (C)

Parameter	Weight (lb)	
	Vented	Nonvented
Pressurization System 3b		
• Hardware (3,500 psia bottle)	240	238
• Helium	132	130
• Residual Gases (H ₂ and F ₂)	110	153
• GH ₂ Boiloff	43	0
Tank Weights		
• LH ₂ (306 ft ³)	217 (70 psia)	290 (97.7 psia)
• LF ₂ (156 ft ³)	166 (73 psia)	219 (95 psia)
Vent-Free Fluorine		
System Weight		
• LH ₂ Zero-g Vent System	15	15
• LF ₂ Heat Exchanger	4	(for emergency vent only) 4
• LF ₂ Mixer	3	—
• Fuel Cell	4	0
Reactant Weights (H ₂ and O ₂)		(normal operation)
Propellant Orientation		
System Weights		
EHD Device (LH ₂ Tank)		
• Electrodes	11	—
• HV Supply	11	—
• Cabling and HV Feedthrough	4	—
• Fuel Cell Reactant Weights (H ₂ and O ₂)	10	—
Surface Tension Device	3 (LF ₂ Tank)	5 (LH ₂ Tank)
		3 (LF ₂ Tank)
Insulation Weight	168	168
(Thickness optimization was not performed)		
TOTAL (LB)	1,141	1,225
ΔW	0	84

CONFIDENTIAL

LOCKHEED MISSILES & SPACE COMPANY

means for providing only LH_2 or GH_2 at the vent intake is required. This may require an electrophoretic propellant orientation device. Studies in Subtask 6 may show also a surface-tension device can be used in the LH_2 tank for vented systems instead of the electrophoretic device because the helium prepressurant provides considerable subcooling of the propellant. Thus, liquid hydrogen trapped under a surface tension device in the sump will probably remain subcooled even with a high local heat leak and, consequently, will not cause pump cavitation during an engine start transient.

(C) The insulation weights shown in Table 2-2 were not optimized for this comparison but held constant. Any optimization tends to favor the already lighter vented system; however, because tank weights increase more rapidly (with pressure increase) as the heat load is varied than does the GH_2 boiloff - i.e., ~0.7-lb tank weight per 1 lb of insulation weight vs. ~0.25-lb GH_2 boiloff weight per 1 lb of insulation weight. Therefore, the conclusion that vented systems are lighter than nonvented systems is valid.

(C) The final tank pressure to which a nonvented system is designed is a direct function of the duty cycle assumed. For the selected pressurization system, duty cycle 3 provides the highest tank pressure rises in nonvented tanks and consequently were used in this comparison. The tank-pressure histories for this duty cycle are shown in Subtask 8. For a vented system, the tank pressures are held constant at the expense of additional boiloff, independent of duty cycle. Thus, the vented system is more flexible in regard to changes in duty cycles than a nonvented system, an important consideration when duty cycles may change later in the program. Extension of the vehicle mission beyond 14 days to 180 days also favors the vented system, as tank pressures for the nonvented system would be higher. The main feature recommending the nonvented mode of operation is the greater system reliability resulting from a simpler design. Considering all of these factors, Lockheed has decided that the advantages of a vented system outweigh those of the nonvented system and selected the vented system for application to the AMPS vehicle.

(U) Other input data derived from the screening analysis include vehicle loads, shell configurations, shell materials, and tank configurations. These data are used in the configuration optimization studies.

CONFIGURATION OPTIMIZATION STUDIES

(C) The principal objectives of the configuration optimization studies are selection of configurations for the external shell, the liquid hydrogen tank, and the liquid fluorine tank. A general summary of the configuration selection parametric study is presented in Fig. 2-7.

(U) A summary of the input data generated to date is presented in the following paragraphs.

Candidate Propellant Loadings

(C) Candidate loadings of usable propellant will be divided on the basis of a 12-to-1 by weight LF_2/LH_2 mixture ratio. Nonusable propellants to be added to the usable quantities are:

<u>Nonusable Propellant</u>	<u>LH_2</u>	<u>LF_2</u>
Liquid Residuals	X	X
Line Entrapment	X	X
PU Residual	X	
Bolloff	X	
Gas Residuals	X	X

These items will be updated as the iteration process proceeds.

CONFIDENTIAL

LMSC-680959

Fixed Weights

(C) Items considered to be fixed weights in the study are as follows:

<u>Item</u>	<u>Weight (lb)</u>
Payload	2,000
Engine system	543
Orientation devices	39
Propellant utilization	29
Attitude-control system	87
ACS propellant	279
Nonvented fluorine system	26
Lines	25
Electrical	12
Liquid residuals in lines, entrapment, P.U. residual	77

Candidate Maximum Tank Pressures

(C) Various tank pressures equal to, or greater than, 70 psia will be selected for the study. These pressures will be optimized using the iteration process to maximize vehicle ΔV .

Candidate Ullage Volumes

(C) Ullage volumes will be varied from a reference value of 5 percent to maximize vehicle ΔV .

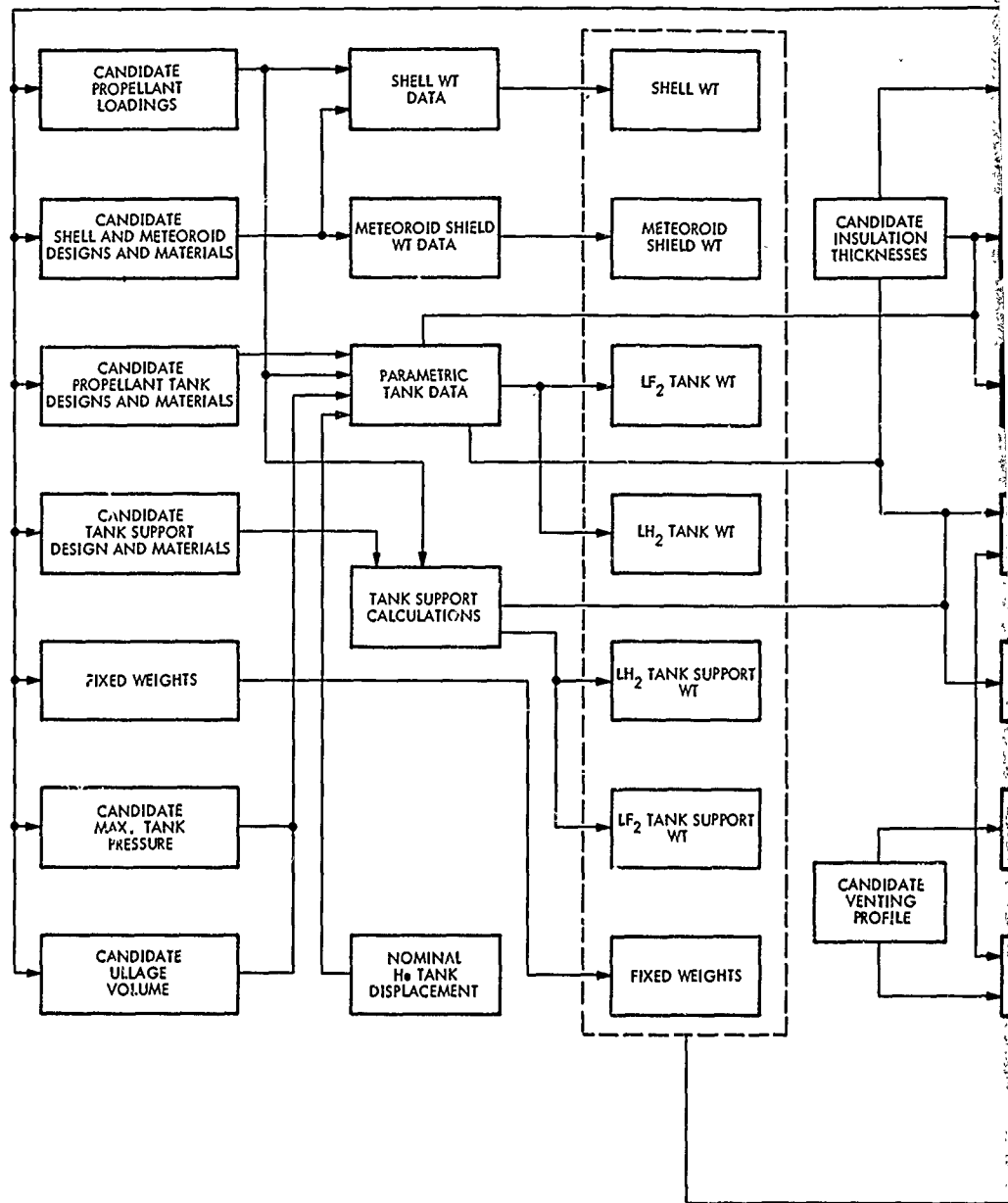
Shell Weight

(C) Shell weights are being developed for cylindrical and cylindrical/conical shell configurations shown in Fig. 2-8. Screening analyses in Subtask 5 show one

CONFIDENTIAL

LOCKHEED MISSILES & SPACE COMPANY

CONFIDENTIAL



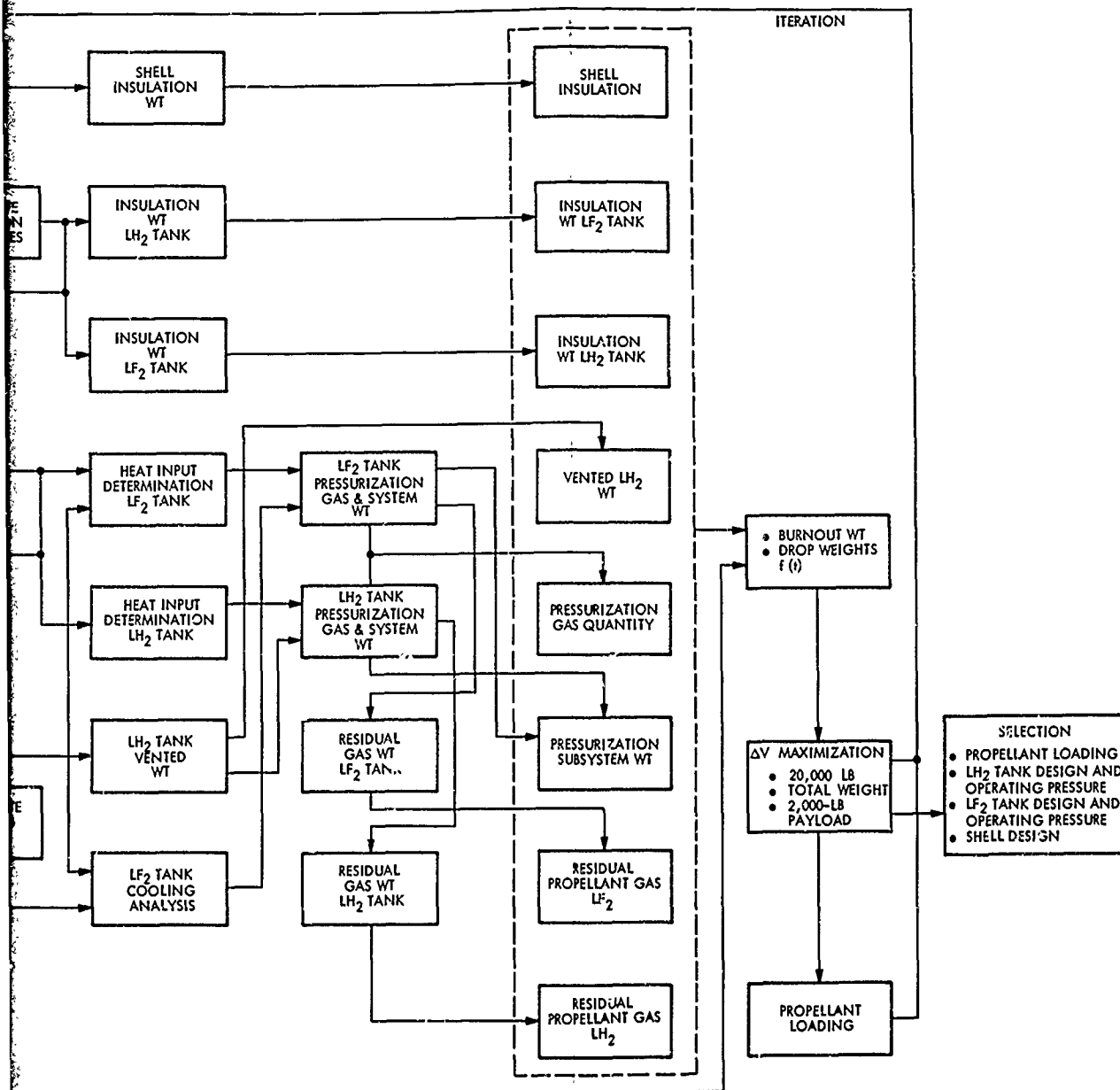


Fig. 2-7 Configuration Selection Optimization Studies (C)

Fig. 2-8 Conical/Cylindrical and Cylindrical Shells (C)

(This page is unclassified.)

promising shell design consisting of internal rings and integral external ribs running vertically along the shell. A promising construction material is HM21A magnesium thorium. Some initial results of the outer-shell analyses are given. The ground rules discussed in Subtask 5 are being used. The shell dimensions and loadings are as follows:

Diam. = 120 in.

L = 79 in.

L/R = 1.32

N_x = Line load, lb/in.

$$N_x = \frac{M}{\pi r^2} + \frac{P}{\pi D}$$

M = ultimate bending moment, in.-lb

P = ultimate axial load, lb

(U) Figure 2-9 depicts cylinder weight vs. an axial-load parameter (which includes temperature effects). The axial load is computed, as shown above, from the axial load in lb and the bending moment in in.-lb. Ultimate loads equal to 1.25 times limit loads are used in all cases.

(U) The temperature factor, K, is the ratio of the modulus of elasticity, E, at the expected temperature divided by the room temperature value of E.

(U) The weights shown do not include end rings, doublers, cutouts, or manufacturing contingencies. Minimum skin gage allowed was 0.012 in.

(U) Figure 2-10 shows cylinder weights in lb per in. of cylinder length for use in weight approximations for other cylinder lengths.

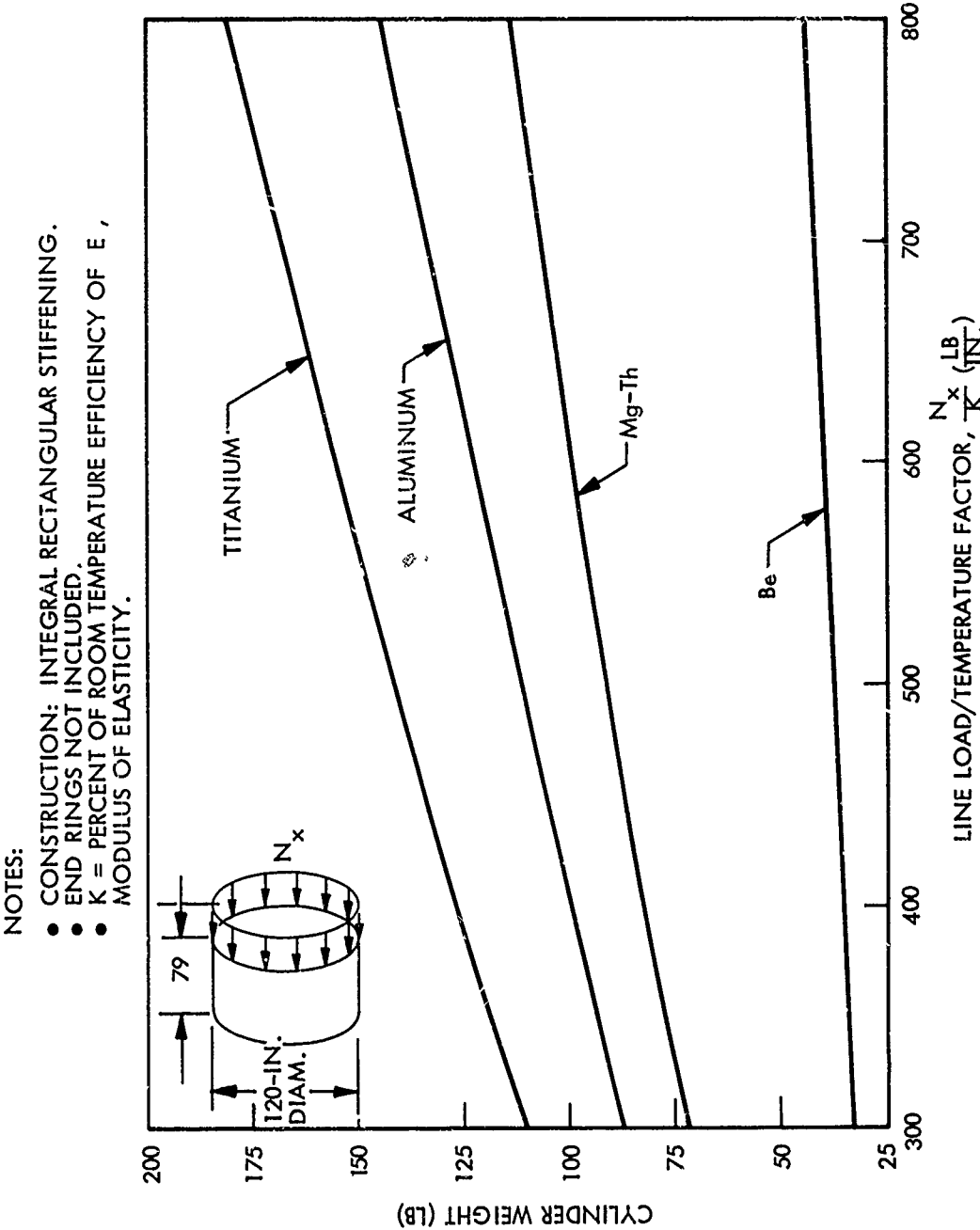


Fig. 2-9 Cylindrical Shell Weight as a Function of Axial Line Load

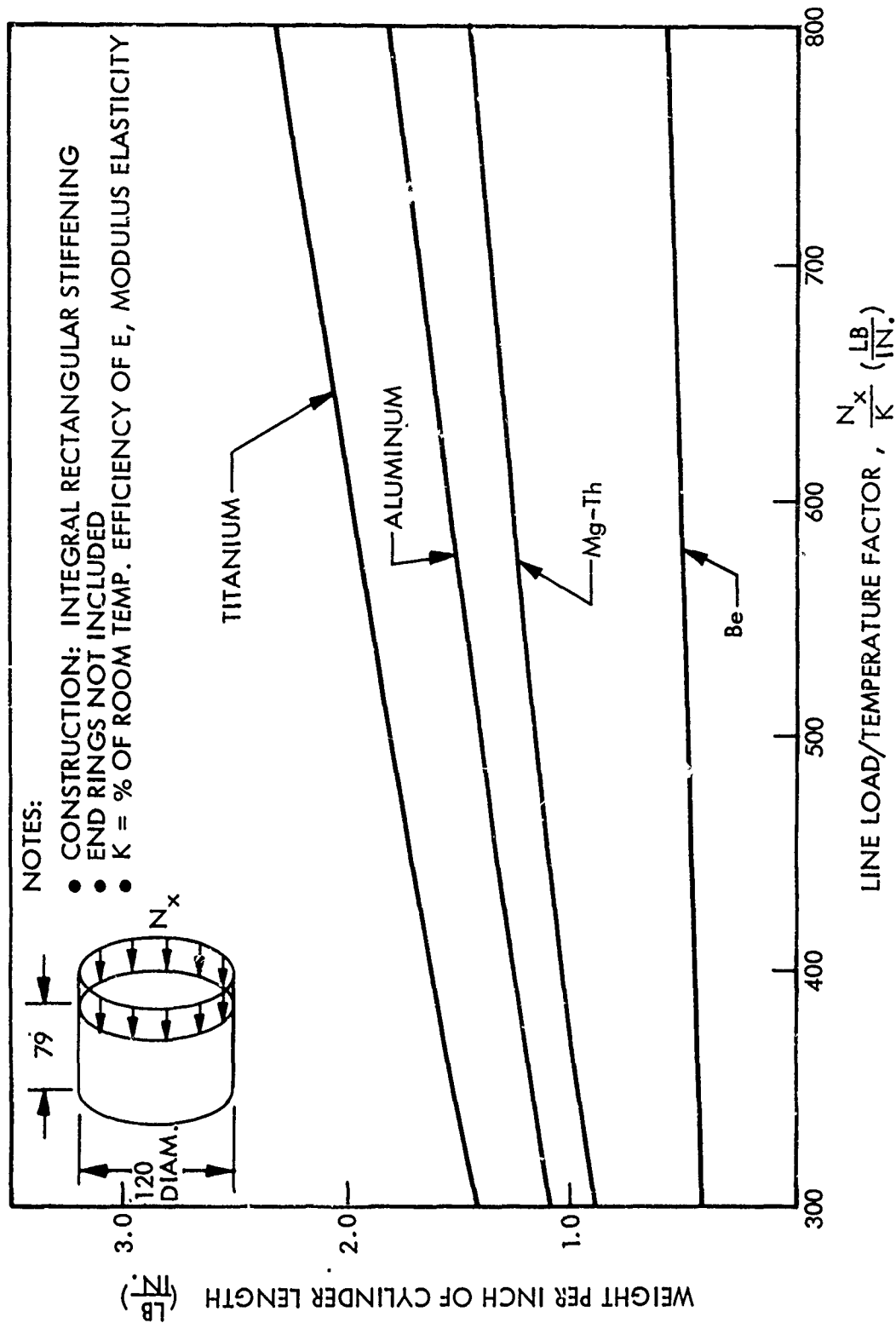


Fig. 2-10 Cylindrical Shell Weight Per Inch of Shell Length as a Function of Axial Line Load

Meteoroid-Shield Weight Data

(U) The meteoroid environment and penetration criteria were taken from Aerospace Meteoroid Environment and Penetration Criteria, Aerospace Corporation Report No. TOR-269 (4560-40)-2. These data were reduced to usable form by plotting thickness vs. $(KA_s + FA_p) T$ where:

T = the time interval

K = the ratio of average rate of sporadic meteoroids during the time interval, T , to the yearly average rate of sporadic meteoroids

A_s = surface area, ft^2

A_p = projected area, ft^2

F = the ratio of the average rate of shower meteoroids during the time interval, T , to the yearly average rate of sporadic meteoroids

(U) These penetration curves are currently being plotted.

Parametric Tank Data

(C) Following selection of 2021-T62 aluminum alloy as the most appropriate material for the liquid hydrogen and liquid fluorine tanks for the flight vehicle, the study for optimizing the most suitable tank configuration and tank arrangement to achieve the vehicle maximum ΔV can be started. Previous Lockheed studies (Ref. 3.) show the advantages of using combinations of ellipsoidal and/or spheroidal LF_2 and LH_2 tanks instead of multiple tank combinations or toroid/spheroid configurations. Consequently, this study is restricted only to spheroids and ellipsoids.

(C) Location of the LF_2 tank above the LH_2 tank on the vehicle was established for three reasons. First, locating the LF_2 tank above the larger LH_2 tank allowed the

shell shape to be conical in this region. Second, the LH_2 line length can be kept short, minimizing loss of trapped propellant after each burn. The higher temperature LF_2 is potentially easier to keep subcooled in a long feed line than the LH_2 . Third, locating the heavier LF_2 tank above the LH_2 minimizes the shift in the vehicle center of gravity as the propellants are depleted. This shift is currently estimated to be only 7.3 in. aft as the propellants are depleted.

(C) The maximum diameter for the LH_2 tank was set at 110 in. based on width of materials available for forming and clearance allowances between the 120-in.-diam. outer structural shell and the tank. To allow adequate clearance between the shell and the 3-in.-diam. LF_2 line that curves around the outside of the LH_2 tank when the 110-in. maximum diameter tank is assumed, the line must be locally flattened to approximately 1.5 in. It is also assumed that the line is insulated in such a manner that the equilibrium temperature within the blanket surrounding the line is in the liquid-fluorine temperature range.

(C) Tank concepts having an a/b ratio of 1.0, 1.2, 1.4 and 1.5 were analyzed. Table 2-3 lists the assumptions used in calculating the LH_2 and LF_2 tank weights as a function of a/b ratios. In this analysis the stage weight was kept constant, while the propellant loading was varied as the component weight fluctuated. Consequently, tank weights were calculated as a function of four volumes for both the LF_2 and LH_2 as shown on Table 2-3. On determination of a specific internal tank pressure, a curve can be constructed showing the weights for each of the four tank a/b ratios as function of the tank volume. The effect of a weight change can then be assessed in terms of tankage volume.

(U) For a constant volume, the semimajor axes were determined by using the equation:

$$a = \sqrt[3]{\frac{3V}{4\pi} \times \frac{a}{b}}$$

CONFIDENTIAL

LOCKHEED MISSILES & SPACE COMPANY

Table 2-3

ASSUMPTIONS USED FOR CALCULATION OF LH₂ AND LF₂
TANK WEIGHTS AS A FUNCTION OF a/b RATIO (C)

Assumptions		LH ₂		LF ₂	
<u>Configuration</u>					
Volume		290 ft ³		150 ft ³	
		306 ft ³		156 ft ³	
		320 ft ³		160 ft ³	
		340 ft ³		170 ft ³	
Major Diameter Limitation		110.0 in.		None	
Pressure Domes		70 psia to 150 psia		70 psia to 150 psia	
Number of Segments for a/b:					
1.0 - 1.2		6		6	
1.4 - 1.5		1		1	
Membrane Thickness		variable taper		variable taper	
Cylindrical Section		see Fig. 2-15		None	
Suspension System					
Number of Points		4		4	
Access Cover		Yes		Yes	
<u>Material</u>					
2021-T62 Aluminum Alloy		Yes		Yes	
Minimum Gage		0.030 in.		0.030 in.	
Material Allowables (ksi)		F _{tu}	F _{ty}	F _{tu}	F _{ty}
140° R	Parent Metal	91.0	74.0	-	-
	Weldment	47.5	-	-	-
200° R	Parent Metal	-	-	86.0	71.0
	Weldment	-	-	44.7	-
530° R	Parent Metal	73.0	61.0	73.0	61.0
	Weldment	38.0	-	38.0	-
		LH ₂ and LF ₂			
Burst Limit Pressure		1.25			
Yield Limit Pressure		1.10			
Proof Limit Pressure		1.05			
Additional Safety Factor for Discontinuity and Weldment Mismatch		1.22			

where

V = volume of tank

a = semimajor axis

b = semiminor axis

(C) A tank-pressure history analysis of the LH_2 tank showed that the maximum liquid head pressure increased the total design pressure by 0.4 psi which was added to the ullage pressure in determining the tank-membrane thickness for both the upper and lower shells. A similar analysis of the LF_2 tank showed that the design of the lower half-shell was determined by the summation of the ullage pressure and the maximum total liquid head. The total range of the pressures due to the liquid head varied from 4.23 psi for the 1.5 ellipsoid (150 ft³ tank) to 5.9 psi for the sphere (170 ft³ tank). The upper half-shell membrane thickness was determined by the summation of the ullage pressure and one half of the maximum liquid head. The following assumptions were made for the solution of the liquid head pressures:

Ullage (both the LH_2 and the LF_2 tanks)	5%
Fuel (LH_2) specific weight at 16 psia	4.395 lb/ft ³
Oxidizer (LF_2) specific weight at 16 psia	94.5 lb/ft ³
Liquid head pressure =	$g \times h \times w$,

where g = acceleration (1.5 g at beginning of firing phase, ~6.2 g at termination)

h = liquid level in tank

w = specific weight

$$g = \frac{30,000}{20,000 - nW_p}$$

where 30,000 = engine thrust, lb

20,000 = vehicle weight, lb

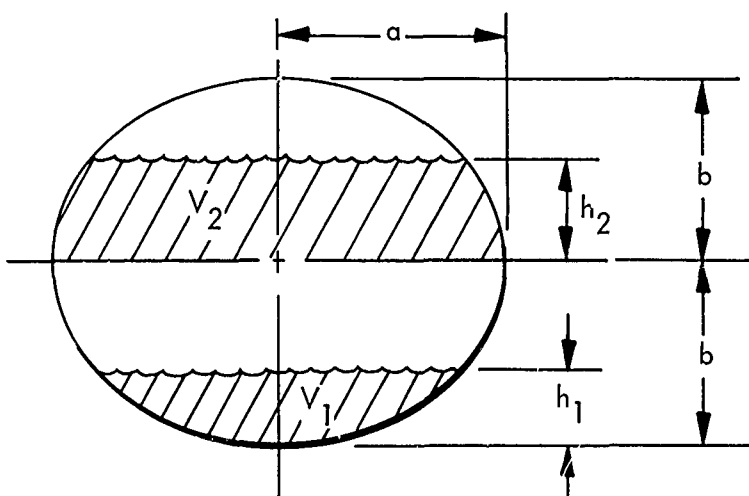
n = percent of propellant used

W_p = propellant weight

The term h was determined by the expressions V_1 and V_2 .

$$V_1 = \pi a^2 \left[h_1 - \frac{(h_1 - b)^3 + b^3}{3b^2} \right]$$

$$V_2 = \pi a^2 \left[h_2 - \frac{h_2^3}{3b^2} \right]$$



(U) On determination of the total internal pressure acting upon the tank membrane, stress analysis for each of the a/b ratio tanks was made to determine the membrane and weld-land thicknesses so that an accurate weight analysis could be made. To achieve minimum weights, the membrane thicknesses were tapered to maintain a constant stress level throughout the tank membrane. The following expressions were used for determining membrane thicknesses:

$$\text{Thickness at the tank poles: } t_p = \frac{pa}{2S} \times \frac{a}{b}$$

$$\text{Thickness at the tank equator: } t_e = \frac{pa}{2S}$$

Variable thicknesses between the pole and equator at point P: $t_v = \frac{p\sqrt{K_2}}{2Sb^2}$

where

t_v = membrane thickness at \underline{P}

$K_2 = a^4b^2 \cos^2 \phi + a^2b^4 \sin^2 \phi$

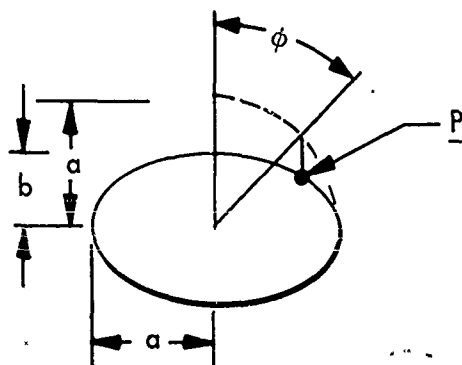
ϕ = angle shown in drawing below

S = allowable tensile stress

p = ullage pressure + liquid head

\underline{P} = designated stress point

(U) Angle ϕ was computed at 10-deg increments beginning at the tank pole.



(U) It can be shown that the hoop stress at the equator is negative for shells having an $a/b > 1.41$ because $S_h = \frac{pa}{2t} [2 - (\frac{a}{b})^2]$. Therefore, tank shells having an a/b ratio of 1.5 will buckle under compression if

$$S_h \geq \frac{0.3 Et}{r_1}$$

where:

$$r_1 = \frac{b^2}{a}$$

S_h = hoop stress

t = membrane thickness at equator

E = modulus of elasticity (10.6×10^6)

(U) As discussed in the preceding paragraphs, the geometry of the tank Y-ring is designed largely in consideration of weld land thicknesses and the tank support attaching flange. After each 1.5 ratio tank Y-ring was designed on this basis, the shell thicknesses were analyzed for buckling at the equator. The results showed that it was unnecessary to provide additional material to the Y-ring because positive margins of safety of 40 percent to 46 percent existed, depending upon the tank size.

(U) After the membrane thicknesses and weld lands were established, total tank-skin surface areas were computed. The following equations were used for these computations:

Ellipsoidal tanks

$$A = K_1 a^2, \text{ where:}$$

$$K_1 = \left[2\pi \left(1 + \left(\frac{b^2}{2a^2 E} \right) \left(\ln \frac{1+E}{1-E} \right) \right) \right]$$

where:

$$E = \sqrt{1 - \left(\frac{b}{a} \right)^2}$$

A = tank surface area

Spherical tanks

$$S = 4\pi r^2$$

(U) When the wall thicknesses are determined, shell weights can be established by slicing the domes into rings and computing the weight of each ring, using an average thickness. Nine rings, one for each 10 deg of angle ϕ , were used for these calculations.

(C) Figure 2-11 shows the LH_2 tank configurations under consideration. Figures 2-12 through 2-15 show the total liquid-hydrogen tank weights as a function of the tank pressures for each a/b ratio considered for tank volumes 290 ft^3 , 306 ft^3 , 320 ft^3 , and 340 ft^3 . Weights were plotted for both 530°R and 140°R material allowables, and, as would be expected, a significant weight saving can be realized by using the improved mechanical properties of 2021-T62 at 140°R . The temperature of 140°R was chosen, because liquid nitrogen can be used as the medium for proof-pressure testing of the tank without difficulty in the testing. These curves show that the 1.2 tank is heavier for both 140°R and 530°R than the 1.4 tank for corresponding temperatures, because the 1.2 half-shell must be formed in gore segments as described in the manufacturing analyses. The spherical tank is also made from gore sections, but the lighter weight of the spherical configuration results in a slightly lighter tank than does the 1.4 configuration. Weld lands are provided at each gore juncture, as shown in Section A-A of Fig. 2-11. These weld lands have a pronounced effect upon tank weight.

(C) Figure 2-16 shows the LF_2 tank configurations which are being considered.

(C) Figures 2-17 through 2-20 show the total liquid-fluorine tank weights as a function of the tank pressures of each tank a/b ratio for tank volumes of 150 ft^3 , 156 ft^3 , 160 ft^3 , and 170 ft^3 . Weights are plotted for a temperature of 530°R material allowables. Weights for 200°R temperature allowables are currently being calculated. As in the case of the LH_2 tanks, the tank having an a/b ratio of 1.2 is heavier than the tank having a ratio of 1.4 for the same reasons explained in the preceding paragraphs.

(C) The initial conclusion can be drawn that, for the AMPS vehicle, the 1.4 elliptical and the spheroidal tank configurations provide the lightest weight tanks, the latter being slightly lighter.

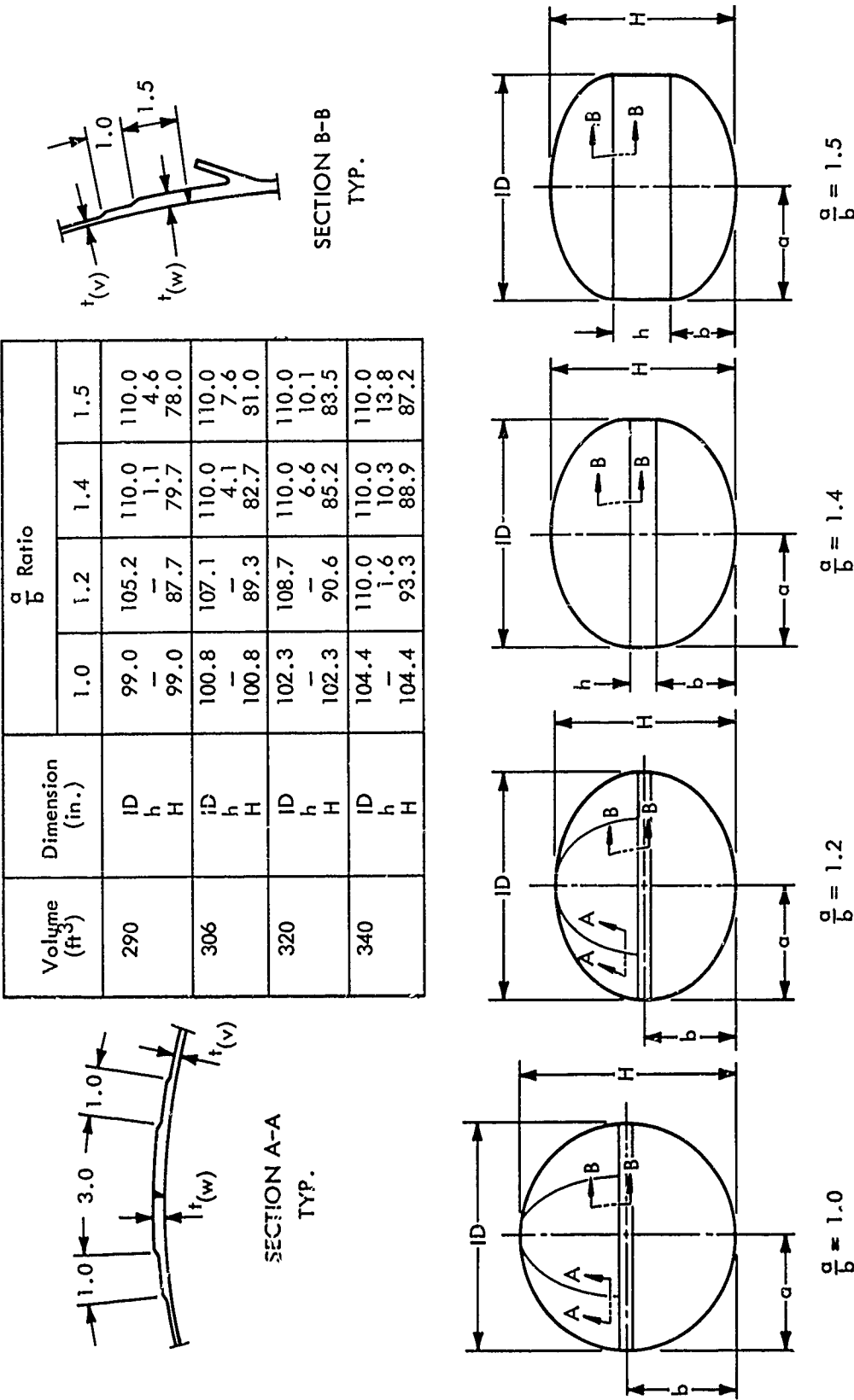


Fig. 2-11 Liquid Hydrogen Tank Configurations (C)

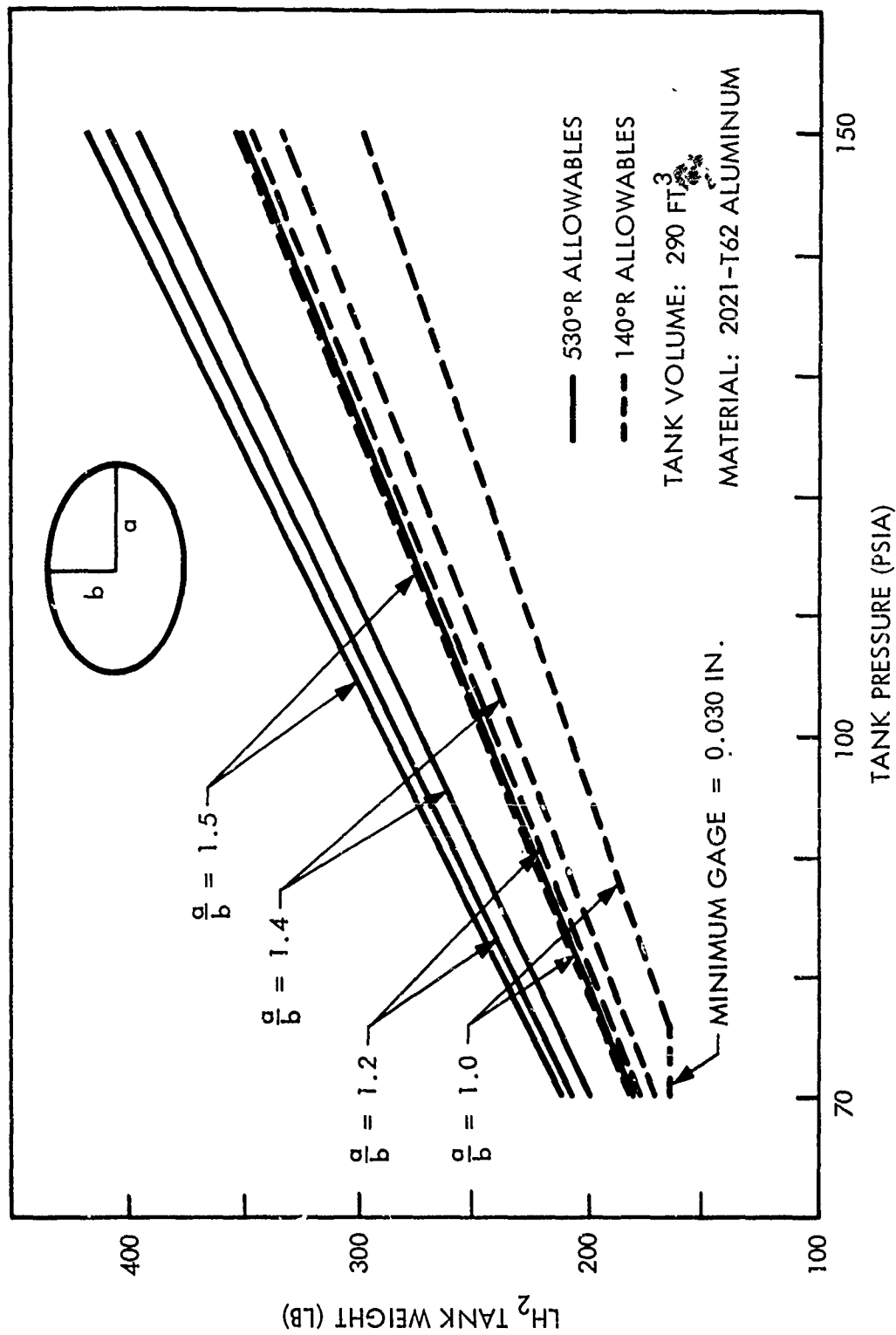


Fig. 2-12 LH₂ Tank Parametric Weights, 290 ft³ Volume (C)

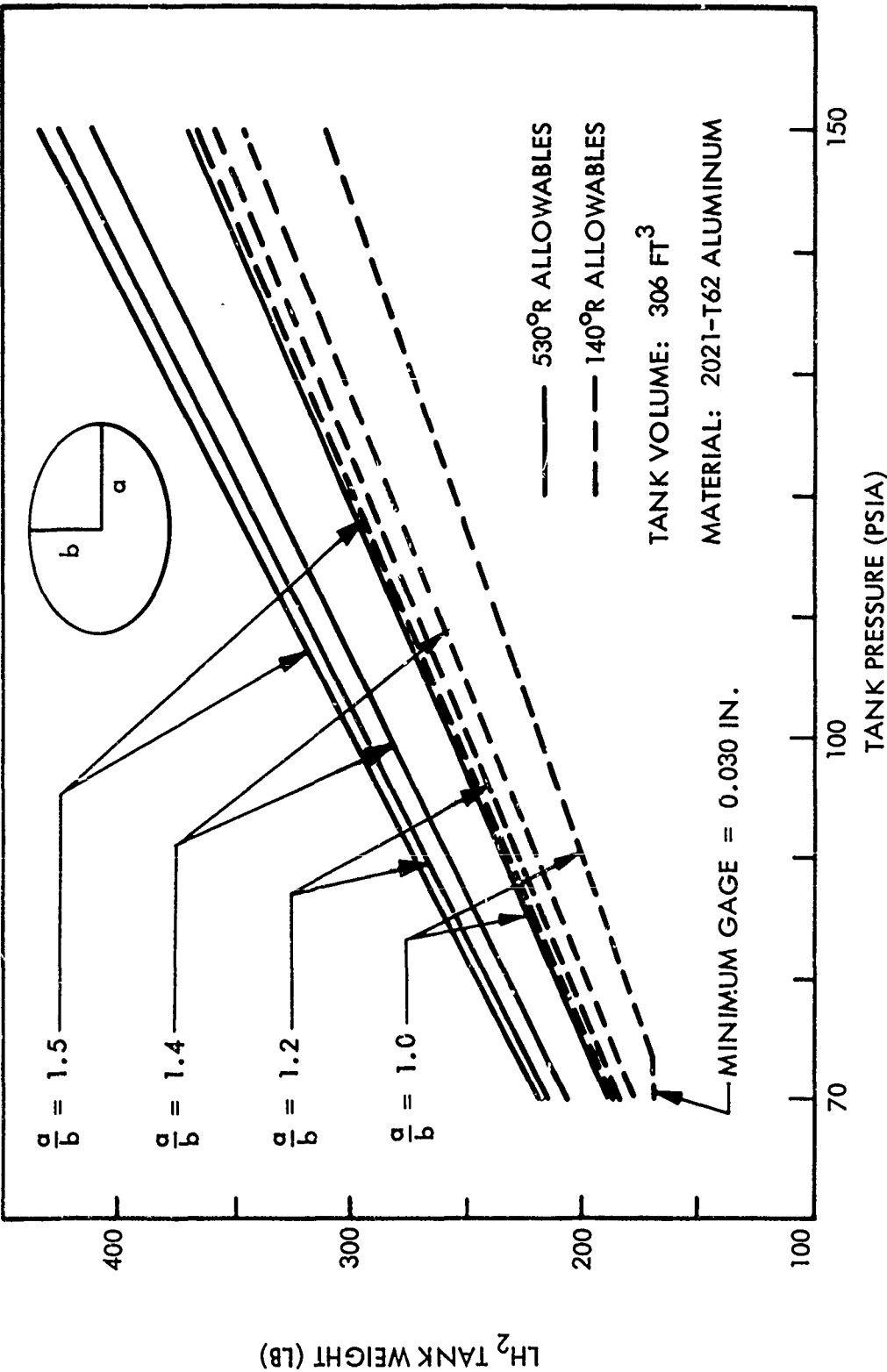


Fig. 2-13 LH₂ Tank Parametric Weights, 306 ft³ Volume (C)

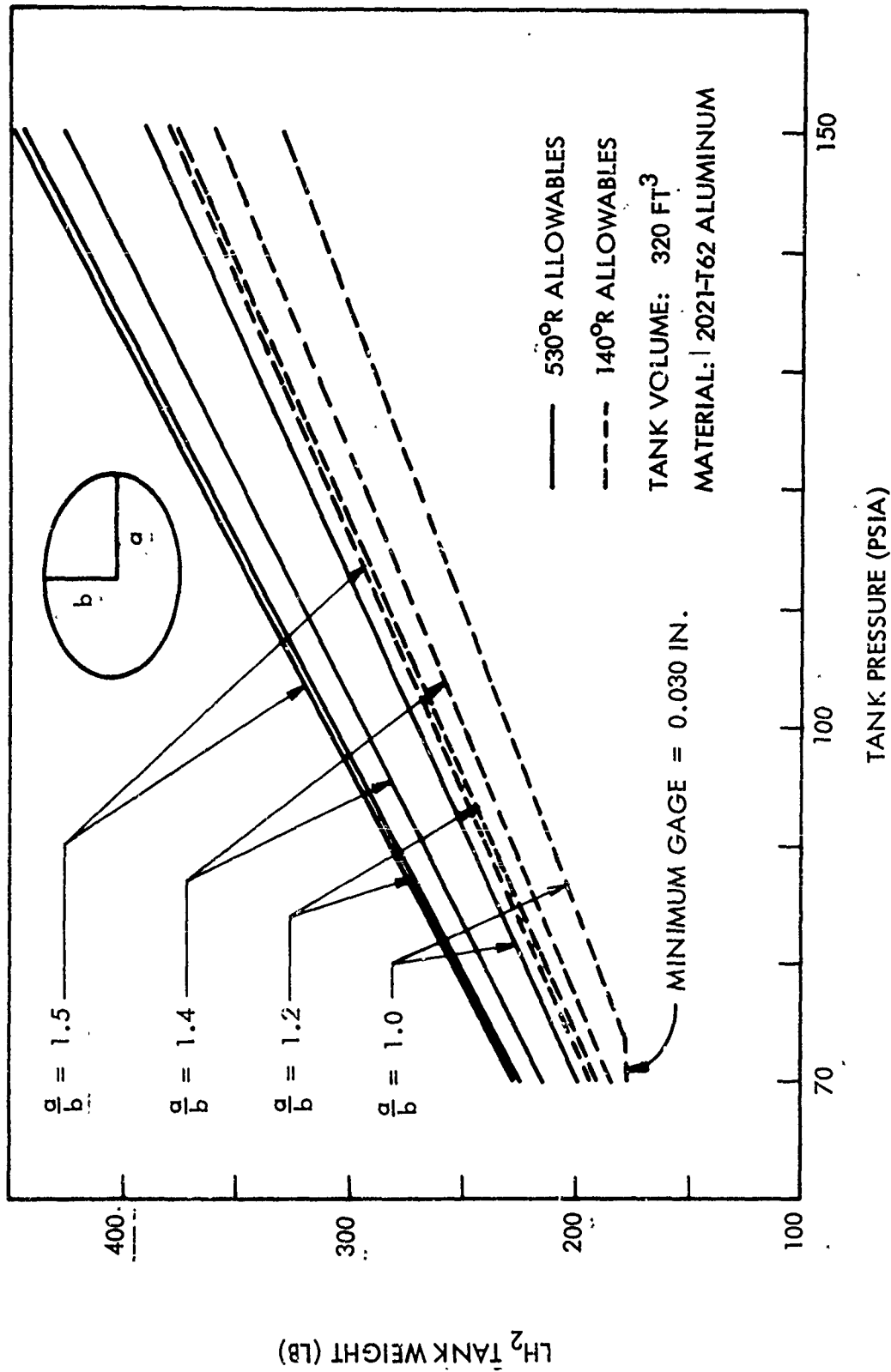


Fig. 2-14 LH₂ Tank Parametric Weights, 320 ft³ Volume (C)

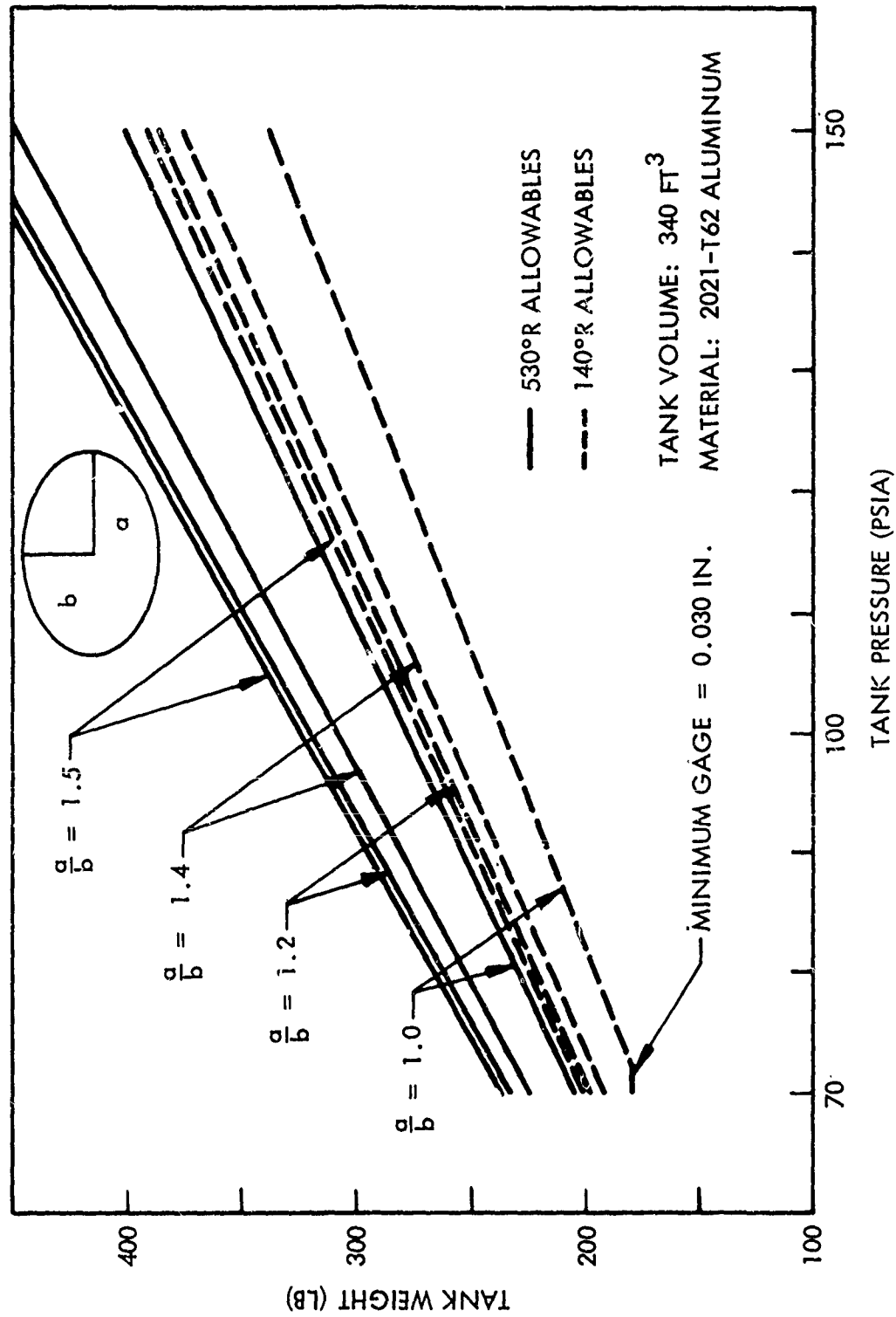


Fig. 2-15 LH₂ Tank Parametric Weights, 340 ft³ Volume (C)

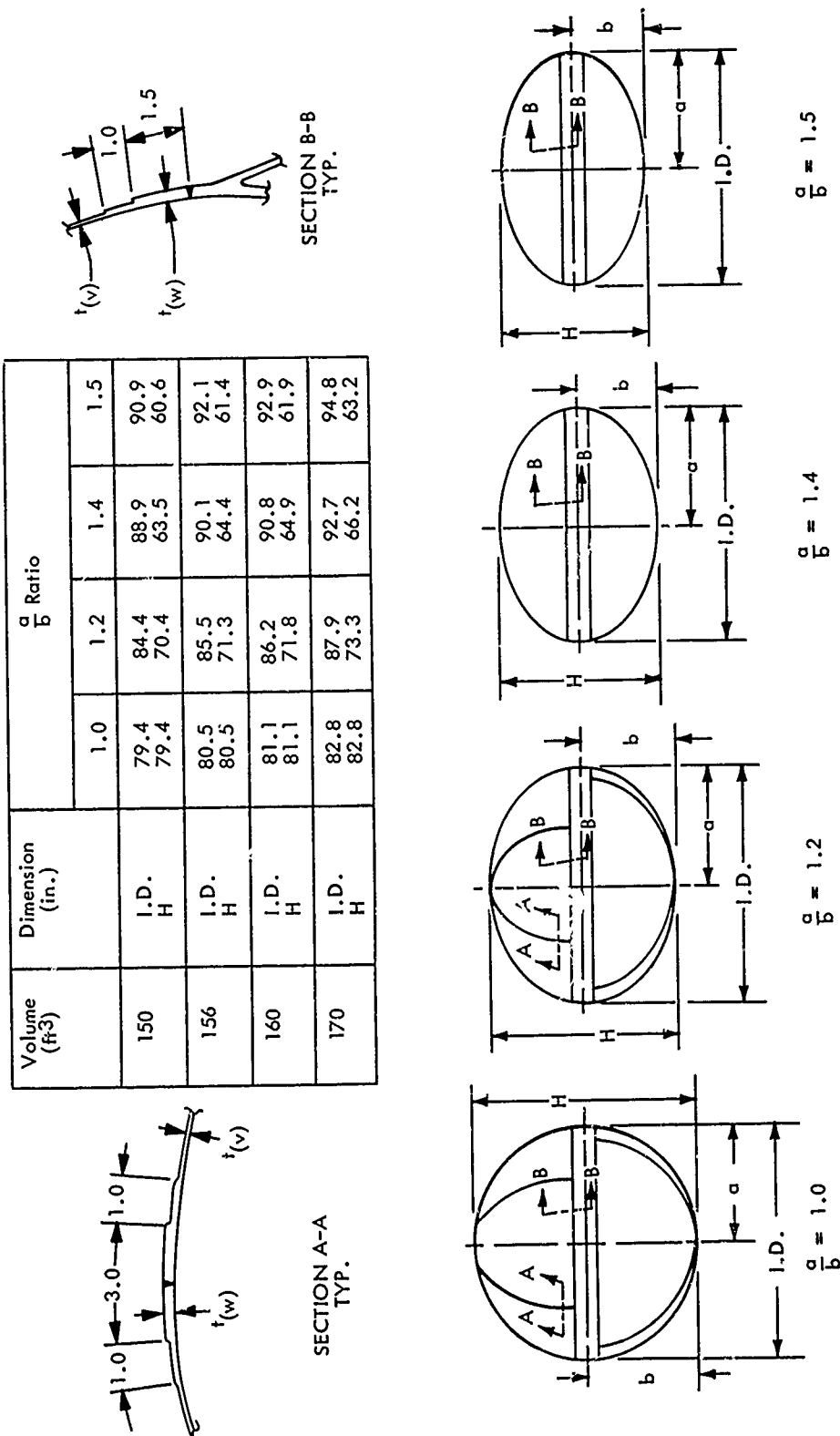


Fig. 2-16 Liquid Fluorine Tank Configurations (C)

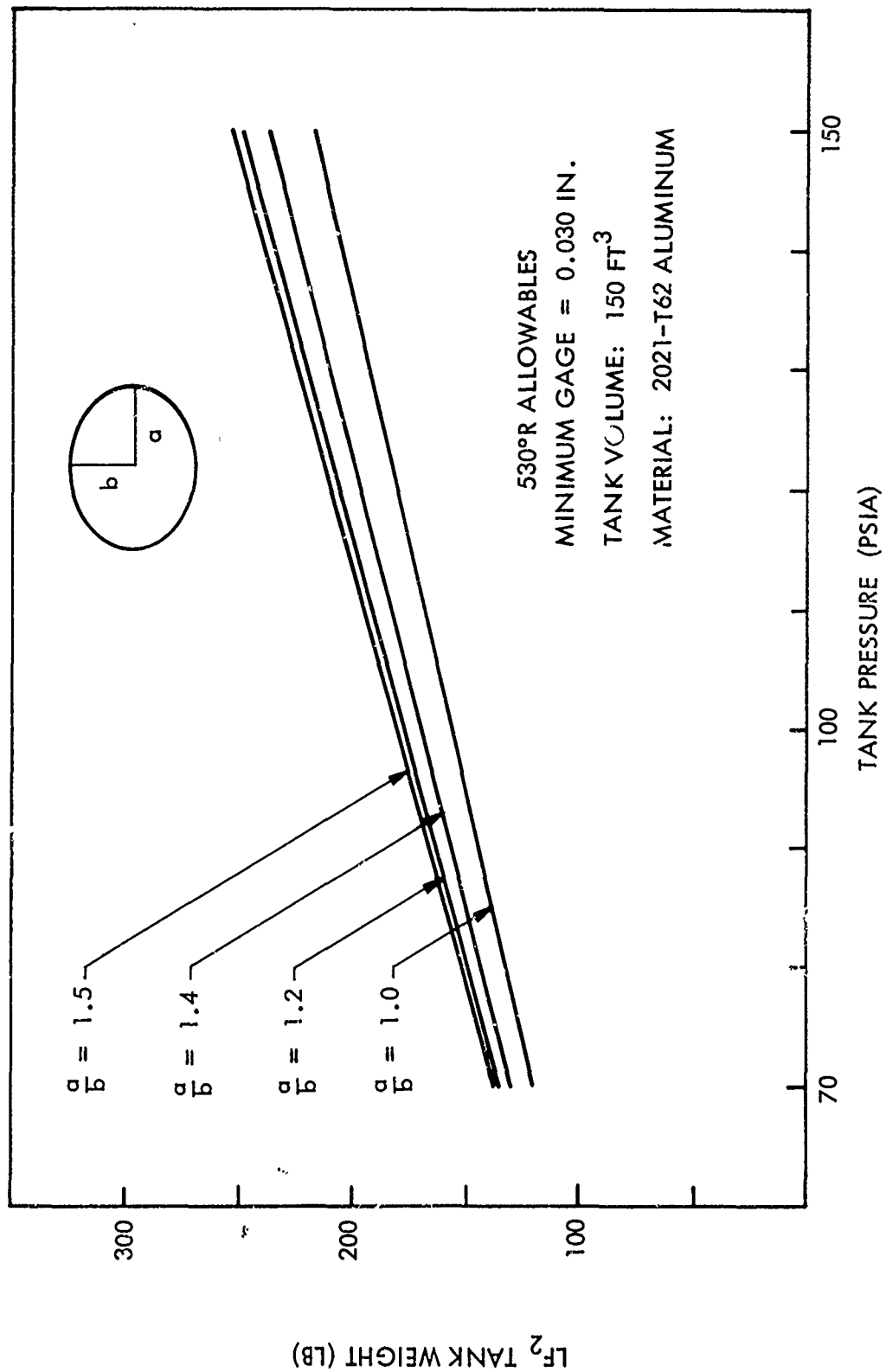
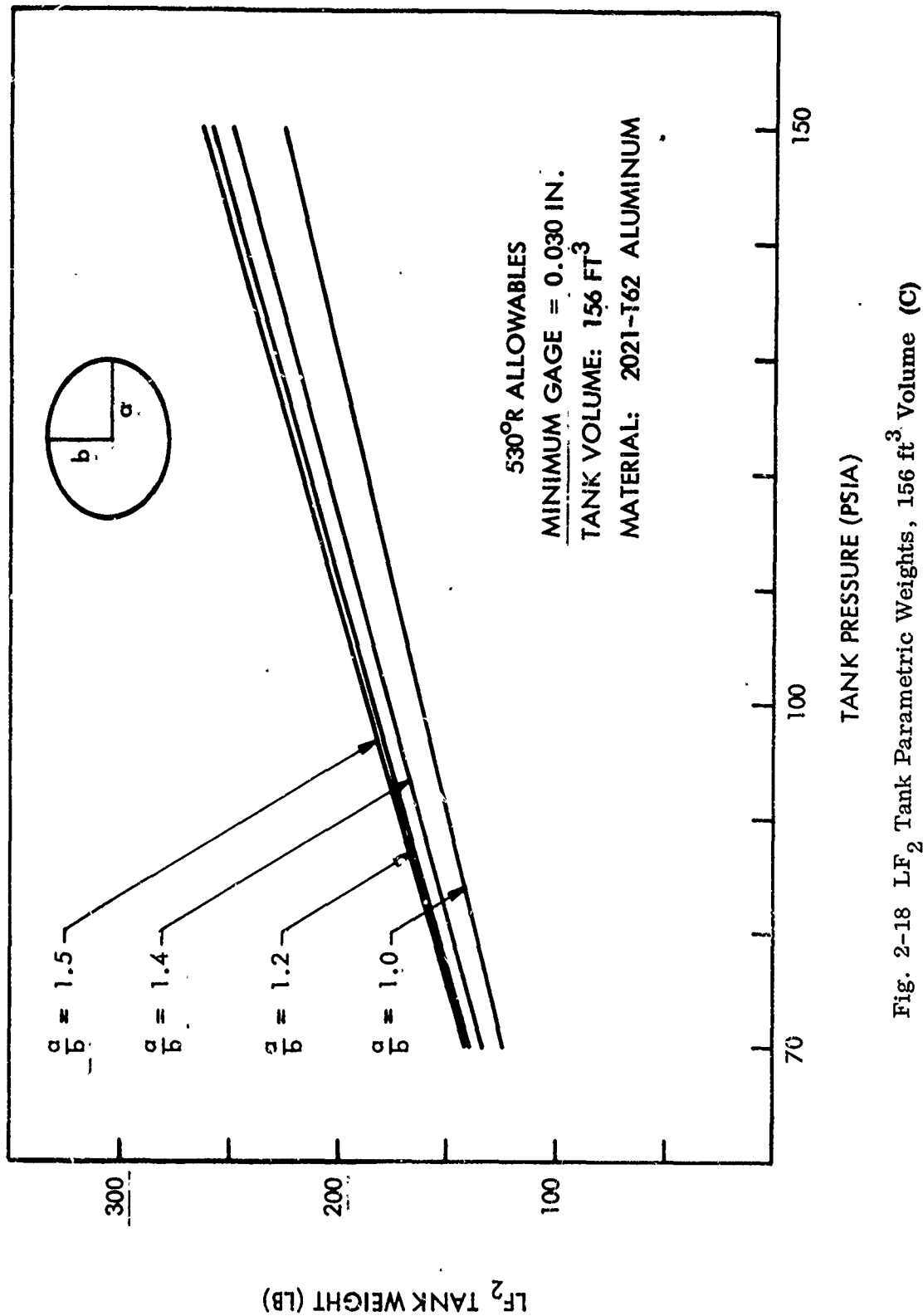


Fig. 2-17 LF₂ Tank Parametric Weights, 150 ft³ Volume (C)



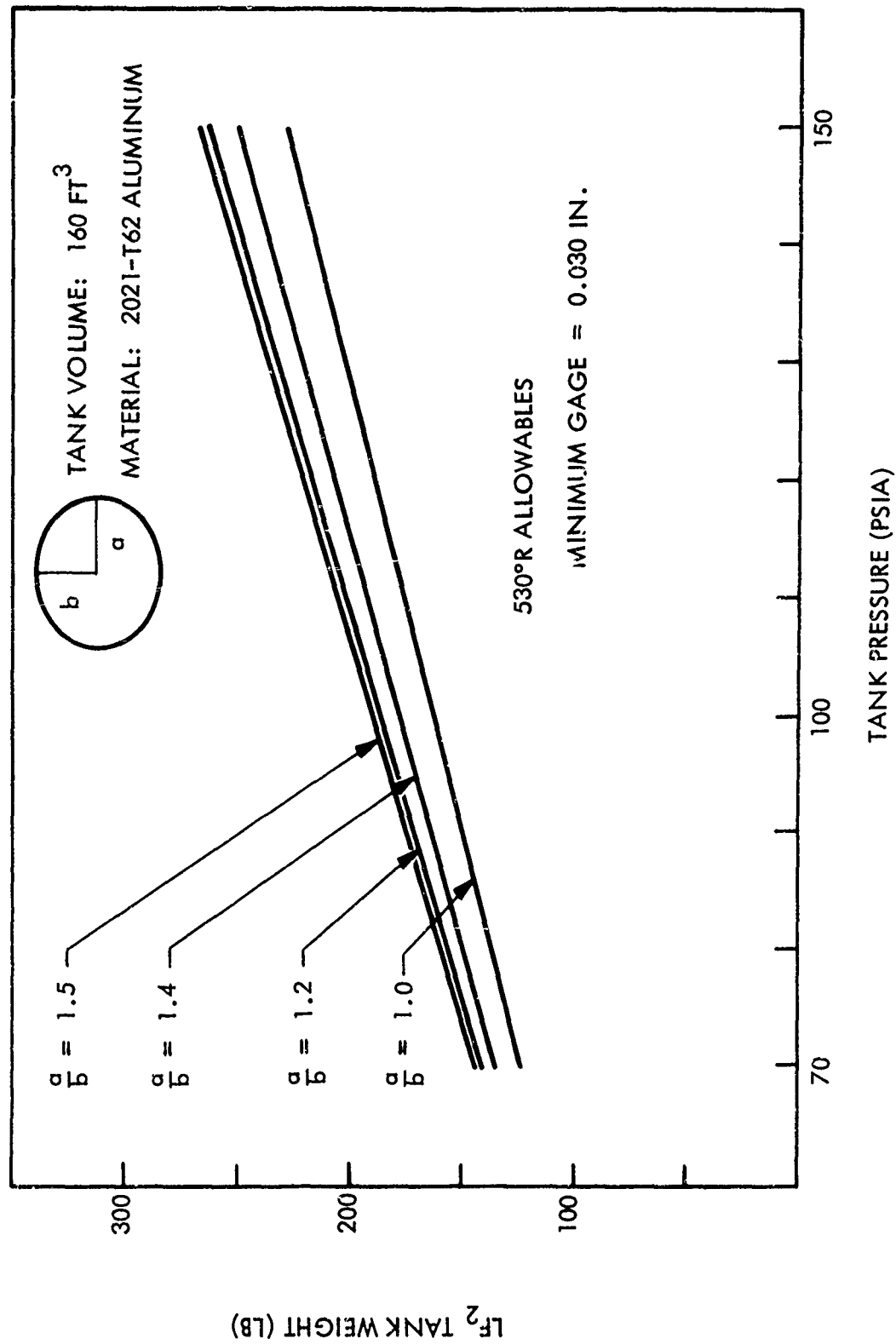


Fig. 2-19 LF₂ Tank Parametric Weights, 160 ft³ Volume (C)

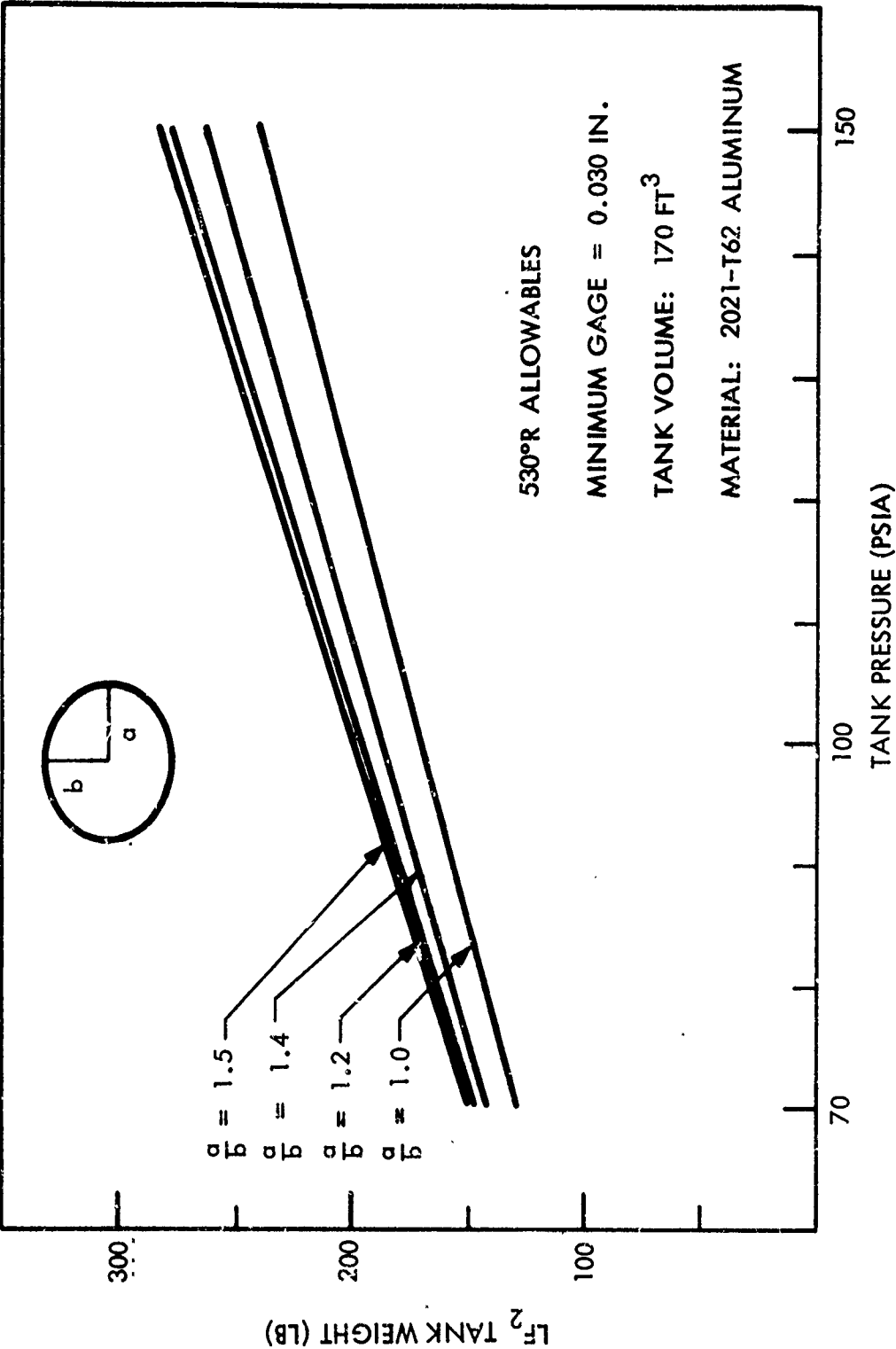


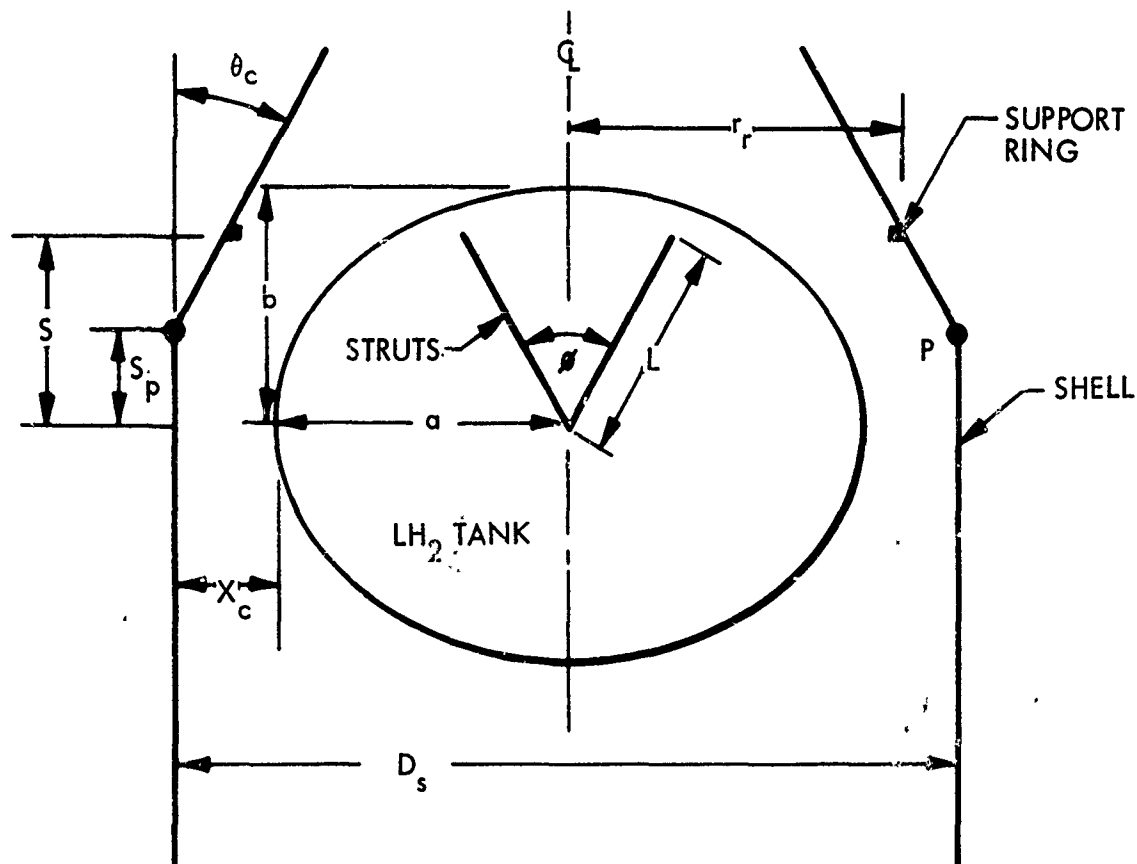
Fig. 2-20 LF₂ Tank Parametric Weights, 170 ft³ Volume (C)

(C) The need for a Y-ring, whatever the final tank configurations, is open to question. Lockheed has begun analyses to determine the weight increase or decrease that may be inherent in the Y-ring vs. no Y-ring design. One influence on this problem area is selection of the tank support system. The screening analyses conducted on the tank support system in Subtask 5 indicate that, for the LF_2 tank, titanium alloy struts are superior to fiberglass struts and to fiberglass semimonocoque cones. Analyses on the Y-ring configuration show that the Y-ring thickness optimized for no support would have to be increased only slightly to react the loads in such a four-point support system. Weight increase is approximately 2 lb, which varies only slightly if the tank diameter is increased. The hydrogen tanks require no change to the nominal Y-ring thickness, because the tank inertial loads are small. It is of interest to note that the "nominal" Y-ring design is established by material properties and manufacturing limitations. The initial thickness of the Y-ring in both the LF_2 and the LH_2 tanks is dictated by the weld allowables and consequent weld-land thicknesses at the girth. The geometry of the juncture of the membrane portion of the Y-ring and the strut attaching flange is not amenable to thinning adjacent to the weld lands; consequently, this material thickness is available for reacting the tank inertial loads. The outstanding tang on the Y-ring is retained the full height only at the four attaching points. This tang is machined away between the attach points to save weight.

Tank Support Calculations

(C) The total weight, length, and cross-sectional area of the tank support struts for both the hydrogen and fluorine tanks are defined in the following paragraphs for use in the parametric studies.

(C) LH₂ Tank Struts. The sketch below shows the LH₂ tank geometry.



(C) By evaluating a worst case, using the maximum propellant load with the longest struts, the rebound condition of compression designs the LH₂ tank fiberglass struts. From this analysis, it was determined that the minimum strut size allowed (2.0-in. diam. \times 0.030-in. thickness) satisfies the worst case analyzed. If the tubing size is held constant, the weight and heat leak associated with the hydrogen tank strut system is a function only of strut length. The total weight of the struts is given by:

$$W_T = n (\pi D_M t L_T) \rho_{FG} + W_{fixed}$$

where

- n = number of struts
- D_M = strut mean diameter
- t = strut-wall thickness
- L_T = tube length ($\approx 0.8L$)
- ρ_{FG} = tube density
- W_{fixed} = fixed weight of attachment and strut hardware

Length of the struts, L, is defined by:

$$L = \left[r_r^2 - 2a \left(r_r^2 - S^2 \tan^2 \frac{\phi}{2} \right)^{1/2} + a^2 + S^2 \right]^{1/2}$$

Constraints on the use of the equations are as follows:

- If $S_p \geq S$, then $\theta_c = 0$.
- The major axis of the tank cannot be above point P.

(C) LF₂ Tank Struts. An analysis performed using titanium struts shows that the major design considerations for the LF₂ tank struts in compression are maximum ascent acceleration and side loads. The total weight of the struts is given by the following equation:

$$W_T = n L_T A_c \rho_{titanium} + W_{fixed}$$

Where

n = number of struts

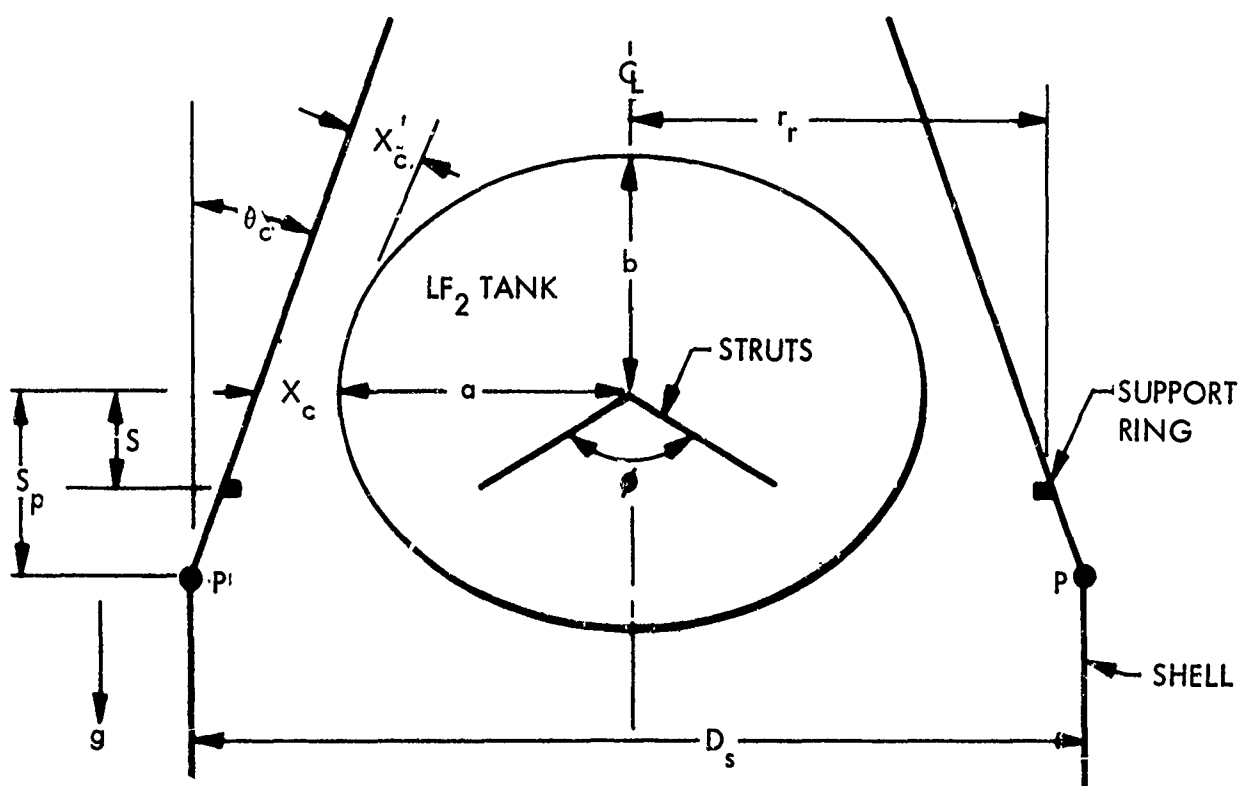
$$L_T = \text{tubing length } (\approx 0.8L)$$

A_c = tubing cross-sectional area

$$\rho_{\text{titanium}} = \text{tube density}$$

W_{fixed} = fixed weight of attachments and strut hardware

The sketch below shows the LiF_2 tank geometry.



(U) The cross section of the titanium tubing is given by

$$A_c = \frac{160}{E} \left[1.125 \frac{W_p L}{S} + 0.27 W_p \right]$$

where

E = modulus of elasticity

W_p = total supported weight

L = geometrical strut length

S = the parameter shown on LF_2 tank geometry illustration

(U) The geometric length of the struts, L , is given by

$$L = \left[r_r^2 - 2a \left(r_r^2 - S^2 \tan^2 \frac{\phi}{2} \right)^{1/2} + a^2 + S^2 \right]^{1/2}$$

where

$$r_r = \frac{D_s}{2} - (S_p - S) \tan \theta_c$$

(U) Constraints on the use of the equations are as follows:

- If $S \geq S_{sp}$, then $\theta_c = 0$.
- The major axis of the tank cannot be below point P

$$\bullet X_c' \geq 5 \text{ in.} = \cos \theta_c \left\{ \frac{D_s}{2} - S_p \tan \theta_c - \left[\frac{\cot^2 \theta_c}{\frac{b^2}{a^4} + \frac{\cot^2 \theta_c}{a^2}} \right]^{1/2} \right\}$$

Nominal Helium Tank Displacement

(C) LH₂ tank weight increments as a function of changing tank volume are shown below for both the spherical and 1.4 elliptical tanks over the range 290 ft³ to 340 ft³. This weight increment must be added to the basic tank weight for different helium-bottle sizes.

LH ₂ Tank Pressure (psia)	LH ₂ Tank Weight Increment (lb)			
	Unit Volume (ft ³)			
	Sphere		1.4 Ellipsoid	
	530° R	140° R	530° R	140° R
70	0.48	0.28 (In minimum gage region)	0.46	0.40
100	0.66	0.56	0.66	0.56

Heat Input Determination

(U) The heat input rate per unit weight (lb/ft²) of insulation (for the tank-mounted insulation) was determined using the maximum heating conditions described in Subtask 5. These parametric data are shown in Figs. 2-21 and 2-22. These curves will be used for given tank geometries to estimate the total heat-input rate (Btu/hr) to the tanks. Similar curves will be prepared for shell-mounted insulation.

Pressurization Gas and System Weight

(U) The configuration optimization study will consider only one type of pressurization subsystem concept. The expulsion temperatures are varied between Systems 3a and 3d, but the pressurization concept is the same. The concept was derived in studies performed in Subtask 8. The parametric pressurization-gas weight data have been collected as shown in Figs. 2-23 and 2-24. These expressions allow the heat input rates to provide the input variable for selecting the weights. This necessarily correlates the thermal protection and pressurization evaluations.

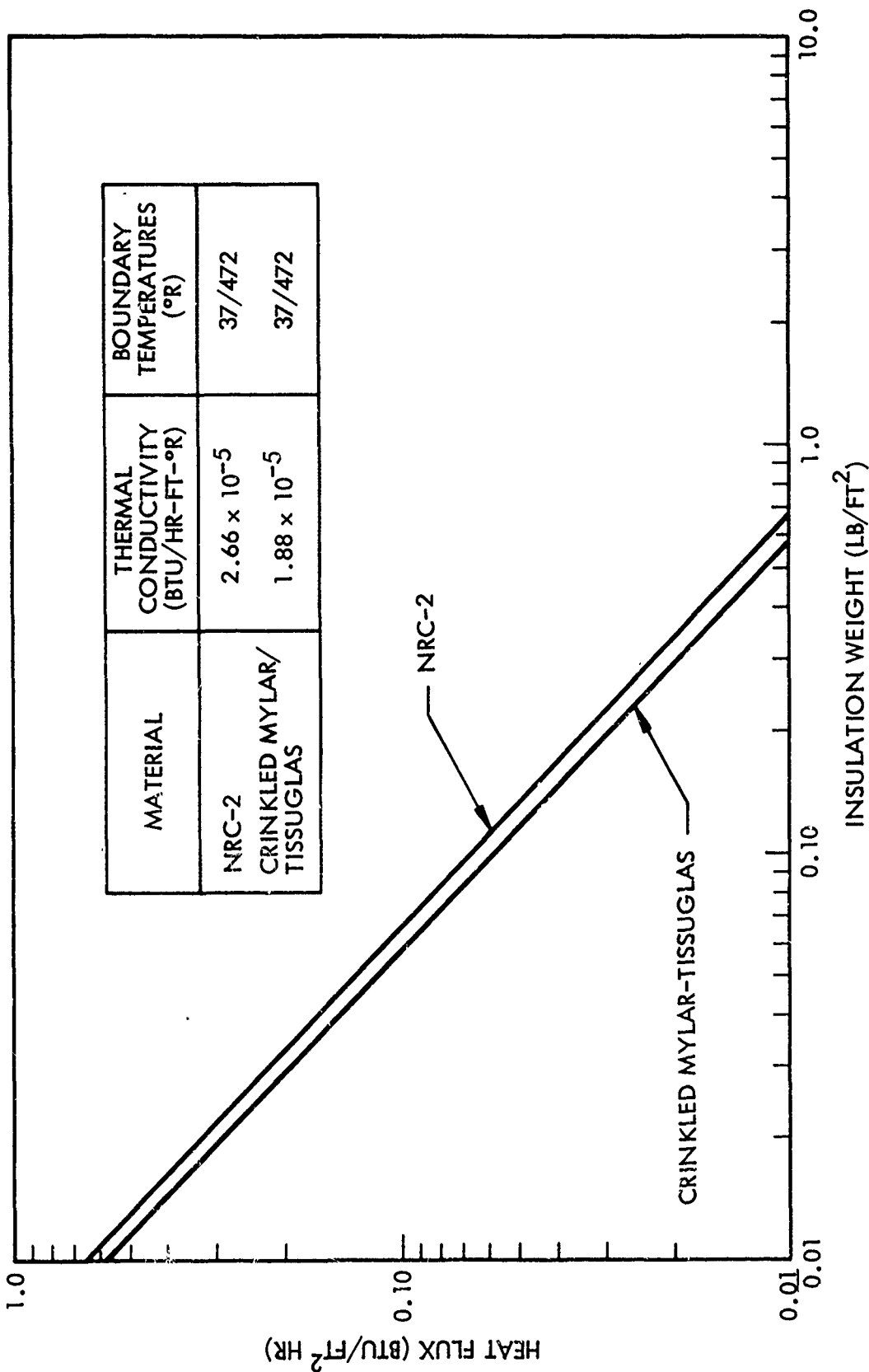


Fig. 2-21 LH₂ Tank Insulation Weight as a Function of Heat Flux (C)

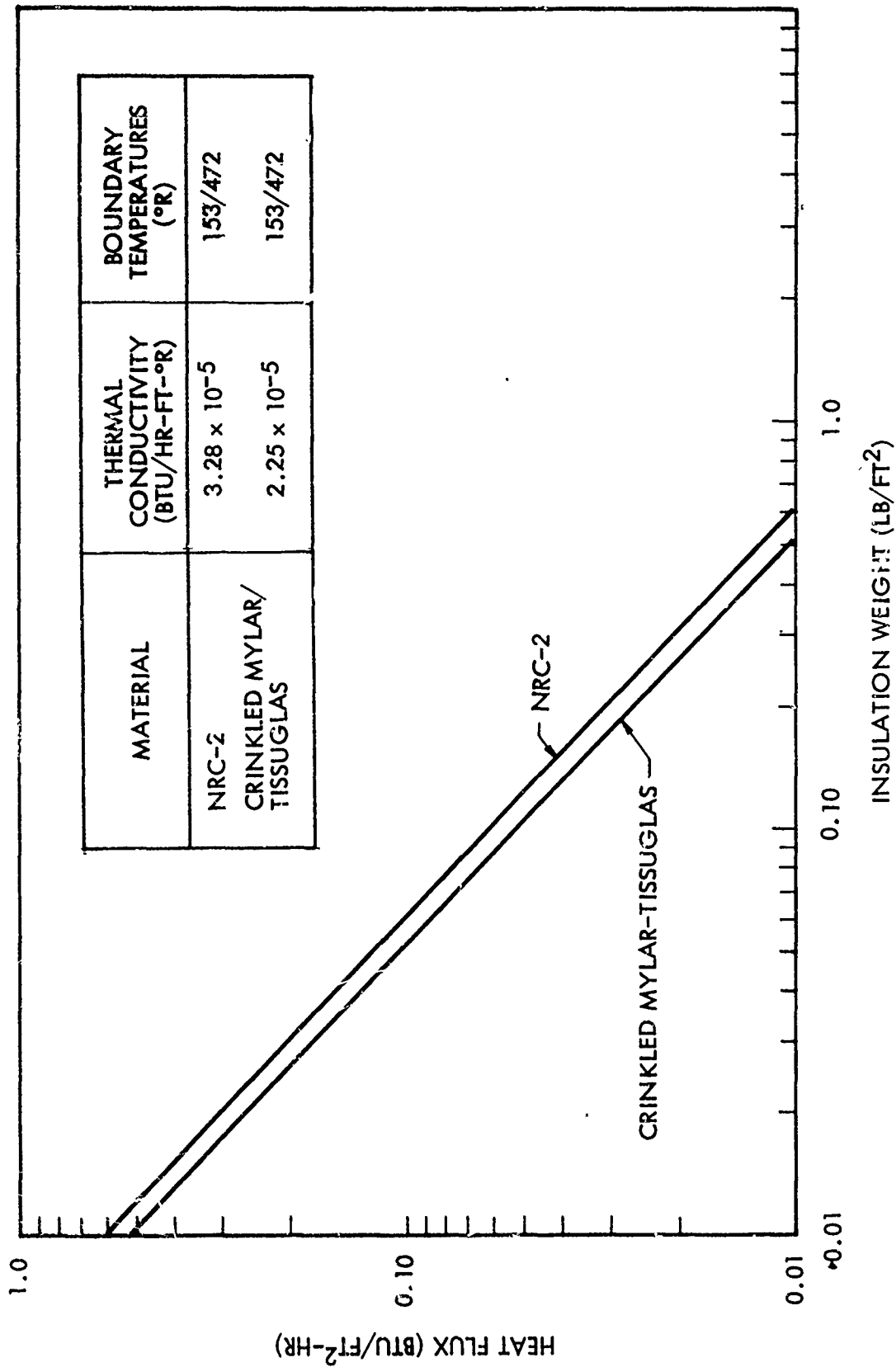


Fig. 2-22 LF₂ Tank Insulation Weight as a Function of Heat Flux (C)

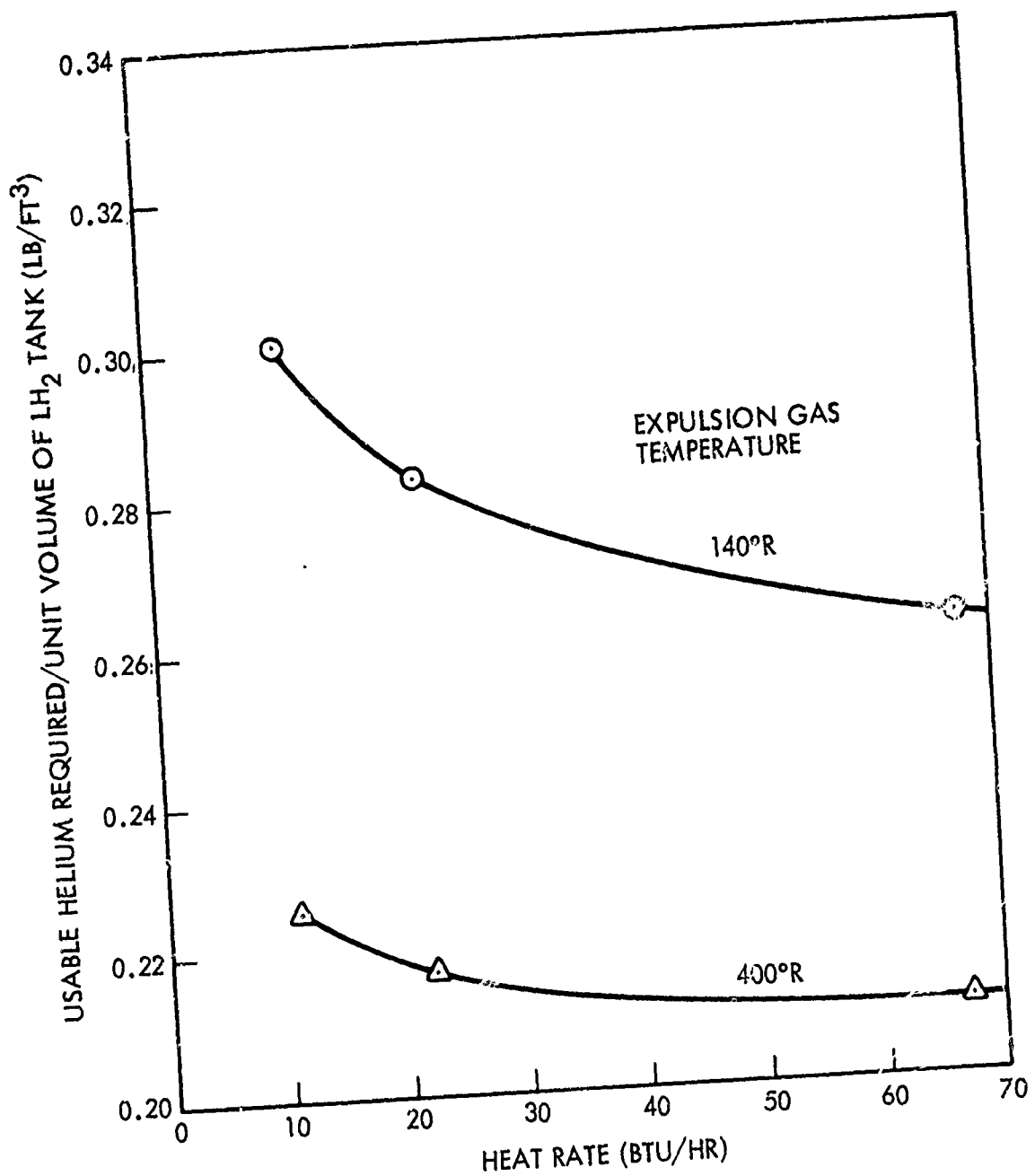


Fig. 2-23 Helium Requirements for LH₂ Tank, Duty Cycle No. 4 (C)

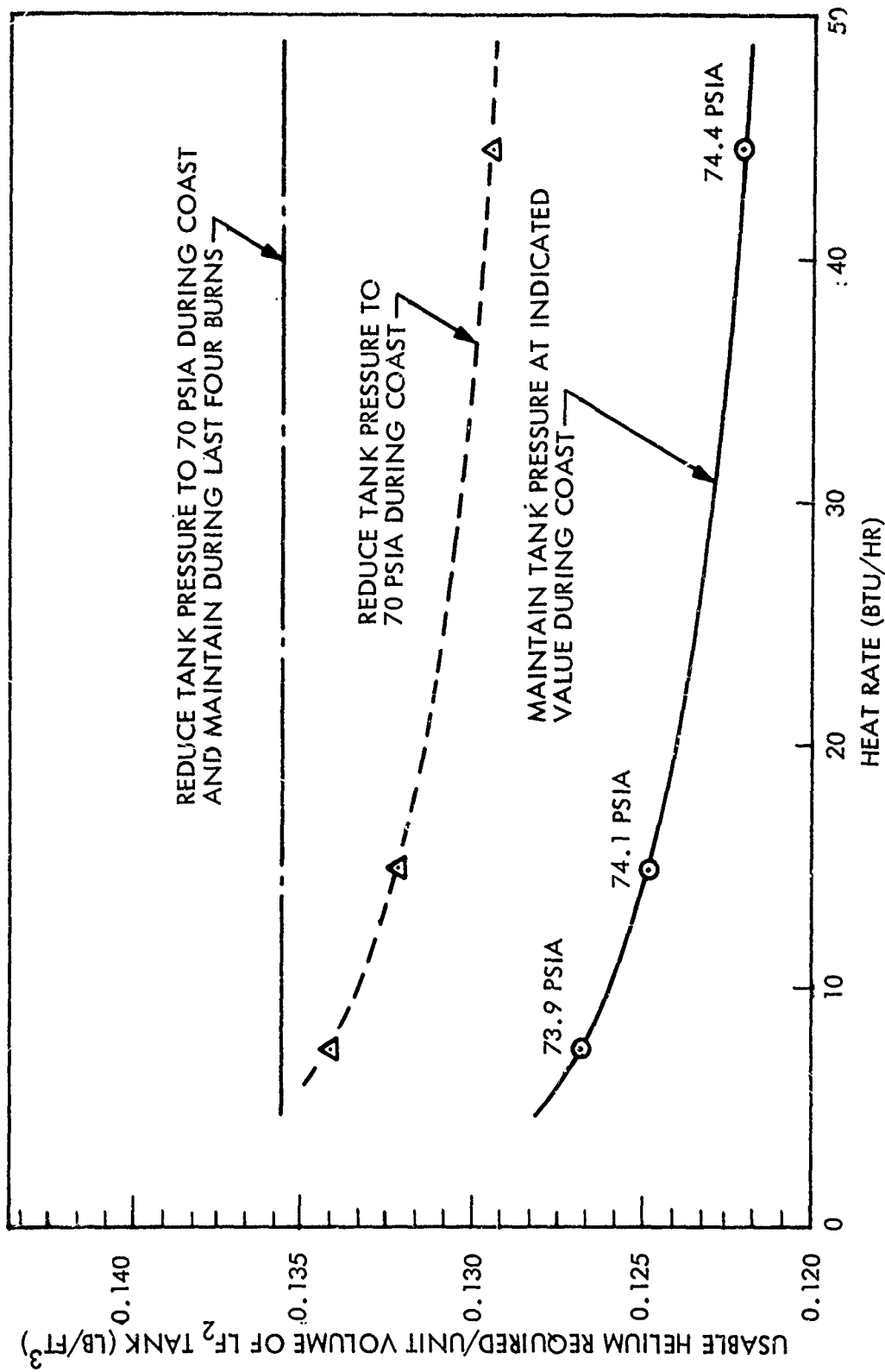


Fig. 2-24 Helium Requirements for LF₂ Tank; Duty Cycle No. 4 (320° R Expulsion) (C)

(C) These parametric gas-weight data are then used in a scaling equation developed for determining the pressurization system weight. The equation includes the effect of hydrogen-tank regulated pressure and volume, fluorine-tank regulated pressure and volume, hydrogen-tank expulsion temperature, and fluorine-tank expulsion temperature. This equation is shown in Fig. 2-25.

(C) The helium-bottle weight was handled separately in the equation because its weight is independent of the flow process. Because the helium-storage bottle constitutes one of the major system weights, a study was performed to determine the optimum storage pressure as described in Subtask 5. This pressure is optimized at 1,250 psia. Consequently, bottle weights are based on this pressure as shown in Fig. 2-26.

(U) The approach used for evaluating lines and valves was to apply the continuity equation and maintain a constant mach number at any given point in the system. In this manner, a required change in flow area as a function of pressure, temperature, and flowrate could be established. This change in area was then applied to a size-to-weight relationship to determine variation in weight of valves and lines. Pressure drop in the lines does not remain constant for all design conditions but will change in proportion to the tank pressure.

(C) A nominal system was sized and the weights of components calculated or estimated. These weights were then used to establish the coefficients for the individual terms of the equation. Each term represents a specific group of components that are influenced by the flow to either the hydrogen tank or fluorine tank. The terms represent components as follows:

First term - helium-bottle weight

Second term - hydrogen bleed lines and fittings

Third term - hydrogen tank repressurization GHe lines and fittings

Fourth term - lines, fittings, and heat exchanger affected by flow to the fluorine tank

Fifth term - hydrogen-tank bleed GH_2 valves

$W_{\text{pressurization system}} =$

$$\begin{aligned}
 \text{Bottle Weight} & \left\{ \frac{V_{F_2 \text{ tank}} W_{GHeF_2} + W_{GHeH_2} V_{H_2 \text{ tank}}}{(1 - 0.000775 T_{H_2 \text{ inj}}) (2.085 - 0.00351 P_{H_2 \text{ tank}})} \right. \\
 \text{Hardware Weight} & \left\{ \begin{aligned} & + \frac{14.04}{(T_{H_2 \text{ inj}})^{1/4}} + \frac{45.9}{(T_{H_2 \text{ inj}})^{3/8}} + 0.801 \left(\frac{W_{GHeH_2} V_{H_2 \text{ tank}}}{P_{H_2 \text{ tank}}} \right)^{1/2} (T_{H_2 \text{ inj}})^{1/4} \\ & + 0.829 \left(\frac{W_{GHeH_2} V_{H_2 \text{ tank}}}{P_{H_2 \text{ tank}}} \right)^{3/4} (T_{H_2 \text{ inj}})^{3/8} + 167.2 \left(\frac{W_{GHeF_2}}{P_{F_2 \text{ tank}}} \right)^{1/2} (T_{F_2 \text{ inj}})^{1/4} \\ & + 461 \left(\frac{W_{GHeF_2}}{P_{F_2 \text{ tank}}} \right)^{3/4} (T_{F_2 \text{ inj}})^{3/8} + 8.5 \end{aligned} \right. \\
 \text{Usable Plus Residual Helium Weight} & \left\{ + \frac{V_{H_2 \text{ tank}} W_{GHeH_2} + W_{GHeF_2} V_{F_2 \text{ tank}}}{1 - 0.001686 P_{H_2 \text{ tank}}} \right.
 \end{aligned}$$

where

W_{GHeH_2} = usable GHe weight (lb) for LH_2 tank per ft^3 of H_2 tank (See Fig. 2-23)

W_{GHeF_2} = usable GHe weight (lb) for LF_2 tank per ft^3 of F_2 tank (See Fig. 2-24)

$P_{H_2 \text{ tank}}$ = regulated pressure (psia) to LH_2 tank

$P_{F_2 \text{ tank}}$ = regulated pressure (psia) to LF_2 tank

$V_{H_2 \text{ tank}}$ = volume (ft^3) of LH_2 tank (minus tie bottle volume)

$V_{F_2 \text{ tank}}$ = volume (ft^3) of LF_2 tank

$T_{H_2 \text{ inj}}$ = GH_2 expulsion temperature ($^{\circ}R$) to LH_2 tank

$T_{F_2 \text{ inj}}$ = GHe expulsion temperature ($^{\circ}R$) to LF_2 tank

* $W_{\text{pressurization system}}$ includes: Bottle, total GHe, lines, valves, fittings, and heat exchanger

Fig. 2-25 Pressurization System Weight Scaling Equation (C)

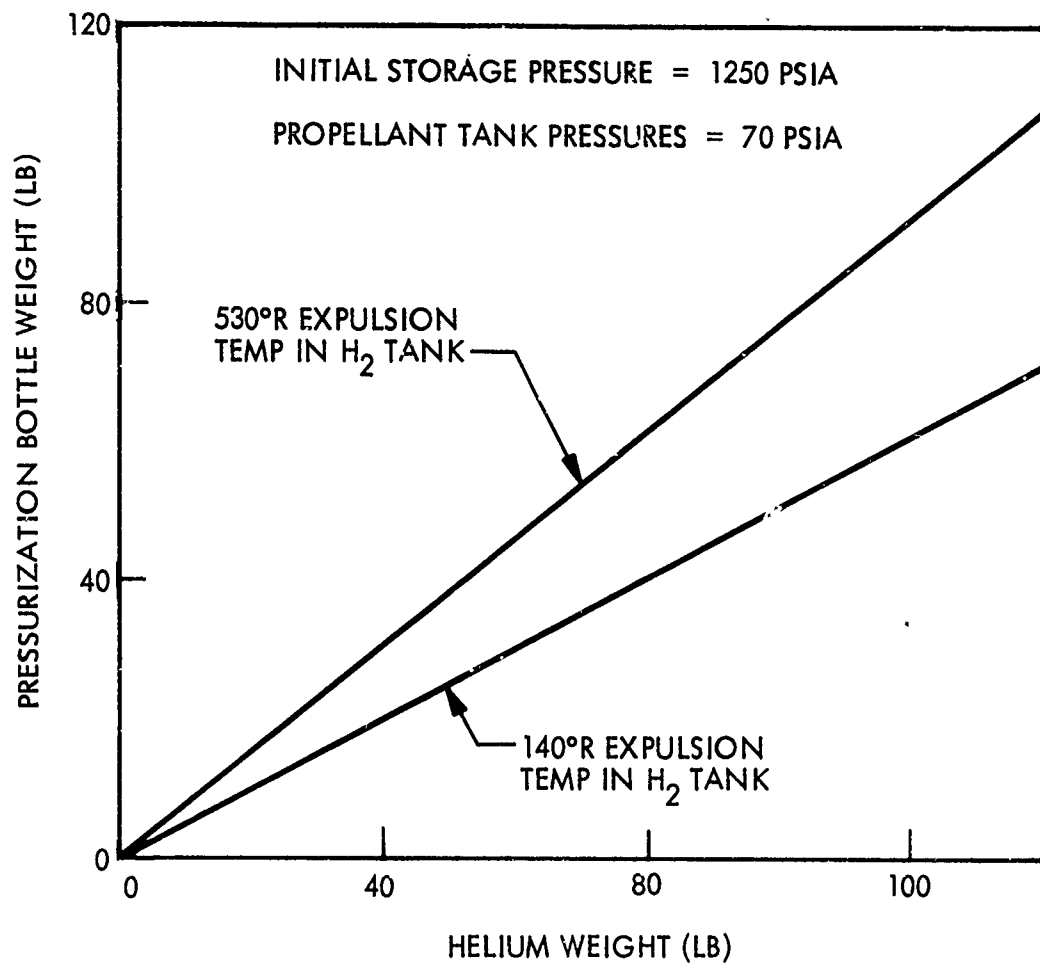


Fig. 2-26 Helium Bottle Weight as a Function of Usable Helium Weight (C)

Sixth term - hydrogen-tank repressurization valves

Seventh term - valves affected by flow to the fluorine

Eighth term - weight of valves, lines, and fittings not affected by flow or mass of pressurant

Ninth term - total weight of GHe loaded

(C) The helium bottle weight is affected by usable mass of helium, expulsion temperature to the hydrogen tank, and regulated pressure to the hydrogen tank. The expulsion temperature influences the material allowables of the bottle, and the regulated pressure affects the final blowdown pressure and, consequently, GHe residuals. Material allowables are varied linearly with temperature. There is some variation from actual allowables due to linearization, but the weight difference is small and should have little effect on the accuracy of the overall pressurization system weight. In the anticipated range of temperature expulsion, the allowables are very accurate.

(C) Line and valve sizes are varied according to flow temperature, pressure, and flowrate as indicated by the mach-number equation below.

$$M = \frac{\dot{w}}{PA} \sqrt{\frac{RT}{\gamma g}}$$

(C) The fluorine lines and valves are sized for expulsion requirements. The hydrogen repressurization GHe lines and valves are sized for a nominal flow requirement but will be modified by the hydrogen expulsion bleed gas temperature. Temperature of the hydrogen tank ullage at shutdown influences the rate of hot gas collapse and, therefore, alters the maximum replenishment flowrate.

LH₂ Tank Venting

(C) The heat-input rate data are used to obtain the LH₂ tank vented weight from Fig. 2-27. An evaluation is made to determine if this vent rate is sufficient for LF₂ tank cooling.

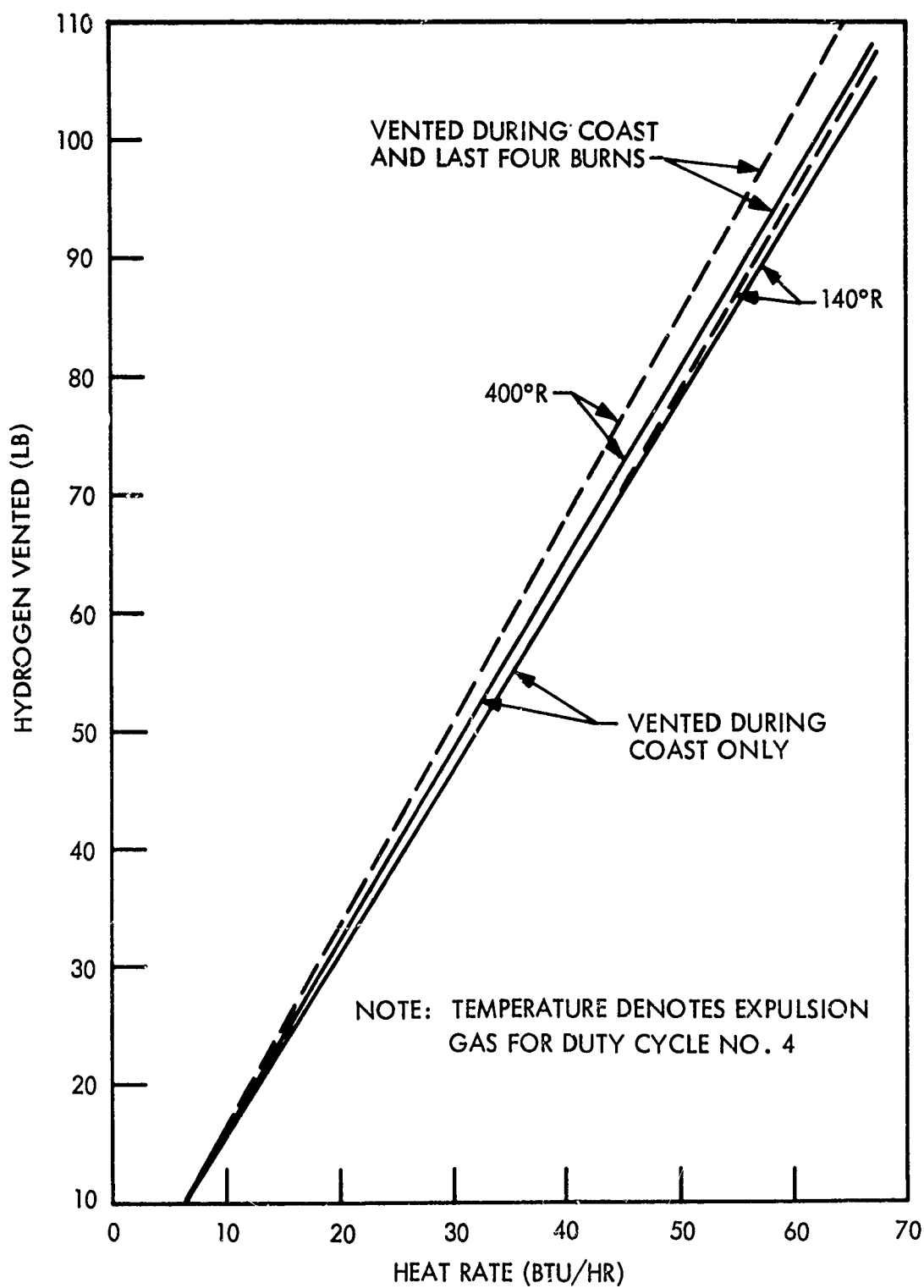


Fig. 2-27 Hydrogen Vented for 14-Day Mission as a Function of Ambient Heat Rate(C)

Residual Propellant Gases

(C) The heat rates to the LH_2 and LF_2 tanks are used again to obtain the residual propellant gases from Figs. 2-28 and 2-29. (The 154°R fluorine curve is not yet plotted.)

 ΔV Maximization

(U) The maximization of ΔV will involve iteration through the procedure shown in Fig. 2-7, establishing propellant loading and varying parameters. Time-dependent drop weights, such as boiloff, will be considered in the calculations.

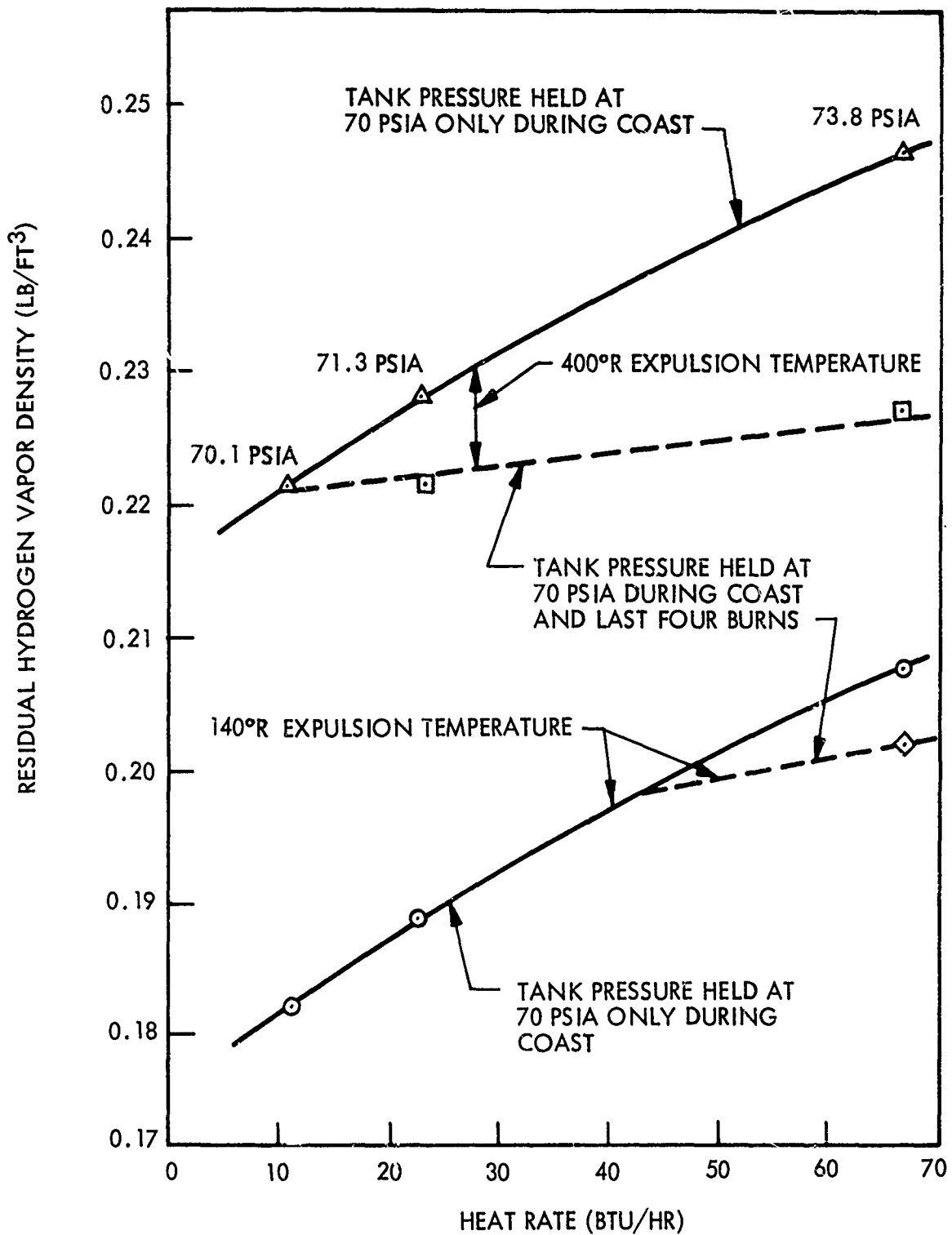


Fig. 2-28 Residual GH_2 Parametric Data, Duty Cycle No. 4 (C)

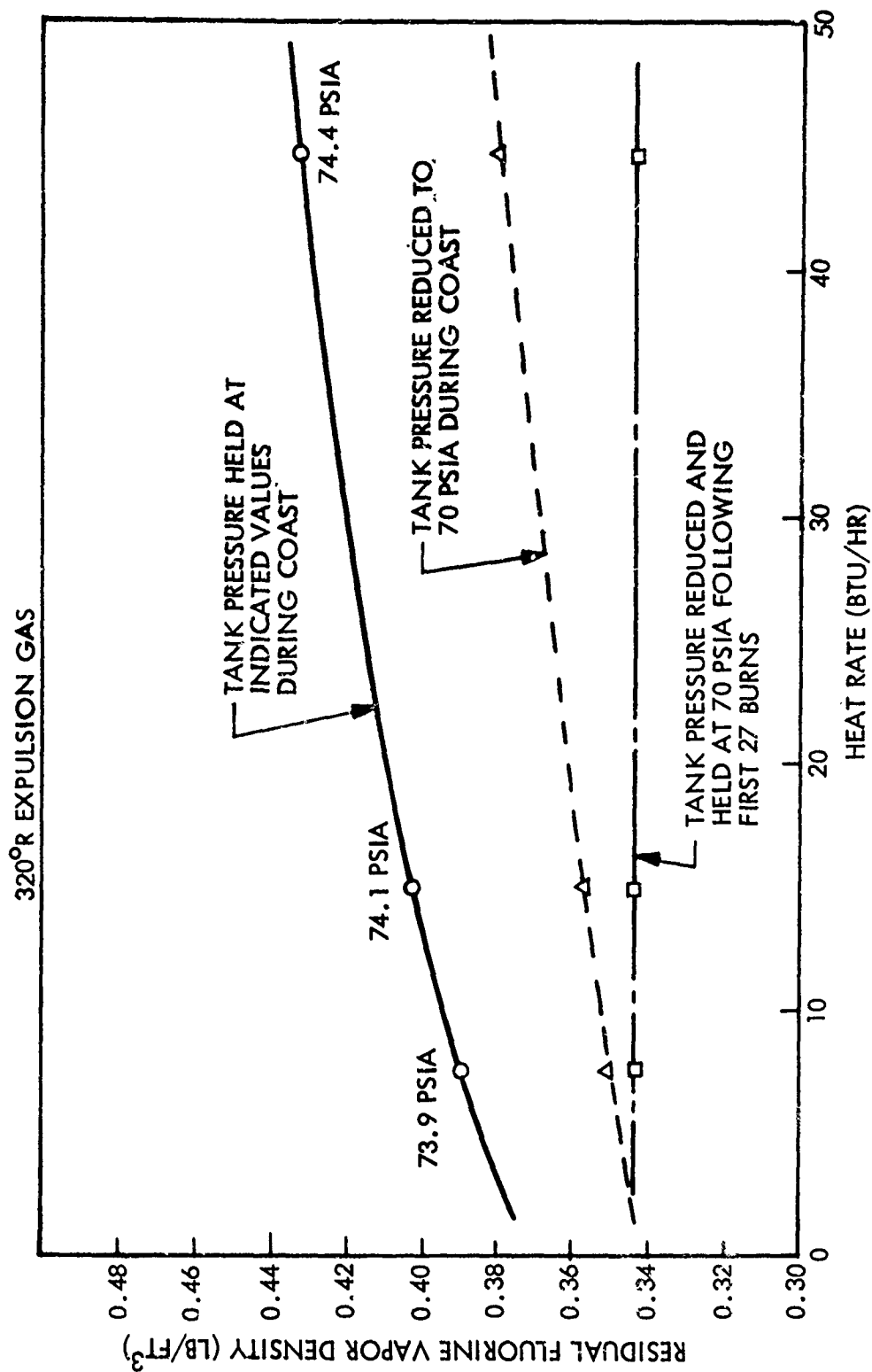


Fig. 2-29 Residual Fluorine Gas Parametric Data, Duty Cycle No. 4 (C)

SUBTASK 4 - ATTITUDE CONTROL SYSTEM INTEGRATION STUDY

(C) Work on integrating the Compound A/MHF-5 system into the AMPS vehicle was initiated in Subtask 4. The first problem is to locate the 16 thrusters on the vehicle. The deciding factors for location are controllability of the vehicle, performance efficiency, problems with plume impingement on the structure, and locally induced accelerations. The optimization study described above requires input derived from location studies of the ACS.

(U) The g-levels produced at the propellant tank sump regions are necessary for propellant orientation and sump design. To calculate these accelerations, vehicle mass properties were determined for the four typical vehicle configurations shown in Fig. 4-1. These calculations are tentative in that only preliminary design data are now available.

(C) The weight statement in the Propellant Feed System Handbook (Ref. 2) served as a baseline. Weights from this source were used for all four configurations because the weight differences between vehicles are not significant for these calculations. The centers of gravity of each subsystem were calculated as necessary. The payload mass was assumed to be uniformly distributed throughout its envelope. Based on these assumptions, the vehicle moments of inertia and CG's for the four configurations are as follows:

Configuration (See Fig. 4-1)	MOI Pitch (lb/ft ²)	Center of Gravity* Location
1	332 (10) ³	121.0
2	308 (10) ³	115.1
3	251 (10) ³	93.4
4	225 (10) ³	89.6

*Distance forward of aft end of shell in inches.

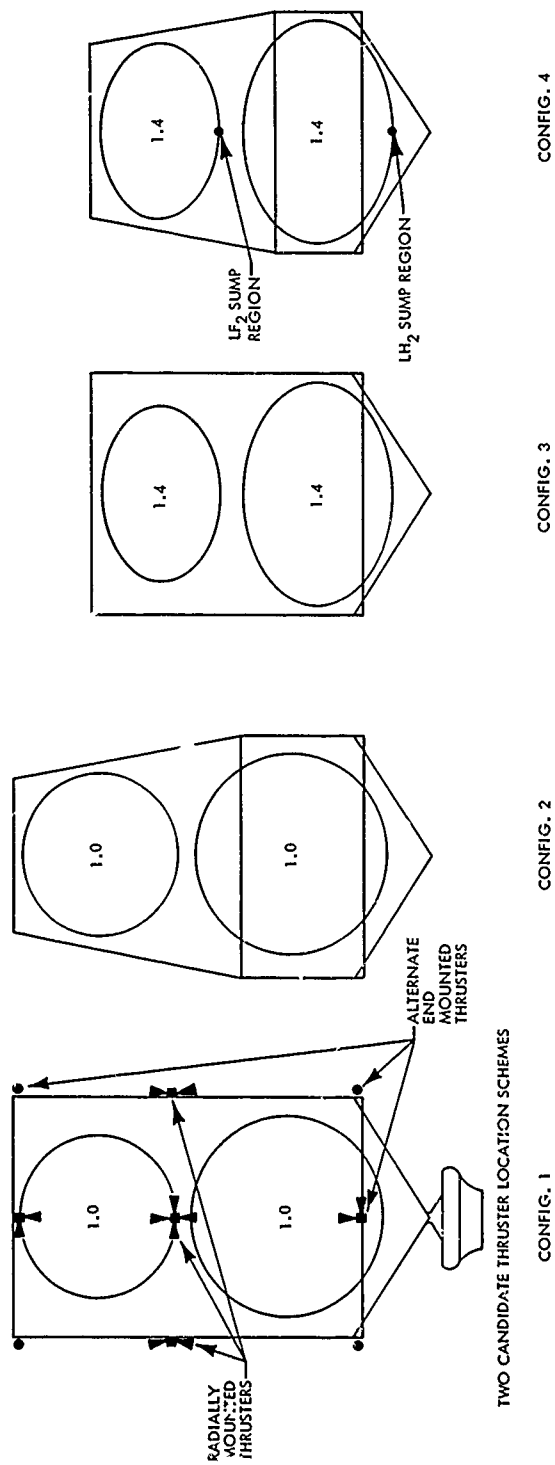


Fig. 4-1 Tank Configurations Examined in the Attitude Control Study (C)

(U) Maximum vehicle accelerations are realized near vehicle burnout and are calculated according to the relationships shown below. Both tangential and centrifugal accelerations were calculated for the empty-propellant condition:

$$a_t = \frac{RFd}{I}$$

$$a_n = \left(\frac{Fd}{I}\right)^2 R\Delta t^2$$

where

a_t = tangential acceleration

a_n = centrifugal acceleration

R = distance between vehicle center of gravity and sump

d = distance between coupled thrusters

I = moment of inertia

Δt = thruster burn time

F = thrust

(U) Coupled nozzles are employed to maintain control of the vehicle with a minimum of undesirable vehicle motion. Thrusters are fired in pairs so that a force couple is effected and so that no sideways acceleration is produced when the vehicle is rotating.

(C) Two general arrangements for locating the thrusters are being considered. One method places all of the thrusters radially on the surface of the shell on a plane normal to the longitudinal axis of the vehicle, as shown in Fig. 4-1. The other arrangement places the thrusters at the forward and aft ends of the shell. The latter concept takes advantage of larger effective moment arms and requires less propellant than the former.

(C) The resultant centrifugal acceleration levels for thrusters located on the ends of the shell are shown in Fig. 4-2. Transverse accelerations, which are independent of time, are as follows:

Configuration	Fluorine Sump Transverse g Level	Hydrogen Sump Transverse g Level
1	1.37×10^{-3}	8.1×10^{-3}
2	1.08×10^{-3}	8.4×10^{-3}
3	1.22×10^{-3}	7.0×10^{-3}
4	1.10×10^{-3}	7.5×10^{-3}

(C) The hydrogen sump g levels are much greater than the fluorine sump because the spinup arm length is greater. Both tangential and centrifugal forces are directly proportional to the distance from the center of gravity.

(C) Acceleration levels for the mid-shell-located thrusters are reduced by the effective coupled thruster moment arms. These reductions amount to 35 percent for the spherical tank configuration (1 and 2) and 16 percent for the elliptical tank configuration (3 and 4).

(C) In all cases, the direction of centrifugal acceleration is aft, and the propellants tend to remain in the sump if only centrifugal acceleration is considered.

(C) If an adverse translation of the vehicle occurs along the vehicle's longitudinal axis, the g level tending to throw liquid toward the top of the tank out of the orientation devices is approximately 7×10^{-3} g (near vehicle burnout). The orientation devices will be designed to hold the propellants against the highest g-levels experienced in any axis.

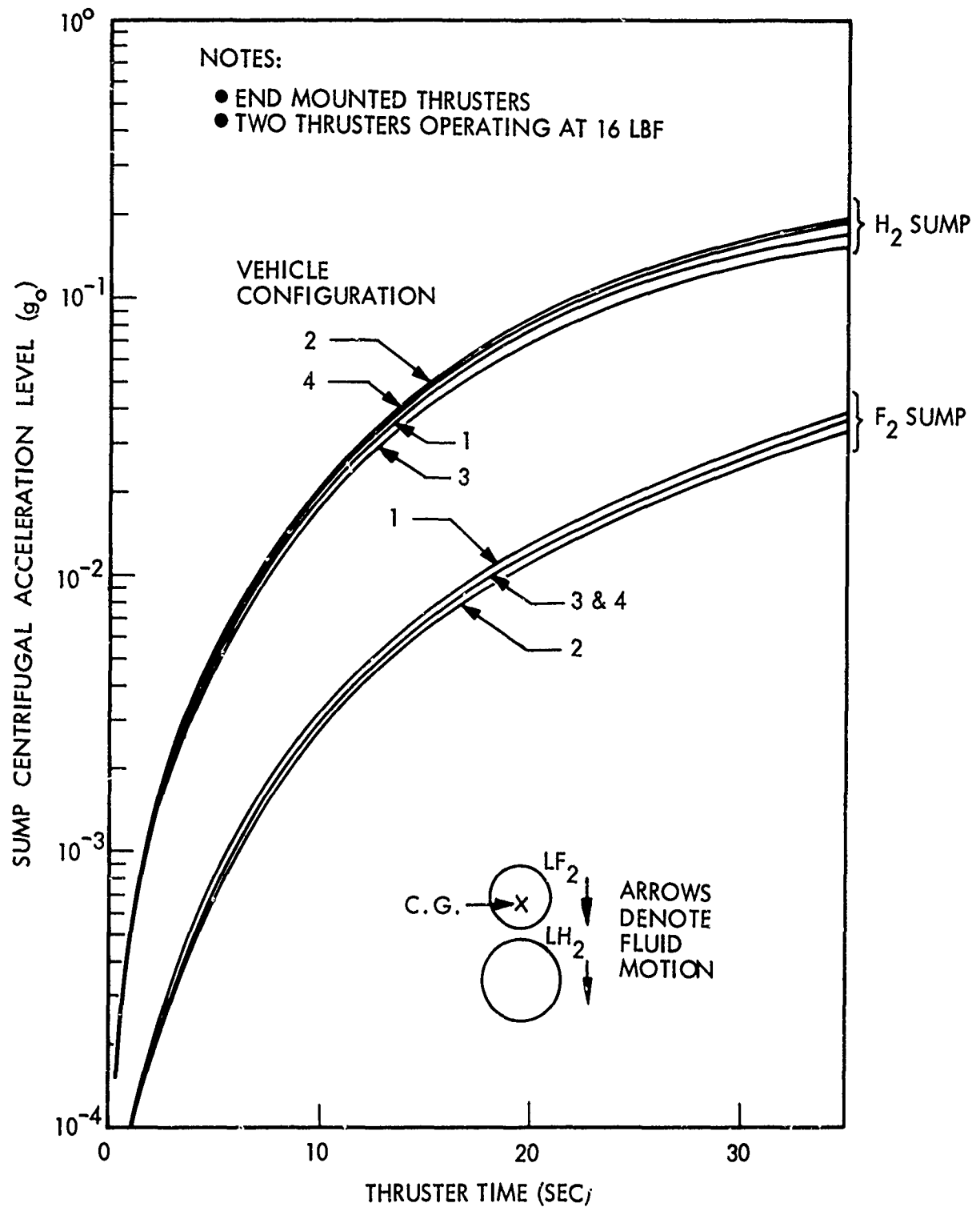


Fig. 4-2 Sump Centrifugal Acceleration Levels as a Function of ACS Thruster Burn Time (C)

SUBTASK 5 - THERMAL CONDITIONING AND SUPPORT STRUCTURE

(U) A series of screening analyses was conducted on shell structures, support structures, and insulation composites to select promising system concepts for the configuration optimization study described in Subtask 2. The results to date of these analyses are presented in the following paragraphs.

SCREENING ANALYSES OF SHELL STRUCTURES

(U) Lockheed has formulated and currently is using several computer programs for performing structural optimization analyses of numerous shell configurations subjected to axial compression and radial pressure. By selecting the appropriate computer program, it is possible to optimize the detail design and corresponding weights for each external shell considered for the AMPS vehicle and maintain consistency with realistic engineering and manufacturing constraints. Figure 5-1 shows a typical configuration and the variable design parameters that the computer analysis will optimize for the integrally stiffened configuration.

(C) A large number of shell configurations can be conceived as possible candidates; however, previous Lockheed screening studies have shown that the following configurations inherently possess the highest strength-to-weight ratio consistent with more realistic manufacturing features and cost benefits. For these reasons, the following design configurations are selected for further evaluation for the AMPS vehicle:

- Aluminum honeycomb sandwich
- Corrugated truss core, face sheets on both surfaces
- Corrugated truss core, face sheets on outside surface only
- Integrally stiffened skin, stringers on outside - rings on inside
- Integrally stiffened skin, stringers and rings on inside

CONFIDENTIAL

LOCKHEED MISSILES & SPACE COMPANY

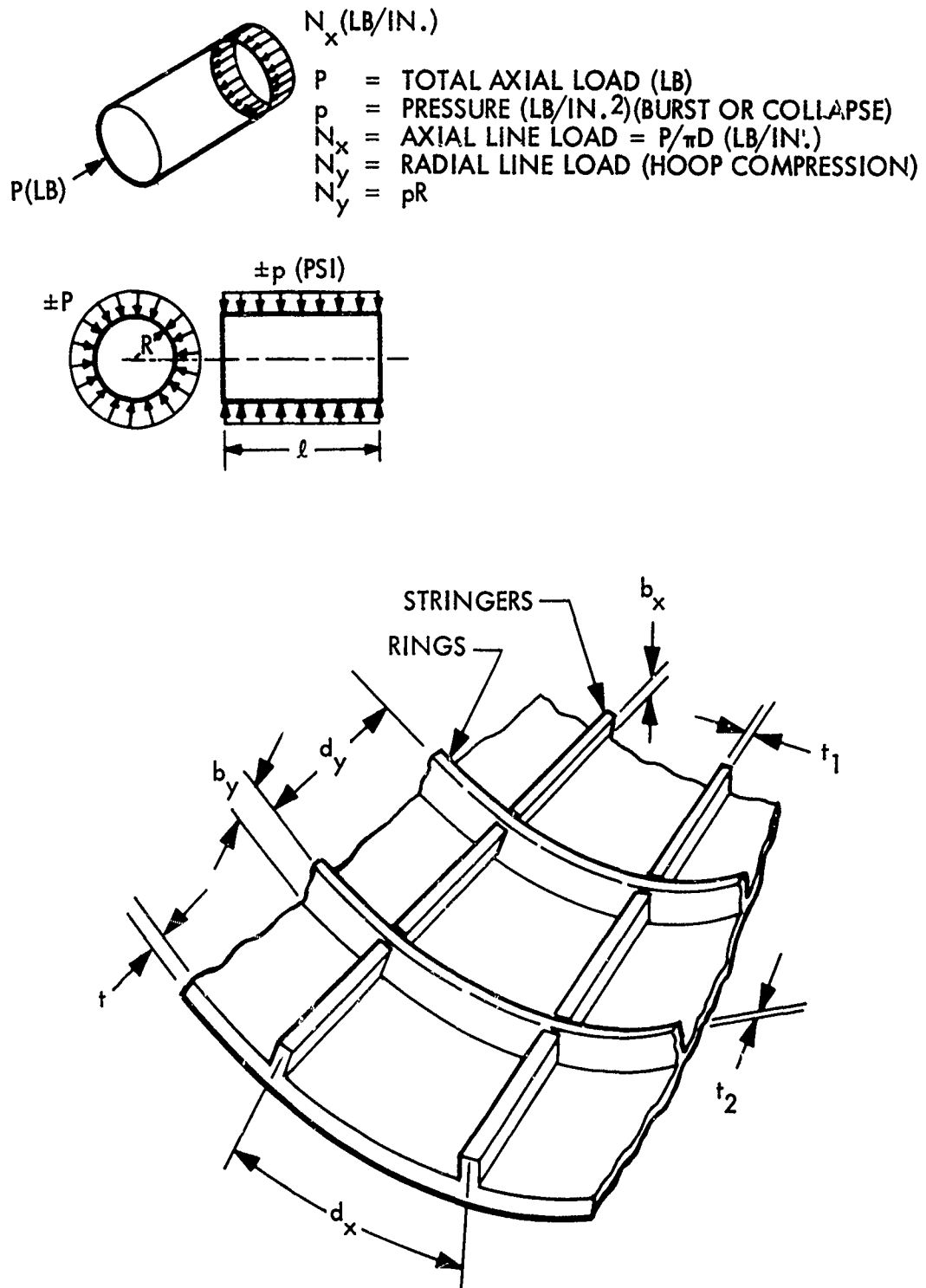


Fig. 5-1 Integrally Stiffened Cylinder Configuration (C)

(C) Aluminum is the only material considered for the honeycomb sandwich. Preliminary stress analyses have shown that the magnitude of the axial compression load will probably dictate small thicknesses of materials available only in aluminum alloys. This construction is relatively easy to fabricate, and the cost is not excessive. Test data have shown, however, that this construction is inferior to other concepts in affording meteoroid protection. The honeycomb cells restrict vaporization of the meteoroid after it strikes the external skin bumper and has been rejected in other programs (e.g., MOL). Corrugated truss core with face sheets on both sides of the corrugations exhibits good compression characteristics. Moreover, it is possible that no additional area is required for meteoroid protection for short-term missions, since the meteoroid must pass through three bumpers. This construction is difficult to fabricate because the closure sheet must be attached by welding or bonding. In addition, the corrugations in the conical section of the cones must be constructed on tapered element lines that will be difficult to manufacture and join at the edges.

(C) Corrugated truss core with face sheets on the outside surface is a compromise to the above system and presents manufacturing problems similar to the preceding truss core, except that the problems are somewhat alleviated because the inside skin is eliminated. This design offers less meteoroid protection because only two bumpers are available.

(C) Integrally stiffened skin with stringers on the outside and rings on the inside surface is a favorable candidate. With the placement of the stringers on the outside, smooth surfaces are provided on the inside shell for attachment of rings and equipment to the shell. This concept is in use on some existing spacecraft. However, it may not be possible to consider this concept for all of the optimum materials when the external skin temperature is high. In addition, optimization of the skin thickness for axial compression loads may dictate that additional protection be provided for meteoroid protection.

(C) The shell configuration utilizing an integrally stiffened skin with the stringers and rings on the inside surface is a strong candidate. Based on preliminary loads

CONFIDENTIAL

LOCKHEED MISSILES & SPACE COMPANY

analysis, it appears that the geometry of this structure is amenable to milling the rings integrally with the skin-stringer combination in a waffle pattern. The skin temperatures due to ascent heating will be lower with this concept. Moreover, the smooth external surface imposes no restrictions on the thermal-control surface selection or flight performance during launch. However, this type of construction does not offer the same degree of flexibility for installing equipment on the internal shell as the configuration with the external stringers.

(C) The materials listed in Table 5-1 have been selected on the basis of inherently possessing characteristics most compatible with the requirements for the external structural shell. Pertinent mechanical properties are tabulated for each material.

Table 5-1
CANDIDATE SHELL MATERIAL PROPERTIES (C)

CONFIDENTIAL

Material	Density (lb/in. ³)	Modulus $E_c^{(a)}$ (lb/in. ²)	Allowable $F_{cy}^{(b)}$ (lb/in. ²)
Be Sheet	0.066	42	51
Al 2014	0.10	10.5	56
Mg-Th HM21A	0.064	6.5	17
Ti 6Al-4V	0.16	16.4	132

(a) 10^6 ; (b) 10^3

CONFIDENTIAL

(C) Previous Lockheed studies of shell designs have shown that for certain configurations (variations of truss core), beryllium exhibited the lightest weight compared with the other materials listed in Table 5-1. However, this material has a number of severe fabrication limitations. First, it will be necessary to develop the rolling process at the mill for producing sheets in much larger sizes than have been fabricated to date. Maximum-size sheets are required to minimize the number of panel splices,

which tend to negate the weight benefit for this material. Rolling-mill companies feel that it is possible to increase the sheet dimensions, but the maximum size must be determined by a developmental program. Lockheed has constructed a large beryllium structural manufacturing facility, but development of large beryllium structures has not yet begun.

(U) One material, 2014 aluminum alloy, offers a comprehensive baseline for evaluating the characteristics of the other candidate materials. This material may be eliminated as a candidate if the thermal analysis shows that skin temperatures are sufficiently high to degrade the mechanical properties during ascent.

(U) Magnesium-thorium alloy could be a strong candidate material where skin temperature becomes a limiting design factor. The mechanical properties and manufacturing capabilities of this material are well established. Additionally, magnesium-thorium alloy has been successfully used for many Agena vehicle components, including the aft equipment rack and the booster adapter.

(U) Table 5-1 shows that the modulus (E_c) of titanium is second to that of beryllium, although the compression yield allowable for titanium is approximately 2.5 times higher than that of beryllium. Because of these values, it may not be possible to consider titanium for the truss core configurations. The shell line load may dictate sheet thicknesses thinner than it is possible to produce. The unit cost of titanium is higher than that of aluminum and magnesium but is less than that of beryllium.

(C) The parametric computer study for optimizing the shell configuration and defining the optimum weights is in progress. In addition to the factors previously discussed, the following constraints are being integrated into the computer inputs for the ring and stringer concept:

- Slenderness Ratio. The slenderness ratio of stringers and rings will be restricted to 15.0 from manufacturing and structural crippling considerations.

- Stringer Height. Since the stringers will likely be integral, a maximum plate thickness of 1-1/4 in. for manufacturing considerations will be used. This allows a maximum stringer height of about 1 in.
- Ring Heights. Ring spacing (optimum) will be in the range of 10 to 15 in., allowing them to be manufactured separately and mechanically attached to the shell. Accordingly, an arbitrary 1.5-in. maximum height has been assigned to the Mark IV computer code. The rings will be analyzed later using more efficient channel sections producing a further weight saving. The ring weight is expected to be between 10 and 20 percent of the total shell weight.
- Elastic Consideration. The instability shell analysis is elastic in nature, requiring cutoff stresses at or below the compressive yield stress.
- Loadings. The loadings will be derived from the axial and lateral loads, bending moments, and collapse pressures occurring during the critical phases (such as maximum $q\alpha$). During loading analyses of the shells, it was noted that the recommended transverse load factor of 1.5 g at the maximum flight bending condition ($q\alpha = 4,200$ psf-deg) resulted in inertia relief loading from the large wind-induced bending moment. Use of a transverse load factor of 1.5 g consequently results in unrealistically light shell weights. Based on Lockheed's previous experience with Titan III launch programs, a more realistic load factor is ± 0.2 g at maximum $q\alpha$. This value results in a heavier shell weight but a more realistic design. Shell loading and weight curves using both ± 0.2 g and ± 1.5 g will be presented and compared in the sixth monthly contract status report.
- Ascent Heating. Structural weight curves and tables will incorporate a K factor to allow correction for temperature effects.
- Operations. Maximum axial-load factors occur during AMPS operation. Portions of the shell may be designed to withstand this condition.
- Meteoroids. Upon completion of the optimization study (which will define the shell configuration and optimize the weights based on flight loads and criteria), it will be necessary to evaluate each configuration to determine the effects of meteoroid penetration. Additional material or separate

meteoroid bumpers may be required to comply with the meteoroid-protection criteria of 99.5-percent probability of no propellant-tank punctures in 14 days.

(U) Some initial results of these computer runs on shell structures are presented in Subtask 2.

(U) Shell temperatures and corresponding heat rates were determined for two 100-nm circular orbits with the vehicle either rotating or nonrotating with respect to its longitudinal axis.

(C) The computer model used consisted of a 120-in.-diameter cylindrical shell enclosing a 105-in.-diameter cylindrical tank covered with 1.5 in. of multilayer insulation. The shell is 2024-T4 aluminum with skin thickness equal to 0.040 in. The outer shell surface α/ϵ ratios selected were 0.3/0.95 and 0.05/0.80, corresponding to thermal paint and optical solar reflector surfaces, respectively. Maximum tolerance values for external incident energy are obtained from the Propulsion Feed Systems Handbook (Ref. 2). The tank was assumed to have a 40° R cold wall covered with 1.5 in. of multilayer insulation having a thermal conductivity of $k = 2.6 \times 10^{-5}$ Btu/hr-ft-° R. The analogous electrical network consists of 12 shell nodes, 12 insulation nodes, 1 sink node, and 4 source nodes representing the direct solar, Earth-reflected, Earth-emitted, and aerodynamic incident fluxes.

(C) Figure 5-2 shows the shell temperature profiles for the case where the vehicle is horizontal with respect to the Earth's surface. The resulting heat rates are seen to be highest for the case of vehicle rotation for both α/ϵ ratios. Orienting the vehicle nose toward Earth results in higher average shell temperatures, as shown in Fig. 5-3. For this orbit, the highest heat rates are for the vehicle roll condition (as in the previous case). It is therefore concluded that the orbital condition shown in Fig. 5-3 results in the highest heat input to the propellant tanks. It is also concluded that the condition of vehicle rotation results in a higher heat input to the tanks than the condition of a nonrotational vehicle.

CONFIDENTIAL

LOCKHEED MISSILES & SPACE COMPANY

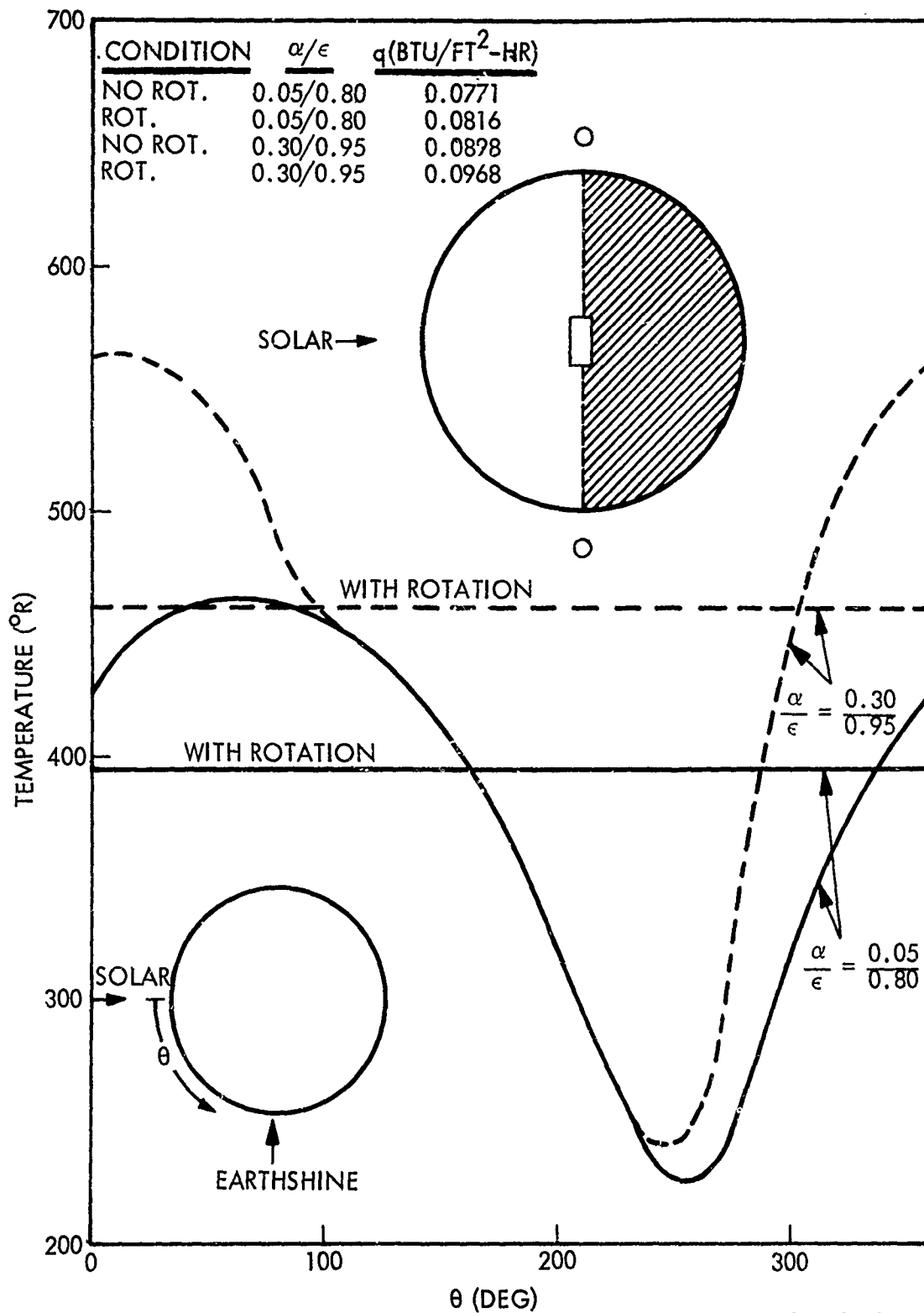


Fig. 5-2 Maximum Shell Temperatures and Heat Fluxes with Vehicle Axis Tangent to the Earth's Surface

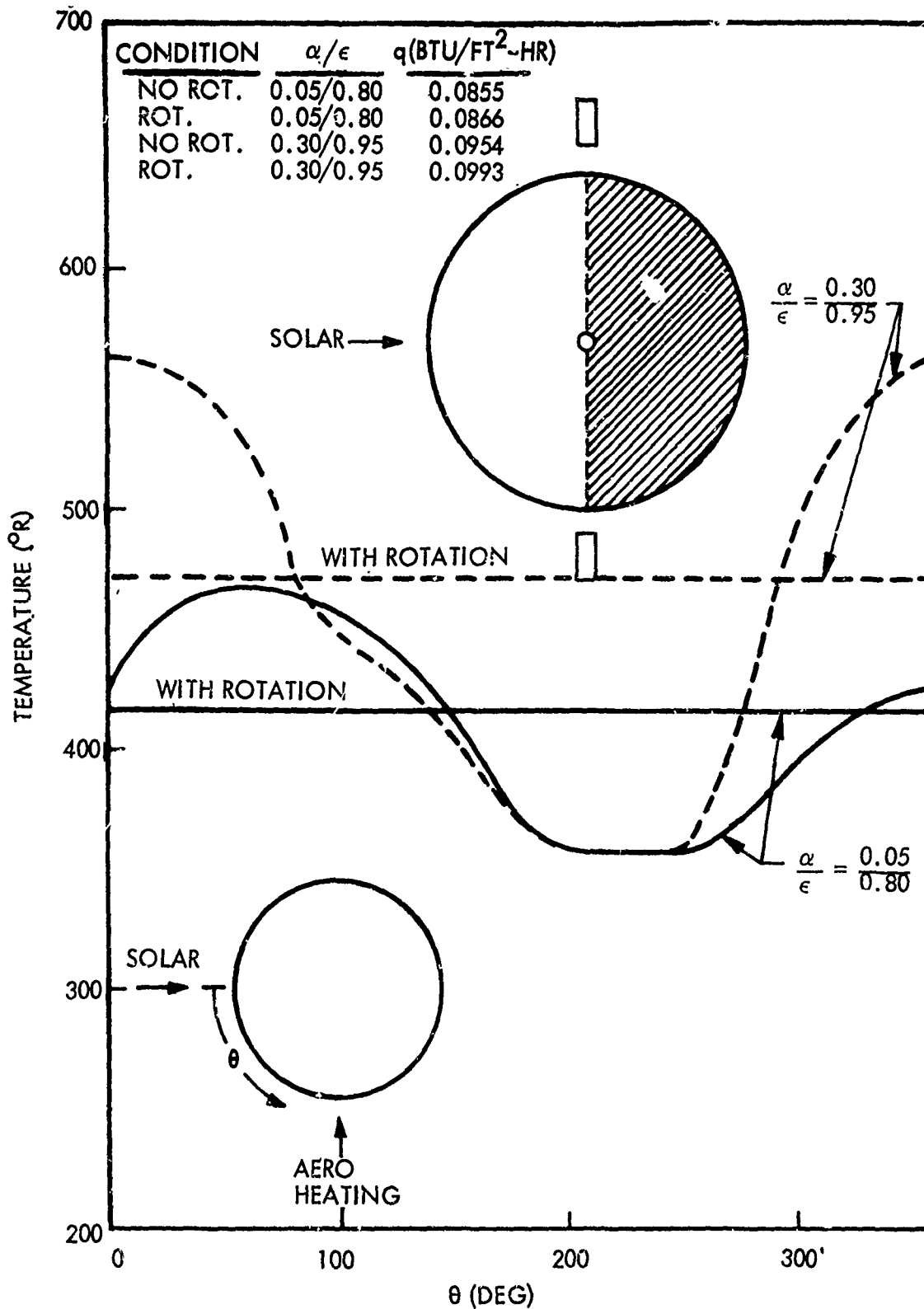


Fig. 5-3 Maximum Shell Temperatures and Heat Fluxes with Vehicle Axis Normal to the Earth's Surface

SCREENING ANALYSES OF TANK SUPPORT SYSTEMS

(U) The design and selection of a structural support system is dictated by considerations of mission duration, vehicle size, and mission environment, as well as mechanical and operational complexity. Lockheed is currently under contract to NASA (LeRC) to evaluate cryogenic tank support systems for a range of tank sizes and mission durations that include those of interest to the AMPS. During the performance of this contract, the following design concepts were originated and evaluated:

- Continuous Supports (Cones)

- Mechanically uncoupling cone
- Pyrotechnically detached cone
- Thermal-barrier tension cone
- Fiberglass cone
- Vapor-cooled titanium cone

- Multiple Point Supports (Struts)

- Torque-tube strut
- Ball and clamp support strut
- Retracting wedge strut
- Titanium strut with stacked washers thermal barrier
- Filament-wound fiberglass strut
- Subliming solid-cooled strut
- Vapor-cooled titanium strut

(U) The most promising of these concepts are examined here for their applicability to the AMPS vehicle.

(C) Although the propellants considered in the NASA study were liquid hydrogen and liquid methane, the results obtained can be adapted to the LF_2 tankage. The results of the analyses of these concepts show that the filament-wound fiberglass strut and cooled titanium struts are the most efficient concepts for LH_2 tankage, as shown in

Fig. 5-4. The titanium strut with stacked washers and the cooled titanium strut are most efficient for LF_2 tankage, as shown in Fig. 5-5. The results are presented in terms of normalized effective weight versus mission time as a means of ranking the most promising systems. The effective weight of a particular concept is defined as the sum of the support structure weight and the boiloff weight. (For the fluorine tank, the boiloff weight consists of sufficient GH_2 to cool the tank and maintain the pressure constant.) The lowest weight system as a function of mission duration was assigned a value of one for comparing with other support system candidates. The normalized effective weight is the ratio of a system effective weight to the lowest weight system at the mission duration considered. For the LH_2 tank, a crossover occurred at 75 days between the fiberglass strut and the cooled titanium strut - the fiberglass strut being the lightest weight system up to 75 days. The cooled titanium strut remained the lightest weight system for the LF_2 tank for all mission durations, although the titanium strut with stacked washers was only slightly heavier.

(C) Note in Fig. 5-5 that the normalized effective weight of the fiberglass struts for the LF_2 tank is higher than both the titanium struts plus stacked washers and cooled titanium strut. This condition is due to the higher inertial loads associated with the LF_2 tank at vehicle rebound, which introduces compression loads in the struts. Since the modulus of elasticity for fiberglass is approximately three times less than that of titanium, the fiberglass tube diameter-to-wall thickness is appreciably increased, resulting in a greater cross-sectional area and consequent increased structure and equivalent boiloff weights. For compression supports, the titanium strut is even more favorable than fiberglass.

(C) On the basis of these rankings, plus considerable hardware experience with these types of support systems, the filament-wound fiberglass strut appears optimum for the LH_2 tank; the titanium strut with stacked washers appears to be a good choice for the fluorine tank when operational and weight considerations are evaluated. The titanium strut plus stacked washers is 10 percent heavier for a 14-day mission than the cooled titanium strut, but the added complications of cooling are not felt to be worthwhile to pick up the additional 2 lb in weight. The optimum washer stack height for the LF_2 tank is 0.25 in. for the 14-day mission.

CONFIDENTIAL

LOCKHEED MISSILES & SPACE COMPANY

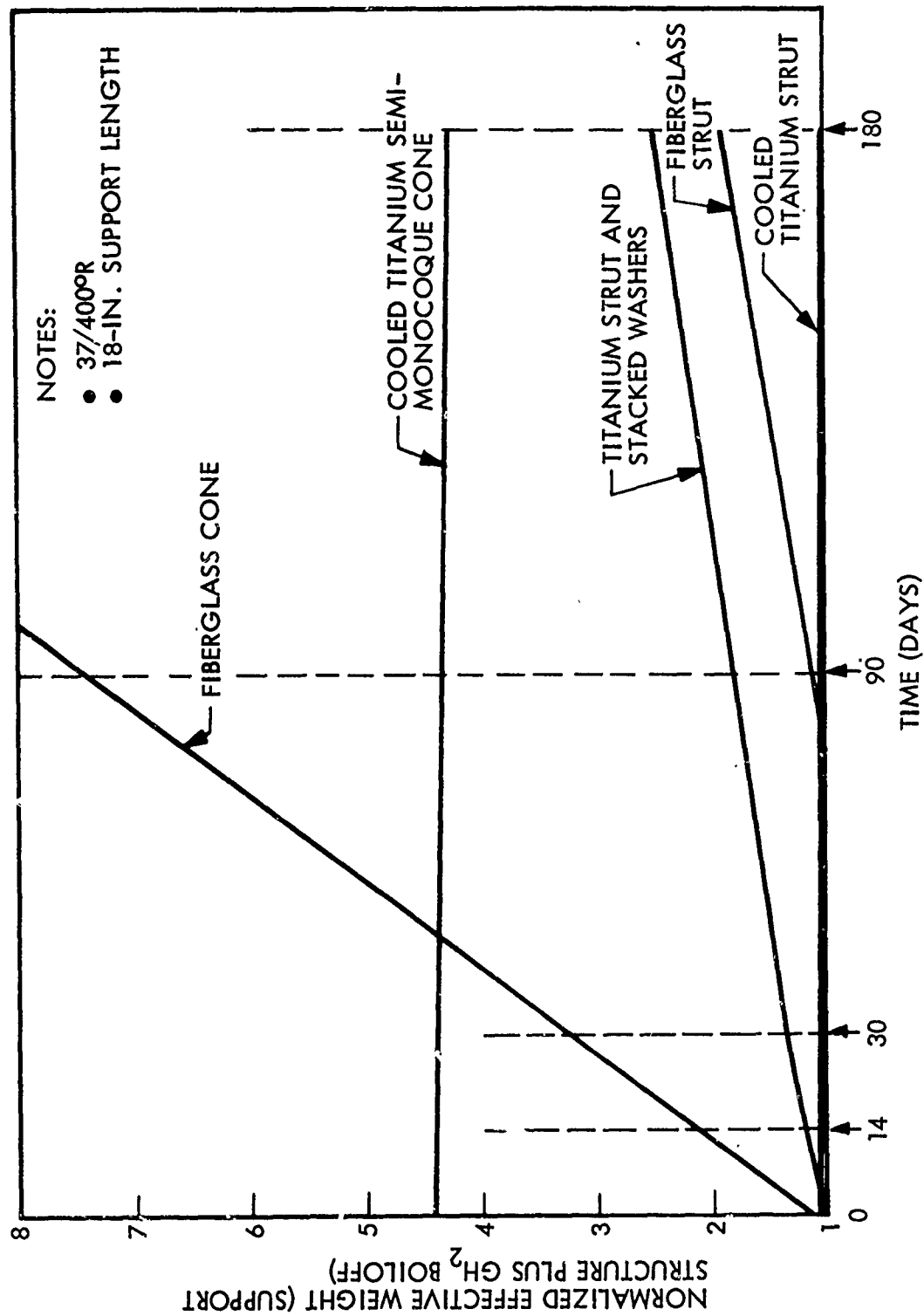


Fig. 5-4 Ranking of LH₂ Tank Support Systems (C)

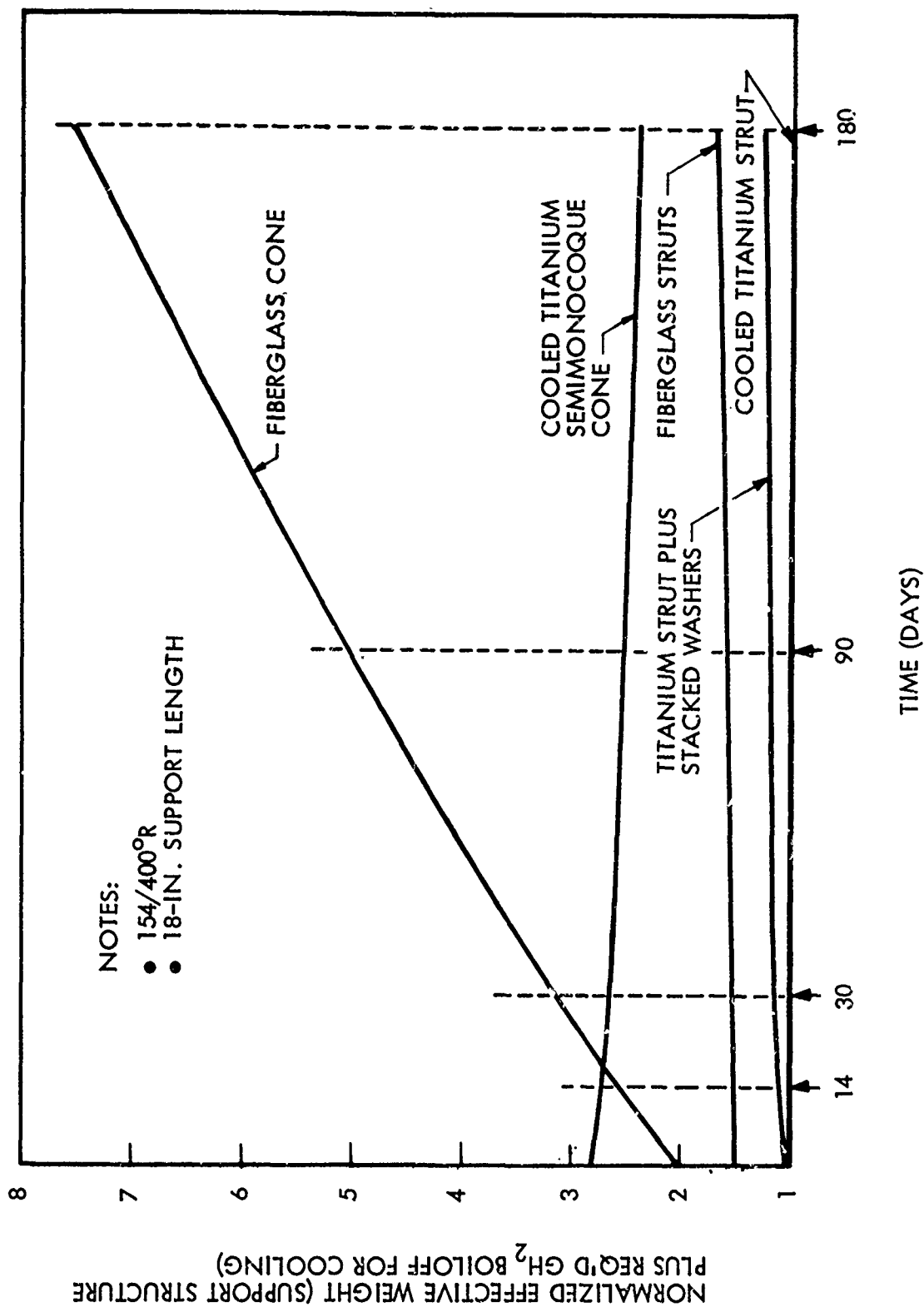


Fig. 5-5 Ranking of LF₂ Tank Support Systems (C)

SCREENING ANALYSES OF INSULATION COMPOSITES

(U) A study was made to evaluate and provide a relative ranking of the four most promising multilayer insulations for use on the AMPS vehicle. The multilayer insulations studied include:

- Superfloc
- NRC-2
- Flat Double-Aluminized Mylar Tissuglas
- Crinkled Double-Aluminized Mylar Tissuglas

(U) The selection of these insulations over others, such as composites of Dimplar, foam spacers, silk netting, etc., is based on results of analytical and test screening evaluations conducted by Lockheed under Contract NAS 8-20758, "Investigations Regarding Development of a High-Performance Insulation System," and under inhouse insulation development programs. The above four concepts emerged from these evaluations as being superior to all others.

(U) The effective conductivity for each insulation concept tested was measured as a function of insulation layer density at insulation boundary temperatures of 140/540° R, and for some concepts at 140/460° R, and 140/630° R. A new analysis technique developed by Lockheed that correlates well with the referenced test data is used to extend these data to the insulation boundary temperatures of interest for the AMPS vehicle, namely, 40/400° R (LH₂ tank) and 153/400° R (LF₂ tank) when the insulation is tank mounted. It is noted that the outer boundary temperature of 400° R used for both tanks was taken as an average shell temperature for the purpose of obtaining a relative ranking of these insulations. Later in this section, where design conductivity data are derived, more refined shell temperatures are employed.

(U) The measured effective thermal conductivities for each insulation are shown in Fig. 5-6. The lowest thermal conductivity measured is that for flat aluminized Mylar/Tissuglas, whereas the highest is for superfloc. The equations that describe the thermal conductivity of each insulation are contained in the Propulsion Feed Systems Handbook.

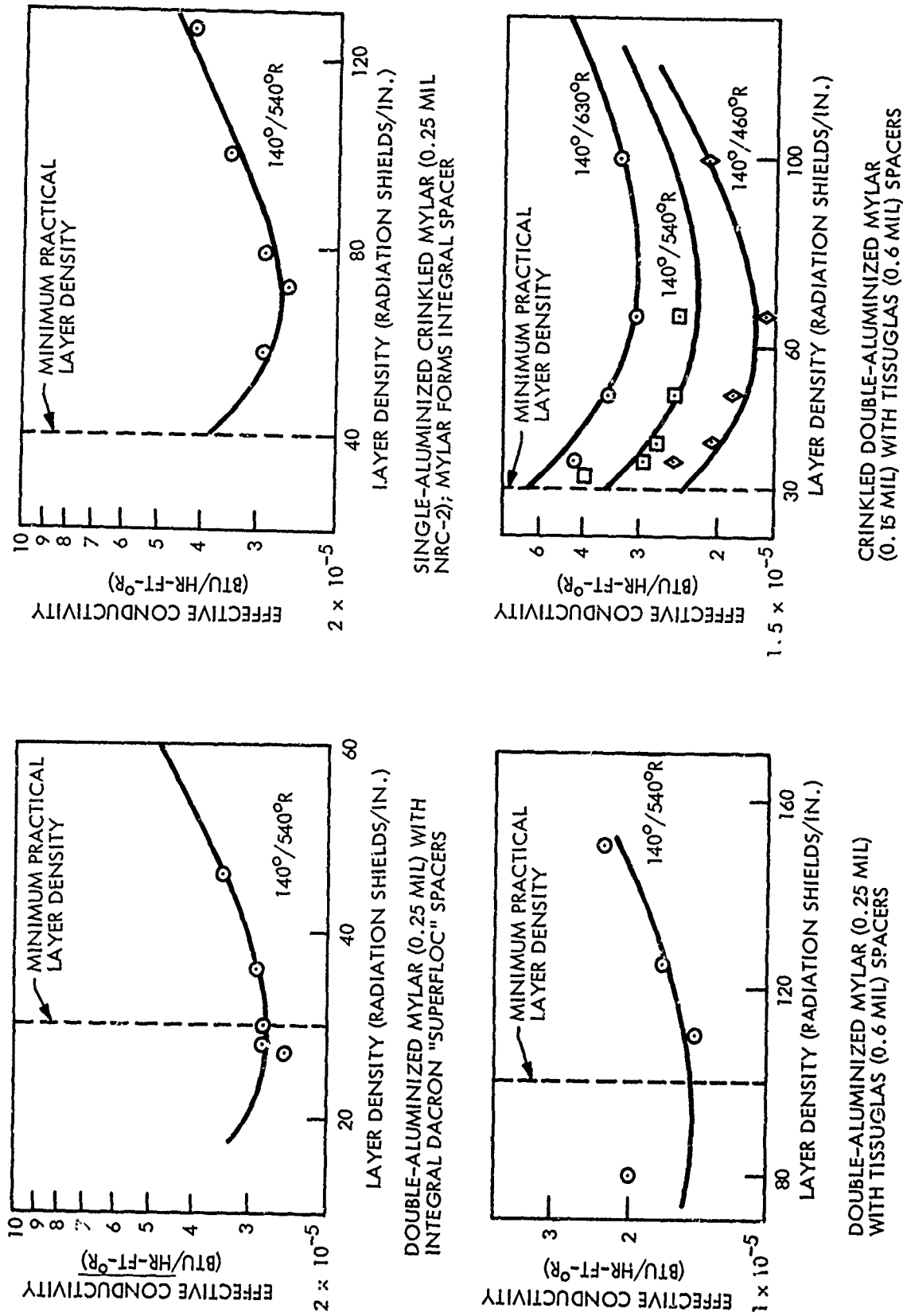


Fig. 5-6 Measured Conductivities of Promising Multilayer Composites

(U) The minimum layer densities at which the composites can be installed on a tank are shown in Table 5-2.

Table 5-2

MINIMUM PRACTICAL LAYER DENSITY

Insulation	Minimum Practical Layer Density (Layers/in.)
Superfloc	30
NRC-2	40
Flat Mylar/ Tissuglas	100
Crinkled Mylar/ Tissuglas	30

(U) The thermal rankings of each of these insulations at or above the minimum practical layer density for the minimum value of conductivity for the insulation material are indicated in Table 5-3.

(U) On the basis of these rankings, superfloc provides approximately twice the heat flow to each cryogen - compared with flat Mylar/Tissuglas - for the same thickness.

(C) A characteristic of an efficient insulation is a low value of the product of density (ρ) times conductivity (k). This characteristic for each insulation is shown in Fig. 5-7 for the LH_2 and LF_2 tanks.

(U) The relative ranking of the insulations is shown in Table 5-4. On the basis of these rankings, NRC-2 is three times more efficient than flat Mylar/Tissuglas.

(C) As shown in Fig. 5-6 the effective thermal conductivity of each insulation is a function of its layer density. Control of the layer density to the design value (minimum practical layer density) is dependent upon (1) the manner in which the insulation is

Table 5-3

RELATIVE RANKING OF INSULATION ON THE
BASIS OF EFFECTIVE CONDUCTIVITY (C)
CONFIDENTIAL

Insulation	Relative Ranking ^(a)	
	LH ₂ Tank	LF ₂ Tank
Flat Mylar/ Tissuglas	1	1
Crinkled Mylar/ Tissuglas	1.2	1.03
NRC-2	1.3	1.35
Superfloc	1.9	2

(a) Lowest is 1.

CONFIDENTIAL

Table 5-4

RELATIVE RANKING OF INSULATION ON THE
BASIS OF ρk PRODUCT (C)
CONFIDENTIAL

Insulation	Relative Ranking ^(a)	
	LH ₂ Tank	LF ₂ Tank
NRC-2	1	1
Crinkled Mylar/ Tissuglas	1.5	1.3
Superfloc	1.6	1.6
Flat Mylar/ Tissuglas	2.9	2.9

(a) Best insulation is lowest ranked.

CONFIDENTIAL

designed and installed on the tank and (2) the physical and thermal properties of the insulation. It is possible for the insulation to be compressed (increased in layer density) during installation and under g-loadings encountered in flight. A worst case

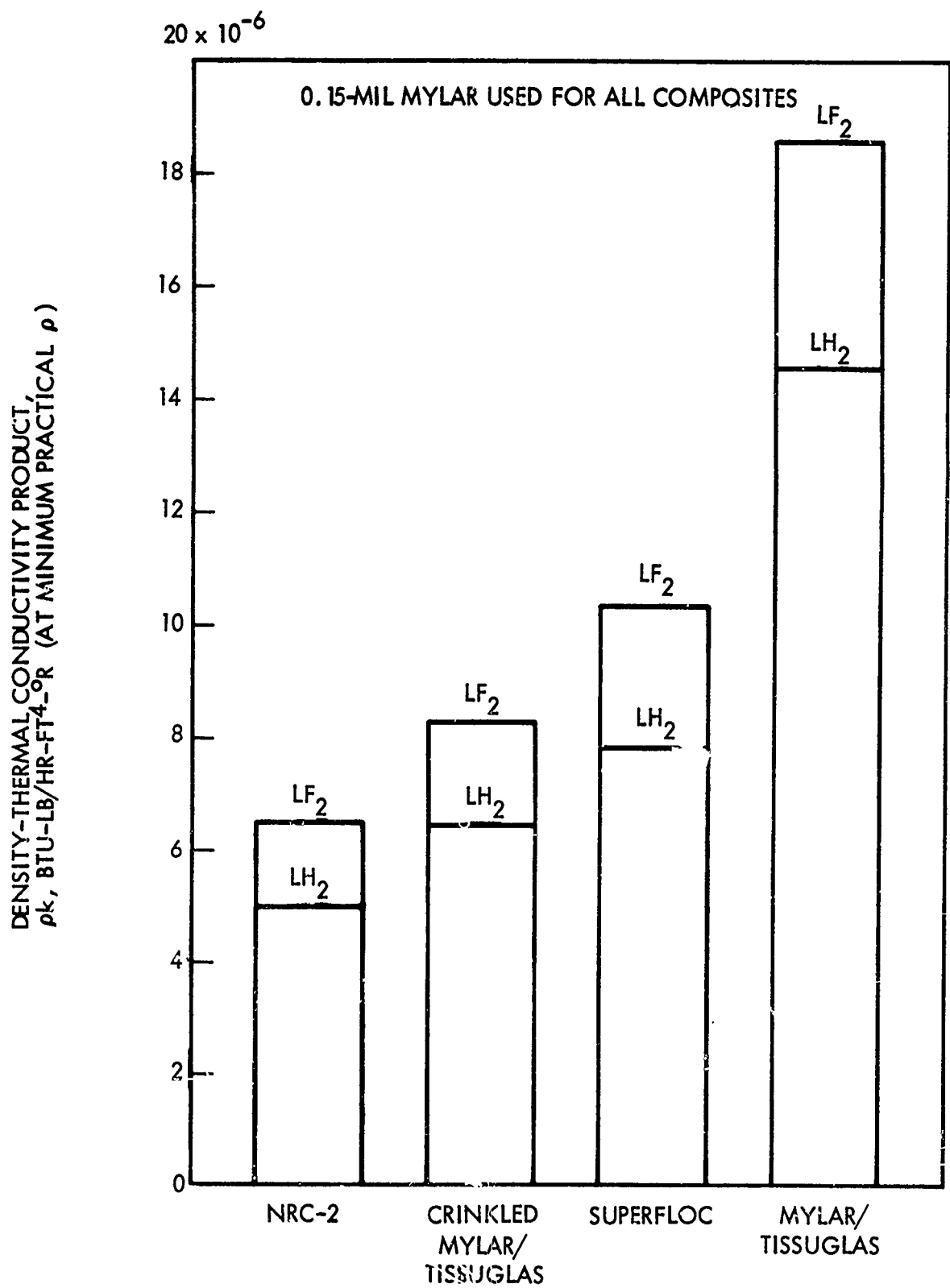


Fig. 5-7 Density-Thermal Conductivity Ranking of Insulation Composites (C)

condition has been considered to provide a ranking of each insulation on the basis of its change in heat rate after experiencing a 6.2-g acceleration load. This acceleration could be experienced near vehicle burnout.

(C) Insulation on the top domes of each tank tends to be compressed, whereas insulation on the bottom domes tends to be expanded. The worst case condition is where the insulation is compressed and where this compression is permanent. (Actual tests on insulations compressed under accelerations up to 20 g show that the insulations return to their original uncompressed k value when the g-load is removed. This ranking is based on the hypothetical assumption that the composites remain compressed.) Figures 5-8 and 5-9 show the effect of compressive load on the insulations for each tank. Taking the weight (converted to pressure load) of each insulation under the 6.2-g loading, accounting for the effect of layer density change under load and using the experimental data of Figs. 5-8 and 5-9, one obtains the insulation rankings shown in Table 5-5.

Table 5-5

RELATIVE RANKINGS OF INSULATION ON THE BASIS OF
HEAT FLOW WITH 6.2-g COMPRESSIVE LOAD (C)

CONFIDENTIAL

Insulation	Relative Rankings ^(a)	
	LH ₂ Tank	LF ₂ Tank
Flat Mylar/ Tissuglas	1	1
Crinkled Mylar/ Tissuglas	1.2	1.1
NRC-2	1.25	1.2
Superfloc	2	2.1

(a) Best insulation is lowest ranked. CONFIDENTIAL

On the basis of this ranking, flat Mylar/Tissuglas is least sensitive thermally to layer density changes.

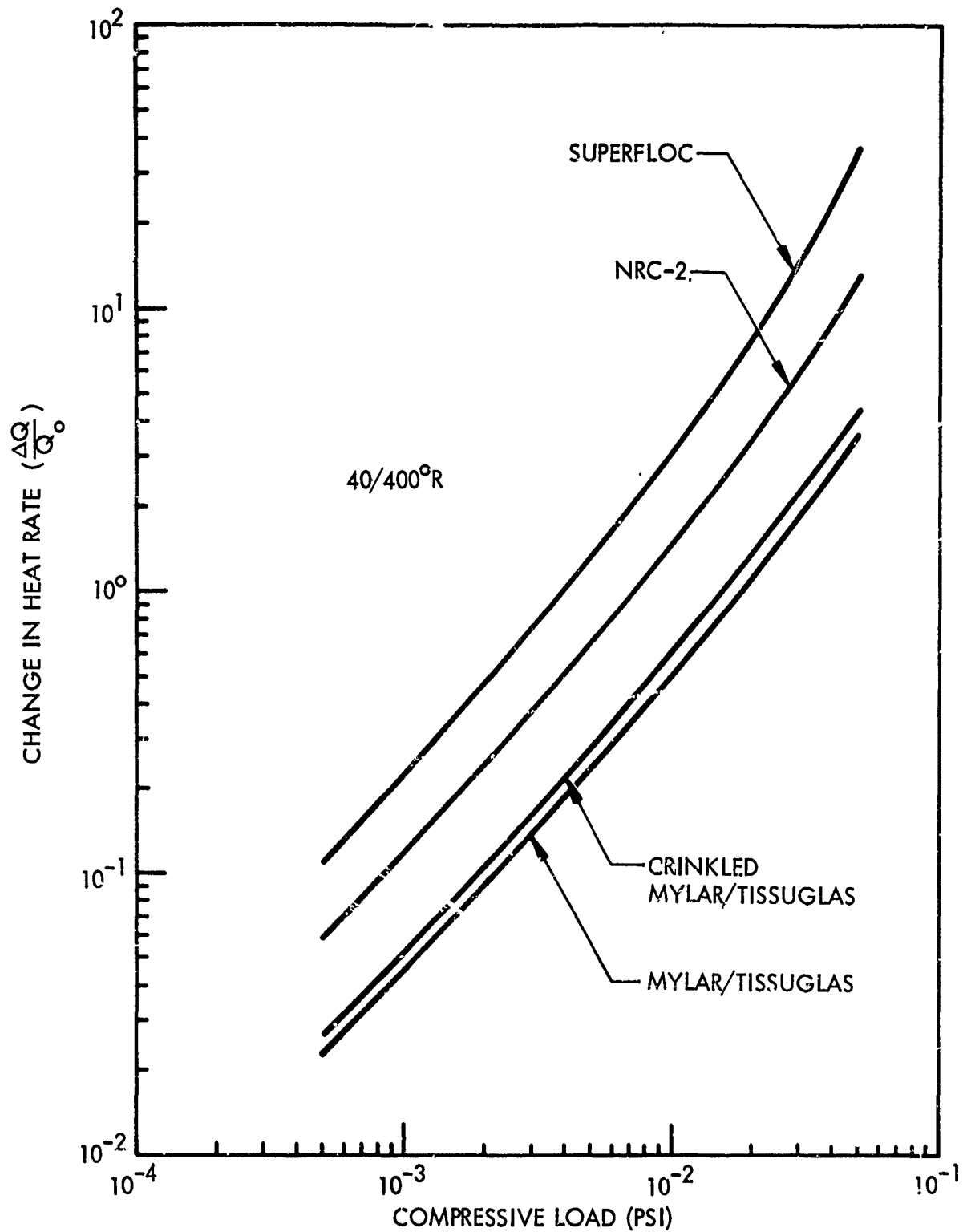


Fig. 5-8 Effect of Compressive Load on Insulation Heat Rates for the LH₂ Tank (C)

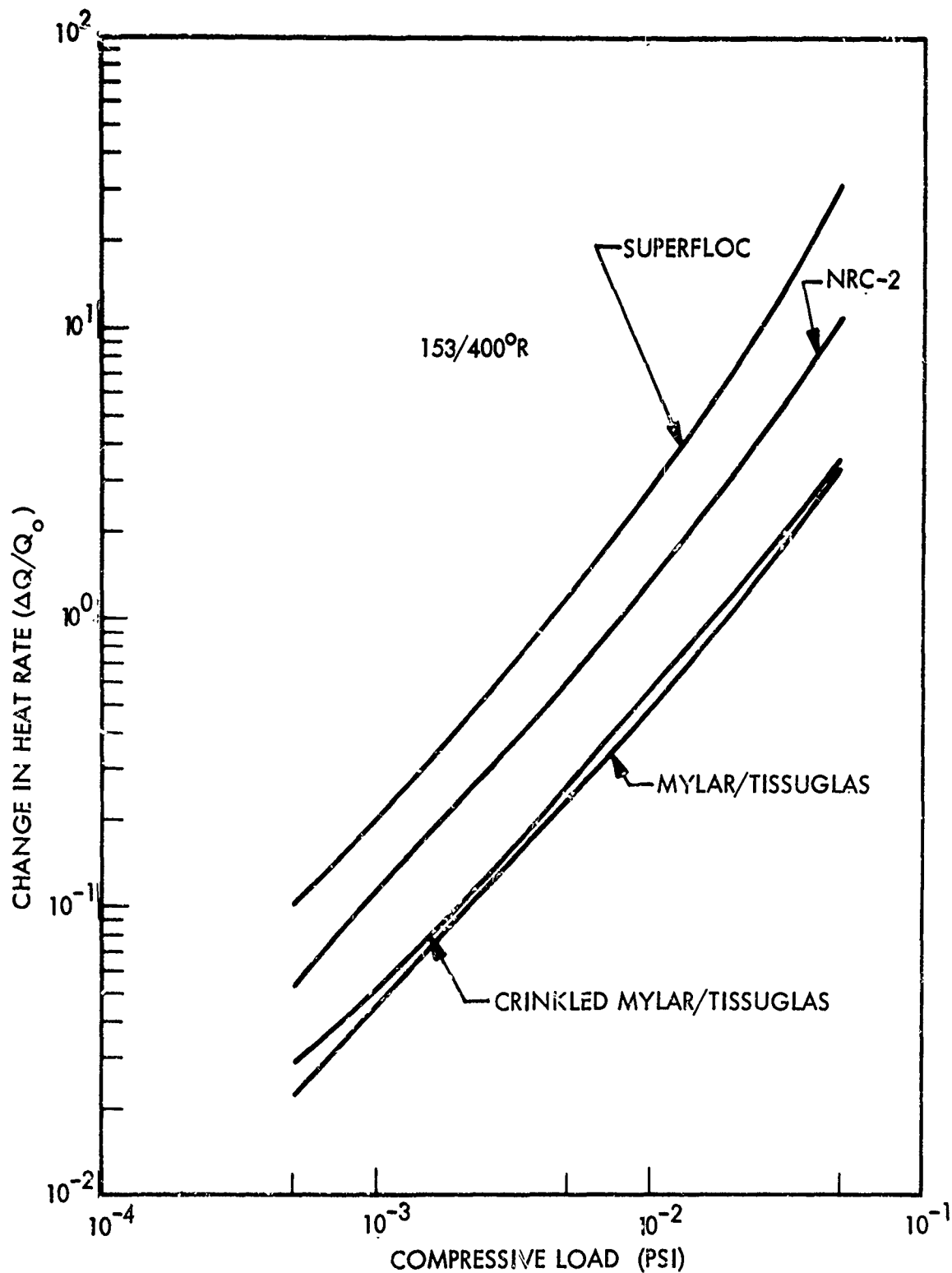


Fig. 5-9 Effect of Compressive Load on Insulation Heat Rates for the LF_2 Tank (C)

(U) The last ranking is a composite evaluation of compression effect and thermal effectiveness per unit weight

$$\rho k \left(\frac{Q_0 + \Delta Q}{Q_0} \right)$$

where Q_0 is the heat flux before compression, and ΔQ is the change during compression (assumed permanent). This composite evaluation is probably the best measure of overall performance to be expected for the insulations. Table 5-6 shows this ranking.

Table 5-6

RELATIVE RANKING OF INSULATION BASED ON
COMPOSITE CHARACTERISTICS $\rho k [(Q_0 + \Delta Q)/Q_0]$ (C)

CONFIDENTIAL

Insulation	Relative Ranking	
	LH ₂ Tank	LF ₂ Tank
NRC-2	1	1
Crinkled Mylar/ Tissuglas	1.2	1.1
Superfloc	2	1.9
Flat Mylar/ Tissuglas	3.2	3.2

CONFIDENTIAL

On the basis of the composite ranking and on previous rankings, NRC-2 and crinkled Mylar/Tissuglas will be further evaluated in the configuration optimization study.

THERMAL DESIGN DATA FOR CONFIGURATION SELECTION PARAMETRIC STUDIES

(U) The flat-plate calorimeter data, applied in conjunction with the new Lockheed analysis technique, provided a relative ranking of the four insulations, which, in turn, permitted selection of the two best candidates. Use of these two candidates, NRC-2 and crinkled aluminized-Mylar/Tissuglas, will be further studied in the configuration optimization study.

(U) To properly apply these insulations in the optimization study, conductivity data used must account for the manner in which these insulations perform after installation on the propellant tanks. The manner in which the design conductivity data were obtained for the two candidate insulations is described in subsequent paragraphs.

(U) Multilayer insulation installed on compound curvature surfaces, such as propellant tankage, can be compressed locally. This compression degrades the insulation's thermal performance over that obtained on flat-plate calorimeters. Consequently, a new approach has been adopted to estimate the as-installed condition of insulation candidates for purposes of the optimization study.

(U) This approach is based on using thermal performance data of as-installed insulation systems on large scale cryogenic tanks and correlating these data with the flat-plate test results. The thermal performance data on double-aluminized Mylar/Tissuglas insulation were derived from the Lockheed 110-in.-diameter LH₂ tank tests. (These data will be substantiated by Lockheed experience on applying crinkled aluminized-Mylar/Tissuglas on the Lockheed slush hydrogen dewar.) These two tankage systems reflect practical data derived from as-installed insulation concepts. The NRC-2 data from the flat-plate calorimeter are correlated with as-installed NRC-2 on a Lockheed 60-in.-diameter tank test. Thus, the two prime candidate insulations that appear to be best, on the basis of analytical and flat-plate calorimeter data, also have been applied to larger, practical tank configurations. These data will be injected into the optimization analysis.

(C) An effective compressive force that takes into account the degradation of the as-installed insulation performance compared with the relatively more idealized flat-plate calorimeter data is calculated. Conductivity at the as-installed layer density is used in the optimization study. These results are shown in Table 5-7 for both the LH₂ and LF₂ tanks at the maximum outer boundary temperature defined previously for the outer shell.

CONFIDENTIAL

LOCKHEED MISSILES & SPACE COMPANY

Table 5-7

AS-INSTALLED TANK INSULATION
THERMAL PERFORMANCE (C)

CONFIDENTIAL

On-Tank Insulation	As-Installed Thermal Conductivity (Btu/hr-ft-° R)	
	LH ₂ (472 to 37° R)	LF ₂ (472 to 153° R)
NRC-2	2.66×10^{-5}	3.28×10^{-5}
Crinkled Mylar/ Tissuglas	1.88×10^{-5}	2.25×10^{-5}

CONFIDENTIAL

(U) These values of thermal conductivity were used to provide heat-input parametric data for the configuration optimization analyses in Subtasks 2 and 3.

CONFIDENTIAL

TABLE 9

CALCULATED VALUES FOR MAIN ENGINE LH₂ INDUCER AND IMPELLER

Parameter	Inducer	Impeller
Inlet Tip Diameter, inches	2.1	2.1
Inlet Hub Diameter, inches	0.63	1.5
Inlet Tip Blade Angle, degrees	7.0	11.1
Discharge Tip Diameter, inches	2.1	4.1
Discharge Hub Diameter, inches	1.5	4.1
Discharge Blade Angle, degrees	12.0	40
Number of Blades	3	20
Head Coefficient	0.10	0.609
Flow Coefficient	0.0704 (inlet)	0.098 (discharge)
Discharge Tip Blade Velocity, ft/sec	687	1342
Discharge Tip Fluid Whirl Velocity, ft/sec	114	1018
Discharge Tip Fluid Axial Velocity, ft/sec	112.3	131.4
Euler Head, feet	2440	40,000

98
CONFIDENTIAL

SUBTASK 6 - PROPELLANT ORIENTATION

(U) Work was started on selection of suitable propellant orientation devices. Initially, surface-tension devices have been being examined for both tanks. Subsequently, this type of component will be compared with a dielectrophoretic device. The approach being used to examine the surface-tension device is described in the following paragraphs.

(C) Use of a partial-orientation passive retention system with LH_2 imposes the requirement that the trapped propellant remain subcooled to prevent boilout of the retention-system volume. To conserve helium pressurant, it is further required that only LH_2 be admitted to the thermal conditioning system throttling unit. Thus, there exists an additional requirement for a liquid collection and feed system to support the demands for thermal conditioning, as well as for engine restart. The operational characteristics of the engine-restart system (ERS) and the thermal conditioning feed system (TCFS) are sufficiently dissimilar to recommend the employment of entirely separate feed and retention systems. Following is a discussion of the considerations associated with each design.

(U) Since the vehicle system will operate in a high-g environment, a partial-retention system should be employed for the ERS as opposed to a system that attempts to control the entire propellant mass. The approach with partial propellant control is to retain sufficient propellant at the tank outlet to assure engine start, prevent the entrance of pressurant gas into the engine feedlines, and settle the bulk of the propellant mass to support the engine flow demand. This implies a retention-system volumetric requirement which, since the system is passive, must be determined using the most stringent combination of vehicle operating conditions that can be anticipated in the prescribed missions.

CONFIDENTIAL

LOCKHEED MISSILES & SPACE COMPANY

(U) A number of considerations impose constraints on the design of the ERS. Each of these must be analyzed to determine the effect it has on proper operation of the restart system. These operational considerations are listed as follows:

- Pullthrough
- Character of propellant settling
- Retention system refill
- False start
- Penultimate shutdown condition
- Capillary stability to environmental accelerations

(C) Preliminary estimates have been made of the quantities of LH_2 and LF_2 that must be trapped by the orientation system for restart. These values, shown in Figs. 6-1 and 6-2, include the following items:

- Propellant Settling. The retention system must contain sufficient liquid to supply the engine while propellant is settled over the drain.
- Fill Drain Lines. The hydrogen line boils out between burns, whereas the fluorine line is kept full. Provision is made to fill the hydrogen line for a given burn plus two false starts.
- Zero-G Start Transient. When the signal to open the fuel valves is given, the time required to fill downstream cavities and lines and to satisfy engine cooling requirements calls for a considerable demand on the retention-system volume. This flow takes place at zero-g or small adverse accelerations; careful sump design is required to prevent suckthrough of pressurant gas.
- Pullthrough Prevention. Pressurant can be drawn into the engine under thrusting conditions. A minimum pullthrough level must be provided for in the retention system during the start transient. This mass of propellant is greater than the maximum residuals for the system weight penalty.
- Two False Starts. Two consecutive demands on the hydrogen-retention device, but not the fluorine device, have been postulated. Further analysis of this requirement will be made to determine its applicability to the vehicle mode of operation.

CONFIDENTIAL

LOCKHEED MISSILES & SPACE COMPANY

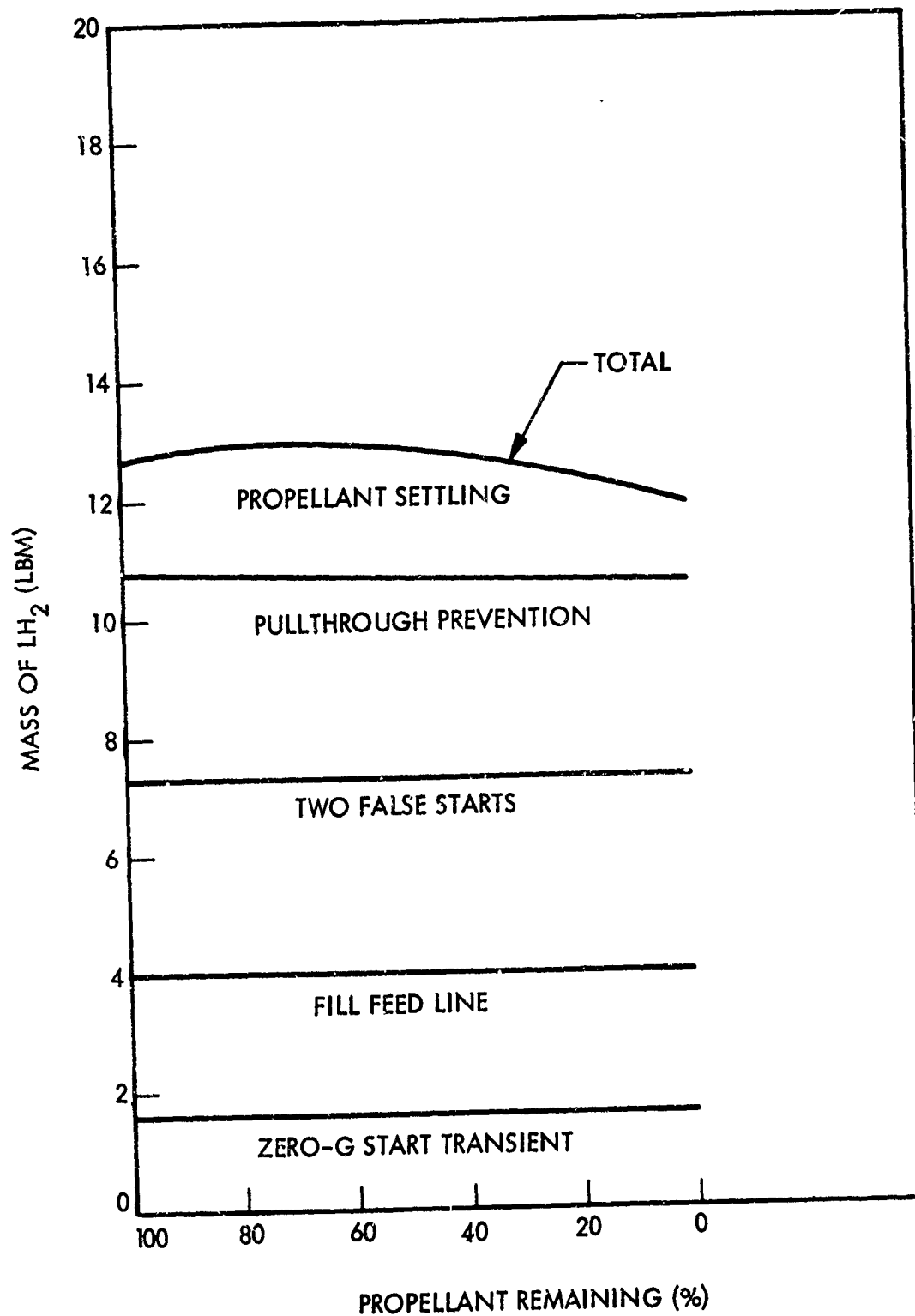


Fig. 6-1 Preliminary Estimate of LH₂ Propellants to be Trapped by the Orientation System for Restart (C)

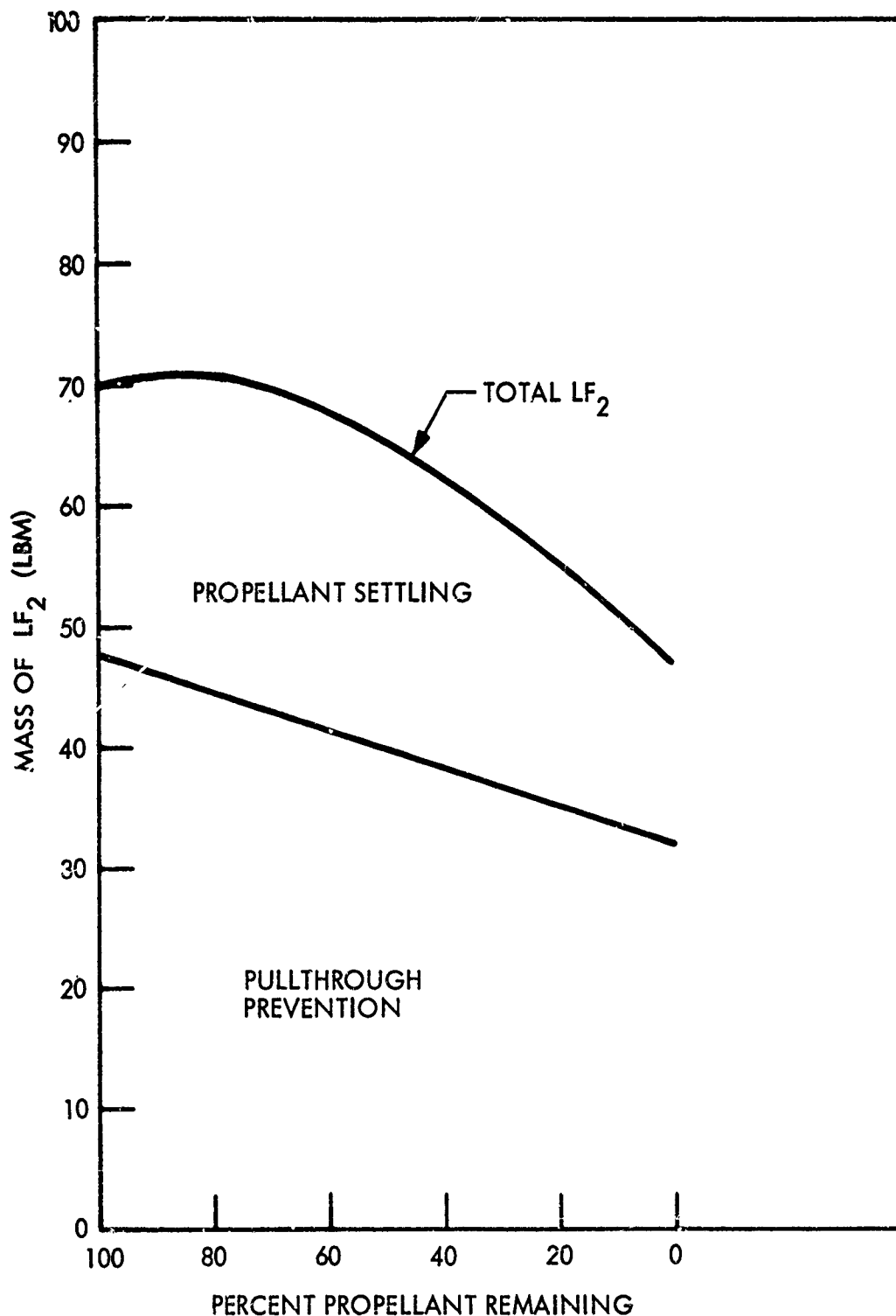


Fig. 6-2 Preliminary Estimate of LF_2 Propellants to be Trapped by the Orientation System for Restart (C)

CONFIDENTIAL

LOCKHEED MISSILES & SPACE COMPANY

- Total LH_2 . This curve represents the sum of the various fuel masses needed for restart. The maximum value of 13 lb occurs with approximately 70 percent of the propellant remaining. The curve does not provide for GH_2 venting demands — a separate supply is used for that purpose.
- Total LF_2 . This curve is the sum of the pullthrough-prevention and propellant-settling curves. A maximum results, as in the LH_2 case, because of the settling-time dependence on settling distance and g level, both of which depend, in turn, on the propellant mass remaining in the tanks. This maximum value, 71 lb, occurs with 86 percent of the propellant remaining.

() Once the above considerations have fixed the gross dimensions and shape of the ERS, it becomes a relatively simple matter to select a screen mesh capable of providing capillary support to some level of vehicle environmental acceleration during engine nonoperational periods.

(C) The operational requirements of a propellant feed system for the tank pressure control unit dictate a different design than that for the ERS. Propellant is withdrawn on a demand basis as dictated by the tank pressure. This withdrawal is at a very low flow rate (approximately 1.4 lb/hr during operation), but the integrated amount (approximately 33 lb), is large compared with that required for any one engine restart sequence. The feed system operates in the low-gravity nonpropulsive periods where the propellant orientation must be considered as random. The above considerations seem to indicate a feed-system design distributed throughout the tank. However, the feed system also must be capable of operation following the high-g periods of main engine operation, which would upset any capillary support capability of the system and necessitate refill following main-engine shutdown. This argues strongly for a separate retention system similar to that of the ERS, with sufficient volumetric capability to support the most extended period of tank pressure control operation. This system could be located near the tank outlet, which can be refilled by engine thrust.

CONFIDENTIAL

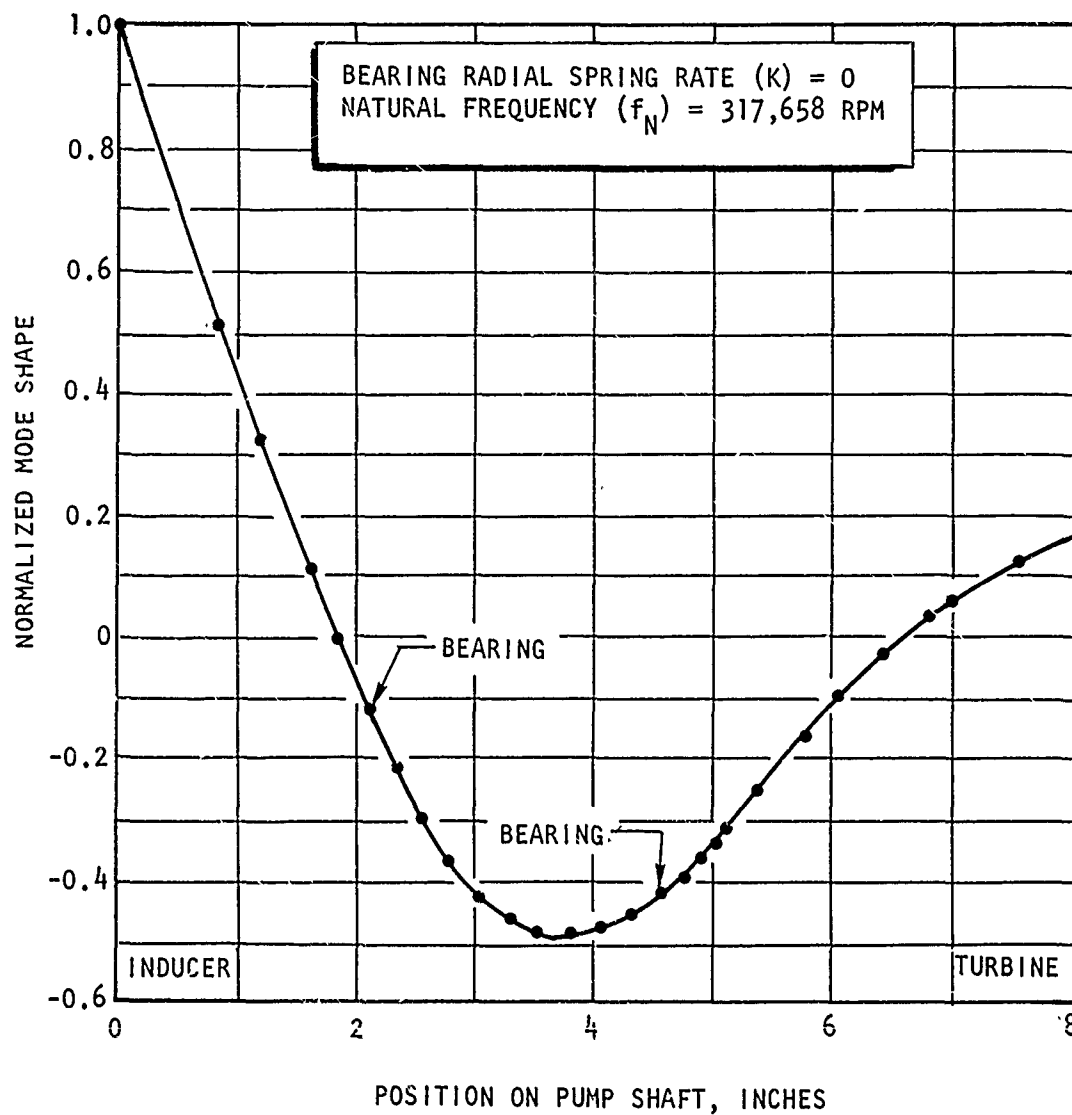


Figure 46. Main Engine Oxidizer Turbopump Shaft Shape for "Free-Free" Mode

CONFIDENTIAL

SUBTASK 7 - PROPELLANT MANAGEMENT SYSTEM

(U) This subtask will begin in July.

CONFIDENTIAL

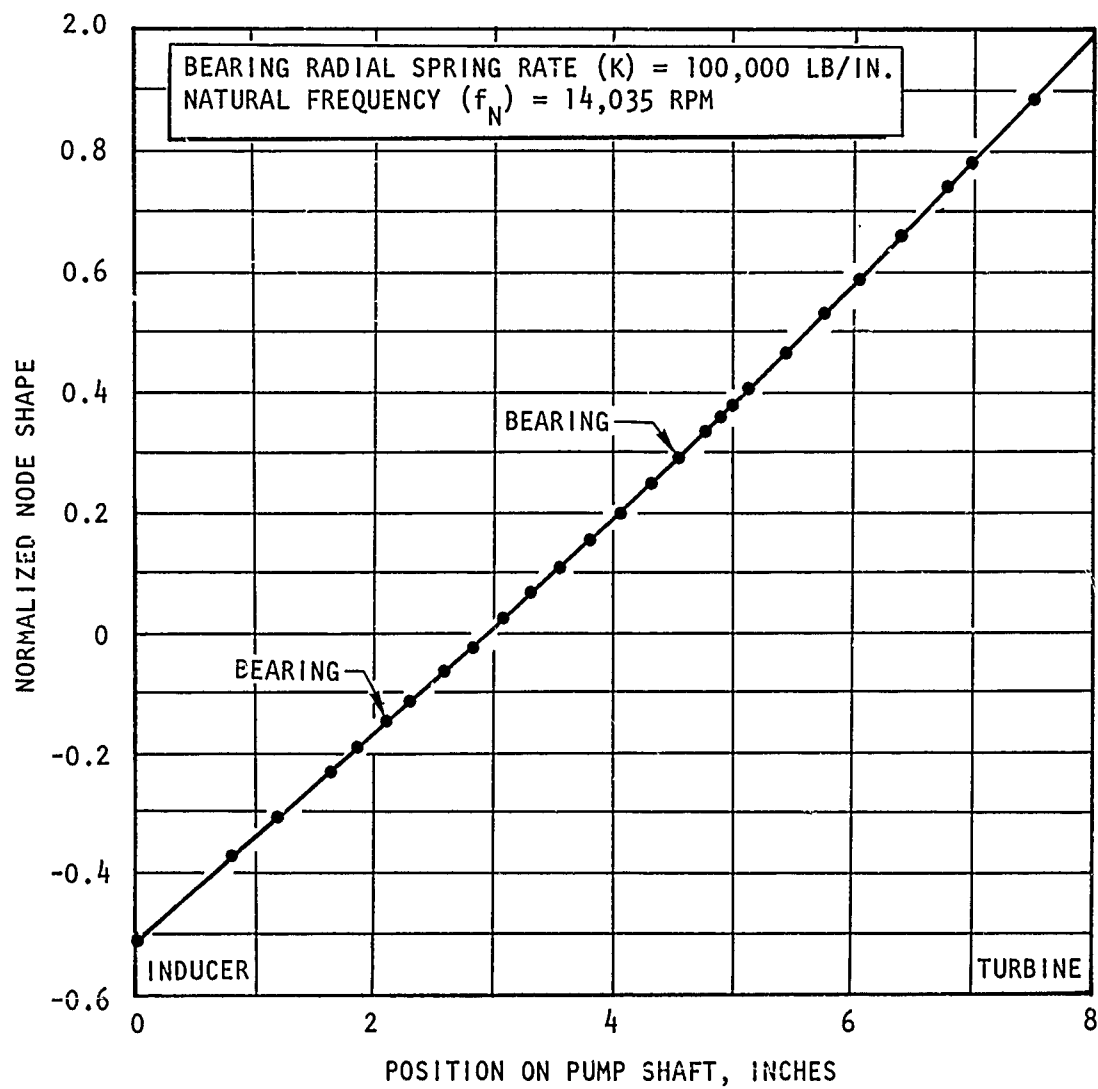


Figure 47. Main Engine Oxidizer Turbopump Shaft Shape for Turbine-End Bearing "Stick" Mode (100,000 lb/in. spring rate)

CONFIDENTIAL

SUBTASK 8 - PRESSURIZATION SYSTEM

(U) Work on screening candidate pressurization systems was initiated early in the study to allow selection of a primary concept for the tank configuration parametric studies. Multiple pressurization system concepts are possible for the AMPS vehicle. To keep the independent variables in the subsequent tank and load carrying shell parametric optimization studies to a workable number, it is necessary to evaluate and select a primary concept early in the evaluation.

(C) Subsequent to this concept selection, certain key influencing data must be derived on the selected system. These data, important to the tank design and configuration evaluations, are as follows:

- Pressurization system weight as a function of GHe weight
- LH₂ tank weight increment due to in-tank helium-bottle displacement of LH₂

(U) Additional parametric tank and outer vehicle shell studies that are impacted by the pressurization system analysis are as follows:

- Evaluation of the vented and nonvented tank modes of operation
- Evaluation of maximum pressurant expulsion temperatures that affect the selected tank material strength allowables
- Evaluation of residual gas weights as a function of pressurant expulsion temperatures

(U) These data related to the pressurization system, plus other influencing data developed in Subtasks 2, 3, and 5, permit optimization of the propellant tanks and outer load-carrying shell of the AMPS vehicle. Therefore, these parametric data are transferred for use into Subtasks 2, 3, and 5.

(U) During this quarter, the candidate screening analysis was completed and a primary pressurization system concept was selected for the tanks/shell optimization studies.

(U) Subtask 8 subsequently will be completed by performing a design of the selected pressurization concept and by integrating it into the final vehicle optimization in Subtask 10.

SCREENING ANALYSES

(U) Screening analyses of the candidate pressurization systems are complete. The analytical approach used is summarized below.

(U) First, a number of candidate pressurization systems for the AMPS vehicle was selected. Influencing factors in this initial selection were the required NPSP, simplicity and reliability, requirement for instant readiness for engine start, effect of pressurization system on other subsystems, and light weight. The 13 initial candidates are listed in Table 8-1. System schematics and hardware weight tables were prepared on these candidates.

(U) Parametric weight data on propellant tanks and helium pressurant bottles were then calculated.

(U) Finally, tank pressure histories and overall weight penalties were calculated for each pressurization system for both vented and nonvented tanks and the four duty cycles listed in Table 8-2.

(C) Table 8-3 is a list of assumptions or input data used in the pressurization system analyses. A vented system refers to a vented LH_2 tank and a nonvented LF_2 tank cooled by GH_2 boiloff, while a nonvented system refers to a nonvented LH_2 tank and a nonvented LF_2 tank.

Table 8-1
PRESSURIZATION SYSTEMS INVESTIGATED (C)

Pressurization System	LH ₂ Tank			LF ₂ Tank		
	Prepressurant		Expulsion	Prepressurant		Expulsion
	Gas	Temp. (°R)		Gas	Temp. (°R)	
1	He	37	37	He	154	154
2	→	400	400	He	154	154
2a		37	140	He	154	154
2b		37	140	He	154	320
3		400	400	He	154	154
3a	→	37	400	He	154	154
3b		37	140	He	154	154
3c		37	140	He	154	320
3d		37	400	He	154	320
4	H ₂	400	400	He	154	154
4a	H ₂	400	400	He	154	154
5	H ₂	400	400	GF ₂	400	400
Tridyne	He	500	1000 to 1500	Tri-dyne	500	500

Table 8-2

DUTY CYCLES^(a) (C)

1. Single burn to propellant depletion on first day after achieving orbit
2. Single burn to propellant depletion at end of 14th day in orbit
3. Two-burn 90/10 mission:^(b)
 - One burn first day using 90 percent of propellant
 - One burn 14th day using remaining 10 percent of propellant
4. Thirty-one burn 90/10 mission:^(b)
 - Twenty-seven equal burns, uniformly spaced on the first day
 - Four equal burns, uniformly spaced on the 14th day

(a) Expulsion rates may vary from maximum to minimum for any of the duty cycles.

(b) The number 10 refers to 10% of usable propellant left for subsequent burn after propellants have come to thermal equilibrium.

(U) To identify the reasons that some pressurization systems were discarded and one concept emerged as the optimum, a general discussion on prepressurization modes is given, followed by weight-penalty data for each system. The systems are ranked based on these data and one system concept is selected. Finally, a description of the selected operation is given.

(U) A non-condensable gas such as helium is desirable to provide the required pressure above the propellant partial pressure in both tanks for the following reasons.

(C) During certain phases of the four mission profiles previously listed, the vehicle will be in a low-gravity coasting mode prior to engine restart. This low-gravity condition may be as low as 10^{-5} or $10^{-6}g$ or it could be higher, e.g., $10^{-2}g$, which is normally associated with attitude-control firings. In either case, which could be random depending upon actual mission operational requirements, rapid restart of this

Table 8-3

ASSUMPTIONS OR INPUT DATA USED IN THE PRESSURIZATION SYSTEM
SCREENING ANALYSES (C)

Assumption	Vented Concept		Nonvented Concept	
	LH ₂ Tank	LF ₂ Tank	LH ₂ Tank	LF ₂ Tank
Tank Operating Pressure (psia)	70	70	70 or greater	70 or greater
Vented Gas	Hydrogen	None	None	None
Total Pressure Requirement Above Vapor Pressure (psia)	11.5	52.4	11.5	52.4
Total Heat Input (Btu)				
• Three-minute non-vented ground hold	4380	3020	4380	3020
• Ascent	2300	1600	2300	1600
Heat Rate in Orbit (Btu/hr)	22.4	14.9	22.4	14.9
Prepressurant				
• Gas	He	He	He	He
• Temperature (°R)	37	154	37	154
• Storage Pressure (psia)	3500		3500	

system is desirable. Under these possible conditions, the precise location of the propellants within the tanks is uncertain. The propellant might be oriented by use of a dielectrophoretic device or surface-tension device which controls the propellant orientation throughout the tank (Fig. 8-1). Lockheed has studied these possibilities in previous contracts for the USAF and NASA (Contracts AF04(611)11403, NAS9-5174, NAS8-20553 and NAS10-4606). This previous work concluded that the orientation devices become excessively heavy when required to orient hydrogen and/or fluorine against gravitational loads as high as $10^{-2}g$. In addition, this type of "complete"

CONFIDENTIAL

LOCKHEED MISSILES & SPACE COMPANY

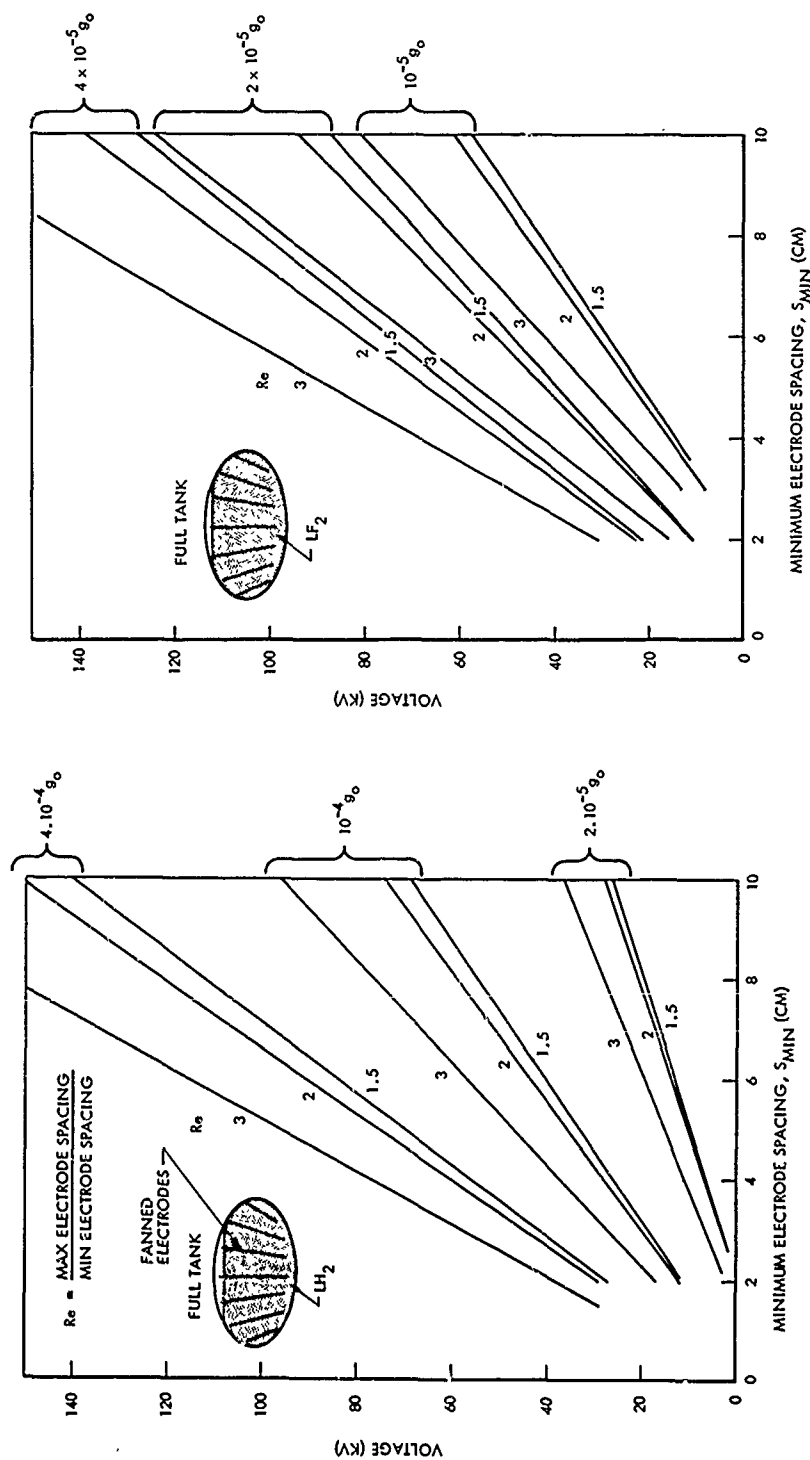


Fig. 8-1 Acceleration Stability Levels of Contained Propellants Vs. Electrode Voltage and Electrode Configuration (Dielectrophoretic Device) (C)

propellant orientation device (the entire tank filled with electrodes or screens) limits the point of ingress into the tanks, which further complicates such system. Assuming, then, that the pressurization system must function reliably even if there is random orientation of the propellants at low-g conditions, the incoming pressurant gas must be capable of entering through liquid or through vapor. Using a condensible gas under these conditions, the required ΔP would be difficult to maintain with any degree of confidence since it would be unknown as to the propellant condition around the injector inlet.

(U) Using warm helium gas as a prepressurant was also found to be undesirable for the following reasons. Location of the propellant under low-g conditions is uncertain; therefore, the heated helium collapse factor is also uncertain. A conservative assumption of complete collapse can be made; this would assume that the NPSP provided by the helium is essentially equivalent to that obtained by introducing helium at the propellant temperature. Actually, the helium requirement would be slightly less than this assumption would incur because the ΔP between the increased propellant partial pressure - caused through heating by the higher temperature helium - and the required tank operating pressure would be less than when cold helium is used. Moreover, the use of heated helium makes an external heat source necessary because the engine is not in operation during low-g coasting.

(C) A rapid start capability using heated prepressurant requires that the external heat source, heat exchanger, and lines must be sized to allow rapid pressurization to 70 psia or higher, depending on the mode of operation. Using a cold prepressurant, the tank is always at 70 psia before and after engine burns. Thus, there is no time lag caused by a prepressurization transient which cannot be avoided when using heated pressurant. In addition, the required prepressurant line sizes and heat exchanger are smaller when using cold helium, since the helium is introduced at a rate just fast enough to maintain constant tank pressure following an engine burn. Another advantage of using cold helium prepressurant is its use as a cooling medium. Following an engine burn, the warm expulsion gas collapses

CONFIDENTIAL

LOCKHEED MISSILES & SPACE COMPANY

in the tank, and cold helium from the LH_2 tank can be added to maintain tank pressure in both the LH_2 and LF_2 tanks. This gas must be warmed slightly to the respective propellant temperatures; therefore, small heat exchangers can be located on the propellant feed lines to accomplish this function. The cold gas is warmed to the propellant temperature by intercepting heat being conducted up the line from engine soakback. This gas is capable of cooling the LH_2 line as well as the LF_2 line. Propellant storability analysis indicates that the heat soakback problem is most severe following an engine burn; consequently, if this heat is intercepted and used, propellant storability, and consequently vehicle performance, is improved.

System 1

(C) System 1 is a basically simple and reliable system that uses cold helium gas for prepressurization and expulsion in both tanks. However, using helium expulsion gas at the propellant temperature causes a pressure rise above 70 psia in both tanks for duty cycle 3 even for the vented system, as shown in the pressure history evaluation. The reason for this is as follows: The He expulsion requirement was based on the assumption that no propellant vaporization occurs during an expulsion. Consequently, the ullage propellant vapor partial pressure decreases during the expulsion and the helium partial pressure increases correspondingly to maintain a constant pressure of 70 psia in the ullage. The liquid is assumed to remain at its initial state prior to expulsion. At the end of an expulsion, the system is assumed to enter into a state of thermal equilibrium because of mixing of the fluid after engine shutdown. When this occurs, propellant is vaporized to provide sufficient ullage vapor so that the remaining propellant is at a new saturated condition which corresponds to a propellant partial vapor pressure less than that before expulsion. When the amount of expelled propellant is small compared to the total tank volume, as for duty cycle 4, the total pressure remains near 70 psia. However, for a large initial expulsion, as in duty cycle 3, the final tank pressure rises above 70 psia. For the vented system, this pressure rise can be limited to some extent depending on the response and capacity of the vent system. For a nonvented system, this pressure rise results in a higher total tank pressure at the end of the coast period than for duty cycle 4. Therefore, the tank design operating pressure would be based on duty cycle 3 requirements.

CONFIDENTIAL

LOCKHEED MISSILES & SPACE COMPANY

(C) To limit this pressure rise in the tanks, heated helium is required for the expulsions. The temperature of the helium is determined from duty cycle 3 requirements, which require the highest degree of collapse of the expulsion vapor to limit the pressure rise above 70 psia, and yet provide a sufficient partial pressure of helium in the tank following each engine burn. As the helium temperature is increased, the partial pressure of the heated fluorine increases, decreasing the helium partial pressure when the total pressure is held constant.

(U) System 1 weight penalties are shown in Fig. 8-2 for vented and nonvented tanks.

System 2

(C) System 2 uses heated helium for both prepressurization and expulsion in the hydrogen tank. This system ranks well on a weight penalty basis; however, it is felt that the previously described instant start problems associated with a heated prepressurant system are sufficient to eliminate this system from further analysis.

Systems 2a and 2b

(U) Systems 2a and 2b use cold helium prepressurant and different helium expulsion temperatures.

(C) System 2b uses heated helium for expelling the LF_2 in place of $154^\circ R$ helium for the reasons described under System 1; otherwise, systems 2a and 2b are identical. Weight penalties for these concepts for both duty cycles 3 and 4 and the vented and nonvented modes of operation are shown in Fig. 8-3. For duty cycle 4, vented or nonvented, cold helium expulsion results in a lighter system weight than warm expulsion because of the use of low-temperature material allowables for System 2a. The higher allowables result in higher LF_2 tank weight.

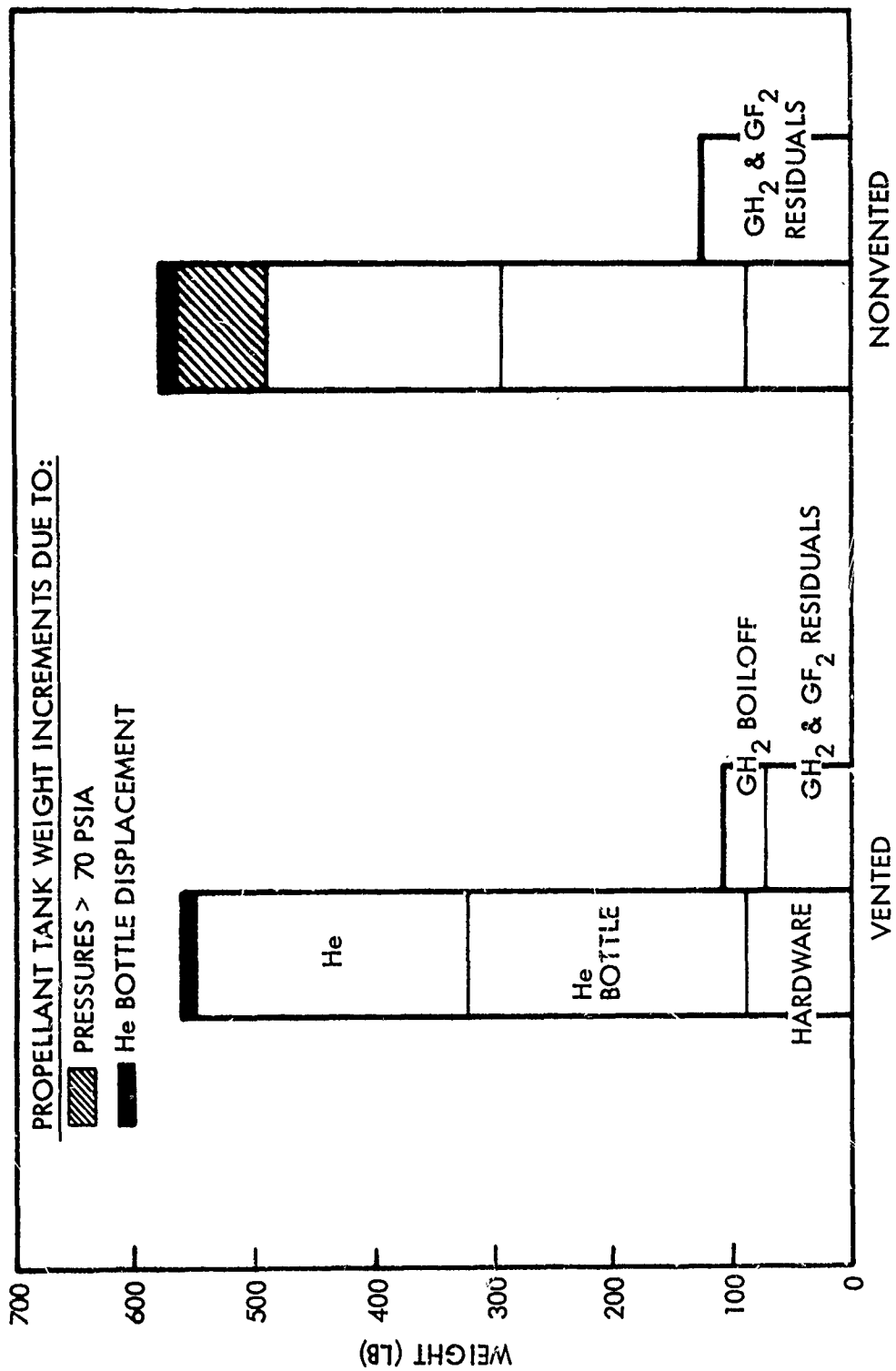
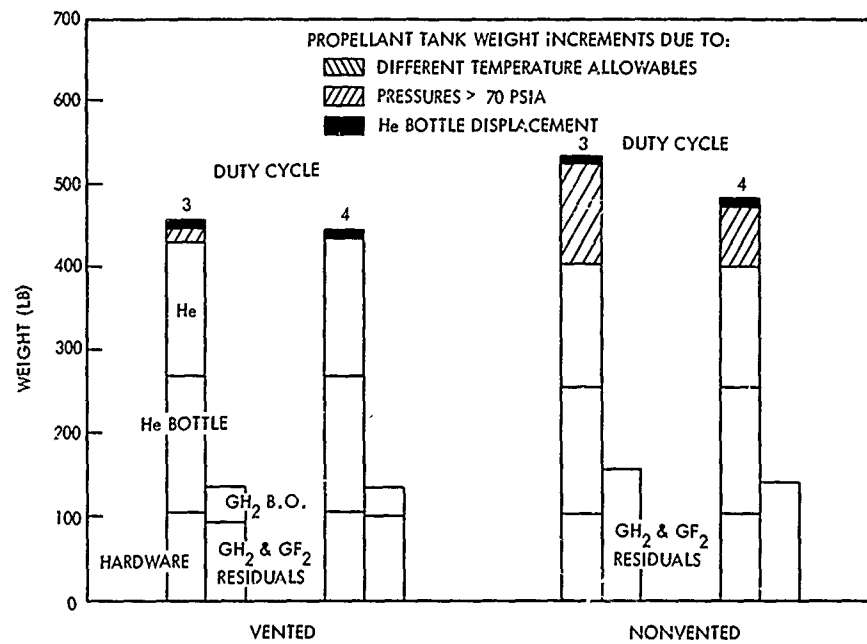
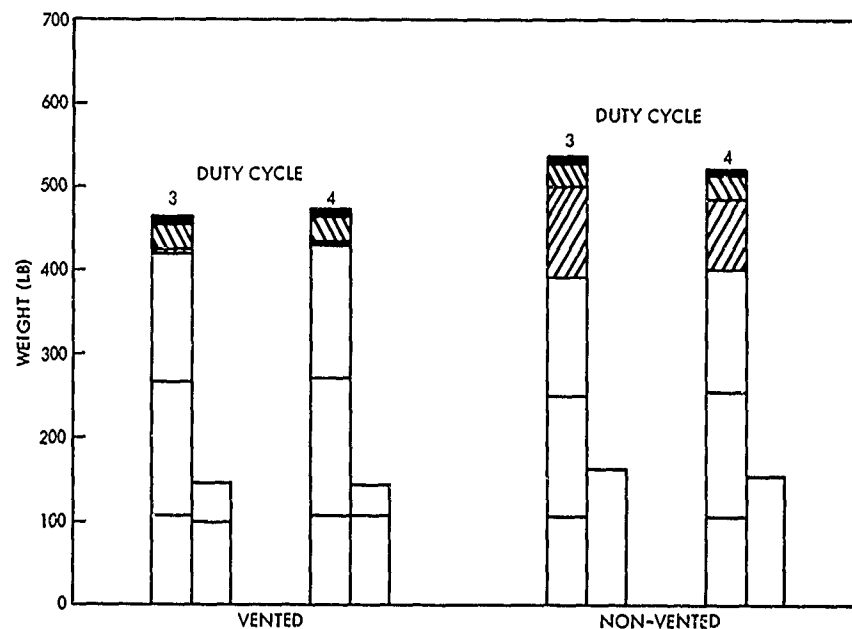


Fig. 8-2 Comparative Weight Penalty - Pressurization System 1, Duty Cycle 4 (C)



2a



2b

Fig. 8-3 Comparative Weight Penalties for Systems 2a and 2b (C)

System 3

(U) The weight penalties for vented System 3 were reported in Ref. 4 for Missions 1, 2, and 3. The vented duty cycle 4 case was reported in Ref. 4. While this system is attractive from a weight penalty standpoint, it is felt that it should not be analyzed further because of instant start problems associated with a heated prepressurant system.

Systems 3a, 3b, 3c, and 3d (Selected Concept)

(C) These systems all use helium prepressurant at the propellant temperatures. Expulsion in the LH_2 and LF_2 tanks is accomplished using warm GH_2 and GHe , respectively. Expulsion temperatures were varied between the four systems to determine the temperature effect on system weight. These analyses are preliminary; therefore, the temperatures selected are not optimum, but were chosen only to indicate trends. Based on the weights shown in Fig. 8-4, the lower temperature expulsion gases provide the lightest weight systems, as shown by the following rankings:

Ranking	System	Expulsion Temperatures ($^{\circ}\text{R}$)		
		LH_2	LF_2	
1	3b	140	154	↓ Heavier system on overall weight basis
2	3c	140	320	
3	3a	400	154	
4	3d	400	320	

(U) This weight trend is caused by several factors. Residual gas weights are less for lower temperature expulsion due to lower propellant partial pressures at burnout. (Refer to Tank Pressure Histories presented in a subsequent paragraph.) Although more helium is required for the lower temperature expulsion systems, the helium bottle weights are lighter because of the use of lower temperature material allowables. Consequently, the weight of the helium plus the 3,500 psia bottle, surprisingly,

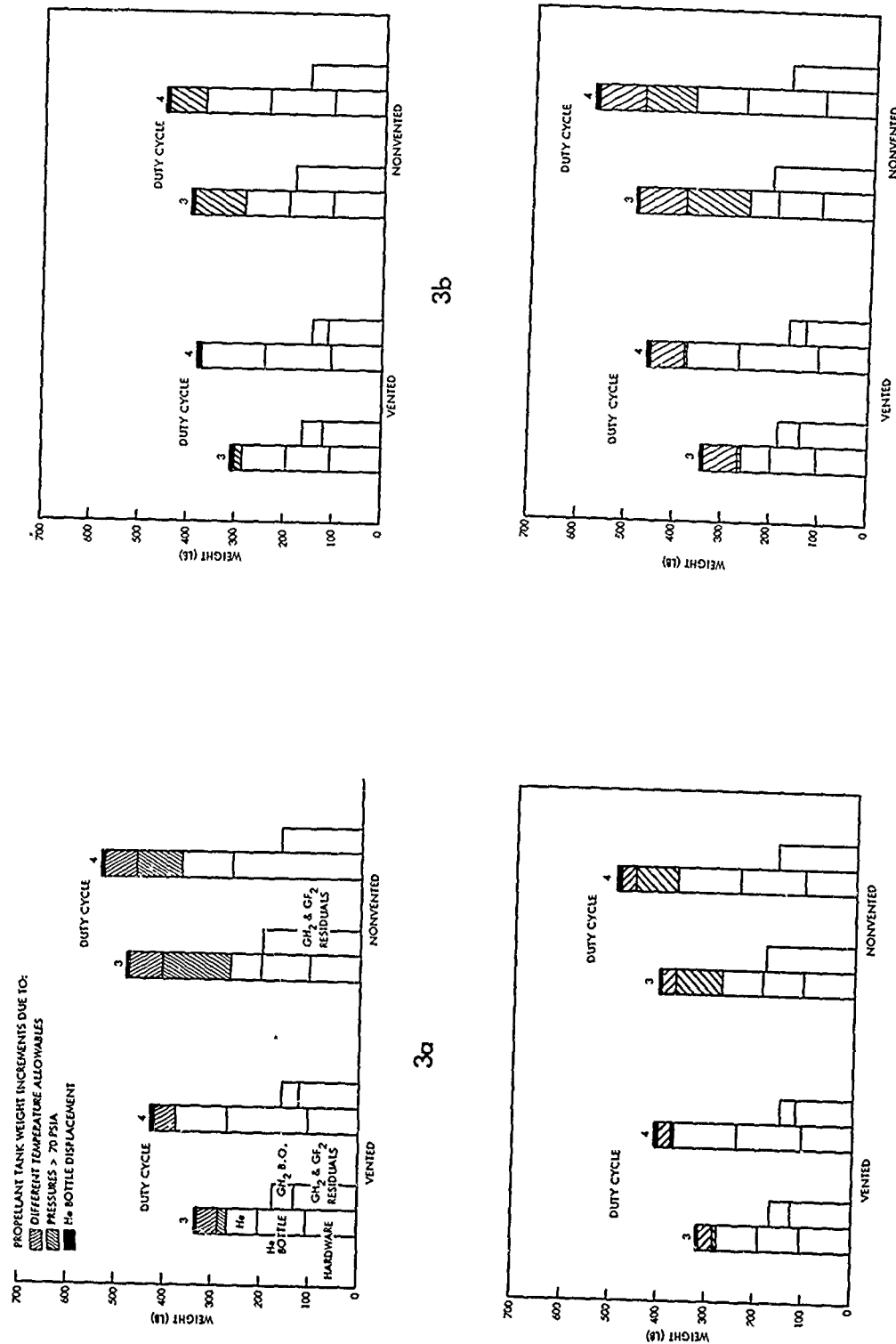


Fig. 8-4 Comparative Weight Penalties for Systems 3a Through 3d (C)

remains relatively constant for 3a through 3d due to these opposing trends. Another weight advantage for low temperature expulsion systems accrues from use of low temperature allowables in the propellant tanks. A more detailed examination of expulsion temperatures as affected by tank and bottle material allowables and bottle pressures is required before optimum expulsion temperatures can be established.

Systems 4, 4a, and 5

(U) References 4 and 5 present system weight penalties for some vented system/mission combinations. No further analyses were performed for these systems because of instant start problems associated with a heated condensable prepressurant system.

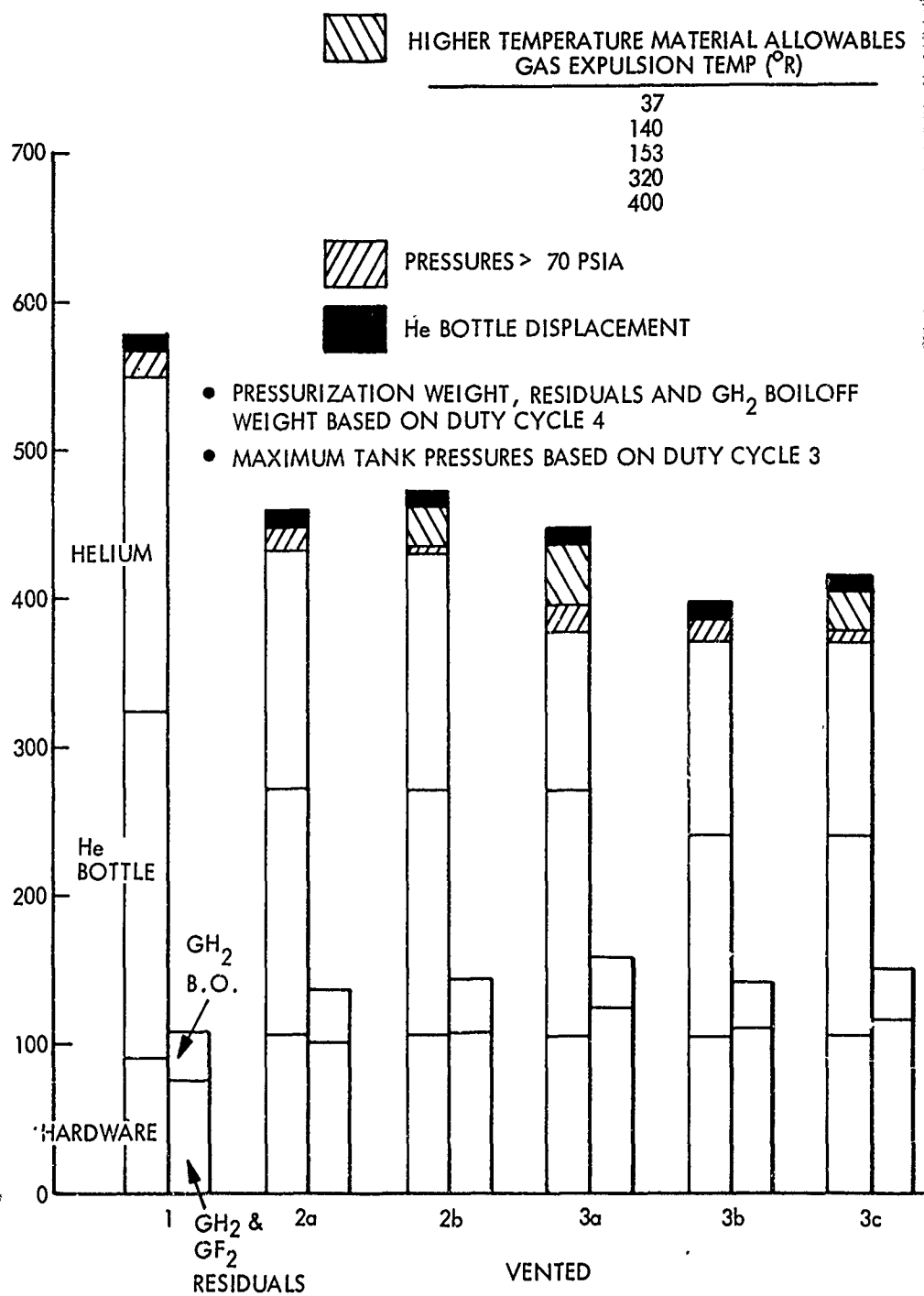
Tridyne System

(C) The Tridyne System uses heated helium for prepressurizing the LH_2 tank, and a mixture of helium, H_2 , and O_2 (Tridyne gas) to prepressurize the fluorine tank. The hydrogen and oxygen are reacted in a catalyst bed to heat the helium prepressurant prior to entering the fluorine tank. This system was eliminated from further consideration because of instant start problems associated with a heated prepressurant gas and the problems that may be encountered by introducing ice crystals into the fluorine tank.

System Rankings

(C) A weight penalty comparison of the promising systems discussed previously is presented in Fig. 8-5 for both vented and nonvented tanks. Duty cycle 4 provided the highest pressurization system weights and, consequently, is used for the ranking. In some cases duty cycle 3 provides higher tank pressures than duty cycle 4. Tank weight increments reflecting duty cycle 3 are included. A 70 psia tank is used as the baseline reference. Propellant tank design temperatures and helium bottle design temperatures as a function of the gas expulsion temperature (used to calculate tank weights) are shown in Fig. 8-5.

● PROPELLANT TANKS AND He BOTTLE WEIGHT INCREMENTS DUE TO



EENTS DUE TO:

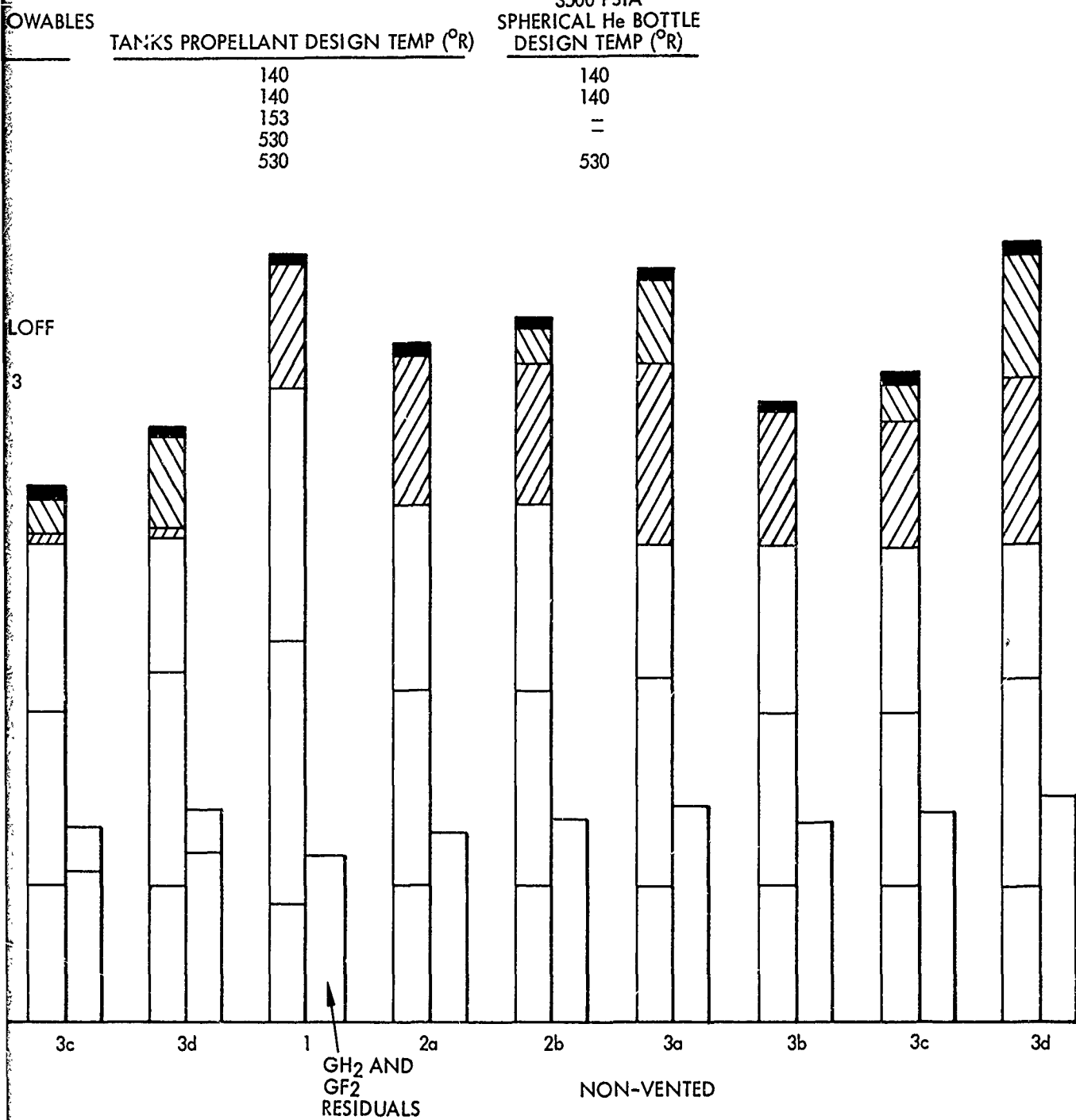


Fig. 8-5 Pressurization System Weight Comparison for Vented and Nonvented Systems (C)

CONFIDENTIAL

LMSC-680959

(C) Weight breakdowns of Fig. 8-5 show that vented systems are consistently lighter than the equivalent nonvented systems. A vented versus nonvented tank comparison based on the lowest weight pressurization system (3b) is shown in Subtasks 2 and 3. This comparison also includes vent-free fluorine system weights, propellant orientation system weights, and insulation weights, as well as the weights shown in Fig. 8-5.

(C) The promising pressurization systems on a normalized weight-penalty basis combining pressurization weight penalties and residual gas weight penalties are shown in Fig. 8-6. System 3b remains the lightest weight system using these criteria for both vented and nonvented tanks. As discussed previously for Systems 3a through 3d, lower expulsion temperatures produce lighter weight systems because of the use of low-temperature material allowables in the propellant tanks and helium bottle. However, optimization of the expulsion temperatures as a part of the overall optimization of the vehicle is still required. Until this optimization is completed, System 3b expulsion temperatures will be used in further analyses.

Operation of Selected System

(C) The selected system uses helium prepressurant in both tanks at the propellant temperature. Expulsion of LH_2 is performed using warm engine bleed GH_2 . Fluorine is expelled with gaseous helium. Helium is stored at 1,250 psia inside the LH_2 tank. (The screening analysis used 3,500 psia bottles. The lower pressure was selected by optimization techniques described in the related analysis section.) Operation of the system shown schematically in Fig. 8-7 is described in the following paragraphs.

(C) Immediately following vehicle injection into orbit, both tanks are pressurized to 70 psia with helium through heat exchangers 1 and 2. The vent-free fluorine system maintains a constant 70 psia pressure (within a specified tolerance band) in both tanks during coast. When the tank prevalues open for an engine burn, three-way valve U3

CONFIDENTIAL

LOCKHEED MISSILES & SPACE COMPANY

WEIGHT PENALTY CONSISTS OF:

- He GAS
- He BOTTLE
- PRESSURIZATION HARDWARE
- PROPELLANT TANK INCREMENTS DUE TO:
 - EXPULSION TEMPERATURE
 - PRESSURES > 70 PSIA
 - He BOTTLE DISPLACEMENT
- GAS RESIDUALS INCREMENT > SYSTEM 1 RESIDUALS (WHERE PREPRESSURANT AND EXPULSION GASES ARE AT PROPELLANT TEMPERATURES)

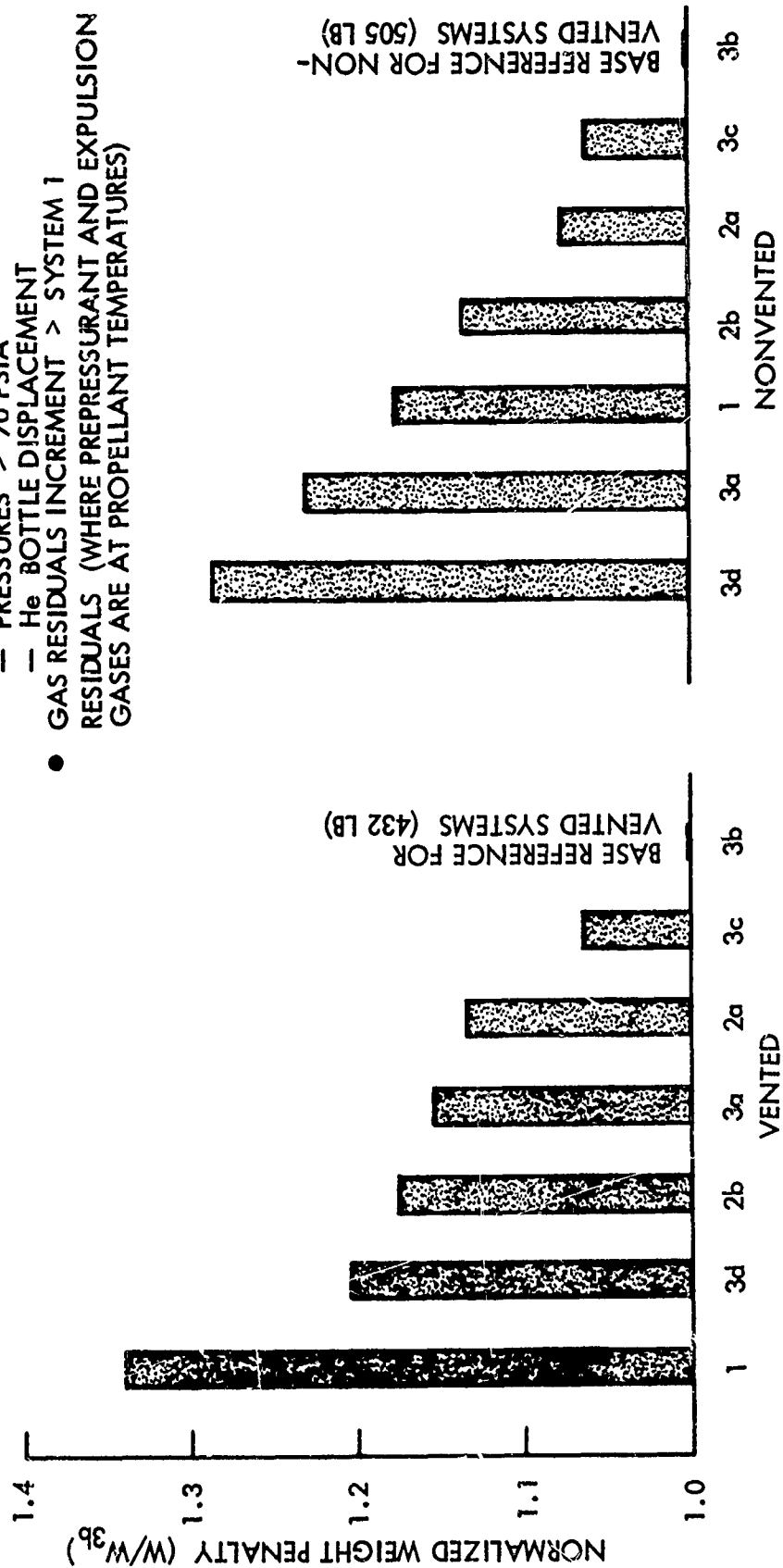


Fig. 8-6 Normalized Weight Penalty Comparison of the Pressurization Systems (C)

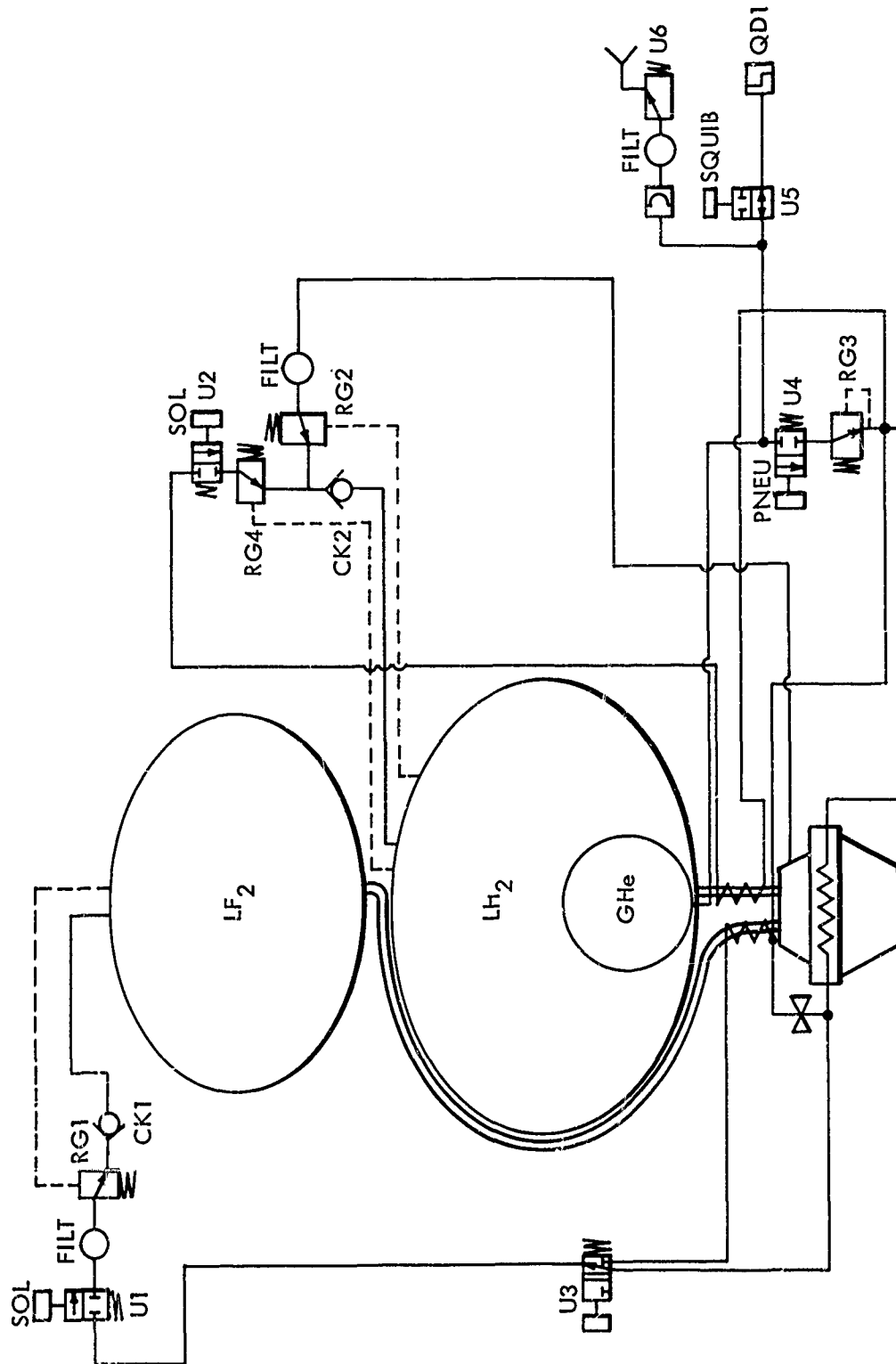


Fig. 8-7 Selected Pressurization System Schematic (C)

switches the helium flow through the engine heat exchanger and a cold bypass line. The proper ratio of cold to hot gas is obtained by use of a fixed orifice to maintain the expulsion temperature. The heat exchanger on the LF_2 feed line is bypassed during expulsion. LF_2 tank pressure is thus maintained at 70 psia during engine burn. At the same time valve U3 operates, valve U2 closes and heated GH_2 bleed is used to maintain 70 psia during LH_2 expulsion.

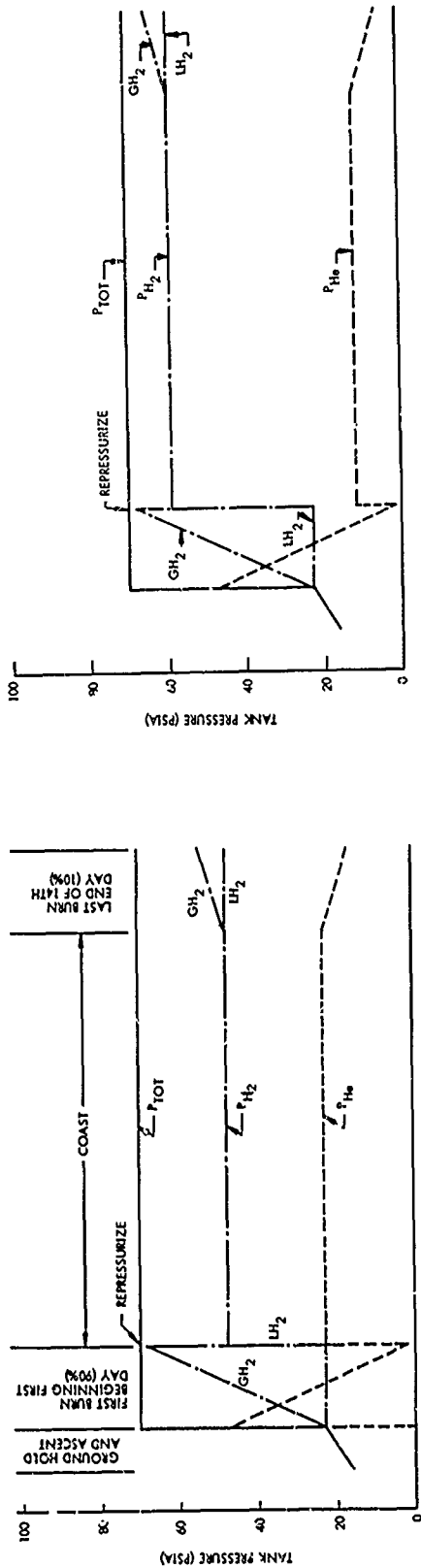
(C) Upon shutdown of the engine and closure of the tank prevalues, operation of valve U3 switches the helium flow from the engine heat exchanger to the LF_2 line heat exchanger. As the residual heated helium in the LF_2 tank collapses (if helium above $154^\circ R$ is used for expulsion), regulator RG1 maintains the tank pressure at 70 psia by introducing more helium at LF_2 temperature. On the hydrogen side at engine shutdown, the hydrogen bleed line is closed and valve U2 is opened. Regulator RG4 maintains the LH_2 tank pressure at 70 psia as the hot hydrogen gas collapses.

Tank Pressure Histories

(C) Tank pressure histories were calculated for each pressurization system and significant duty cycle to determine maximum tank operating pressures and to ensure that total pressure requirements above propellant vapor pressure are met during the 14-day duration. These maximum tank pressures were used in the previously described pressurization weight penalty analyses to calculate tank weight penalties. Pressure history curves for the selected system concept (3a through 3d) are shown here and are typical of the other pressurization system pressure histories.

(C) Hydrogen Tank. Figure 8-8 shows hydrogen tank pressure histories for different expulsion temperatures and a vented or nonvented condition. Duty cycle 3 was chosen because it provides maximum tank pressure rise. The partial pressure noted " LH_2 " on Fig. 8-8 refers to a partial pressure corresponding to the propellant temperature. " GH_2 " refers to the ullage partial pressure. The higher expulsion temperature of $400^\circ R$ versus $140^\circ R$ reduces the helium requirement for both vented and nonvented

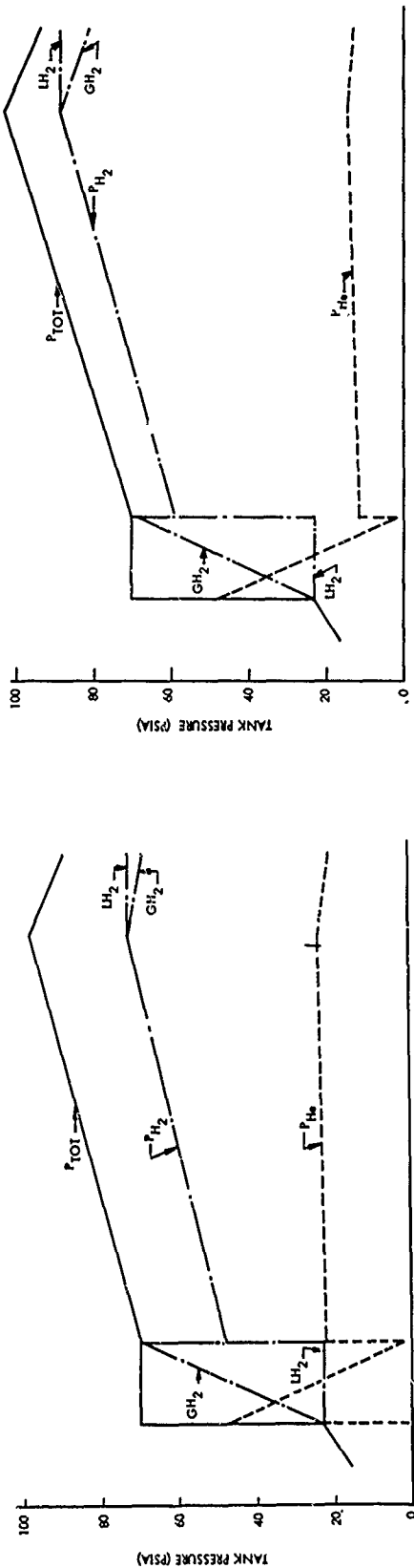
140°R HYDROGEN EXPULSION TEMPERATURE 400°R



VENTED

140°R

400°R



NONVENTED

Fig. 8-8 Hydrogen Tank Pressure Histories, Duty Cycle 3, 37° R Helium Prepressurization (C)

systems. This is caused by the lower helium partial pressure. However, this higher temperature increases the hydrogen residual weights because of higher hydrogen partial pressure at burnout - 64 versus 54 psia for vented tanks and 81 versus 64 psia for nonvented tanks.

(C) The minimum tank operating pressure of 70 psia is held constant for the vented system over the 14-day period. The nonvented tank pressure that rises above 70 psia is allowed to decay during the last engine burn. The pressure does not reach 70 psia; therefore, no additional helium or hydrogen pressurant is required after the first burn. The maximum tank pressure (102 psia) is reached using the 400° R expulsion gas, versus 98 psia for the 140° R gas.

(C) Fluorine Tank. Figure 8-9 shows fluorine tank pressure histories for different expulsion temperatures and a vented or nonvented condition. Comments on required helium weight and residual weights as a function of expulsion temperature given in the hydrogen tank pressure discussion also apply here. However, the maximum tank pressure trend is reversed; i. e., the highest tank pressure is reached with helium expulsion gas at 154° R rather than 320° R. The reason for this reversal for both the vented and nonvented tanks is the assumption that no fluorine vaporization occurs during expulsion. Consequently, the fluorine partial pressure drops and the helium partial pressure rises to maintain the tank pressure constant as the ullage volume increases. For 154° R expulsion, no pressure collapse occurs following engine burn; therefore, the total tank pressure rises when fluorine evaporation occurs at engine shutdown. Using 320° R gas (the maximum temperature that can be used and still meet the total pressure requirements above the propellant vapor pressure) the pressure decreases following an engine burn; however, this decrease is not enough (lacking 3 psi) to prevent the tank pressure from exceeding 70 psia. During the optimization study, mass transfer across the fluorine interface will be considered during expulsion to more accurately define the tank pressure histories.

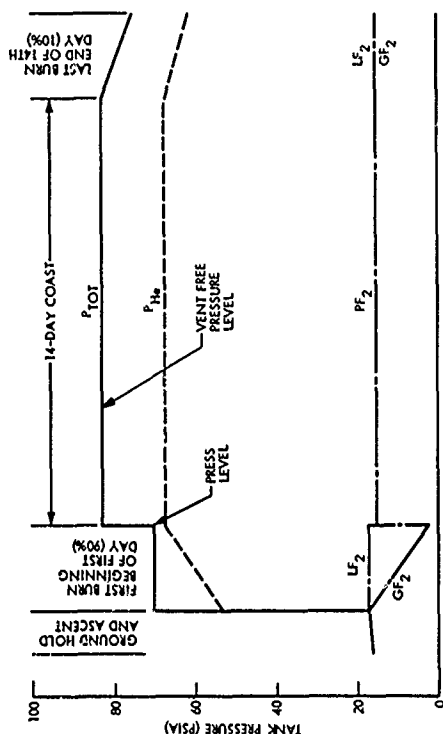
CONFIDENTIAL

LOCKHEED MISSILES & SPACE COMPANY

154°R

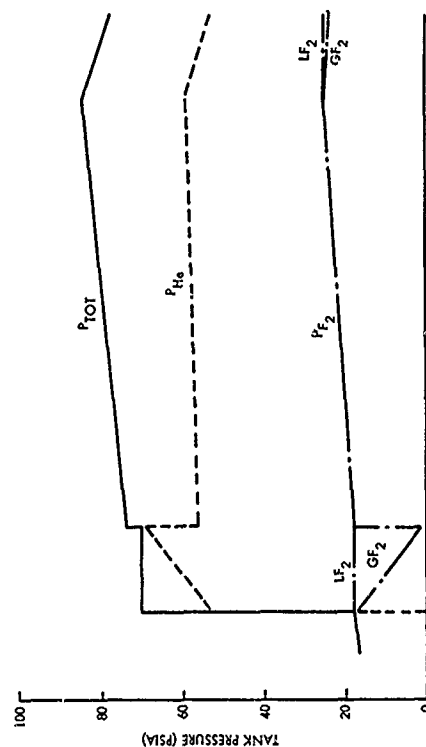
HELIUM EXPULSION TEMPERATURE

320°R



VENTED

320°R



NONVENTED

154°R

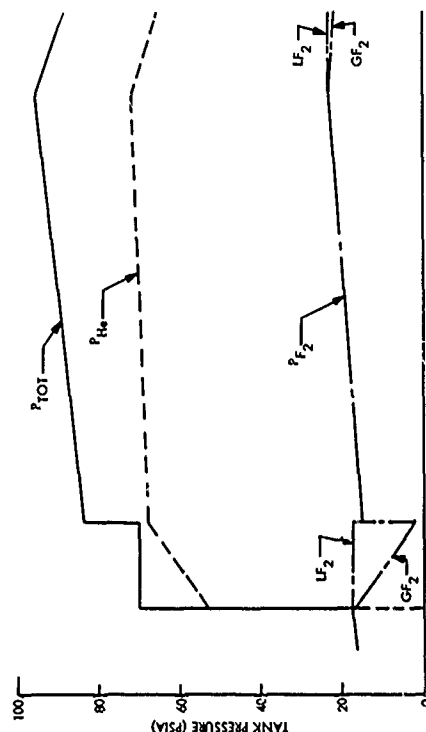


Fig. 8-9 Fluorine Tank Pressure Histories, Duty Cycle 3, 154°R Helium Prepressurization (C)

Supporting Analyses

(U) Tank weight analyses performed in Subtasks 2 and 3 and helium bottle-weight analyses were required to support the pressurization screening analyses. The results of these analyses are summarized in the following paragraphs.

(C) Tank Weight Analyses. Weights of the LH_2 and LF_2 tanks as a function of volume, temperature allowables, and pressure were required to provide tank-weight increment penalties for the various systems.

(C) Tank-weight increments caused by pressures above 70 psia and varying gas expulsion temperatures were obtained from Figs. 8-10 and 8-11. Figure 8-12 shows LH_2 tank weight versus volume. These data are used for calculating the tank weight penalty increment associated with the in-tank helium bottle displacement of LH_2 .

(C) Helium Bottle Weight and Size Analyses. Analyses were conducted on helium bottle sizes and weights as a function of the helium mass requirements (gas stored at 37°R) to aid in the pressurization system weight analyses. Inconel 718 was selected as a candidate material for the bottle because of its excellent low-temperature properties and heat-treatable age-hardening capabilities.

(C) A storage pressure of 3,500 psia was selected for the screening analyses. (Following the screening analyses, the storage pressure was optimized for the selected concept.) Both spheres and cylinders with spherical ends were examined. Sphere sizes were becoming too large to fit through a reasonably sized access opening, as is possible with cylindrical bottles; consequently, the problems associated with building a fully qualified spherical helium bottle into the LH_2 tank were examined. From Ref. 6, the failure rate for standard high-pressure bottles of this type is 7×10^{-8} failures/hr. For a period of 14 days, this failure rate converts to a reliability value of 0.999977. Extending the mission duration to 180 days decreases the reliability value to 0.99970. These values are high enough to assume that once the helium bottle

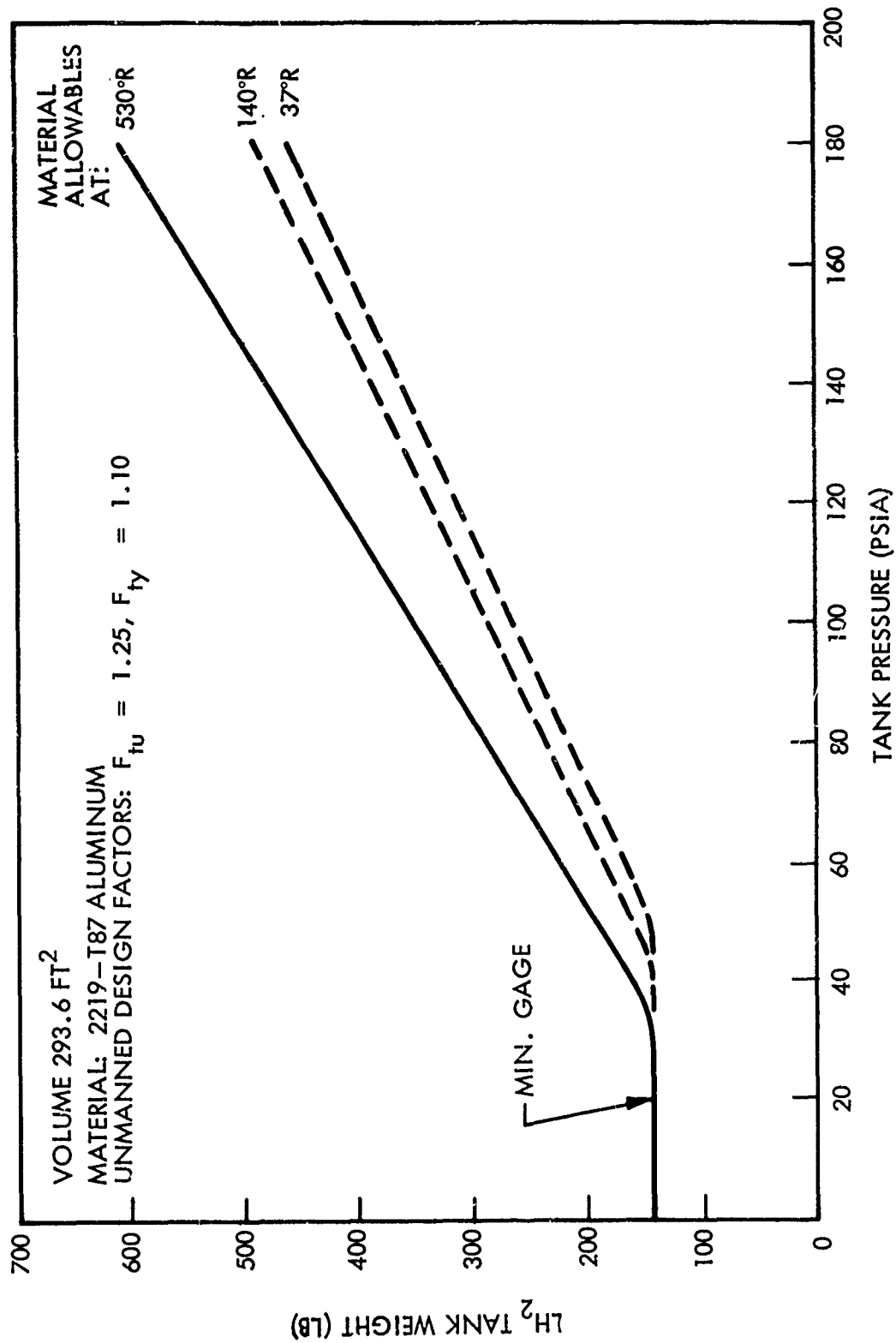


Fig. 8-10 Effect of Pressure and Low Temperature Allowables on LH₂ Tank Weight (C)

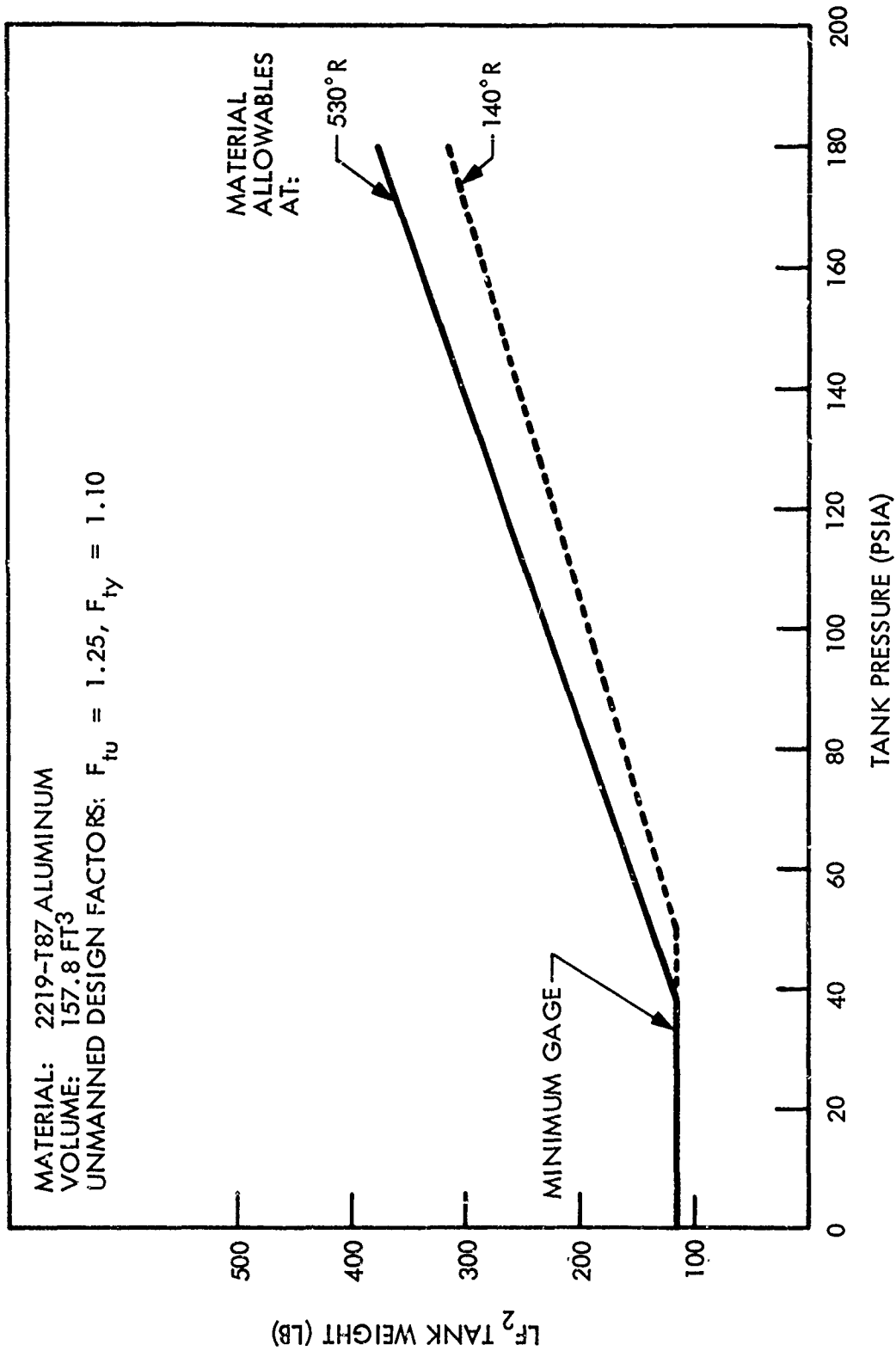


Fig. 8-11 Effect of Pressure and Low-Temperature Allowables on LF₂ Tank Weight (C)

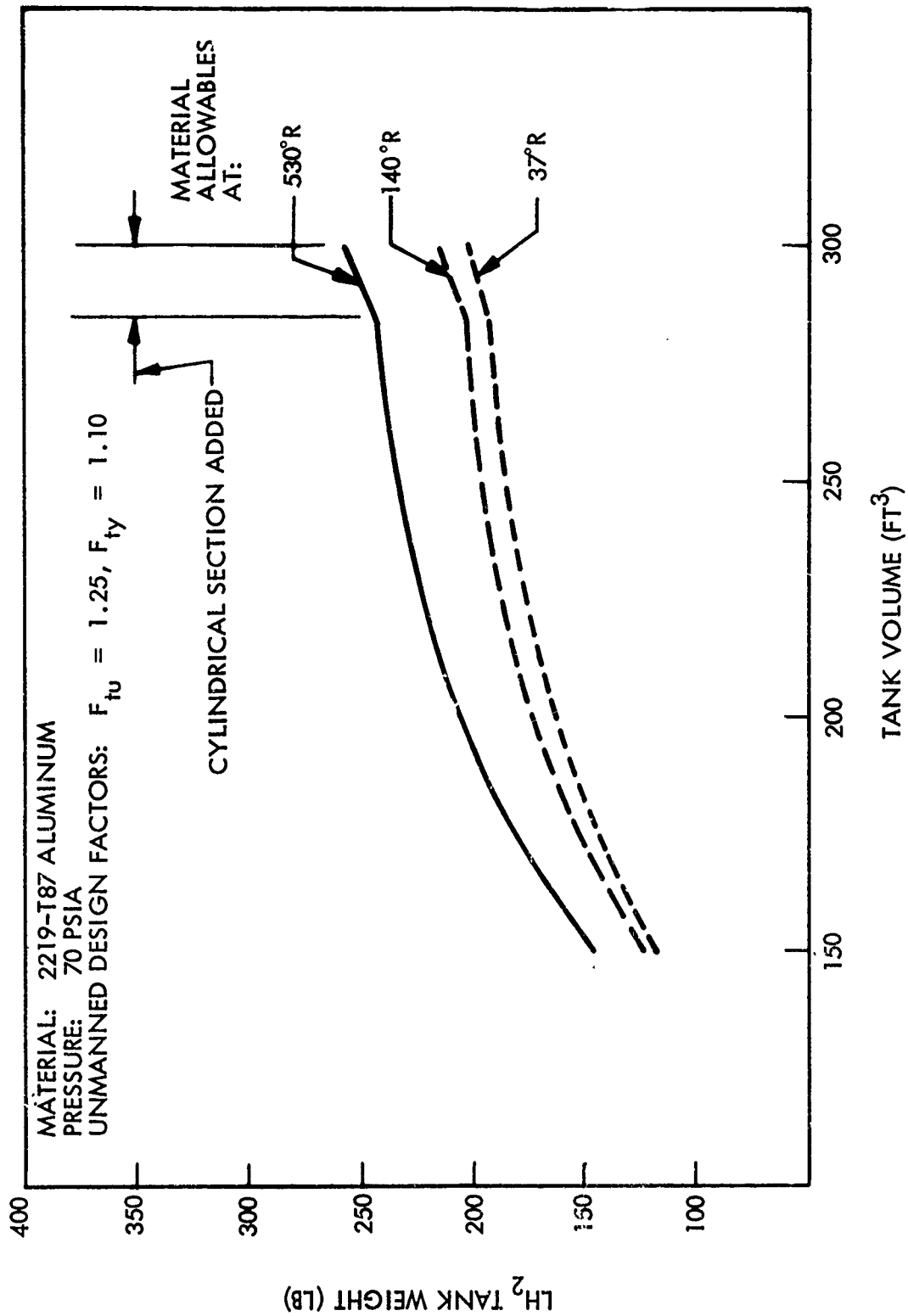


Fig. 8-12 Effect of Volume and Low Temperature Allowables on LH₂ Tank Weight (C)

is installed in the LH_2 tank prior to the final Y-ring closure weld, it will never have to be removed (assuming that the bottle is not damaged during fabrication). Consequently, the lighter spherically shaped bottle was selected for this study over the cylindrical bottle. Fabrication costs will be higher using the spherical bottle because of the added complexity of assembly.

(U) The following data were generated to support the pressurization analyses. First, required storage volumes were determined as a function of the helium mass, as shown in Fig. 8-13. Helium bottle weights were then calculated as a function of storage volume for spheres, 23-in. -diameter cylinders, and two temperature allowables, as shown in Fig. 8-14. The same curves were replotted substituting GHe weight for volume, as shown in Fig. 8-15. Tank sizes were obtained from Fig. 8-16.

Optimization of Helium Bottle Pressure

(U) For the pressurization screening analyses, a helium bottle pressure of 3,500 psia was used. Use of a fixed pressure was considered adequate for ranking the systems. Following selection of a pressurization system concept, optimization of the helium pressure for that concept was performed. Weight data based on this optimized pressure will be used in the configuration selection parametric studies.

(C) Weights considered in the optimization were the bottle, bottle residuals, LH_2 tank increment due to bottle displacement of LH_2 insulation system, and hydrogen boiloff.

(U) The general optimization approach used was to derive an expression for mass of helium loaded as a function of usable mass, and express the affected system weights as a function of mass loaded.

(U) For an isothermal blowdown at the end of mission, the total mass loaded is

$$W_L = \frac{W_{GHe}}{1 - \frac{P_f Z_1}{Z_f P_1}}$$

134

Appendix II

CONFIDENTIAL

LOCKHEED MISSILES & SPACE COMPANY

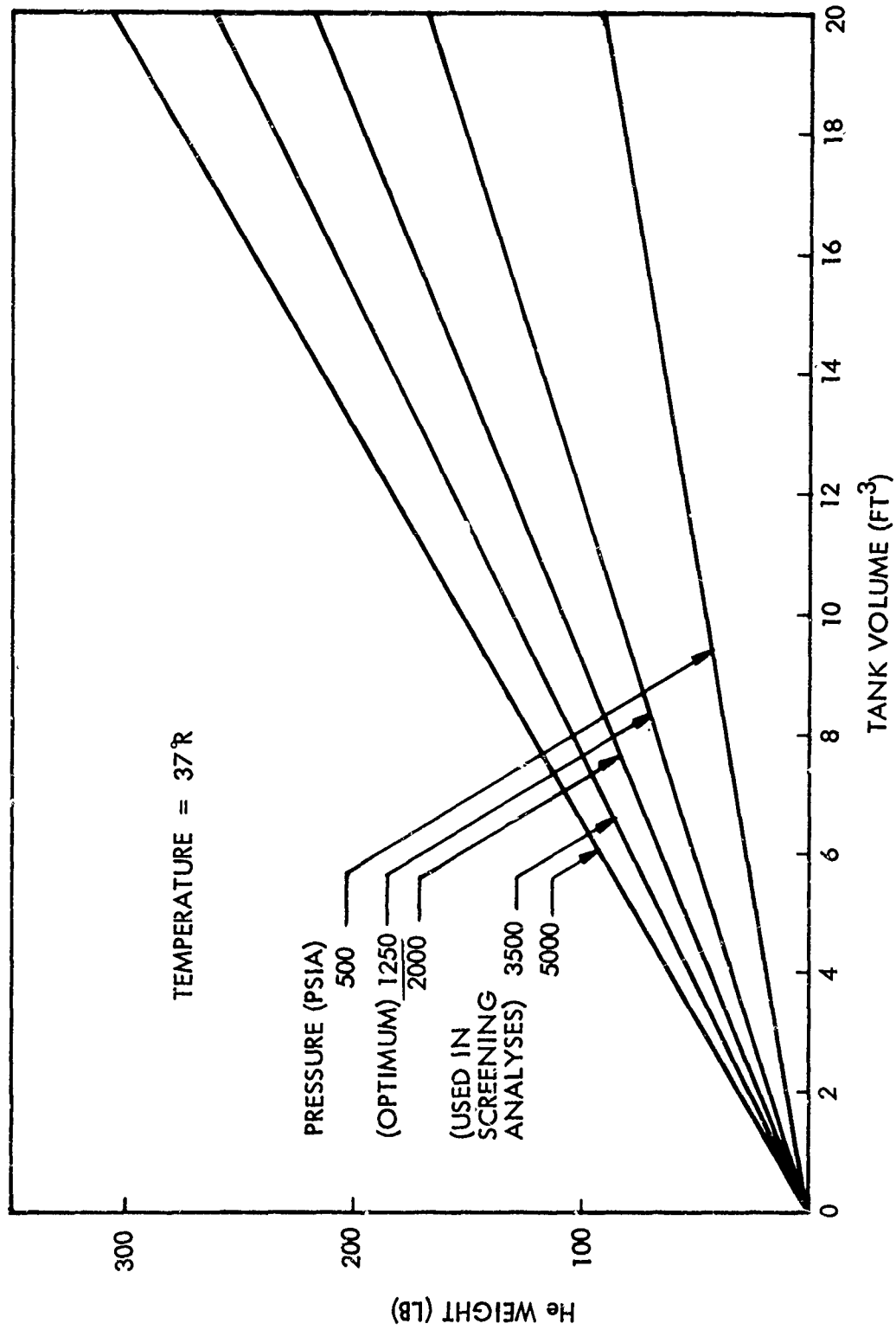


Fig. 8-13 Helium Storage Volume Required as a Function of Helium Mass and Storage Pressure (C)

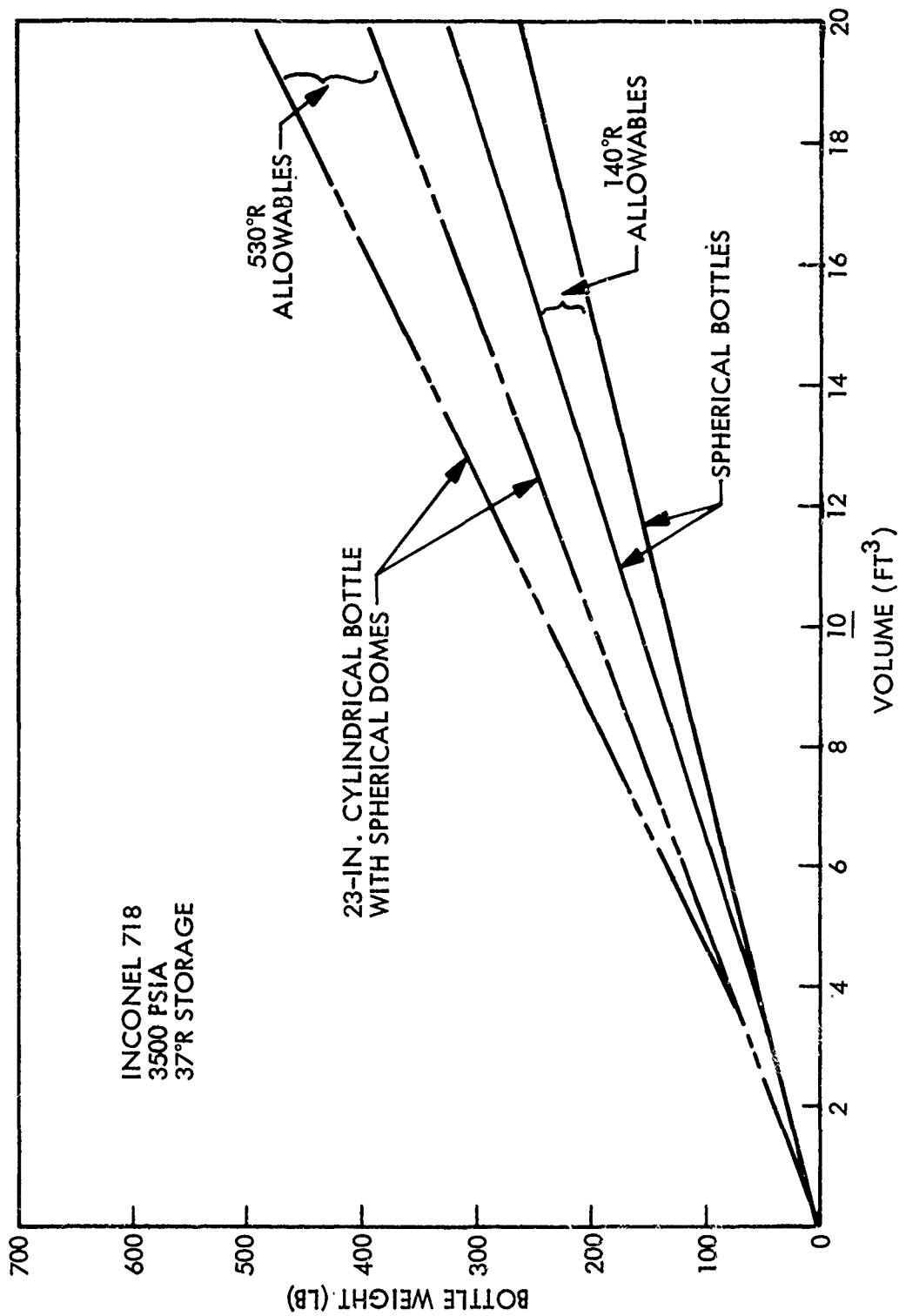


Fig. 8-14 Pressurant Bottle Weight as a Function of Volume, Tank Shape, and Material Allowables (at 3,500 psi) (C)

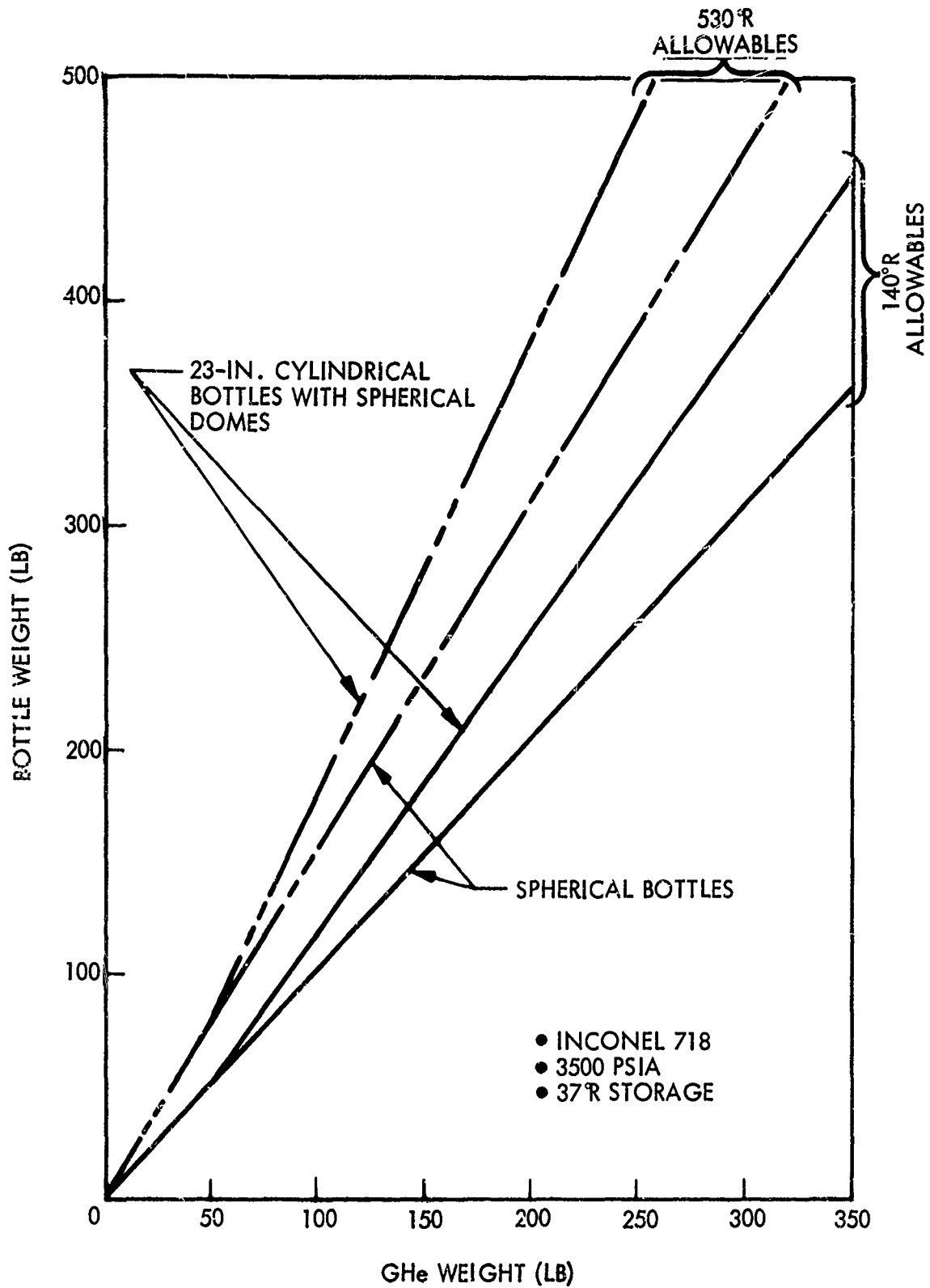


Fig. 8-15 Pressurant Bottle Weight as a Function of GHe Weight, Tank Shape, and Material Allowables (at 3,500 psia) (C)

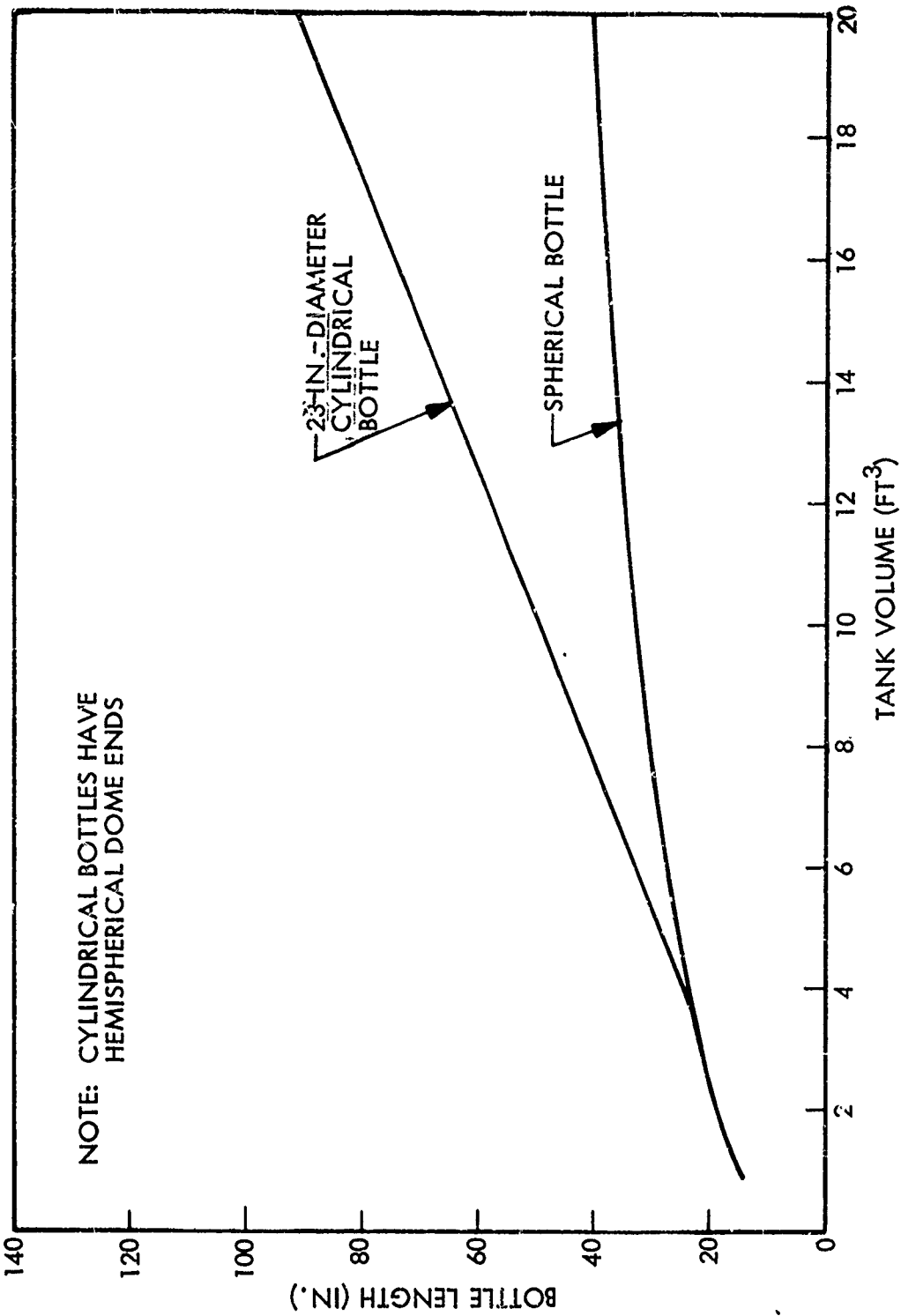


Fig. 8-16 Bottle Size as a Function of Volume (C)

where

W_L = total mass of helium loaded

W_{GHe} = usable helium

P_f = minimum blowdown pressure

P_1 = initial storage pressure

Z_f = compressibility factor at minimum pressure

Z_1 = compressibility factor at initial conditions

The results of the analyses are shown in Fig. 8-17.

(C) From Fig. 8-17 it can be seen that different temperature allowables for the bottle and different LH_2 tank pressures had a negligible effect on the optimum pressure (approximately 1,250 psia). Bottle weights for this pressure as a function of volume are shown in Fig. 8-18. The major reason the pressure optimized at this low value is that the compressibility factor of helium at 37° R (i. e., the mass of helium stored) is not a linear function of pressure. Consequently, helium bottle weight increases more rapidly with pressure than mass of helium stored. Another significant factor in selecting the optimum pressure is the choice of final blowdown pressure. This effect is shown in Fig. 8-19 for two pressures - 100 psia and 500 psia. Note the higher system weights and shift in optimum storage pressure upward for higher final blowdown pressure caused by the increased residuals. A 500 psia pressure, consistent with pneumatic valve operation, was examined to determine if gas from the helium bottle could serve a dual function. The large increase in weight penalty between 500 and 100 psia (approximately 120 lb), indicates that a separate helium supply is required for pneumatic valve operation. For the 31-burn mission, this separate ambient temperature helium supply is estimated to weigh 15 lb.

(C) The lowest blowdown pressure possible consistent with line pressure drops therefore produces the lightest weight system. On this basis, a 100-psia blowdown pressure was chosen. This pressure will be optimized during detail design, consistent with line pressure drops not to exceed $P_{Blowdown} - P_{LH_2}$ tank.

CONFIDENTIAL

LOCKHEED MISSILES & SPACE COMPANY

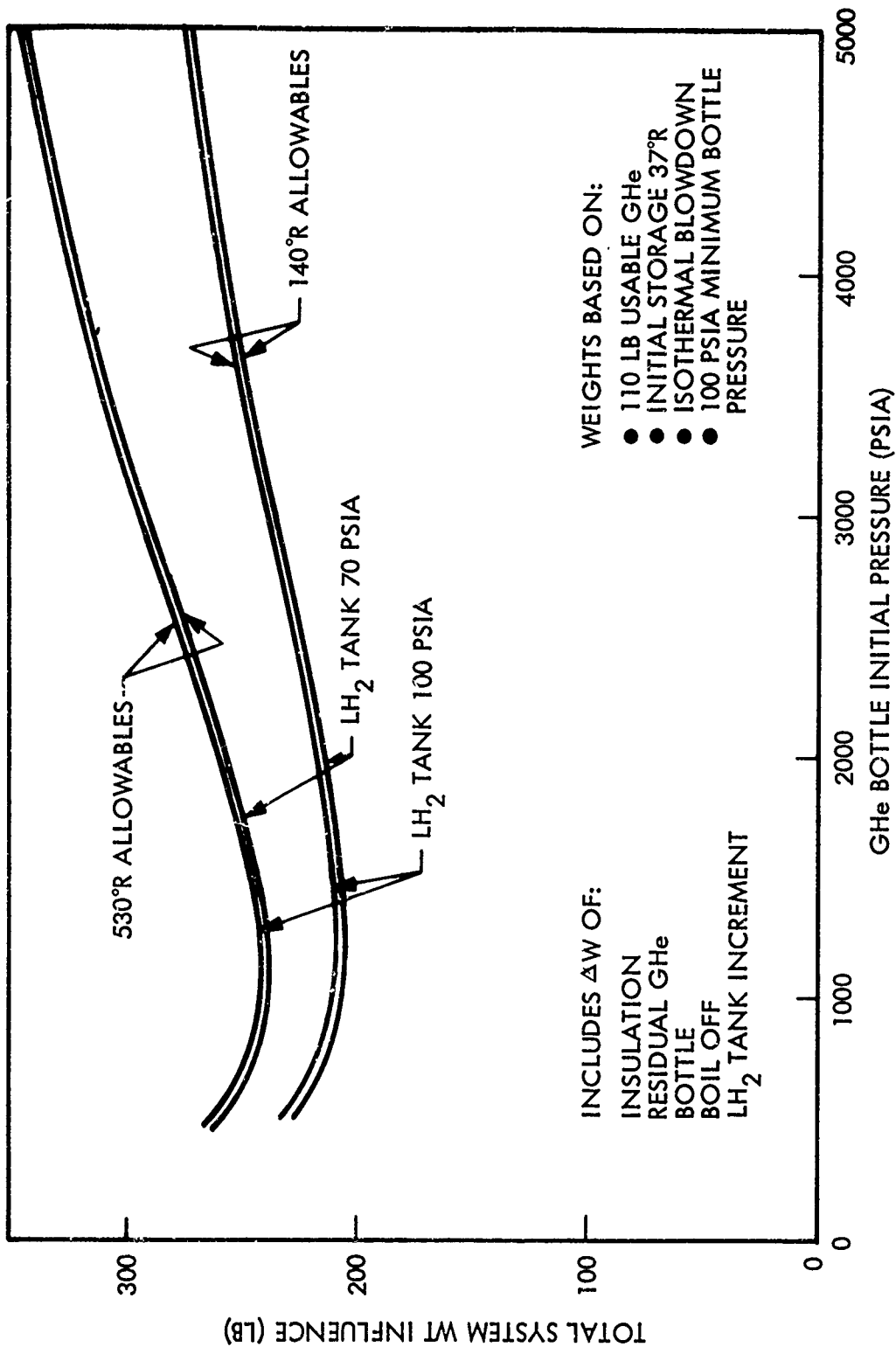


Fig. 8-17 Helium Bottle Pressure Optimization (C)

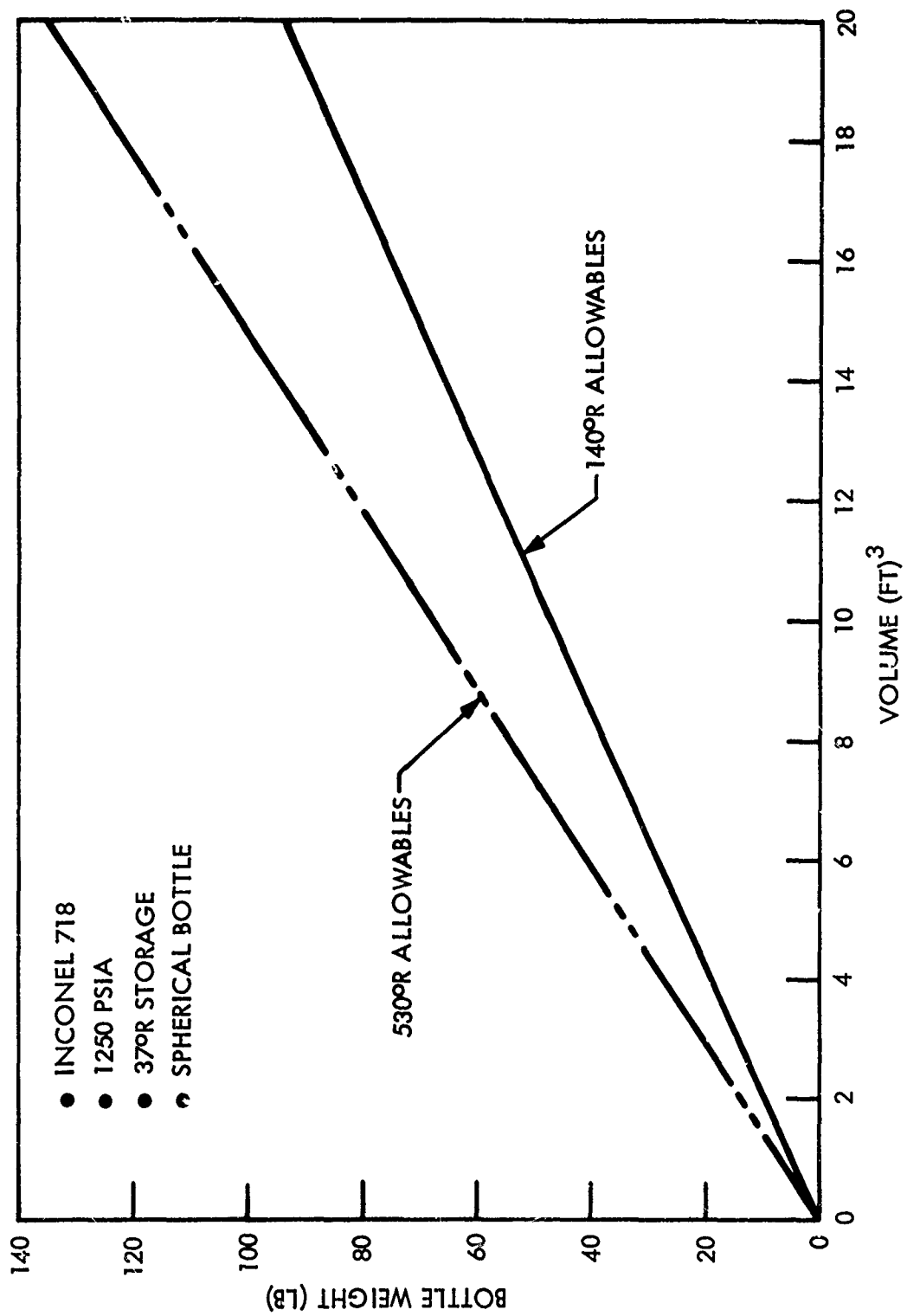


Fig. 8-18 Pressurant Bottle Weight as a Function of Volume and Material Allowables at 1,250 psia (C)

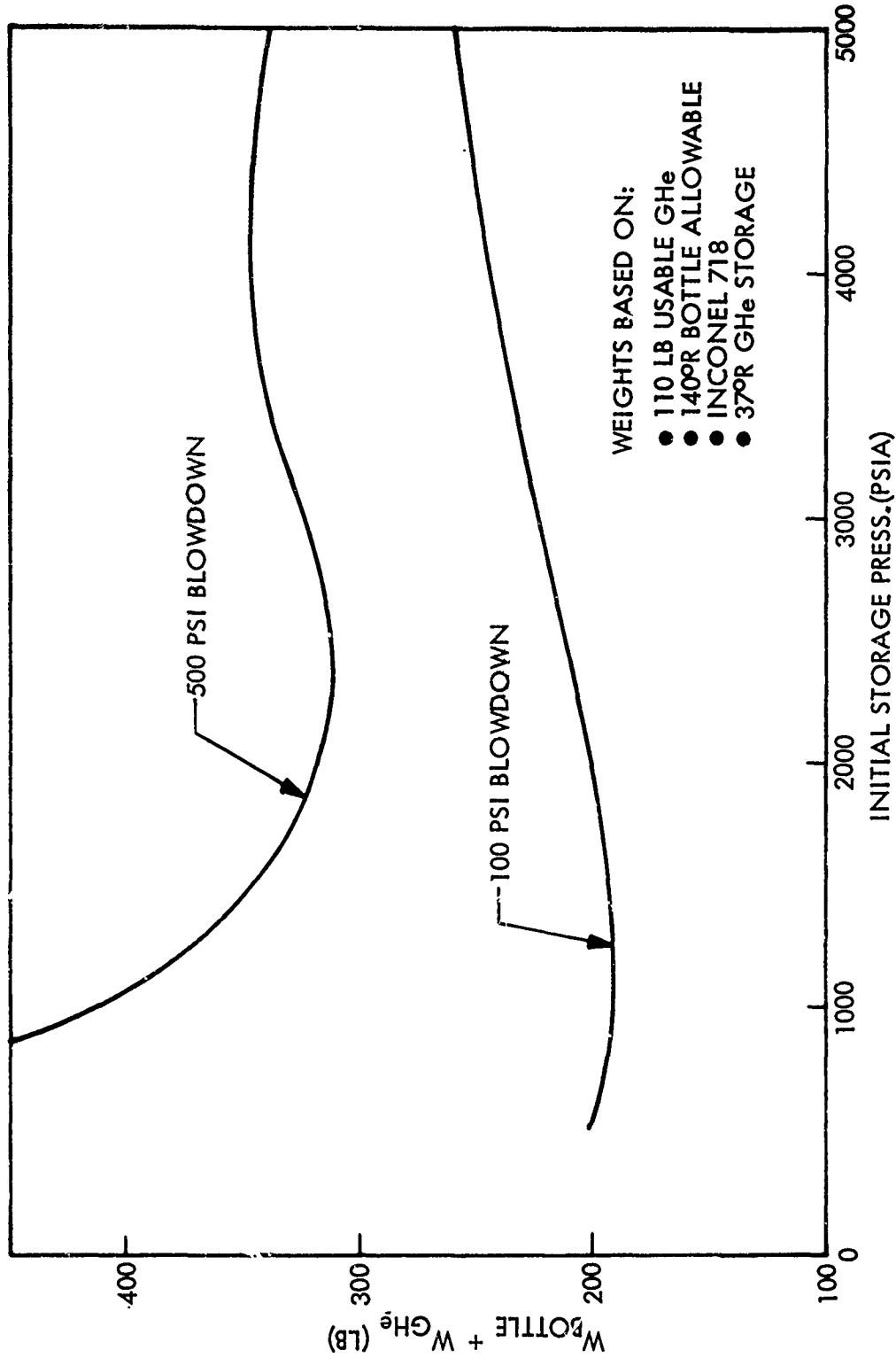


Fig. 8-19 Effect of Final Blowdown Pressure on Optimum Storage Pressure and System Weight (C)

PARAMETRIC PRESSURIZATION DATA FOR SELECTED CONCEPT

(U) Parametric pressurization weight data for the selected system concept (3b) is provided in Subtasks 2 and 3 as part of the overall configuration optimization studies.

CONFIDENTIAL

LMSC-680953

SUBTASK 9 - FILL, VENT, AND FEED PRESSURIZATION LINES STUDY

(C) Preliminary configuration screening analyses of the fill, feed, and vent systems are underway. The primary objective here is to provide data input for the optimization study. The synergistic effect of one system on another may then be properly evaluated in more detail. The most critical design of these systems is the feed lines - and especially the fluorine feed line. Of major concern is vapor formation and control of vapor. Fill-line design for some candidate configurations will affect the heat leak into the tank and/or feed line. Vent system size is affected by fill-line size; it is therefore important that these three systems be analyzed together.

(U) Initial analyses on feed-line pressure drops are presented here.

(C) The major variable in feed-line pressure drop is the line diameter. For reference purposes, pressure drops at full thrust were calculated for line sizes equal to the engine inlet diameters of 2.75 in. The pressure drop in the hydrogen line was 2.5 psi; in the fluorine line, it was 18.6 psi. Because of this high pressure drop in the fluorine line, other line sizes were investigated to see what effect increased line diameters have on reducing this value. The results are shown in Fig. 9-1. Note that increasing the line from 2.75 to 3 in. in diameter decreases the pressure drop from 18.6 to 12 psi. A major portion of the LF_2 feed-line pressure drop is associated with the tank pre valve. For example, the shutoff valve accounted for an 11.8-psi drop at the 2.75-in. diameter. This value is high but is consistent with present bellows-actuated, inline poppet valves being designed for flight-type fluorine service.

CONFIDENTIAL

LOCKHEED MISSILES & SPACE COMPANY

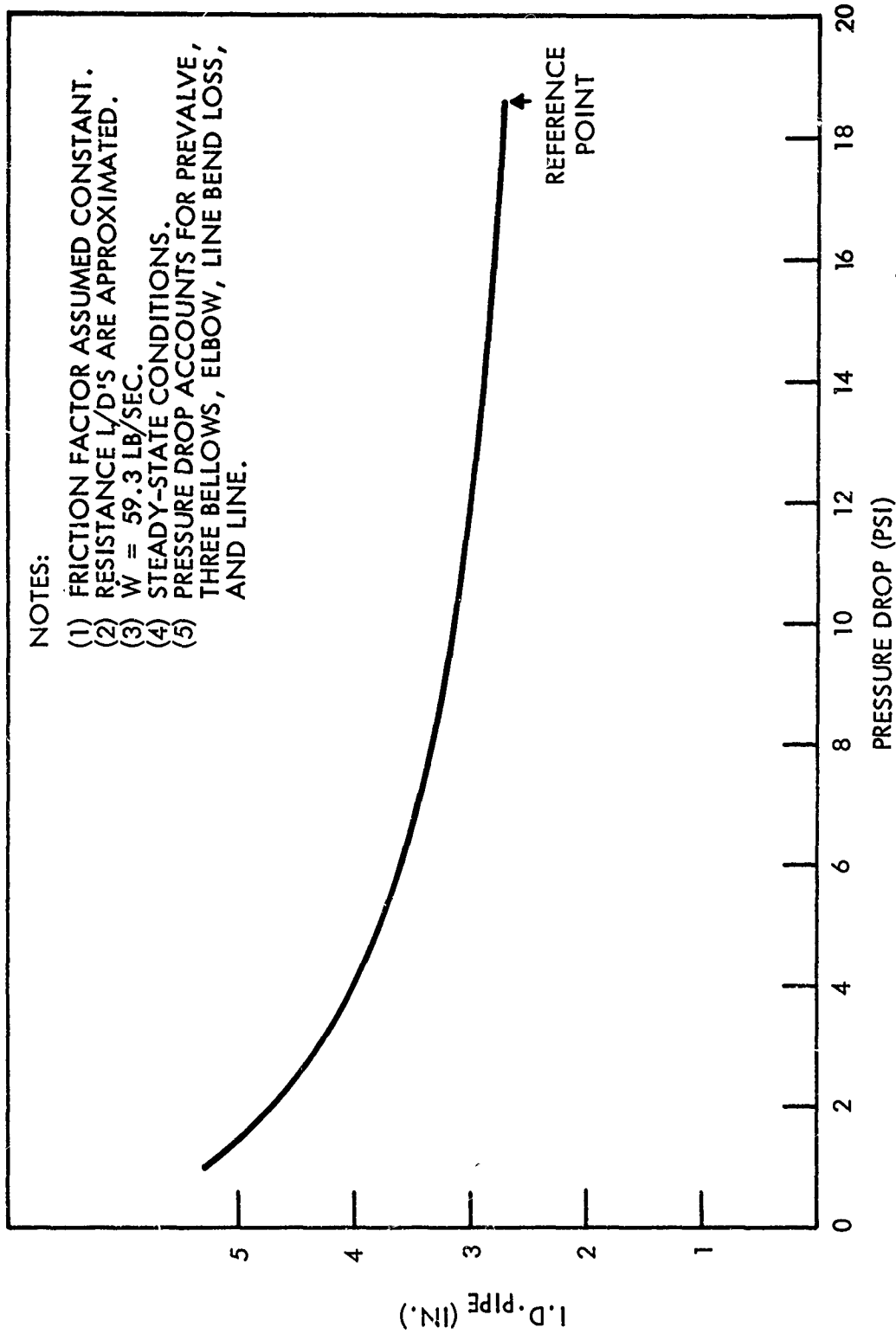


Fig. 9-1 Liquid Fluorine Feed-Line Pressure Drop as a Function of Line Diameter (C)

SUBTASK 10 - FINAL FEED SYSTEM DESIGN

(U) This subtask will begin in January 1969.

CONFIDENTIAL

LMSC-680959

FUTURE ACTIVITIES

(C) During the next quarter, the configuration optimization studies will be completed, as will the stress analysis and design of both propellant tanks. In addition, design of the outer shell will be finished. The compound A/MHF-5 attitude-control system will be integrated into the vehicle. Investigation of the influence of the integrated attitude-control system on the vehicle design will be in progress. Design of the tank supports and insulation system will be completed. Design of the vent-free fluorine system will be in progress. Screening analyses on the propellant orientation system will be finished. Optimization of the pressurization system design and mode of operation will be in progress. Screening analyses and parametric studies on the fill, vent, and feed pressurization lines will be continuing.

The following selections will have been made by the end of the next quarter:

- Tank materials will be selected.
- Tank configurations will be selected.
- Tank design details will be established.
- The outer shell materials will be selected.
- The outer shell configuration will be selected.
- The outer shell design details will be established.
- The compound A/MHF-5 ACS system will be integrated into the AMPS vehicle.
- The tank-support system will be selected.
- The tank-support design details will be established.
- The insulation concept will be selected.
- The insulation design details will be established.
- The propellant orientation system concept will be selected.
- The pressurization system concept will be selected.

CONFIDENTIAL

LOCKHEED MISSILES & SPACE COMPANY

LMSC-680959

REFERENCES

1. Martin-Marietta Company, Titan III-C Payload Users Guide, IR-68-3, Jan 1968
2. Lockheed Missiles & Space Company, Propulsion Feed Systems Handbook, LMSC-T-41-67-1, Sunnyvale, Calif.
3. -----, Propellant Tankage Evaluation for Cryogenic Space Propulsion Stages, LMSC-A796408, Sunnyvale, Calif., Mar 1968
4. -----, First Quarterly Progress Report, Advanced Maneuvering Propulsion System, Propellant Feed System Analytical and Design Study, LMSC-685056, Sunnyvale, Calif., 9 Feb 1968
5. -----, Advanced Maneuvering Propulsion System, Propellant Feed System Analytical and Design Study, Monthly Contract Status Report No. 3, Sunnyvale, Calif., 5 Mar 1968
6. U. S. Navy, Fleet Missile Systems Analyses and Evaluation Group, Bureau of Naval Weapons Failure Rate Data Handbook, (FARADA), SP63-470, Corona, Calif.

Enclosure A

PRESSURIZATION ANALYSES

(C) The pressurization analyses were based on quasi-steady-state conditions existing prior to and immediately after each engine burn. The equation relating the initial and final conditions in the tanks is

$$\left(M_{L_i} U_{L_i} + M_{V_i} U_{V_i} \right)_p + \left(M_i U_i \right)_{He} + \left(M_i U_i \right)_w + \dot{Q} \theta + M_s U_s + M_{ex} h_{ex} - p_{ex} (\Delta V)_d J - \dot{m}_d \bar{h}_d \theta = \left(M_{L_f} U_{L_f} + M_{V_f} U_{V_f} \right)_p + \left(M_f U_f \right)_{He} + M_f U_{f_w}$$

where

$$\left(M_{L_i} U_{L_i} + M_{V_i} U_{V_i} \right) = \text{total internal energy of the propellant prior to expulsion}$$

$$\left(M_i U_i \right)_{He} = \text{total internal energy of helium in the ullage prior to prepressurization}$$

$$\left(M_i U_i \right)_w = \text{total internal energy of the tank wall prior to expulsion}$$

$$\dot{Q} \theta = \text{total energy due to heat transfer that enters the system during expulsion}$$

$$M_s U_s = \text{total internal energy of the prepressurant gas}$$

$$M_{ex} h_{ex} = \text{total internal energy of the expulsion gas}$$

$p_{ex}(\Delta V)_d$ = work performed by the fluid due to a volume change

$\dot{m}_d \bar{h}_d \theta$ = energy of the propellant expelled

$\left(M_{L_f} U_{L_f} + M_{V_f} U_{V_f} \right)_p$ = total internal energy of the remaining propellant after expulsion

$\left(M_f U_f \right)_{He}$ = total internal energy of the helium in the ullage after expulsion

$\left(M_f U_f \right)_w$ = total internal energy of the tank wall after expulsion

(C) It is assumed that the system is in thermal equilibrium before and after an expulsion when the conditions are calculated. Energy entering the system between burns is assumed to be distributed in a mixed model for determining partial pressures and vent requirements when necessary. A collapse factor of 2 was used for warm expulsion gases. This collapse factor will be varied during the optimization study based on experimental data.

CONFIDENTIAL

LOCKHEED MISSILES & SPACE COMPANY

CONFIDENTIAL

Security Classification

DOCUMENT CONTROL DATA - R & D

(Security classification of title, body of abstract and indexing annotation must be entered when the overall report is classified)

1. ORIGINATING ACTIVITY (Corporate author) Rocketdyne, a Division of North American Rockwell Corporation, 6633 Canoga Avenue, Canoga Park, California 91304		2a. REPORT SECURITY CLASSIFICATION CONFIDENTIAL	
		2b. GROUP 4	
3. REPORT TITLE Advanced Maneuvering Propulsion Technology Program (Second Quarterly Progress Report)			
4. DESCRIPTIVE NOTES (Type of report and inclusive dates) Quarterly Progress Report, 1 February 1968 to 30 April 1968			
5. AUTHOR(S) (First name, middle initial, last name)			
6. REPORT DATE May 1968		7a. TOTAL NO. OF PAGES 680	7b. NO. OF REFS 4
8a. CONTRACT OR GRANT NO. F04611-67-C-0116		3a. ORIGINATOR'S REPORT NUMBER(S) R-7380-2	
b. PROJECT NO.			
c.		9b. OTHER REPORT NO(S) (Any other numbers that may be assigned this report)	
d.		AFRPL-TR-68-20	
10. DISTRIBUTION STATEMENT Qualified users may obtain copies of this report from the Defense Documentation Center			
11. SUPPLEMENTARY NOTES		12. SPONSORING MILITARY ACTIVITY AFRPL, Edwards, California	
13. ABSTRACT (U) Analysis and design effort on the Advanced Maneuvering Propulsion System (AMPS) progressed satisfactorily during the second quarterly period. Engine system mixture ratio, operating range, and operational requirements were conducted. Thrust chamber, turbopump, and control subsystem design analysis were performed. Propellant feed system analysis and design effort was accomplished on the propellant tanks, outer shroud and tank supports, insulation, and pressurization subsystems. (C) Engine critical component demonstration testing was accomplished on the main engine thrust chamber segment hardware. Forty firing tests were accomplished with the 5-inch solid-wall segment configuration over a chamber pressure range of 650 psia to 72 psia, which meets the design requirement.			

DD FORM 1473
1 NOV 65CONFIDENTIAL
Security Classification

14.	KEY WORDS	LINK A		LINK B		LINK C	
		ROLE	WT	ROLE	WT	ROLE	WT
	Propellant System Advanced Engines System Performance Propellant Storage						